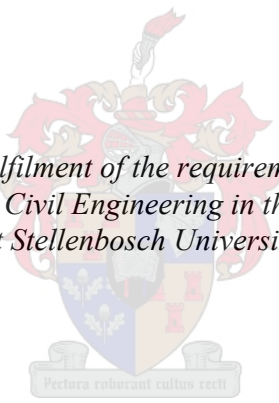


# **An Assessment of the In-situ State and Staged Construction of a Tailings Storage Facility in South Africa**

by  
Yusuf Simjee



*Thesis presented in fulfilment of the requirements for the degree of  
Master of Engineering in Civil Engineering in the Faculty of Engineering  
at Stellenbosch University*

Supervisor: Dr Charles MacRobert

March 2020



UNIVERSITEIT • STELLENBOSCH • UNIVERSITY  
jou kennisvenoot • your knowledge partner

## Plagiaatverklaring / Plagiarism Declaration

- 1 Plagiaat is die oorneem en gebruik van die idees, materiaal en ander intellektuele eiendom van ander persone asof dit jou eie werk is.  
*Plagiarism is the use of ideas, material and other intellectual property of another's work and to present it as my own.*
- 2 Ek erken dat die pleeg van plagiaat 'n strafbare oortreding is aangesien dit 'n vorm van diefstal is.  
*I agree that plagiarism is a punishable offence because it constitutes theft.*
- 3 Ek verstaan ook dat direkte vertalings plagiaat is.  
*also understand that direct translations are plagiarism.*
- 4 Dienooreenkomstig is alle aanhalings en bydraes vanuit enige bron (ingesluit die internet) volledig verwys (erken). Ek erken dat die woordelike aanhaal van teks sonder aanhalingstekens (selfs al word die bron volledig erken) plagiaat is.  
*Accordingly, all quotations and contributions from any source whatsoever (including the internet) have been cited fully. I understand that the reproduction of text without quotation marks (even when the source is cited) is plagiarism.*
- 5 Ek verklaar dat die werk in hierdie skryfstuk vervat, behalwe waar anders aangedui, my eie oorspronklike werk is en dat ek dit nie vantevore in die geheel of gedeeltelik ingehandig het vir bepunting in hierdie module/werkstuk of 'n ander module/werkstuk nie.  
*declare that the work contained in this assignment, except where otherwise stated, is my original work and that I have not previously (in its entirety or in part) submitted it for grading in this module/assignment or another module/assignment.*

<b>Y Simjee</b> <b>Voorletters en van / Initials and surname</b>	<b>March 2020</b> <b>Datum / Date</b>



## Abstract

Due to the sizeable dimensions, in cases of failure, tailings dams represent high-risk not only to the mining operations but also to surrounding communities and the environment. The recent catastrophic failures of Mount Polley (Canada), Fundão (Brazil) and Brumadinho (Brazil) Tailings Storage Facilities (TSF's) between 2014 and 2019, due to static liquefaction caused by the loss of containment of mine tailings, have placed the worldwide mining industry under even greater pressure to ensure that risks associated with TSF's in their global portfolios are assessed according to industry best practice and sound engineering frameworks.

Internationally detailed assessments of the in-situ state of tailings and staged construction are common in design and construction stages as well as post-construction monitoring of these facilities. Recent failures of TSF's globally have prompted mining companies to review their TSF risk evaluation approach and design standards in terms of their current and future assets in their portfolios. Therefore, the need for more specialised studies is likely to gather pace and may possibly become a more frequent requirement in South African TSF design, operation and monitoring studies.

This research covers an array of multifaceted aspects such as material (tailings) behaviour, in-situ and laboratory testing and numerical simulations. The main objectives of the research were to determine the static liquefaction potential of tailings by characterising its in-situ state using in-situ and laboratory test data available for the tailings dam and to perform a staged construction of a tailings dam under static loading conditions by using an appropriate soil constitutive model.

This research describes the application of the Shuttle and Jefferies (2016) methodology to estimate the state parameter for silt-like materials. A comparison with more conventional approaches (developed for sand-like materials) namely, Robertson (2010) as well as Jefferies and Been (2016) was performed. The state parameters spatial distribution was determined by assessing each CPTu along its respective monitoring line. The following pertinent findings were observed:

- The state parameter using Shuttle and Jefferies (2016) procedure is systematically higher than the Robertson (2010) and Jefferies and Been (2016) methodologies.
- The Shuttle and Jefferies (2016) methodology shows that underflow tailings display predominantly dilative (strain-hardening) behaviour at most of the CPTu. Only a few CPTu show minor contractive layers within some portions of the underflow tailings.
- The Shuttle and Jefferies (2016) methodology shows that overflow tailings show contractive (strain-softening) behaviour with interbedding of dilative layers in some portions of the overflow tailings.
- Good correlations were found between SBTn classifications and interpretation of state parameter using Shuttle and Jefferies (2016) methodology in that similar behavioural responses of the underflow (i.e. dilative) and overflow (i.e. contractive) were noted.

In summary, the Shuttle and Jefferies (2016) methodology is based on a more fundamental understanding of the physics involved in cone penetration and uses a constitutive model built around the concept of state parameter, making it more reliable for silt-like tailings than empirically-based procedures (Sottile, et al., 2019).

The staged construction of the tailings dam was numerically modelled using the commercial FEM package RS2. The software was used to generate a 2-D FEM model that involves defining type of materials and associated input parameters, phreatic surface and boundary conditions. Also, the software was used to calibrate the Softening-Hardening soil constitutive model with drained and undrained triaxial test data. As part of this research the pore pressure distribution, drainage conditions and location of phreatic surface were assessed at varying rates of rise using hydraulic gradients representative of hydrostatic and sub-hydrostatic pore pressure conditions. The following pertinent findings were observed:

- The RoR has a more noticeable impact on the location of the phreatic surface than the pore pressure regime. With an increasing rate of rise, there is a corresponding rise of the phreatic surface.
- The largest pore pressures are developed in the overflow zone that has the lowest permeability. Underflow tailings are unsaturated following construction due to its higher permeability.
- Phreatic surface and pore pressure trends observed in the analyses are comparable to the literature. Maximum bulbs/zones of pore water pressure form at the overflow-foundation interface.
- For RoR of 3.0 m/yr and 6.0 m/yr using hydraulic gradients representative of sub-hydrostatic pore pressure conditions, the lower portion of the overflow tailings demonstrate a drained-like behaviour during staged construction. This is reflected by the continuous increases in effective confining pressure ( $p'$ ) that are notably higher than their corresponding pore pressure ( $pp$ ). It can also be observed that drainage conditions become poorer into the TSF-A basin as the differences between  $p'$  and  $pp$  progressively decrease from Points 1 to 4 (Figure 6-14).
- For RoR of 3.0 m/yr and 6.0 m/yr using hydraulic gradients representative of hydrostatic pore pressure conditions, the lower portion of the overflow tailings from Points 1 to 3 demonstrate a drained-like behaviour during staged construction. On the other hand, Point 4 demonstrates undrained-like behaviour. This is reflected by the continuous increases in  $pp$  that are notably higher than their corresponding  $p'$  (Figure 6-15).

The staged construction using fully coupled transient FEM analyses was found to be a valuable tool to understanding the pore pressure distribution, drainage conditions and location of phreatic surface within a tailings dam.

## Opsomming

Vanweë die aansienlike groote, in die geval van faaling, hou slikdamme 'n hoë risiko vir nie net mynbedrywighede nie, maar ook vir die omliggende gemeenskappe en die omgewing. Die onlangse katastrofiese faalings van Mount Polley (Kanada), Fundão (Brasilië) en Brumadinho (Brasilië) se opbergingsfasiliteite tussen 2014 en 2019, weens statiese vervloeiing wat veroorsaak word deur die verlies aan behoud van mynafval, het die mynboubedryf wêreldwyd onder nog groter druk geplaas om te verseker dat die risiko's verbonde aan slikdamme in hul wêreldwye portefeuljes, volgens beste praktyke en vertoubare ingenieursraamwerke beoordeel word.

Internasionale gedigitalleerde assesserings van die in-situ toestand van die slikdamme en gefaseerde konstruksie van 'n numeriese model is algemeen in ontwerp en konstruksie fases. Dit word ook toegepas op post-konstruksie monitering van hierdie fasiliteite. Onlangse faalings van slikdamme wêreldwyd het mynmaatskappye aangespoor om hul slikdam-risikoevalueringsbenadering en ontwerpstandaarde in terme van hul huidige en toekomstige bates in hul portefeuljes te hersien. Dus, die behoefte aan meer gespesialiseerde studies is dus geneig om meer in aanvraag te wees, en kan moontlik 'n vereiste in die Suid-Afrikaanse slikdamontwerp bedryf en moniteringsstudies wees.

Hierdie navorsing dek 'n verskeidenheid van aspekte aan soos materiaal (slik) gedrag, in-situ en laboratoriumtoetsing, en numeriese simulaties. Die belangrikste doelwite van die navorsing was om eerstens, die statiese vervloeiing potensiaal van slik te bepaal deur die eienskappe van die in-situ toestand van die slikdam te gebruik. Dit word met behulp van in-situ en laboratoriumtoetsdata wat beskikbaar is vir die slikdam bepaal. Tweedens om 'n gefaseerde numeriese model konstruksie van 'n slikdam te analiseer onder statiese lading toestande. Die numeriese analise was gedoen met behulp van 'n toepaslike grondkonstitutiewe model gebruik te maak.

Hierdie navorsing beskryf die toepassing van Shuttle en Jefferies (2016) se metodologie deur die staatsparameter vir slik-agtige materiaal te beraam. 'n Vergelyking was ook getrek deur van meer konvensionele benaderings (ontwikkel vir sand-agtige materiaal) gebruik te maak naamlik, Robertson (2010) asook Jefferies en Been (2016). Die staatsparameters se ruimtelike verspreiding is bepaal deur elke CPTu langs die onderskeidelike moniteringslyn te assesseer. Die volgende bevindinge is waargeneem:

- Die staatsparameter wat bepaal is deur behulp van Shuttle en Jefferies (2016) se prosedure, is hoër as die wat bepaal word deur Robertson (2010), en Jefferies en Been (2016) se prosedures.
- Die Shuttle en Jefferies (2016) metode toon dat ondervloeiislik oorwegend dilatiewe (spanning-verharding) gedrag toon by meeste van die CPTu. Slegs 'n paar CPTu vertoon klein kontrakktiewe lae binne sommige gedeeltes van die ondervloeiislik.
- Die Shuttle en Jefferies (2016) metode toon dat die oorloopslik kontrakktiewe (spanning-versagting) gedrag toon, met dilatiewe interbedingslae in sommige gedeeltes van die oorloopslik.
- Goeie korrelasies is gevind tussen SBTn klassifikasies en die interpretasie van Shuttle en Jefferies (2016) se prosedure van die staatsparameter, deurdat soortgelyke gedrag met betrekking tot die ondervloeiislik (dilatiewe) en oorloopslik (d.w.s. kontrakktiewe), gevind is.

In opsomming, die Shuttle en Jefferies (2016) metodologie is gebaseer op 'n meer fundamentele begrip van die Fisika wat betrokke is by kegel penetrasie, en gebruik 'n konstitutiewe model, gebou rondom die konsep van die staat parameter. Dit maak dit meer betroubaar vir silt-agtige slik as empiries-gebaseerde prosedures (Sottile, et al., 2019).

Die fase numeriese model konstruksie van die slikdam is gemodelleer met behulp van die kommersiële sagteware pakket FEM-pakket RS2. Die sagteware is gebruik om 'n 2-D FEM model op te stel deur die tipe materiale te definieer asook gepaardgaande inset parameters, watertafel vlak, en grenstoestande. Die sagteware is ook gebruik om die versagting-verharding grond konstitutiewe model te kalibreer met behulp van gedreineerde en ongedreineerde triaksiale toets data. As deel van hierdie navorsing word die porieëdrukverspreiding, dreineringsstoestande en ligging van die watertafel vlak teen wisselende tempo van verhooging (RoR) geassesseer. Die assessering was uitgevoer deur middel van die hidrouliese gradiënte wat hidrostatiese en sub-hidrostatiese porieëdruktoestande verteenwoordig te gebruik. Die volgende tersaaklike bevindinge is waargeneem:

- Die “RoR” het 'n meer merkbare impak op die ligging van die watertafelvlak as wat die porieëdrukregime het. Soos wat die “RoR” toeneem is daar 'n ooreenstemmende toeneeming van die watertafel vlak.
- Die grootste porieëdruk word ontwikkel in die oorloopslikone wat die laagste deurlaatbaarheid het. Ondervloei is onversadig na konstruksie as gevolg van die hoër deurlaatbaarheid.
- Die Watertafel vlak en porieëdruk tendense wat waargeneem is in die ontledings, is vergelykbaar met die literatuur. Maksimum sones van porieëwaterdruk vorm tussen die oorloopslik en fondasievlak.
- Die onderste gedeelte van die oorloopslik toon 'n gedreineerdagtige gedrag tydens die fasekonstruksie van die numeriese model. Dit vertoon spesifiek by 'n tempo van verhooging van 3,0 m/jaar en 6,0 m/jaar deur gebruik te maak van hidrouliese gradiënte verteenwoordigend is van sub-hidrostatiese porieëdruktoestande. Dit word weerspieël deur die deurlopende verhoging in effektiewe beperkende druk wat veral hoër is as die ooreenstemmende porieëdruk. Swakker dreineringsstoestande is waargeneem in slikdam A as gevolg van die verskille tussen beperkendedruk en porieëdruk wat progressief afneem van punte 1 tot 4 (Figuur 6-14).
- Vir RoR, van 3,0 m/jaar en 6,0 m/jaar met behulp van hidrouliese gradiënte verteenwoordiger van hidrostatiese porieëdruk toestande, word die volgende waargeneem: Die onderste gedeelte van die oorloopslik, van punt 1 tot 3, toon 'n gedreineerd-agtige gedrag tydens die fase konstruksie van die numeriese model; punt 4 toon ongedreineerde-agtige gedrag. Dit word weerspieël deur die deurlopende styging in porieëdruk wat veral hoër is as hul ooreenstemmende behoudendedruk (Figuur 6-15).

Die fasekonstruksie van 'n numeriese model wat ten volle gekoppel is aan “transient” FEM-ontledings, is 'n waardevolle hulpmiddel om die porieëdrukverspreiding, dreineringsstoestande en-ligging van die watertafelvlak binne 'n slikdam te verstaan.

## Acknowledgements

I would like to thank the following people:

- Dr Charles MacRobert, for his guidance as my supervisor during this project.
- Mauro Sottile and Dr Alejo Sfriso at SRK Consulting (Argentina) as well as Adriaan Meintjes at SRK Consulting (South Africa) for their support and guidance throughout this project.
- SRK Consulting (South Africa) work colleagues, for their support and understanding during this project.
- My wife and children as without their prayers, love, sacrifices and support (mental and motivational) I may never have completed this thesis.
- My parents for their love and support throughout my life. Thank you both for giving me strength to challenge myself and chase my dreams. My brothers, sister, aunties and cousins deserve my wholehearted thanks as well.
- My grandparents, for their love and support during my studies. A special mention to my paternal grandfather who passed away last May. Thank you for always being there and for setting such an immaculate example for me and my siblings to follow. I wish you could have been here and I hope I have made you proud.

# Contents

Abstract .....	ii
Acknowledgements.....	vi
List of Tables .....	ix
List of Figures .....	x
Chapter 1 : Introduction .....	1
1.1. Problem Definition .....	1
1.2. Scope and Objectives.....	2
1.3. Approach.....	2
1.4. Limitations of the Study .....	3
1.5. Thesis Structure.....	3
Chapter 2 : Literature Review.....	4
2.1. Tailings Dam Failures .....	4
2.2. Theoretical Considerations for Liquefaction of Tailings.....	9
2.3. Characterisation of Tailings Behaviour.....	12
2.3.1. Critical State Soil Mechanics .....	14
2.3.2. NorSand Constitutive Model.....	15
2.3.3. Measuring In-Situ State of Tailings.....	20
2.3.4. Note on Characterisation of Tailings Behaviour and CSSM.....	25
2.4. Staged Construction of Tailings Dams .....	25
2.5. Static and Dynamic Tailings Parameters.....	30
2.6. Tailings Dam Surveillance .....	30
2.7. Conclusion .....	33
Chapter 3 : Overview of TSF-A and Testing Data.....	34
3.1. TSF-A.....	34
3.2. Laboratory Data .....	35
3.3. In-Situ Data .....	35
Chapter 4 : Determination of In-Situ State Parameters.....	37
4.1. Calibration of NorSand Constitutive Model.....	39
4.1.1. Overflow Tailings Calibration .....	39
4.1.2. Underflow Tailings Calibration.....	39
4.2. Calibration of $k$ and $m$ Coefficients .....	42
4.3. Interpretation of The State Parameter from CPTu Data.....	45

4.4.	State Parameter Variability and Spatial Distribution.....	50
4.5.	Summary of State Parameter Assessment At TSF-A .....	52
Chapter 5 : Soil Constitutive Model for Staged Construction .....		53
5.1.	Softening Hardening Soil Constitutive Model .....	53
5.2.	Calibration of Softening-Hardening Constitutive Model.....	55
5.3.	Calibration at Elemental Level .....	56
5.3.1.	Overflow Tailings .....	56
5.3.2.	Underflow Tailings .....	59
Chapter 6 : Staged Construction Numerical Modelling .....		62
6.1.	Software.....	62
6.2.	Numerical Model Setup .....	62
6.2.1.	Constitutive Models .....	62
6.2.2.	Material Parameters .....	63
6.2.3.	Hydraulic Parameters .....	63
6.2.4.	Geometry and Mesh .....	64
6.2.5.	Model Stages .....	66
6.2.6.	Boundary Conditions .....	66
6.3.	Results and Discussion of Staged Construction.....	69
6.4.	Summary of Staged Construction At TSF-A.....	71
Chapter 7 : Conclusions .....		84
7.1.	Future Research .....	85
Chapter 8 : References.....		86
Appendix A: CPTu Interpretation – Monitoring Line A .....		97
Appendix B: CPTu Interpretation – Monitoring Line B .....		110
Appendix C: CPTu Interpretation – Monitoring Line C .....		126
Appendix D: CPTu Interpretation – Monitoring Line D .....		139
Appendix E: CPTu Interpretation – Monitoring Line E .....		152
Appendix F: CPTu Interpretation – Monitoring Line F .....		171
Appendix G: CPTu Interpretation – Monitoring Line G.....		196
Appendix H: CPTu Interpretation – Monitoring Line H .....		212
Appendix I: CPTu Interpretation – Monitoring Line I.....		225
Appendix J: CPTu Interpretation – Monitoring Line O.....		241
Appendix K: CPTu Interpretation – Monitoring Line P .....		263

## List of Tables

Table 2-1:	Example of Information Captured in WISE Database. ....	4
Table 2-2:	Cases and Causes of Static Liquefaction Failures. ....	6
Table 2-3:	Summary of NorSand Soil Properties (Shuttle and Jefferies, 2010). ....	18
Table 2-4:	Recommended Laboratory Tests for Tailings (Been, 2016). ....	18
Table 2-5:	Summary of Important Literature Related to Interpretation of $\psi$ (Been, 2016). ....	21
Table 2-6:	Summary of Pore Pressures Regimes (Martin, 1999). ....	28
Table 2-7:	Proposed Guidelines in Tailings Facility Design and Construction (Caldwell, 2016). ....	32
Table 2-8:	Instrumentation and Associated Outputs for Monitoring Slope Stability (Du Toit, 2015). ....	32
Table 3-1:	Summary of CIUC and CIDC Triaxial Tests Conducted on Overflow and Underflow Tailings. ....	35
Table 4-1:	Calibrated NorSand Parameters for Overflow Tailings. ....	39
Table 4-2:	Calibrated NorSand Parameters for Underflow Tailings. ....	39
Table 4-3:	Summary of Calibrated $k$ and $m$ Coefficients for Overflow and Underflow Tailings. ....	45
Table 4-4:	Criterion to Define $k$ and $m$ Coefficients Used to Interpret $\Psi$ (Jefferies and Been, 2016). ....	45
Table 4-5:	State Parameter Interpretation Across the Various Monitoring Lines. ....	51
Table 4-6:	SBTn Interpretation Across the Various Monitoring Lines. ....	51
Table 5-1:	Overflow Tailings Parameters Calibrated for S-H Constitutive Model. ....	56
Table 5-2:	Pertinent Observations for Overflow Parameters Calibrated for S-H Constitutive Model. ....	57
Table 5-3:	Underflow Tailings Parameters Calibrated for S-H Constitutive Model. ....	59
Table 5-4:	Pertinent Observations for Overflow Parameters Calibrated for S-H Constitutive Model. ....	60
Table 6-1:	Hydraulic Parameters Used in Numerical Modelling in RS2. ....	64



## List of Figures

Figure 2-1:	(a) Kingston TSF Failure (b) Mount Polley TSF Failure (c) Fundao TSF Failure (d) Brumadinho TSF Failure (Skytruth, 2016; TheStar, 2006; The Guardian, 2019; Wikipedia, 2019) .....	7
Figure 2-2:	(a) Merriespruit TSF Failure Showing the Path of the Destructive Mudflow That Occurred (b) Bafokeng TSF Failure (c) Two of the Three Failures That Occurred at the Saaiplaas TSF (Boulanger and Duncan, n.d.; Fourie, et al., 2001). .....	8
Figure 2-3:	CSL and the Meaning of Parameters $\Gamma$ , $\lambda_{ln}$ , and $\psi$ (Torres-Cruz, 2011). .....	10
Figure 2-4:	Ideal Behaviour of Loose, Saturated Cohesionless Tailings Under Monotonic and Cyclic Loading (Davies, et al., 2002).....	11
Figure 2-5:	Tailing Gradations Illustrating Dominance of Silt Fraction (Shuttle and Jefferies, 2016) .....	12
Figure 2-6:	Measured Silt Densification from In-Situ to As-Tested Conditions (Shuttle and Jefferies, 2016). .....	13
Figure 2-7:	Instability Limit in Relation to Limiting Stress Ratio from Drained Tests on Dense Samples (Been, 2016). .....	14
Figure 2-8:	Definition of $\Psi$ and $R$ (Jefferies and Shuttle 2002).....	16
Figure 2-9:	NorSand Yield Surfaces and Limiting Stress Ratios. (a) Very Loose Soil; (b) Very Dense Soil (Jefferies and Shuttle 2005).....	17
Figure 2-10:	Comparison of NorSand With Reconstituted Silt Behaviour In (a) Drained and (b) Undrained Triaxial Compression (Shuttle and Jefferies, 2016). .....	20
Figure 2-11:	Example of Soil Behaviour Identified by CPTu on Soil Classification Chart (Been, 2016). ....	22
Figure 2-12:	Updated SBTn Chart Showing Behaviour Based Descriptions (Robertson, 2016).....	22
Figure 2-13:	CPTu Profile in Massive Silt Tailings Deposit (Shuttle and Jefferies, 2016). .....	23
Figure 2-14:	Pore Pressure Measured at $u_1$ and $u_2$ Locations on a CPTu (Robertson, 2013).....	24
Figure 2-15:	Graphical Representation of Pore Pressure Regimes (Martin, 1999). .....	29
Figure 2-16:	Risk Management Via The Observational Method (Martin and Davies, 2000). .....	31
Figure 2-17:	Failure Modes, Warning Signs and Surveillance Measures (Martin and Davies, 2000). .....	31
Figure 3-1:	Schematic of Upstream TSF-A Showing Underflow Wedge and Impounded Overflow.....	34
Figure 3-2:	Schematic Drawing of TSF-A Monitoring Line Layout Plan. ....	36
Figure 4-1:	Correlations of $\lambda_{10}$ with $k$ and $m$ (Jefferies and Been, 2016).....	37
Figure 4-2:	Scheme to Compute the Cavity Expansion Limit Effective Pressure ( $p'_{lim}$ ) Using NorSand and a Large Strain 1D FEM Code (Shuttle and Jefferies, 2016).....	38
Figure 4-3:	Comparison Between CIUC CIDC Test Data and NorSand Calibration for Overflow. ....	40
Figure 4-4:	Comparison Between CIUC CIDC Test Data and NorSand Calibration for Underflow. ....	41
Figure 4-5:	CPTWidget Results for Drained Analyses on the Overflow Tailings. ....	43
Figure 4-6:	CPTWidget Results for Undrained Analyses on the Overflow Tailings. ....	43
Figure 4-7:	CPTWidget Results for Drained Analyses on the Underflow Tailings. ....	44
Figure 4-8:	CPTWidget Results for Undrained Analyses on the Underflow Tailings. ....	44
Figure 4-9:	Cone Resistance, Friction Ratio, Soil Behaviour Type ( $I_c$ ), Interpreted State Parameter Along Depth ( $\psi$ ), Contractive and Dilative Zones with Depth for Shuttle and Jefferies (2016), Jefferies and Been (2016) and (Robertson 2010) Methodologies, Robertson (2010) SBTn Analysis for CPTu PC1.....	47

Figure 4-10:	Frequency of Shuttle and Jefferies (2016), Jefferies and Been (2016) and Robertson (2010) Derived State Parameters Along Depth of CPTu PC1. ....	48
Figure 4-11:	Difference of State Parameter Between Shuttle and Jefferies (2016) and Jefferies and Been (2016) as well as Shuttle and Jefferies (2016) and Robertson (2010) for CPTu PC1. ....	49
Figure 5-1:	The Yield Surfaces of the S-H model; a) Deviatoric Yield Surface (red) and the Vertical Cap (green); b) Deviatoric Yield Surface (red) and Elliptical Cap (blue) (Rocscience Inc B, n.d.).	54
Figure 5-2:	Yield Surface of S-H Model With Vertical Cap In 3D Stress Space (Rocscience Inc B, n.d.).	54
Figure 5-3:	Yield Surface of S-H Model With Elliptical Cap in 3D Stress Space (Rocscience Inc B, n.d.).	55
Figure 5-4:	Comparison Between CIUC CIDC Test Data and S-H Calibration for Overflow Tailings. ....	58
Figure 5-5:	Comparison Between CIUC CIDC Test Data and S-H Calibration for Underflow Tailings. ....	61
Figure 6-1:	Example of Hydraulic Conductivity Function for the Overflow Tailings. ....	63
Figure 6-2:	Monitoring Line F Showing Modelled Zones. ....	65
Figure 6-3:	Monitoring Line F Showing the Modelled 2-D Full Finite Element Mesh. ....	65
Figure 6-4:	Monitoring Line F Showing the Modelled 2-D Zoomed-In Finite Element Mesh. ....	65
Figure 6-5:	Summary of TSF-A Construction Stages as Modelled in RS2. ....	67
Figure 6-6:	Hydraulic Boundary Conditions for Final Stage of Construction. ....	68
Figure 6-7:	Mechanical Boundary Conditions for Final Stage of Construction as well as Points 1 to 4 and Section A to D Used to Extract and Compare Data. ....	68
Figure 6-8:	The Evolution of Total Head and the Location of the Phreatic Surface for a Rate of Rise of 3.0 m/yr and 6.0 m/yr, Using a Sub-Hydrostatic Hydraulic Gradient. ....	73
Figure 6-9:	The Evolution of Total Head and the Location of the Phreatic Surface for a Rate of Rise of 3.0 m/yr and 6.0 m/yr, Using a Hydrostatic Hydraulic Gradient. ....	75
Figure 6-10:	Contours of Pore Water Pressure at the End of Construction, for a Rate of Rise of 3.0 m/yr, Using a Sub-Hydrostatic Hydraulic Gradient. ....	76
Figure 6-11:	Contours of Pore Water Pressure at the End of Construction, for a Rate of Rise of 6.0 m/yr, Using a Sub-Hydrostatic Hydraulic Gradient. ....	76
Figure 6-12:	Contours of Pore Water Pressure Developed at the End of Construction, for a Rate of Rise of 3.0 m/yr, Using a Hydrostatic Hydraulic Gradient. ....	77
Figure 6-13:	Contours of Pore Water Pressure Developed at the End of Construction, for a Rate of Rise of 6.0 m/yr, Using a Hydrostatic Hydraulic Gradient. ....	77
Figure 6-14:	Time History of Pore Pressure (PP) and Effective Confining Pressure ( $p'$ ) at Points 1 to 4, Using a Sub-Hydrostatic Hydraulic Gradient. ....	78
Figure 6-15:	Time History of Pore Pressure (PP) and Effective Confining Pressure ( $p'$ ) at Points 1 to 4, Using a Hydrostatic Hydraulic Gradient. ....	79
Figure 6-16:	Pore Pressures Along Section Line A at the End of Construction, Using Sub-Hydrostatic and Hydrostatic Hydraulic Gradients at Rates of Rise Ranging Between 3.0 m/yr and 6.0 m/yr. .	80
Figure 6-17:	Pore Pressures Along Section Line B at the End of Construction, Using Sub-Hydrostatic and Hydrostatic Hydraulic Gradients at Rates of Rise Ranging Between 3.0 m/yr and 6.0 m/yr. .	81
Figure 6-18:	Pore Pressures Along Section Line C at the End of Construction, Using Sub Hydrostatic and Hydrostatic Hydraulic Gradients at Rates of Rise Ranging Between 3.0 m/yr and 6.0 m/yr. .	82
Figure 6-19:	Pore Pressures Along Section Line D at the End of Construction, Using Sub-Hydrostatic and Hydrostatic Hydraulic Gradients at Rates of Rise Ranging Between 3.0 m/yr and 6.0 m/yr. .	83

# Chapter 1 : Introduction

Major mining operations have increased their production by an order of magnitude every 30 years, for the past 120 years (Robertson, 2012). This has resulted in a significant rise in tailings production over time, which in turn has led to a significant increase in volume, area and height of tailings dams. Robertson (2012) referred to these structures as “*giants of the landscape*” that must remain stable long after monitoring and maintenance have ceased. The largest tailings dams are by volume the largest manmade structures ever created (Morgenstern and Kupper 1988; Aubertin and Chapuis 1991). In the event of a breach, a large volume of tailings could potentially undergo flow liquefaction causing serious damage to downstream environments, infrastructure and populations (WISE, 2018).

Tailings are residual materials that is the by-product of mineral extraction from mined ores. In southern Africa, they usually are non-cohesive, sandy silt to silt-sized particles that show complex behaviour depending on the pore pressure regime to which they are exposed (Martin, 1999). Tailings are usually pumped in the form of a slurry via a delivery pipeline to the tailings dam. They are hydraulically deposited via several methods, namely: subaerial discharge (with spigots and hydrocyclones), subaqueous discharge (slurry is injected below the water surface), thickened discharge (slurry with low water content) and open-end discharge behind a mechanically formed containment wall (McPhail and Wagner, 1989; Jewell, 1998). Tailings dams constructed by mechanical means involve the construction of containment walls using imported materials (McPhail and Wagner, 1989). Tailings dams are generally constructed using the upstream, downstream or centreline methods that involve staged construction over the operational life of the facility with compacted in-situ material, tailings and/or waste rock (Vick, 1990).

Tailings dams constructed using the upstream method require low volumes of mechanically placed fill material for initial starter wall construction. Subsequently, hydraulic deposition is used to raise the tailings dam in the upstream slope direction. This leads to the upstream construction method being the most economical and as a result the most adopted in the mining industry (Vick, 1983; Vick, 1990; Martin and McRoberts, 1999; WISE, 2004; Saad and Mitri, 2010). However, whilst this method is economically favourable, it involves several dam stability related risks associated with high Rates of Rise (RoR), rapid rise in phreatic surface, hydraulic fracturing and internal erosion (piping), static and seismic liquefaction as well as excessive settlements and horizontal deformations resulting from foundation instability (WISE, 2004). It should be noted that these risks need to be assessed and continuously monitored from the design stage right through to post-closure of the facility.

## 1.1. Problem Definition

Due to the sizeable dimensions (area, height and storage volume) of these so-called “*giants of the landscape*”, in cases of failure, tailings dams represent high-risk not only to the mining operations but also to surrounding communities and the environment. The recent catastrophic failures of Mount Polley (Canada), Fundão (Brazil) and Brumadinho (Brazil) Tailings Storage Facilities (TSF's) between 2014 and 2019, due to static liquefaction caused by the loss of containment of mine tailings, have placed the worldwide mining industry under even greater pressure to ensure that risks associated with TSF's in their global portfolios are assessed according to industry best practice and sound engineering frameworks.

Internationally detailed assessments of the in-situ state of tailings and staged construction are common in design and construction stages as well as post-construction monitoring of these facilities. As mentioned above, recent failures of TSF's globally have prompted mining companies to review their TSF risk evaluation approach and design standards in terms of their current and future assets in their portfolios. Therefore, the need for more specialised studies is likely to gather pace and may possibly become a more frequent requirement in South African TSF design, operation and monitoring studies.

## 1.2. Scope and Objectives

Taking cognisance of the complexity surrounding numerical assessments of TSF's, research covers an array of multifaceted aspects such as material (tailings) behaviour, in-situ and laboratory testing and numerical simulations.

The main objectives of the research presented in this thesis are:

- To review available information with focus placed on studies related to in-situ state and static liquefaction potential of tailings, static liquefaction failures, hydromechanical behaviour of tailings during staged construction as well as tailings dam monitoring and surveillance;
- To determine the static liquefaction potential of a tailings dam by characterising its in-situ state using in-situ and laboratory test data available for the tailings dam;
- To perform a staged construction of a tailings dam under static loading conditions by using an appropriate soil constitutive model.

## 1.3. Approach

In order to accomplish the above-mentioned objectives, the following approach was adopted:

- A literature review was conducted on in-situ state and static liquefaction potential of tailings, static liquefaction failures, hydromechanical behaviour of tailings during staged construction as well as tailings dam monitoring and surveillance;
- The data from the literature review was used to highlight the presence/absence of published tailings dam static liquefaction and staged construction studies in South Africa;
- In-situ state parameters ( $\psi$ ) were determined for platinum tailings using the methodology proposed by Shuttle and Jefferies (2016) that focuses on silt-like materials;
- Contractive and dilative behaviour of tailings (based on  $\psi$ ) were used to infer layering (material boundaries) within the tailings dam;
- A commercial Finite Element Modelling (FEM) package was selected as a numerical tool for modelling staged construction of the tailings dam. The software was used to generate a 2-D FEM model that involves defining type of materials and associated input parameters, phreatic surface and boundary conditions. Also, the software was used to calibrate the selected soil constitutive model with drained and undrained triaxial laboratory test data.

## 1.4. Limitations of the Study

The limitations of this thesis are:

- Apparent biases/uncertainties regarding the triaxial testing performed in a commercial laboratory, seem to have influenced the results. The author balanced these various sources of uncertainty to produce a reasonable and credible set of calibration parameters presented in this study.
- The study is limited to aspects specifically related to determining the in-situ state of the platinum tailings and staged construction of the TSF. The CPTu results used in determining the tailings in-situ state, were limited to tailings beneath the TSF slopes. This is primarily due to safety and access constraints associated with probing within the TSF basin. The purpose of the staged construction was not to perform a static trigger analyses that goes beyond the scope of this study.
- Routine slope stability analyses and associated factors of safety were considered in this study.

## 1.5. Thesis Structure

This thesis consists of the following chapters:

Chapter 1 outlines TSF's in mining operations. The background, problem definition, scope and objectives of the thesis are described.

Chapter 2 presents a literature review focussed on studies related to a Critical State Soil Mechanics (CSSM) framework to characterise the in-situ state and static liquefaction potential of tailings, static liquefaction failures, hydromechanical behaviour of tailings during staged construction as well as tailings dam monitoring and surveillance.

Chapter 3 presents an overview of the tailings dam considered in this study as well as a summary of the in-situ and laboratory test data that will be used in this thesis.

Chapter 4 presents the analyses performed to estimate the state parameter on tailings following Shuttle and Jefferies (2016) methodology, which combines the use of CPTu data and numerical element tests using the NorSand constitutive model.

Chapter 5 presents the calibration process and the performance in element tests of the selected soil constitutive model used for numerically modelling the staged construction of the tailings dam.

Chapter 6 presents an assessment of the staged construction using numerical modelling techniques.

Chapter 7 presents the conclusions of the dissertation and recommendations for future research. The proceeding sections include the list of the references and appendices.

## Chapter 2 : Literature Review

The chapter starts with a review of tailings dam failures related to static liquefaction. The second part of the chapter provides an overview of theoretical considerations for liquefaction of tailings. The third part reviews the characterisation of tailings behaviour within the CSSM framework. The fourth part provides a brief overview of staged construction and a review of some recent staged construction studies related to tailings dams. The fifth part provides a brief overview of the mechanical and dynamic properties of tailings and how they are determined. The final two parts of the chapter respectively review the tailings dam monitoring and surveillance practices as well as conclusions of the literature review.

It was initially planned to primarily focus the literature review on South African tailing dam studies. However, upon investigation and review of the available literature, South African related studies with regards to the topics mentioned above, were limited. Therefore, the literature review was expanded to include international tailings dam studies of which extensive literature is available.

### 2.1. Tailings Dam Failures

The improvement of mineral extraction technology has allowed reserves with even lower grade ore to be exploited, resulting in significant increases in tailing dams volumes which is more than likely to be the cause of more frequent, severe and very serious tailings dam failures (Davies 2002; Psarropoulos and Tsompanakis, 2008; Rico et al., 2008; Azam and Li, 2010; Ferdosi et al., 2015a, 2015b; Bowker and Chambers, 2015; Wanderley et al., 2016). The US National Committee on Large Dams (1994) defines "failure" as *"any breach in the embankment leading to a release of the impounded tailings"*. Of concern is the rate of failure of tailings dams being notably greater than that of water retention dams even though improvements in design, construction and monitoring methods of tailings dams are continuously being improved (ICOLD 2001; Aubertin et al., 2002a, 2002b; Davies, 2002; Hardy and Engels, 2007; Azam and Li, 2010).

There are several sources that aim to summarise the worldwide tailings dam failure incidents in databases that are continuously updated (Davies et al., 2000). The most popular database referenced in the literature seems to be the WISE Internet site (<https://www.wise-uranium.org/mdaf.html>). An example of the information that the WISE database captures is presented in Table 2-1.

Table 2-1: Example of Information Captured in WISE Database.

Date	Location	Parent Company	Ore Type	Type of Incident	Release	Impacts
10 July 2019	Cobriz mine, San Pedro de Coris district, Churcampa province, Huancavelica Region, Peru	Doe Run Perú S.R.L	Copper	Tailings dam failure	67 488 m <sup>3</sup> of tailings	Tailings covered an area of 41 574 m <sup>2</sup> and reached Mantaro River

A review and evaluation of these tailings dam failure databases in terms of their geographical location, mechanisms of failure, relation to mining activity and dam construction methods have been conducted by several authors (USEPA, 1997; Davies, et al., 2002; Blight and Fourie, 2003; Rico, et al., 2008; Rodriguez et al., 2009) with the causes (triggers) and trends noted as follows:

- **Triggers:**

- Overtopping caused by a loss of freeboard;
- Excess pore water pressure generation due to high RoR or rapid rise in phreatic surface, resulting in static liquefaction;
- Excess pore water pressure generation due to cyclic loading, resulting in seismic liquefaction;
- Foundation, seepage and structural issues, which include foundation shear or piping failure, piping through the dam wall, erosion of tailings dam toe and inward collapse of a penstock tower or outfall pipeline.

- **Trends:**

- Operational tailings dams are more susceptible to failure;
- In non-operational tailings dams, overtopping is the primary trigger in nearly half the failures;
- Upstream tailings dams present most of the failures and are responsible for all major static liquefaction failures;
- Slope instability accounts for two-thirds of all upstream tailings dam failures;
- The main failure modes for non-upstream tailings dams are related to foundation, seepage and structural issues;
- Earthquakes have little effect on most non-upstream tailings dams.

Tailings dams constructed using the upstream, centreline or downstream methods typically comprise engineered starter walls or impoundment dykes to retain tailings and supernatant water. They also occasionally retain stormwater during heavy rainfall events, where insufficient decanting of stormwater in the TSF basin may occur (for example due to a blocked penstock intake). It should be noted that to minimise the cost of TSF construction, starter walls or impoundment dykes do not typically extend to the full height of the tailings dam. This results in the TSF being constructed solely from tailings above the height of the starter walls or impoundment dykes, with the coarser fraction of the tailings stream being used to form an outer wedge that acts to retain the finer fraction of the tailings stream deposited in the TSF basin. If the outer impoundment (comprised of engineered fill or tailings) is breached there is a high possibility that impounded tailings within the TSF will be released.

Failures of this nature are typically associated with tailings dams constructed using the upstream method, as low volumes of engineered fill material are required for initial starter wall construction, with the remainder of the TSF constructed using tailings. This upstream method of tailings dam construction is the most economical resulting in them being the most adopted in the mining industry (Vick, 1983; Vick, 1990; Martin and McRoberts, 1999; WISE, 2004; Saad and Mitri, 2010). However, tailings are typically poorly consolidated (Mittal and Morgenstern, 1975; Martin and McRoberts 1999), which creates an environment for large excess pore pressures and low shear strengths to develop, thereby increasing the risk of static or seismic liquefaction to occur.

It should be noted that liquefaction is a phenomenon most often linked with seismicity. However, more static liquefaction related failures have occurred in tailings dams than seismic liquefaction related failures (Davies, et al., 2002; da Fonseca, 2012; Been, 2016). It should be borne in mind that several static liquefaction failures are amongst the most destructive tailings dam failures in history. In order to contextualise and visualise the



impacts of these failures, several case histories are outlined in Table 2-2 and graphically shown in Figure 2-1 and Figure 2-2.

*Table 2-2: Cases and Causes of Static Liquefaction Failures.*

<b>Case</b>	<b>Reason for Failure</b>
Aberfan (1968, UK)	Triggered by excess pore pressures from heavy rainfall. Resulted in the death of 144 people; tailings travelled 600 m downstream.
Bafokeng (1974, South Africa)	Dam wall breach from concentrated seepage and piping through cracks. 12 deaths due to flooding of a mine shaft with tailings; tailings flowed 45 km downstream.
Merriespruit (1994, South Africa)	Dam wall breach following heavy rainfall; 17 deaths with widespread damage to housing; tailings travelled 4 km downstream.
Aznalcollar (1998, Spain)	Foundation failure causing loss of containment and contamination of farmland.
Kingston (2008, USA)	Loss of containment resulting in substantial environmental damage.
Mt Polley (2014, Canada)	Foundation failure causing loss of containment and environmental damage.
Fundao (2015, Brazil)	Static liquefaction flow slide caused by insufficient drainage, which resulted in the death of at least 17 people and with billions of dollars in damage.
Brumadinho (2019, Brazil)	Investigations still underway to determine cause but initial reports suggest dam wall breach due to foundation failure, resulting in flow liquefaction of tailings. Resulted in the death of at least 300 people and with billions of dollars in damage.

In summary, tailings dams, especially those constructed using the upstream construction method, are extremely susceptible to failure as a result of static liquefaction as well as seismic liquefaction, which can result from a single or a combination of triggers.

Furthermore, a noteworthy lesson from the case histories presented in Table 2-2, together with the findings of Poulsen, et al. (2014), is the importance of analysing the stability of both tailings and founding material, especially sites where cohesive soils are present. From the few case histories presented it can be seen that the onset of tailings liquefaction was triggered by loss of containment due to instability of the outer tailings dam wall.





(a)



(b)



(c)



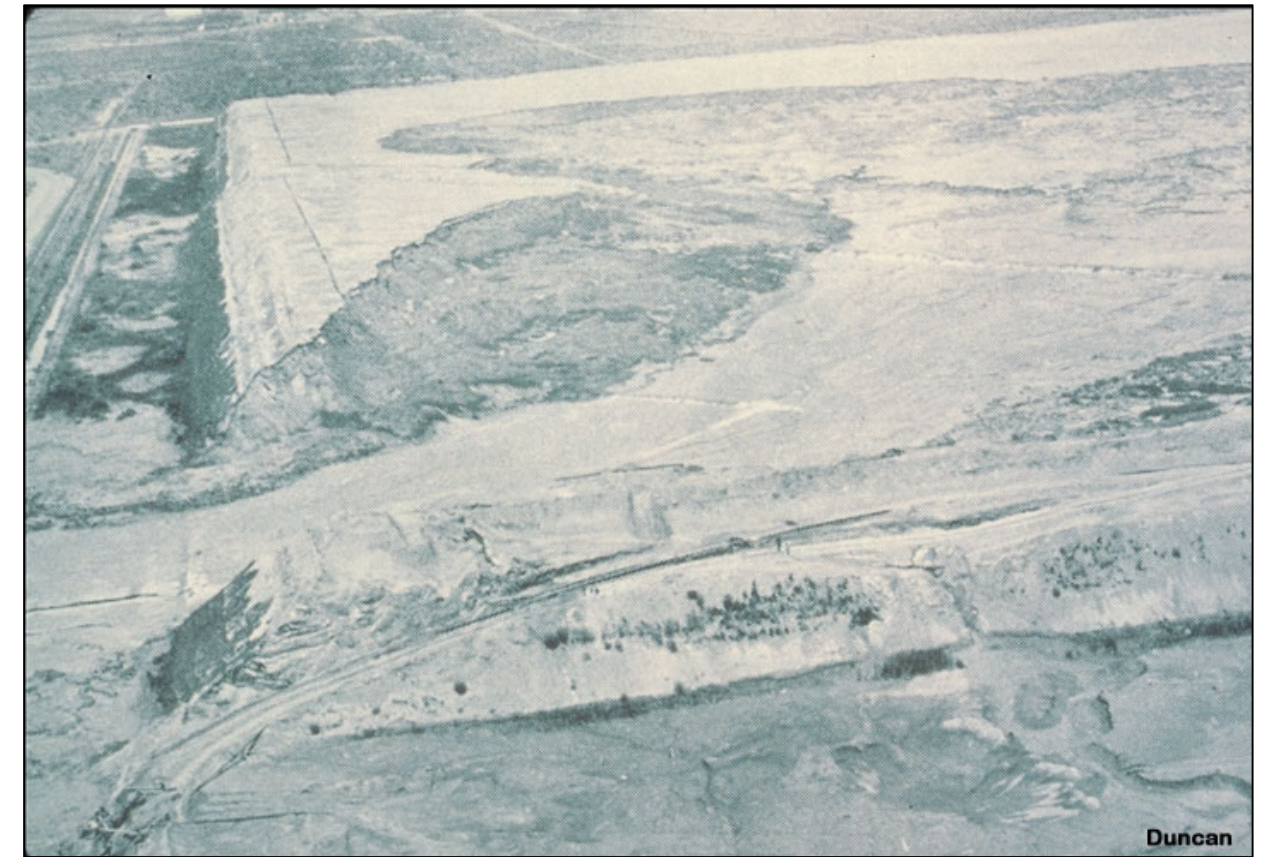
(d)

Figure 2-1: (a) Kingston TSF Failure (b) Mount Polley TSF Failure (c) Fundao TSF Failure (d) Brumadinho TSF Failure (Skytruth, 2016; TheStar, 2006; The Guardian, 2019; Wikipedia, 2019)





(a)



(b)



(c)

Figure 2-2: (a) Merriespruit TSF Failure Showing the Path of the Destructive Mudflow That Occurred (b) Bafokeng TSF Failure (c) Two of the Three Failures That Occurred at the Saaiplaas TSF (Boulanger and Duncan, n.d.; Fourie, et al., 2001).

## 2.2. Theoretical Considerations for Liquefaction of Tailings

Liquefaction is associated with a reduction in shear strength of saturated, cohesionless soil/tailings material, that experiences significant deformation under load (James, et al., 2003). Most tailings dam failures are attributed to increases in pore water pressure and resulting liquefaction of retained tailings due to loss of containment (Dobry et al., 1967; Ishihara, 1984; Finn, 1980; Finn, 1996; ICOLD, 2001; Aubertin et al., 2002a; Azam and Li 2010; GEER, 2010; Chambers and Higman 2011; WISE, 2014).

Soils that display sand-like behaviour, i.e. shear strength being largely governed by the friction angle of particle to particle contacts, can be more prone to liquefaction (Torres-Cruz, 2011). It should be noted that this sort of behaviour is characteristic of tailings, as the finer fraction in tailings is typically cohesionless (Ishihara, 1993).

The fundamental concept of liquefaction is to understand whether a soil will display contractive (strain-softening) or dilative (strain-hardening) behaviour when sheared. According to Casagrande (1936), a low-density loose sand will contract and a high-density dense sand will dilate when sheared until reaching the same critical void ratio ( $e_c$ ). If the void ratio ( $e$ ) is greater than  $e_c$  the sand will contract and if the  $e$  is less than  $e_c$  the sand will dilate. In other words, the critical void ratio is basically the density of material that will mitigate against the rapid change from drained (no excess pore pressure) to undrained (generation of excess pore pressure) loading conditions resulting in static liquefaction. The relationship between critical void ratio and mean effective stress ( $p'$ ) is denoted as the Critical State Locus (CSL) (Been, 2016). The CSL can usually be treated as semi-logarithmic for all soils and is expressed mathematically using Equation 1.

$$e_c = \Gamma - \lambda_{ln} \cdot \ln(p') \quad (1)$$

where  $\lambda_{ln}$  is the slope of the CSL and  $\Gamma$  is the value of  $e_c$  when  $p' = 1$  kPa. Caution should be taken with cited values of  $\lambda$ , as both log base 10 ( $\lambda_{10}$ ) and natural logarithms ( $\lambda_{ln}$ ) are used.  $\lambda_{ln}$  is more suitable for constitutive modelling, whereas  $\lambda_{10}$  is derived from plotting laboratory test data. Distinguishing between  $\lambda_{ln}$  and  $\lambda_{10}$  can be accomplished by using the notation  $\lambda_{10} = 2.303\lambda_{ln}$ .

Figure 2-3 shows the principle of flow liquefaction susceptibility based on state parameter concept. Soils that plot above their respective CSL will display contractive behaviour that will be susceptible to liquefaction, while soils that plot below their respective CSL are dilative and thus not susceptible to liquefaction. Furthermore, a soil plotting slightly ( $\psi \leq 0.05$ ) above the CSL will initially contract at smaller strains and will then dilate at larger strains (Been, 2016).

Casagrande also observed that a soil will undergo larger contraction or dilation with increasing deviation of a soils current void ratio above or below the CSL, respectively. Consequently, Been and Jefferies (1985) introduced the state parameter ( $\psi$ ) to characterise a soils contractive and or dilative behaviour. The  $\psi$  is a measure of the  $e$  relative to  $e_c$  at the same  $p'$  (Equation 2).

$$\psi = e - e_c \quad (2)$$

According to Been and Jefferies (1985), soils with a  $\psi > 0$  are contractive and when  $\psi < 0$  are dilative.



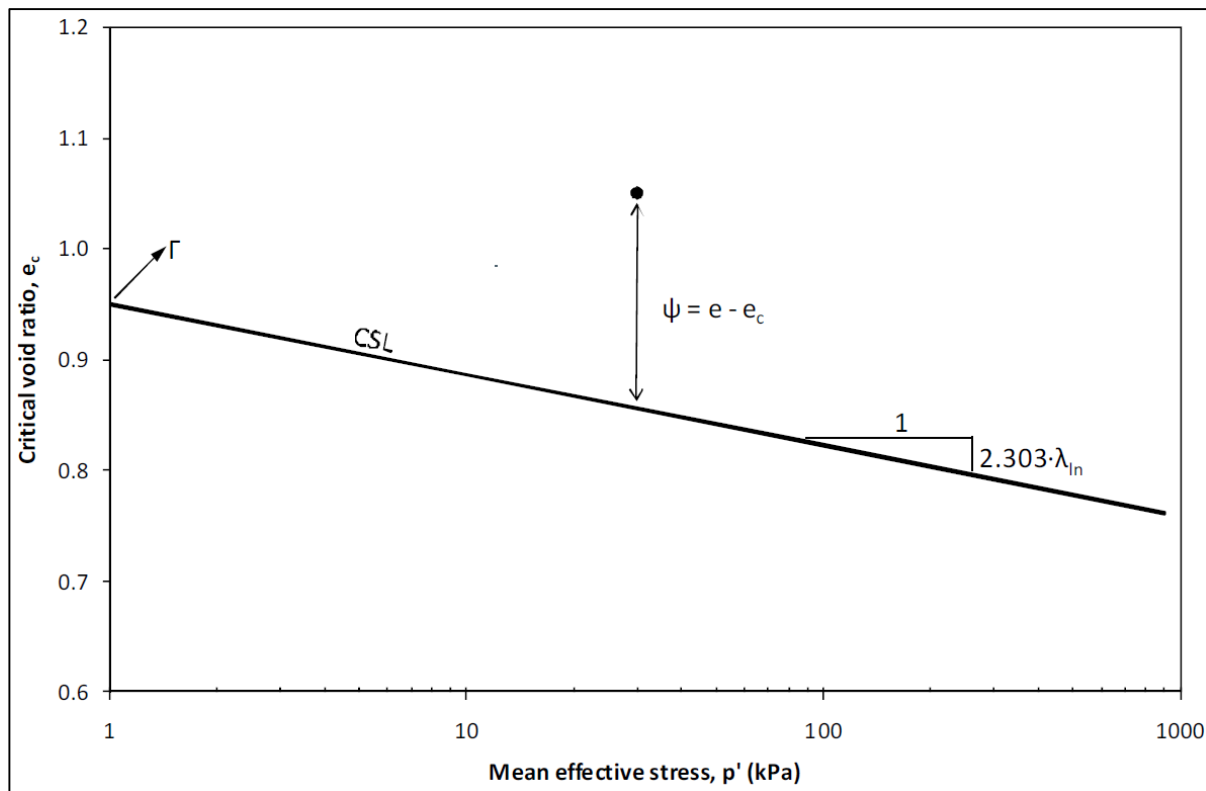


Figure 2-3: CSL and the Meaning of Parameters  $\Gamma$ ,  $\lambda_{in}$ , and  $\psi$  (Torres-Cruz, 2011).

Although Casagrande (1936), as well as Been and Jefferies (1985) studies, were conducted on sand, the same principles apply to cohesionless sandy silts, silts and silt-like tailings. This was shown by Davies, et al. (2002) that concisely describes the concept of liquefaction with emphasis placed on static liquefaction by reviewing several tailings dam static liquefaction case histories and their associated failure mechanisms. An important concept from this paper is that tailings could possibly have one of four characteristics upon shear loading:

- Brittle strain softening (complete liquefaction with the potential for unlimited deformation) – contractive behaviour upon shear up to the steady-state condition;
- Limited strain softening (limited liquefaction with limited deformation) – some initial contraction followed by dilation of tailings;
- Ductile behaviour with undrained shearing but no significant degree of strain-softening (no liquefaction);
- Strain hardening (no appreciable liquefaction or deformation) – only dilation.

Figure 2-4 illustrates the strain-softening response to both monotonic and cyclic shear loading conditions.

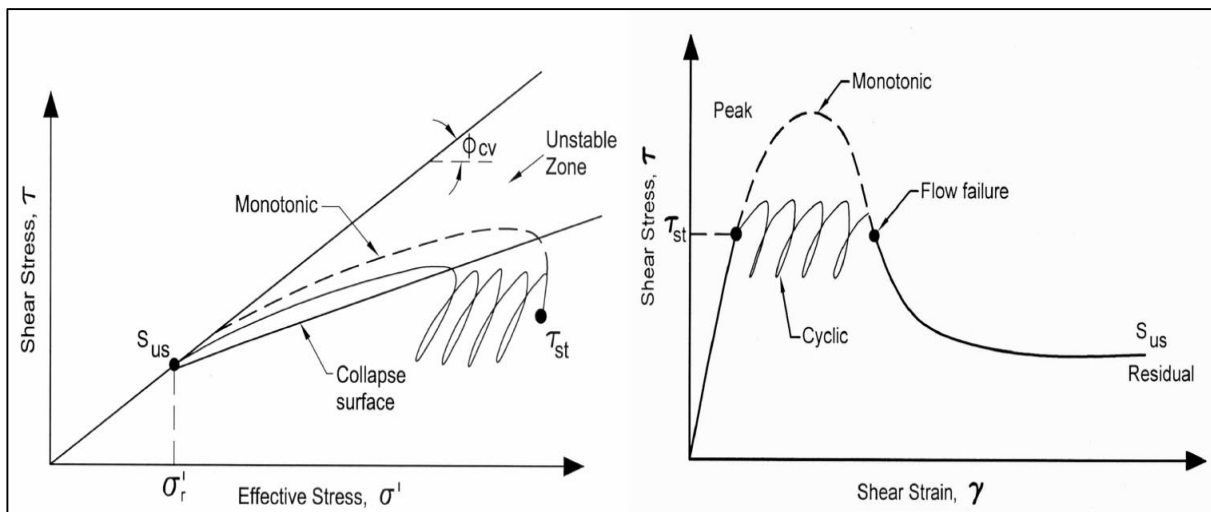


Figure 2-4: *Ideal Behaviour of Loose, Saturated Cohesionless Tailings Under Monotonic and Cyclic Loading* (Davies, et al., 2002)

According to Cruz (2011), in addition to the presence of pore water, for brittle strain-softening flow liquefaction failures to occur in tailings dams three conditions need to exist:

- Tailings must display contractive behaviour, which will allow for excess pore water pressures to develop and as a result cause a significant reduction in effective stress and shear strength;
- A triggering condition (as discussed in Section 2.1) that invokes a big enough shearing stress for contraction to occur (Poulos et al., 1985; Ishihara et al., 1990; Olson and Stark 2003; Blight, 2010);
- Post-liquefaction, a load inducing shear stress greater than the residual shear strength of the tailings must exist. If this situation develops for tailings dams located on sloping ground, large flow failures can occur (Ishihara et al. 1990; Olson 2001).

Based on the information discussed in this section it becomes apparent that understanding the behaviour and state of tailings materials are of vital importance to assess/predict liquefaction potential of tailings dams. The characterisation of tailings dam behaviour and the framework used to accomplish this is described in further detail in Section 2.3.

## 2.3. Characterisation of Tailings Behaviour

Tailings are typically transported to a tailings dam as a slurry that comprises coarser (sands) and predominantly finer tailings (sandy silts and silts) that are either hydraulically segregated via spigoting or mechanically separated using hydrocyclones. Figure 2-5 illustrates some examples of dominance of the silt fraction in tailings particle size distributions. The coarser fractions settle near the discharge points while the finer silt fractions settle out along the beach and comprise a significant volume of tailings dams, which is typical of tailings dams in southern Africa (Martin, 1999; Shuttle and Cuning, 2007; Shuttle and Jeffries, 2016).

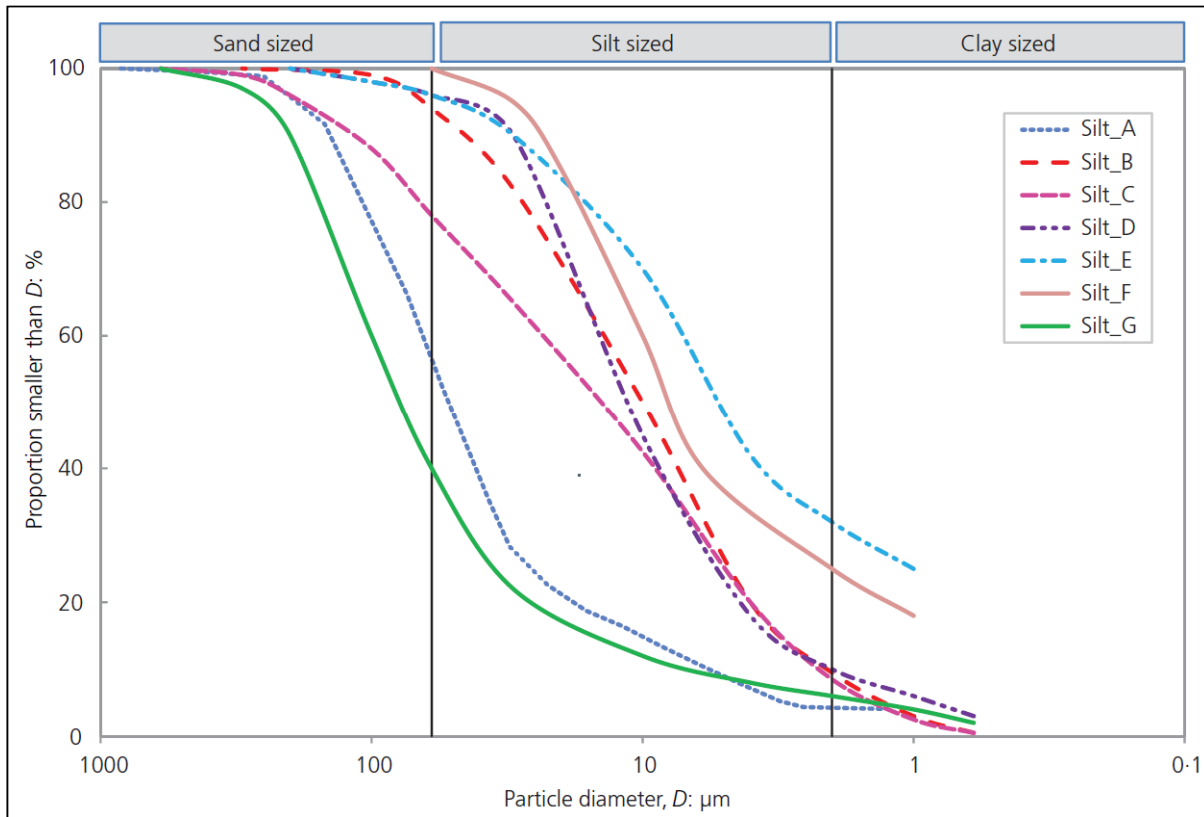


Figure 2-5: Tailing Gradations Illustrating Dominance of Silt Fraction (Shuttle and Jeffries, 2016)

This means that to effectively assess the geotechnical performance of such tailing's dams, tailings need to be characterised in terms of silt behaviour. However, this poses a challenge as almost all the understanding found in the literature relates to either the mechanical behaviour of sands or clays. It should be noted that the reasons for this bias towards sand and clay behaviour is discussed in detail by Shuttle and Jeffries (2016); however, some main reasons are described. For sands, CPTu calibration chamber studies have allowed development of mappings between void ratio, confining stress and penetration resistance. Also, there is a considerable amount of engineering data for sands in the literature. For clays, undisturbed samples can be tested using 'element' tests, such as triaxial compression or simple shear. Clay behaviour can also be investigated by remoulding samples across a range of void ratios. Furthermore, clays are agreeable to in-situ tests that use few assumptions and are readily compared to laboratory data.

The evaluation of tailings behaviour during construction and operational conditions is of vital importance to validate design assumptions, with attention paid to upstream and thickened tailings dams comprised of mainly

silts (Been, 2016; Shuttle and Jeffries, 2016). Silts and sandy silts can be sampled using a thin-wall unsprung (uniform diameter) Shelby tube. However, sample transportation and laboratory preparation results in considerable densification (Been, 2016; Shuttle and Jeffries, 2016). This is apparent when comparing the as-recovered void ratio and the as-tested void ratios (Figure 2-6) for natural silts (Mohajeri and Ghafghazi, 2012). Sample densification will result in non-conservative results because the sample will be in stronger state when tested in the laboratory than in-situ.

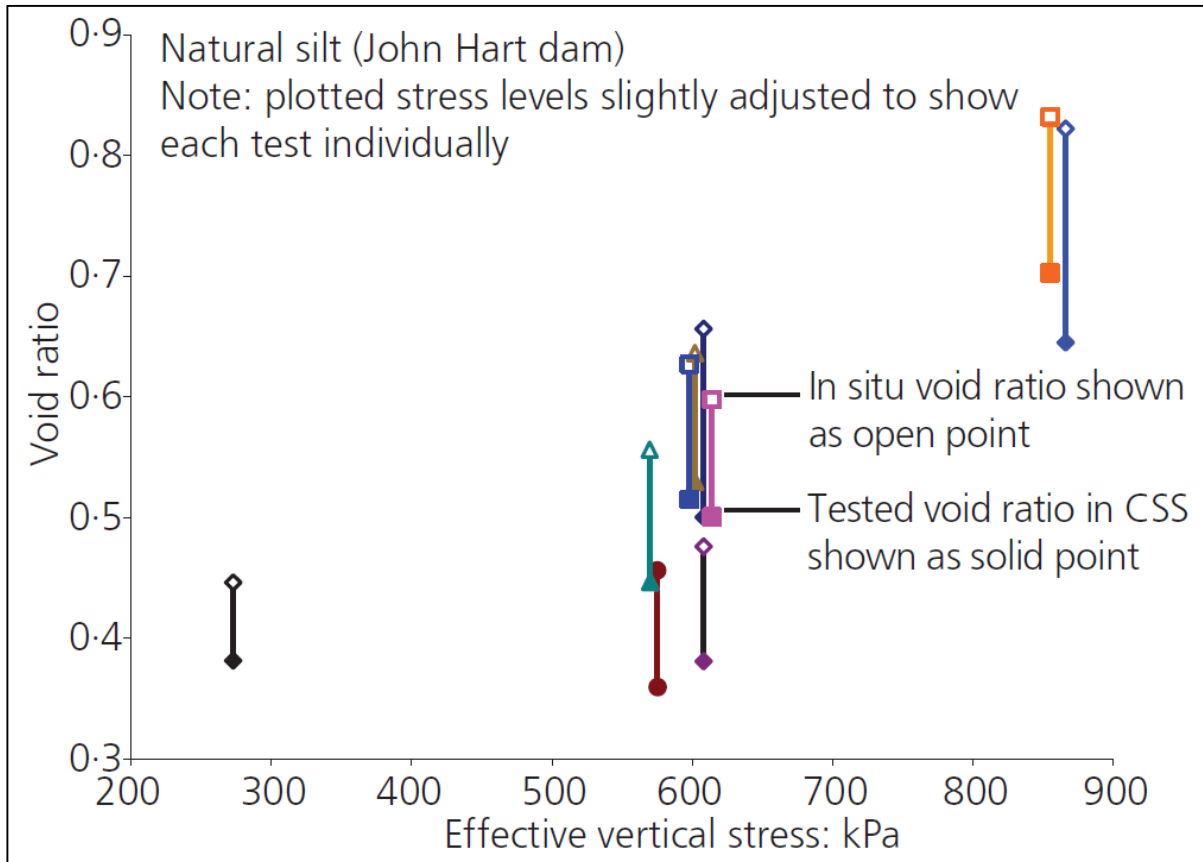


Figure 2-6: Measured Silt Densification from In-Situ to As-Tested Conditions (Shuttle and Jeffries, 2016).

To address this issue Been (2016) as well as Shuttle and Jeffries (2016), proposed two alternative methods that can be used for characterising tailings in terms of silt behaviour:

- Correct strengths measured in the laboratory for the measured densification from 'as-recovered' (in-situ) to 'as-tested' void ratios;
- Adopting a similar approach to sand-like materials for silt tailings, by measuring the in-situ  $\psi$  to calculate in-situ strengths from measured soil properties by using reconstituted samples.

It should be noted that this thesis addresses the second approach and proceeding sections describe the framework in which the in-situ state of silt tailings is characterised. Briefly, the framework implements Critical State Soil Mechanics (CSSM) to characterise how silt behaviour changes with void ratio by using CPTu data and numerical element tests in conjunction with the NorSand soil constitutive model (Been, 2016).

### 2.3.1. Critical State Soil Mechanics

Soils occur over a range of void ratios with the in-situ void ratio (or density) having a major effect on soils constitutive behaviour. A good soil constitutive model must effectively capture changes in soil behaviour (most notably strength and stiffness) as a result of changes in density. This density dependence is incorporated in CSSM with the Cam Clay (Schofield and Wroth, 1968) and Modified Cam Clay (Roscoe and Burland, 1968) models. These are possibly the most common soil constitutive models in commercial software packages. It should be noted that two schools of thought exist with regards to Cam Clay. The one school sees Cam Clay as one of the most fundamental contributions to soil mechanics in the 20<sup>th</sup> century while the other school sees it as being completely unsuitable to capture real soil behaviour (Been, 2016).

An axiom of CSSM is the concept of critical void ratio, CSL and state parameter that have been described in Section 2.2, which have led to the development of state-based models. Important features of state-based models are: (a) the yield surface; (b) the 'flow rule' giving relative plastic strain increments which invokes stress dilatancy and (c) the hardening law which controls how the yield surface responds to plastic strain (Shuttle and Jefferies, 2016).

The trends in sand and silt behaviour described by Been and Jefferies (1985) as well as Jefferies and Been (2015) showed that yield surfaces (the limits of elastic behaviour) evolve to the CSL with shear strain (Figure 2-7). Based on these findings, two types of constitutive models were developed namely the Drucker et al. (1957) framework and Manzari and Dafalias, (1997) bounding surface plasticity model. Currently, there are several good soil constitutive models that have common features such as a CSL; a critical friction ratio (or angle); dilation and strength controlled by  $\psi$ ; plastic hardening that partly scales with the slope of the CSL and isotropic elasticity with stress-level dependence (Been, 2016). These soil constitutive models are very similar with small differences between them and it typically depends on user preference as to which is implemented.

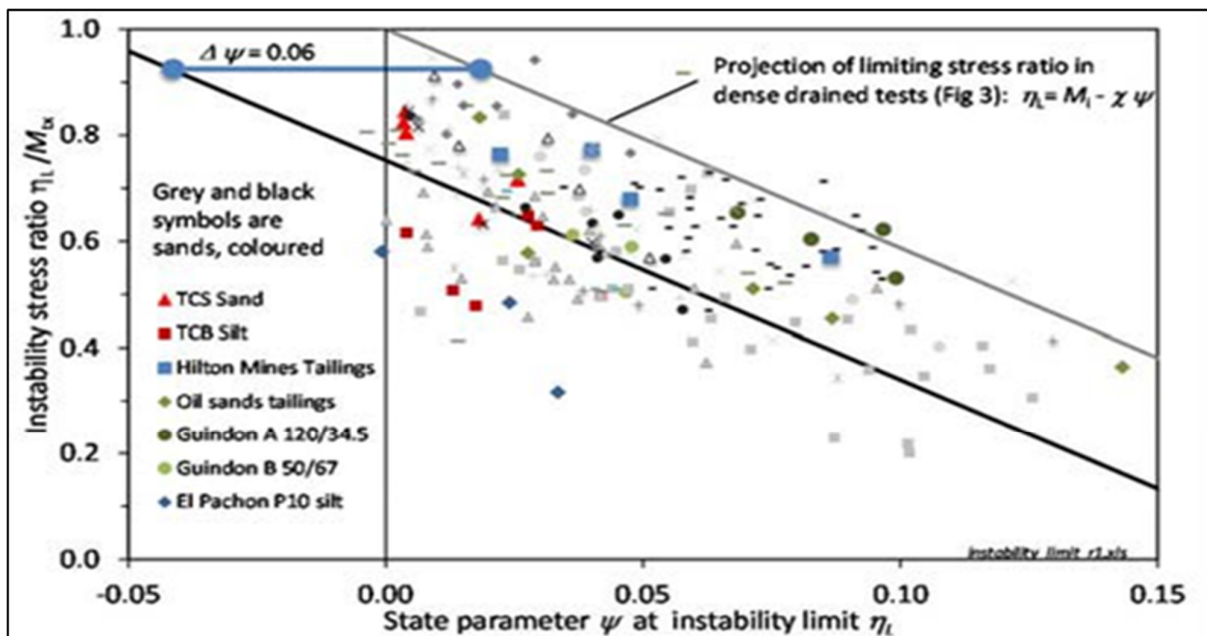


Figure 2-7: Instability Limit in Relation to Limiting Stress Ratio from Drained Tests on Dense Samples (Been, 2016).



Additionally, from Figure 2-7 it was found that best-fit trend lines for drained and undrained test data were parallel and offset by  $\Delta\psi = 0.06$ . Taking this into consideration, Been (2016) described an instability principle that states if  $\psi < -0.06$  the material will display dilative or strain-hardening behaviour. If  $\psi > -0.06$  the material will display contractive or strain-softening behaviour.

As described above, CSSM models such as Cam Clay and Modified Cam Clay can capture the effect of void ratio on soil behaviour to a certain degree. However, these models cannot accurately capture the dilative behaviour of dense soils (which form a major part of engineered construction). Also, these original CSSM models do not accurately predict the liquefaction behaviour of loose sands (Shuttle and Jefferies, 2010). Furthermore, a recurring assessment of CSSM is that the CSL displays non-uniqueness and changes with stress path to reach CSL (Been, 2016). This is where the capabilities of NorSand make up for the deficiencies of other soil constitutive models in terms of effectively capturing the constitutive behaviour of soils. NorSand will be described in greater detail in Section 2.3.2.

It should be noted that the book written by Jefferies and Been (2016) is an excellent reference that combines substantial amounts of data on soil liquefaction and CSSM and contextualises this topic within an integrated and simple framework that can also be applied to tailings. This book cuts through much of the empiricism in standard liquefaction procedures enabling civil and geotechnical engineers to gain a solid understanding of concepts of CSSM and liquefaction.

### **2.3.2. NorSand Constitutive Model**

The aim of selecting an appropriate constitutive soil model to characterise sand and silt is to capture behavioural changes over a spectrum of void ratios and confining stress levels. There are several state parameter-based models that can do this. NorSand (Jefferies 1993; Jefferies and Shuttle 2002, 2005) was the original CSSM (state parameter-based) model developed for sands. Although the model name contains 'sand', this was done to distinguish NorSand from Cam Clay. In fact, NorSand is applicable to any soil (such as clayey silt, silt and sand) in which particle interactions are controlled by frictional forces rather than bonds (Shuttle and Jefferies, 2010). It should be noted that when modelling and assigning material parameters for silt, typical values for sand may not be applicable (Shuttle and Jefferies, 2010).

NorSand can be applied to several applications and is typically used for conditions that require accurate representation of volume changes as a result of large strain, confinement, or excess pore pressure generation. So, naturally, the use of NorSand would gravitate towards engineering scenarios focussed on improving soil density, static and cyclic liquefaction as well as soil-structure interaction (Shuttle and Jefferies, 2010).

An advantage of NorSand is that it can be implemented as easily and effortlessly as the basic Mohr-Coulomb constitutive model because similarly, NorSand requires a few input parameters that can easily be determined (Shuttle and Jefferies, 2010).

#### **2.3.2.1. Model Description**

NorSand is a critical state model and is based on four simple features that build upon the CSSM framework discussed in Section 2.3.1. Shuttle and Cunniff (2007) describe these features as follows:

- NorSand can recognise an infinity of normal compression loci (NCL) / yield surfaces in  $e - \ln p'$  space. The infinity of NCL allow  $\psi$  and overconsolidation ratio ( $R$ ) to characterise the state of a soil. The  $\psi$  is a measure of the location of an individual NCL in  $e - \ln p'$  space and  $R$  represents the proximity of a state point to its yield surface (Figure 2-8);
- The  $\psi$  tends to zero as shear strain accumulates i.e. the yield surface intersects the CSL;
- Dilation that occurs at peak strength is linearly related to  $\psi$ ;
- Softening (shrinking) of the yield surface will always occur with principal stress rotation and loading beyond the internal cap and principal stress rotation.

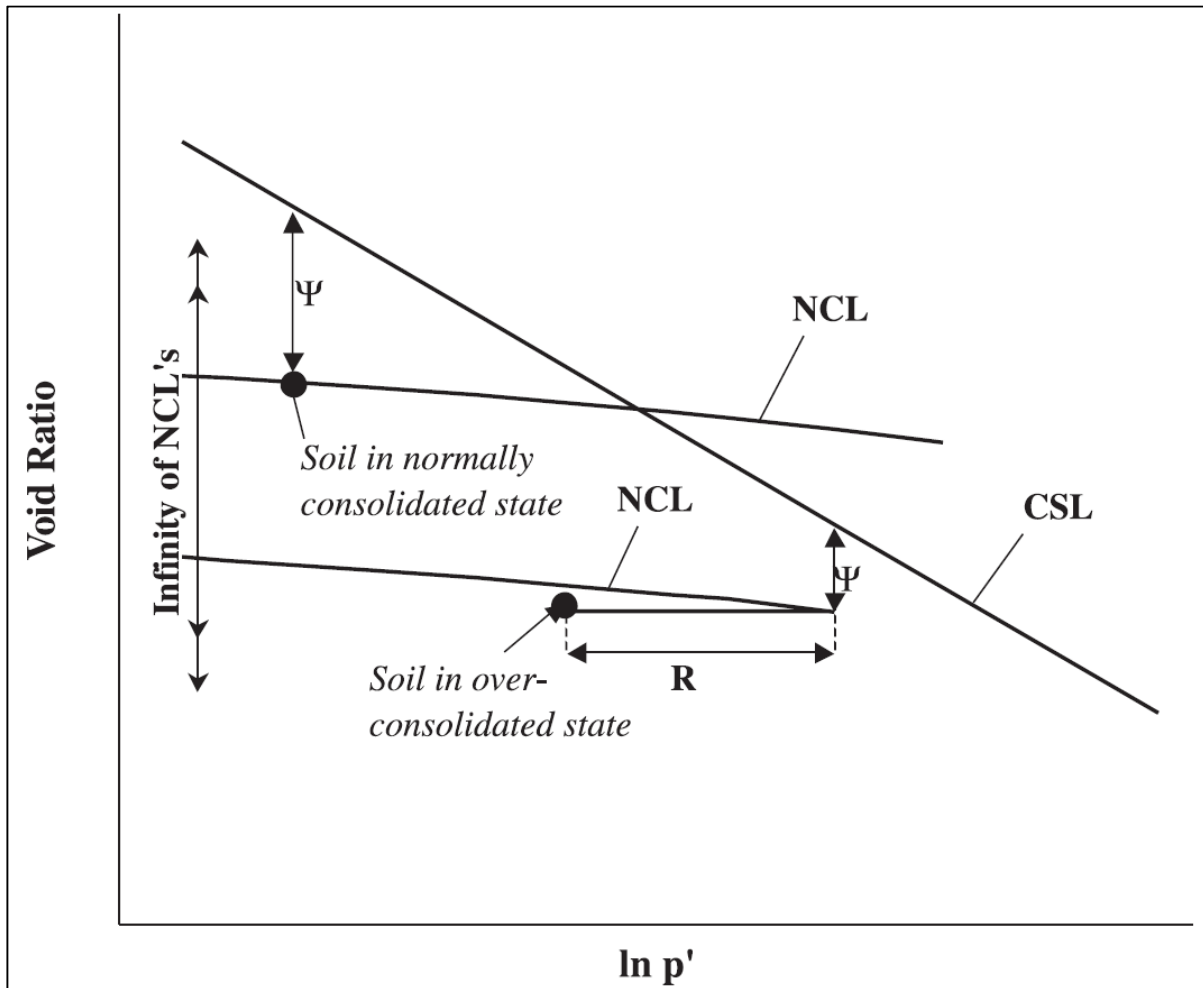


Figure 2-8: Definition of  $\psi$  and  $R$  (Jefferies and Shuttle 2002).

NorSand is like other soil plasticity models in that it has a yield surface; a flow rule and a hardening law. NorSand generates yield surfaces (Figure 2-9) that can accurately capture the full range of soil behaviour i.e. dilation and contraction of dense to very loose soils respectively (Shuttle and Jefferies, 2016), whilst displaying a unique CSL that effectively captures the range of soil behaviour used to assert non uniqueness (Jefferies and Shuttle, 2005).

NorSand differs from standard critical state models by two features. Firstly, an internal cap that changes with the changing state parameter allows NorSand to predict accurate dilatancy. Secondly, the yield surface diverges from the critical state (i.e. does not typically intersect). This feature forms the basis of the hardening

law, which functions to shift the yield surface towards the critical state under plastic shear strain. In doing so, it directly captures the core of critical state principles (Shuttle and Cuning, 2007). Strain hardening or softening of the yield surface depends on the current state parameter and on the direction of loading.

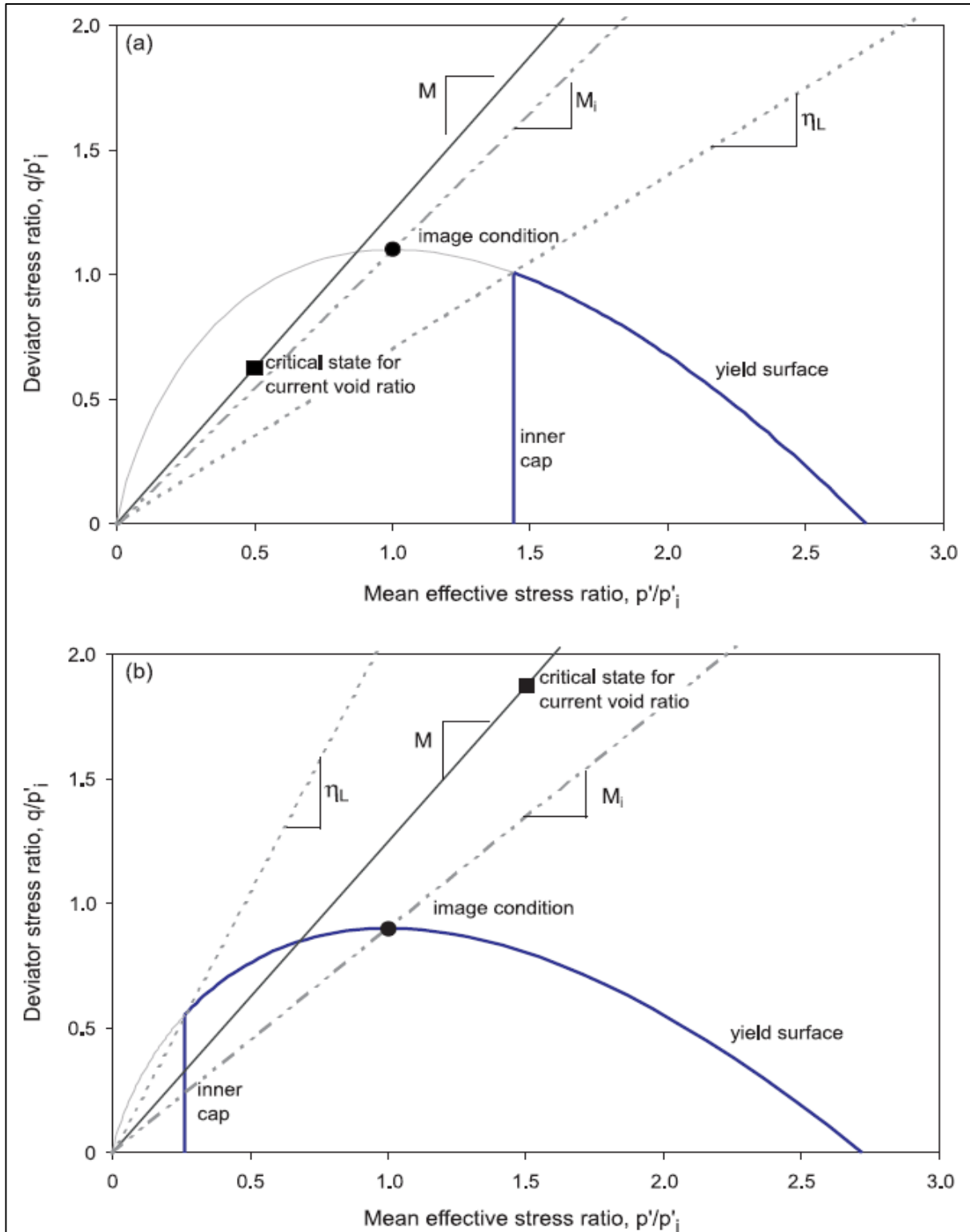


Figure 2-9: NorSand Yield Surfaces and Limiting Stress Ratios. (a) Very Loose Soil; (b) Very Dense Soil (Jefferies and Shuttle 2005).

### 2.3.2.2. Properties of NorSand

The soil properties used in NorSand are for the most part not exclusive to NorSand (i.e. they can be implemented in other CSSM constitutive models) and capture the fundamental behaviour of any particulate material (Been, 2016). Using a semi-log CSL there are five soil properties ( $\Gamma$ ,  $\lambda_{10}$ ,  $M$ ,  $N$  and  $\chi$ ) that can be determined by plotting isotropically consolidated drained (CIDC) and undrained triaxial (CIUC) compression tests, with the equations of NorSand facilitating the generalisation to three-dimensional (3D) stress conditions (Jeffries and Shuttle, 2002; Been, 2016). The properties used in NorSand are presented in Table 2-3 below.

Table 2-3: Summary of NorSand Soil Properties (Shuttle and Jeffries, 2010).

Model	Property	Description
CSL	$\Gamma$	Void ratio at critical state, for a $p_0'$ of 1 kPa, assuming a linear CSL in the semi-log plot.
	$\lambda_{10}$	Intrinsic soil compressibility representing the slope of the CSL in $e - \log p'$ space.
	$M_{tc}$	Intrinsic soil friction and defines the CSL in $p'-q$ space (*)
Plasticity	$N$	Defines the stress-dilatancy rule: $D = (M - \eta)/(1 - N)$ (**)
	$\chi$	Defines the lower bound for dilation based on the state parameter: $D_{min} = \chi^\psi$
	$H_0$	Defines plastic hardening
	$H_\psi$	Incorporates the effect of $\psi$ on the plastic hardening modulus: $H = H_0 + H_\psi \cdot \psi$
Elasticity	$I_r$	Rigidity Index
	$b$	Exponent for the pressure dependence of the shear stiffness
	$\nu$	Poisson's ratio

$$(*) p' = (\sigma_1' + \sigma_2' + \sigma_3')/3; q = \sigma_1 - \sigma_3 \quad (**) \eta = q/p' \quad I_r = (G_{max}/p')$$

The soil properties  $\Gamma$ ,  $\lambda_{10}$ ,  $M$ ,  $N$ ,  $\chi$  (all associated with soil behaviour) are familiar and simply defined (Shuttle and Jeffries, 2016). These properties are independent of any constitutive model (i.e. no constitutive model is used) and can be determined from plotting triaxial test data in several ways (Been, 2016; Shuttle and Jeffries, 2016).

Once more, undisturbed samples of silt do not accurately capture in-situ behaviour due to densification of the sample (Figure 2-6), therefore reconstituted samples can be used to determine soil properties of silts. Representative samples need to be retrieved from different material zones determined from CPTu and particle size distributions. Table 2-4 provides a schedule of laboratory tests that can be used to characterise the static and cyclic behaviour of tailings and indicates which tests provide which properties.

Table 2-4: Recommended Laboratory Tests for Tailings (Been, 2016).

Test Type	No of Tests	Purpose
Particle Size Distribution	20	Define heterogeneity of material, identify representative materials.
Specific Gravity	2	Basic property to calculate void ratio.
Max. and Min. Density	2	Not part of CSL framework, helpful for sample preparation.
Triaxial CIUC	5 – 8	Define CSL, undrained strength, brittleness ( $\Gamma$ , $\lambda$ , $M$ ).
Triaxial CIDC	5 – 8	Define CSL, stress-dilatancy, state-dilatancy ( $M$ , $N$ , $\chi$ ) as well as basic stress-strain data for calibrating constitutive model.
Oedometer/Rowe Cell	3 – 5	Consolidation behaviour ( $C_c$ , $c_v$ )
Bender Element Tests	2 set of 8	Measure $G_{max}$ as a function of stress level at two initial void ratios. Measure consolidation curves.

Test Type	No of Tests	Purpose
Cyclic Simple Shear Tests	8	Two sets of four tests. Each set at same $\psi$ . Include post-liquefaction settlement if possible.
Resonant column testing	2	Optional, but avoids reliance on published curves for $G$ and $D_r$

The oedometer or Rowe Cell tests are conducted to gain an understanding of the tailing's consolidation behaviour. Understanding this behaviour is important because consolidation affects the storage capacity of the TSF and because life of mine is typically 25 years, it is expected that the strength of the tailings will increase with time (Been, 2016).

It is also important to determine the small strain shear stiffness ( $G_{max}$ ) which allows for more precise assessments of  $\psi$  from CPTu and seismic response (Been, 2016). The use of triaxial apparatus with bender elements is preferred over the in-situ measurement of  $G_{max}$  because the relationship between  $G_{max}$ , void ratio and stress level is better understood in the laboratory (Been, 2016). It also allows for further understanding of the consolidation behaviour of the tailings to be determined.

There are several useful constitutive soil models that can capture a soil's static strength and stiffness behaviour with the parameters determined from the standard laboratory tests. However, to assess strain-softening behaviour triggered by dynamic loading, cyclic simple shear tests are required for seismic slope stability and ground response work on tailings dams (Been, 2016).

The method to accurately determine void ratio involves closing drainage and pore pressure measurement lines immediately after the shearing phase. The triaxial cell is then depressurised and placed in a freezer for a couple of hours which is enough to remove the sample without water loss. The moisture content of the whole sample is then converted to void ratio using the measured  $G_{max}$  (Been, 2016).

There are a few ways to determine plastic modulus with each constitutive model having its own approach (Been, 2016; Shuttle and Jeffries, 2016). The approach used by Been (2016) as well as Shuttle and Jeffries (2016) to determine plastic shear modulus from triaxial testing is Iterative Forward Modelling (IFM), which will be discussed in the proceeding section.

### 2.3.2.3. Calibration of NorSand

Procedures for calibration of sand properties in NorSand are outlined in Shuttle and Jefferies (2010) with a more detailed explanation presented in Jefferies and Been (2016). Calibration of silt properties requires more effort, as current laboratory procedures are incapable of reconstituting silt samples that are representative of in-situ void ratios (Shuttle and Jefferies, 2016).

IFM is a procedure where all properties are estimated (initial void ratio and test confining stress are known) and the stress-strain behaviour calculated. The modelled behaviour is compared to the laboratory test behaviour. The properties are adjusted and the procedure is repeated (iterated) until best-fit curves of modelled behaviour to laboratory test behaviour are obtained (Figure 2-10). IFM requires a criterion covering what is an acceptable fit of the model to laboratory data because not all parts of a stress-strain curve are of equal importance. A good fit of the modelled and laboratory test behaviour to the volumetric strain or the stress path for undrained tests is important (Shuttle and Jefferies, 2016). According to Shuttle and Jefferies (2016)

engineering judgement to determine an acceptable fit of modelled to laboratory data is preferred over statistical best-fit criteria.

To efficiently conduct IFM, the number of iterated properties should be reduced by focussing on properties that have a notable effect on the modelled behaviour (Shuttle and Jefferies, 2016). Properties  $\Gamma$ ,  $\lambda$  and  $M$  should be determined directly from test data with the values of  $H$ ,  $\chi$  and  $N$  determined by iteration (Shuttle and Jefferies, 2016). IFM allows for optimisation of soil properties and the use of the same property values across the whole data set. This is because properties do not change with void ratio or confining stress when using sound modelling approaches, such as IFM (Shuttle and Jefferies, 2016). According to Shuttle and Jefferies (2016), IFM shows how well a selected constitutive model (in this case NorSand) replicates the whole data set (Figure 2-10).

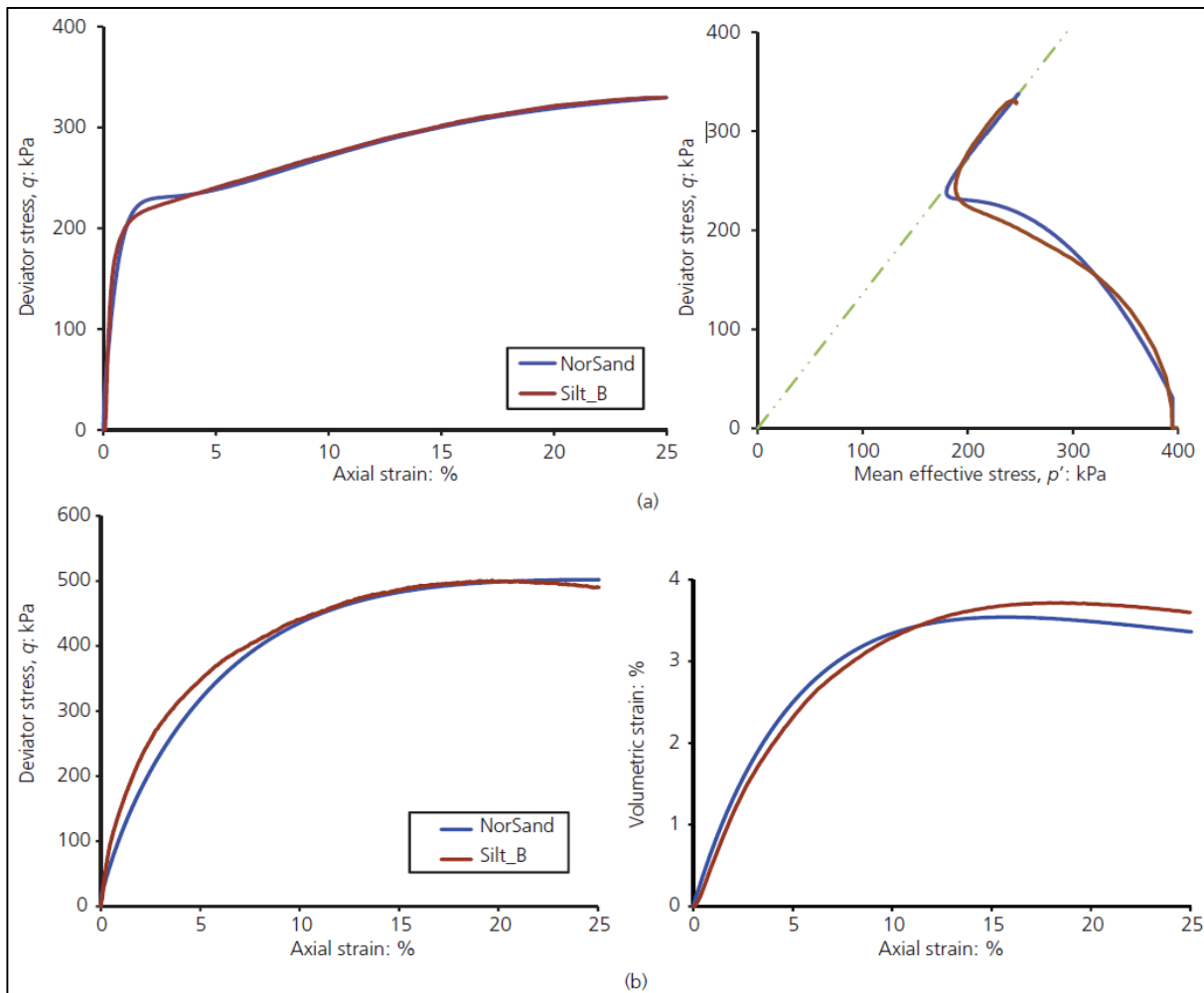


Figure 2-10: Comparison of NorSand With Reconstituted Silt Behaviour In (a) Drained and (b) Undrained Triaxial Compression (Shuttle and Jefferies, 2016).

### 2.3.3. Measuring In-Situ State of Tailings

There are several parameters that can be used to characterise the in-situ state of tailings, such as void ratio; relative density; dilatancy index and gamma-ray absorption from downhole logging, to name a few. However, it must be recognised that determining these parameters requires a great deal of technical input and precise

calibration to in-situ conditions (Been, 2016). Instead, Been (2016) recommends that the in-situ  $\psi$  should be measured using a CPTu, for the following reasons:

- Undisturbed samples of tailings are difficult to retrieve. However, the CPTu allows for a continuous accurate profile of a tailings dam to be determined;
- The  $\psi$  is the major control on contractive and dilative behaviour of soils and this applies to the CPTu resistance, friction angle and cyclic stress;
- Even if void ratio or density could accurately be determined, there is still an issue with relating the void ratio to  $\psi$  and engineering behaviour because a soil will display a range of CSLs in-situ.

Been (2016) highlights some important studies that have contributed to the interpretation of  $\psi$  from CPTu over the past thirty years. These studies are summarised in Table 2-5.

Table 2-5: Summary of Important Literature Related to Interpretation of  $\psi$  (Been, 2016).

Literature	Comment
Been et al. (1987)	Methods are applicable if good calibration chamber testing data is available. However, this rare.
Plewes et al. (1992)	Established a screening level procedure to determine the in-situ state of tailings, whereby $\lambda$ is related to the CPTu friction ratio (F%).
Shuttle and Jeffries (1998)	Developed a basic method to determine in-situ $\psi$ .
Been (2016)	Outlined a CSSM based procedure that can be applied irrespective of fines content. Similarly, the procedure requires in-situ CPTu and laboratory testing as well as calibrated spherical cavity expansion implemented in NorSand for assessing the in-situ state of silt tailings. It also requires the characterisation of the static and seismic CSSM properties over a range of in-situ state parameters in terms of CSL and Cyclic Resistance Ratio (CRR), respectively.
Shuttle and Cuning (2007)	Developed a CSSM framework that combines in-situ CPTu and laboratory testing as well as calibrated spherical cavity expansion implemented in the NorSand constitutive model (i.e. a critical state soil model) for assessing the in-situ state of silt tailings. It also identified the contractive/dilatant boundary for all soils, i.e. $\psi = -0.05$ (Figure 2-11) i.e. almost equal to the $\Delta\psi = 0.06$ between drained and undrained behaviour (Figure 2-7).
Shuttle and Jeffries (2016)	Developed a procedure for determining silt state from CPTu and expands upon the Shuttle and Cuning (2007) framework. It considers undrained CPTu soundings required for silts as well as scaling factors used in spherical cavity expansion.
Robertson (2009, 2010, 2012, 2016)	Published several papers on what he considers to be best practice. Robertson (2016) provided an updated soil behaviour type (SBTn) classification chart from using textural-based descriptions, such as sand and clay, to using behaviour-based descriptions such as Clay-like-contractive or Clay-like-dilative (Figure 2-12).

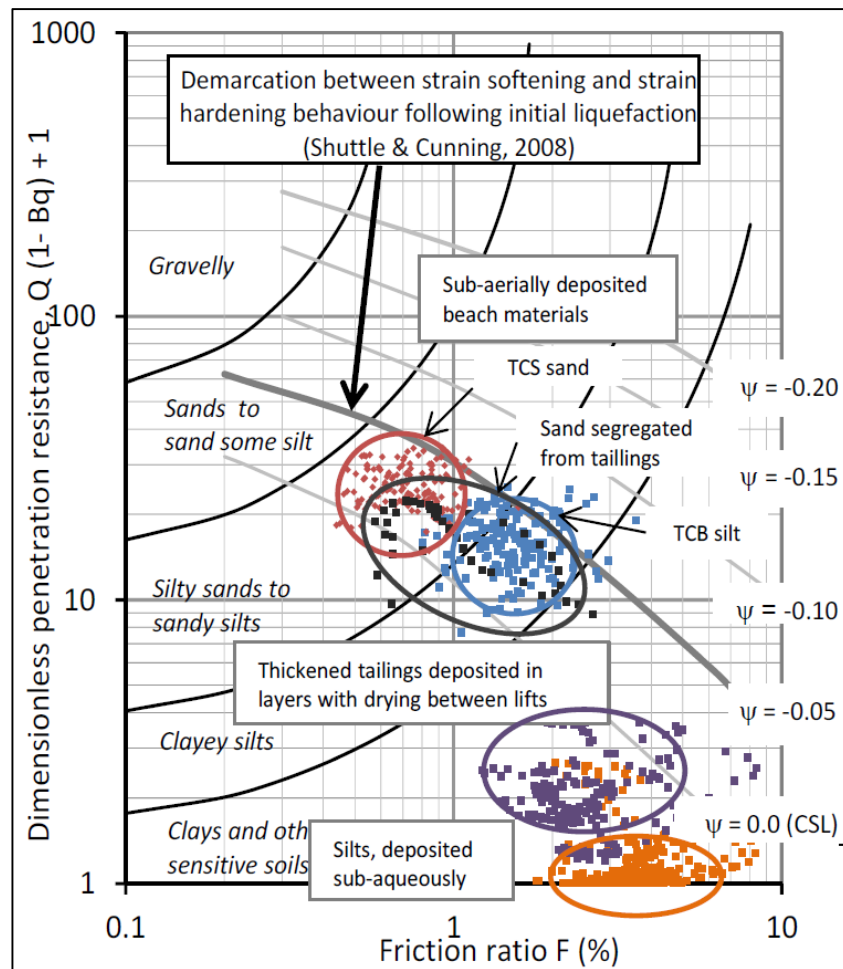


Figure 2-11: Example of Soil Behaviour Identified by CPTu on Soil Classification Chart (Been, 2016).

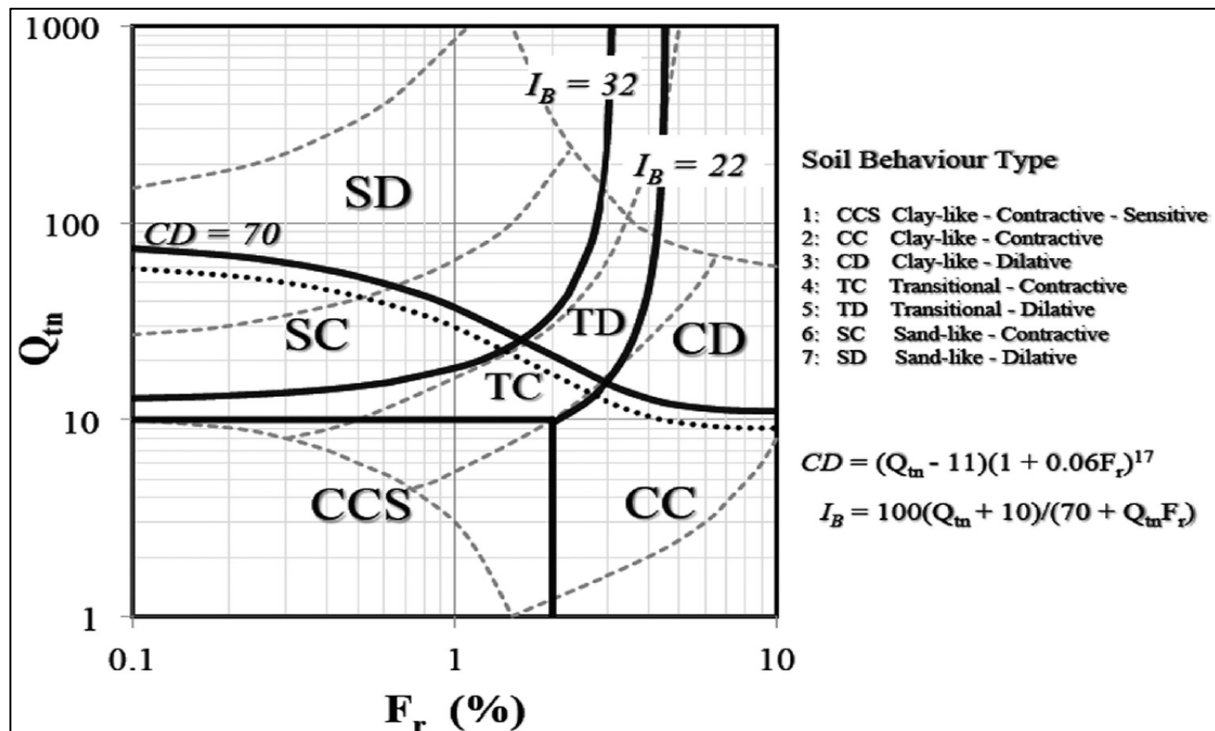


Figure 2-12: Updated SBTn Chart Showing Behaviour Based Descriptions (Robertson, 2016).



For sands, the relationship between  $\psi$  and the CPTu resistance was first determined from calibration chamber tests (Been, 2016). Although sands are found in tailings, nearly all tailings dams will comprise silts and may be dominated by silts (Martin, 1999; Shuttle and Cuning, 2007; Shuttle and Jeffries, 2016). However, no correctly executed calibration chamber investigations for the CPTu in silt exist (Been, 2016).

According to Been (2016), CPTu in silts occur under undrained conditions that result in large excess pore pressures (Figure 2-13). With respect to clays, undrained CPTu are assessed based on total stress by calibrating the undrained shear strength determined from the CPTu to undrained shear strength determined in the laboratory triaxial tests (Been, 2016). Now the issue with silts arises when trying to calibrate CPTu derived undrained strength to a reference laboratory strength because sample densification (discussed above) results in non-conservative undrained shear strengths (Been, 2016).

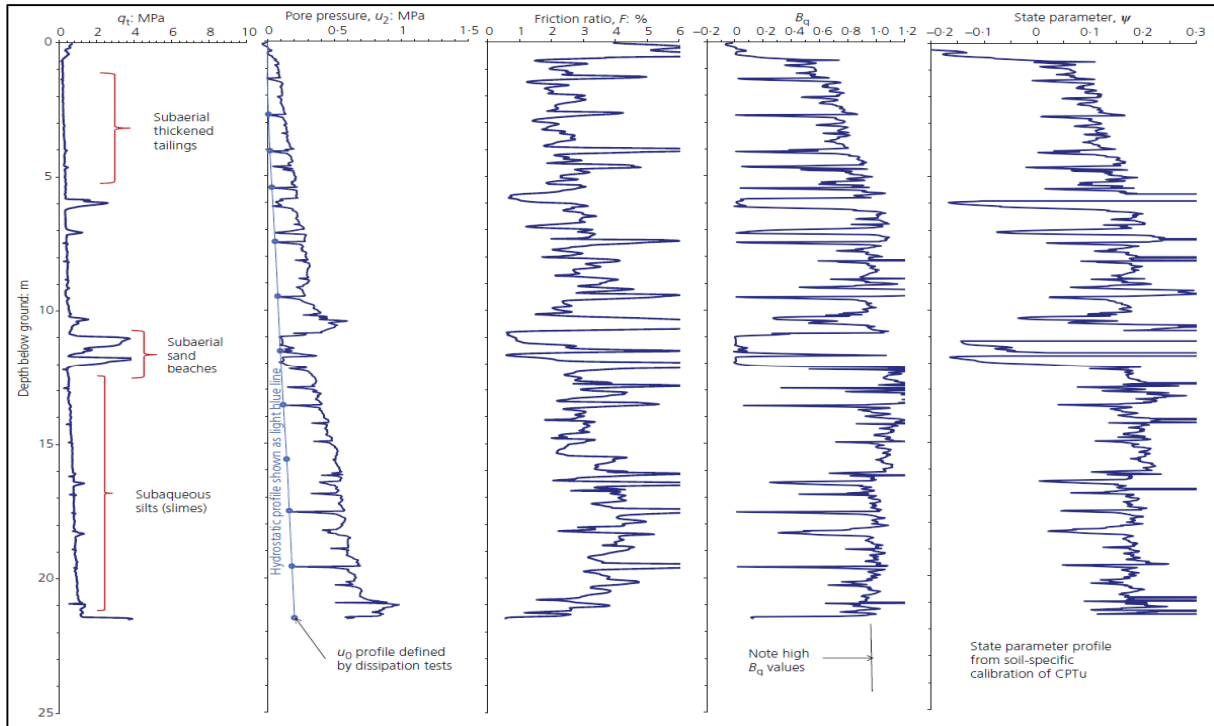


Figure 2-13: CPTu Profile in Massive Silt Tailings Deposit (Shuttle and Jeffries, 2016).

Instead, certain CSSM models can compute the drained and undrained stress-strain behaviour of silts with Been (2016) suggesting that the  $\psi$  must be the basis for characterising silts and predominantly silty soils. Subsequently, the basis for assessing CPTu in undrained conditions should be according to Equation 3 (Been et al, 1988).

$$\psi = -\ln(Q_p/k)/m \quad (3)$$

where  $Q_p = Q(1 - B_q) + 1$  with  $k$ ,  $m$  being the soil-specific coefficients for undrained conditions. Shuttle and Cuning (2007) used Shuttle and Jeffries (1998) cavity expansion method to determine  $K'$ ,  $m'$  for undrained conditions. This suggests that pore pressure should be measured at the  $u_1$  location because desaturation of the pore pressure sensor at the  $u_2$  location can occur in highly stratified or heavily overconsolidated soils from suction pressures generated in dilative soils (Peuchen et al., 2010). If pore water pressure is measured at the  $u_1$  location, an equation developed by Peuchen et al., (2010) allows pore water

pressure at the  $u_2$  location to be calculated. The locations on the CPTu where the pore pressure is measured are shown in Figure 2-14.

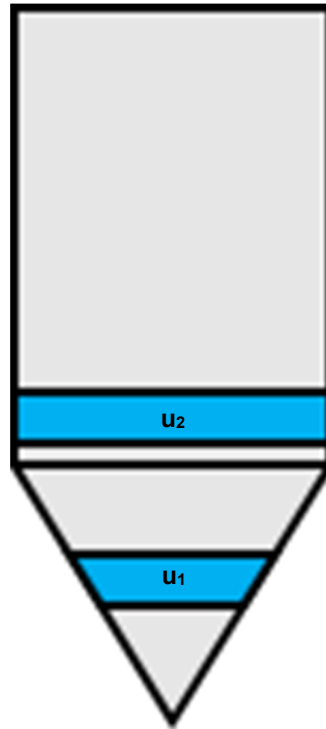


Figure 2-14: Pore Pressure Measured at  $u_1$  and  $u_2$  Locations on a CPTu (Robertson, 2013).

Typically, the piezometric regime of a tailings dam is governed by the degree to which tailings have consolidated and the drainage conditions (Been, 2016). The degree of consolidation and the drainage conditions can be determined in-situ from a CPTu by conducting dissipation tests (usually at 1 m intervals) measuring the horizontal coefficient of consolidation ( $c_h$ ) and the current pore pressure ( $u_o$ ), respectively (Been, 2016).

It should be noted that CPTu analyses can be augmented by using in-situ  $G_{max}$  from Seismic Cone Penetration Tests (SCPT). Ideally, the in-situ testing programme should include 1 SCPTu for every 5 CPTu scheduled. Furthermore, a  $G_{max}$  profile is the basis for any earthquake ground response analysis (Been, 2016).

Representative samples of both sand and silt-sized tailings were tested as part of the (Been, 2016) study. The properties of CSL's show an interesting relationship, with  $\lambda_{10} = 0.115$  for sand tailings (with 22% fines) and  $\lambda_{10} = 0.086$  for silty tailings (51% fines). The  $\lambda_{10}$  (slope of CSL) can be directly compared with the compression index ( $C_c$ ) used with clays (Been, 2016). On this basis, it is shown that silt tailings with a higher fines content are less compressible than the sand tailings. This is a result of additional fines occupying voids that will, in turn, reduce the amount of shear-induced movement (Been, 2016). These findings show that caution must be taken when using fines content to represent compressibility in the interpretation of CPTu results (Been, 2016).

Once the in-situ  $\psi$  is measured, the soil behaviour at that state must be characterised using laboratory test data in conjunction with a suitable constitutive soil model to capture the drained and undrained behaviour of silts (Been, 2016).

### 2.3.4. Note on Characterisation of Tailings Behaviour and CSSM

As discussed in this section there seems to be a satisfactory framework in place to characterise the behaviour (state) of tailings. However, there have been four recent tailings dam failures that resulted in huge environmental damage and loss of life. According to Been (2016), the problem is not the mining companies or shareholders, *“It is the lack of teaching of critical state concepts to geotechnical engineers and the application of rigorous mechanical approaches that has caused this problem”*.

The continued use of “fines content corrections” in tailings dam design is completely incorrect, as most tailings dams will have higher fines content than those published in the literature for sands and many tailings dams may comprise entirely of fines. This leads to engineering parameters being non-representative of actual site conditions as entirely corrected data is used instead of actual data (Been, 2016).

As shown by Been (2016) and described above, the mechanical properties of tailings do not correlate well with “fines content”. To alleviate these issues the CSSM framework should be used to capture tailings behaviour and will provide good engineering practice because: 1) CSL’s allow constitutive models with the CSSM framework to capture the effect of void ratio and confining stress on soil behaviour for all stress paths and loadings; 2) Few dimensionless and constant soil properties are required; 3) Stress-strain behaviour can be modelled in a spreadsheet; 4) In-situ  $\Psi$  can be reliably calculated from CPTu data.

## 2.4. Staged Construction of Tailings Dams

Three main stages characterise the lifecycle of most large tailing’s dams. The first stage involves the starter wall construction. The second stage involves the construction of the rest of the tailings dam until termination (closure) elevation. The third stage involves closure of the tailings dam (Energy, Mines and Resources Canada, 1977; Aubertin and Chapuis, 1991).

The construction stage of a tailings dam is critical for dam stability. During construction of an embankment, positive excess pore water pressure may develop in the tailings or in the foundation soil. When a tailings dam is raised in height, the weight of the newly deposited tailings may generate excess pore pressures. Although some portion of excess pore pressures may dissipate, complete pore pressure dissipation will not occur and some residual pore pressures will remain. The residual pore pressures will accumulate over time with increasing height of the tailings dam until termination (closure) elevation is reached (Zardari, 2011). For example, Martin (1999) observed a large upstream tailings dam that developed high excess pore pressures and had a rate of rise as low as 2.1 m/year.

Martin (1999) provides a detailed discussion on the characterisation of pore pressure conditions that commonly exist in upstream tailings dams. He identified six idealised pore pressure regimes that are described in Table 2-6 and illustrated in Figure 2-15. He also mentions that hydrostatic pore pressure conditions are typically assumed within upstream tailings dams for convenience in slope stability analysis due to lack of piezometric monitoring network or misinterpretation of piezometric data. In this thesis, pore pressure conditions will be varied during staged construction to assess the impacts on pore pressures and level of phreatic surface.

Staged construction analyses (that includes seepage and stability analyses) are typically conducted for upstream tailings dams and should be conducted at a suitable rate of rise to allow pore pressure dissipation,

consolidation and strength gain of tailings. This is very important when constructing upstream tailings dams with monitoring of phreatic surface and pore pressures to determine drained or undrained conditions (Been, 2016). Priscu (1999) demonstrated the importance of such analyses by studying the effects that normal and increased rates of rise at various stages of construction have on the structural behaviour of an upstream gold tailings dam, located in South Africa. In doing so the author found that suitable rates of rise could be forecast for different types of mining operations.

Staged construction analyses can be conducted as either uncoupled or coupled under steady-state or transient seepage flow conditions. Uncoupled analyses do not allow changes in pore pressure to effect deformation and vice versa. Whereas, fully coupled analyses allows changes in pore pressure to effect deformation and deformation to affect pore pressure. The main difference between steady-state and transient flow is the hydraulic head (and possibly the permeability coefficient) changes with respect to time (Fredlund et al., 2012).

The number of tailings dam failures that occur every year (Davies 2002; Hamade and Mitri, 2013; Bowker and Chambers, 2015) indicates that conventional uncoupled staged construction analyses may not fully capture the complex behaviour of tailings dams (Naeini and Akhtarpour, 2018). Therefore, it is suggested that fully coupled (hydromechanical) analyses be used to more accurately capture tailings behaviour during staged construction (Saad and Mitri, 2010).

According to Naeini and Akhtarpour (2018), there are three types of numerical analyses conducted for tailings dams. The first type comprises seepage analyses used to locate the position of the phreatic surface, which in turn can be used in stability analyses (Rykaart et. al., 2001; Yuan and Lei, 2015). The second type comprises numerical or limit equilibrium stability analyses to determine static and/or pseudo-static factors of safety (Zardari, 2011; Rout, et al., 2013; Ozcan et. Al., 2013; Rout, et al., 2013; Xu and Wang, 2015; Wei et. al., 2016 and Zhang et. al., 2016). The third type is hydromechanical analyses that involves transient coupled non-linear analyses. It should be noted that this thesis focusses on the first and third type of numerical analyses. To gain an understanding of what seepage and hydromechanical analyses entails, the proceeding paragraphs briefly describe the findings and outcomes of more recent seepage and hydromechanical studies that have been conducted.

According to Saad and Mitri (2010), the traditional steady-state seepage analyses give no consideration to transient flow conditions caused by continuous self-weight consolidation during construction and operation of a TSF. This means that for a steady-state seepage analysis, the flow of fluid in the TSF is not affected by its mechanical response, which does not represent porous media behaviour at all (Biot, 1941). On this basis, the authors used transient coupled non-linear analyses in the ABAQUS code to study the hydromechanical behaviour of three upstream tailings dams during staged construction. The analyses incorporated transient partially saturated flow within the tailings, consolidation, nonlinear material response and staged construction rates of rise of the tailings. The results of the numerical analyses showed comparable hydromechanical behaviour to upstream tailings dams in the literature.

A more recent staged construction study was also conducted by Naeini and Akhtarpour (2018) of high centreline tailings dams using coupled stress-pore pressure analyses in SIGMA/W. The effect of foundation permeability, rate of rise, tailings anisotropic permeability and variations of starter wall geometry on the structural response were studied. It was found that foundation permeability and anisotropic permeability of

tailings have a major impact on pore pressure development whilst varying the geometry of the starter walls results in substantial displacements. Similarly, Hamade, et al. (2011) conducted numerical modelling in FLAC using the Mohr-Coulomb constitutive model as well as transient coupled stress-pore pressure and stochastic analyses to evaluate the static slope stability of a tailings dam during its staged construction. Ormann et. al. (2013) evaluated the increase in strength during the consolidation process by using a fully coupled analysis. Hu et. al. (2015) further supported the use of coupled hydromechanical analysis to more accurately capture the long-term behaviour of a tailings dam. Additional examples of coupled hydromechanical analyses with respect to tailings dams can be found in Tanriseven (2012); Holmqvist (2014); Zardari, et al. (2014) and Barrero, et al. (2015).

Using RS2 (Rocscience Inc., 2018), Xu (2019) as part of his thesis performed FEM transient uncoupled staged construction analyses of an upstream tailings dam to investigate different methods of phreatic surface control. Several factors such as beach width, permeability anisotropy, rate of rise and slope inclination were varied to assess their influence on the phreatic surface. It should be noted that the main theoretical considerations of modelling and assessing seepage flow through tailings dams has not been described in this thesis. This is covered in detail under Chapter 3 of Xu (2019) and should be referred to for further information.

Table 2-6: Summary of Pore Pressures Regimes (Martin, 1999).

Regime	Fig Ref.	Foundation Conditions		Plasticity of Tailings Slimes	Rate of Rise	Beach Width	Comments
		Hydrogeology	K (foundation)				
Hydrostatic	1a	Natural groundwater table at or near the ground surface.	$\leq k$ (tailings)	None to low plasticity	Slow (< 6-8 m/year)	Sufficiently wide such that slimes do not underlie slope.	Indicative of essentially horizontal seepage flow within deposit due to lack of underdrainage at the base.
Over Hydrostatic	1b	Groundwater discharge area or groundwater table near ground surface, and/or compressible foundation soils.	Usually $\leq k$ (tailings)	Low to high plasticity	Rapid (> 8 m/year)	Narrow with slimes underlying slope.	Under-consolidated conditions within portion of the deposit and its foundation, with lack of underdrainage at base.
Over Hydrostatic with Bottom Drainage	1c	Groundwater recharge area.	> k (tailings) by factor of 10 to 100	Low to high plasticity	Rapid (> 8 m/year)	Narrow with slimes underlying slope.	Under-consolidated conditions within portion of the deposit but foundation is fully consolidated and provides for double drainage conditions.
Positive Pore Pressure Below	1d	Low groundwater table (recharge area).	> k (tailings) by factor of 10 to 100	Low to moderate plasticity	Intermediate	Narrow with slimes underlying slope.	Can indicate an underconsolidated condition where seepage is entirely vertical, or fully consolidated condition where flow has horizontal and vertical components.
Pore Pressures Near Zero	1e	Low groundwater table (recharge area).	> k (tailings) by factor of 10 to 100	Non-plastic	Slow (<6-8 m/year)	Wide beach, with slimes not underlying slope.	Indicates a fully consolidated condition with downward seepage due to good underdrainage at base.
Unsaturated	1f	Low groundwater table, arid climate.	> k (tailings) by factor of 10 to 100	Non-plastic	Slow (<<6-8 m/year)	Wide beach, with slimes not underlying slope.	A condition that can probably only be achieved in operating impoundments in arid climates, with wide tailings beaches and systematic discharge and drying cycles.



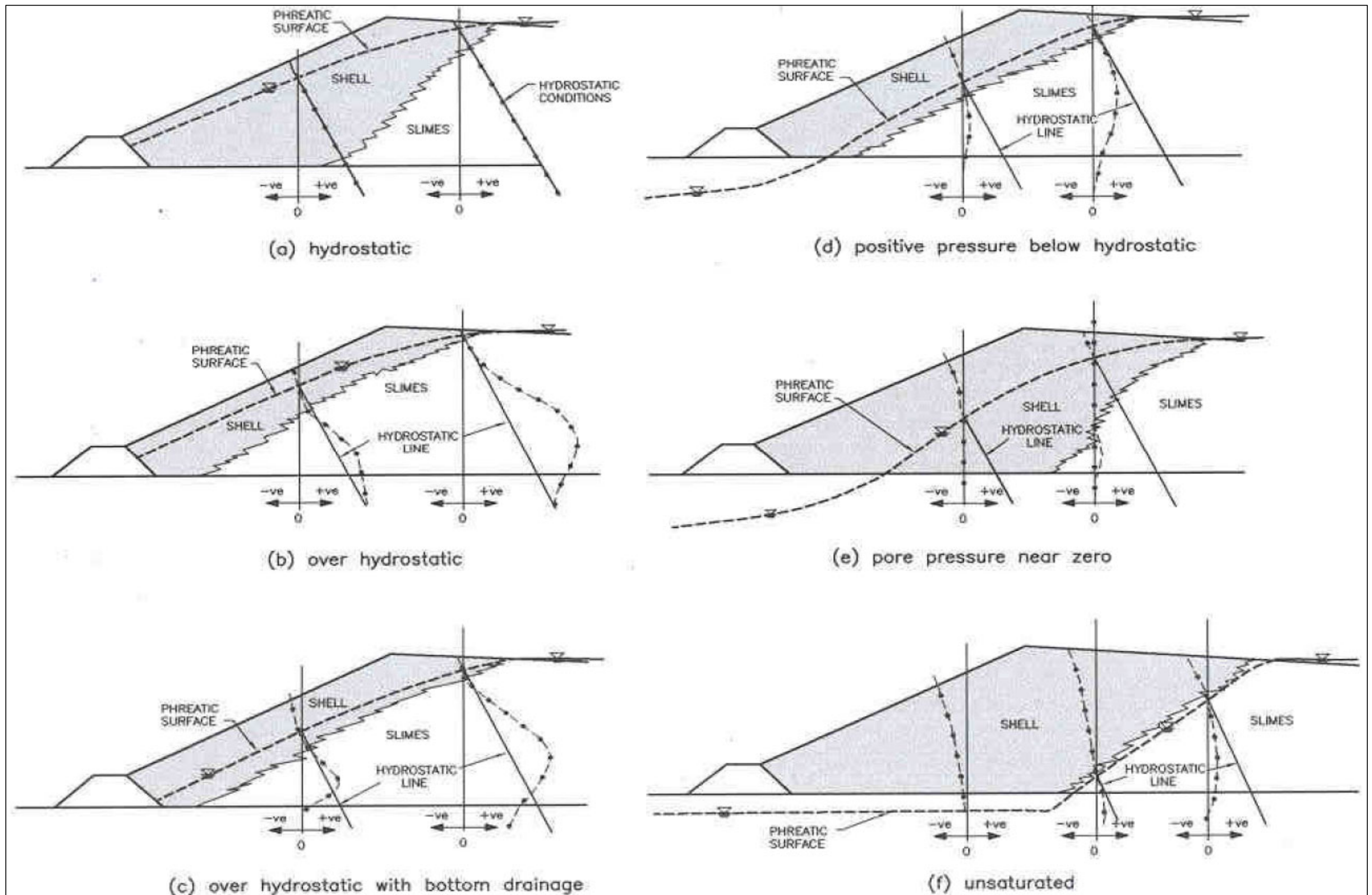


Figure 2-15: Graphical Representation of Pore Pressure Regimes (Martin, 1999).

## 2.5. Static and Dynamic Tailings Parameters

Assessing the geotechnical parameters of tailings through in-situ and laboratory testing is vitally important to safely design and construct tailings dams. These parameters are highly dependent on the static and cyclic behaviour of the tailings as well as the geological and hydrogeological setting of the site. (Davies and Lighthall 2001; WISE 2014; Hu, et al., 2017). It should be noted that tailings properties under unsaturated conditions require several unique, complex apparatus, which is associated with additional time and cost. Nevertheless, these tests if performed properly will produce reliable estimates of a tailing dam's behaviour and stability (Bella, 2017).

The static and cyclic characteristics of tailings have been evaluated from various studies with different findings based on the type of tailings that were tested (Jantzer et al. 2001; Qiu and Sego 2001; Bjelkevik 2005; Bjelkevik and Knutsson 2005; Wijewickreme et al. 2005; James et al. 2007; Shamsai et al. 2007; Guo and Su 2007; Riemer et al. 2008; Wong et al. 2008; Khalili et al. 2010; Wijewickreme et al. 2010; James et al. 2011; Adamczyk, 2012; Geremew and Yanful 2012; Geremew and Yanful 2013; Bonin et al. 2014; Mukerjee, et al., 2015; Zhang et al. 2015; Adajar and Zarco 2016; Bhanbhro, 2017; Xu, et al., 2017).

## 2.6. Tailings Dam Surveillance

As mentioned previously, the failure of the Samarco and Córrego de Feijão tailings dams in Brazil have led the industry to review their tailings facility risk evaluation approach and standards in terms of design, construction, operation and closure (Boshoff, et al., 2018). Construction and operation monitoring of tailings dams are vitally important as characteristics of deposited tailings may change during operation as a result of changes in ore and extraction processes (Caldwell, 2016).

Martin and Davies (2000) and Vanden Berghe, et al. (2011) provide a detailed discussion on the important requirements of tailings dam surveillance. Martin and Davies (2000) place emphasis on a method of risk management known as the observational method (Figure 2-16) that must be reinforced by a surveillance program and describe how this method is applied to tailings dam design and construction.

The steps involved in detecting possible failure modes by implementation of a surveillance program schedule are shown in Figure 2-17. It should be noted that every tailings dam must be considered on a site-specific basis in terms of adverse conditions, warning signs and surveillance measures (Martin and Davies, 2000). Skau, et al. (2013) reported on the benefits of combining numerical analyses with in-situ measurements and the observational method. An example of a site-specific instrumentation and monitoring plan was prepared by Radue (2017) for Poly Met Mining, Incorporated.



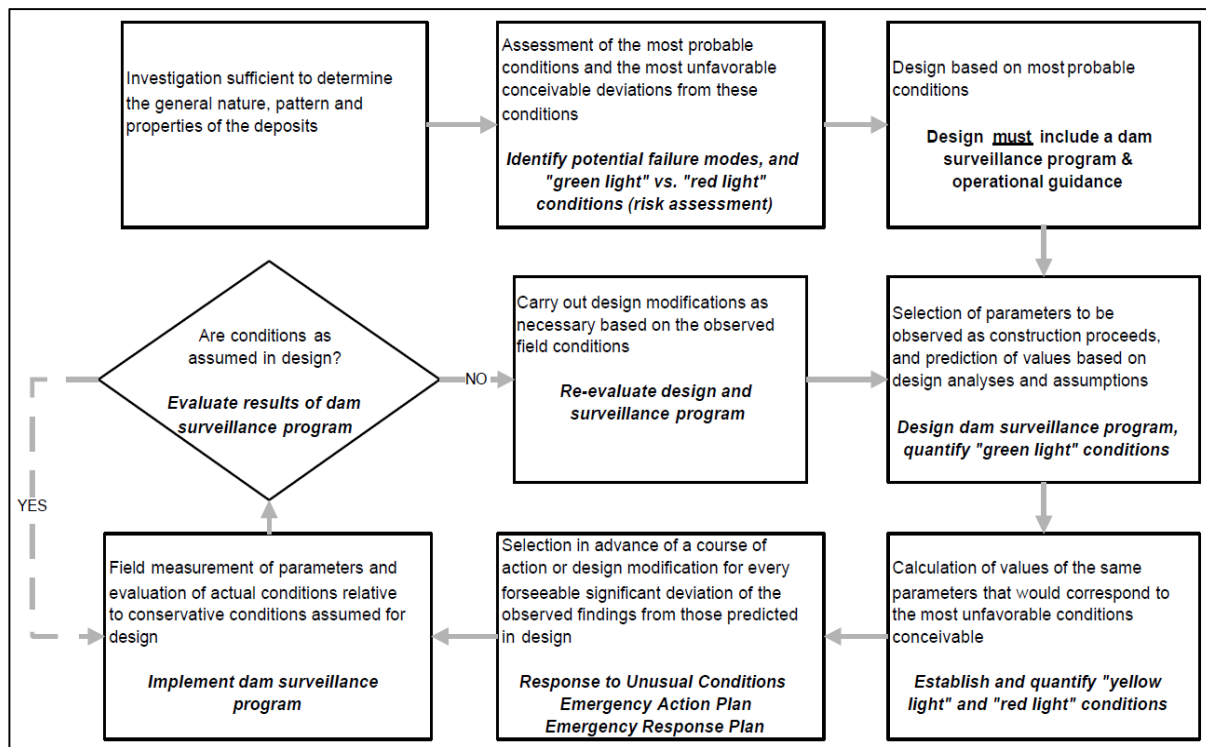


Figure 2-16: Risk Management Via The Observational Method (Martin and Davies, 2000).

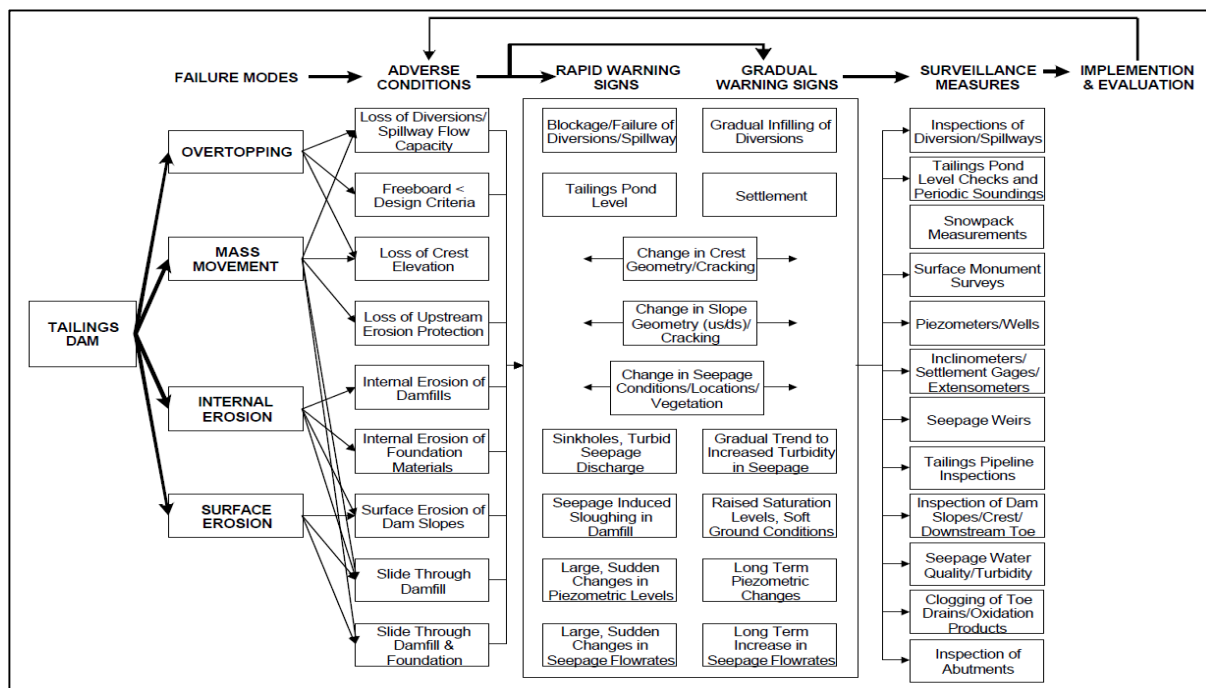


Figure 2-17: Failure Modes, Warning Signs and Surveillance Measures (Martin and Davies, 2000).

Additionally, Caldwell (2016) presented several guidelines in tailings facility design and construction that may reduce the risk profile and failure rate of these facilities. These guidelines have been summarised and are presented in the Table 2 6.

Table 2-7: *Proposed Guidelines in Tailings Facility Design and Construction (Caldwell, 2016).*

Guidelines	Description
Design FoS	Appropriate application of design FoS.
Human Habitation	No tailings facilities upstream of human settlements or sensitive environments.
Upstream Tailings Dams	Avoid upstream construction, use only if construction can be safely established
Cascading Dams	No cascading tailings dams.
Clay Foundations	Limit or avoid clay in the foundations.
Dam Height	Try limiting height to less than 100m.
Water in Basin	No or very small pool or pool distance from crest = 5 x embankment height.
Flat Embankments	Tailings embankments slopes of 5H:1V.
Penstocks	No penstocks through tailings or adjacent abutments.
Perimeter Slimes	No slimes near the perimeter or in the zone of potential slope failure.
Independent Review	An independent peer review of tailings dam design is highly recommended.
Educated Regulators	Governments in charge of review and approval of tailings dams to have above-average training and experience related to the facilities that they permit and to recognize when advice from an external specialist may be required.
Tailings Professionals	Qualified and competent tailings engineer is required for the design, construction and monitoring of tailings facilities.
Management Systems	A tailings management plan, adequate financial resources and processes to oversee design, operation, maintenance and closure.

Hu and Liu (2011) highlighted the change in tailings dam monitoring from being predominantly manual (labour intensive) to more automated real-time monitoring systems with the evolution of computer technology and instrumentation. This has led to the development and implementation of multi-user real-time monitoring networks that provide the client with real-time monitoring data that can be used to assess the safety of a tailings dam at any given time (Wang, et al., 2018). Similarly, Du Toit (2015) described commonly utilised geotechnical and survey instrumentation and their associated outputs (Table 2-8) currently being utilised for monitoring various aspects of slope stability.

Table 2-8: *Instrumentation and Associated Outputs for Monitoring Slope Stability (Du Toit, 2015).*

Sensor	Output
Vibrating Wire Piezometers	Pore water pressure can be measured within soil and rock at various depths allowing for flow gradient to be determined.
Inclinometers and Extensometers	Lateral movement and deformation
Settlement Cells and Horizontal Inclinometers	Vertical movement and deformation
Levelling	Vertical movement and deformation
Weather Stations	Rainfall could potentially be related to pore water pressure readings and barometric pressure is used to correct measurements for certain sensors.
Prism-Based Monitoring using Total Stations	Three-dimensional movement of prisms measured on a slope.
GPS or GNSS using Total Stations	Three-dimensional movement of reference beacons measured on a slope.
Satellite and Terrestrial Radar	Measures and characterises ground deformation using dense point clouds of deformation measurements together with a history of movement over time.

Examples of some of these monitoring systems being practically implemented to monitor various aspects of a tailings facility are discussed in the proceeding paragraphs.

Martin (1999) discussed the importance of correctly characterising pore pressure regimes in upstream tailings dams by implementing piezometer monitoring networks appropriate for various pore pressure regimes. Abancó, et al. (2016) and Boshoff, et al. (2018) demonstrated the effectiveness of implementing vibrating wire piezometer networks to monitor the real-time pore water pressures and temperatures for tailings dam in Spain and South Africa, respectively.

Several authors (Campbell and Fitterman, 2000; Fonseca, 2012; Vargas, et al., 2014; Mainali, et al., 2015; Quiroz, et al., 2016; Yaya et al., 2017; de Wit and Olivier, 2018) showed the effectiveness of using geophysical methods to monitor tailings dams in terms of locating phreatic surfaces and potential zones of seepage as well as characterising multi-layered subsurface profiles of the tailings dam and foundation soils.

Again several authors (Leica Geosystems AG, 2008; Wei and Wang, 2011; Chetty, 2013; Thomas, et al., 2019; Navarro, et al., 2019) showed how Lidar and satellite technology are used to monitor tailings dam deformation, monitoring of supernatant water volumes (operating pool) and potential seepage emanating from embankment slopes.

Fibre Optic Cable (FOC) systems can enable near real-time monitoring of strain, deformation and seepage of tailings dams. As part of a research and development initiative by an international mining company, an FOC system has been installed at a new tailings dam in South Africa. The FOC system has been installed above and beneath the geomembrane HDPE liner to monitor strain and temperature as well as the performance of the liner (Inaudi, et al. 2013; SMARTEC, n.d.; Todd Roberts, n.d.). This initiative aims to assess the effectiveness of the FOC system for lined tailings dams. This will be done by focussing on the liner tailings interface in terms of dam stability and seepage conditions and to incorporate the FOC monitoring data into the planned surveillance monitoring for the facility. The benefits and lessons learned from the FOC system are planned to be implemented within the mining companies portfolio for future lined tailings dam applications

## **2.7. Conclusion**

After carefully reviewing all available literature, determining the in-situ state and static liquefaction potential of tailings dams are typically assessed using one of several methodologies within the framework of CSSM that involves the use of in-situ and laboratory testing in conjunction with numerical analyses. Also, the literature review highlights the importance of performing staged construction to determine the seepage and hydromechanical behaviour of tailings dams. From the literature review, it can be concluded that there is a lack of available literature and studies related to determining the in-situ state and static liquefaction potential as well as staged construction of tailings dams from a South African perspective.

## Chapter 3 : Overview of TSF-A and Testing Data

This chapter presents an overview of an existing tailings dam, located in Limpopo, South Africa as well as a summary of in-situ and laboratory test data considered in this study. The tailings dam case study used in this thesis will henceforth be referred to as TSF-A. The mining company responsible for TSF-A will henceforth be referred to as Mining Company A.

### 3.1. TSF-A

The major TSF failure (Fundão TSF) that occurred at the Samarco Mine in Brazil on November 2015, prompted the mining industry to review their TSF risk evaluation as well as design and monitoring standards. Subsequently, renewed focus was placed on TSF slope stability, mainly in terms of undrained loading conditions where tailings are highly susceptible to static liquefaction. As a result, the evaluation of risk exposure in this regard was set in motion. Mining Company A engaged with its various operations and consulting teams globally to initiate risk screening of all tailings dams in their portfolios, specifically those being constructed using the upstream method.

The risk screening evaluated existing monitoring data to rank each TSF based on a defined risk profile, which considered the likelihood of typical liquefaction triggers such as high RoR, rapid rise in phreatic surface, build-up of excess pore water pressure, foundation materials prone to deformation etc. Subsequently, stability assessments on high-risk tailings dams identified where more data would be required to assess the liquefaction potential of deposited tailings in-situ state i.e. contractive and or dilative behaviour. The risk screening identified TSF-A, which is an upstream platinum tailings dam located in Limpopo Province, South Africa as a high-risk facility that required further detailed investigations, which involved comprehensive laboratory and in-situ testing. The results of these investigations are used in this thesis to assess the in-situ state and conduct a staged construction of TSF-A.

TSF-A was commissioned in October 2006 and has a final elevation of 1145 metres above mean sea level (mamsl) measured at the penstock, that is intended to be reached during 2020. TSF-A is designed to receive 200 000 tons per month (tpm) of dry tailings that are pumped and distributed via a steel spigot ring-feed to hydro-cyclones for deposition. The hydro-cyclones split the combined tailings feed into coarse (underflow) and fine (overflow) fractions. The underflow is used to construct the outer wedge that impounds overflow tailings deposited in the basin (Figure 3-1).

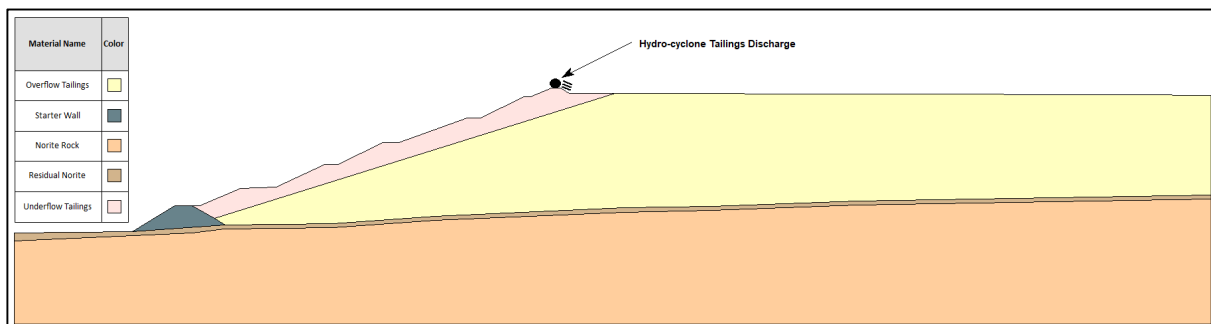


Figure 3-1: Schematic of Upstream TSF-A Showing Underflow Wedge and Impounded Overflow.

### 3.2. Laboratory Data

The following routine classification tests were conducted on forty (40) reconstituted tailings samples retrieved using either Shelby or Mostap sampling techniques: natural moisture content; specific gravity; bulk density; dry density; particle size distribution and Atterberg limits.

Using the Unified Soil Classification System (USCS), the tailings predominantly classify as low plasticity silts (ML) and silty sands (SM). The silt content ranges from 60 % to 85 % and the clay content from 1 % to 10 %, depending on whether the material corresponds to underflow (i.e. coarser silty sand) or overflow (i.e. finer silt) tailings. The results of the Atterberg limits showed the tailings to be non-plastic to slightly plastic with a low expansive potential and a linear shrinkage between 0 – 1 %. The specific gravity and void ratio ranged between 3.44 to 3.75 and 0.45 to 1.09, respectively.

Isotopically-consolidated undrained and drained triaxial compression tests (CIUC and CIDC, respectively) were performed on reconstituted samples representative of the overflow and underflow tailings. These tests are summarised in Table 3-1.

*Table 3-1: Summary of CIUC and CIDC Triaxial Tests Conducted on Overflow and Underflow Tailings.*

Tailings	Triaxial	Quantity	$p_{o'}$ (kPa)	$e_0$ – Test 1	$e_0$ – Test 2	$e_0$ – Test 3	$e_0$ – Test 4
Overflow	CIUC	3	400	0.771	0.884	0.940	-
	CIDC	1	200	0.736	-	-	-
Underflow	CIUC	4	400	0.657	0.761	0.804	0.903
	CIDC	1	200	0.760	-	-	-

It should be noted that apparent biases on the commercial laboratory testing procedures seem to have influenced the results. For example, some results show non-concave stress paths that may indicate seating errors/non-uniform loading, void ratios measured before saturation as well as consolidation and shearing conducted at different triaxial frames.

### 3.3. In-Situ Data

A total of sixty (60) CPTu with dissipation tests at 1 m intervals were conducted at various downstream monitoring lines located around the perimeter of TSF-A between 2017 and 2019. The CPTu reached final depths between 7.30 m and 39.80 m below ground level. Figure 3-2 is a schematic plan of TSF-A that shows the layout of monitoring lines where CPTu were conducted.

It should be noted that the laboratory and in-situ data are presented and interpreted in Section 4 to determine the in-situ state parameters of the tailings.

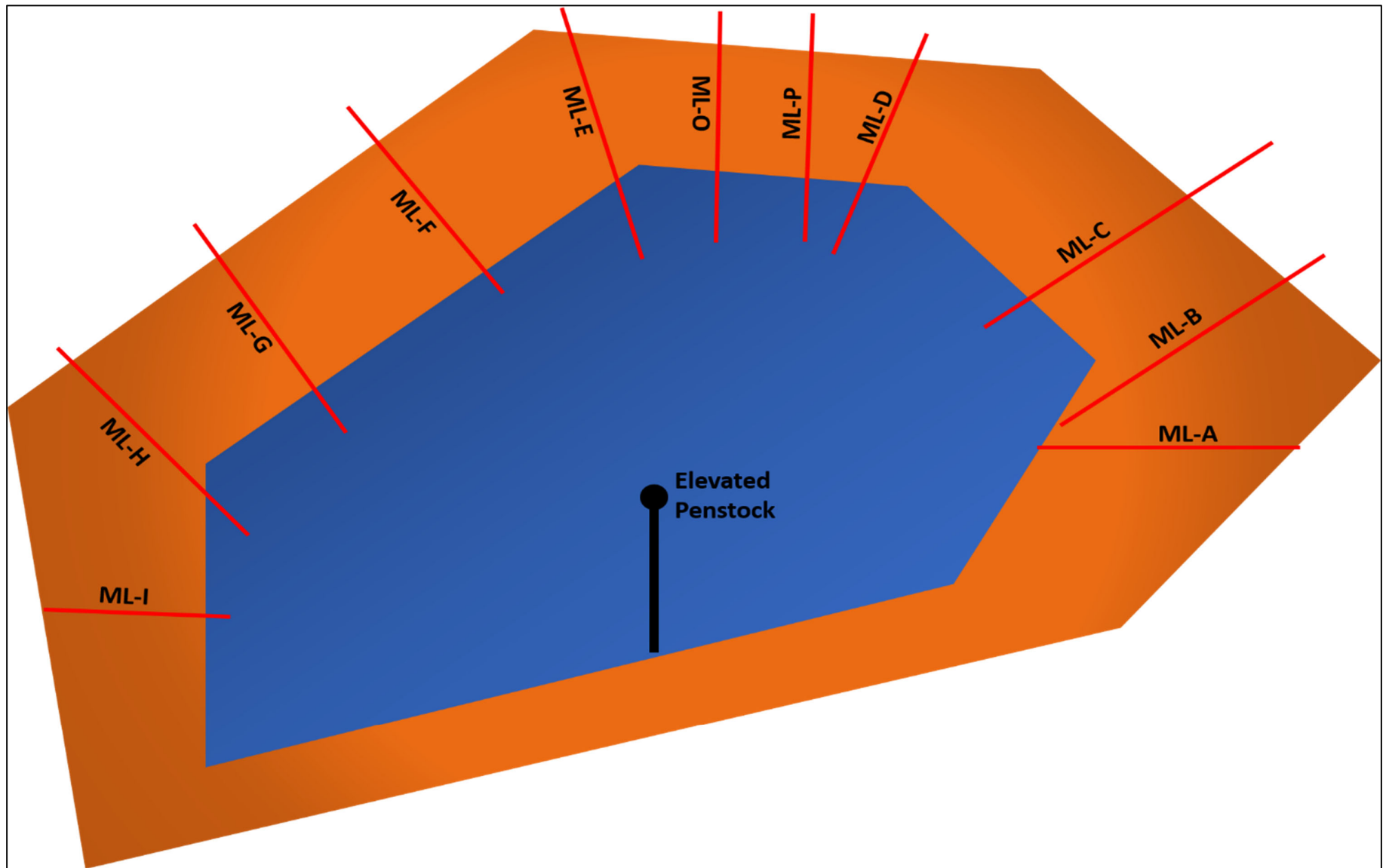


Figure 3-2: Schematic Drawing of TSF-A Monitoring Line Layout Plan.

## Chapter 4 : Determination of In-Situ State Parameters

This chapter presents analyses conducted to determine the in-situ state of TSF-A tailings following the Robertson (2010), Jefferies and Been (2016) as well as Shuttle and Jefferies (2016) methodologies. Results are contrasted and the differences between these methodologies are evaluated and discussed.

As described in Section 2.3 and according to Sottile et al. (2019), sand-like tailings have been well-defined by the CSSM framework (e. g. Bedin et al 2012, Been 2016, Jefferies and Been 2016). Using this framework, the  $\psi$  proposed by Been and Jefferies (1985), has been extensively used to determine a granular (coarse-grained) materials contractive or dilative behaviour based on the distance of the current  $p'-e$  state above or below the CSL (refer to Section 2.2, Figure 2-3).

The classification tests described in Section 3.2 above, show that TSF-A tailings are predominantly silt-like. According to Sottile et al. (2019) these types of tailings combine aspects from clay-like and sand-like materials in that: 1) they behave like clay in terms of low hydraulic conductivity; 2) they behave like sand in terms of having their strength controlled by frictional forces; 3) display dilative and or contractive behaviour depending on the state parameter; 4) densification caused by handling and transportation can result in a significant change in the material response (refer to Section 2.3, Figure 2-6).

The near-impossible task of retrieving good quality undisturbed samples has led to correlations and methods to estimate  $\psi$  of tailings from CPTu data. Robertson (2010) and Jefferies and Been (2016) methodologies have been widely used to determine the in-situ distribution of the state parameters from CPTu data (Sottile, et al., 2019). Nevertheless, they were developed for sand-like materials; hence, a difference is expected when dealing with silt-like tailings. This difference can be seen by the red circles in Figure 4-1. The red circles indicate silt-like tailings outliers when compared to sand-like tailings using the Jefferies and Been (2016) method. It should be noted that some empirical correlations have been developed specifically for tailings (e.g. Been et al 2012, Dienstmann et al 2018); however, these correlations require extensive calibration on a site by site basis.

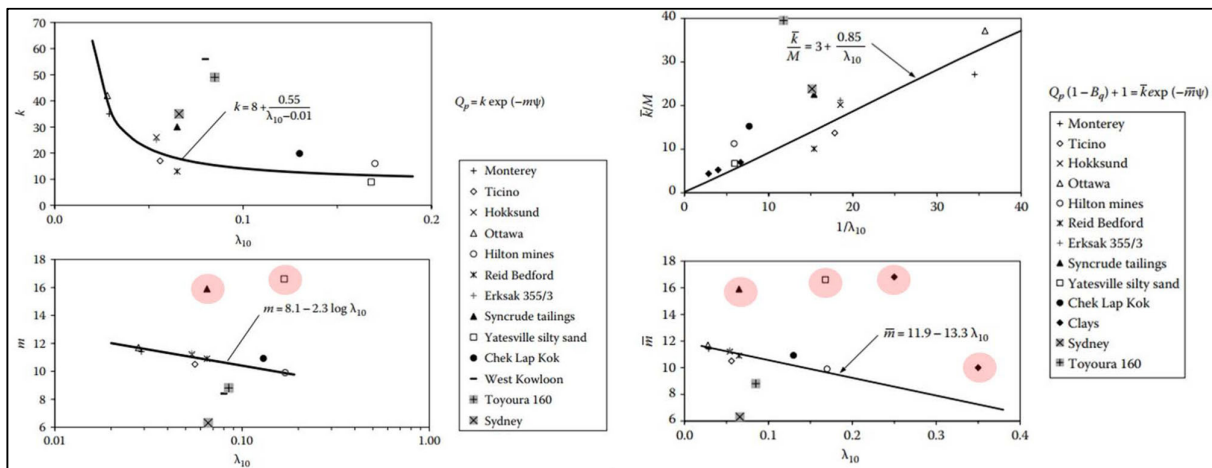


Figure 4-1: Correlations of  $\lambda_{10}$  with  $k$  and  $m$  (Jefferies and Been, 2016).

Shuttle and Jefferies (2016) chose a more fundamental approach where cavity expansion theory is recalled establishing a correlation between the tip resistance of CPTu and the state parameter. The methodology



combines the use of CPTu data and numerical element tests using NorSand. According to the authors, this method is considered to accurately capture calibration data and allows determination of the in-situ state parameter in silt-like tailings from CPTu data.

Firstly, NorSand was calibrated for overflow and underflow tailings, using CIUC and CIDC triaxial compression tests on reconstituted tailings samples. The calibrated NorSand parameters were then used to determine coefficients  $k$  and  $m$  for underflow and overflow tailings undergoing drained and undrained cavity expansion. Cavity expansion effective limit pressures were computed for different confining pressures, state parameters and rigidity indexes (Figure 4-2). Finally, the state parameters were calculated using CPTu data as well as  $k$  and  $m$  coefficients in Equation 3 from Chapter 2.

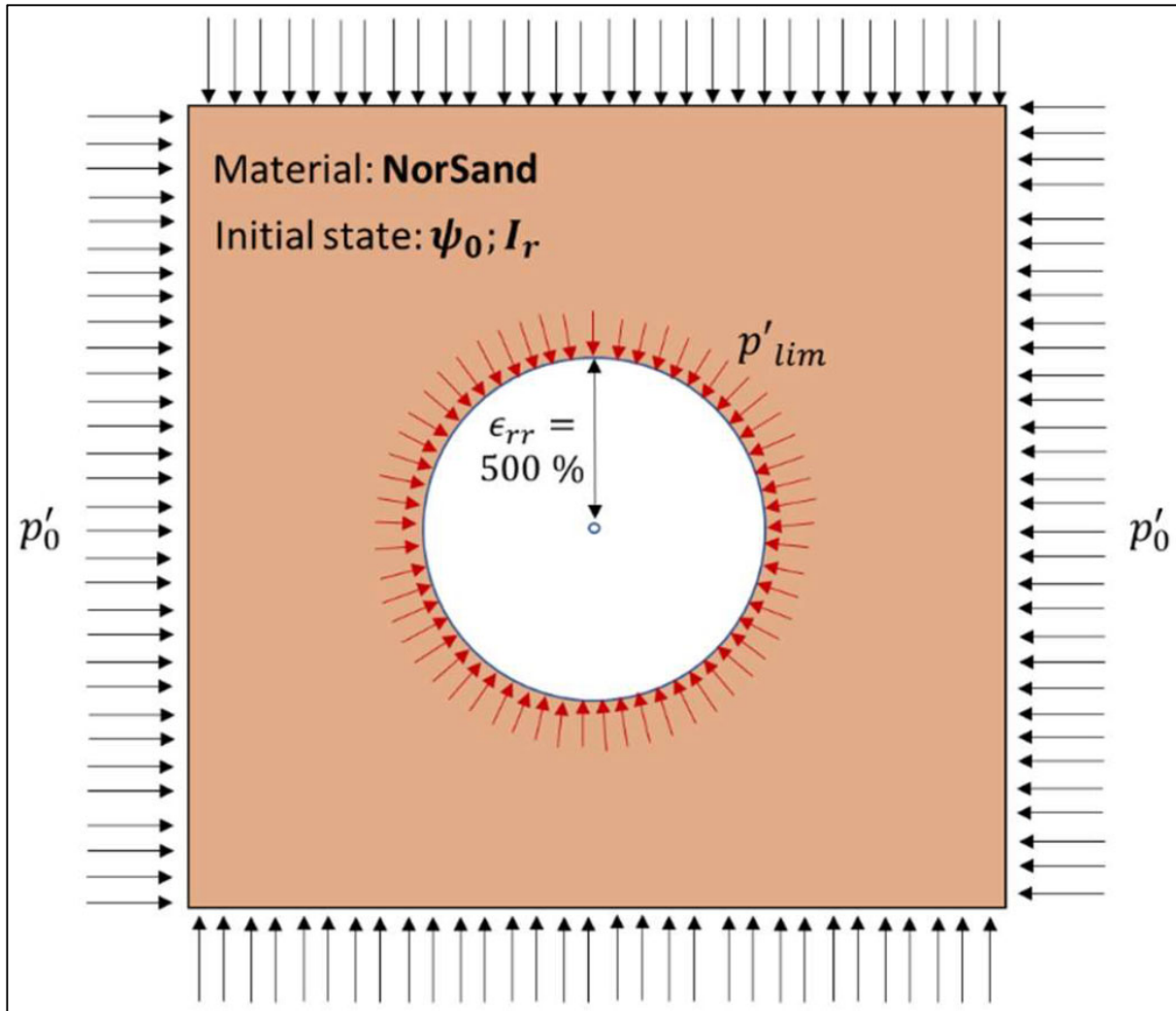


Figure 4-2: Scheme to Compute the Cavity Expansion Limit Effective Pressure ( $p'_{lim}$ ) Using NorSand and a Large Strain 1D FEM Code (Shuttle and Jefferies, 2016).

Although this procedure is more complex than the Robertson (2010) and Jefferies and Been (2016) methods, it results in more reliable and user-independent approximation of the state parameter, thus avoiding the direct use of many correlations available in the literature for natural sands and clays (Sottile, et al., 2019).



## 4.1. Calibration of NorSand Constitutive Model

NorSand was calibrated for overflow and underflow tailings using the CIUC and CIDC triaxial test data. The aim is to determine parameters to be used for drained and undrained cavity expansion analyses required to extract the state parameter from CPTu data, as proposed by Shuttle and Jefferies (2016). NorSand has ten parameters, which have been presented in Table 2-3 above. The various sources of uncertainty in the laboratory results (Section 3.2) were balanced to produce a reasonable set of calibration parameters used in this study.

### 4.1.1. Overflow Tailings Calibration

Figure 4-3 shows the comparison of the NorSand calibration with three CIUC tests and the one CIDC test for the overflow tailings. A notable agreement is obtained between the CIUC results and the NorSand calibration especially in the  $p'-q$  and  $q-\epsilon_a$  space. The CIDC (CD1) test show less agreement. This is primarily due to calibrating one set of parameters by using both CIUC and CIDC tests as well as focussing the calibration on capturing undrained contractive behaviour shown by the CIUC tests. The calibrated parameters for the overflow are shown in Table 4-1.

Table 4-1: Calibrated NorSand Parameters for Overflow Tailings.

$\Gamma$	$\lambda_{10}$	$M_{tc}$	$N$	$\chi$	$H_0$	$H_\psi$	$I_r$	$b$	$v$
1.10	0.205	1.47	0.27	3.5	80	200	90	0.70	0.20

### 4.1.2. Underflow Tailings Calibration

Figure 4-4 shows the comparison of the NorSand calibration with four CIUC tests and the CIDC test for underflow tailings. A good agreement in terms of  $p'-q$  and  $q-\epsilon_a$  is obtained for two CIUC tests (i.e. CU1 and CU2, red and yellow curves) and a poor match is obtained for the other two CIUC tests (i.e. CU3 and CU4, green and purple curves). For the CU3 test, a mean effective stress of around 300 kPa was measured at critical state, while NorSand prediction is approximately 40 kPa. In addition, the measured deviatoric stress at critical state is around 400 kPa, while NorSand entails about 50 kPa. On the other hand, CU4 data shows post-peak softening, while NorSand predicts a considerable post-peak hardening due to an initial negative value of the state parameter  $\psi \cong -0.10$ . The laboratory data for CU3 and CU4 show an initial increase of mean effective pressure, which is inconsistent with a CIUC test on a normally consolidated sample. As a result, the calibration for this set of data focused on achieving a closer fit with better quality laboratory data (i.e. CU1, CU2 and CD1). The calibrated parameters for the underflow material are shown in Table 4-2. A relatively good match is obtained between the NorSand calibration and the CIDC test result when compared to the overflow CIDC calibration.

Table 4-2: Calibrated NorSand Parameters for Underflow Tailings.

$\Gamma$	$\lambda_{10}$	$M_{tc}$	$N$	$\chi$	$H_0$	$H_\psi$	$I_r$	$b$	$v$
0.867	0.089	1.36	0.27	2.00	150	200	90	0.70	0.20

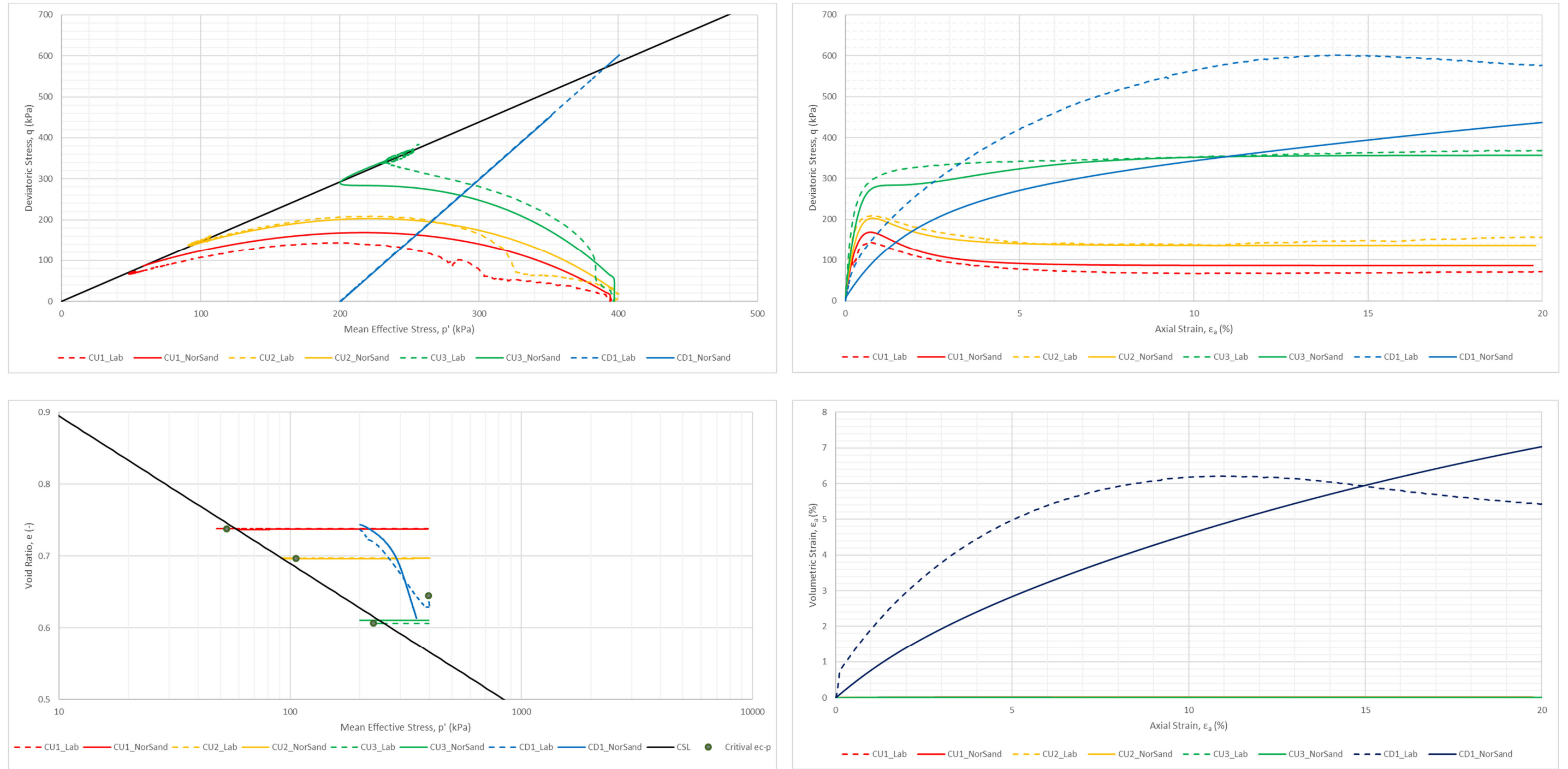


Figure 4-3: Comparison Between CIUC/CIDC Test Data and NorSand Calibration for Overflow.

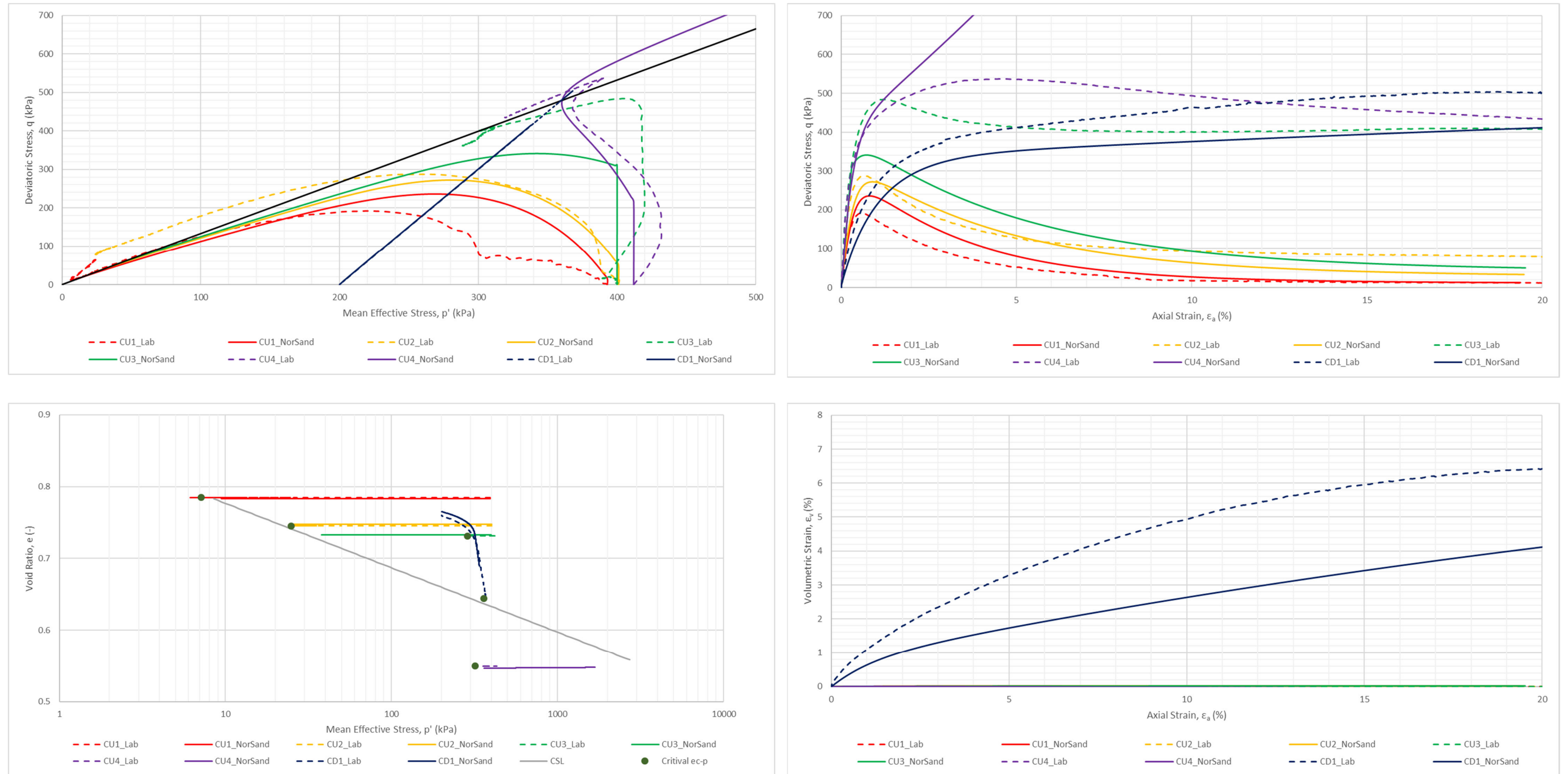


Figure 4-4: Comparison Between CIUC|CIDC Test Data and NorSand Calibration for Underflow.

## 4.2. Calibration of $k$ and $m$ Coefficients

Shuttle and Jefferies (2007), as well as Shuttle and Jefferies (2016), assume that the CPT dimensionless tip resistance ( $Q_p$ ) can be expressed as Equation 4.

$$Q_p = Q_{sph} \times C_q \quad (4)$$

where  $Q_{sph}$  is the spherical cavity expansion and  $C_q$  is a mapping factor that basically relates the sphere with the cone geometry.  $Q_{sph}$  depends on the soil properties, initial mean effective pressure and state parameter.

The methodology uses NorSand to compute limit cavity expansion pressure based on different combinations of initial confining pressures, state parameters and rigidity indexes. This is done by a large-strain finite element analysis code called CPTWidget that is freely available from the authors, Shuttle and Jefferies. The spherical limit pressures are mapped into the cone normalized resistance  $Q_p(1 - B_q) + 1$ . Finally, the coefficients  $k$  and  $m$  are determined and the state parameter is computed from CPTu data.

The NorSand calibration for overflow tailings was combined with drained and undrained cavity expansion analyses using CPTWidget. For drained analyses, a total of thirty-six combinations of different rigidity indexes  $I_r = 50|100|150$ , initial mean effective pressures  $p' = 100|500$  kPa and initial state parameters  $\psi = -0.05|0.00|0.05|0.10|0.15|0.20$  were chosen. For undrained analyses, a total of twenty-four combinations were modelled, using the same initial mean effective stresses and state parameters as for drained simulations, but only analysing rigidity indexes  $I_r = 50|150$  because the limit pressure for undrained cavity expansion is ideally independent of soil stiffness.

Figure 4-5 shows results for overflow tailings drained analyses. It is shown that the rigidity index determines different calibration coefficients for  $I_r = 50$ ,  $k = 28.5$  and  $m = 6.10$ ; for  $I_r = 100$ ,  $k = 30.5$  and  $m = 6.40$ ; and for  $I_r = 150$ ,  $k = 32.5$  and  $m = 6.70$ . Figure 4-6 shows results of overflow tailings undrained analyses which are almost independent of the rigidity index; thus, a unique line is fitted using  $k = 11.5$  and  $m = 9.50$ .

The same procedure was applied to underflow tailings data and Figure 4-7 shows results of drained analyses. It is shown that the rigidity index determines different calibration coefficients for  $I_r = 50$ ,  $k = 29.5$  and  $m = 5.10$ ; for  $I_r = 100$ ,  $k = 33.1$  and  $m = 5.40$ ; and for  $I_r = 150$ ,  $k = 36.7$  and  $m = 5.70$ .

Figure 4-8 shows results for undrained analyses of underflow tailings and it shows that the relationship cannot be accurately represented by a single line. Therefore, two combinations of  $k$  and  $m$  are proposed, based on the normalized tip resistance when  $Q_p(1 - B_q) + 1 > 4$ ,  $k = 10.5$  and  $m = 19.0$ ; when  $Q_p(1 - B_q) + 1 < 4$ ,  $k = 5.5$  and  $m = 6.0$ . It must be noted that CPTu penetrating under undrained conditions in underflow tailings has a low chance of occurring in-situ since the underflow tailings zone is likely to be unsaturated and predominantly located above the phreatic surface.

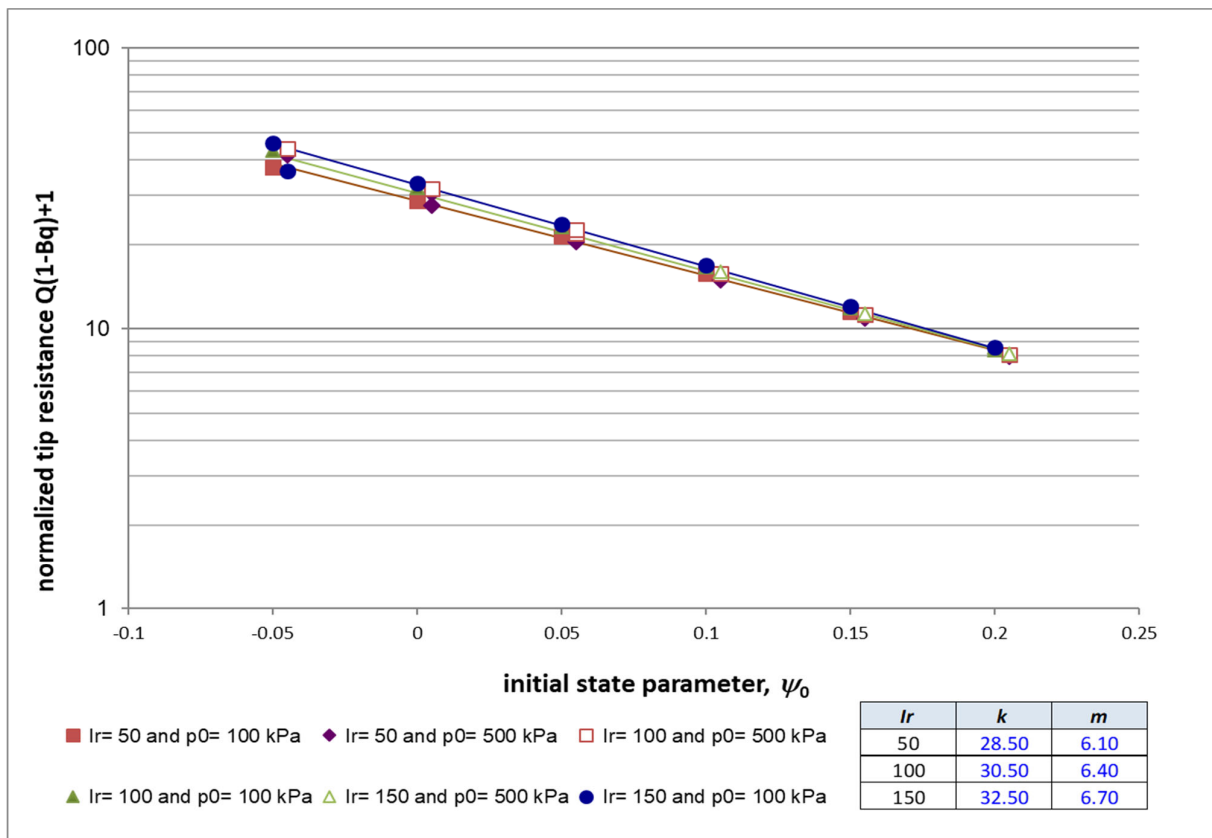


Figure 4-5: CPTWidget Results for Drained Analyses on the Overflow Tailings.

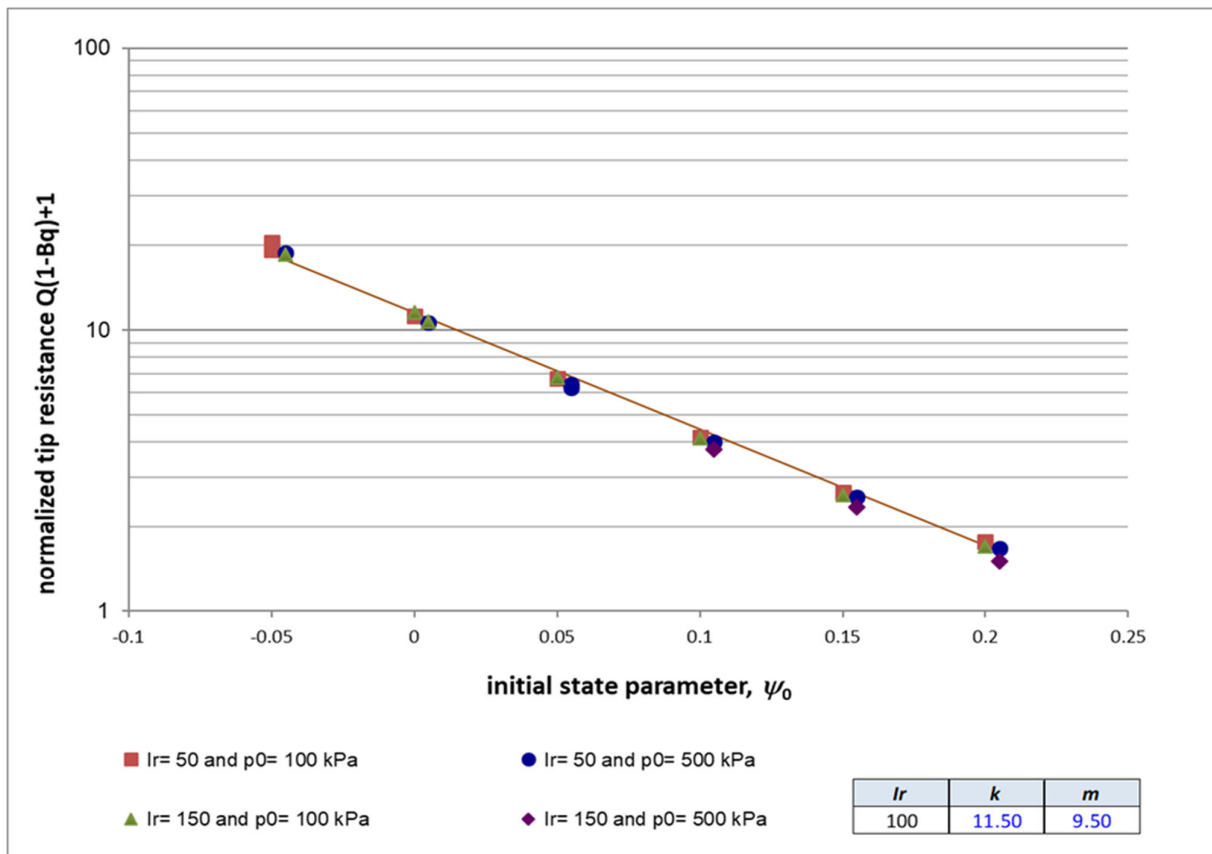


Figure 4-6: CPTWidget Results for Undrained Analyses on the Overflow Tailings.

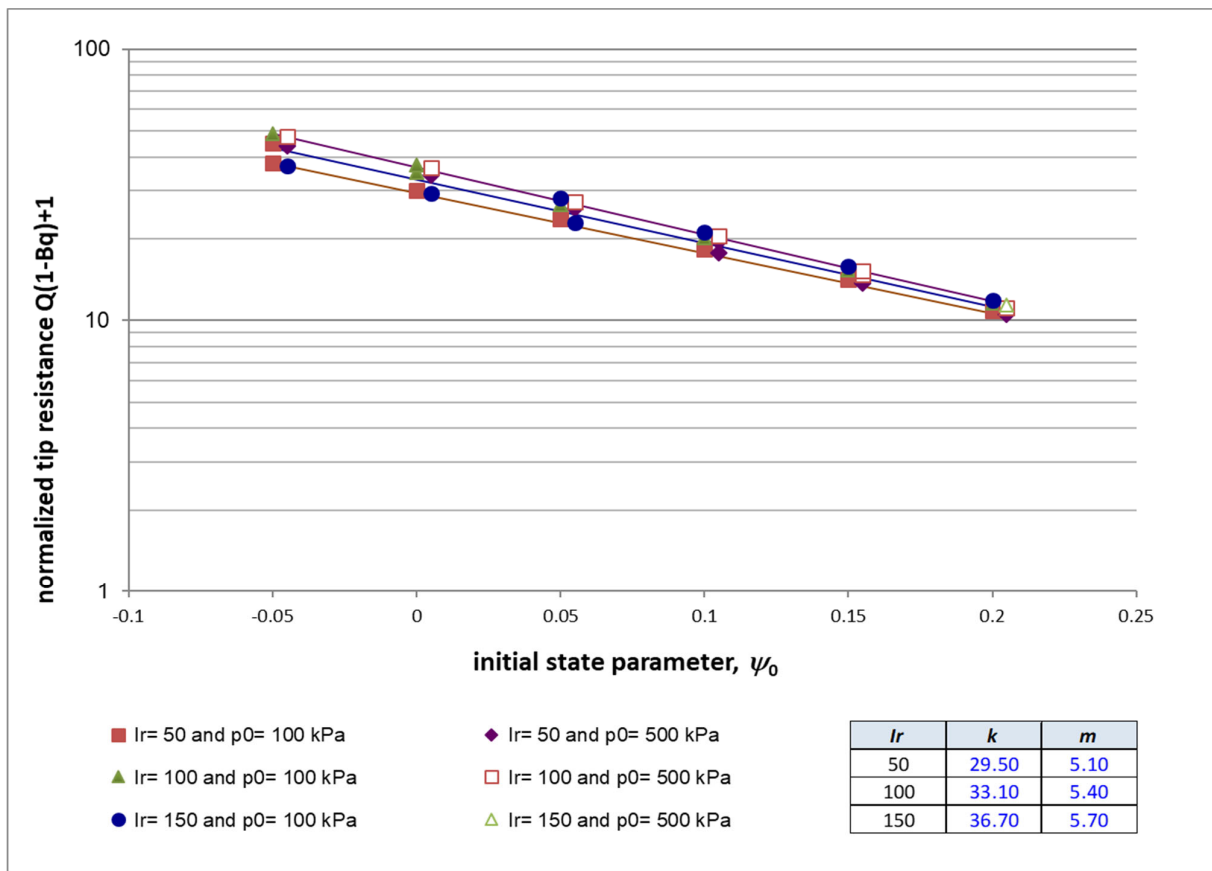


Figure 4-7: CPTWidget Results for Drained Analyses on the Underflow Tailings.

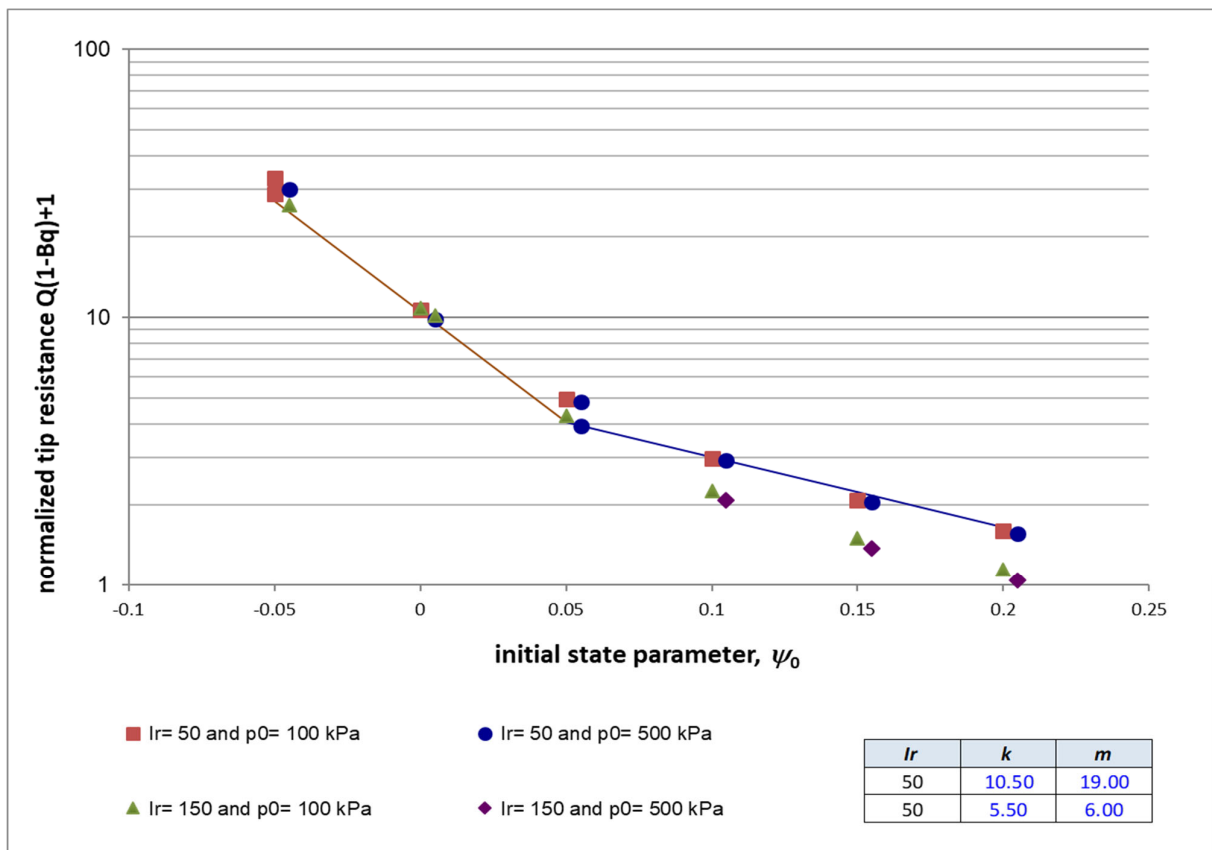


Figure 4-8: CPTWidget Results for Undrained Analyses on the Underflow Tailings.

A summary of coefficients  $k$  and  $m$ , determined from drained and undrained analyses for overflow and underflow tailings, are presented in Table 4-3.

Table 4-3: Summary of Calibrated  $k$  and  $m$  Coefficients for Overflow and Underflow Tailings.

Analysis Type	Overflow	Underflow
Drained	$I_r = 50, k = 28.5 \mid m = 6.10$	$I_r = 50, k = 29.5 \mid m = 5.10$
	$I_r = 100, k = 30.5 \mid m = 6.40$	$I_r = 100, k = 33.1 \mid m = 5.40$
	$I_r = 150, k = 32.5 \mid m = 6.70$	$I_r = 150, k = 36.7 \mid m = 5.70$
Undrained	$k = 11.5 \mid m = 9.50$	$Q_p(1 - B_q) + 1 > 4 \mid k = 10.5 \mid m = 19.0$
		$Q_p(1 - B_q) + 1 < 4 \mid k = 5.5 \mid m = 6.00$

### 4.3. Interpretation of The State Parameter from CPTu Data

State parameter profiles were interpreted for all 60 CPTu positions by using an Excel spreadsheet developed by Oelofse and Kruger (2019). For the sake of simplicity, the results of CPTu PC1 are presented below with the rest of the CPTu interpretations presented in Appendix A to Appendix K. Figure 4-9 shows the following:

- Corrected tip resistance ( $q_c$ ).
- Pore pressure measurement ( $u_0$ ).
- Friction ratio ( $R_f$ ).
- Soil behaviour type ( $I_c$ ).
- Pore pressure ratio ( $B_q$ ).
- Interpreted state parameter along depth of CPTu ( $\Psi$ ).
- Dilative ( $\Psi < -0.06$ ) and Contractive ( $\Psi > -0.06$ ) zones.
- Robertson (2010) SBTn analysis.

The state parameter is determined based on the type of tailings (i.e. underflow or overflow) and whether the cone penetration occurs under drained or undrained conditions. The distinction between overflow and underflow tailings is made based on the  $I_c$  value proposed by Jefferies and Been (2016). Drained and undrained penetration are distinguished based on the absolute value of  $B_q$  also proposed by Jefferies and Been (2016). Subsequently, coefficients  $k$  and  $m$  are obtained from Table 4-3 and state parameters are calculated based on which of the four cases apply (Table 4-4). It must be noted that in the absence of small strain stiffness ( $G_0$ ) in-situ measurements, average rigidity indexes values are adopted for drained cases.

Table 4-4: Criterion to Define  $k$  and  $m$  Coefficients Used to Interpret  $\Psi$  (Jefferies and Been, 2016).

Case	$I_c$	Absolute $B_q$	Tailings	Drainage
1	$< 2.00$	$< 0.02$	Underflow	Drained
2	$< 2.00$	$> 0.02$	Underflow	Undrained
3	$> 2.00$	$< 0.02$	Overflow	Drained
4	$> 2.00$	$> 0.02$	Overflow	Undrained

From Figure 4-9 a distinction is observed between the underflow and overflow tailings from the  $I_c$  value of approximately 2.00. The underflow tailings display  $I_c$  values between 1.25 and 2.00 i.e. clean to silty sands to sandy silt. The overflow tailings are predominantly characterised by  $I_c$  values greater than 2.00 and typically display  $I_c$  values between 2.40 and 3.22 i.e. sandy silt to silty clay. In addition, there is good agreement between state parameters interpreted using the Jefferies and Been (2016) and Shuttle and Jefferies (2016) methodologies. However, it should be noted that the Shuttle and Jefferies (2016) calibrations entail a wider dispersion (distribution range) and a generally higher mean value (Figure 4-10). On the other hand, the Robertson (2010) method entails a narrower dispersion and a lower mean value, which shows a relatively poor



agreement with the Jefferies and Been (2016) methodology and even lesser agreement with the Shuttle and Jefferies (2016) methodology.

To assess the state parameter variation between the Shuttle and Jefferies (2016) methodology versus the Robertson (2010) and Jefferies and Been (2016) methodologies, Equation 5 and 6 are defined as:

$$\Delta\Psi = \Psi_{S\&J} - \Psi_R \quad (5)$$

$$\Delta\Psi = \Psi_{S\&J} - \Psi_{J\&B} \quad (6)$$

where  $\Delta\Psi$  is the difference between the state parameters;  $\Psi_{S\&J}$ ,  $\Psi_R$  and  $\Psi_{J\&B}$  are the state parameters determined using Shuttle and Jefferies (2016), Robertson (2010) and Jefferies and Been (2016) methodologies, respectively.

The  $\Delta\Psi$  for each CPTu are interpreted and plotted as box and whisker plots (Figure 4-11). From these plots, the following is observed:

- The state parameter derived using the Shuttle and Jefferies (2016) method, is systematically higher than the state parameters derived using Robertson (2010) and Jefferies and Been (2016) methods;
- The  $\Delta\Psi$  median and mean values are all positive;
- The largest  $\Delta\Psi$  is observed between the Shuttle and Jefferies (2016) and Robertson (2010) methods;
- The maximum  $\Delta\Psi$  can be up to 0.35 and 0.49 when comparing the Shuttle and Jefferies (2016) method to the Jefferies and Been (2016) and Robertson (2010) methods, respectively.

A similar study was conducted by Sottile, et al. (2019) that compared the state parameters for silt-like tailings determined using the Shuttle and Jefferies (2016) and Jefferies and Been (2016) methods. The observations described above are comparable to those of Sottile, et al. (2019). According to Sottile, et al. (2019), large differences in state parameters (in this case  $\Delta\psi = 0.35$  and  $0.49$ ) observed between the Shuttle and Jefferies (2016) method and the empirically-based methods will have serious impacts on tailings dam design. For example, if one of the empirically based methods developed for sand-like tailings were used to characterise the in-situ state of a tailings dam comprised of silt-like tailings, this may lead to a less robust (non-conservative) design being adopted due to the tailings being characterised as less contractive or even dilative.

According to Sottile, et al. (2019), the Shuttle and Jefferies (2016) methodology has two important features. Firstly, the methodology does a good job at capturing the physics involved in a CPTu and secondly, the methodology has a calibration procedure dependent on a state-parameter based constitutive model. On this basis, the Shuttle and Jefferies (2016) methodology is more reliable for silt-like tailings than empirically-based procedures like Robertson (2010) as well as Jefferies and Been (2016). However, this statement must be used carefully on a project-specific basis that involves analysis of tailings in undrained shear (Sottile, et al., 2019).



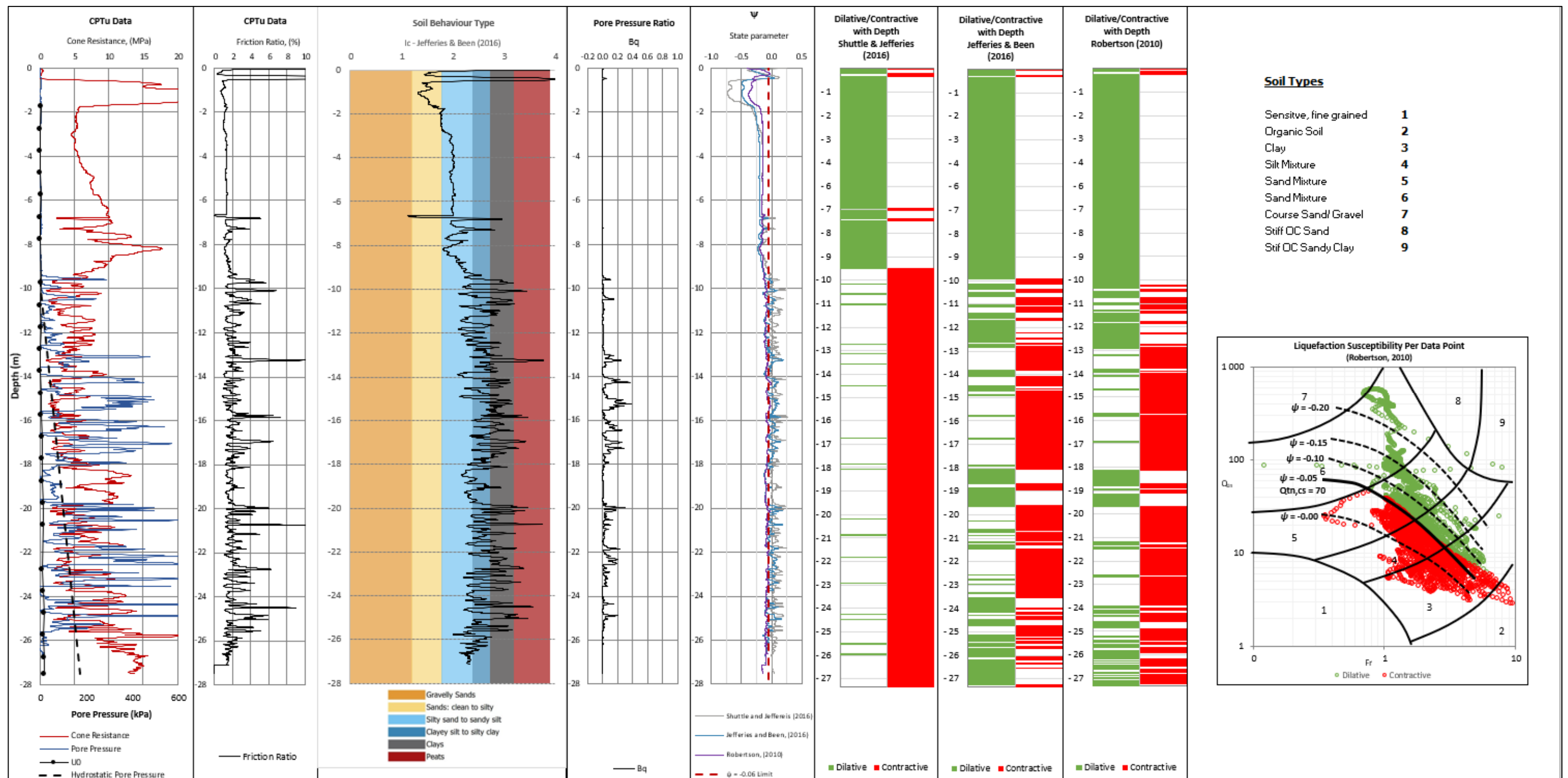


Figure 4-9: Cone Resistance, Friction Ratio, Soil Behaviour Type ( $I_c$ ), Pore Pressure Ratio ( $B_q$ ) Interpreted State Parameter Along Depth ( $\psi$ ), Contractive and Dilative Zones with Depth for Shuttle and Jefferies (2016), Jefferies and Been (2016) and (Robertson 2010) Methodologies, Robertson (2010) SBTn Analysis for CPTu PC1.

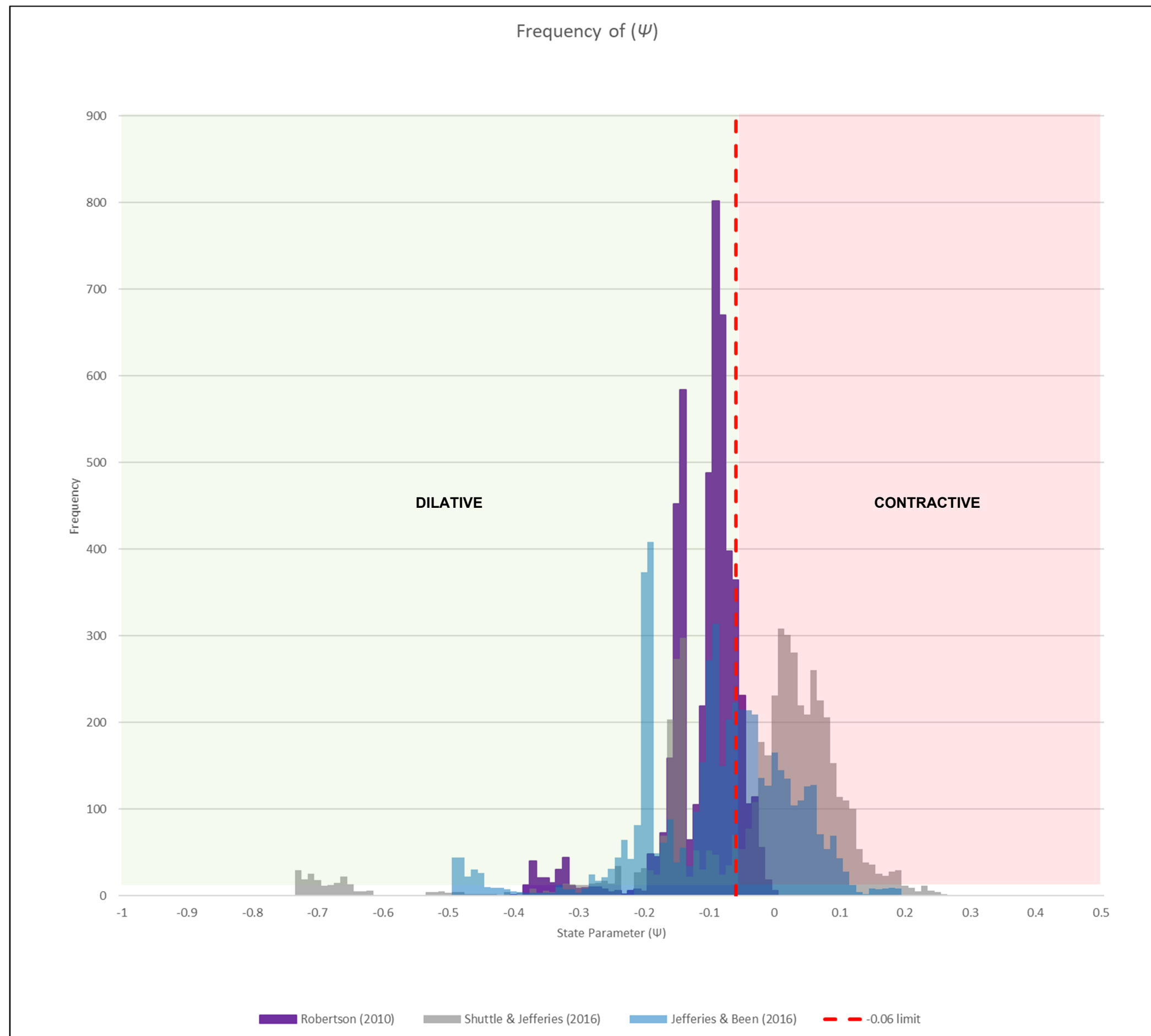


Figure 4-10: Frequency of Shuttle and Jefferies (2016), Jefferies and Been (2016) and Robertson (2010) Derived State Parameters Along Depth of CPTu PC1.

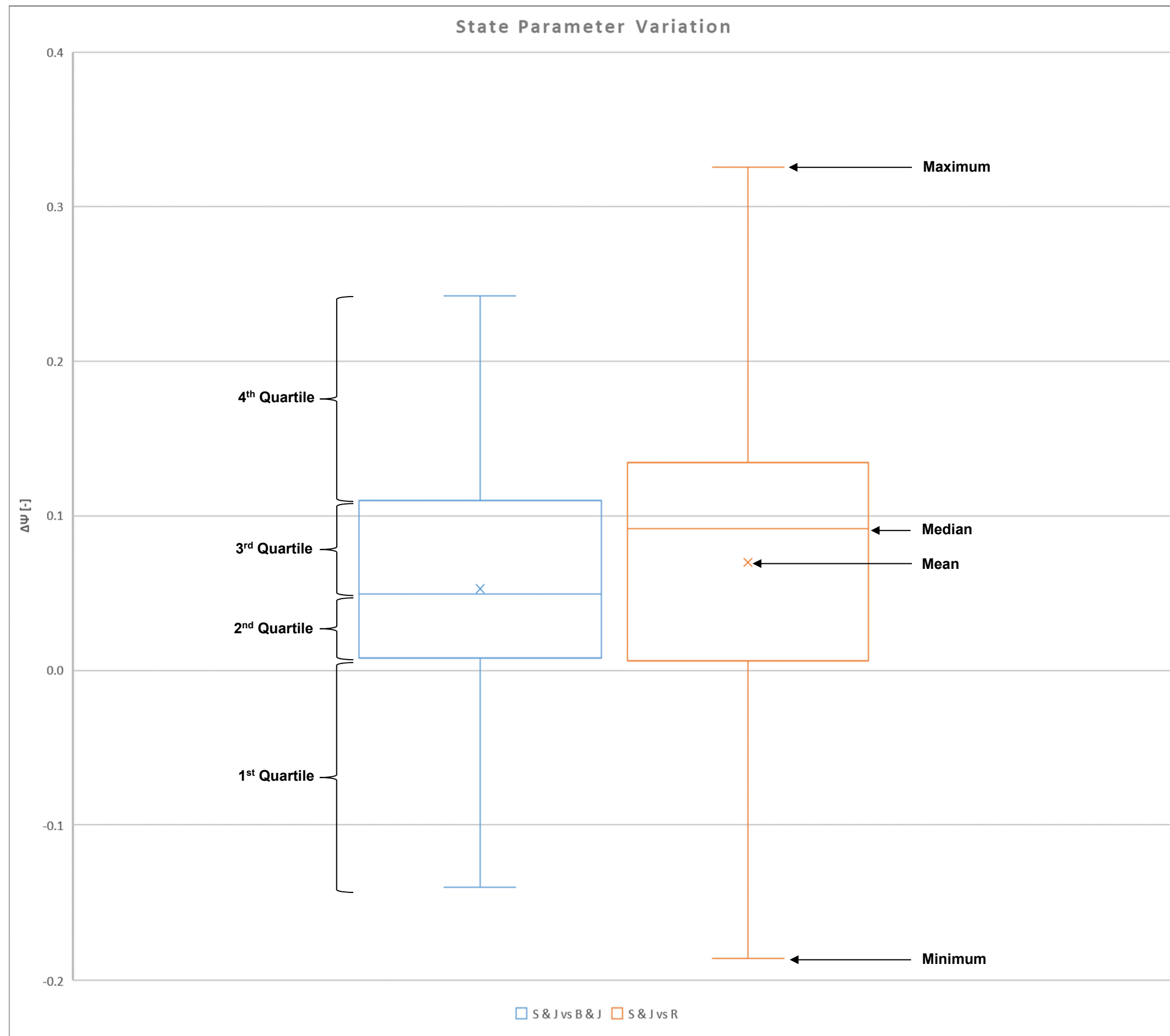


Figure 4-11: Difference of State Parameter Between Shuttle and Jefferies (2016) and Jefferies and Been (2016) as well as Shuttle and Jefferies (2016) and Robertson (2010) for CPTu PC1.

#### 4.4. State Parameter Variability and Spatial Distribution

This part of the chapter studies the spatial distribution of the state parameter at eleven monitoring lines at TSF-A and the variability along each section was then studied. The data from CPTu was also used to estimate the soil behaviour type based on Robertson (2010) SBTn chart. The SBTn chart divides soil behaviour into nine groups based on whether the material is:

- |                            |                                   |                            |
|----------------------------|-----------------------------------|----------------------------|
| 1. Sensitive, fine-grained | 2. Organic                        | 3. Clay                    |
| 4. Silt-mixtures           | 5. Sand-mixtures                  | 6. Sand                    |
| 7. Gravelly sand to sand   | 8. Very stiff sand to clayey sand | 9. Very stiff fine-grained |

According to the Robertson (2010) SBTn chart, all the above groups could display contractive or dilative behaviour except for groups 7 to 9 that will just display dilative behaviour. State parameter and SBTn interpretations for each monitoring line are presented in Table 4-5 and Table 4-6, respectively.

Table 4-5: State Parameter Interpretation Across the Various Monitoring Lines.

Monitoring Line	State Parameter Interpretation		Comment
	Underflow	Overflow	
A	Mainly dilative behaviour across all CPTu locations.	Mainly contractive behaviour across all CPTu locations.	Some minor interbedded dilative/contractive layers are observed within the overflow.
B	Mainly dilative behaviour across all CPTu locations.	Mainly contractive behaviour across all CPTu locations.	CPTu PC18 shows a highly interbedded overflow is predominantly dilative.
C	Mainly dilative behaviour across all CPTu locations.	Mainly contractive behaviour across all CPTu locations.	Some minor interbedded dilative/contractive layers are observed within the overflow.
D	Mainly dilative behaviour across all CPTu locations.	Mainly contractive behaviour across all CPTu locations.	Some minor interbedded dilative/contractive layers are observed within the overflow. Upper 3 m of the overflow in CPTu PC13 shows predominantly dilative behaviour.
E	Mainly dilative behaviour across all CPTu locations.	Mainly contractive behaviour across all CPTu locations.	Some minor interbedded dilative/contractive layers are observed within the overflow. Upper 4 m of the overflow at CPTu PC11 and PC11 Q3 show high interbedding of contractive and dilative layers
F	Mainly dilative behaviour across all CPTu locations.	Mainly contractive behaviour across all CPTu locations.	Some minor interbedded dilative/contractive layers are observed within the overflow at most CPTu locations except for CPTu PC8 and PC8 Q3. These locations show a greater degree of interbedded dilative layers within the predominantly contractive overflow.
G	Mainly dilative behaviour across all CPTu locations.	Mainly contractive behaviour across all CPTu locations.	Some minor interbedded dilative/contractive layers are observed within the overflow at most CPTu locations except for CPTu PC5. This location shows a greater degree of interbedded dilative layers within the predominantly contractive overflow.
H	Mainly dilative behaviour across all CPTu locations.	Mainly contractive behaviour across all CPTu locations.	Some minor interbedded dilative/contractive layers are observed within the overflow.
I	Mainly dilative behaviour across all CPTu locations.	Mainly contractive behaviour across all CPTu locations.	Some minor interbedded dilative/contractive layers are observed within the overflow.
O	Mainly dilative behaviour across all CPTu locations.	Mainly contractive behaviour across all CPTu locations.	Some minor interbedded dilative/contractive layers are observed within the overflow.
P	Mainly dilative behaviour across all CPTu locations.	Mainly contractive behaviour across all CPTu locations.	Some minor interbedded dilative/contractive layers are observed within the overflow.

Table 4-6: SBTn Interpretation Across the Various Monitoring Lines.

Monitoring Line	SBTn Interpretation		Comment
	Underflow	Overflow	
A	Dominant sand-mixture and silt-mixture like dilative.	Dominant silt-mixture and clay-like contractive.	-
B	Dominant sand-mixture and silt-mixture like dilative.	Dominant silt-mixture and clay-like contractive.	CPTu PC19 also displays sand-mixture contractive behaviour within the overflow.
C	Dominant sand-mixture and silt-mixture like dilative.	Dominant silt-mixture and clay-like contractive.	CPTu PC17 predominantly displays a dilative sand-like behaviour within the underflow. CPTu PC17 also displays sand-mixture contractive behaviour within the overflow.
D	Dominant sand-mixture and silt-mixture like dilative.	Dominant silt-mixture and clay-like contractive.	CPTu PC13 and PC29-Q3 also displays dominant sand-mixture contractive behaviour within the overflow.
E	Dominant sand-mixture and silt-mixture like dilative.	Dominant silt-mixture and clay-like contractive.	-
F	Dominant sand-mixture and silt-mixture like dilative.	Dominant sand-mixture, silt-mixture and clay-like contractive.	-
G	Dominant sand-mixture and silt-mixture like dilative.	Dominant silt-mixture and clay-like contractive.	-
H	Dominant sand-mixture and silt-mixture like dilative.	Dominant silt-mixture and clay-like contractive.	-
I	Dominant sand-mixture and silt-mixture like dilative.	Dominant silt-mixture and clay-like contractive.	-
O	Dominant sand-mixture and silt-mixture like dilative.	Dominant silt-mixture and clay-like contractive.	-
P	Dominant sand-mixture and silt-mixture like dilative.	Dominant silt-mixture and clay-like contractive.	-

## 4.5. Summary of State Parameter Assessment At TSF-A

Characterisation of the state parameter of silt-like tailings can be performed in the framework of CSSM. Shuttle and Jefferies (2016) used cavity expansion theory to establish a correlation between the tip resistance of CPTu and the state parameter. The methodology is briefly explained and results are compared with more empirical approaches Robertson (2010) as well as Jefferies and Been (2016).

It is observed that the state parameter using Shuttle and Jefferies (2016) procedure is systematically higher than the Robertson (2010) and Jefferies and Been (2016) methodologies. The Shuttle and Jefferies (2016) methodology shows that underflow tailings display predominantly dilative (strain-hardening) behaviour at most of the CPTu soundings. Only a few soundings show minor contractive layers within some portion of the underflow tailings. The overflow tailings show contractive (strain-softening) behaviour with interbedding of dilative layers in some portions of the overflow tailings.

Data from CPTu were also used to estimate the soil behaviour type along soundings, based on Robertson (2010) SBTn charts. Good correlations were found between SBTn classifications and interpretation of state parameter using Shuttle and Jefferies (2016) methodology in that similar behavioural responses of the underflow (i.e. dilative) and overflow (i.e. contractive) were noted.

In Summary, the Shuttle and Jefferies (2016) methodology is based on a more fundamental understanding of the physics involved in cone penetration and uses a constitutive model built around the concept of state parameter, making it more reliable for silt-like tailings than empirically-based procedures (Sottile, et al., 2019).



## Chapter 5 : Soil Constitutive Model for Staged Construction

This chapter presents the calibration process of the soil constitutive model used to perform the staged construction of TSF-A. The Softening-Hardening (S-H) soil constitutive model was selected to reproduce the dam behaviour during staged construction phases. The model was calibrated for overflow and underflow tailings using isotopically CIUC and CIDC triaxial compression tests on reconstituted overflow and underflow samples.

### 5.1. Softening Hardening Soil Constitutive Model

It is well documented in the literature that experimental data shows plastic deformation in soils occurs from initial stages of loading. To capture such behaviour, the typical elasto-perfect plastic constitutive models are not suitable. Therefore, constitutive models such as S-H soil constitutive model in Rocscience, Rock and Soil 2-D (RS2) analysis program that utilises a hardening law after initial yielding is required (Rocscience Inc B, n.d.). Based on the formulations of this constitutive model, there are three different mechanisms/yield surfaces that include: (1) deviatoric (shear); (2) volumetric (cap) and (3) tension cut off, which are illustrated in Figure 5-1 along with the hardening characteristics of this model in  $p$ - $q$  space. Figure 5-2 and 5-3 show the yield surfaces in 3D stress space. The model is very flexible with several options and formulations. It should be noted that by activating several different functions, the model can be analogous to either the Mohr-Coulomb; Duncan-Chang, ChSoil, Hardening Soil, Double yield and CySoil constitutive models (Rocscience Inc B, n.d.). These models are briefly defined as follows:

- Mohr-Coulomb model – typically used to characterise shear failure in soils and rocks and can be applied to slope stability and underground excavation (ITASCA Consulting Group. Inc., 2019).
- Duncan-Chang model – developed to address nonlinear mechanical behaviour of soils and is based on stress-strain curves from drained triaxial tests on clays and sands (Rocscience Inc C, n.d.).
- Chsoil model – is a basic version of the CySoil model. This model has a friction-hardening law that uses hyperbolic model parameters as direct input and a Mohr-Coulomb failure envelope with two built-in dilation laws (ITASCA Consulting Group. Inc., 2019).
- Hardening Soil model – is an effective stress hardening plasticity model, able to represent the behaviour of materials undergoing plastic compression, consolidation and monotonic shear. The model can be used for soil-structure interaction problems, excavations, tunnelling and settlements analysis, etc (ITASCA Consulting Group. Inc., 2019).
- Double-yield model – simulates materials where substantial permanent compaction and shear yielding occurs, such as hydraulically placed backfill or lightly cemented granular material (ITASCA Consulting Group. Inc., 2019).
- Cysoil model – the model is used to represent the nonlinear behaviour of soils and provides a better representation of the loading/unloading response of soils. The model comprises strain-hardening and softening shear behaviour, an elliptic volumetric cap with strain-hardening behaviour and an elastic modulus function of plastic volumetric strain (ITASCA Consulting Group. Inc., 2019).

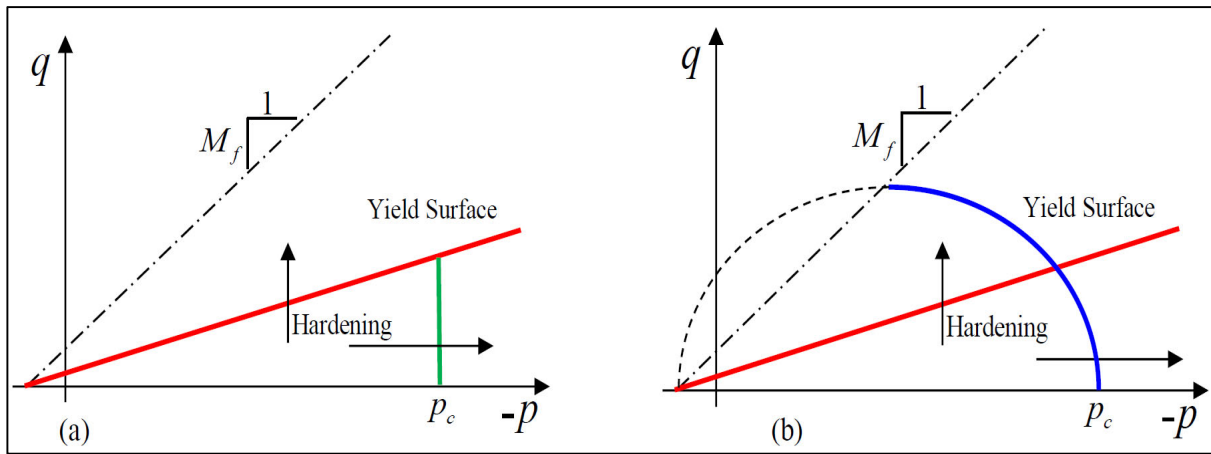


Figure 5-1: The Yield Surfaces of the S-H model; a) Deviatoric Yield Surface (red) and the Vertical Cap (green); b) Deviatoric Yield Surface (red) and Elliptical Cap (blue) (Rocscience Inc B, n.d.).

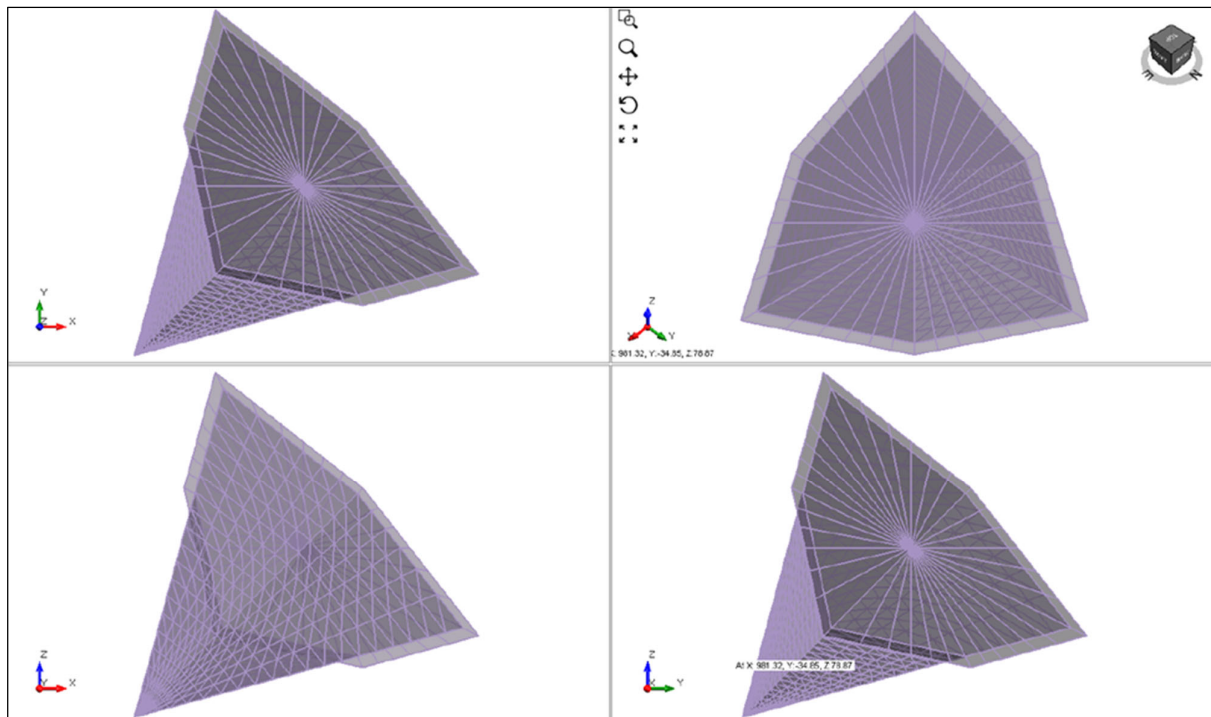


Figure 5-2: Yield Surface of S-H Model With Vertical Cap In 3D Stress Space (Rocscience Inc B, n.d.).

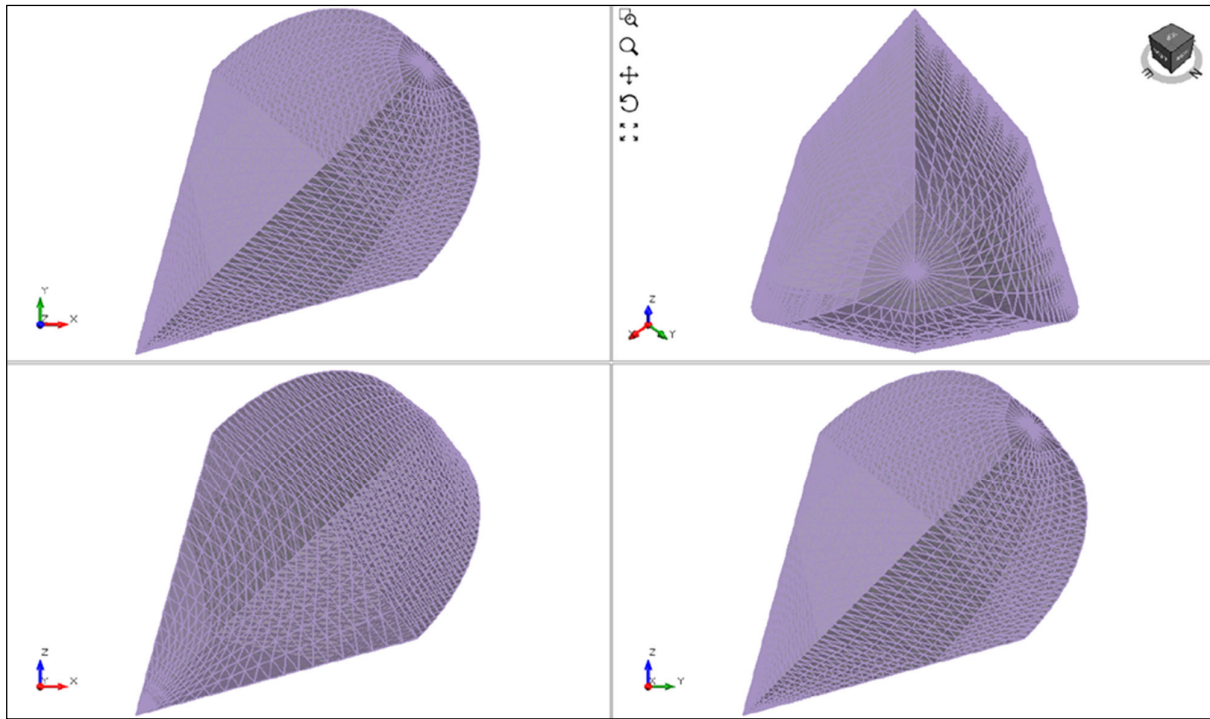


Figure 5-3: Yield Surface of S-H Model With Elliptical Cap in 3D Stress Space (Rocscience Inc B, n.d.).

## 5.2. Calibration of Softening-Hardening Constitutive Model

The S-H soil constitutive model was used to simulate the staged construction of TSF-A. The model can capture most of the observed behaviour of these materials including strain-softening and strain hardening, which were accounted for by varying the compaction-dilation angle and employing the non-linear isotropic stiffness function (Equation 7) in RS2.

$$E = E_0 \left( \frac{p}{p_{ref}} \right)^\alpha \quad (7)$$

$E_0$  is the elastic modulus at reference pressure ( $p_{ref}$ );  $\alpha$  is a material parameter and  $p$  is the mean stress, assuming compression positive. The parameters calibrated in the S-H soil constitutive model are:

- Strength
  - $\phi'$ : Mohr-Coulomb effective friction angle.
  - $c'$ : Mohr-Coulomb effective cohesion.
- Stiffness
  - $\nu$ : Poisson's Ratio
  - $E_0$ : Initial Young's Modulus at reference pressure,  $p_{ref}$ .
  - $p_{ref}$ : Reference Pressure
  - $\alpha$ : Material Parameter.
- Hardening
  - $A$ : Hardening Parameter (positive and constant)
- Dilation
  - $\psi$ : Dilation Angle (can be set to compaction dilation or dilation).

### 5.3. Calibration at Elemental Level

To calibrate the S-H constitutive model, the CIUC and CIDC triaxial tests were modelled in RS2 by assigning the necessary boundary conditions (loads and displacements) to replicate drained and undrained behaviour. Numerous iterations were performed by varying the parameters listed above until the best fit possible between the model and laboratory results were achieved for each test. For a detailed guide on modelling drained and undrained triaxial tests in RS2 using the S-H constitutive model, please refer to Rocscience Inc A (n.d.).

#### 5.3.1. Overflow Tailings

The model was calibrated for three CIUC triaxial tests and one CIDC triaxial test completed on reconstituted overflow samples. When tested, all CIUC tests were confined to an initial mean effective stress  $p_0 = 400$  kPa, but at different initial void ratios. Therefore, the effective stress path for undrained shear differ among the tests. To account for this and considering the model limitation of void ratio independence, the drained and undrained tests were calibrated using the non-linear isotropic stiffness function in RS2, which was used to match the different effective stress paths. A summary of calibrated parameters is presented in Table 5-1.

Table 5-1: Overflow Tailings Parameters Calibrated for S-H Constitutive Model.

Parameter	Unit	CU1	CU2	CU3	CD1
$\phi'$	°	36.0	36.0	36.0	37.0
$c$	°	0	0	0	0
$v$	-	0.3	0.3	0.3	0.25
$E_0$	kPa	13 000	7 000	6 000	30 000
$p_{ref}$	kPa	100	100	100	100
$\alpha$	-	0.7	1.35	1.0	0.2
$A$	-	0.0088	0.005	0.0035	0.005
$\psi$	°	34.5	35.6	35.7	37.0

Table 5-2 below presents pertinent observations made for undrained and drained test calibrations. A comparison between the test data and the S-H soil constitutive model calibration for overflow tailings is presented in Figure 5-4. The contrast is made in terms of mean effective stress ( $p'$ ), deviatoric stress ( $q$ ), axial strains ( $\epsilon_a$ ), volumetric strains ( $\epsilon_v$ ) and shear-induced pore pressures ( $p_w$ ) i.e.  $p' - q$ ,  $q - \epsilon_a$ ,  $p_w - \epsilon_a$  and  $\epsilon_v - \epsilon_a$ .

Table 5-2: Pertinent Observations for Overflow Parameters Calibrated for S-H Constitutive Model.

Calibrated Parameters	CU1 (Red)	CU2 (Orange)	CU3 (Green)	CD1 (Blue)
$p' - q$	There is a good match between the lab data and the calibration especially closer to the CSL.	There is a good match between the lab data and the calibration, especially closer to the CSL.	There is an excellent match between the laboratory data and the calibration	There is an excellent match between the laboratory data and the calibration
$q - \epsilon_a$	The peak strength and strain are slightly overpredicted at peak, but the strength for $\epsilon_a > 5\%$ is well calibrated.	The peak strength and the strain are slightly overpredicted at peak, but the strength for $\epsilon_a > 1\%$ is well calibrated.	There is an excellent match between the laboratory data and the calibration for $\epsilon_a > 2\%$	Overall, peak strength and stiffness are well-calibrated.
$p_w - \epsilon_a$	The modelled shear-induced pore pressures are under-predicted for $\epsilon_a < 5\%$ , but there is an excellent match for larger strains.	The modelled shear-induced pore pressures agree with the laboratory data.	The modelled shear-induced pore pressures are under-predicted for $\epsilon_a < 10\%$ , but there is an excellent match for larger strains.	Zero excess pore pressure can develop during the shearing phase of a drained triaxial compression test.
$\epsilon_v - \epsilon_a$	Zero volumetric strain in undrained triaxial compression test, as sample volume kept constant during the shearing phase.	Zero volumetric strain in undrained triaxial compression test, as sample volume kept constant during the shearing phase.	Zero volumetric strain in undrained triaxial compression test, as sample volume kept constant during the shearing phase.	The numerical model reaches a maximum of approximately $\epsilon_v = 4\%$ , while the measured laboratory value reaches a peak of $\epsilon_v = 6\%$ .

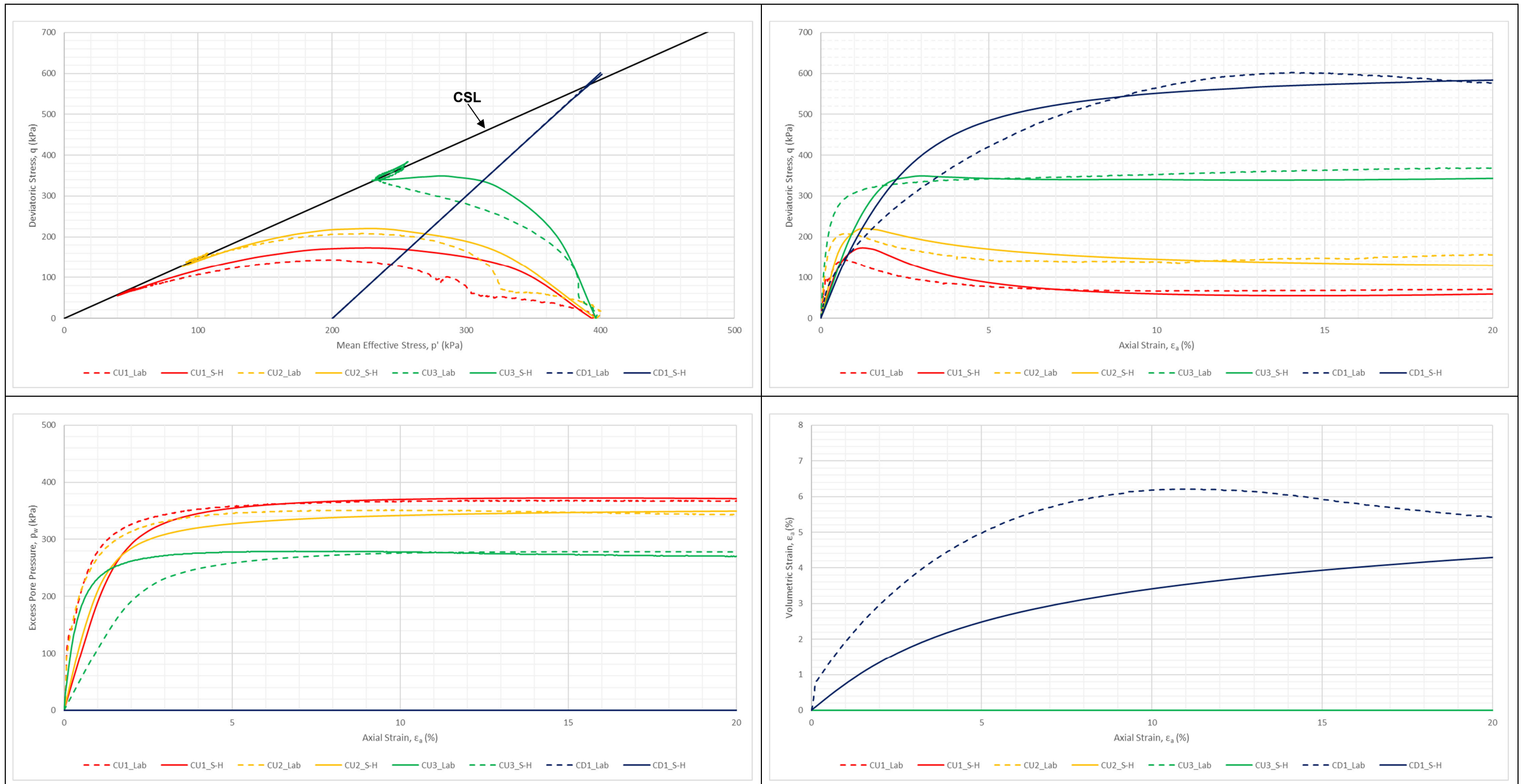


Figure 5-4: Comparison Between CIUC/CIDC Test Data and S-H Calibration for Overflow Tailings.



### 5.3.2. Underflow Tailings

The model was calibrated for four CIUC triaxial tests and one CIDC triaxial test completed on reconstituted underflow samples. When tested, all CIUC tests were confined to an initial mean effective stress of  $\sigma_3 = 400$  kPa, but at different initial void ratios. Therefore, the effective stress path for the undrained shear differ among the tests. To account for this and considering the model limitation of void ratio independence, the drained and undrained tests were calibrated using the non-linear isotropic stiffness function in RS2, which was used to match the different effective stress paths. A summary of the parameters is presented in Table 5-3.

Table 5-3: Underflow Tailings Parameters Calibrated for S-H Constitutive Model.

Parameter	Units	CU1	CU2	CU3	CU4	CD1
$\phi'$	°	33.0	33.0	33.0	33.0	34.0
$c$	°	0	0	0	0	0
$v$	-	0.3	0.3	0.3	0.3	0.3
$E_0$	kPa	26 000	43 000	7 500	8 300	70 000
$p_{ref}$	kPa	100	100	100	100	100
$\alpha$	-	0.65	0.25	0.15	0.60	0.20
$A$	-	0.0032	0.0015	0.0026	0.0010	0.0040
$\psi$	°	32.8	33.0	33.0	33.0	34.0

Table 5-3 below presents pertinent observations made for undrained and drained tests. A comparison between the test data and the S-H soil constitutive model calibration for underflow tailings is presented in Figure 5-5. The contrast is made in terms of  $p'$ ,  $q$ ,  $\epsilon_a$ ,  $\epsilon_v$  and  $p_w$  i.e.  $p' - q$ ,  $q - \epsilon_a$ ,  $p_w - \epsilon_a$  and  $\epsilon_v - \epsilon_a$ .

Table 5-4: Pertinent Observations for Overflow Parameters Calibrated for S-H Constitutive Model.

Calibrated Parameters	CU1 (Red)	CU2 (Orange)	CU3 (Green)	CU4 (Green)	CD1 (Blue)
$p' - q$	Good match between the lab data and the calibration.	Relatively good match between the lab data and the calibration at lower strains. However, the stress path is under-predicted at larger strains.	Poor match between the laboratory data and the calibration.	Poor match between the laboratory data and the calibration	There is an excellent match between the laboratory data and the calibration
$q - \epsilon_a$	The peak strength and axial strain are slightly overpredicted at peak. However, there is an excellent match at larger strains.	The peak strength is slightly under-predicted. Strengths are slightly over-predicted up to $\epsilon_a = 10\%$ . At larger strains $\epsilon_a > 10\%$ strengths are slightly under-predicted.	The peak strength is under-predicted, but there is an excellent match for the strengths at larger strains	The peak strength is under-predicted, but there is an excellent match for the strengths at larger strains	The model under-predicts the peak strength at the corresponding axial strain. Strength at axial strains $\epsilon_a > 10\%$ , show much better agreement.
$p_w - \epsilon_a$	Good match between the lab data and the calibration. The modelled shear-induced pore pressure is slightly under-predicted for $\epsilon_a = 1\%$	The measured shear-induced pore pressures are under-predicted by the numerical model.	The model shear-induced pore pressures are under-predicted for axial strains of up to $\epsilon_a = 10\%$ , but there is a good match for large strains	The model shear-induced pore pressures are under-predicted for axial strains of up to $\epsilon_a = 3\%$ , but there is a good match for larger strains	Zero excess pore pressure is allowed to develop during the shearing phase of a drained triaxial compression test.
$\epsilon_v - \epsilon_a$	Zero volumetric strain in undrained triaxial compression test, as sample volume kept constant during the shearing phase.	Zero volumetric strain in undrained triaxial compression test, as sample volume kept constant during the shearing phase.	Zero volumetric strain in undrained triaxial compression test, as sample volume kept constant during the shearing phase.	Zero volumetric strain in undrained triaxial compression test, as sample volume kept constant during the shearing phase.	The numerical model reaches a maximum of approximately $\epsilon_v = 2\%$ , while the measured laboratory value reaches a peak of $\epsilon_v = 6\%$

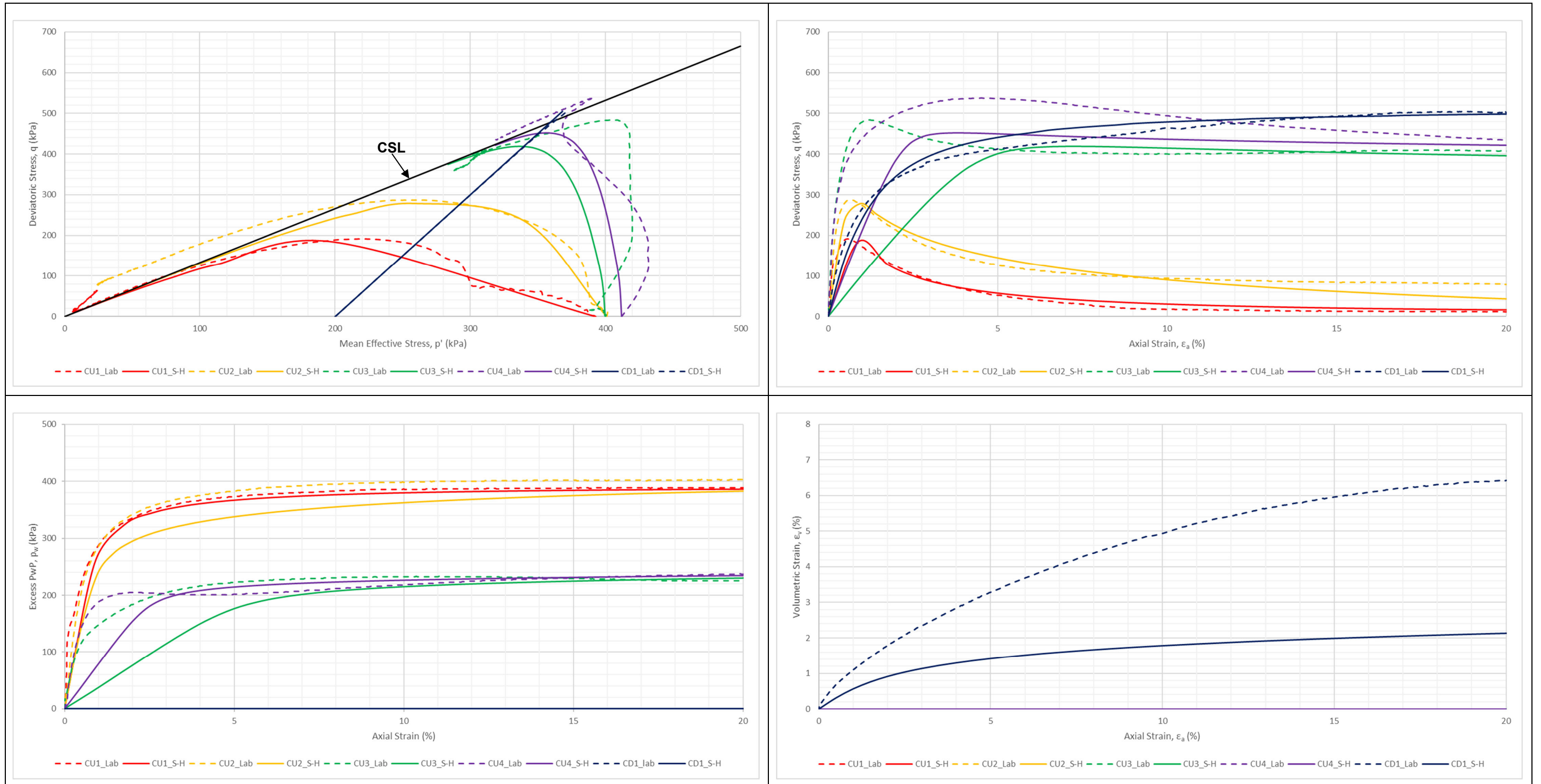


Figure 5-5: Comparison Between CIUC/CIDC Test Data and S-H Calibration for Underflow Tailings.

## Chapter 6 : Staged Construction Numerical Modelling

In this chapter, the staged construction of TSF-A is assessed using numerical modelling techniques. These investigations are primarily conducted to predict the location of the phreatic surface as well as to assess pore pressure and drainage conditions within a tailings dam (Saad and Mitri, 2010).

### 6.1. Software

RS2 Version 9.0 was used for the analyses. RS2 is a program for 2-D finite element analysis of geotechnical structures for civil and mining applications. RS2 can conduct a numerical groundwater seepage analysis for saturated and unsaturated soils using steady-state and transient groundwater seepage formulations through both homogeneous and heterogeneous earth and tailings dams (Xu, 2019).

### 6.2. Numerical Model Setup

Figure 6-2 illustrates a 2-D cross-section on which the numerical analyses are conducted. From previous studies conducted at TSF-A, Monitoring Line F is the highest most critical section and was chosen to conduct the numerical analyses.

Fully coupled transient FEM was performed, which simulated full interaction between ground, construction materials and pore water to reproduce the behaviour of solid and fluid phases of various materials that form the tailings dam. This approach allows the model to achieve a more accurate representation of consolidation and pore pressures distribution, which will result in a more realistic location of the phreatic surface during staged construction of the tailings dam (Saad and Mitri, 2010).

A plane strain formulation (assumes deformations are zero in the longitudinal direction of the dam) was selected as the default type of analysis, which is typical for 2D analyses of dams, which have a constant (prismatic) cross-section (Xu, 2019). Gaussian elimination was chosen as the default solution method and time units were set to months.

#### 6.2.1. Constitutive Models

Constitutive models employed for staged construction were:

- Linear Elastic (LE) for the rock foundation;
- Mohr-Coulomb (MC) for starter wall and residual soils;
- Softening-Hardening, for underflow and overflow tailings.

## 6.2.2. Material Parameters

Identified Geotechnical Zones are as follows:

- Underflow and Overflow Tailings;
- Starter and Toe Wall;
- Foundation – Residual Norite overlying Norite bedrock.

Selected parameter sets used in the numerical modelling are based on the following considerations:

- Although the overflow tailings are expected to be fully saturated below the phreatic surface and state parameter interpretations suggest that they are predominantly contractive. The purpose of the model is not to perform trigger analyses during construction phases; therefore, TSF-A staged construction was conducted using drained overflow set of parameters (CD1, Table 5-1). It should be noted that calibrated undrained overflow parameters would have been used if the model was developed specifically for static liquefaction trigger analyses, which go beyond the scope of this study.
- Underflow tailings are expected to be located above the phreatic level and state parameter interpretations suggest that they are predominantly dilatant. Thus, drained behaviour was assumed and S-H parameters calibrated from the drained test were used (CD1, Table 5-3 and Table 5-2).

## 6.2.3. Hydraulic Parameters

The hydraulic conductivity (permeability) for each material was determined by adjusting a sample function for silt from the Geoslope SEEP/W guide (GEO-SLOPE International Ltd., 2015). An example of the function for overflow tailings is presented in Figure 6-1.

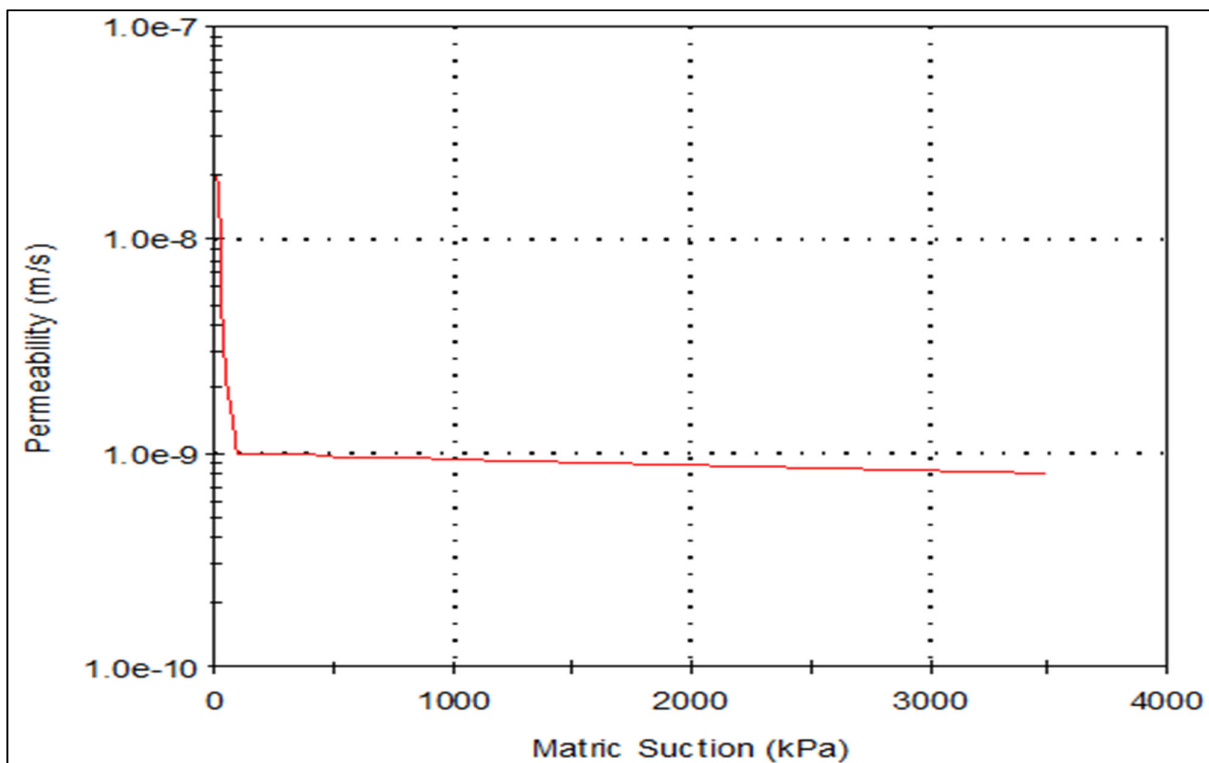


Figure 6-1: Example of Hydraulic Conductivity Function for the Overflow Tailings.

The hydraulic conductivity parameters which were used in the numerical modelling are presented in Table 6-1.

Table 6-1: Hydraulic Parameters Used in Numerical Modelling in RS2.

Material Name	$K_{sat}$ Permeability (m/s)	Anisotropy Ratio ( $K_2 / K_1$ )	$K_1$ Angle (°)
Overflow	2.00E-08	10	90
Underflow	2.00E-07	2	90
Starter Wall	1.00E-07	1	0
Toe Wall	1.00E-07	1	0
Toe Drains	1.00E-05	1	0
Residual Norite	2.00E-07	1	90
Norite Bedrock	2.00E-07	1	0

The analyses and interpretations for  $k_{sat}$  for underflow and overflow tailings were determined through CPTu dissipation data performed across TSF-A. The  $K_2 / K_1$  factor specifies the relative permeability orthogonal to the  $K_1$  direction (Rocscience Inc D, n.d.). It should be noted that the  $K_1$  permeability is the "primary" permeability defined by the saturated permeability ( $K_s$ ) and the unsaturated permeability model (Rocscience Inc D, n.d.). The  $K_1$  angle specifies the direction of the  $K_1$  permeability and is specified relative to the positive X (horizontal) direction (Rocscience Inc D, n.d.).

Permeability in the overflow tailings zone is assumed anisotropic, with anisotropy ratio  $K_2 / K_1$  of 10, whereas the permeability of the underflow tailings zone is assumed to be less anisotropic with anisotropy ratio of  $K_2 / K_1$  of 2 (Abadjiev, 1976; Vick, 1983; Witt, 2004). According to Vick (1990), the anisotropy ratio generally ranges from 2 to 10 for coarse (underflow) and fine (overflow) tailings. It should be noted that the permeability of overflow tailings is assumed one order of magnitude lower than the permeability of underflow tailings.

#### 6.2.4. Geometry and Mesh

The configuration adopted for TSF-A numerical modelling is presented in Figure 6-2. The finite element mesh is illustrated in Figure 6-3 and 6-4. The geometry and mesh setup can be summarised as follows:

- Underflow and Overflow Tailings;
- Foundation at starter wall toe: 1082 mamsl;
- Starter wall: 9.5m maximum height, external slope 1.5H:1.0V, internal slope 1.33H:1.0V;
- Toe Wall: 2.0 m maximum height, external slope 2.0H:1.0V, internal slope 2.0H:1.0V;
- Toe drains located on the inner and outer toe of the starter wall;
- The model has a total width of 490 m and a maximum height of 54.20 m at the crest;
- The finite element mesh comprises of 49075 triangular 6-node elements.



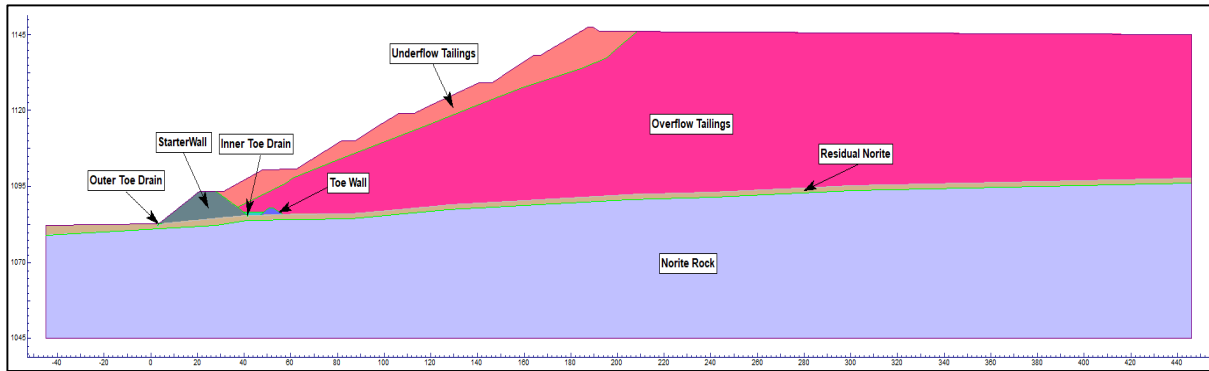


Figure 6-2: Monitoring Line F Showing Modelled Zones.

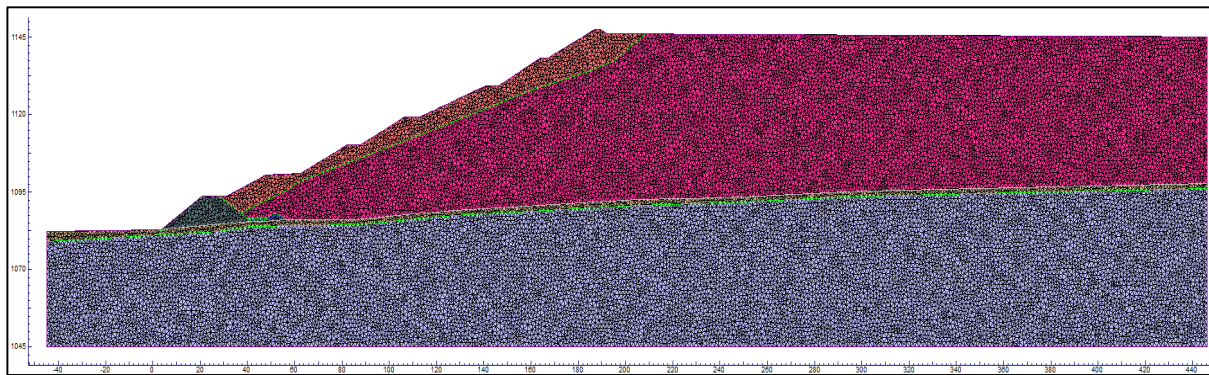


Figure 6-3: Monitoring Line F Showing the Modelled 2-D Full Finite Element Mesh.

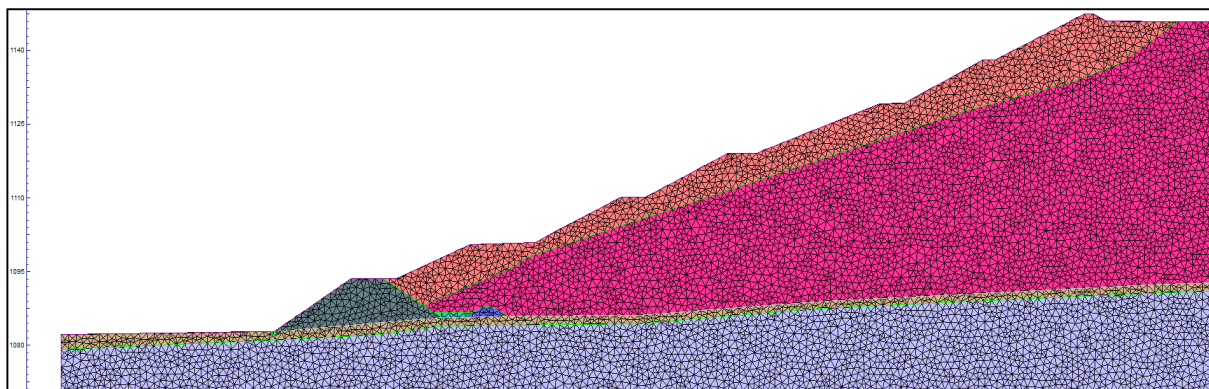


Figure 6-4: Monitoring Line F Showing the Modelled 2-D Zoomed-In Finite Element Mesh.

### 6.2.5. Model Stages

A total of ten stages (presented in Figure 6-5) were modelled and can be described as follows:

- Stage 1 – computation of initial stress state at the foundation;
- Stage 2 – construction of the starter and toe wall, as well as activation of inner and outer toe drains;
- Stage 3 to Stage 10 – TSF-A Construction:
  - Modelling eight construction stages of TSF-A from 1098 to 1145 mamsl. All stages were raised in 6.0 m increments;
  - The staged construction was run using several rates of rise i.e. 3.0 m/yr, 3.5 m/yr, 4.0 m/yr, 4.5 m/yr, 5.0 m/yr, 5.5 m/yr and 6 m/yr to study the effect that increased rates of rise have on pore pressures and location of phreatic surface within TSF-A;
  - The staged construction at different rates of rise was conducted using hydraulic gradients representative of hydrostatic and sub-hydrostatic pore pressure conditions. For hydrostatic conditions, a hydraulic gradient of 9.81 kPa/m was used. For sub-hydrostatic conditions, an average hydraulic gradient estimated from CPTu along Monitoring Line F of 6.24 kPa/m was used;
  - Transient groundwater flow was computed at each phase and total pore pressures were computed based on construction times and material consolidation, stiffness and permeability properties.

### 6.2.6. Boundary Conditions

For the toe drains, zero-pressure nodes were applied where outflow occurs. The permeability of the filter layers leading into the drains was adjusted to reduce the efficiency of the zero-pressure nodes to represent more realistic drains.

The transient response of the system was assessed by performing a consolidation analysis with a new set of hydraulic and mechanical boundary conditions set for each stage of construction (Saad and Mitri, 2010). A total head equal to the applicable construction stage elevation was applied to edges of the model to ensure accurate pore pressure distributions throughout the model.

It should be noted that the top surfaces of the overflow and underflow tailings are fully drained. Therefore, a boundary condition of  $p = 0$  was applied to these boundaries for each construction stage (Saad and Mitri, 2010; Xu, 2019). The remaining side of the model are impermeable and have zero flux. For the mechanical boundary conditions, the model has a fixed base and the right vertical edge is fixed in the horizontal direction (i.e. zero horizontal displacement). Figure 6-6 and Figure 6-7 illustrate the hydraulic and mechanical boundary conditions for the last construction stage, respectively.

The self-weight of elements that comprise the finite element mesh is applied as a gravity force to each stage. This allows pore pressures induced by the weight of the fluid in deposited tailings to be considered. The load related with each stage is applied progressively over the period assigned to each stage. This mitigates against the generation of undrained conditions that could occur due to instantaneous loading from a construction stage. It should be noted that in reality, semiradial flow of tailings deposited via hydrocyclones may lead to uneven rates of rise over time (Saad and Mitri, 2010).

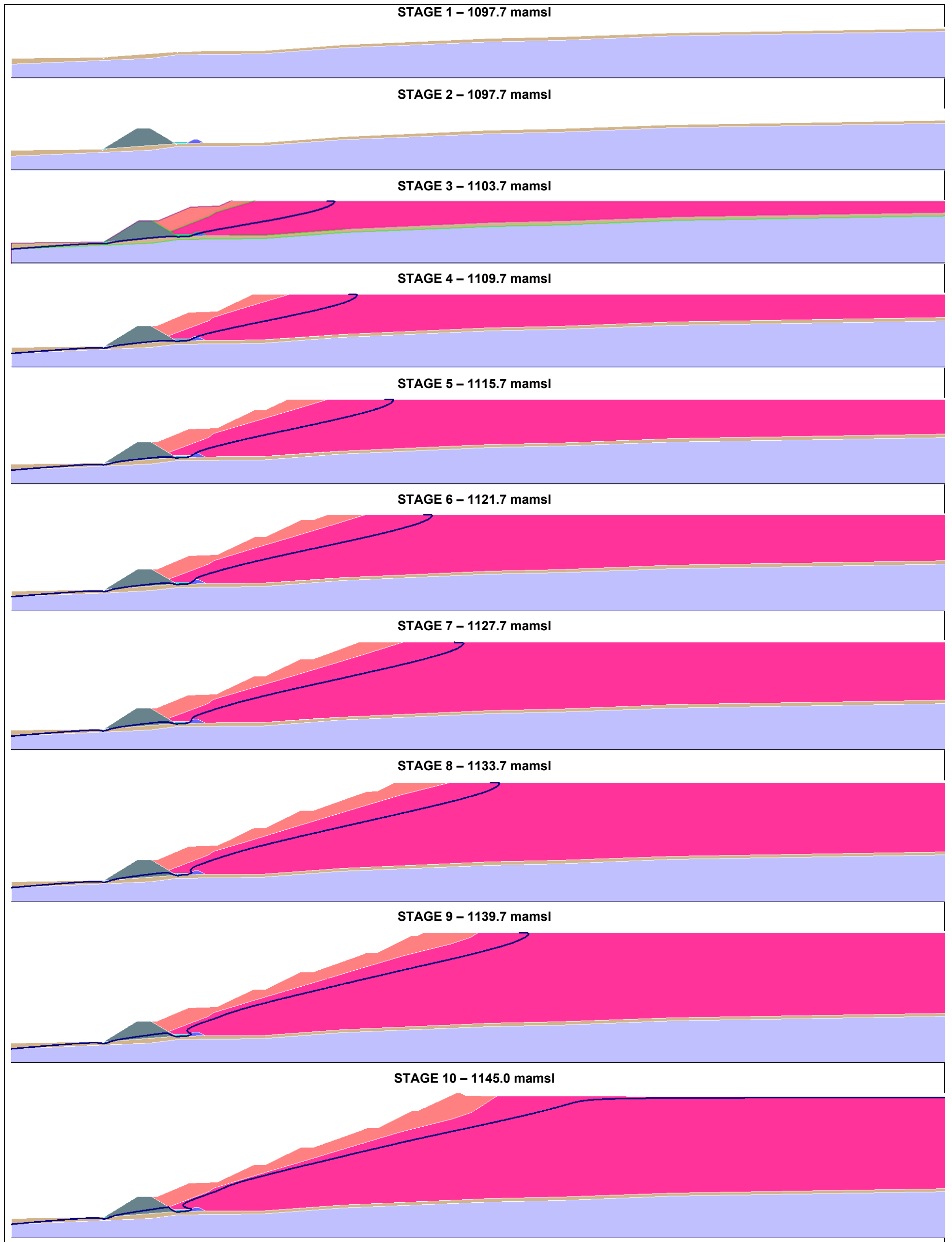


Figure 6-5: Summary of TSF-A Construction Stages as Modelled in RS2.

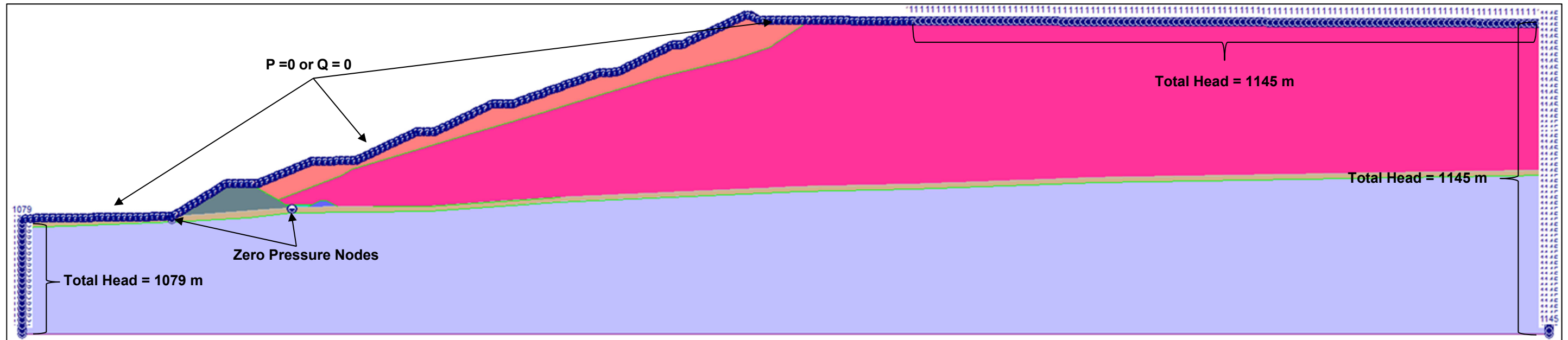


Figure 6-6: Hydraulic Boundary Conditions for Final Stage of Construction.

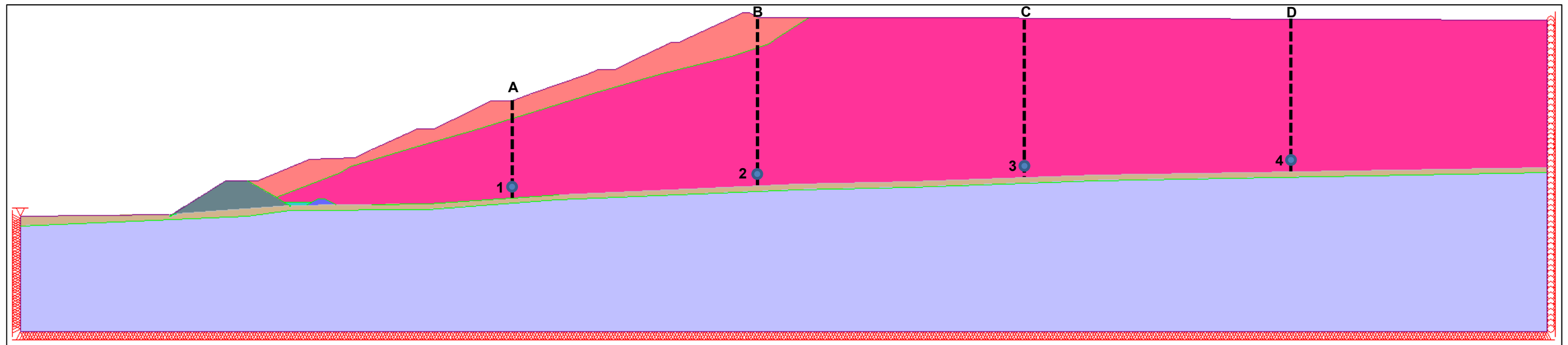


Figure 6-7: Mechanical Boundary Conditions for Final Stage of Construction as well as Points 1 to 4 and Section A to D Used to Extract and Compare Data.

### 6.3. Results and Discussion of Staged Construction

The results show that the phreatic surface is delineated by the internal boundary of the underflow tailings that has a higher permeability than the overflow tailings, which is almost fully saturated. The evolution of total head and the location of phreatic surface for a RoR of 3.0 m/yr and 6.0 m/yr, using hydraulic gradients representative of sub-hydrostatic and hydrostatic pressure conditions, are presented in Figure 6-8 and Figure 6-9, respectively. From the figures, the RoR has a more noticeable impact on the location of the phreatic surface than the pore pressure regime (be it hydrostatic or sub-hydrostatic hydraulic gradients). With an increasing RoR, there is a corresponding rise of the phreatic surface.

Figure 6-10 to Figure 6-13 show the contours of the pore water pressure developed in the tailings dam at the end of construction, for rates of rise of 3.0 m/yr and 6.0 m/yr, using hydraulic gradients representative of sub-hydrostatic and hydrostatic pore pressure conditions. From the figures, the largest pore pressures are generated in the overflow tailings, as this zone has the lowest permeability. Also, the figures show that underflow tailings are unsaturated following its construction due to its higher permeability. According to Holmqvist (2014), negative pore pressures above the phreatic surface shown in the figures will have minimal impact on the seepage analysis. This is because low water content is expected in this material zone and would thereby result in low seepage.

It should be noted that phreatic surface and pore pressure trends described above are comparable to the findings of Saad and Mitri (2010), Ormann et al (2013) and Zardari, et al. (2014) for upstream tailings dams. Notably, the largest pore pressures are developed in the lower third of the overflow (slime) zone, which are similar to the findings of Priscu (1999), Saad and Mitri (2010), Ormann et al (2013), Zardari, et al. (2014), Naeini and Akhtarpour (2018) and Xu (2019).

Also, Figure 6-10 to Figure 6-13 show maximum pore water pressure zones at the overflow-foundation interface that extend over the bottom 20-25 % of the tailings dam foundation. This was first observed by Gassner and Fourie (1998) that when tailings dams are constructed on a low permeability foundation, a high pore pressure 'bulb'/zone typically forms near the base. Subsequently, similar observations were made by Saad and Mitri (2010), Ormann et al (2013) and Naeini and Akhtarpour (2018) for upstream and centreline tailings dams with low permeability foundations.

To carefully study drainage conditions in TSF-A, the time history of pore pressure ( $pp$ ) is plotted against the time history of the effective confining pressure ( $p'$ ) at Points 1, 2, 3, and 4 (Figure 6-7) for rates of rise of 3.0 m/yr and 6.0 m/yr at hydraulic gradients representative of sub-hydrostatic and hydrostatic pressure conditions and are presented in Figure 6-14 and Figure 6-15, respectively.

The following pertinent observations can be made from Figure 6-14 for rates of rise of 3.0 m/yr and 6.0 m/yr using hydraulic gradients representative of sub-hydrostatic pore pressure conditions:

- Points 2 to 4 show a continuous increase in  $p'$  at approximately the same rate during the staged construction. At point 1 between Stage 3 and Stage 5,  $p'$  increased at roughly the same rate as Points 2 to 4. However, much higher  $p'$  values were observed due to greater heights of tailings placed over these stages. Subsequently, with deposition progressing upstream and with loading moving further away from

Point 1, the increase in  $p'$  gradually decreased and became relatively constant after Stage 7 with points 2 to 4 reaching higher  $p'$  between Stages 7 and 10;

- $p'$  decreases into the TSF-A basin (i.e. moving from Point 1 to 4), which is due to the decreasing height of overlying tailings as TSF-A is constructed in the upstream direction. In contrast, a continuous increase in  $pp$  and rates of increase can be observed moving into the TSF-A basin during the staged construction. This is likely due to the distance from the internal drainage, i.e. Point 1 located nearest to the toe drains, shows the lowest  $pp$  and rates of increase, while Point 4 located furthest away from the toe drains shows the highest  $pp$  and rates of increase;
- Overall Points 1 to 4 indicate that the lower portion of the overflow tailings demonstrate a drained-like behaviour during staged construction. This is reflected by the continuous increases in  $p'$  that are notably higher than their corresponding  $pp$ . It can also be observed that drainage conditions become poorer into the TSF-A basin as the difference between  $p'$  and  $pp$  progressively decreases from Points 1 to 4.

The following pertinent observations can be made from Figure 6-15 for rates of rise of 3.0 m/yr and 6.0 m/yr using hydraulic gradients representative of hydrostatic pore pressure conditions:

- Points 2 to 4 show a continuous increase in  $p'$  at approximately the same rate during the staged construction. At Point 1 between Stage 3 and Stage 5,  $p'$  increased at roughly the same rate as Points 2 to 4. However, much higher  $p'$  values were observed due to greater heights of tailings placed over these stages. Subsequently, with deposition progressing upstream and with loading moving further away from Point 1, the increase in  $p'$  gradually decreased and became relatively constant after Stage 7 with Points 2 and 3 reaching higher  $p'$  between Stages 7 and 10;
- $p'$  decreases into the TSF-A basin (i.e. moving from point 1 to 4), which is due to the decreasing height of overlying tailings as TSF-A is constructed in the upstream direction. In contrast, a continuous increase in  $pp$  and rates of increase can be observed moving into the TSF-A basin during the staged construction, which is likely due to distance from the internal drainage, i.e. Point 1 located close to the toe drains shows the lowest  $pp$  and rates of increase, while Point 4 located furthest away from the toe drains shows the highest  $pp$  and rates of increase;
- Points 1 and 2 indicate that lower portions of the overflow tailings, closer to the underflow tailings zone, demonstrate drained-like behaviour during staged construction, which is reflected by the continuous increases in  $p'$  that are notably higher than their corresponding  $pp$ ;
- $p'$  and  $pp$  at Point 3 show relatively small differences in pressure when compared to Point 3 in Figure 6-14 between Stages 3 and 6. Nevertheless, drained-like conditions still prevail with the curves beginning to diverge (after Stage 6) with an increase in  $p'$  and a decrease in  $pp$ ;
- At Point 4,  $p'$  initially starts off higher than the  $pp$  but approximately halfway through Stage 3, up to the end of the staged construction, the  $pp$  generated and the rate of increase is greater than  $p'$ . On this basis, it is inferred from the results that the lower portion of the overflow tailings in this zone experiences undrained-like conditions.

To gain a better understanding of pore pressures generated within the underflow and overflow tailings over the full height of TSF-A, pore pressures along Section Lines A to D (Figure 6-7) were analysed and plotted against the hydrostatic pore pressure at the end of construction and presented in Figure 6-16 to Figure 6-19.



It is observed from Figure 6-16 to Figure 6-19 that Section Lines A to D are indicative of sub-hydrostatic pressure conditions for both vertical hydraulic gradients of 6.24 kPa/m and 9.81 kPa/m with rates of rise ranging from 3.0 m/yr to 6.0 m/yr.

As mentioned above, the rate of rise has a more noticeable impact on the location of the phreatic surface than vertical flow gradients representing sub-hydrostatic or hydrostatic pore pressure conditions. With an increasing rate of rise, there is a corresponding rise of the phreatic surface. This can be more clearly seen in Figure 6-16 and Figure 6-17 (circled in red) where the changes from negative to positive pressures (indicating the depth of the phreatic surface) occur progressively higher in the section with increasing rate of rise.

#### 6.4. Summary of Staged Construction At TSF-A

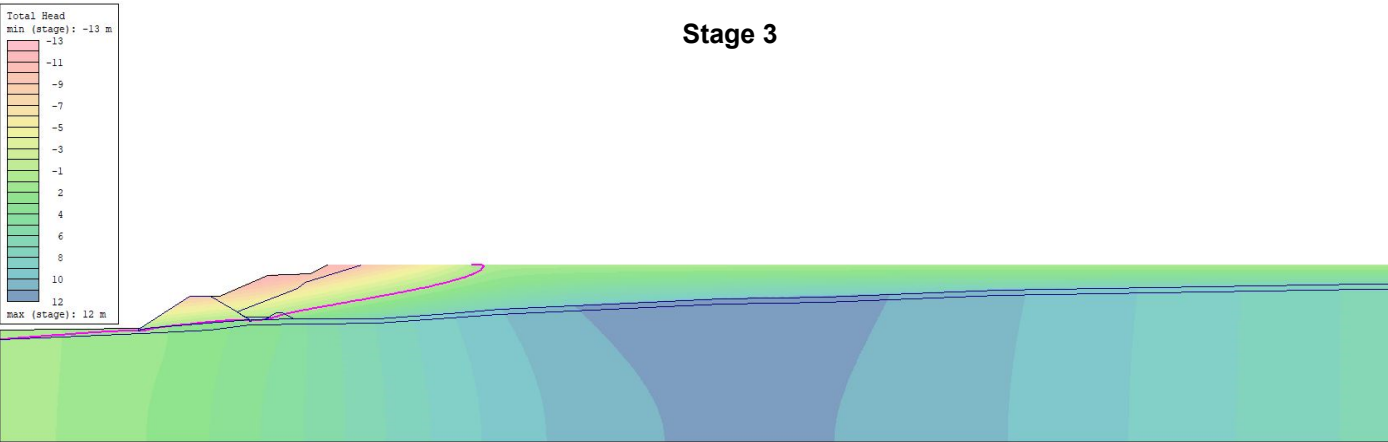
The rate of rise has a more noticeable impact on the location of the phreatic surface than the pore pressure regime. With an increasing rate of rise, there is a corresponding rise of the phreatic surface.

The figures show that the largest pore pressures are developed in the overflow zone as this zone has the lowest permeability. Underflow tailings is unsaturated following its construction due to its higher permeability. Phreatic surface and pore pressure trends observed in the analyses are comparable to the literature. Maximum bulbs/zones of pore water pressure form at the overflow-foundation interface.

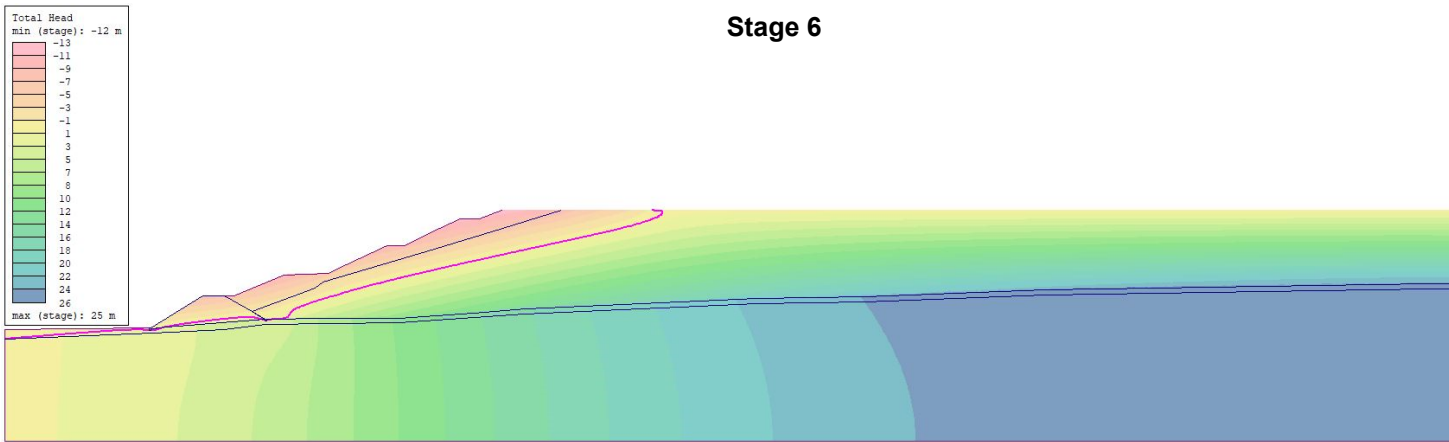
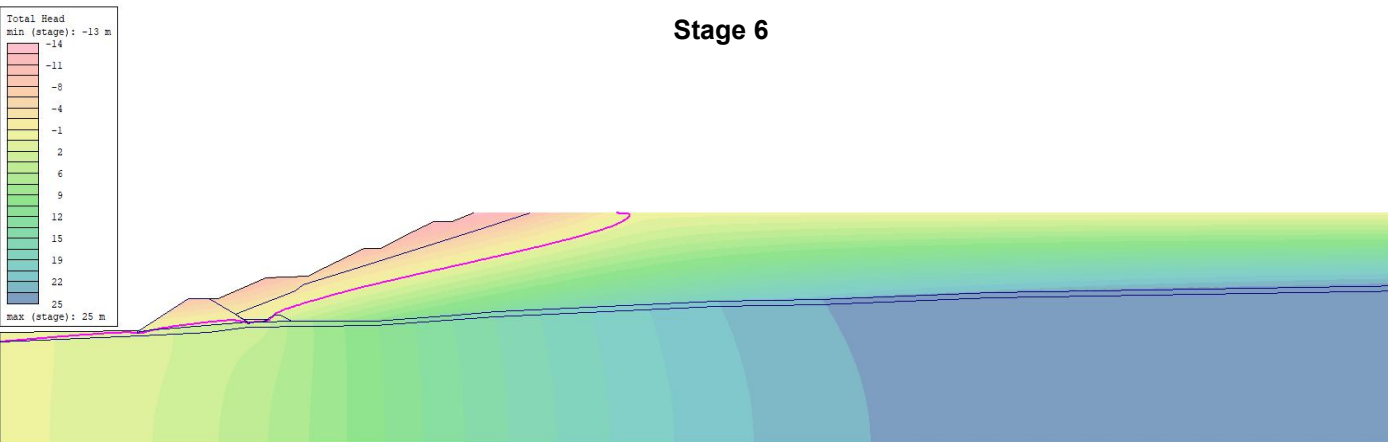
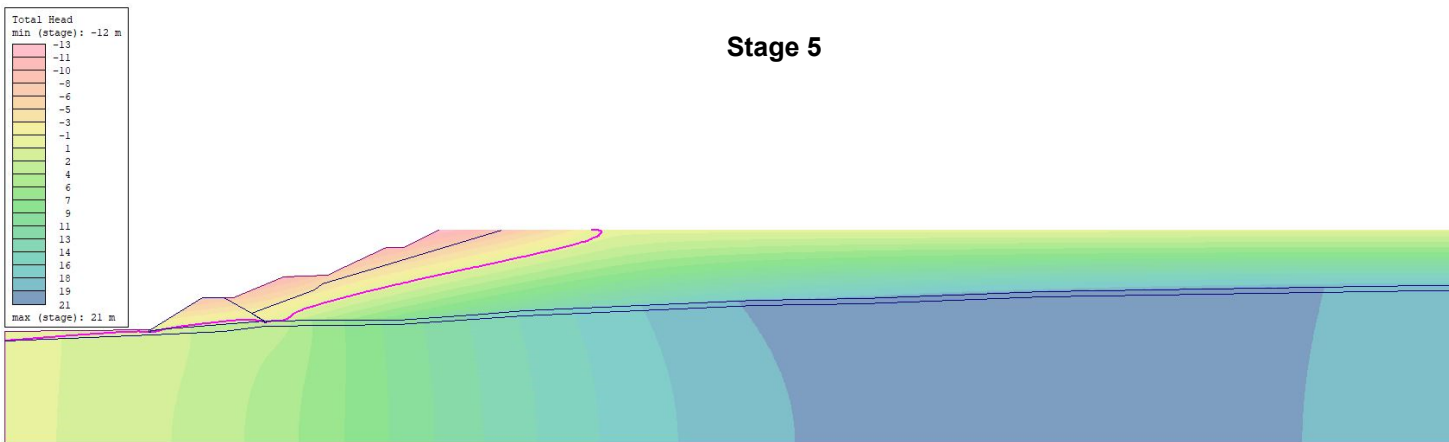
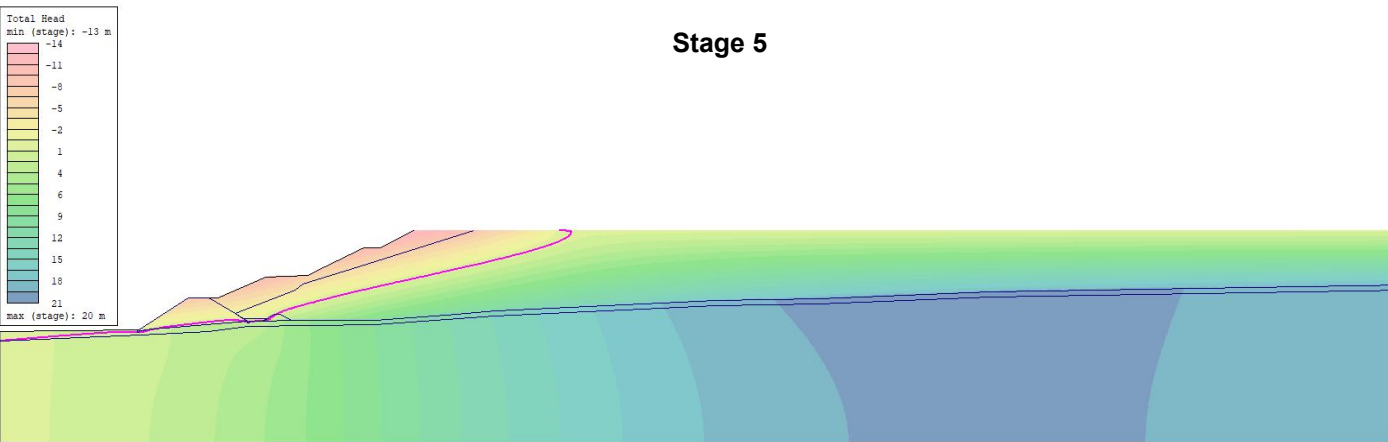
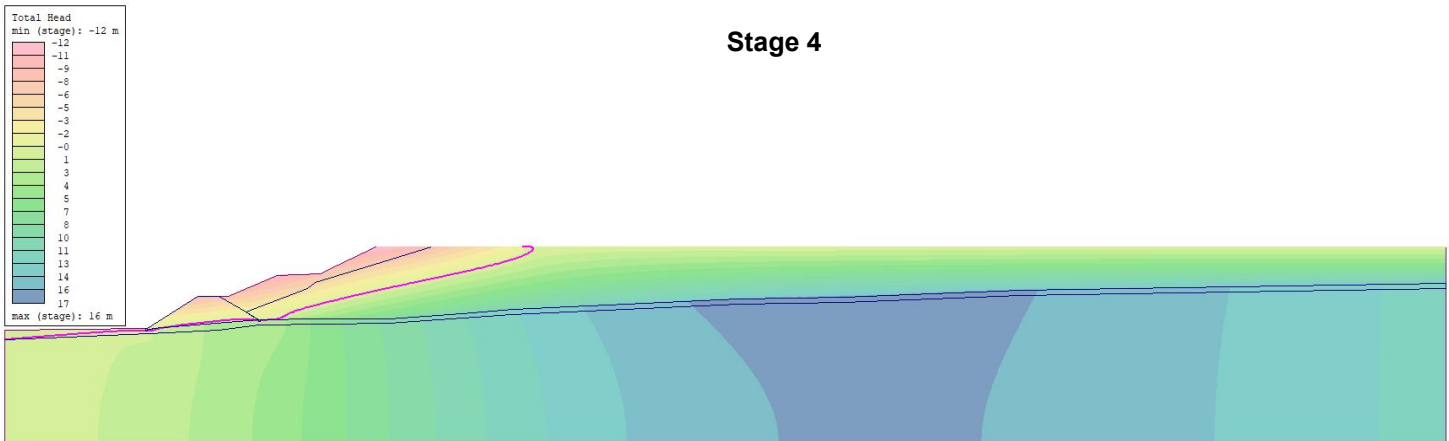
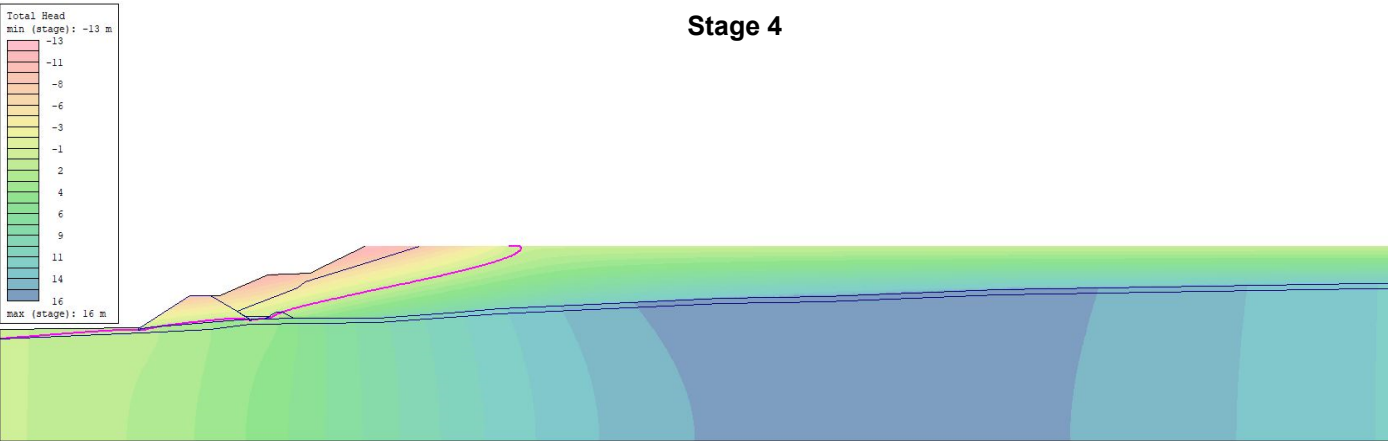
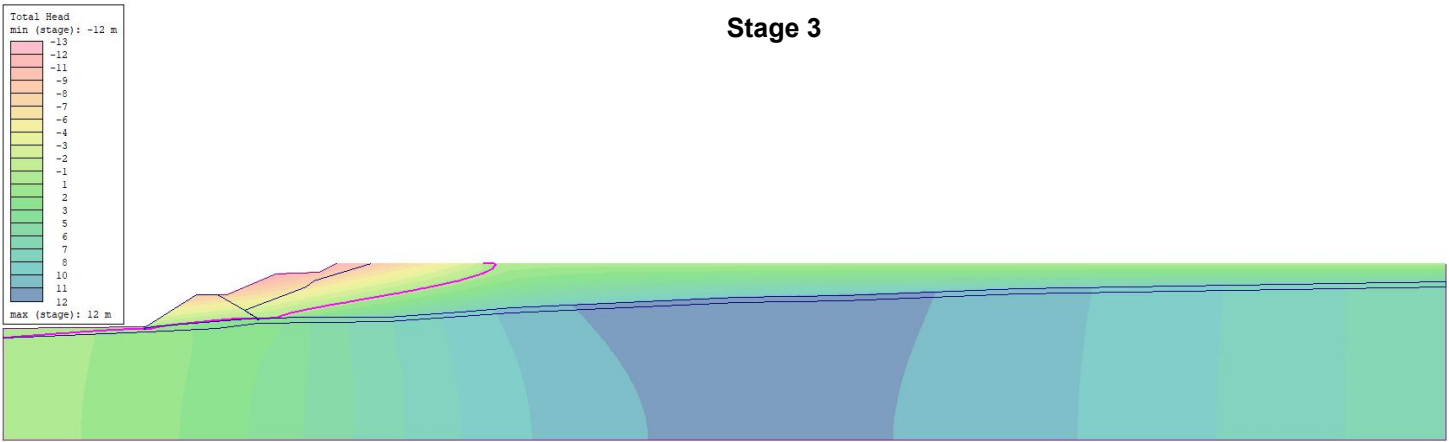
For rates of rise of 3.0 m/yr and 6.0 m/yr using hydraulic gradients representative of sub-hydrostatic pore pressure conditions, the lower portion of the overflow tailings demonstrate a drained-like behaviour during staged construction. This is reflected by the continuous increases in  $p'$  that are notably higher than their corresponding  $pp$ . It can also be observed that drainage conditions become poorer into the TSF-A basin as the differences between  $p'$  and  $pp$  progressively decrease from Points 1 to 4.

For rates of rise of 3.0 m/yr and 6.0 m/yr using hydraulic gradients representative of hydrostatic pore pressure conditions, the lower portion of the overflow tailings from Points 1 to 3 demonstrate a drained-like behaviour during staged construction. On the other hand, Point 4 demonstrates undrained-like behaviour. This is reflected by the continuous increases in  $pp$  that are notably higher than their corresponding  $p'$ . Section Lines A to D are indicative of sub-hydrostatic pressure conditions for both hydraulic gradients of 6.24 kPa/m and 9.81 kPa/m, with rates of rise ranging from 3.0 m/yr to 6.0 m/yr.

RoR = 3.0 m/yr, Hydraulic Gradient = 6.24 kPa/m



RoR = 6.0 m/yr, Hydraulic Gradient = 6.24 kPa/m



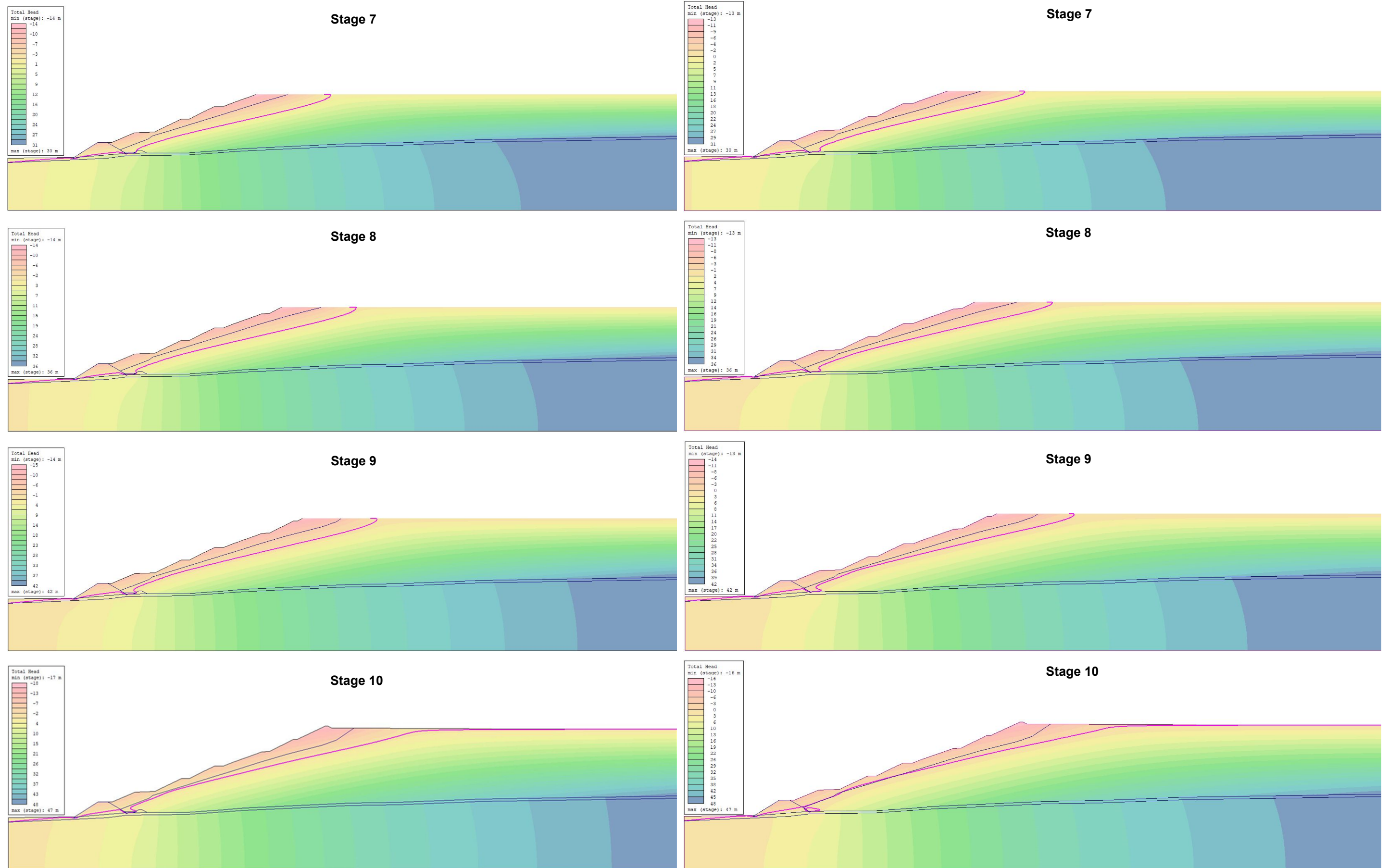
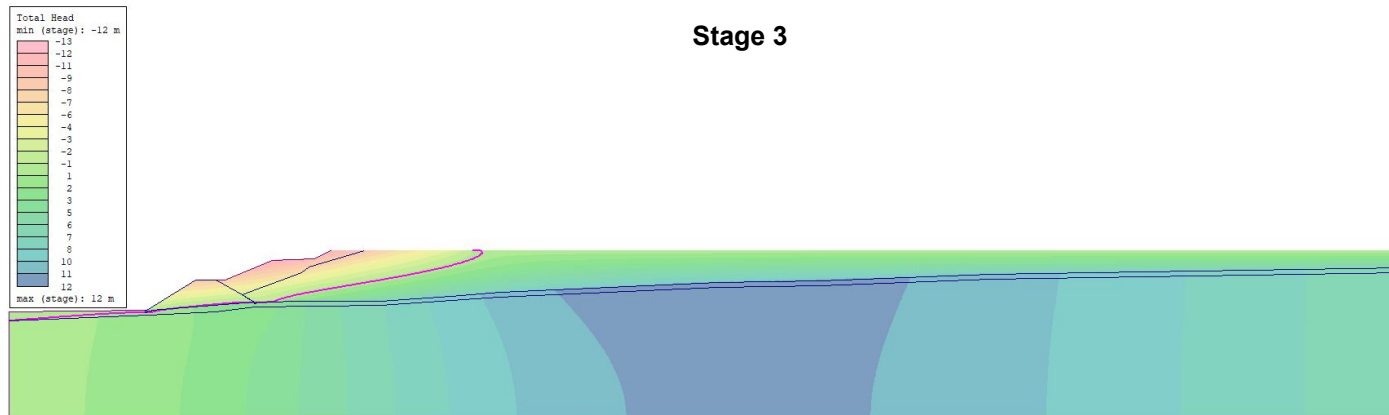


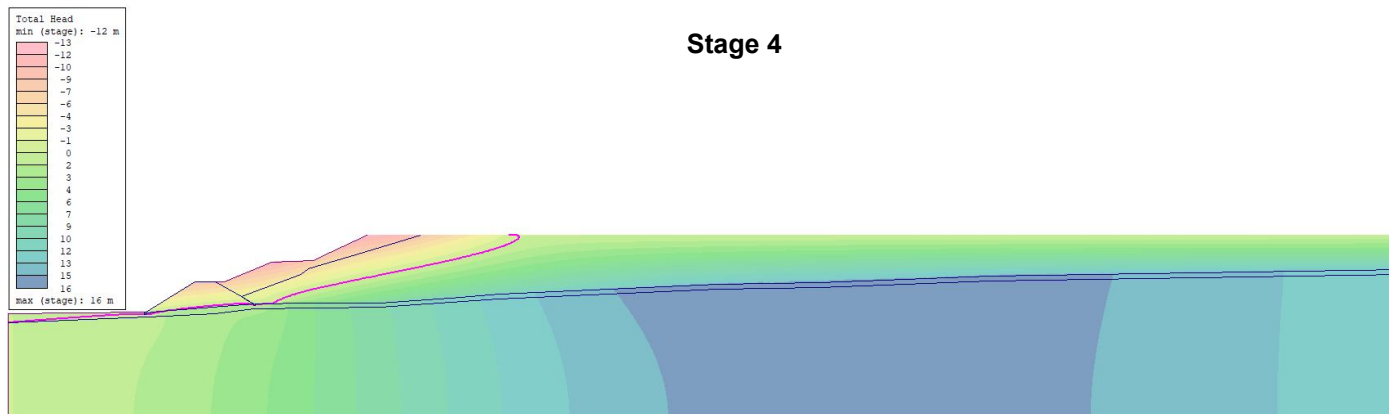
Figure 6-8: The Evolution of Total Head and the Location of the Phreatic Surface for a Rate of Rise of 3.0 m/yr and 6.0 m/yr, Using a Sub-Hydrostatic Hydraulic Gradient.

RoR = 3.0 m/yr, Hydraulic Gradient = 9.81 kPa/m

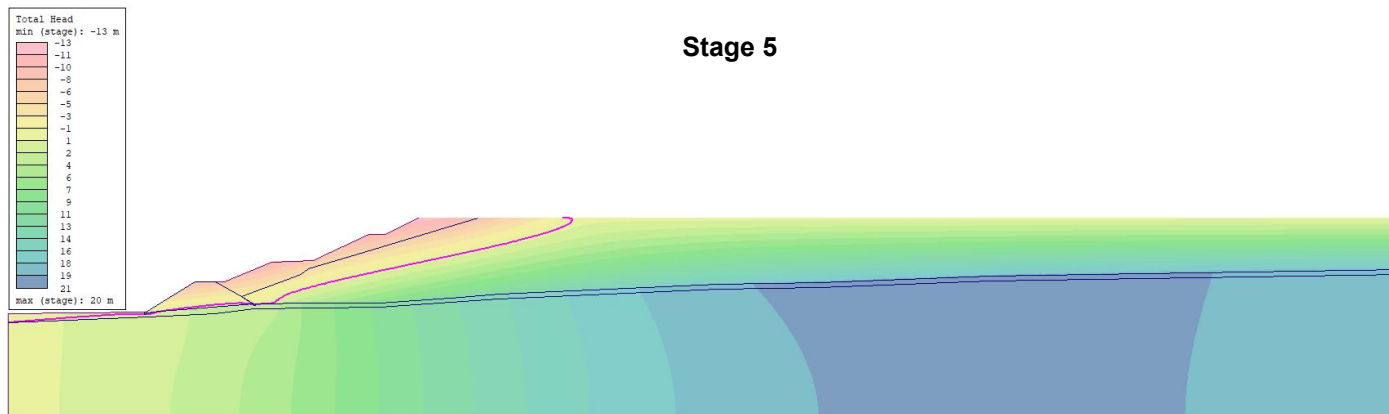
Stage 3



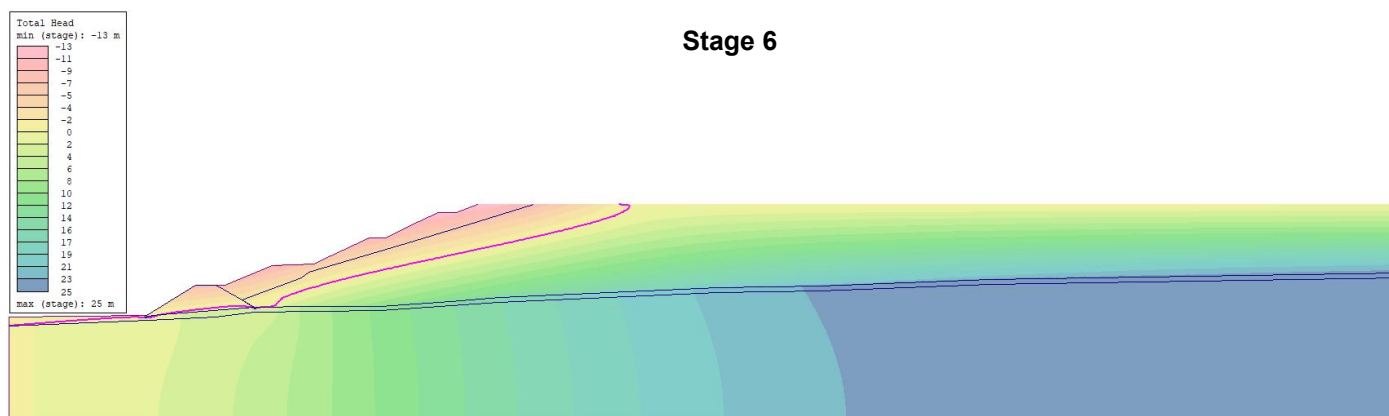
Stage 4



Stage 5

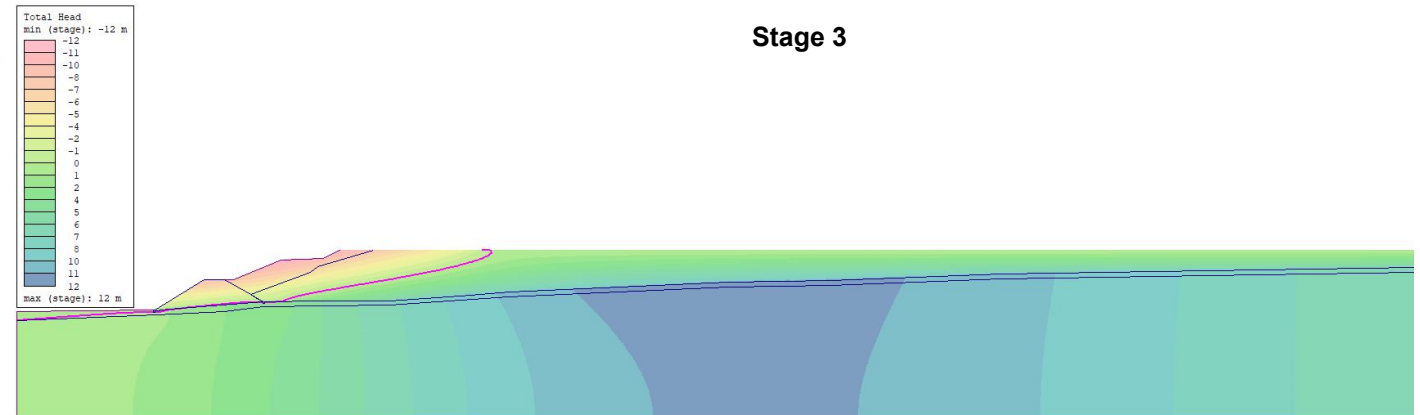


Stage 6

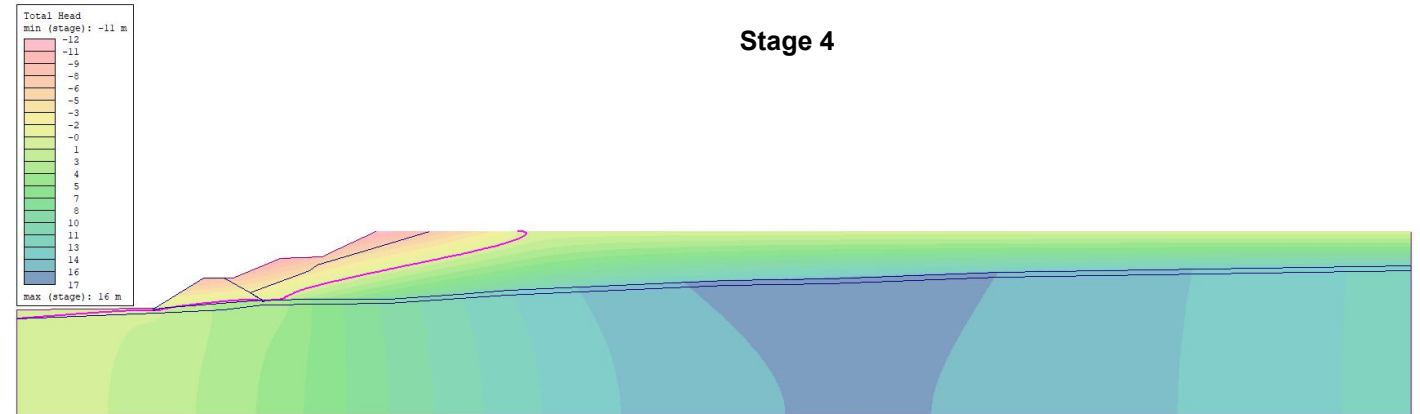


RoR = 6.0 m/yr, Hydraulic Gradient = 9.81 kPa/m

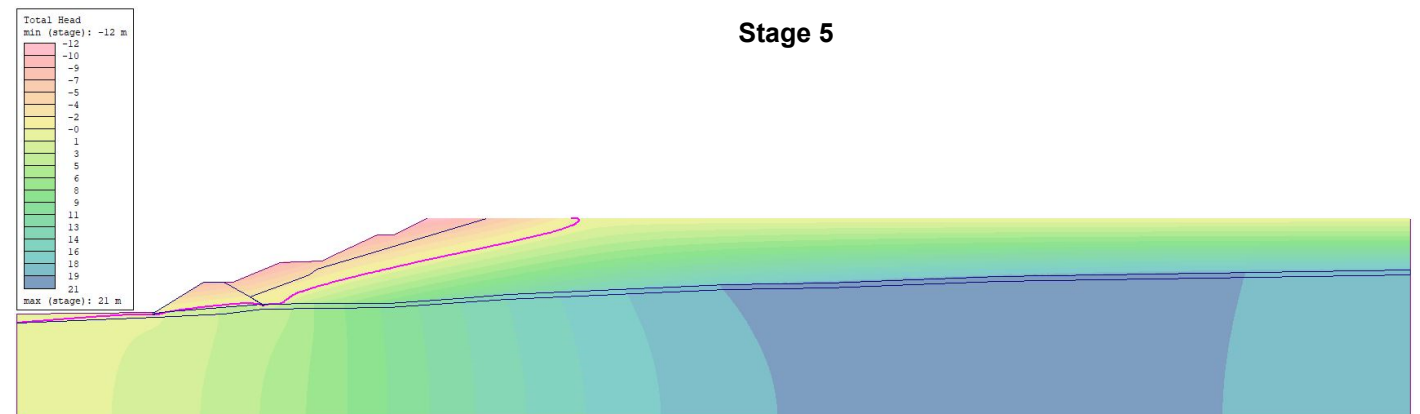
Stage 3



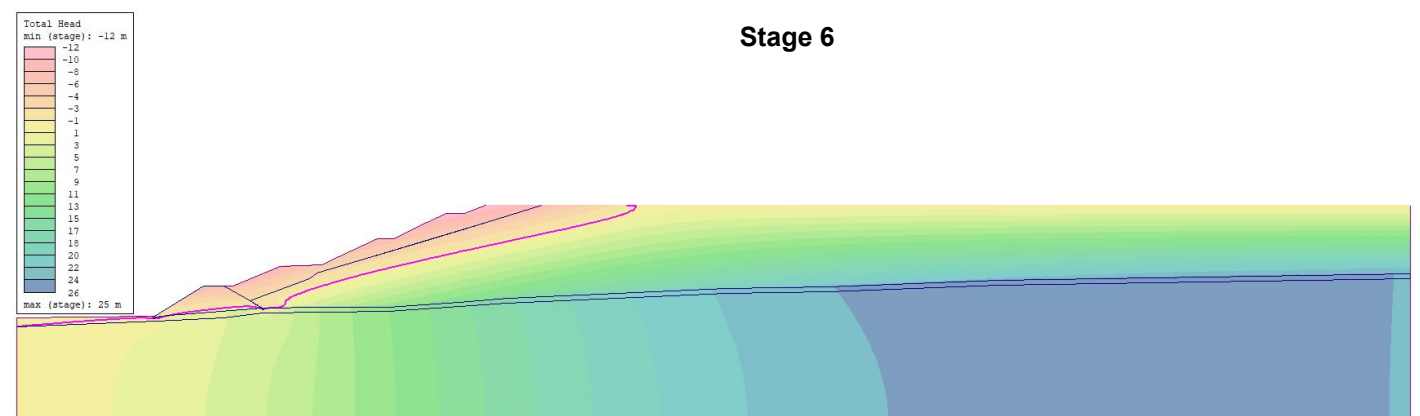
Stage 4



Stage 5



Stage 6





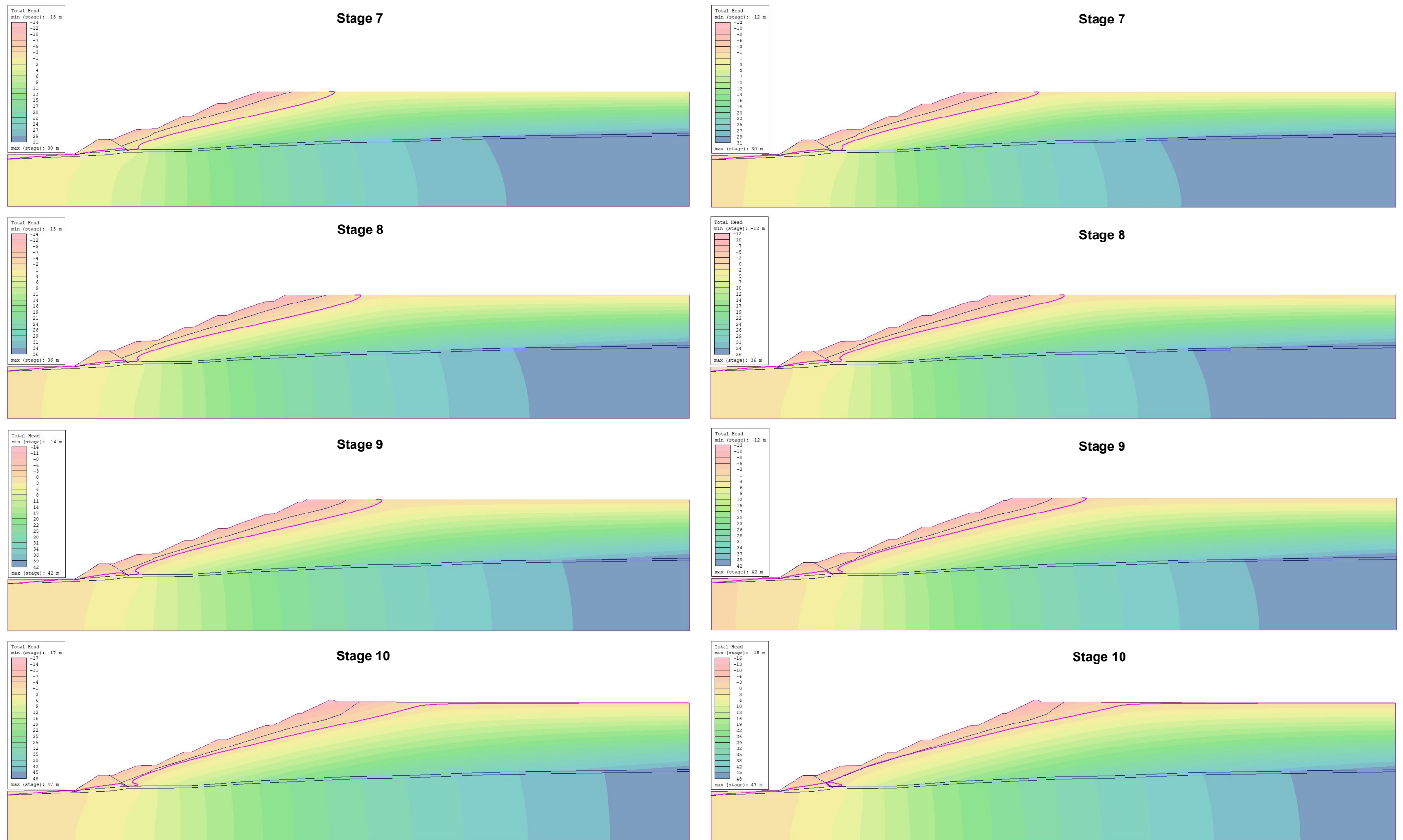


Figure 6-9: The Evolution of Total Head and the Location of the Phreatic Surface for a Rate of Rise of 3.0 m/yr and 6.0 m/yr, Using a Hydrostatic Hydraulic Gradient.

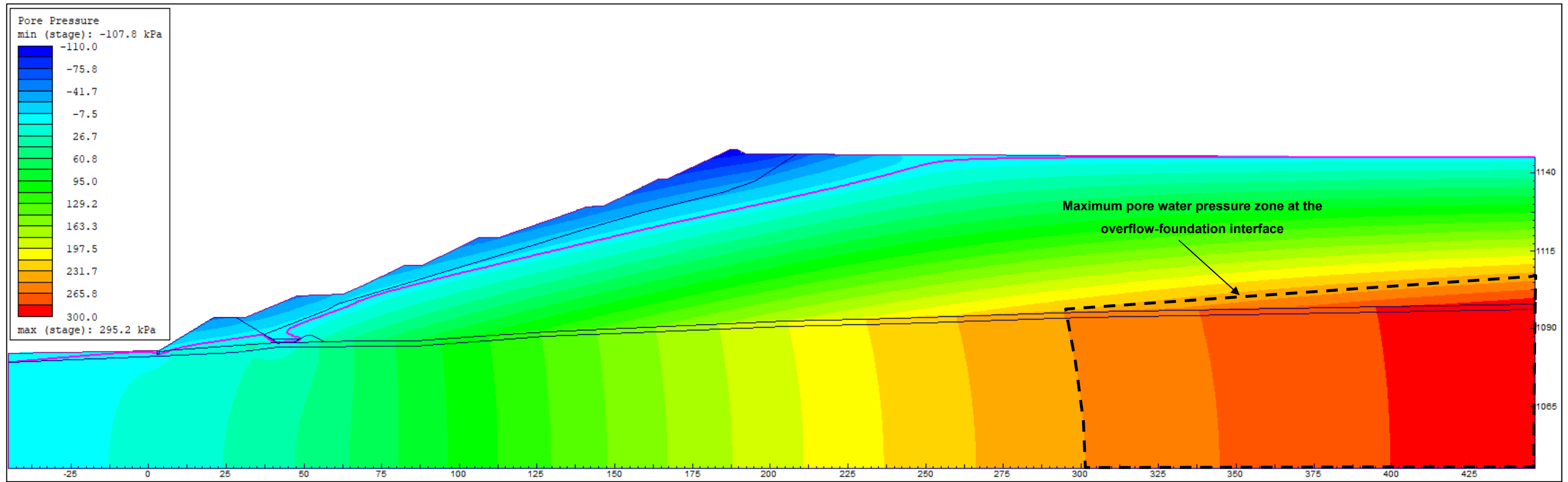


Figure 6-10: Contours of Pore Water Pressure at the End of Construction, for a Rate of Rise of 3.0 m/yr, Using a Sub-Hydrostatic Hydraulic Gradient.

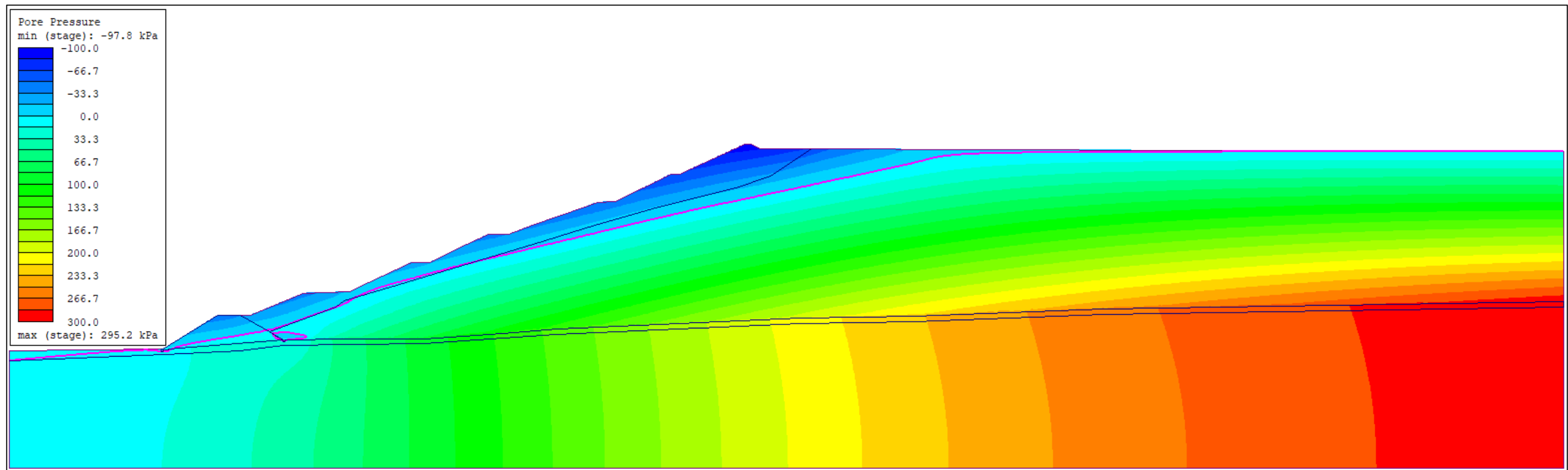


Figure 6-11: Contours of Pore Water Pressure at the End of Construction, for a Rate of Rise of 6.0 m/yr, Using a Sub-Hydrostatic Hydraulic Gradient.



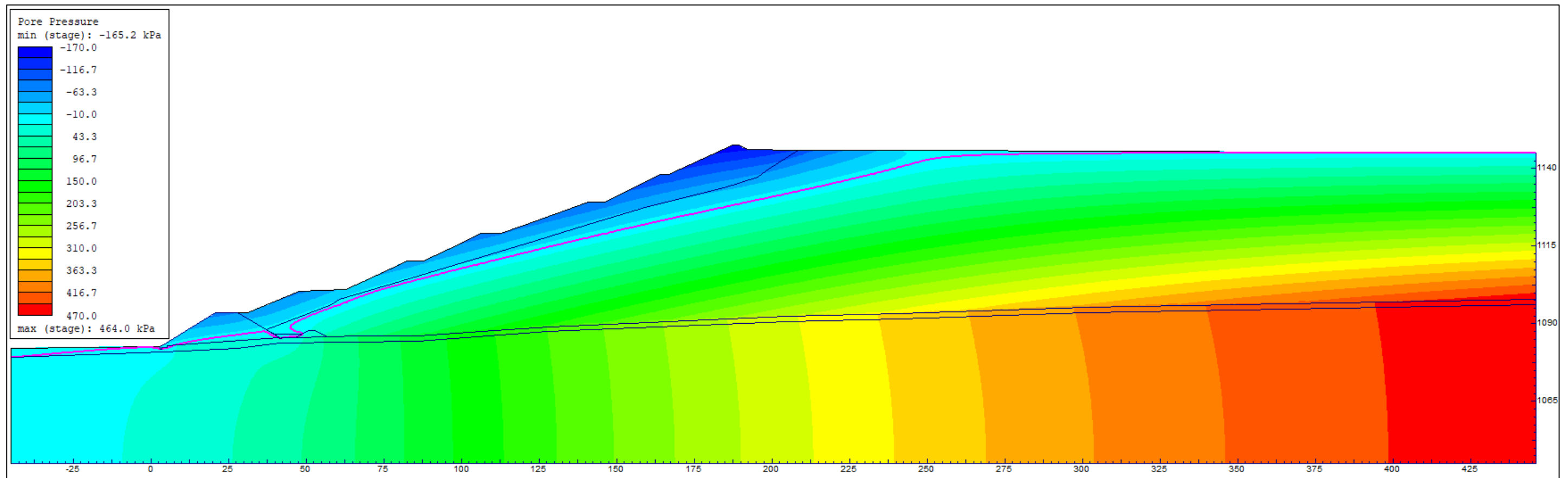


Figure 6-12: Contours of Pore Water Pressure Developed at the End of Construction, for a Rate of Rise of 3.0 m/yr, Using a Hydrostatic Hydraulic Gradient.

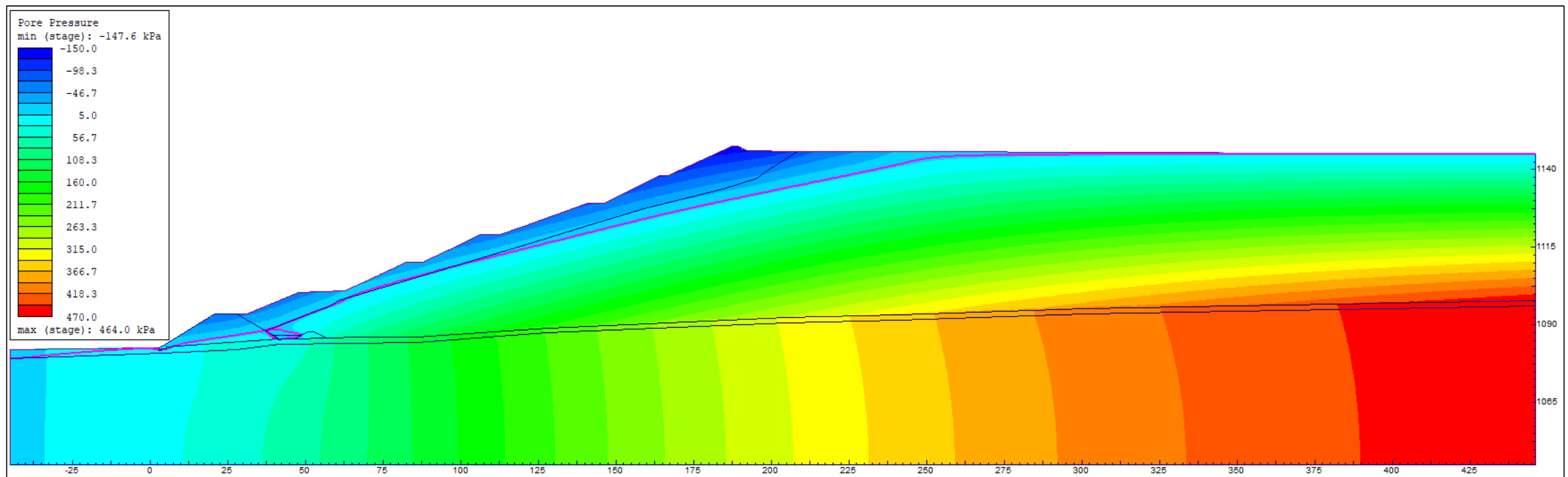


Figure 6-13: Contours of Pore Water Pressure Developed at the End of Construction, for a Rate of Rise of 6.0 m/yr, Using a Hydrostatic Hydraulic Gradient.

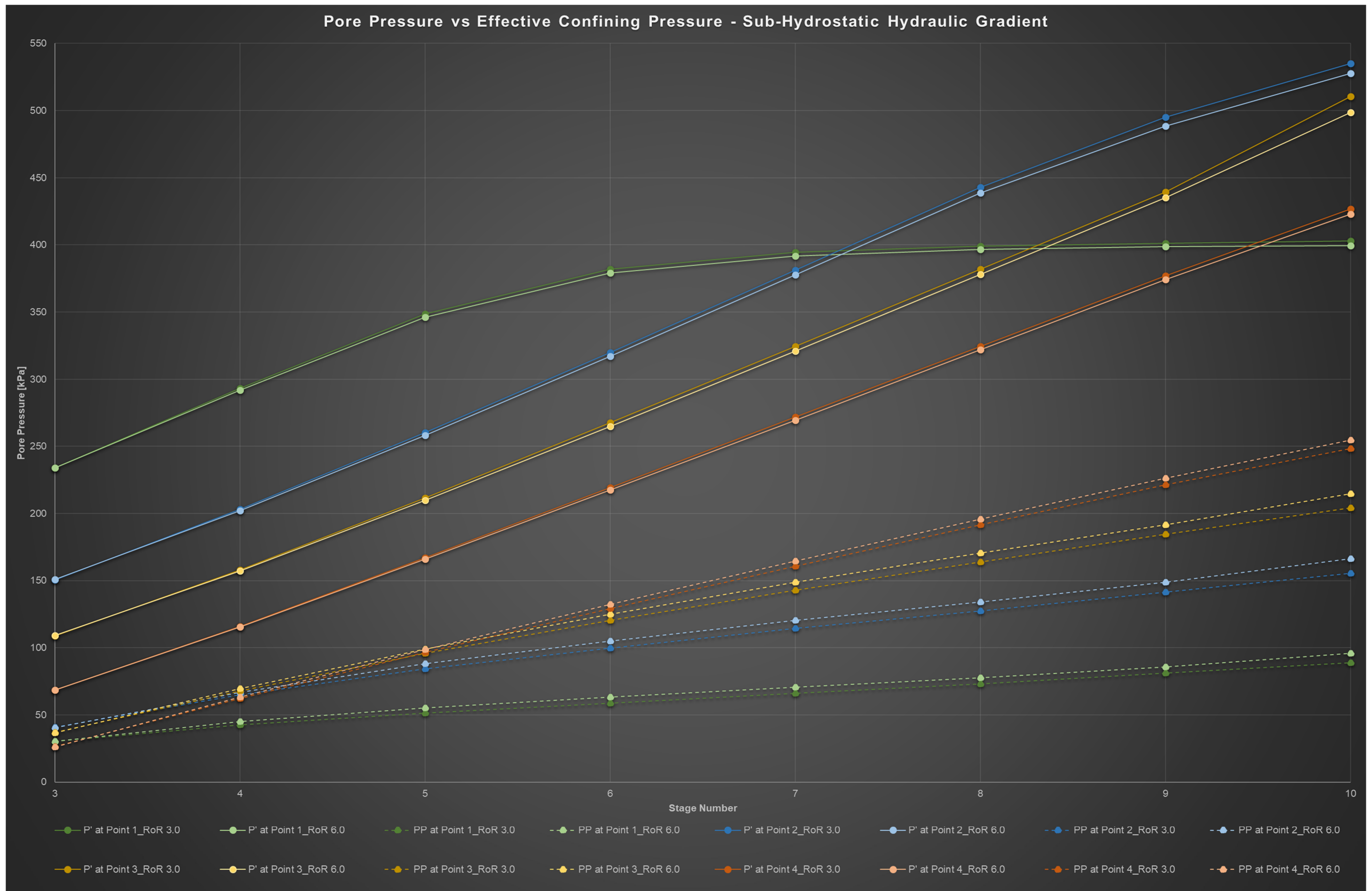


Figure 6-14: Time History of Pore Pressure (PP) and Effective Confining Pressure ( $p'$ ) at Points 1 to 4, Using a Sub-Hydrostatic Hydraulic Gradient.

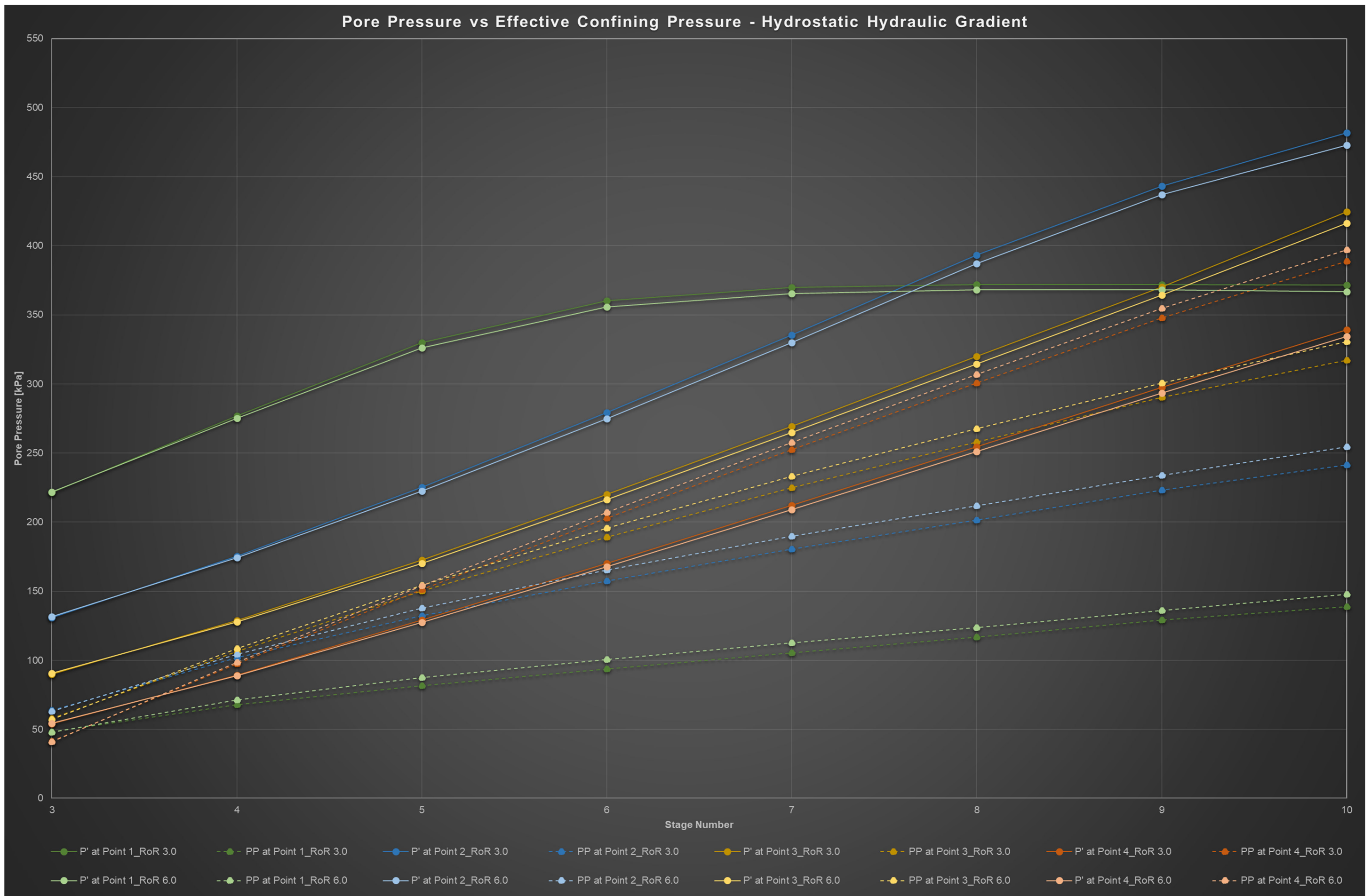


Figure 6-15: Time History of Pore Pressure (PP) and Effective Confining Pressure ( $p'$ ) at Points 1 to 4, Using a Hydrostatic Hydraulic Gradient.

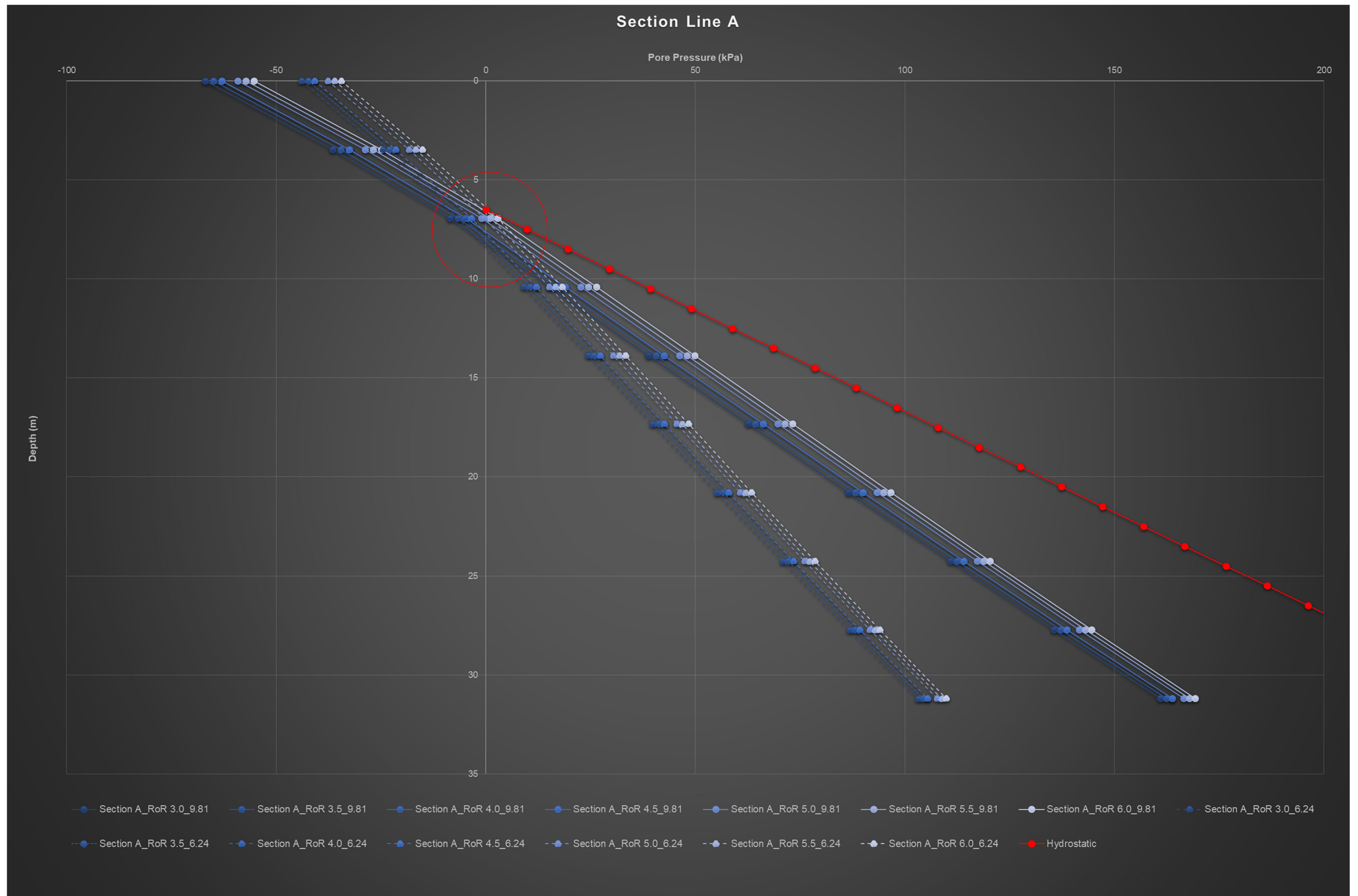


Figure 6-16: Pore Pressures Along Section Line A at the End of Construction, Using Sub-Hydrostatic and Hydrostatic Hydraulic Gradients at Rates of Rise Ranging Between 3.0 m/yr and 6.0 m/yr.



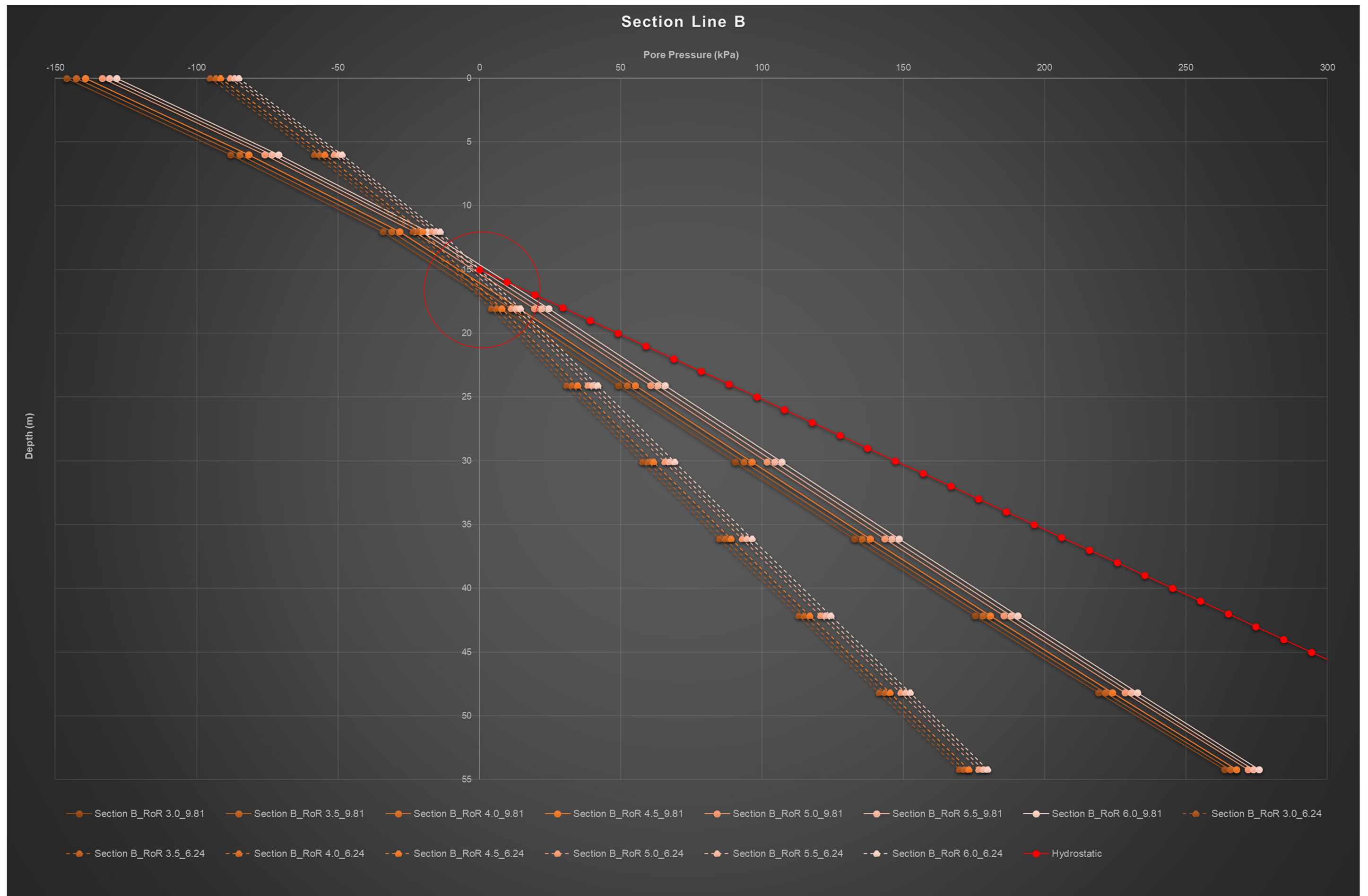


Figure 6-17: Pore Pressures Along Section Line B at the End of Construction, Using Sub-Hydrostatic and Hydrostatic Hydraulic Gradients at Rates of Rise Ranging Between 3.0 m/yr and 6.0 m/yr.

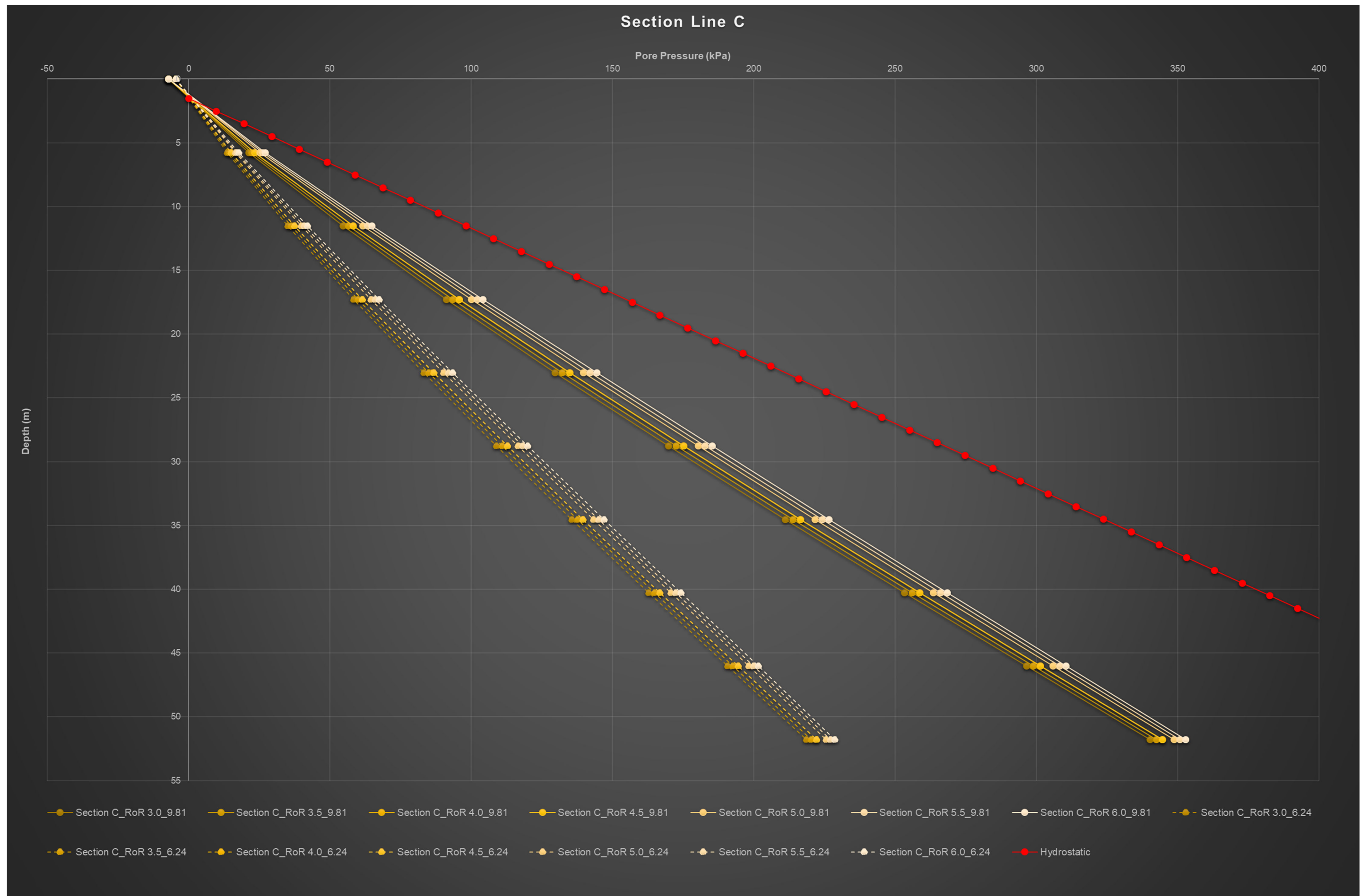


Figure 6-18: Pore Pressures Along Section Line C at the End of Construction, Using Sub Hydrostatic and Hydrostatic Hydraulic Gradients at Rates of Rise Ranging Between 3.0 m/yr and 6.0 m/yr.



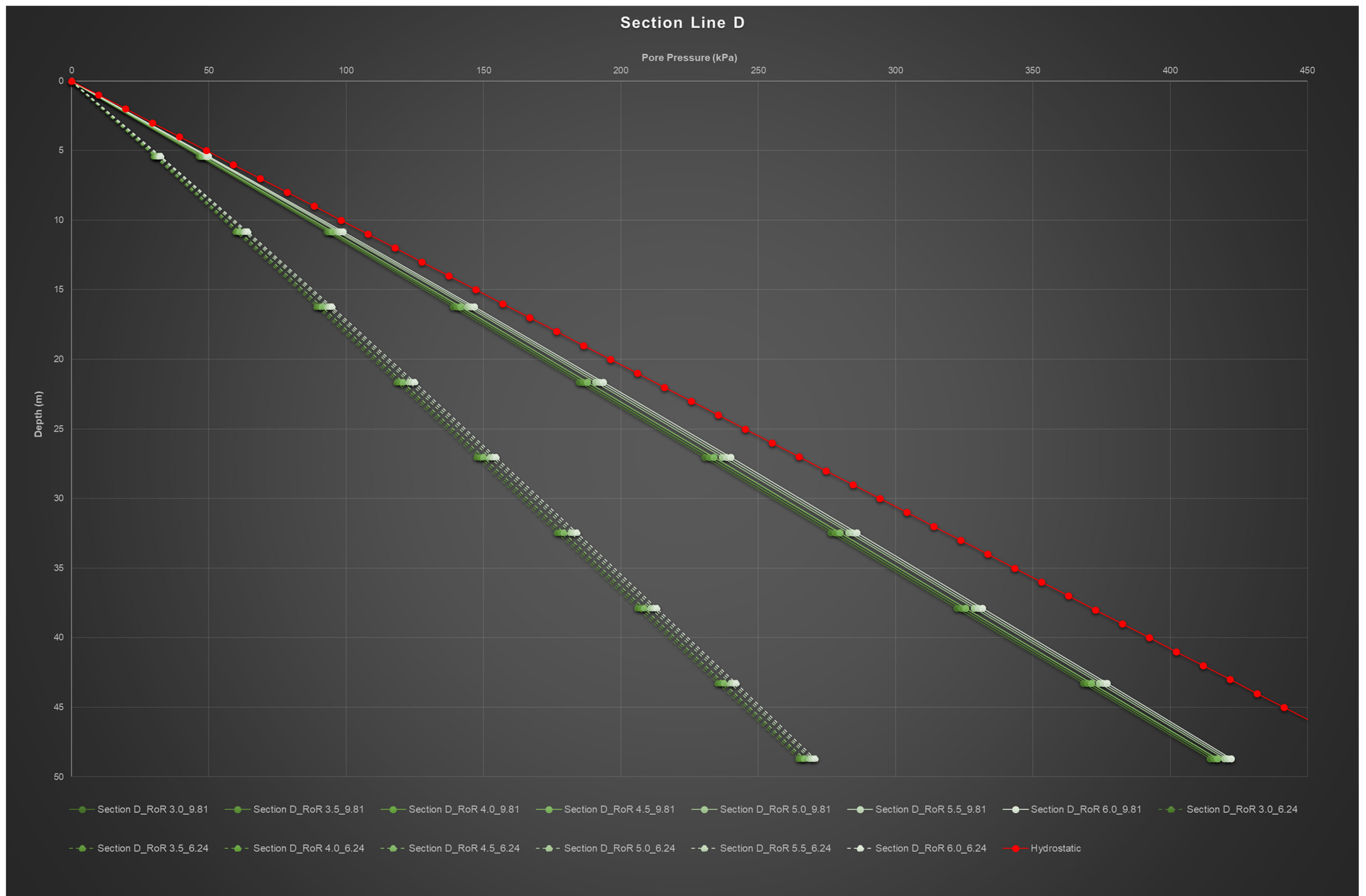


Figure 6-19: Pore Pressures Along Section Line D at the End of Construction, Using Sub-Hydrostatic and Hydrostatic Hydraulic Gradients at Rates of Rise Ranging Between 3.0 m/yr and 6.0 m/yr.

## Chapter 7 : Conclusions

After carefully reviewing all available literature, determining the in-situ state and static liquefaction potential of tailings dams is typically assessed using one of several methodologies within the framework of CSSM that involves the use of in-situ and laboratory testing in conjunction with numerical analyses. The review also highlights the importance of performing staged construction to determine the hydromechanical behaviour of tailings dams. From the literature review, it can be concluded that there is a lack of available literature and studies related to determining the in-situ state and static liquefaction potential as well as staged construction of tailings dams from a South African perspective.

Characterisation of the state parameter of silt-like tailings can be performed in the framework of CSSM. The methodology is briefly explained and results are compared with more empirical approaches Robertson (2010) and Jefferies and Been (2016). It is observed that the state parameter using Shuttle and Jefferies (2016) procedure is systematically higher than the Robertson (2010) and Jefferies and Been (2016) methods. The Shuttle and Jefferies (2016) methodology shows that underflow tailings display predominantly dilative (strain-hardening) behaviour at most of the CPTu soundings. Only a few soundings show minor contractive layers within some portion of the underflow tailings. The overflow tailings show contractive (strain-softening) behaviour with interbedding of dilative layers in some portions of the overflow tailings. Data from CPTu was also used to estimate the soil behaviour type along soundings, based on Robertson (2010) SBTn charts. Good correlations were found between SBTn classifications and interpretation of state parameter using Shuttle and Jefferies (2016) methodology in that similar behavioural responses of the underflow (i.e. dilative) and overflow (i.e. contractive) were noted. In Summary, the Shuttle and Jefferies (2016) methodology is based on a more fundamental understanding of the physics involved in cone penetration and uses a constitutive model built around the concept of state parameter, making it more reliable for silt-like tailings than empirically-based procedures (Sottile, et al., 2019).

Staged construction using fully coupled transient FEM analyses is a useful tool to understanding the pore pressure distribution, drainage conditions and location of phreatic surface within a tailings dam. As part of this research these were assessed at varying rates of rise using hydraulic gradients representative of hydrostatic and sub-hydrostatic pore pressure conditions. The rate of rise has a more noticeable impact on the location of the phreatic surface than the pore pressure regime. With an increasing rate of rise, there is a corresponding rise of the phreatic surface. It is observed that the largest pore pressures develop in the overflow tailings, as this zone has the lowest permeability. Underflow tailings are unsaturated following its construction due to its higher permeability and phreatic surface located at the underflow-overflow contact boundary. Phreatic surface and pore pressure trends observed in the analyses are comparable to the literature. For rates of rise of 3.0 m/yr and 6.0 m/yr, using hydraulic gradients representative of sub-hydrostatic pore pressure conditions, the lower portion of the overflow tailings demonstrate a drained-like behaviour during staged construction. Also, poorer drainage conditions are observed in the TSF-A basin. For rates of rise of 3.0 m/yr and 6.0 m/yr, using hydraulic gradients representative of hydrostatic pore pressure conditions, the lower portion of the overflow tailings predominantly demonstrates a drained-like behaviour during staged construction. Section Lines A to D are indicative of sub-hydrostatic pressure conditions for both hydraulic gradients of 6.24 kPa/m and 9.81 kPa/m, with rates of rise ranging from 3.0 m/yr to 6.0 m/yr.

## 7.1. Future Research

Future research, building on this work, should include the following:

- Apply the Shuttle and Jefferies (2016) methodologies to characterise the in-situ state (contractive and or dilative behaviour) of tailings dams comprised of sand, silt and clay-sized tailings that have been deposited and constructed using different approaches;
- Investigation of the effect of coupled seepage and stress analysis to perform static liquefaction trigger analyses and slope stability assessment in which a factor of safety can be established under different operating scenarios;
- Investigation of the effect of coupled seepage and stress analysis to perform dynamic liquefaction trigger analyses and slope stability assessment in which a factor of safety can be established under different operating scenarios.

## Chapter 8 : References

- Abancó, C. et al., 2016. Wireless low power real-time solutions for tailings dams — a case study. In: P. M. Dight, ed. *Proceedings of the First Asia Pacific Slope Stability in Mining Conference*. Perth: Australian Centre for Geomechanics, pp. 685-694.
- Adajar, M. A. Q. & Zarco, M. A. H., 2016. Predicting the Stress-Strain Behavior of Mine Tailings Using Modified Hyperbolic Model. *International Journal*, 10(21), pp. 1834-1841.
- Adamczyk, J., 2012. Basic Geotechnical Properties of Mining and Processing Waste — A State of the Art Analysis. *AGH Journal of Mining and Geoengineering*, 36(2), pp. 31-41.
- Aubertin, M., Bussière, B. & Bernier, L., 2002b. *Environnement et gestion des rejets miniers [Manual on CD-ROM]*, Montréal: Les Presses Internationales de Polytechnique.
- Aubertin, M. & Chapuis, R. P., 1991. Critères de conception pour les ouvrages de retenue des résidus miniers dans la région de l'Abitibi. In: *Proceedings of the First Canadian Conference on Environmental Geotechnics*. Montréal: s.n., pp. 113-127.
- Aubertin, M. et al., 2002a. Stabilité géotechnique des ouvrages de retenue pour les résidus miniers: Problèmes persistants et méthodes de contrôle. In: Rouyn-Noranda, ed. *Proceedings of Symposium 2002 on Mines and the Environment, Rouyn-Noranda*. Montréal: CIM, pp. 526-552.
- Azam, S. & Li, Q., 2010. Tailings Dam Failures: A Review of the Last One Hundred Years. *Geotechnical News*, 28(4), pp. 50-54.
- Barrero, A. R., Taiebat, M. & Lizcano, A., 2015. *Application of an advanced constitutive model in nonlinear dynamic analysis of tailings dam*. Quebec, GEOQuebec.
- Bedin, J., Schnaid, F., Fonseca, A. & Costa Filho, L., 2012. Gold tailings liquefaction under critical state soil mechanics. *Geotechnique*, 62(3), pp. 263-267.
- Been, K., 1985. A state parameter for sands. *Géotechnique*, 35(2), pp. 99-112.
- Been, K., 2016. Characterizing mine tailings for geotechnical design. In: Lehane, Acosta-Martínez & Kelly, eds. *Geotechnical and Geophysical Site Characterisation 5*. Sydney, Australia: Australian Geomechanics Society, pp. 41-55.
- Been, K. & Jefferies, M. G., 1985. A state parameter for sands. *Géotechnique*, 35(2), pp. 99-112.
- Been, K., Jefferies, M. G., Crooks, J. H. A. & Rothenberg, L., 1987. The cone penetration test in sands: Part II, general inference of state. *Géotechnique*, 37(3), pp. 285-299.
- Been, K., Romero, S., Obermeyer, J. & Hebel, G., 2012. Determining the in situ state of silt and sand tailings with the CPT. In: *Proceedings of the 16th International Conference on Tailings and Mine Waste*. Vancouver : Information Technology, Creative Media, University of British Columbia, pp. 325-333.
- Bella, G., 2017. *Hydro-Mechanical Behaviour of Tailings in Unsaturated Conditions*, Italy: Politecnico di Torino.

- Bhanbhro, R., 2017. *Mechanical Behavior of Tailings Laboratory Tests from a Swedish Tailings Dam*, Luleå : Luleå University of Technology.
- Biot, M. A., 1941. General theory of three-dimensional consolidation. *J. Appl. Phys*, Volume 122, p. 155–164.
- Bjelkevik, A., 2005. *Stability of Tailings Dams Focus on Water Cover Closure*, Sweden: Luleå University of Technology.
- Bjelkevik, A. & Knutsson, S., 2005. Swedish tailings—comparison of mechanical properties between tailings and natural geological materials. In: *Proceedings securing the future, International Conference on Mining and the Environment Metals and Energy Recovery*. Skellefteå, Sweden: SveMin, p. 117.
- Blight, G., 2010. *Geotechnical engineering for mine waste storage facilities*. 1st Edition ed. London: Taylor and Francis.
- Blight, G. E. & Fourie, A. B., 2003. *A Review of Catastrophic Flow Failures of Deposits of Mine Waste and Municipal Refuse*, Johannesburg,: University of the Witwatersrand.
- Bonin, M. D., Nuth, M., Dagenais, A. M. & Cabral, A. R., 2014. Experimental study and numerical reproduction of self-weight consolidation behavior of thickened tailings. *Journal Geotechnical and Geoenvironmental Engineering* , 140(12).
- Boshoff, L., Meintjies, H. A. C. & Boroko, M., 2018. *Learnings from a real-time Pore Pressure Monitoring at a Platinum Tailings Facility*, Johannesburg: SRK Consulting (South Africa) (Pty) Ltd..
- Boulanger, R. W. & Duncan, J. M., n.d. *UCDAVIS Civil and Environmental Engineering - Tailings Dams Failures*. [Online]  
Available at: <https://research.engineering.ucdavis.edu/gpa/embankment-dams/tailings-dam-failures/>  
[Accessed 12 September 2019].
- Bowker, L. N. & Chambers, D. M., 2015. *The Risk, Public Liability, & Economics of Tailings Storage Facility Failures*. Stonington: s.n.
- Caldwell, J. A., 2016. *Tailings Failures and How to Avoid Them*. s.l.:Robertson Geoconsultants.
- Campbell, D. L. & Fitterman, D. V., 2000. Geoelectrical methods for investigating mine dumps. In: *Proceeding Fifth International Conference on Acid Rock Drainage*. Denver, Colorado: Society for Mining, Metallurgy, and Exploration, Inc, pp. 1513-1523.
- Casagrande, A., 1936. Characteristics of cohesionless soils affecting the stability of earth fills. *Journal of Boston Society of Civil Eng*, Volume 23, pp. 257-276.
- Chambers, D. & Higman, B., 2011. Long term risks of tailings dam failure. *Alaska Park Science* , 13(2).
- Chetty, P., 2013. Monitoring of mine tailings using satellite and lidar data. In: *SASGI Proceedings 2013 – Stream 1*. Ekurhuleni: EE Publishers.

- da Fonseca, A. V., 2012. Application of in situ testing in tailing dams, emphasis on liquefaction: case-history.. In: Coutinho & Mayne, eds. *Proceedings of the 4th international conference on geotechnical and geophysical site characterization (ISC'4)*. Porto de Galinhas, Pernambuco, Brazil: Taylor & Francis Group, pp. 181-203.
- Davies, M., Martin, T. & Lighthall, P., 2000. Mine Tailings Dams: When Things Go Wrong. In: *Proceeding of Tailing Dams*. Las Vegas: Association of State Dam Safety Officials, US Committee of Large Dams, pp. 261-273.
- Davies, M., McRoberts, E. & Martin, T., 2002. Static liquefaction of tailings—Fundamentals and case histories. In: *Proceedings, Tailings Dams*. Las Vegas, Nevada: ASDSO/USCOLD, pp. 233-255.
- Davies, M. P., 2002. Tailings impoundment failures: are geotechnical engineers listening?. *Geotechnical News*, 20 September, pp. 31-36.
- Davies, M. P. & Lighthall, P. C., 2001. Geotechnical Aspects of Several Recent Mine Tailings Impoundment Failures. In: *Proceedings of the 54th Canadian Geotechnical Society Conference*. Calgary, Alberta: s.n., pp. 321-326.
- de Wit, T. & Olivier, G., 2018. Imaging and monitoring tailings dam walls with ambient seismic noise. In: R. J. Jewell & A. B. Fourie, eds. *Proceedings of the 21st International Seminar on Paste and Thickened Tailings*. Perth: Australian Centre for Geomechanics, pp. 455-464.
- Dienstmann, G., Schnaid, F., Maghous, S. & DeJong, J., 2018. Piezocone Penetration Rate Effects in Transient Gold Tailings. *Journal of Geotechnical and Geoenvironmental Engineering ASCE*, 144(2).
- Dobry, R. & Alvarez, L., 1967. Seismic Failures of Chilean Tailings Dams. *Journal of Soil Mechanics and Foundation, ASCE*, 93(SM6), pp. 237-260.
- Drucker, D. C., Gibson, R. E. & Henkel, D. J., 1957. Soil mechanics and work hardening theories of plasticity. *Transactions American Society of Civil Engineers*, Volume 122, pp. 338-346.
- Du Toit, I., 2015. *Combining different technologies for better assessing slope stability on a mine*. Ekurhuleni, Geomatics Indaba Proceedings.
- Energy, Mines and Resources Canada, 1977. Chapter 9: Waste Embankments. In: *Pit Slope Manual*. s.l.:Mining Research Laboratories.
- Ferdosi, B., James, M. & Aubertin, M., 2015a. Effect of waste rock inclusions on the seismic stability of an upstream raised tailings impoundment: a numerical investigation. *Canadian Geotechnical Journal*, Volume 52, pp. 1930-1944.
- Ferdosi, B., James, M. & Aubertin, M., 2015b. Numerical simulations of seismic and post-seismic behavior of tailings. *Canadian Geotechnical Journal*, Volume 53, pp. 85-92.
- Finn, W., 1980. Seismic Response of Tailings Dams. In: *Proceeding Seminar on Design and Construction of Tailings Dams*. USA: Colorado School of Mines.



- Finn, W., 1996. Seismic Design and Evaluation of Tailings Dams: State of the Art . In: *Int. Symposium on Seismic and Environmental Aspects of Dam Design: Earth, Concrete and Tailing Dams*. Chile: s.n.
- Fourie, A. B., Blight, G. E. & Papageorgiou, G., 2001. Static liquefaction as a possible explanation for the Merriespruit tailings dam failure. *Canadian Geotechnical Journal*, Volume 38, pp. 707-719.
- Fredlund, D. G., Rahardjo, H. & Fredlund, M., 2012. *Unsaturated Soil Mechanics in Engineering Practice*. s.l.:John Wiley & Sons, Inc.
- Geo-Engineering Extreme Events Reconnaissance (GEER), 2010. Geo-engineering reconnaissance of the 2010 Maule, Chile Earthquake. In: J. D. Bray & D. Frost, eds. *Report of the NSF Sponsored GEER Association Team*. s.l.:NSF-Sponsored GEER-022, Version 2.
- GEO-SLOPE International Ltd., 2015. *Seepage Modeling with SEEP/W*, Calgary, Alberta, Canada: GEO-SLOPE International Ltd..
- Geremew, A. M. & Yanful, E. K., 2012. Laboratory Investigation of the Resistance of Tailings and Natural Sediments to Cyclic Loading. *Geotechnical and Geological Engineering*, 30(2), pp. 431-447.
- Geremew, A. M. & Yanful, E. K., 2013. Dynamic Properties and Influence of Clay Mineralogy Types on the Cyclic Strength of Mine Tailings. *International Journal of Geomechanics, ASCE*, 13(4), pp. 441-453.
- Guo, P. & Su, X., 2007. Shear strength, interparticle locking, and dilatancy of granular materials. *Canadian Geotechnical Journal*, 44(5), pp. 579-591.
- Hamade, T. & Mitri, H., 2013. Reliability-based approach to the geotechnical design of tailings dams. *International Journal of Mining, Reclamation and Environment*, Volume 27, p. 377–392.
- Hamade, T., Saad, B. & Pouliot, S., 2011. Stochastic analysis of tailing dams stability using numerical modelling. In: *Conference proceedings - 2011 Pan-Am CGS Geotechnical Conference : 64th Canadian Geotechnical Conference and 14th Pan-American Conference on Soil Mechanics and Geotechnical Engineering*. Toronto: Canadian Geotechnical Society .
- Hardy, D. & Engels, J., 2007. Guidelines and recommendations for the safe operation of tailings management facilities. *Environmental Engineering Science*, 24(5), pp. 625-637.
- Holmqvist, M., 2014. *Seepage, Solute transport and Strain-stress Analysis of Ashele Tailings Dams*. Uppsala: Uppsala University.
- Hu, J. & Liu, X., 2011. Design and implementation of tailings dam security monitoring system. *Procedia Engineering*, Volume 26, pp. 1914-1921.
- Hu, L. et al., 2017. Geotechnical Properties of Mine Tailings. *Journal of Materials in Civil Engineering*, 29(2), pp. 04016220-1-10.
- Hu, S. et al., 2015. Effect of seepage control on stability of a tailings dam during its staged construction with a stepwise-coupled hydro-mechanical model. *International Journal of Mining, Reclamation and Environment*, Volume 29, p. 125–140.

- ICOLD, 2001. *Tailings dams - risk of dangerous occurrences - lessons learnt from past experiences*, Paris: International Commission on Large Dams and United Nations Environmental Program (ICOLD).
- Inaudi, D., Cottone, I. & Figini, A., 2013. Monitoring Dams and Levees with Distributed Fiber Optic Sensing. In: *Proceedings of The 6th International Conference on Structural Health Monitoring of Intelligent Infrastructure*. Hong Kong: s.n.
- Ishihara, K., 1984. Post-Earthquake Failure of a Tailings Dam Due to Liquefaction of the Pond Deposit. In: *Int. Conference on Case Histories in Geotechnical Engineering*. St. Louis, USA: s.n.
- Ishihara, K., 1993. Liquefaction and flow failure during earthquakes. *Geotechnique*, 43(3), pp. 351-415.
- Ishihara, K., Yasuda, S. & Yoshida, Y., 1990. Liquefaction-induced flow failure of embankments and residual strength of silty sands. *Soils and Foundations*, 30(3), pp. 69-80.
- ITASCA Consulting Group. Inc., 2019. *FLAC Constitutive Models*. [Online] Available at: <https://www.itascacg.com/software/flac-constitutive-models> [Accessed 20 October 2019].
- James, M., Aubertin, M., Wijewickreme, D. & Ward Wilson, G., 2011. A laboratory investigation of the dynamic properties of tailings. *Canadian Geotechnical Journal*, Volume 48, pp. 1587-1600.
- James, M., Gomes, P. & Schwenger, R., 2007. The liquefaction resistance of tailings and the stability of impoundments. In: *Proc., 60th Canadian Geotechnical Conf., Canadian Geotechnical Society*. Edmonton, Canada: s.n.
- James, M., Jollette, D., Aubertin, M. & Bussière, B., 2003. An experimental set-up to investigate tailings liquefaction and control measures. In: *Proceedings of the International Symposium on Major Challenges in Tailings Dams (ICOLD)*. Montréal: Que, pp. 153-164.
- Jantzer, I., Bjelkevik, A. & Pousette, K., 2001. *Material properties of Tailings from Swedish mines*, Lulea: Norsk Geoteknisk Forening. ICOLD and UNEP.
- Jefferies, M. & Been, K., 2016. *Soil liquefaction: a critical state approach*. 2nd ed. s.l.:CRC Press.
- Jefferies, M. G., 1993. NorSand: a simple critical state model for sand. *Géotechnique*, Volume 43, pp. 91-103.
- Jefferies, M. G. & Shuttle, D. A., 2002. Dilatancy in general Cambridge-type models. *Géotechnique*, 52(9), pp. 625-638.
- Jefferies, M. G. & Shuttle, D. A., 2005. NorSand: features, calibration and use. In: J. A. Yamamuro & V. N. Kaliakin, eds. *ASCE Geotechnical Special Publication No. 128, Soil Constitutive Models: Evaluation, Selection, and Calibration*. s.l.:s.n., pp. 204-236.
- Jewell, J. R., 1998. An Introduction to Tailings. *Case Studies on Tailings Management*.
- K, B., Crooks, J. H. A. & Jefferies, M. G., 1988. Interpretation of material state from CPT in sands and clays. In: *Proc. Conf. Penetration Testing*. s.l.:Thomas Telford, pp. 215-218.

- Khalili, A., Wijewickreme, D. & Ward Wilson, G., 2010. Mechanical response of highly gap-graded mixtures of waste rock and tailings. Part I: Monotonic shear response. *Canadian Geotechnical Journal*, 47(5), pp. 552-565.
- Leica Geosystems AG, 2008. *Monitoring a dam wall in a Polish Copper Ore Enrichment Facility (PL)*, Heerbrugg: Leica Geosystems AG.
- Mainali, G., Nordlund, E., Knutsson, S. & Thunehed, H., 2015. Tailings Dams Monitoring in Swedish Mines using Self-Potential and Electrical Resistivity Methods. *Electrical Journal of Geotechnical Engineering*, 20(13), pp. 5859-5875.
- Manzari, M. T. & Dafalias, Y. F., 1997. A critical state two surface plasticity model for sands. *Géotechnique*, Volume 47, pp. 255-272.
- Martin, T. E., 1999. Characterization of pore pressure conditions in upstream tailings dams. In: *Proc., 6th Int. Conf. on Tailings and Mine Waste '99*. Rotterdam: Balkema, pp. 303-313.
- Martin, T. E. & Davies, M. P., 2000. Development and Review of Surveillance Programs for Tailings Dams. In: *Proceedings, Tailings Dams 2000*,. Las Vegas: Association of State Dam Safety Officials (ASDSO), Lexington, KY, pp. 367-380.
- Martin, T. E. & McRoberts, E. C., 1999. Some considerations in the stability analysis of upstream tailings dams.. In: *proceedings of sixth International Conference on Tailings and Mine Waste '99*. Fort Collins, Colorado: A.A Balkema Rotterdam, pp. 1-17.
- McPhail, G. I. & Wagner, J. C., 1989. Disposal of residues, Chapter 11. In: G. G. Stanley, ed. *The Extractive Metallurgy of Gold in South Africa*. s.l.:The Chamber of Mines of South Africa, pp. 655-707.
- Mittal, H. K. & Morgenstern, N. R., 1975. Parameters for the design of tailings dams. *Canadian Geotechnical Journal*, 12(2), pp. 235-261.
- Mohajeri, M. & Ghafghazi, M., 2012. Ground sampling and Laboratory testing on low plasticity clays. In: *Proc. 15th World Conference on Earthquake Engineering*. Lisbon: s.n.
- Morgenstern, N. R. & Kupper, A. A. G., 1988. Hydraulic fill structures - a perspective. In: *Proceedings of the Conference on Hydraulic Fill Structure (ASCE)*. Fort Collins, Colorado: s.n., pp. 1-13.
- Mukerjee, S., Raj, D. & Bharathi, M., 2015. *Liquefaction Susceptibility of Tailings Material*. Pune, India, Indian Institute of Technology Roorkee.
- Naeini, M. & Akhtarpour, A., 2018. A numerical investigation on hydro-mechanical behaviour of a high centreline tailings dam. *Journal of the South African Institution of Civil Engineering*, 60(3), pp. 49-60.
- Navarro, L., Aravena, G., Engels, J. & Turner, J., 2019. Satellite bathymetry for the monitoring of supernatant water volumes within tailings storage facilities. In: A. B. Fourie & D. Reid, eds. *Proceedings of the 22nd International Conference on Paste, Thickened and Filtered Tailings*. Perth: Australian Centre for Geomechanics, pp. 205-217.

- Oelofse, P. & Kruger, W., 2019. *Centre of Monitoring Excellence - CPTu Analysis Spreadsheet*. South Africa/Gauteng.
- Olson, S. M., 2001. *Liquefaction analysis of level and sloping ground using field case histories and penetration resistance*, PhD Thesis, Urbana: Univ. of Illinois-Urbana-Champaign.
- Olson, S. M. & Stark, T. D., 2003. Yield strength ratio and liquefaction analysis of slopes and embankments. *Journal of Geotechnical and Geoenvironmental Engineering*, 129(8), pp. 727-737.
- Ormann, L. et al., 2013. Numerical analysis of strengthening by rockfill embankments on an upstream tailings dam. *Canadian Geotechnical Journal*, Volume 50, p. 391–399.
- Peuchen, J., Vanden Berghe, J. F. & Coulais, C., 2010. Estimation of  $u_1/u_2$  conversion factor for piezocone. In: *CPT'10, 2nd International Symposium on Cone Penetration Testing*. s.l.:s.n.
- Plewes, H. D., Davies, M. P. & Jefferies, M. G., 1992. CPT based screening procedure for evaluating liquefaction susceptibility. In: *Proc 45th Canadian Geotechnical Conference*. Toronto: s.n.
- Poulos, S. J., Castro, G. & France, J. W., 1985. Liquefaction evaluation procedure. *J. of Geotech. Eng*, 111(6), pp. 772-792..
- Poulsen, B. et al., 2014. Mine Overburden Dump Failure: A Case Study. *Geotechnical and Geological Engineering*, pp. 1-13.
- Priscu, C., 1996. *Behavior of Mine Tailings Dams Under High Tailings Deposition Rates*. Montreal: Department of Mining and Metallurgical Engineering, McGill University.
- Psarropoulos, P. N. & Tsompanakis, Y., 2008. Stability of Tailings Dams Under Static and Dynamic Loading. *Canadian Geotechnical Journal*, Volume 45, pp. 663-675.
- Qiu, Y. & Sego, D. C., 2001. Laboratory properties of mine tailings. *Canadian Geotechnical Journal*, Volume 38, pp. 183-190.
- Quiroz, C. T., Rafael, H. M. A. M. & Romanel, C., 2016. Seismic Analysis for the Foundation of a Tailings Dam in Peru. In: *XVIII Brazilian Conference on Soil Mechanics and Geotechnical Engineering*. Belo Horizonte, Minas Gerais, Brazil: ABMS.
- Radue, T. J., 2017. *Tailings Basin Geotechnical Instrumentation and Monitoring Plan*, Minneapolis: Barr Engineering.
- Rico, M. et al., 2008. Reported tailings dam failures review of the European incidents in the worldwide context. *Journal of Hazardous Materials*, Volume 152, pp. 846-852.
- Riemer, M., Moriwaki, Y. & Obermeyer, J., 2008. Effect of high confining stresses on static and cyclic strengths of mine tailing materials. In: *Proceedings of the ASCE Congress: Geotechnical Earthquake Engineering and Soil Dynamics IV, Sacramento, California. GSP 181*. Reston, Va: American Society of Civil Engineering.
- Robertson, A., 2012. Tailings: dammed, damned or damless. *Newsletter*, December, pp. 14-15.

- Robertson, P. K., 2009. Interpretation of cone penetration tests - a unified approach. *Canadian Geotechnical Journal*, Volume 46, pp. 1337-1355.
- Robertson, P. K., 2009. Performance based earthquake design using the CPT. In: T. Kokusho, Y. Tsukamoto & M. Yoshimine, eds. *Proceedings of the international conference on performance-based design in earthquake geotechnical engineering (IS-Tokyo 2009)*. Tokyo : s.n.
- Robertson, P. K., 2010. Evaluation of flow liquefaction and liquefied strength using the cone penetration test. *Journal of Geotechnical and Geoenvironmental Engineering, ASCE*, 136(6), pp. 842-853.
- Robertson, P. K., 2012. Evaluating flow (static) liquefaction using the CPT: an update. In: *Proceedings Tailings and Mine Waste '12*. Keystone, Co., USA: s.n.
- Robertson, P. K., 2013. *CPTu Dissipation Tests – Theory and practice*. [Online]  
Available at: <http://www.greggdrilling.com/webinars/cptu-dissipation-tests-theory-and-practice/>  
[Accessed 19 September 2019].
- Robertson, P. K., 2016. CPT-based Soil Behaviour Type (SBT) Classification System – an update. *Canadian Geotechnical Journal*, pp. 1-18.
- Rocscience Inc A, n.d. *Drained and Undrained Triaxial Tests on Sand*, s.l.: Rocscience Inc.
- Rocscience Inc B, n.d. *Softening-Hardening Material Model*, Canada: Rocscience Inc.
- Rocscience Inc C, n.d. *Duncan-Chang Hyperbolic Material Model*, Canada: Rocscience Inc.
- Rocscience Inc D, n.d. *Define Hydraulic Properties*. [Online]  
Available at: [https://www.rocscience.com/help/slide2/slide\\_model/groundwater/Hydraulic\\_Properties.htm](https://www.rocscience.com/help/slide2/slide_model/groundwater/Hydraulic_Properties.htm)  
[Accessed 2 August 2019].
- Rocscience Inc. (2018), 2019. *RS2 User's Manual*. [Online]  
Available at: [www.rocscience.com](http://www.rocscience.com)  
[Accessed 16 January 2019].
- Rodriguez, L., Ruiz, E., Alonso-Azcarate, J. & Rincon, J., 2009. Heavy metal distribution and chemical speciation in tailings and soils around a Pb–Zn mine in Spain. *The Journal of Environmental Management*, Volume 90, pp. 1106-1116.
- Roscoe, K. H. & Burland, J. B., 1968. On the generalized stress-strain behaviour of 'wet' clay". In: J. Heyman & F. A. Leckie, eds. *In Engineering plasticity*. London: Cambridge University Press, pp. 535-609.
- Rout, S. K., Sahoo, T. & Das, S. K., 2013. Design of tailing dam using red mud. *Central European Journal of Engineering*, 3(2), pp. 316-328.
- Rykaart, M., Fredlund, M. & Stianson, J., 2001. Solving tailings impoundment water balance problems with 3-D seepage software. *Geotechnical News*, Volume 19, p. 50–54.

- Saad, B. & Mitri, H., 2010. Staged construction analysis of surface tailings disposal facilities. *International Journal of Mining, Reclamation and Environment*, 24(1), pp. 44-63.
- Schofield, A. & Wroth, C. P., 1968. *Critical State Soil Mechanics*. London: McGraw-Hill.
- Shamsai, A., Pak, A., Bateni, S. M. & Ayatollahi, S. A. H., 2007. Geotechnical characteristics of copper mine tailings: a case study. *Geotechnical and Geological Engineering*, 25(5), pp. 591-602.
- Shuttle, D. A. & Cunning, J., 2007. Liquefaction potential of silts from CPTu. *Canadian Geotechnical Journal*, Volume 44, pp. 1-19.
- Shuttle, D. A. & Jefferies, M. G., 1998. Dimensionless and unbiased CPT interpretation in sand. *International Journal of Numerical and Analytical Methods in Geomechanics*, Volume 22, pp. 351-391.
- Shuttle, D. & Jefferies, M., 2010. *NorSand: Description, Calibration, Validation and Applications*, s.l.: s.n.
- Shuttle, D. & Jefferies, M., 2016. Determining Silt State from CPTu. *Institution of Civil Engineers*, pp. 1-29.
- Skau, K. et al., 2013. *Stability and Deformations of Želazny Most Dam - One of the World's Largest Deponies For Copper Tailings*, Oslo: Fjellsprengning-steknikk-bergmekanikk-geoteknikk.
- Skytruth, 2016. *Skytruth*. [Online]  
Available at: <https://skytruth.org/tech/skytruth-imagery/flickr-content/5417802-72157623161226096/72157616144968039/#!>  
[Accessed 9 September 2019].
- SMARTEC, n.d. *SMARTEC Main Projects for Tailings Dams*, Switzerland: SMARTEC.
- Sottile, M., Kerguelen, A. & Sfriso, A., 2019. *A comparison of procedures for determining the state parameter of silt-like tailings*, Buenos Aires, Argentina: SRK Consulting.
- Tanriseven, E. N., 2012. *Stability investigation of eti copper mine tailings dam using finite element analysis*, Ankara: Middle East Technical University.
- The Guardian, 2019. *Brazil dam disaster: firm knew of potential impact months in advance*. [Online]  
Available at: <https://www.theguardian.com/world/2018/feb/28/brazil-dam-collapse-samarco-fundao-mining>  
[Accessed 9 September 2019].
- TheStar, 2006. *Four years since Mount Polley mine disaster and no charges*. [Online]  
Available at: <https://www.thestar.com/vancouver/2018/08/03/four-years-since-mount-polley-mine-disaster-and-no-charges.html>  
[Accessed 9 September 2019].
- Thomas, A. et al., 2019. Earth observation data and satellite InSAR for the remote monitoring of tailings storage facilities: a case study of Cadia Mine, Australia. In: A. B. Fourie & D. Reid, eds. *Proceedings of the 22nd International Conference on Paste, Thickened and Filtered Tailings*. Perth: Australian Centre for Geomechanics, pp. 183-195.



- Todd Roberts, P. G., n.d. *Distributed Fiber Optic Sensors for Dams and Levee Deformation Monitoring*, Denver: RocTest, Ltd.
- Torres-Cruz, L. A., 2011. *Assessment of Two Cone Penetration Test Based Methods for Evaluating the Liquefaction Potential of Tailings Dams*, Johannesburg: University of Witwatersrand Faculty of Engineering and Built Environment.
- United States Committee on Large Dams (USCOLD), 1994. *Tailings Dam Incidents*. . 82 pps., s.l.: USCOLD.
- USEPA, 1997. *Damage Cases and Environmental Releases from Mines and Mineral Processing Sites*, Washington, DC: U.S. Environmental Protection Agency, Office of Solid Waste.
- Vanden Berghe, J. F., Ballard, J. C., Wintgens, J. F. & List, B., 2011. Geotechnical Risks Related to Tailings Dam Operations. In: *Proceedings Tailings and Mine Waste*. Vancouver, BC: s.n.
- Vargas, R., Paihua, S., Ordoñez, A. & Herrera, F., 2014. *Seismic response analysis for the stability of waste rock dumps and tailings dams*, Lima, Peru: Knight Piésold Consultores S.A..
- Vick, S. G., 1983. *Planning, Design, and Analysis of Tailings Dams*. New York; Chichester; Brisbane; Toronto; Singapore: John Wiley & Sons.
- Vick, S. G., 1990. *Planning, design, and analysis of tailings dams*. Canada: BiTech Publishers Ltd.
- Wanderley, L. J., Mansur, M. S., Milanez, B. & Pinto, R. G., 2016. Desastre da Samarco/Vale/BHP no Vale do Rio Doce: aspectos econômicos , políticos e socio ambientais. *Ciência e Cultura*, 68(3).
- Wang, L., Yang, X. & He, M., 2018. Research on Safety Monitoring System of Tailings Dam Based on Internet of Things. *IOP Conference Series: Materials Science and Engineering*, Volume 322.
- Wei, L. & Wang, C., 2011. First International Symposium on Mine Safety Science and Engineering: GPS in the tailings dam deformation monitoring. *Procedia Engineering*, Volume 26, pp. 1648-1657.
- Wei, Z., Yin, G., Wan, L. & Li, G., 2016. A case study on a geotechnical investigation of drainage methods for heightening a tailings dam. *Environmental Earth Science*, 75(106), pp. 1-10.
- Wijewickreme, D., Khalili, A. & Ward Wilson, G., 2010. Mechanical response of highly gap-graded mixtures of waste rock and tailings. Part II: Undrained cyclic and post-cyclic shear response. *Canadian Geotechnical Journal*, 47(5), pp. 566-582.
- Wijewickreme, D., Sanin, M. V. & Greenaway, M. R., 2005. Cyclic shear response of fine-grained mine tailings. *Canadian Geotechnical Journal*, Volume 42, pp. 1408-1421.
- Wikipedia, 2019. *Brumadinho dam disaster*. [Online]  
Available at: [https://en.wikipedia.org/wiki/Brumadinho\\_dam\\_disaster](https://en.wikipedia.org/wiki/Brumadinho_dam_disaster)  
[Accessed 9 September 2019].

WISE, 2004. *Safety of Tailings Dams*. [Online]

Available at: <http://www.wise-uranium.org/mdas.html#INTRO>

[Accessed 28 July 2018].

WISE, 2018. *Chronology of major tailings dam failures*. [Online]

Available at: <http://www.wise-uranium.org/mdaf.html>

[Accessed 28 July 2018].

WISE, 2019. *Chronology of major tailings dam failures*. [Online]

Available at: <https://www.wise-uranium.org/mdaf.html>

[Accessed 08 September 2019].

Wong, R. C. K., Mills, B. N. & Liu, Y. B., 2008. Mechanistic model for one-dimensional consolidation behavior of nonsegregating oil sands tailings. *Journal Geotechnical Geoenvironmental Engineering*, 134:2(195), pp. 195-202.

Xu, B. & Wang, Y., 2015. Stability analysis of the Lingshan gold mine tailings dam under conditions of a raised dam height. *Bulletin of Engineering Geology and the Environment*, 74(1), pp. 151-161.

Xu, C., 2019. *Long-Term Seepage Assessment Using Numerical Modeling for Upstream-Type Tailings Dam*, Montreal, Quebec, Canada: Concordia University.

Xu, H., Jing-yu, S., Wei, W. & Dong-hui, M., 2017. Dynamic Triaxial Tests on Dynamic Characteristics of Tailings. *The Electronic Journal of Geotechnical Engineering*, 22(4), pp. 1495-1509.

Yaya, C., Tikou, B. & LiZhen, C., 2017. Numerical analysis and geophysical monitoring for stability assessment of the Northwest tailings dam at Westwood Mine. *International Journal of Mining Science and Technology*, Volume 27, pp. 701-710.

Yuan, L. & Lei, J., 2015. The analysis of the seepage characteristics of tailing dams based on FLAC 3D numerical simulation. *The Open Civil Engineering Journal*, Volume 9, p. 400–407..

Zardari, A. M., 2011. *Stability of Tailings Dams - Focus on Numerical Modelling*, Sweden: Luleå University of Technology.

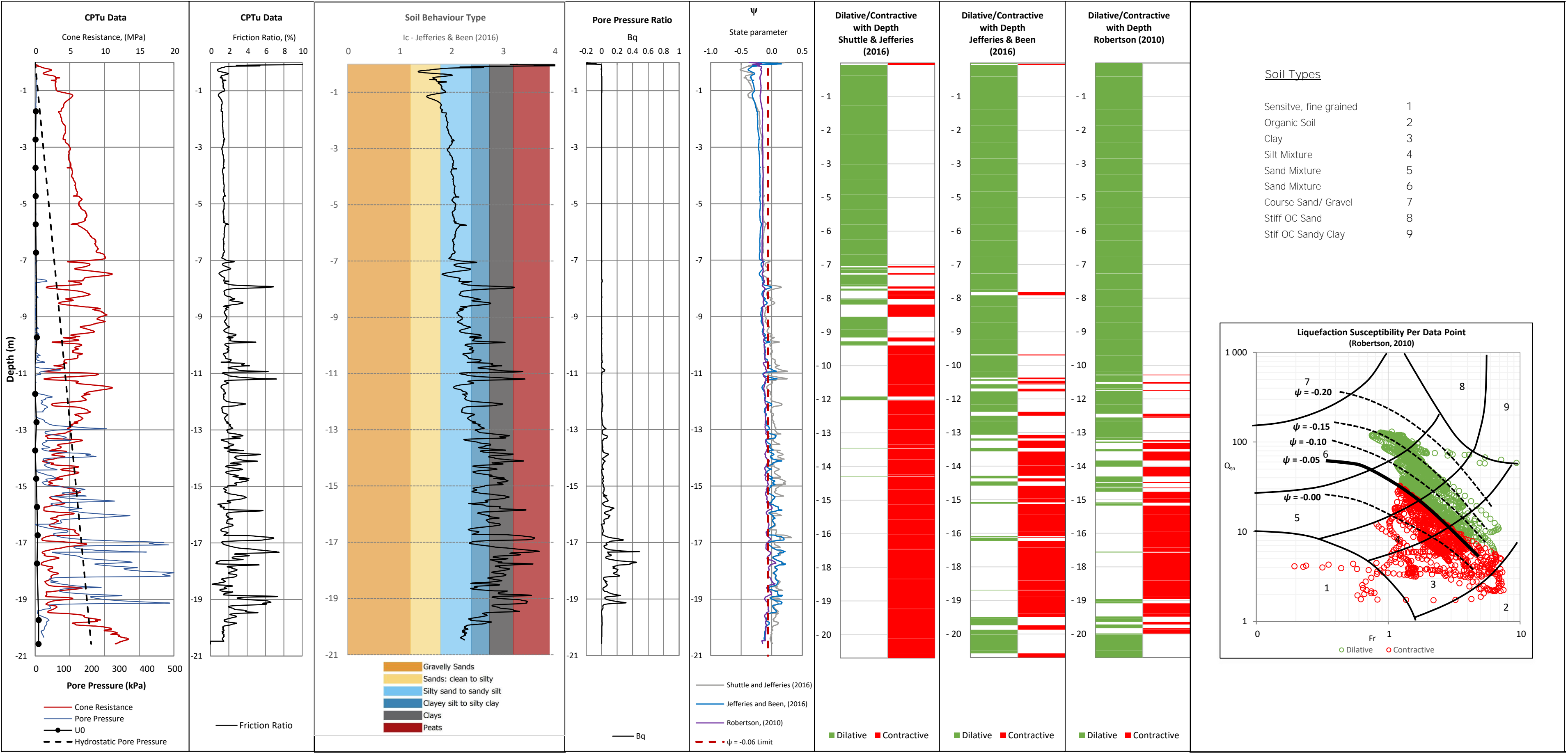
Zardari, M. A., Ormann, L., Mattsson, H. & Knutsson, S., 2014. Numerical Analysis of Staged Construction of an Upstream Tailings Dam. In: *Proceedings of 1st National Conference on Civil Engineering (NCCE 2013-14): (Modern Trends and Advancements)*. Quest Nawabshah, Pakistan: Department of Civil Engineering, Quest Nawabshah, Pakistan, pp. 150-160.

Zhang, C., Liu, H., Yang, C. & Wu, S., 2016. Mechanical characteristics of non-saturated tailings and dam stability. *International Journal of Mining, Reclamation and Environment*, 32(1), pp. 1-14.

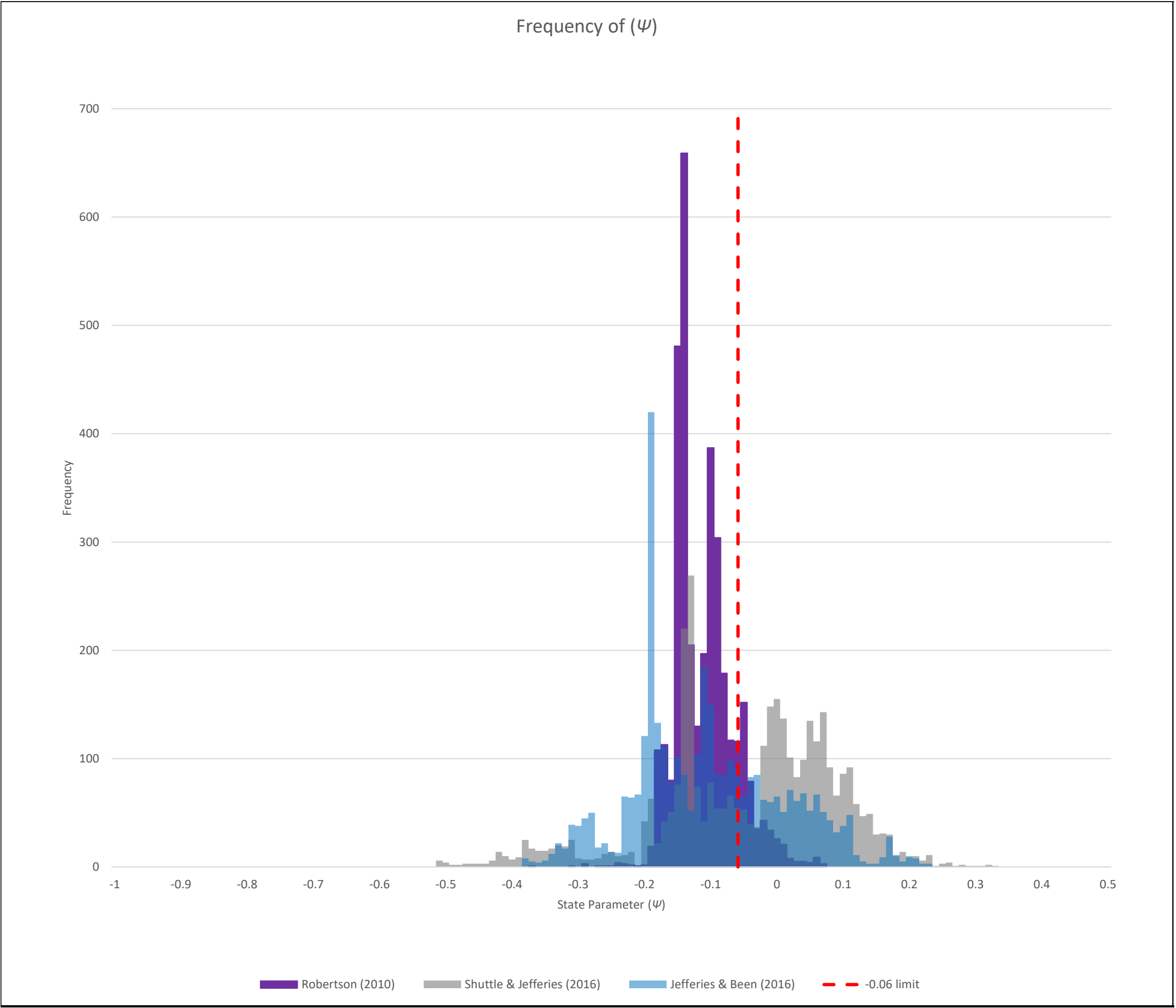
Zhang, Q. et al., 2015. An experimental study of the mechanical features of layered structures in dam tailings from macroscopic and microscopic points of view. *Engineering Geology*, Volume 195, pp. 142-154.

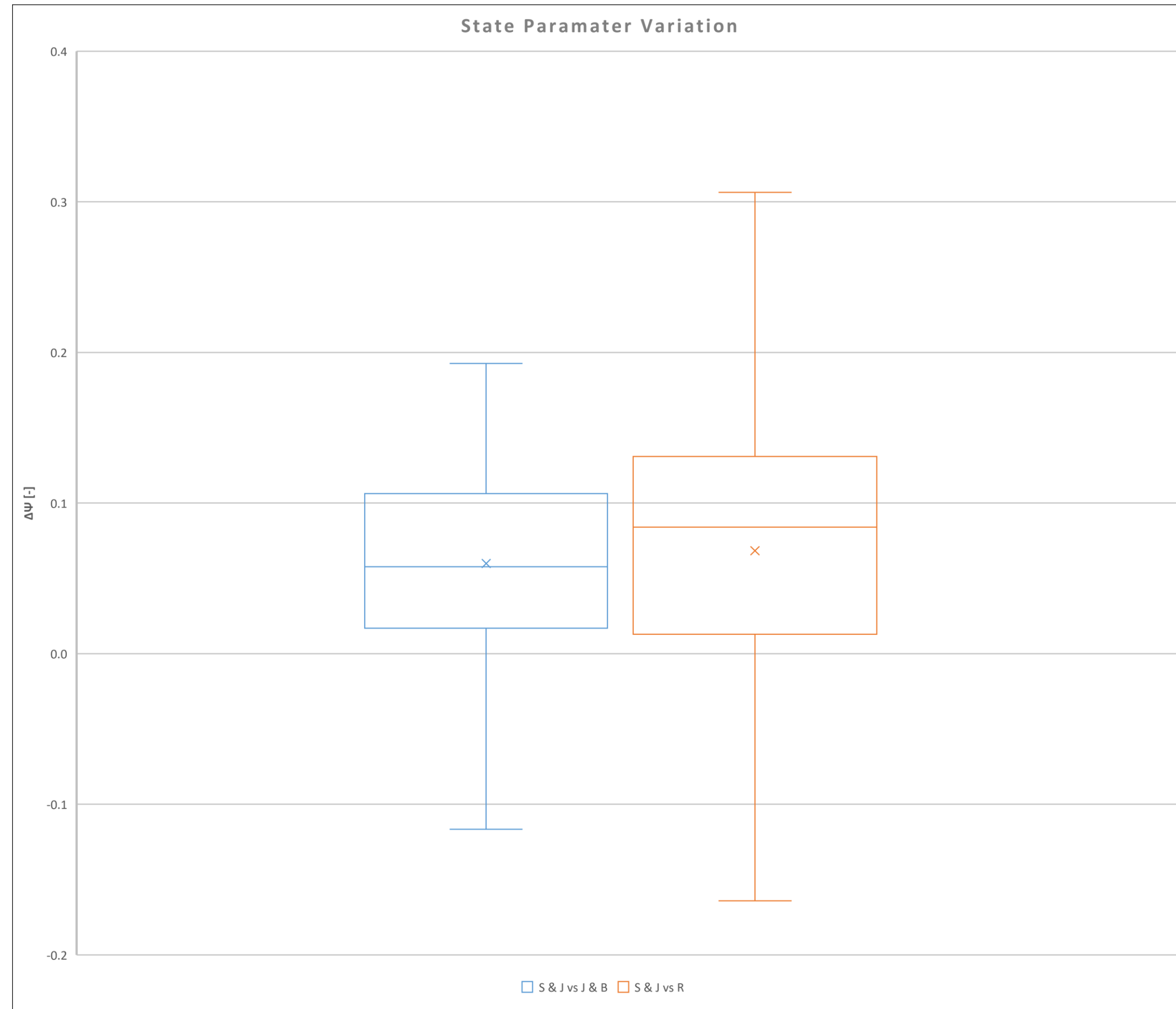
## **Appendix A: CPTu Interpretation – Monitoring Line A**

CPTu PC20



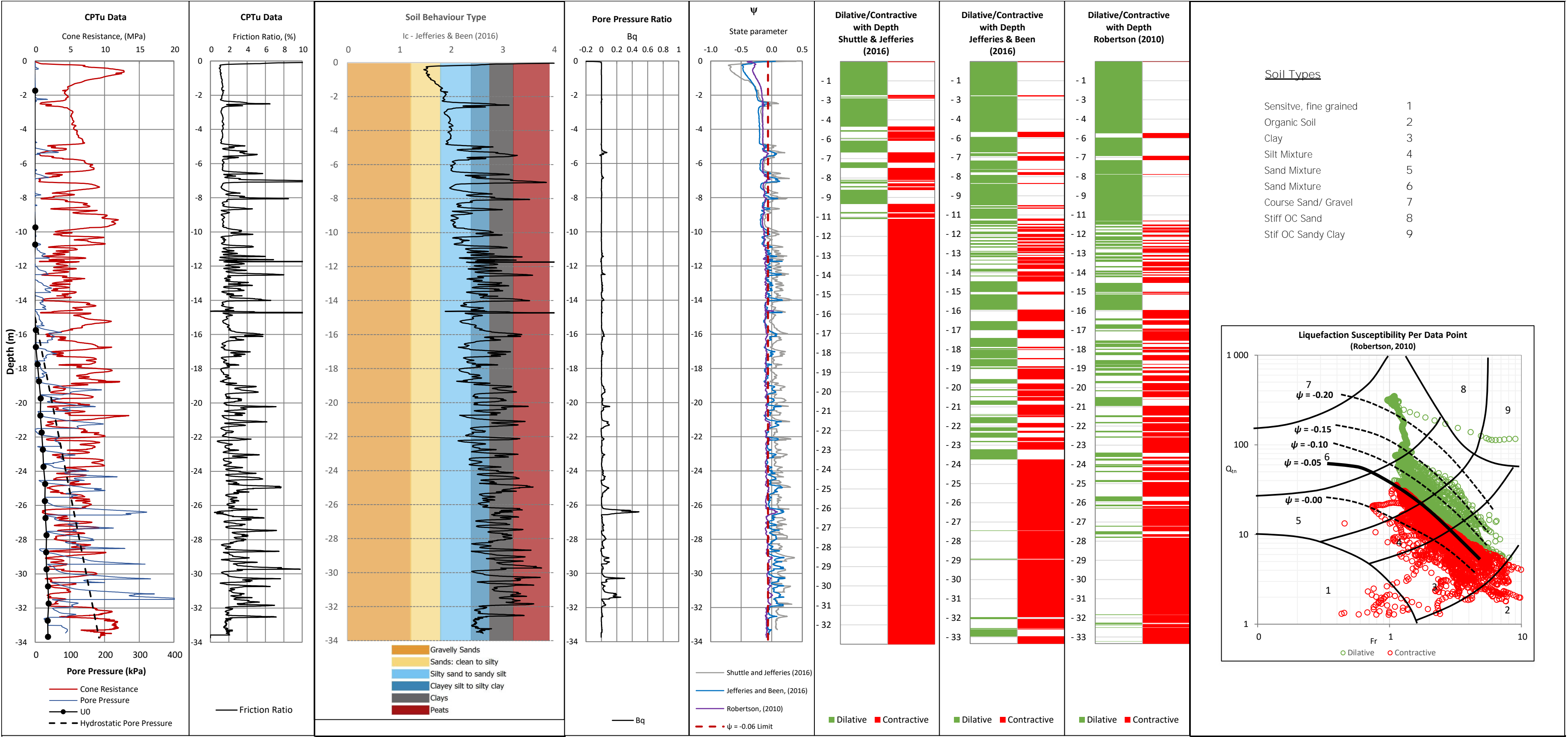
CPTu PC20



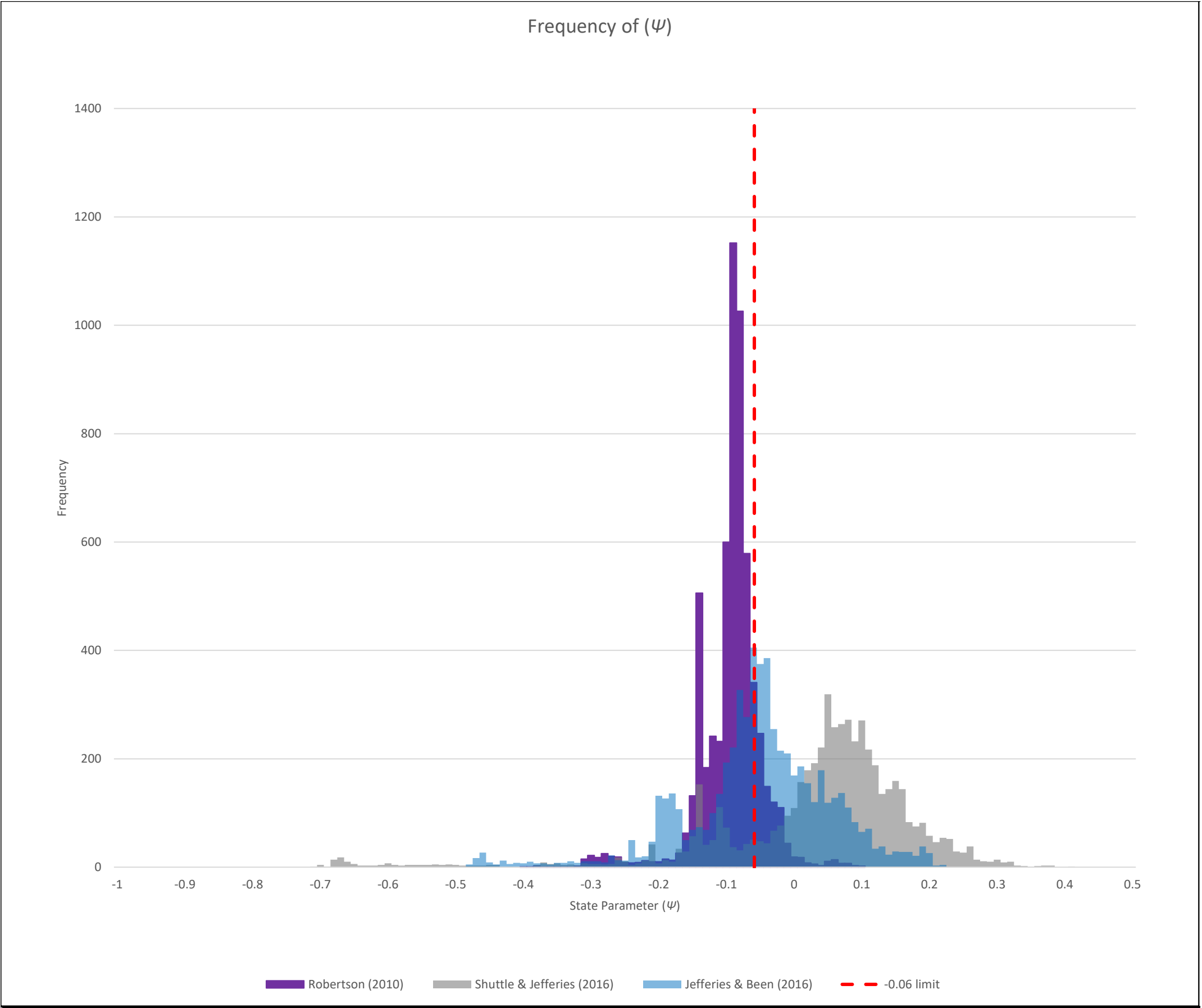
**CPTu PC20**



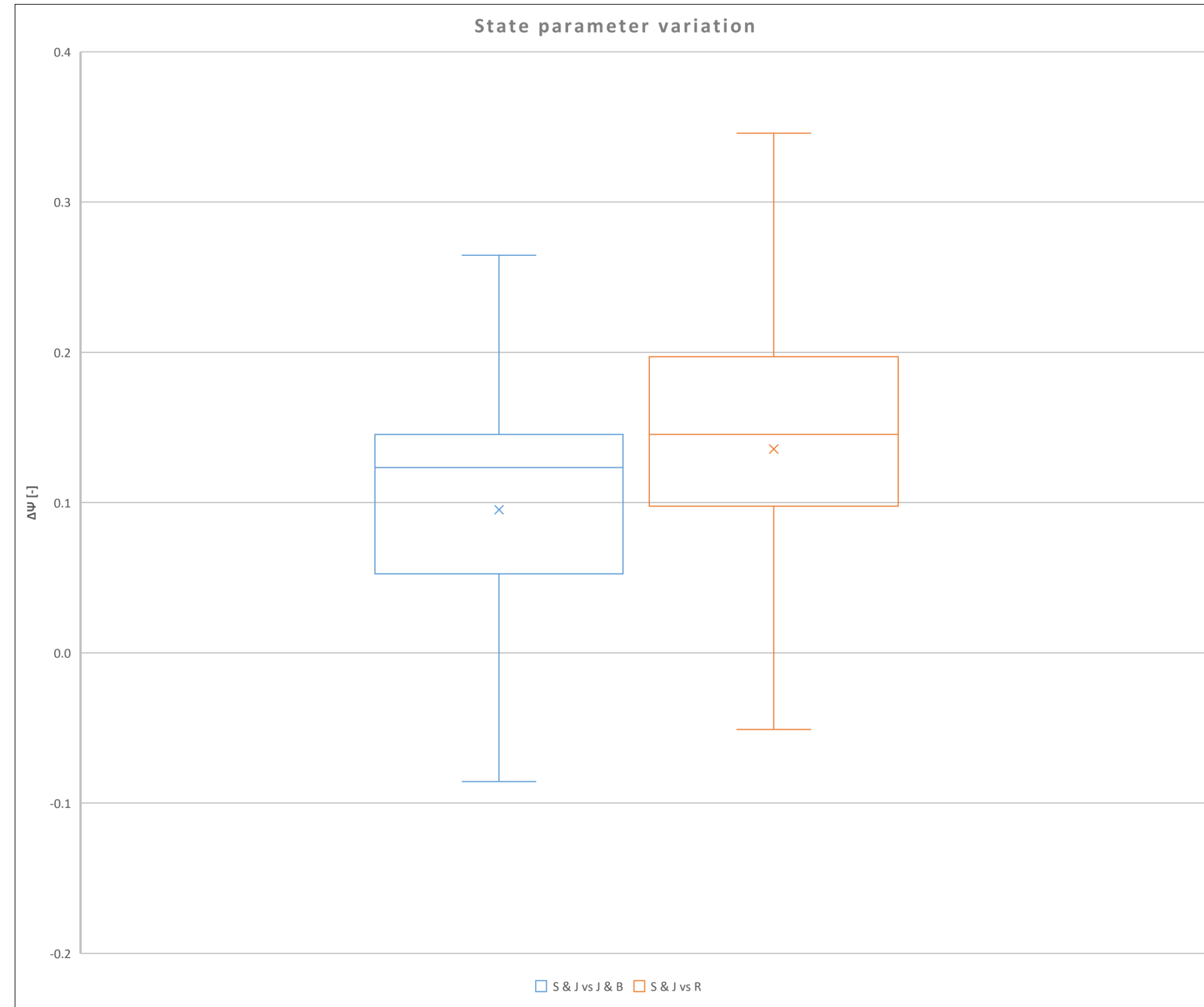
CPTu PC21



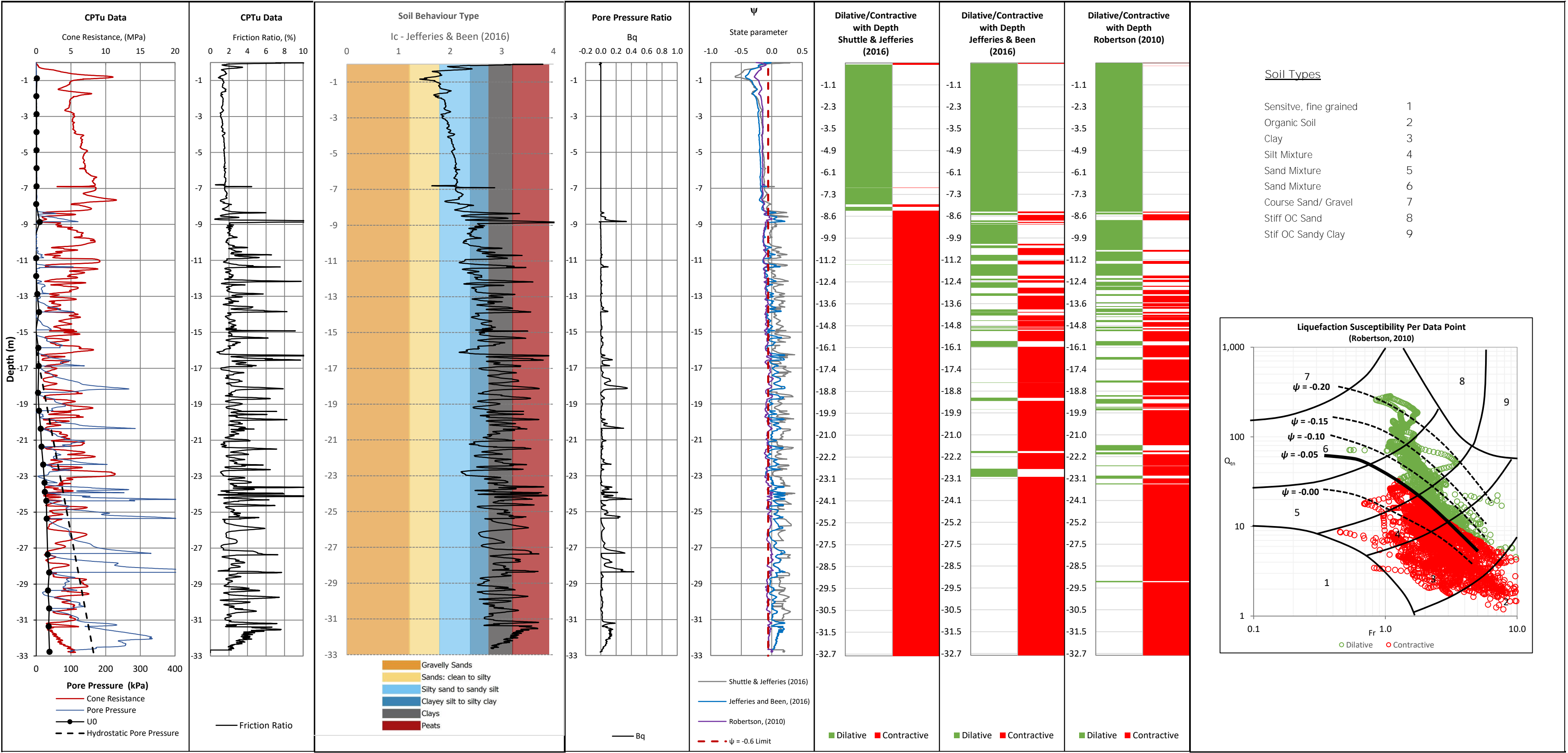
CPTu PC21



## CPTu PC21



PCA2



Pore Pressure Ratio

Bq

-0.20.00.20.40.60.81.0

-1

-3

-5

-7

-9

-11

-13

-15

-17

-19

-21

-23

-25

-27

-29

-31

-33

Bq

$\Psi$

State parameter

-1.0-0.50.00.5

-1

-3

-5

-7

-9

-11

-13

-15

-17

-19

-21

-23

-25

-27

-29

-31

-33

Shuttle & Jefferies (2016)

Jefferies and Been, (2016)

Robertson, (2010)

$\psi = -0.6$  Limit

Dilative/Contractive with Depth Shuttle & Jefferies (2016)

Dilative/Contractive with Depth Jefferies & Been (2016)

Dilative/Contractive with Depth Robertson (2010)

Dilative

Contractive

Dilative

Contractive

Dilative

Contractive

Soil Types

Sensitive, fine grained

1

Organic Soil

2

Clay

3

Silt Mixture

4

Sand Mixture

5

Sand Mixture

6

Course Sand/ Gravel

7

Stiff OC Sand

8

Stif OC Sandy Clay

9

Liquefaction Susceptibility Per Data Point (Robertson, 2010)

1,000

100

10

1

$\psi = -0.20$

$\psi = -0.15$

$\psi = -0.10$

$\psi = -0.05$

$\psi = -0.00$

7

6

5

1

8

9

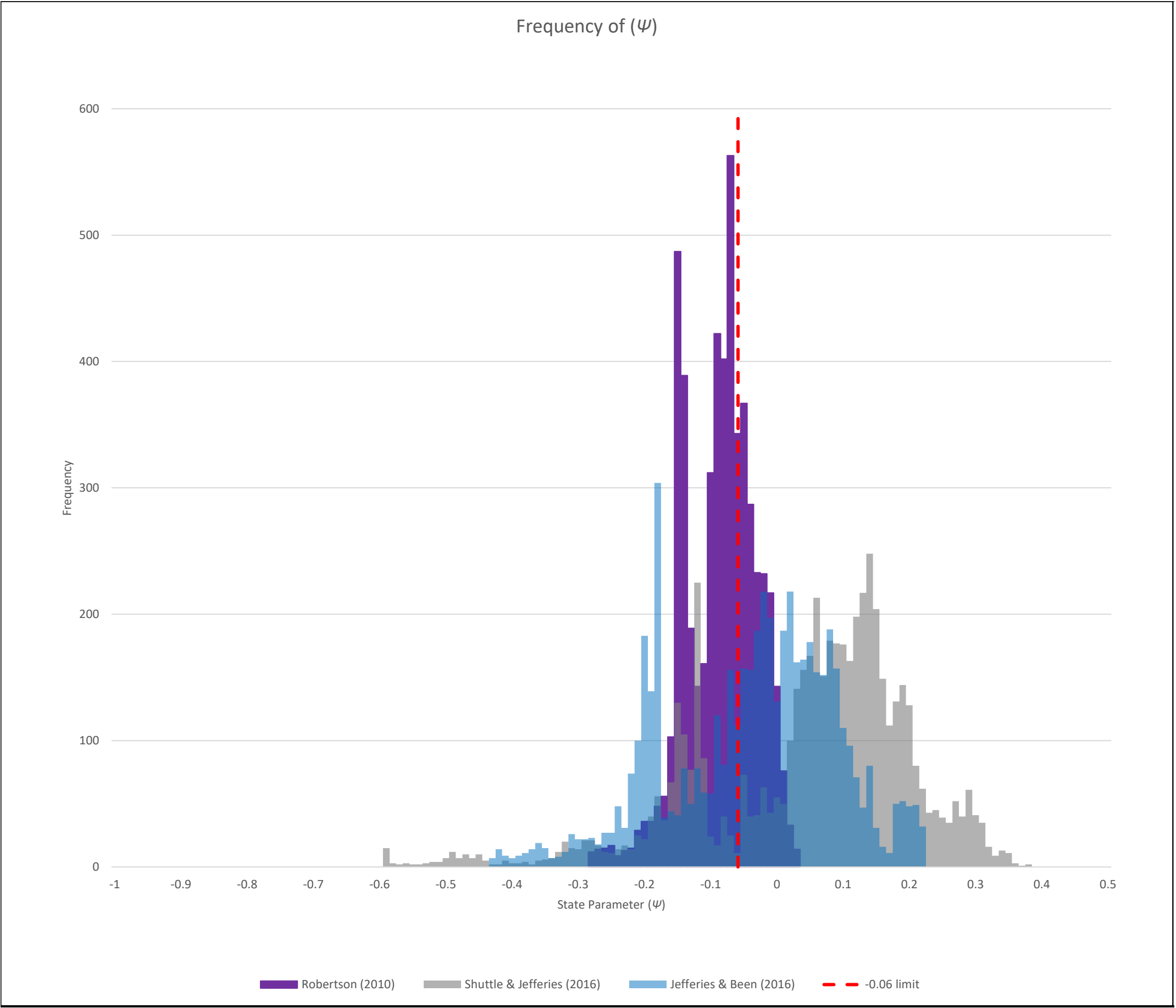
$Q_{tn}$

$F_r$

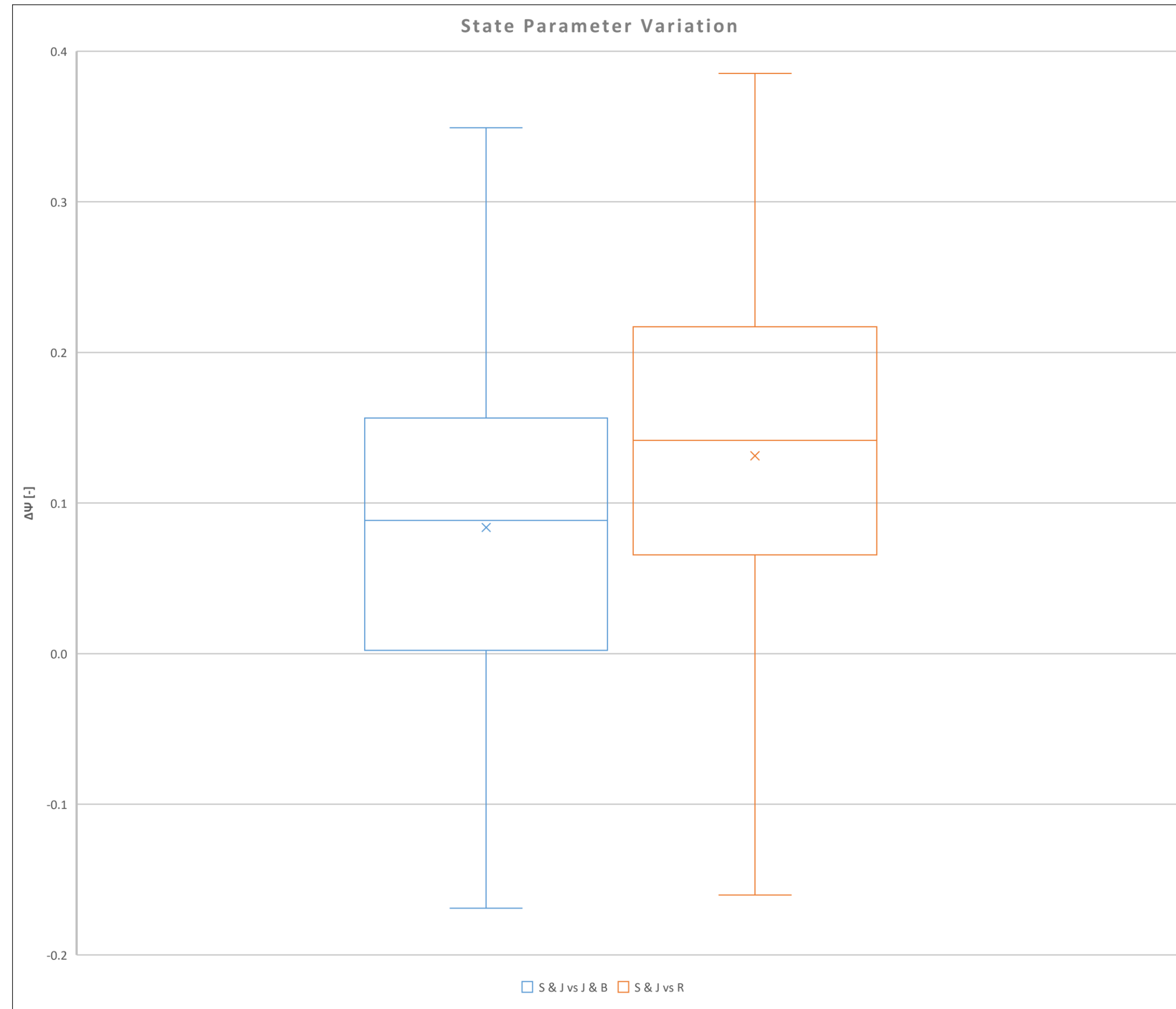
Dilative

Contractive

PCA2

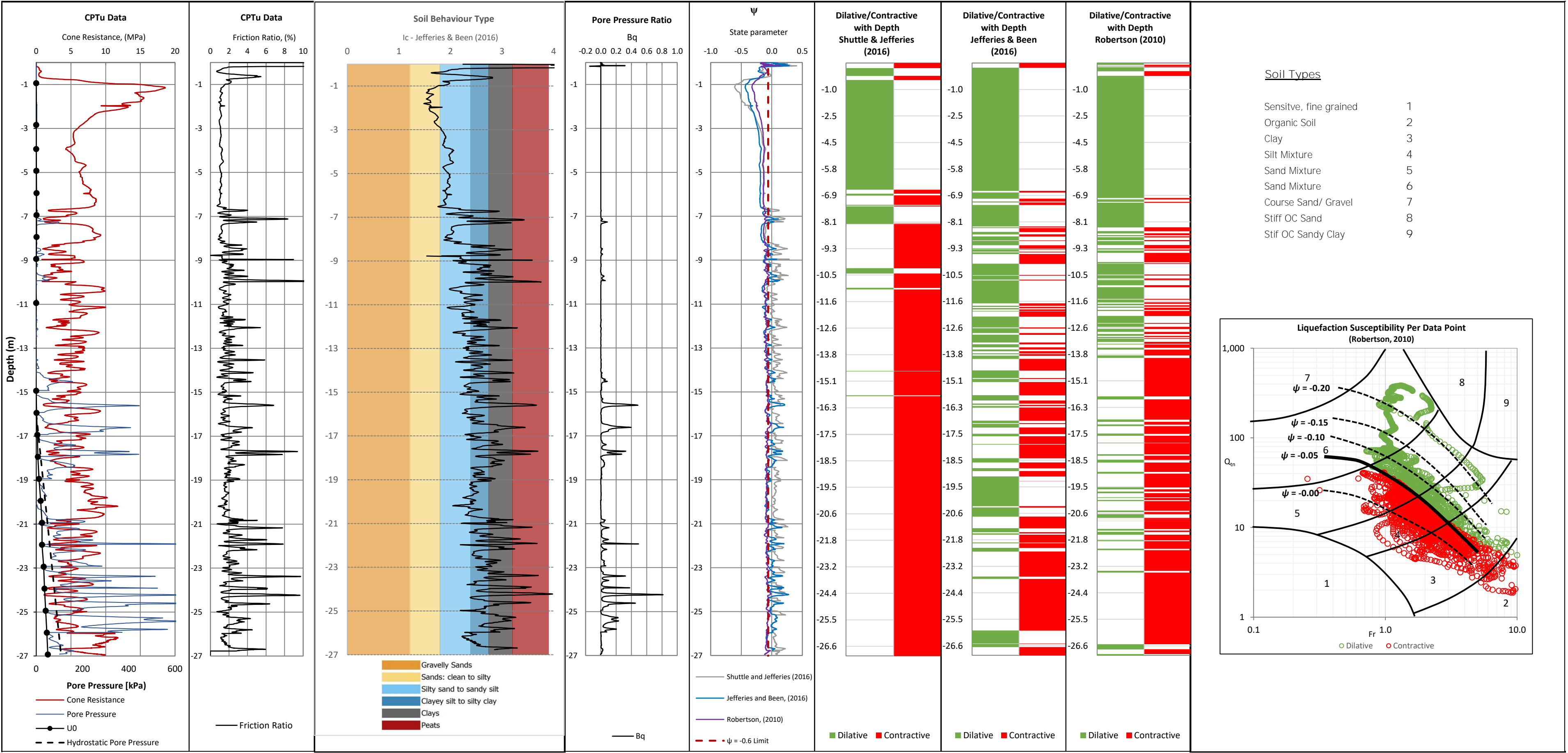


## PCA2

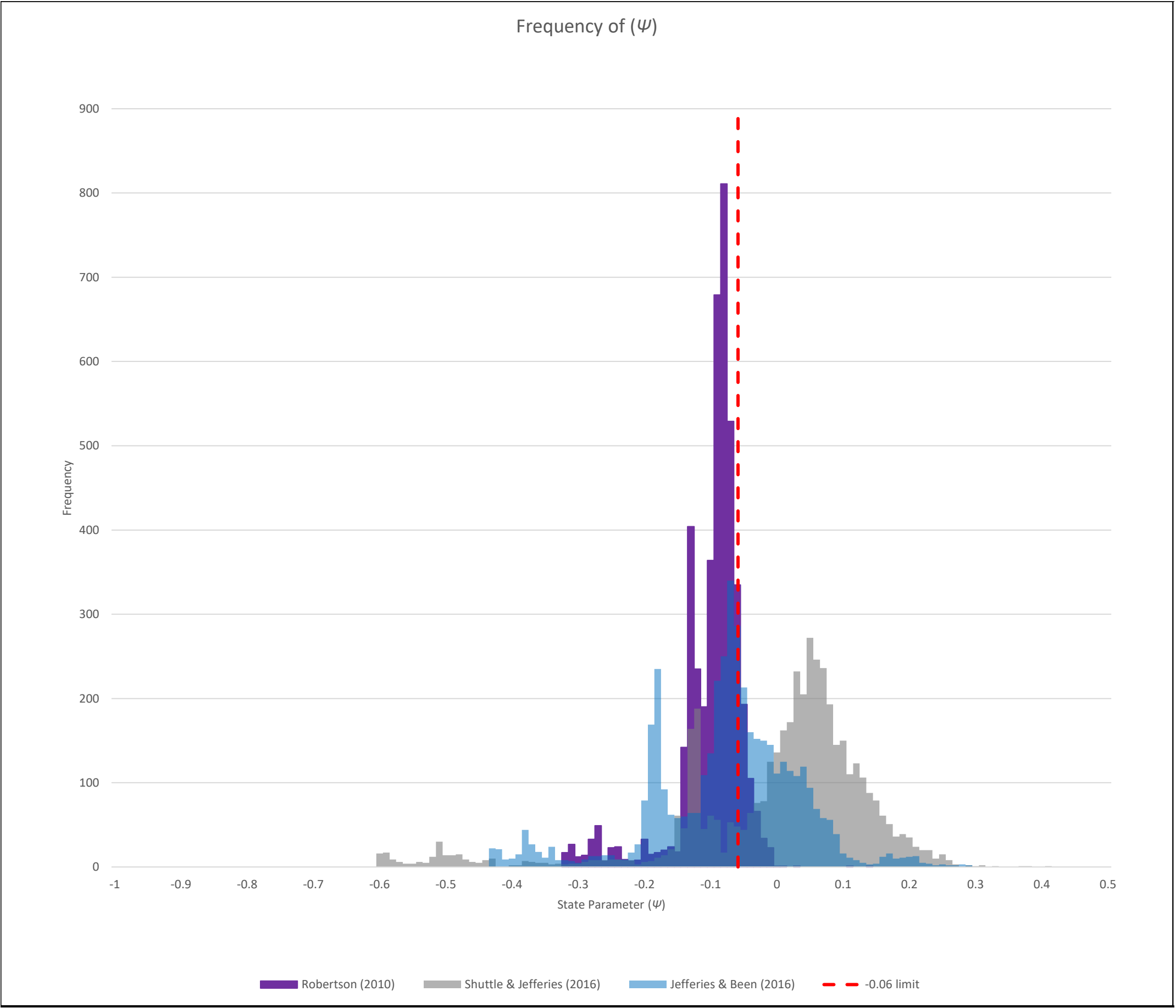




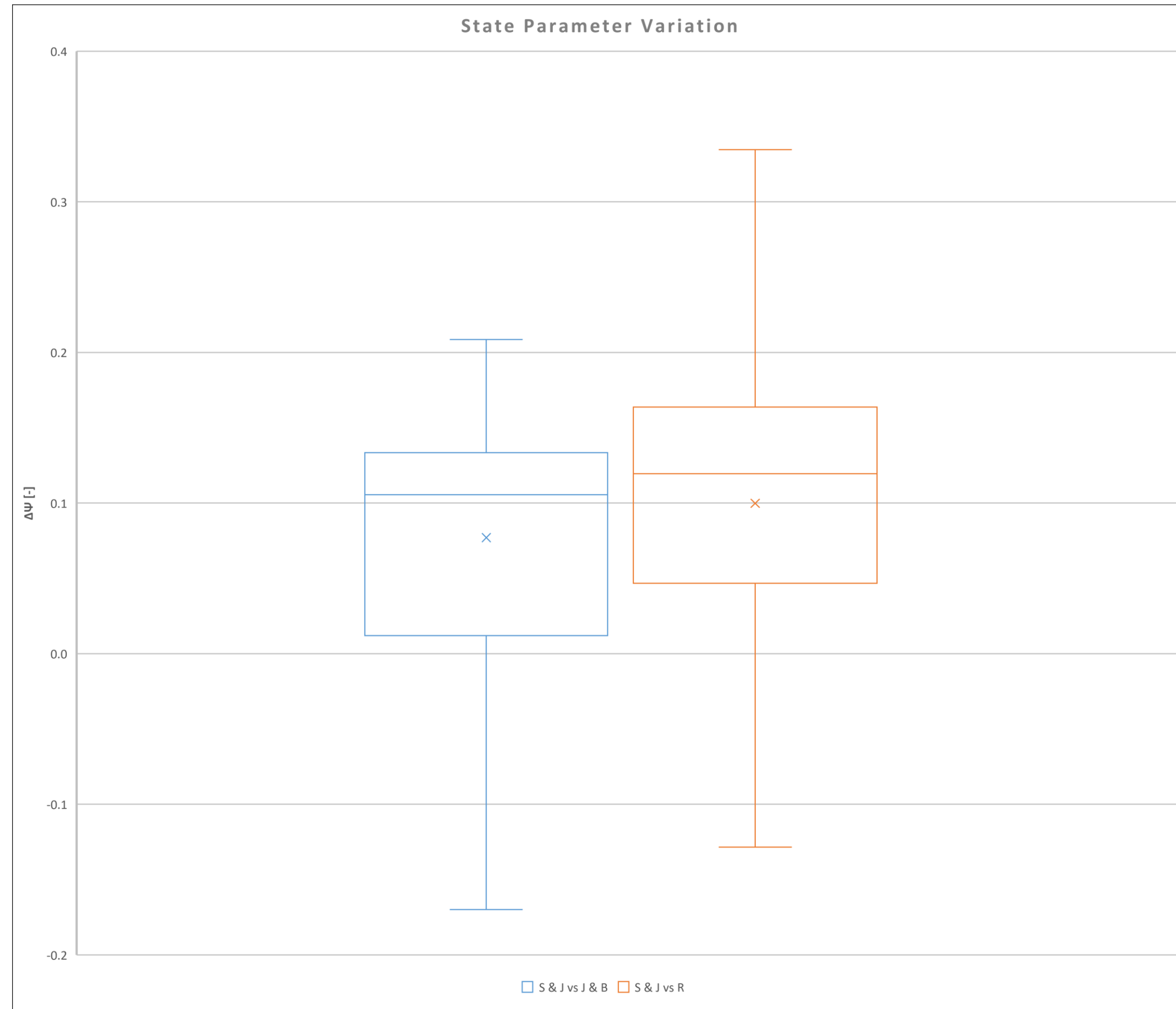
PCA3



PCA3

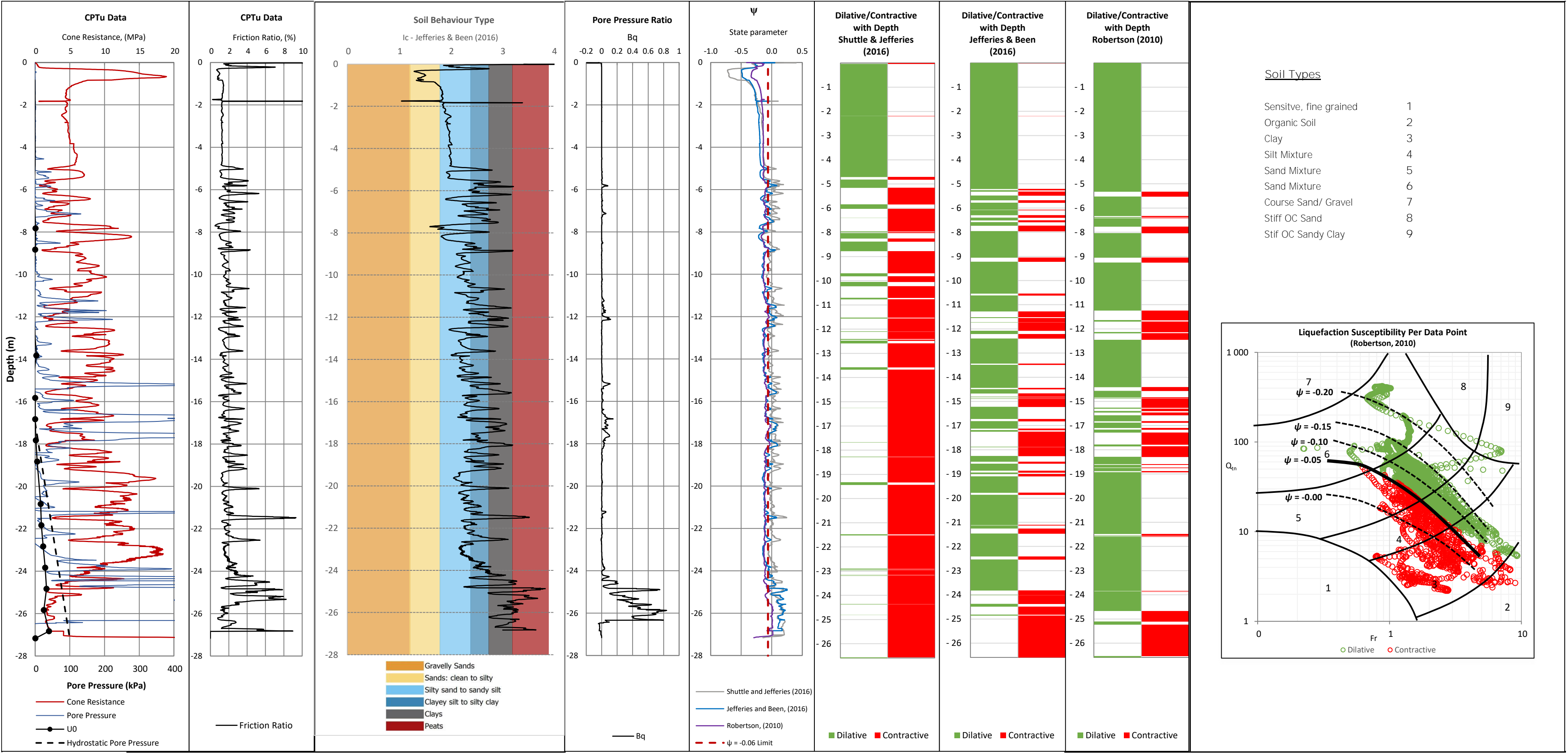


# PCA3

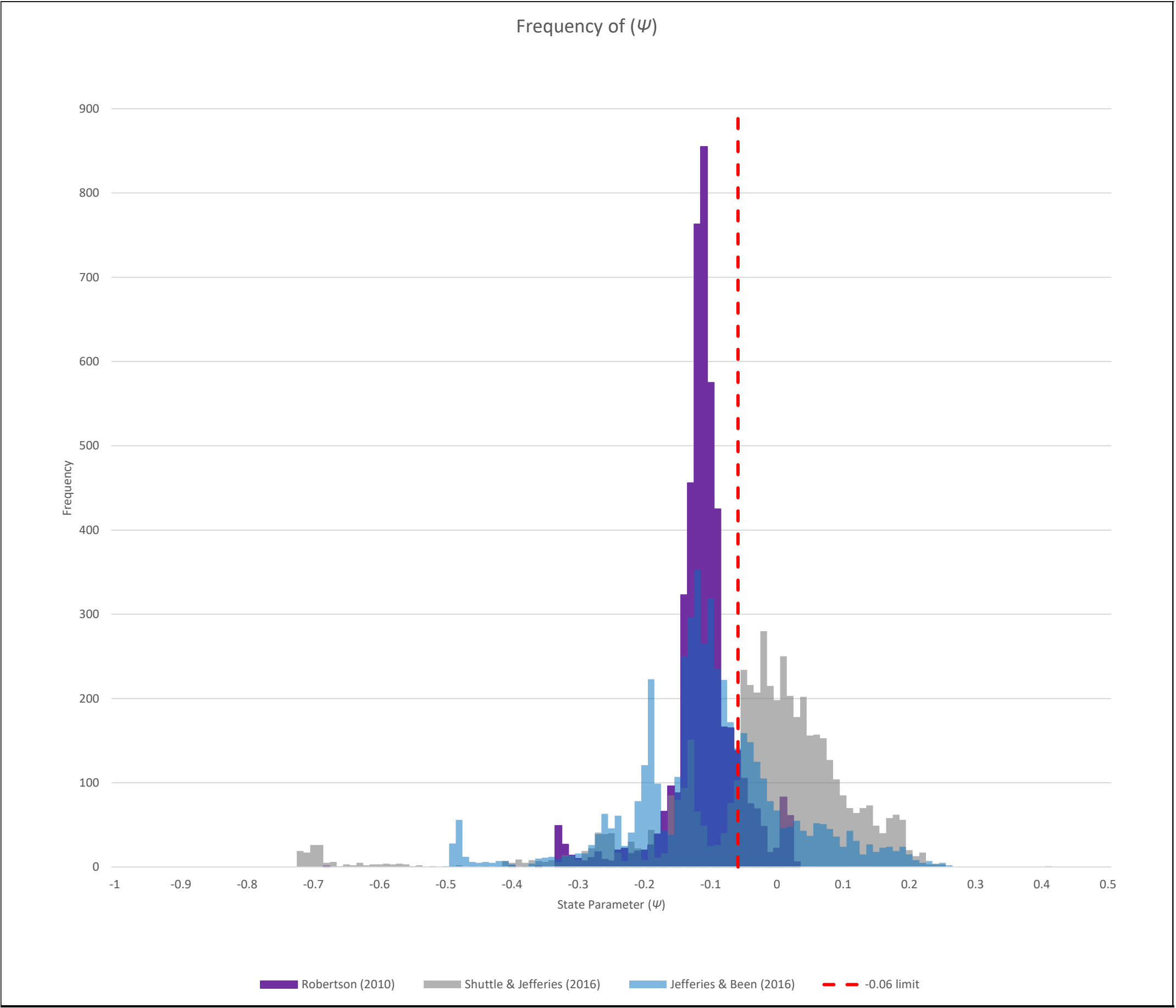


## **Appendix B: CPTu Interpretation – Monitoring Line B**

CPTu PC18

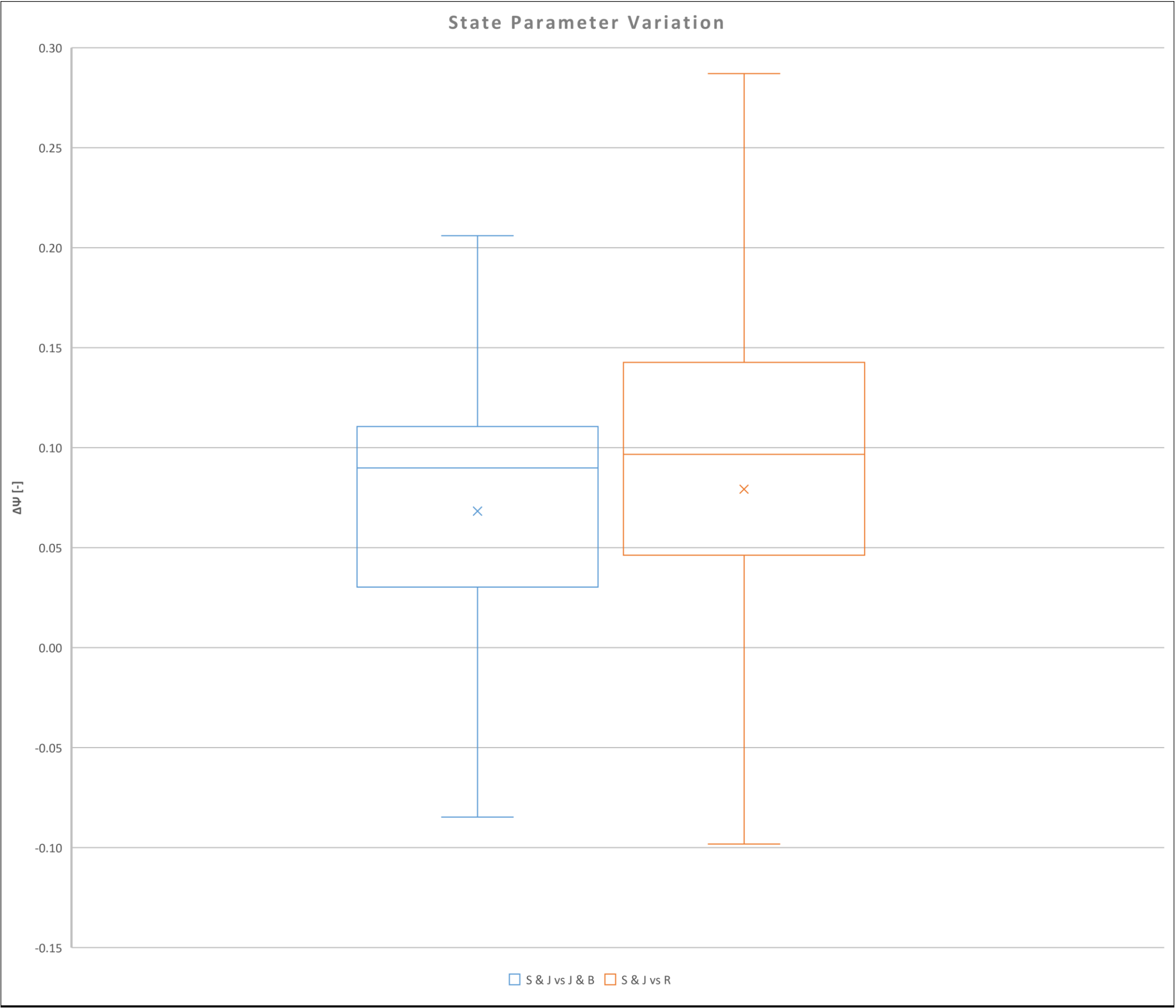


CPTu PC18

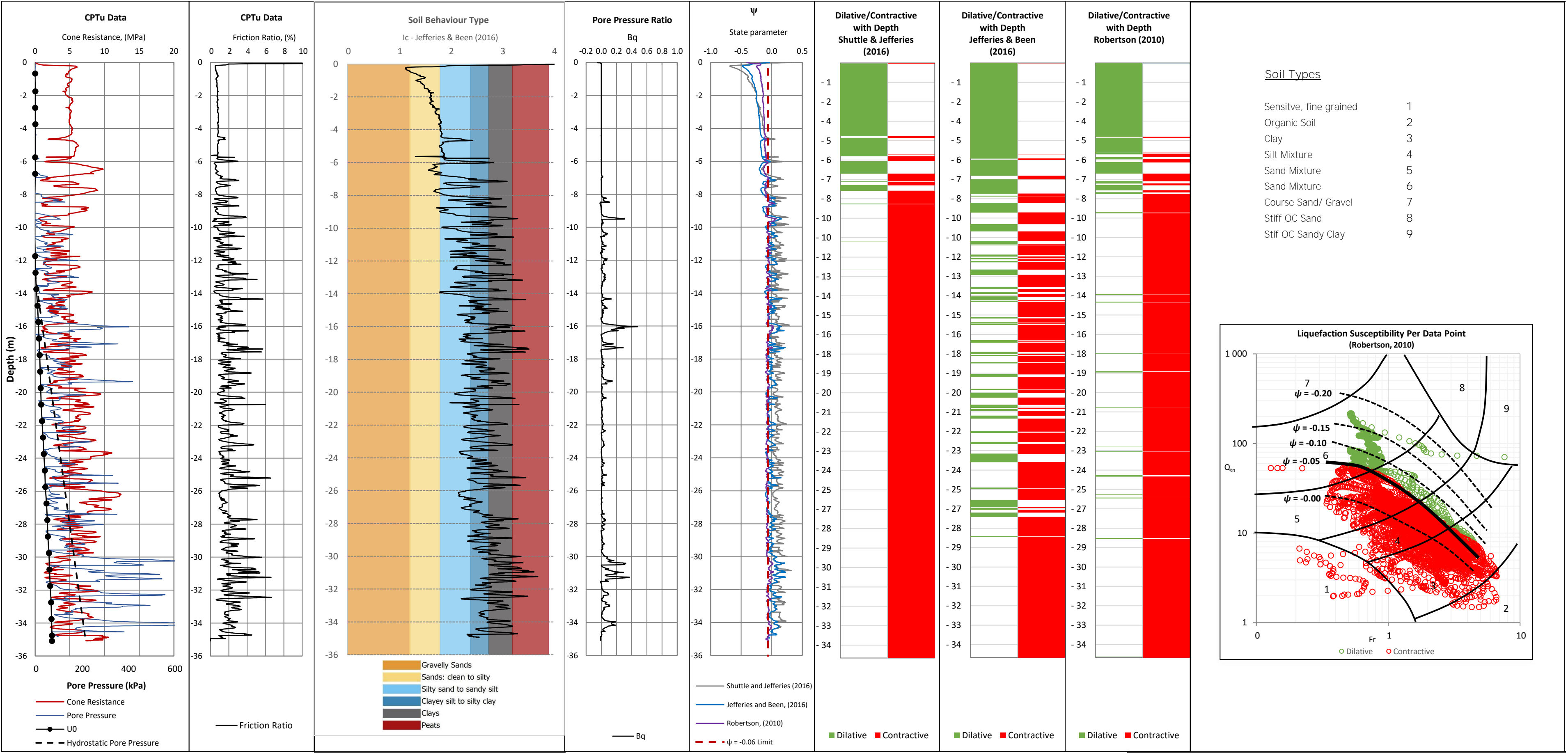




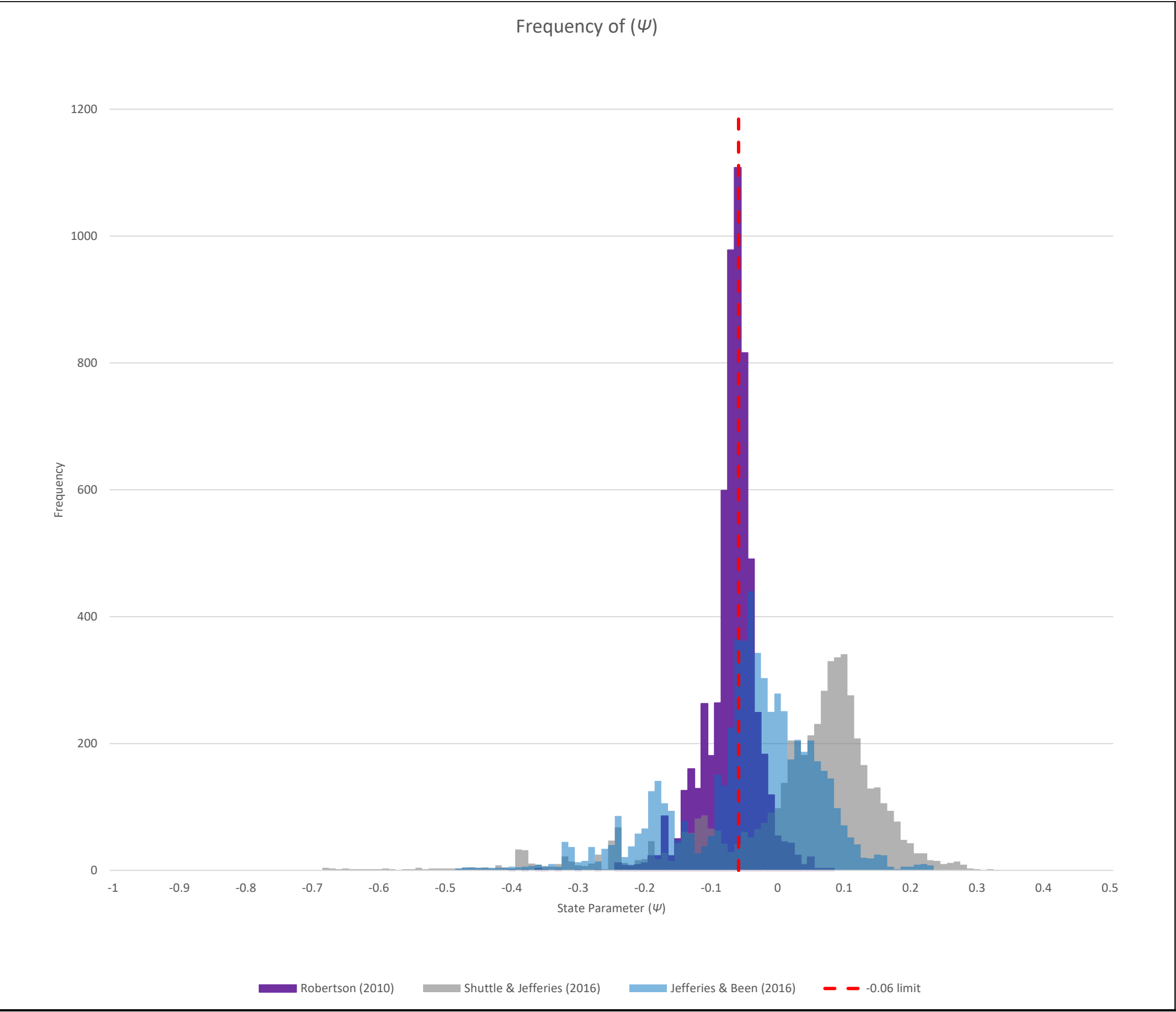
CPTu PC18



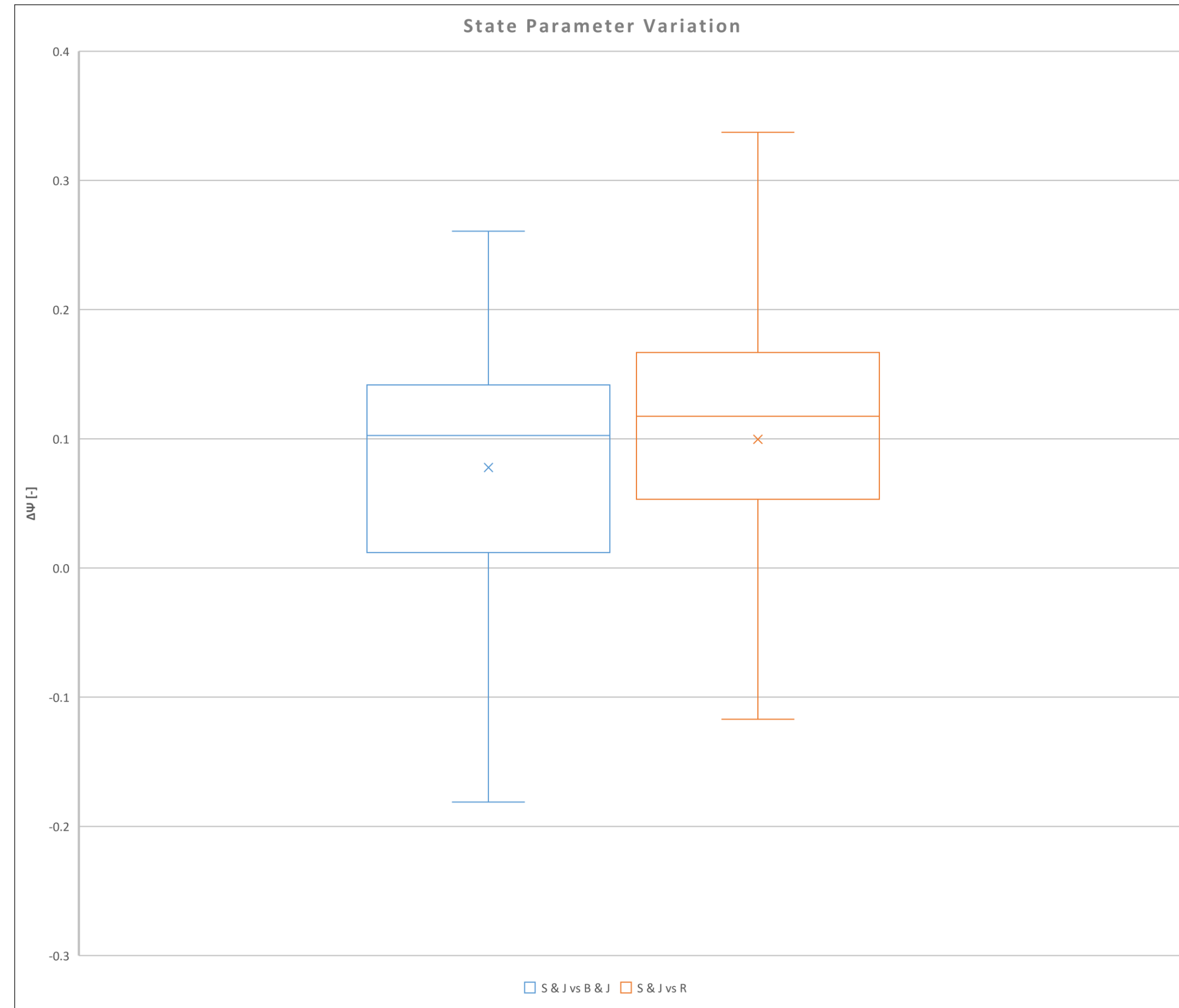
CPTu PC19



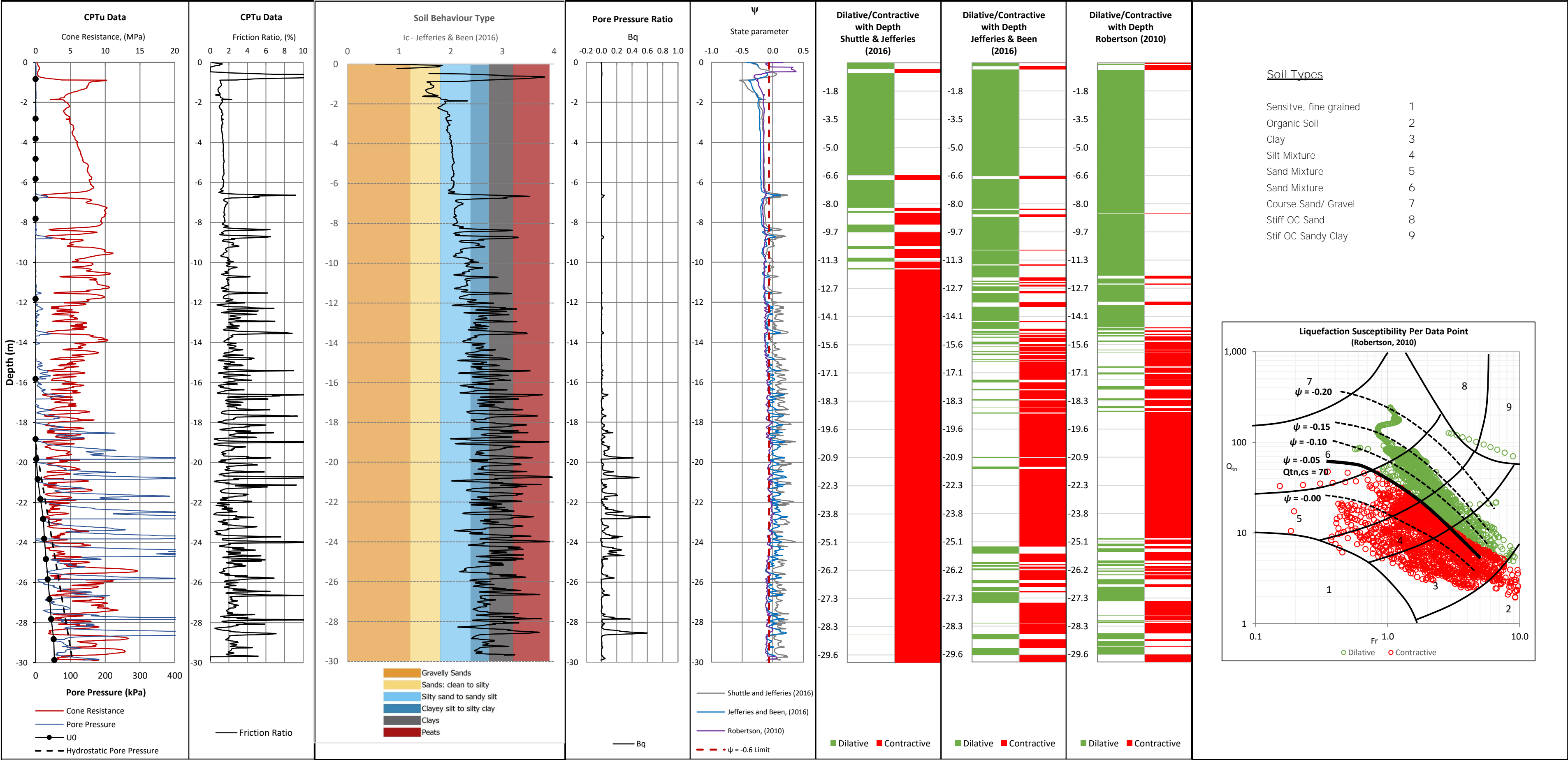
CPTu PC19



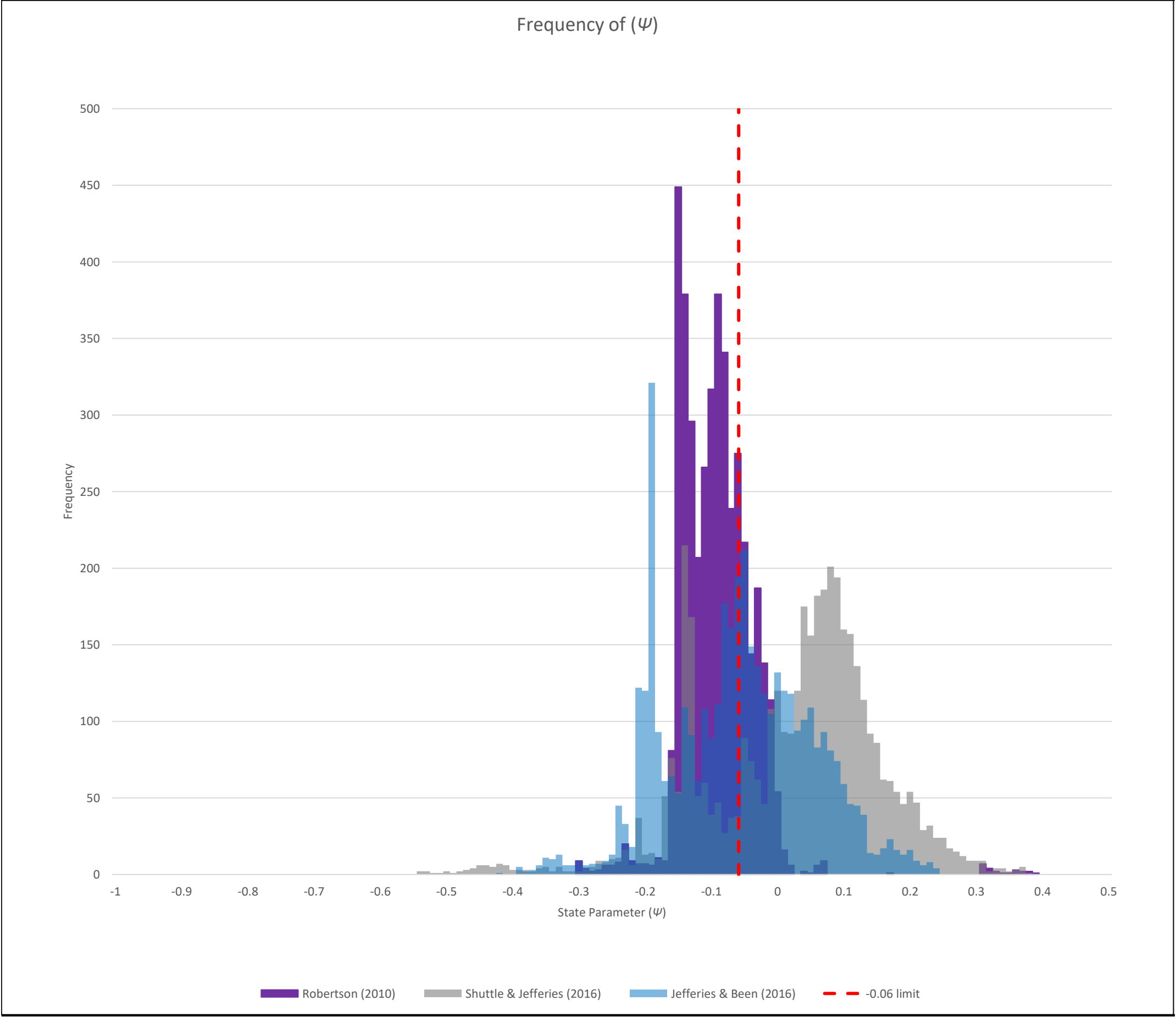
## CPTu PC19



PCB2

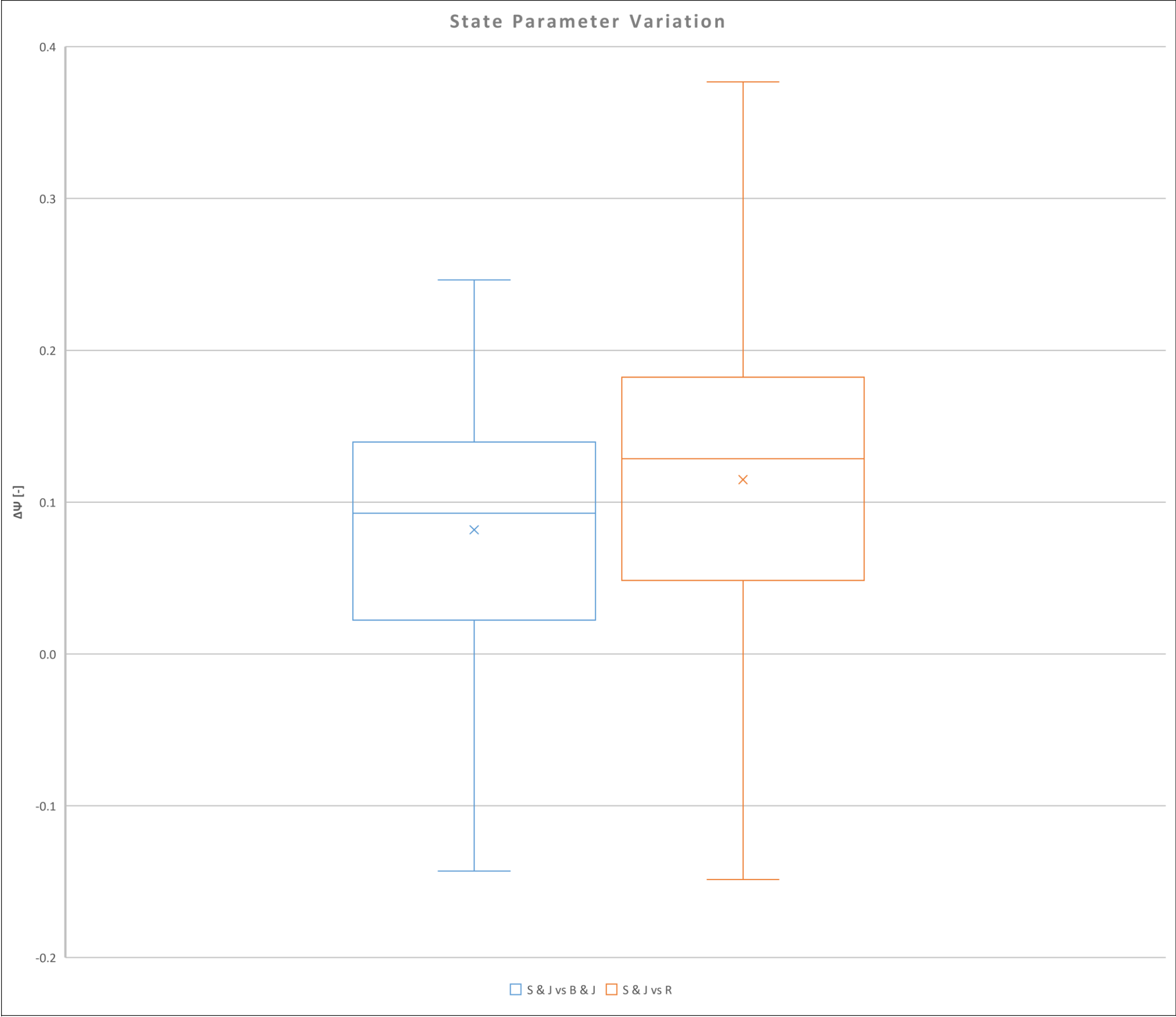


PCB2

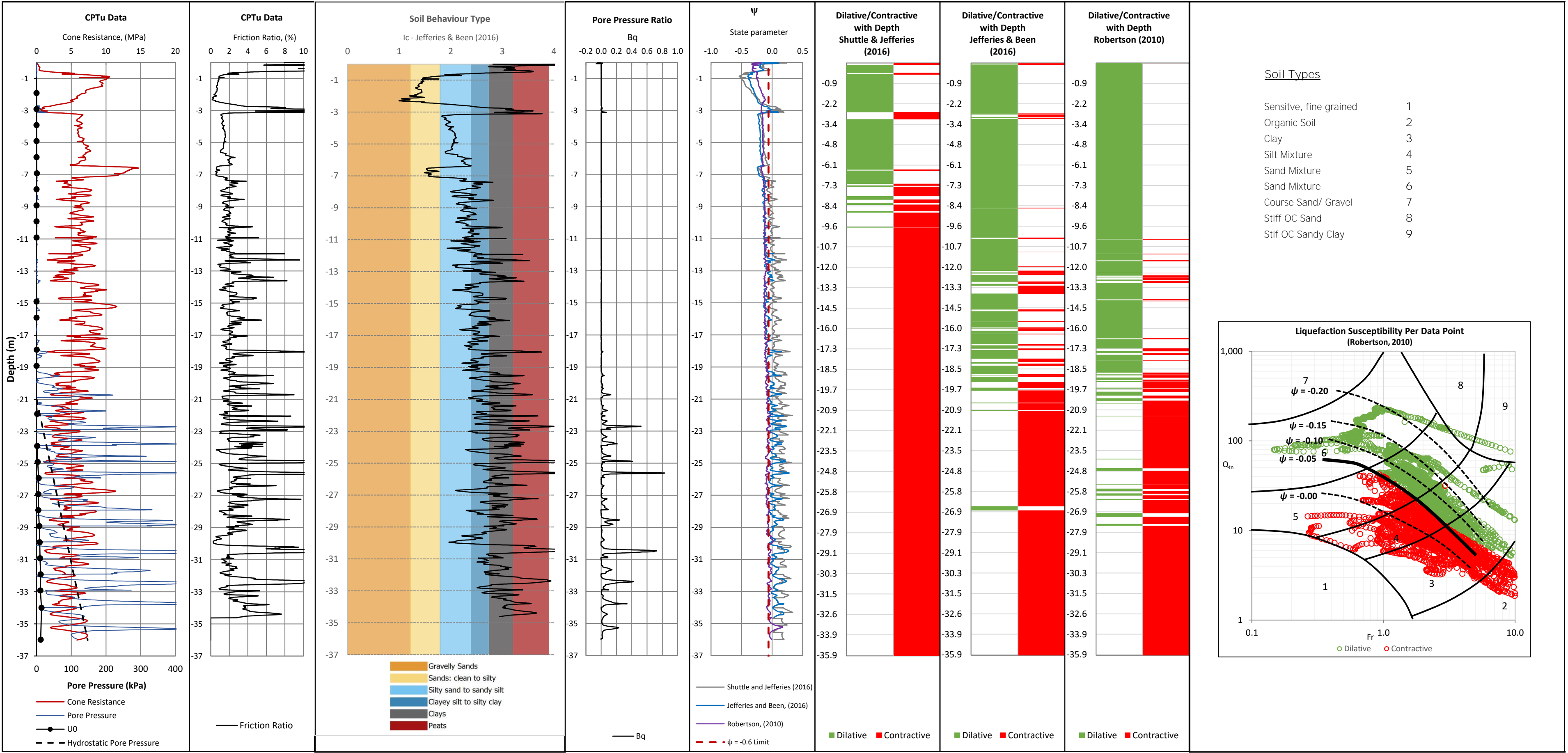




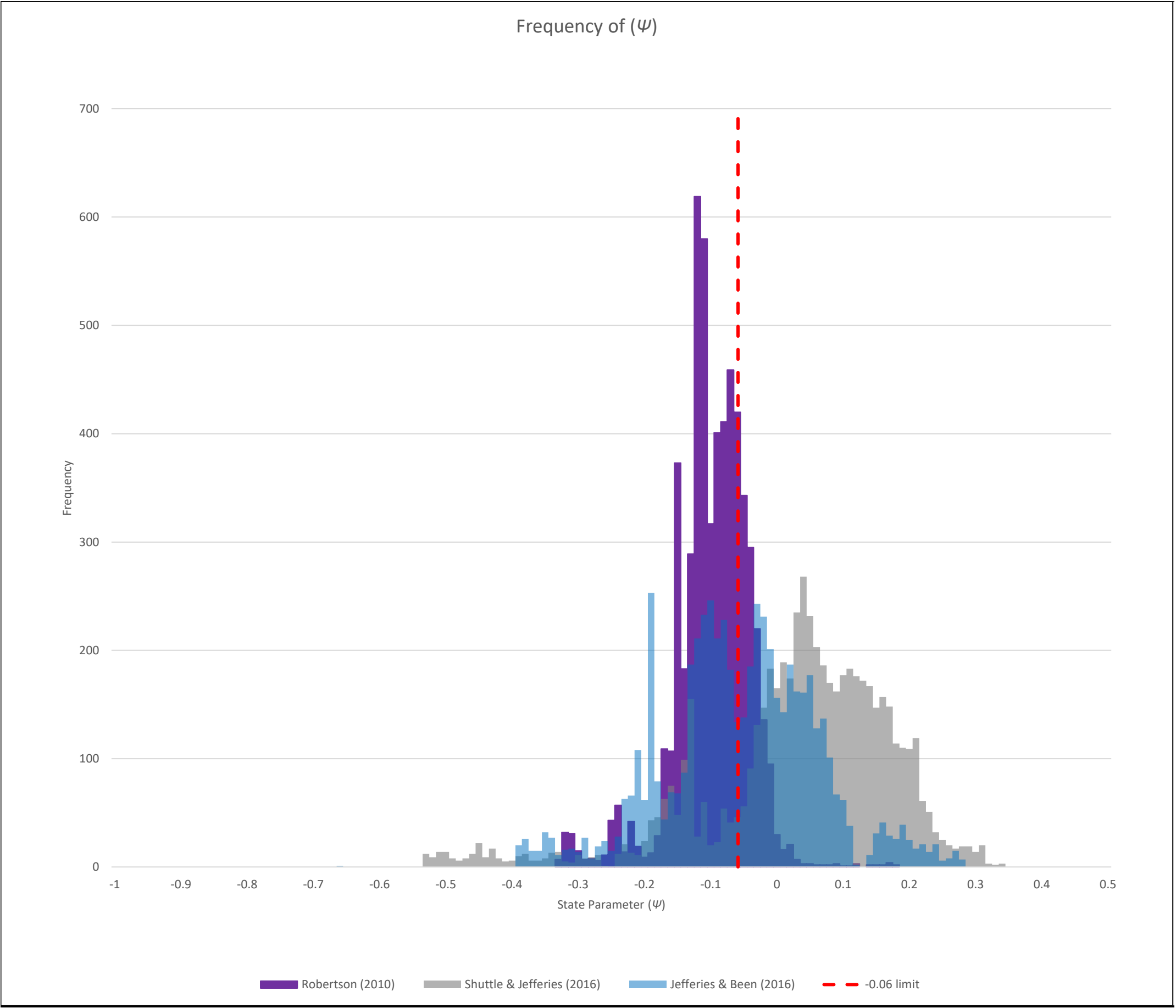
PCB2

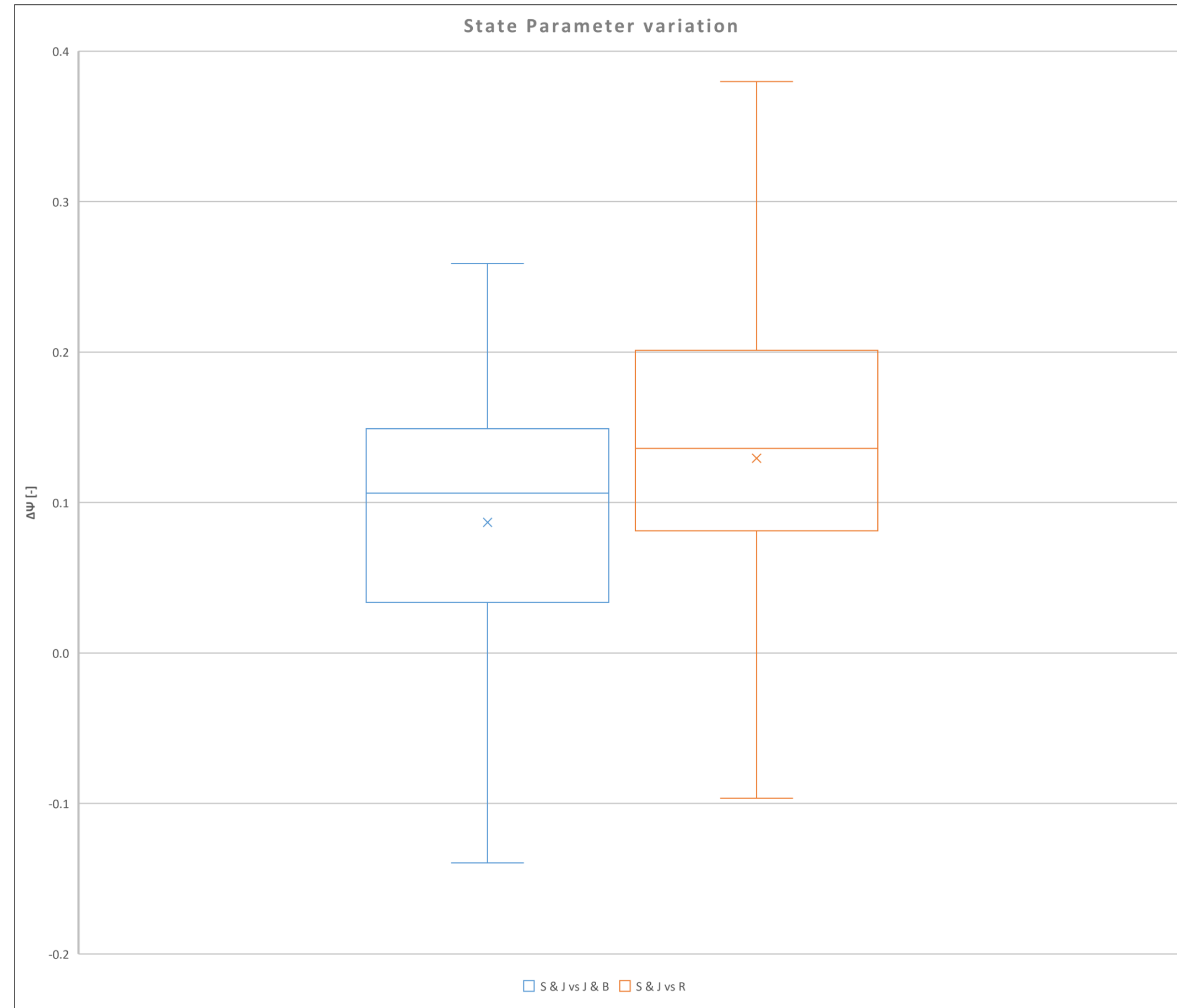


PCB3

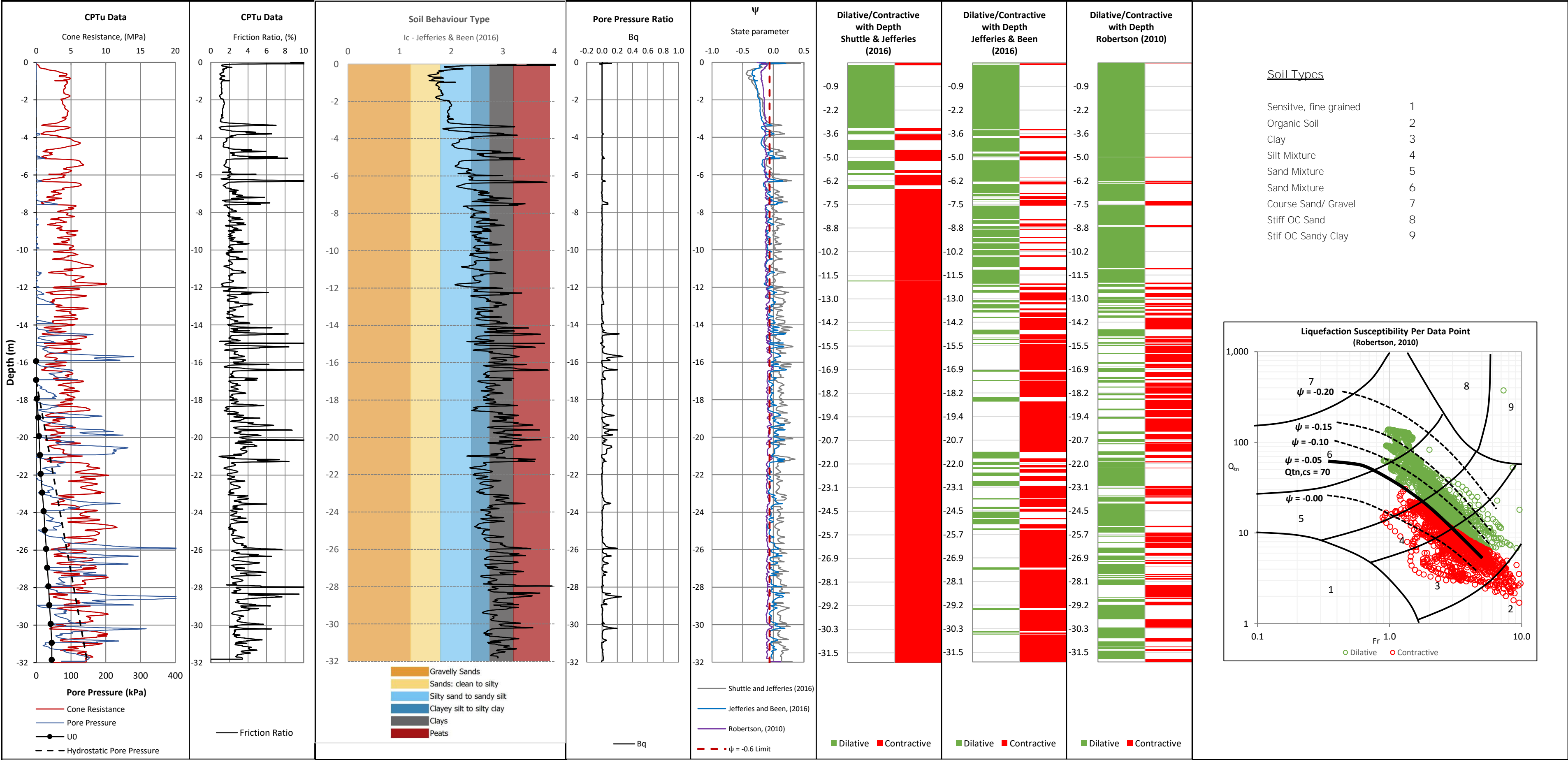


PCB3

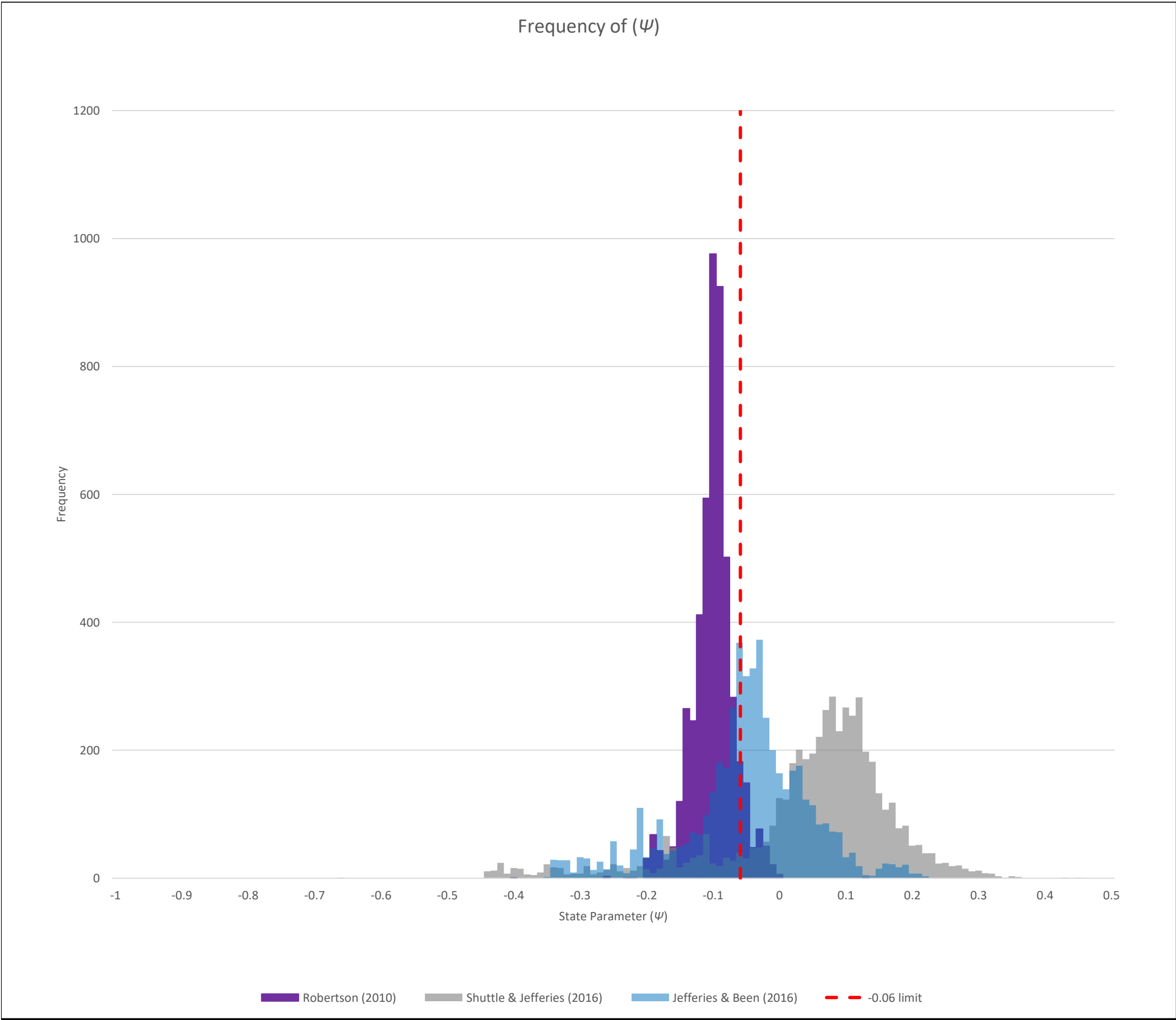


**PCB3**

PCB4

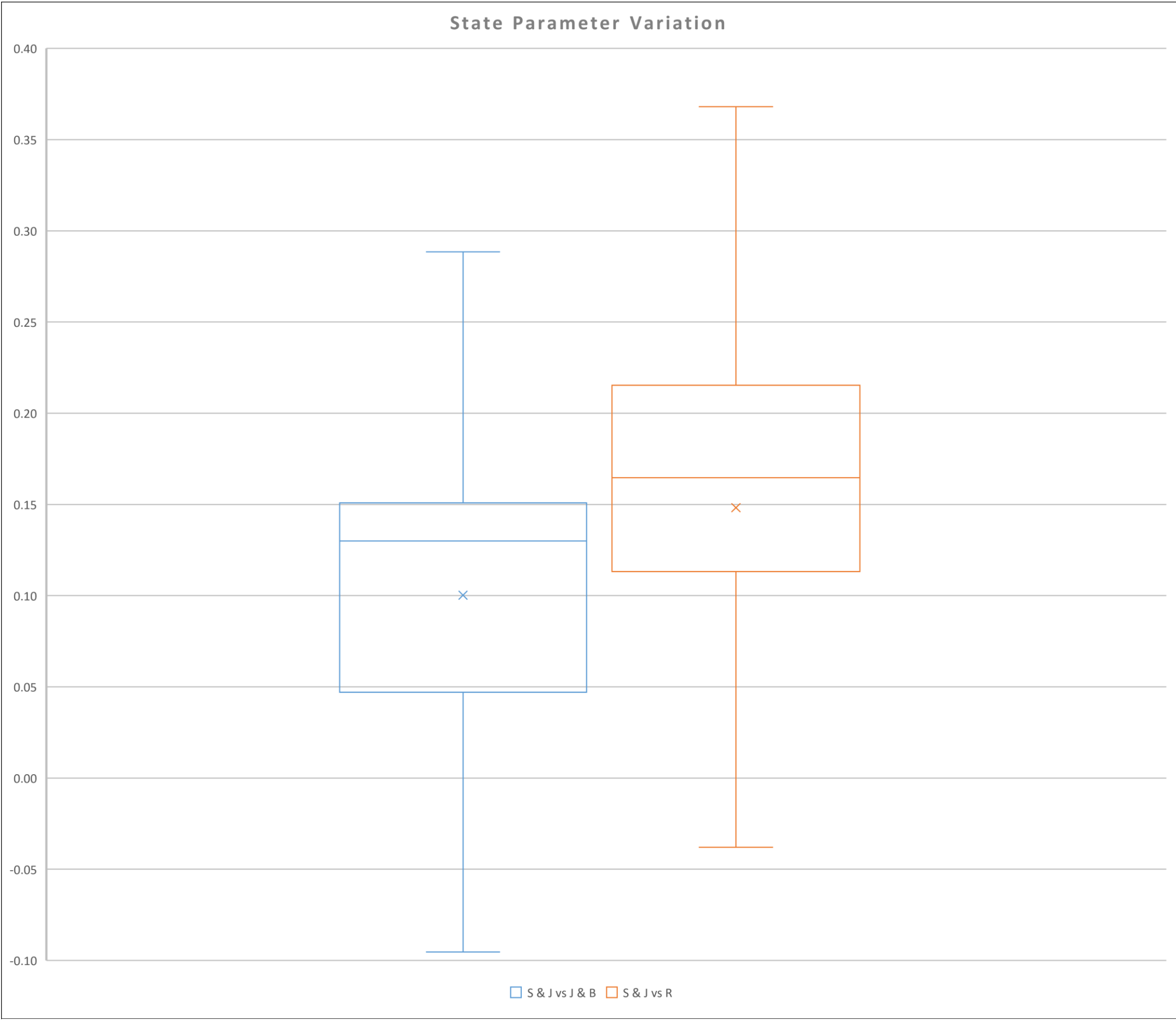


PCB4

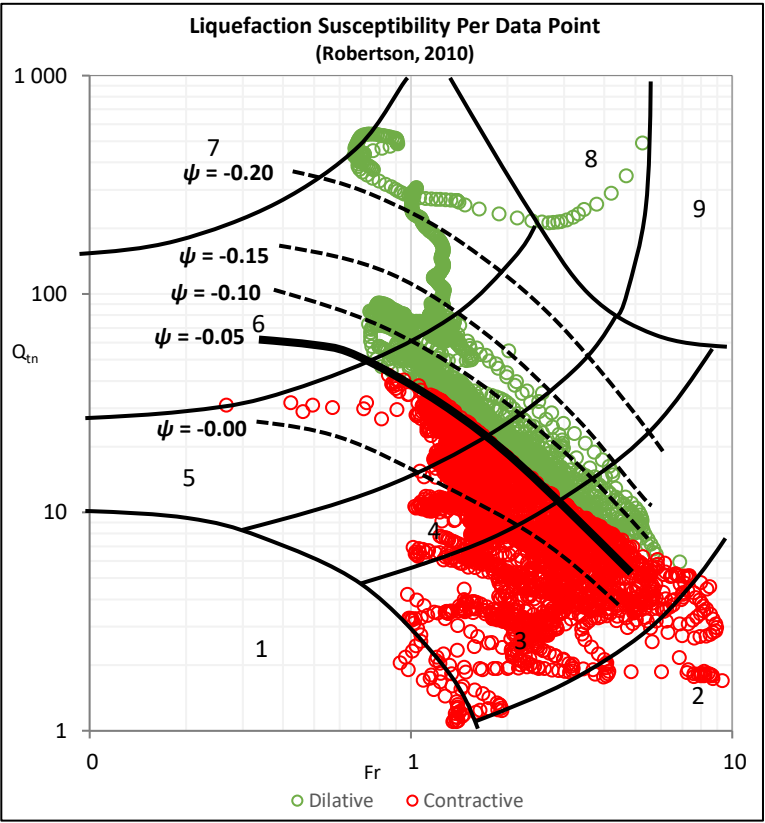




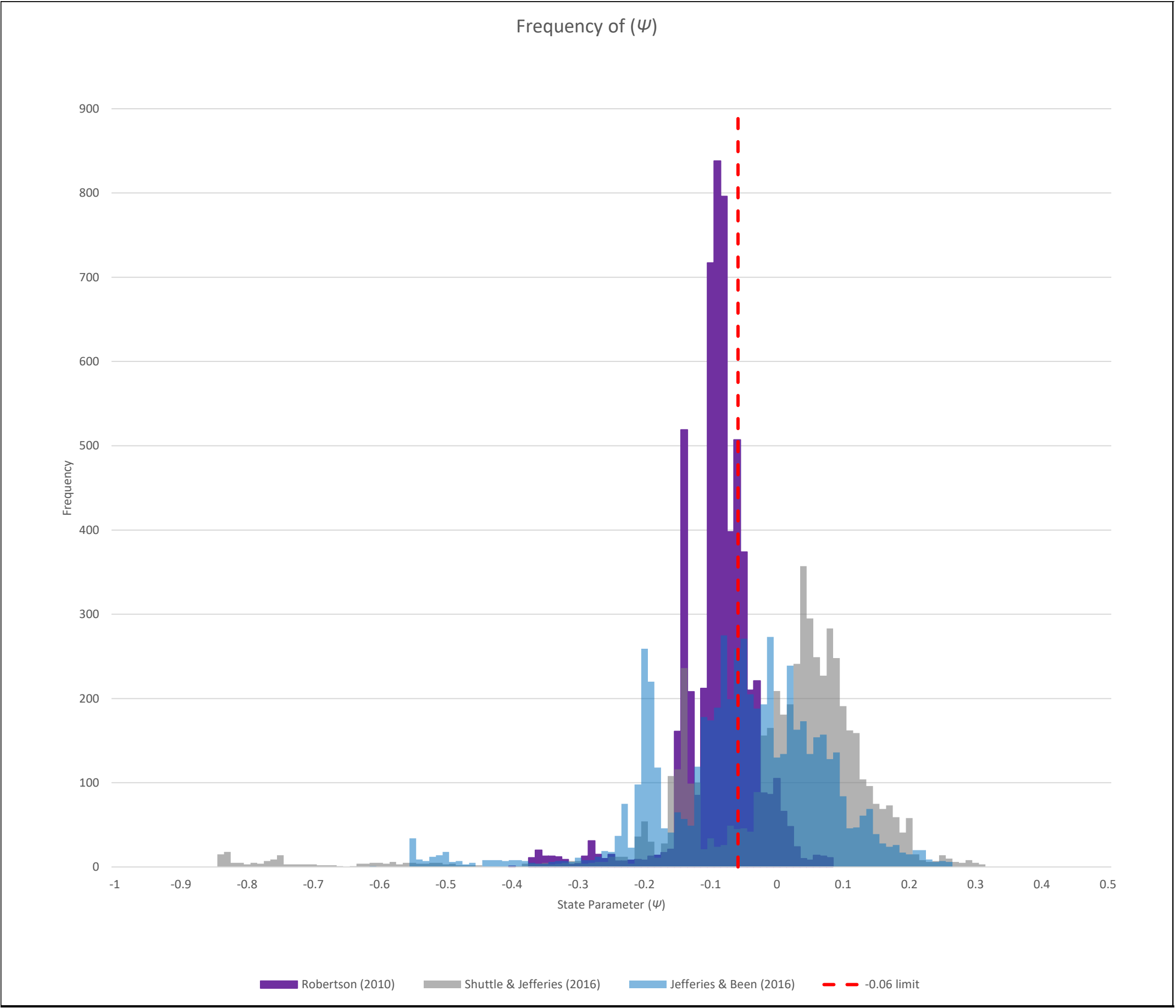
PCB4



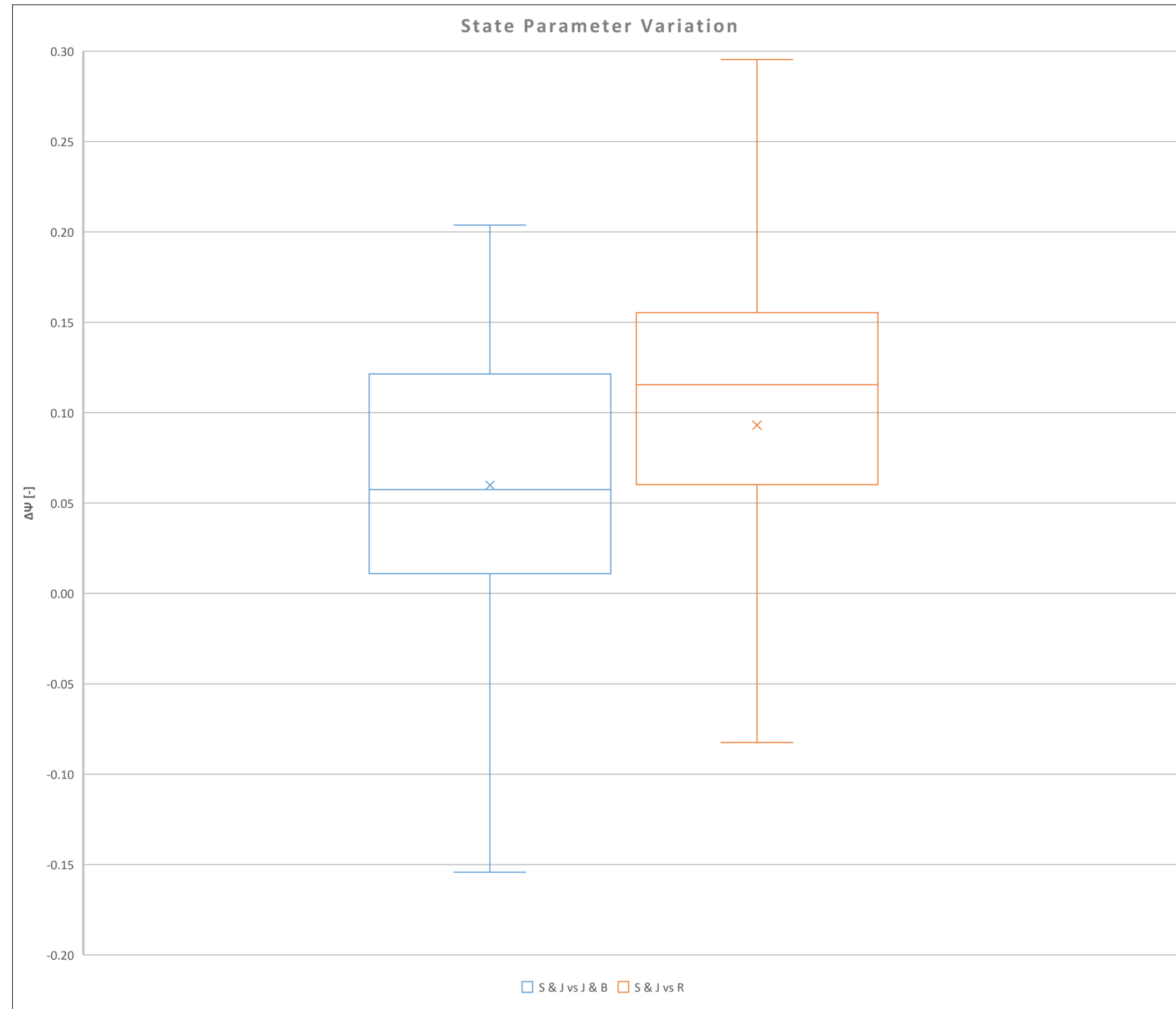
## **Appendix C: CPTu Interpretation – Monitoring Line C**



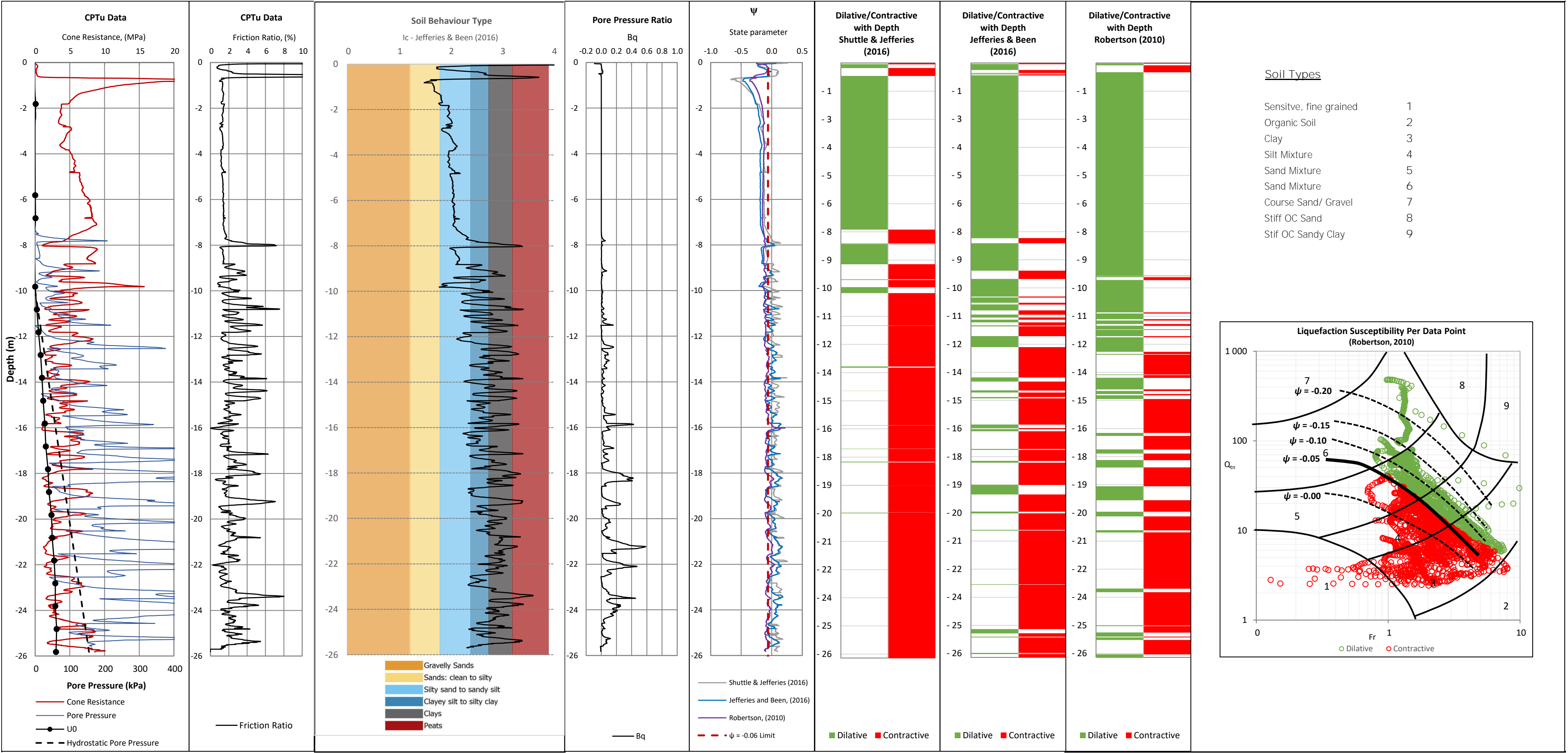
CPTu PC15



# CPTu PC15



CPTu PC16



Dilative/Contractive with Depth

Shuttle & Jefferies (2016)

Dilative

Contractive

Dilative/Contractive with Depth

Jefferies & Been (2016)

Dilative

Contractive

Dilative/Contractive with Depth

Robertson (2010)

Dilative

Contractive

Soil Types

Sensitive, fine grained

1

Organic Soil

2

Clay

3

Silt Mixture

4

Sand Mixture

5

Sand Mixture

6

Course Sand/ Gravel

7

Stiff OC Sand

8

Stif OC Sandy Clay

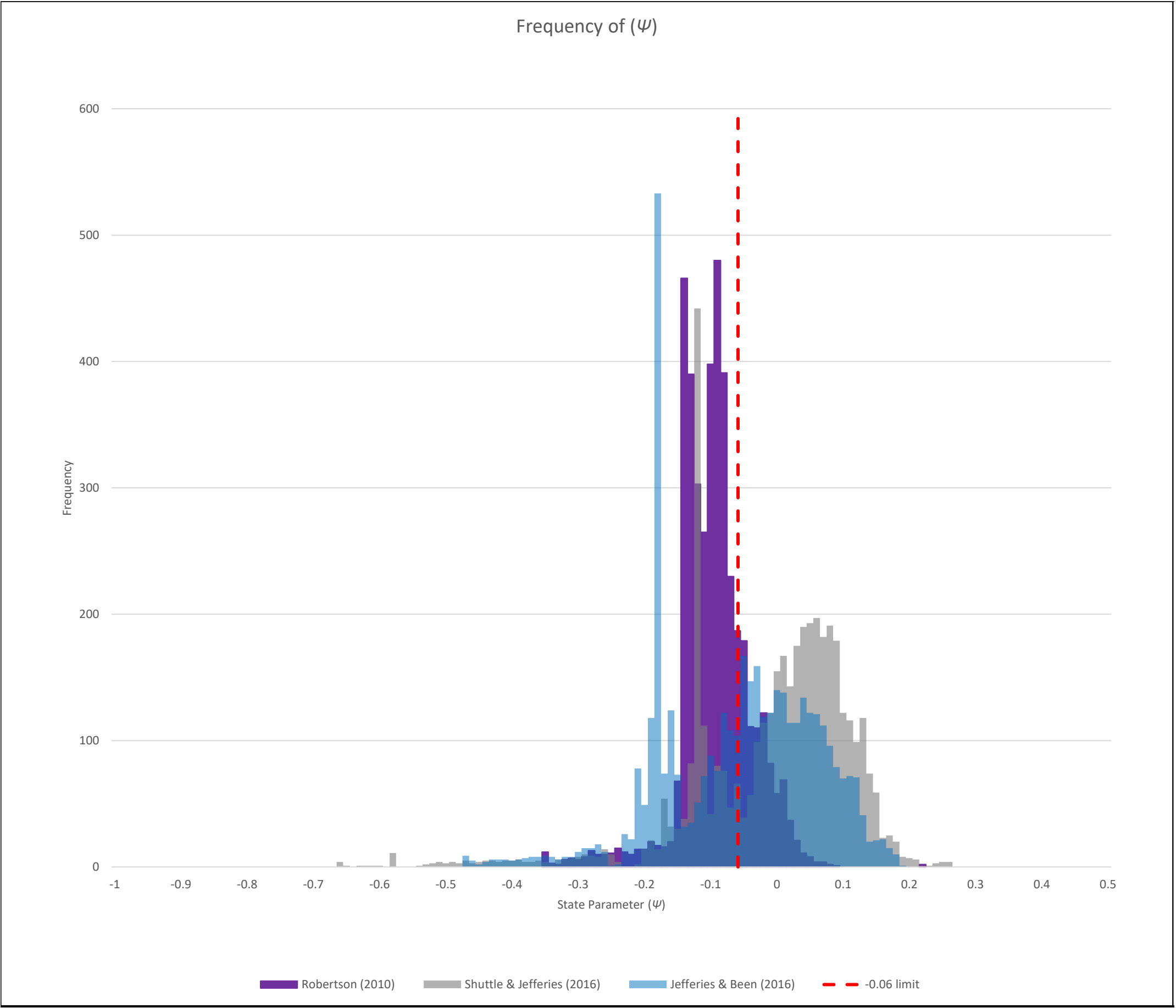
9

Liquefaction Susceptibility Per Data Point

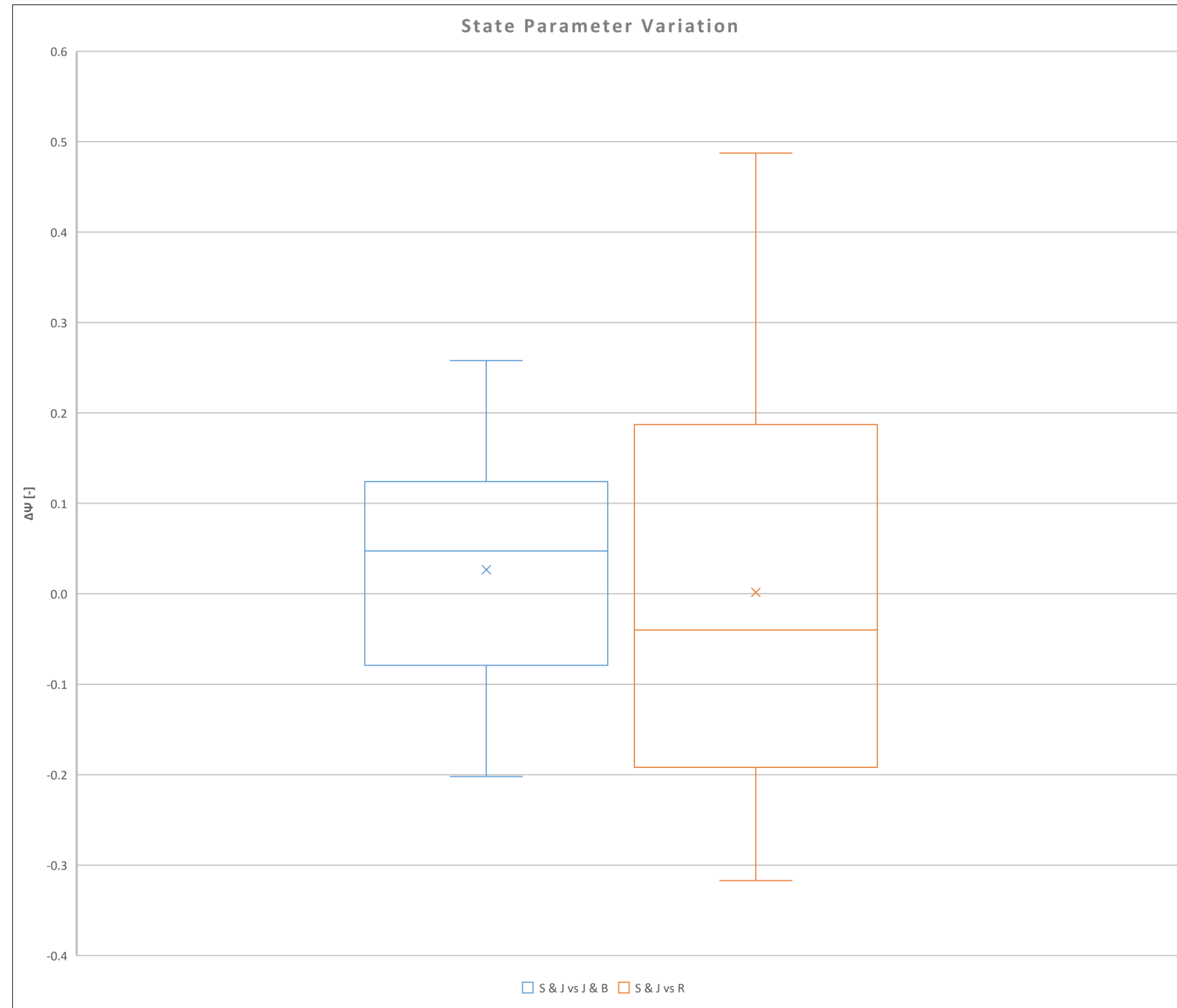
(Robertson, 2010)



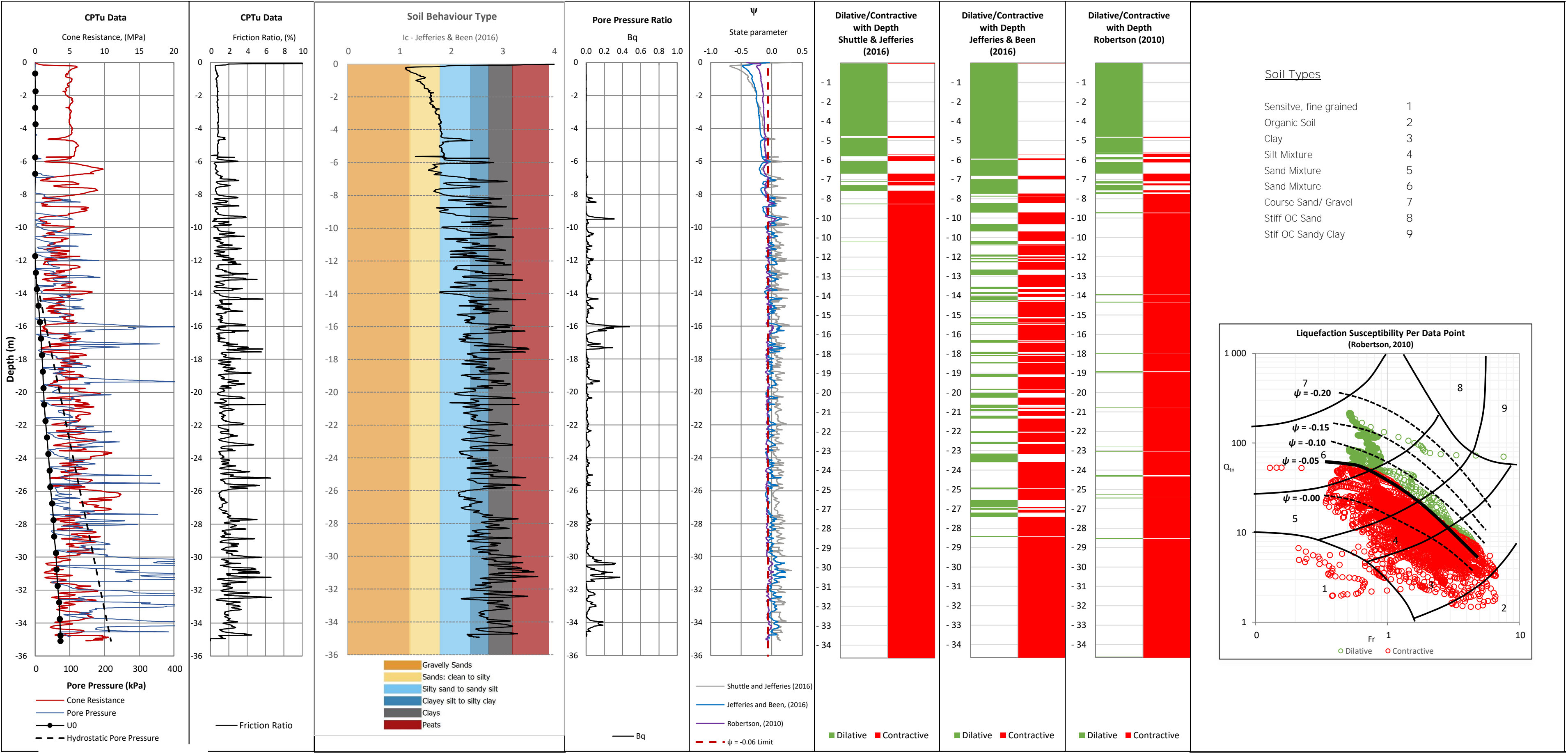
CPTu PC16



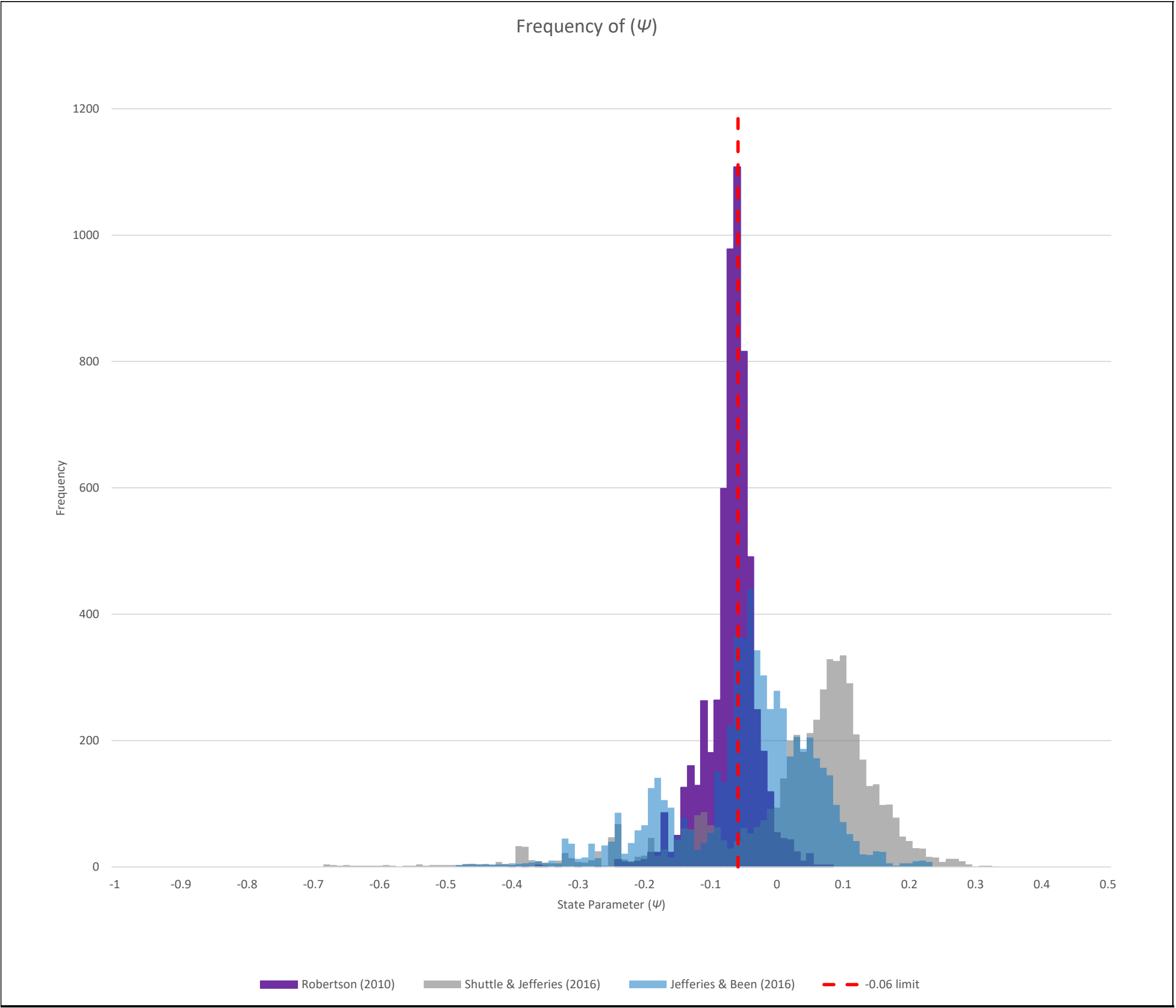
# CPTu PC16



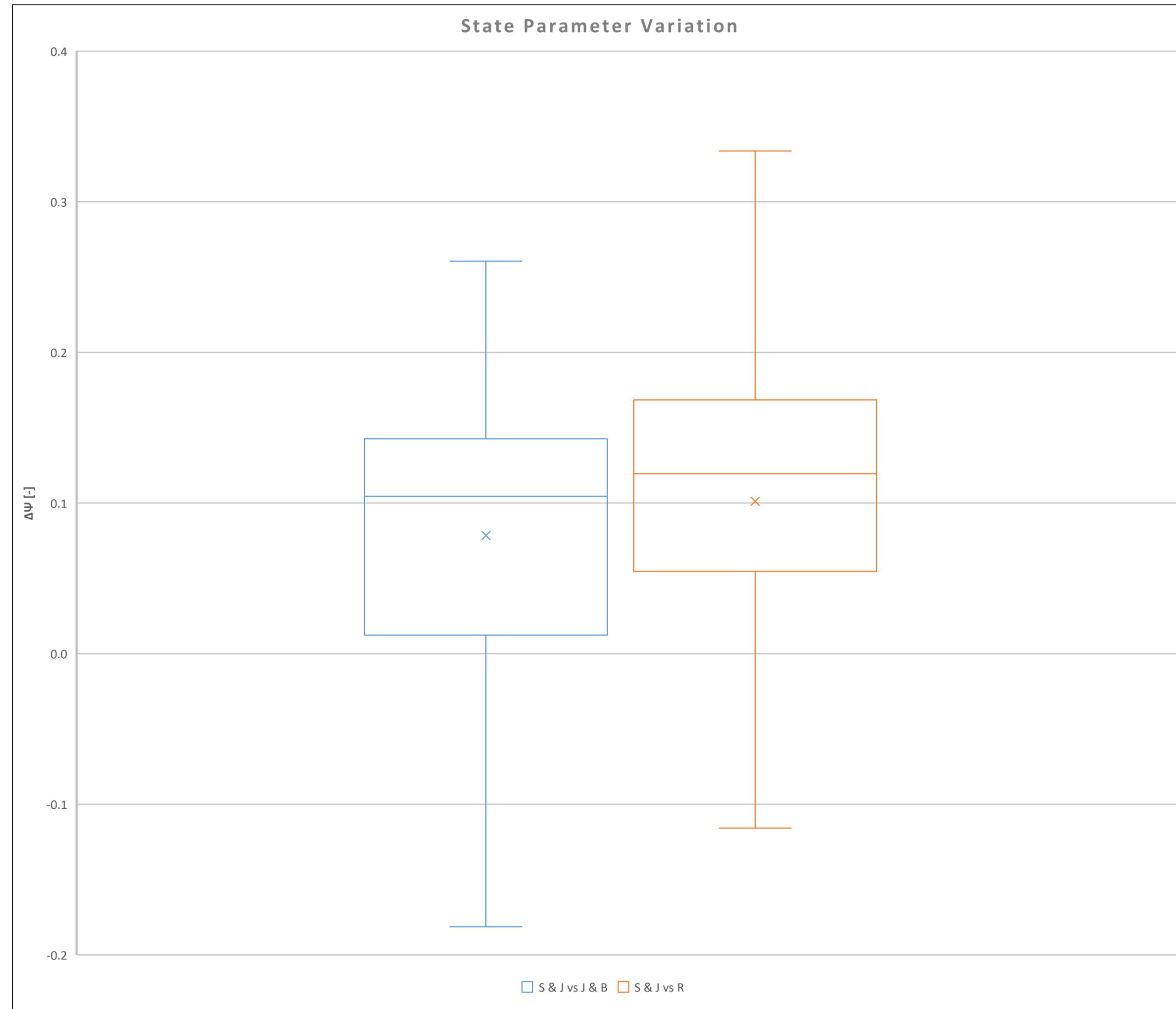
CPTu PC17



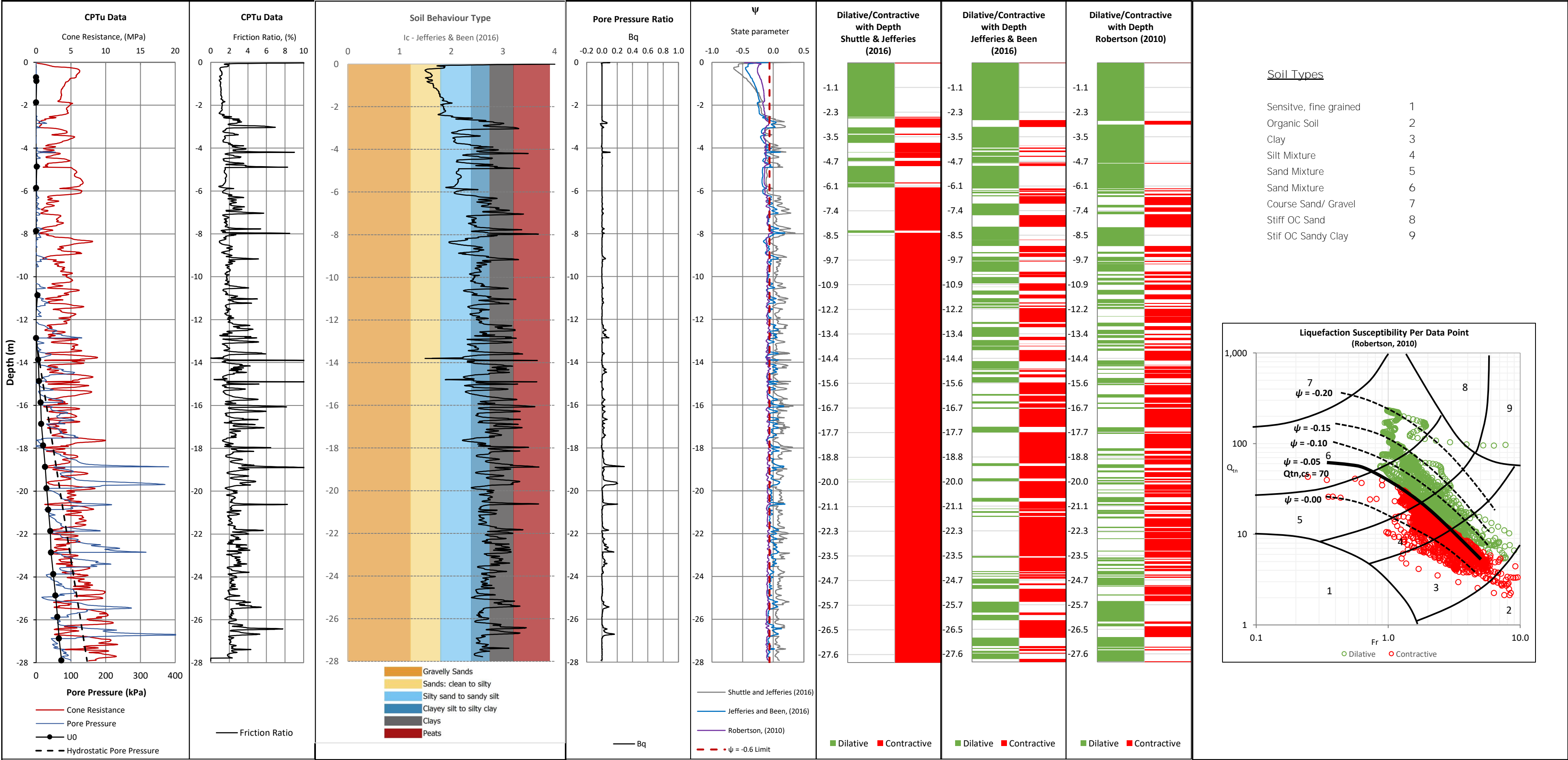
CPTu PC17



## CPTu PC17

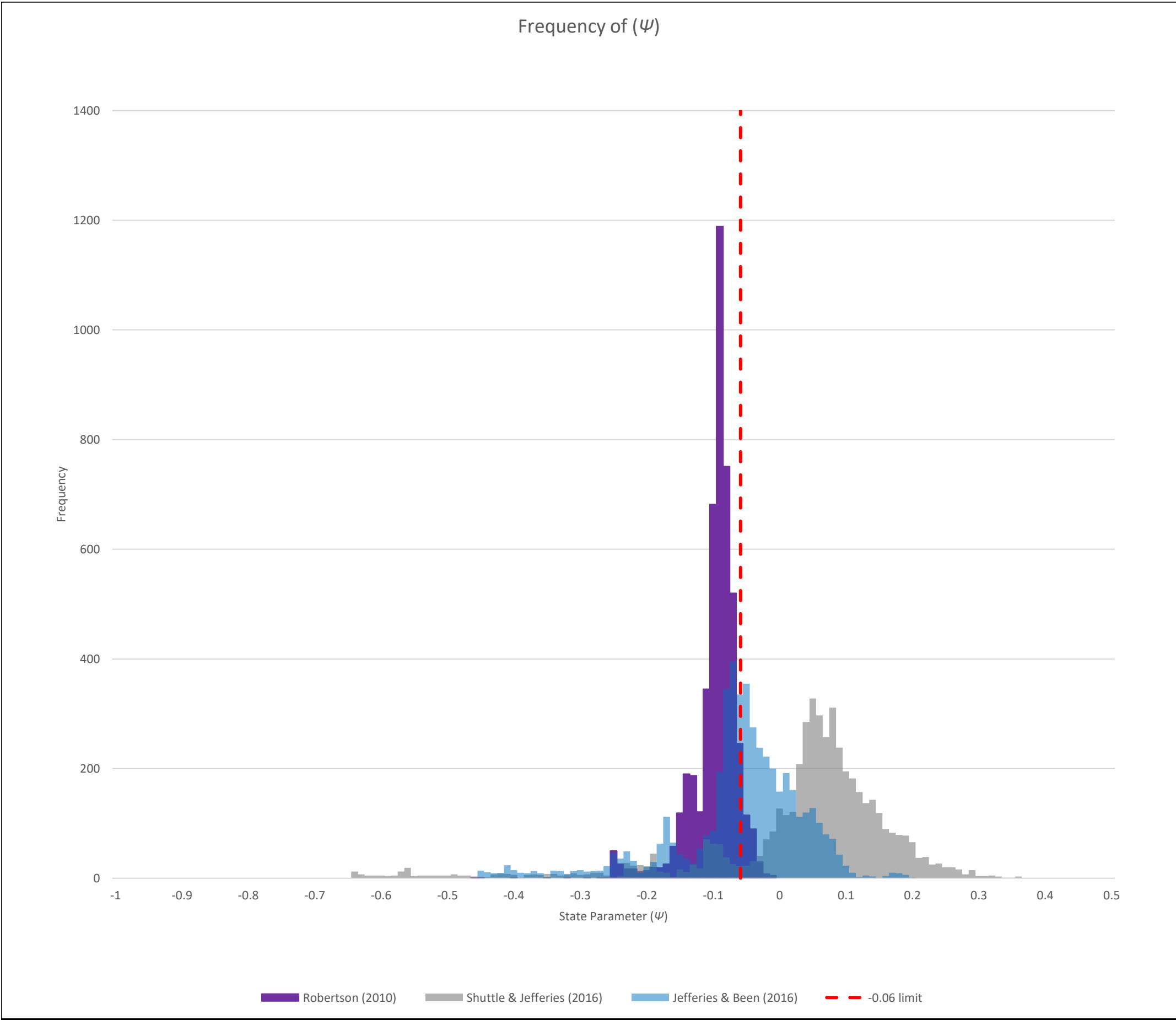


PCC2

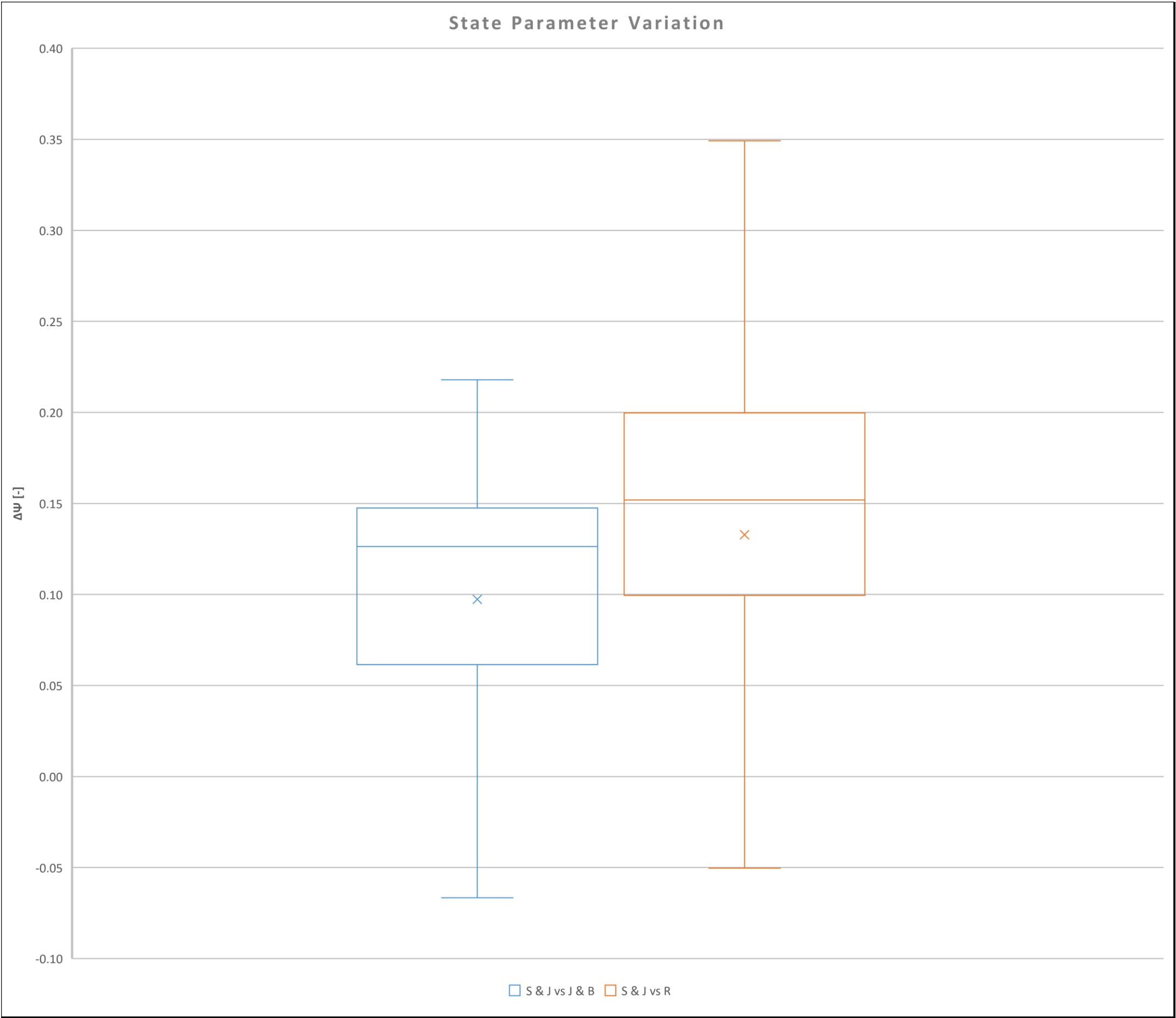




PCC2

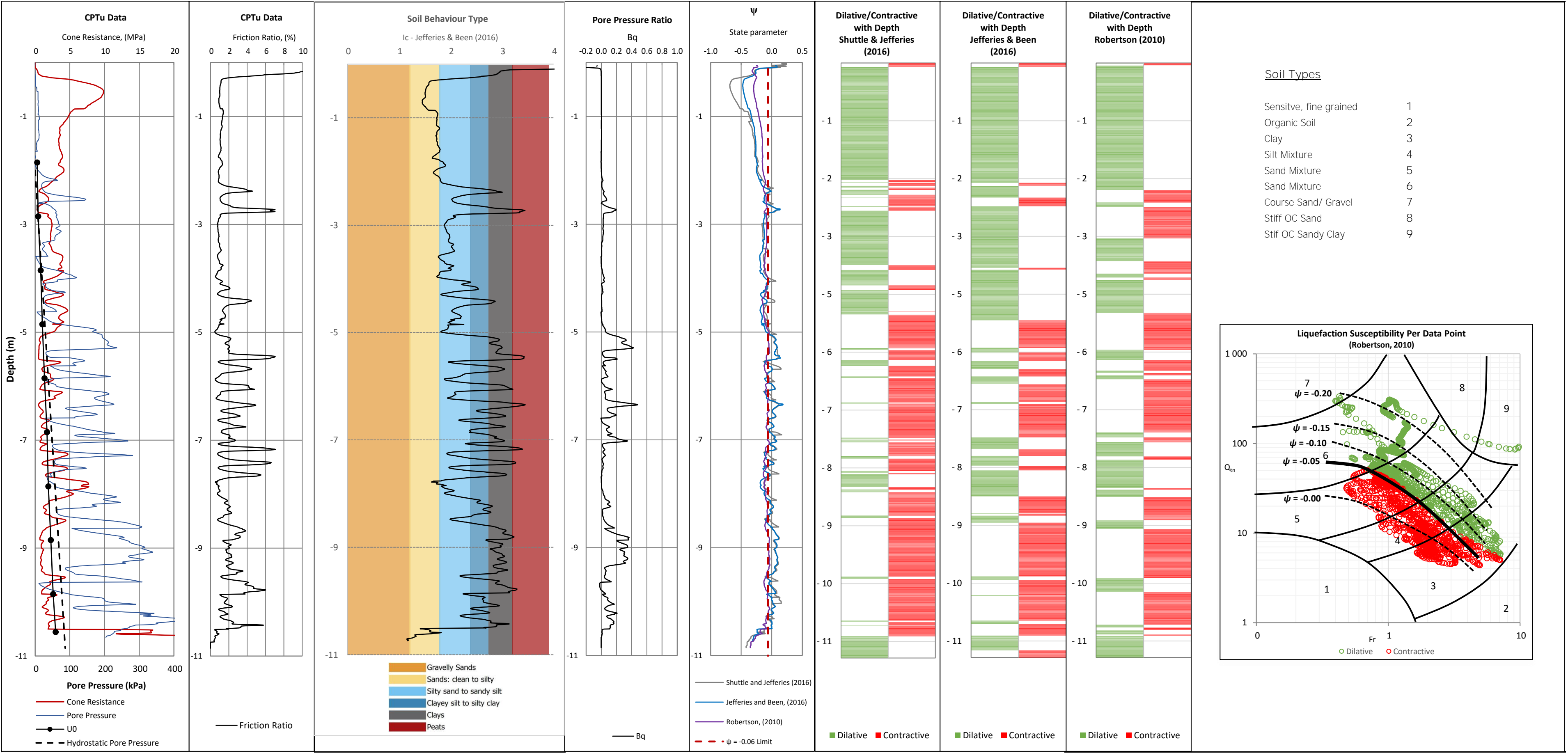


PCC2

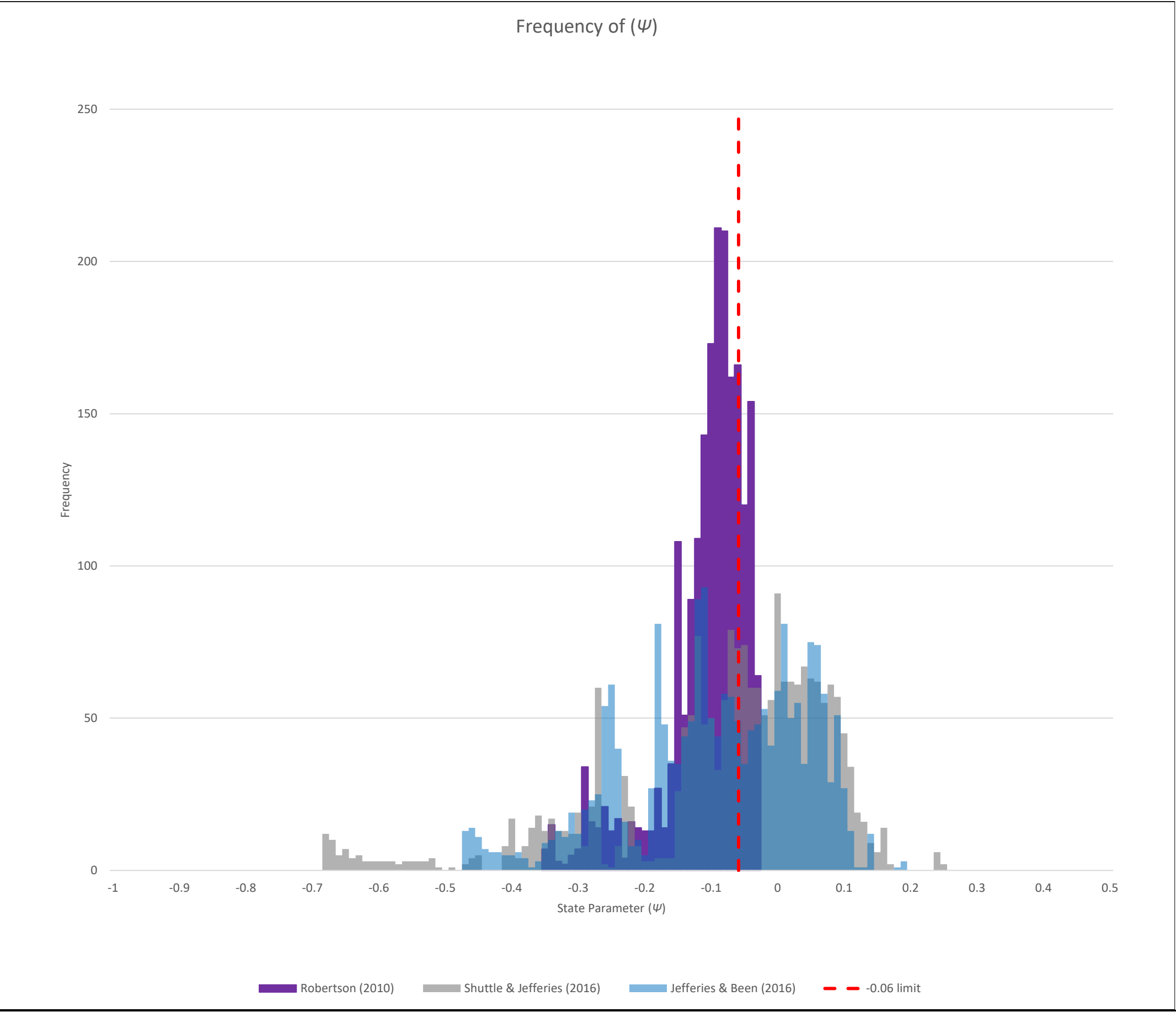


## **Appendix D: CPTu Interpretation – Monitoring Line D**

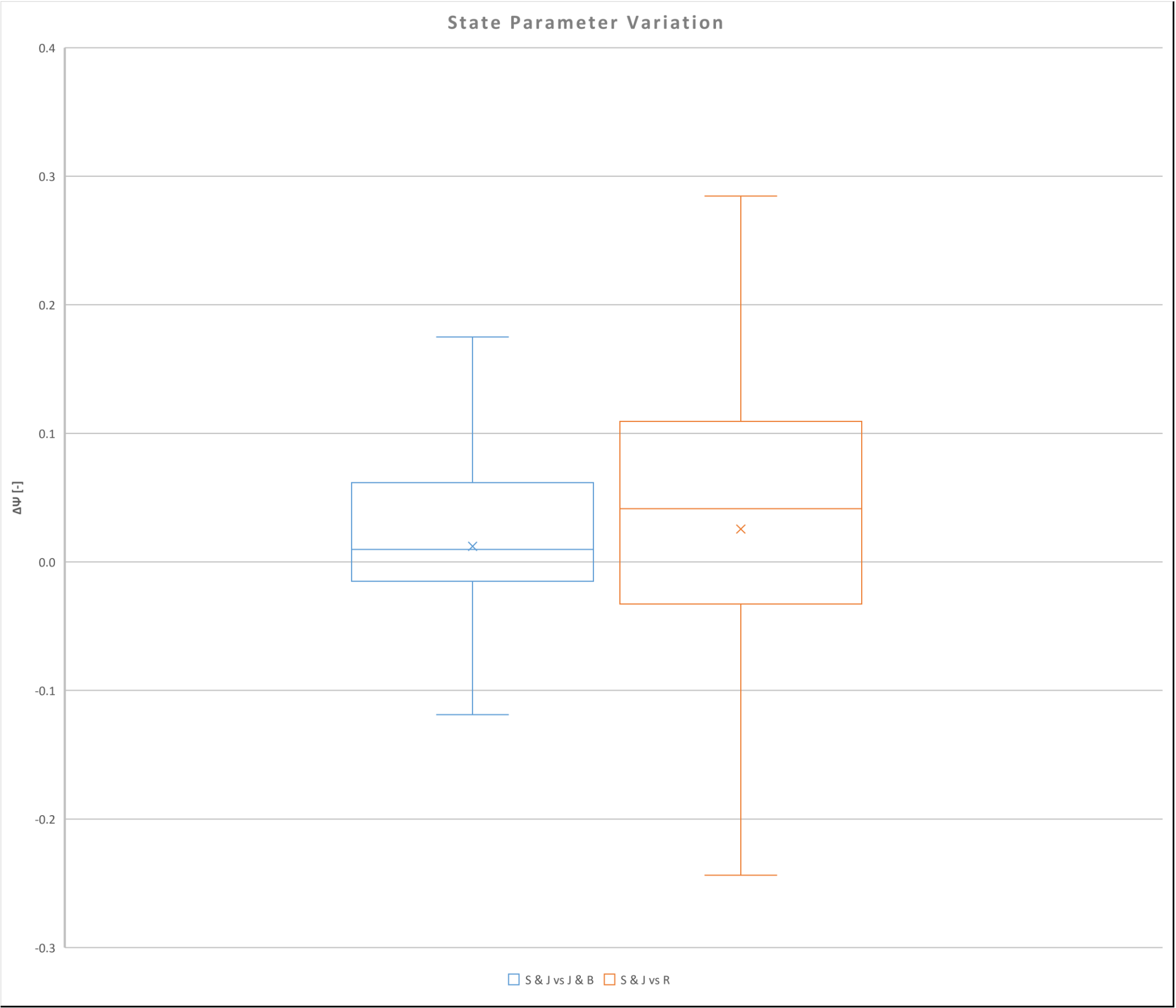
CPTu PC13



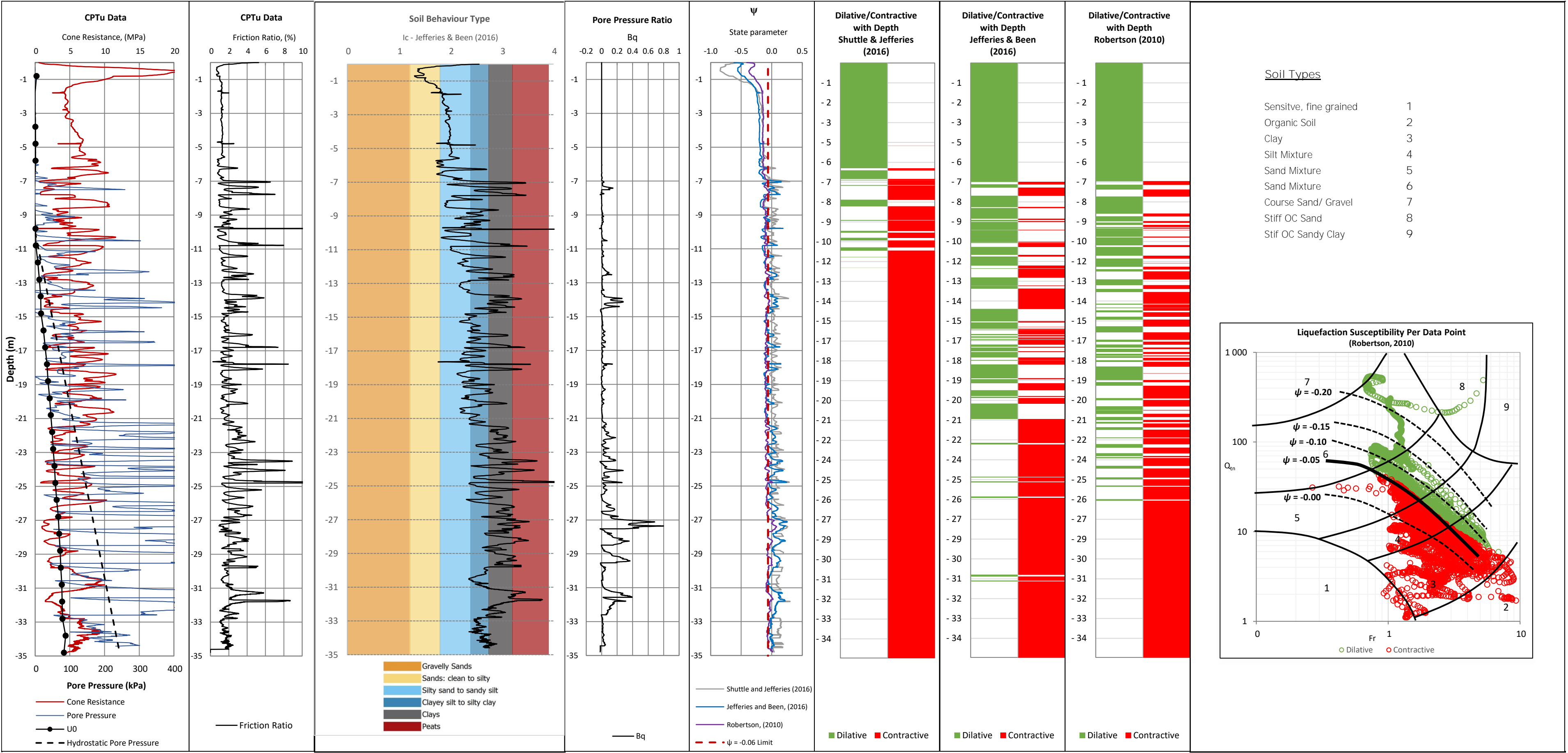
CPTu PC13



CPTu PC13

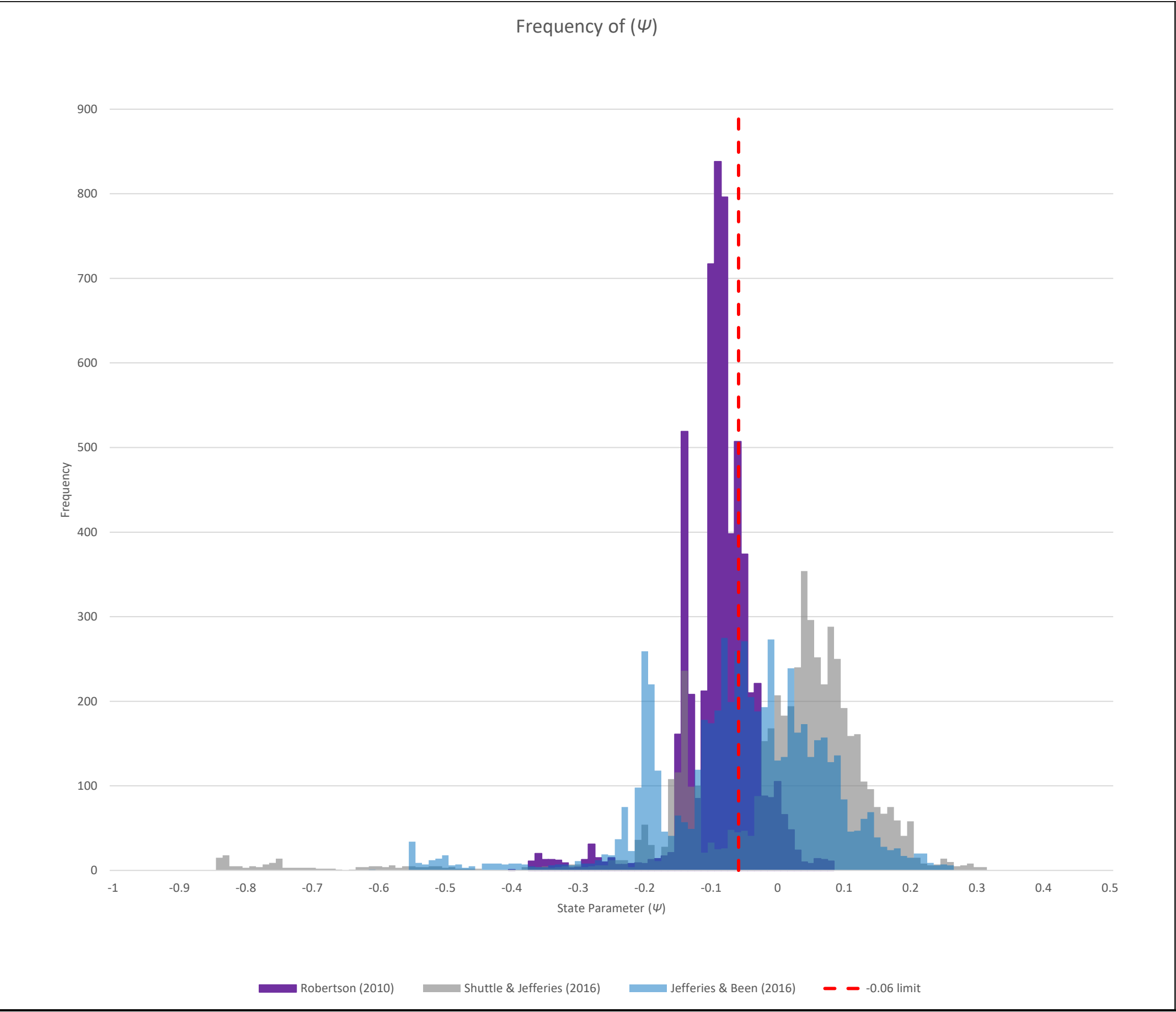


CPTu PC14

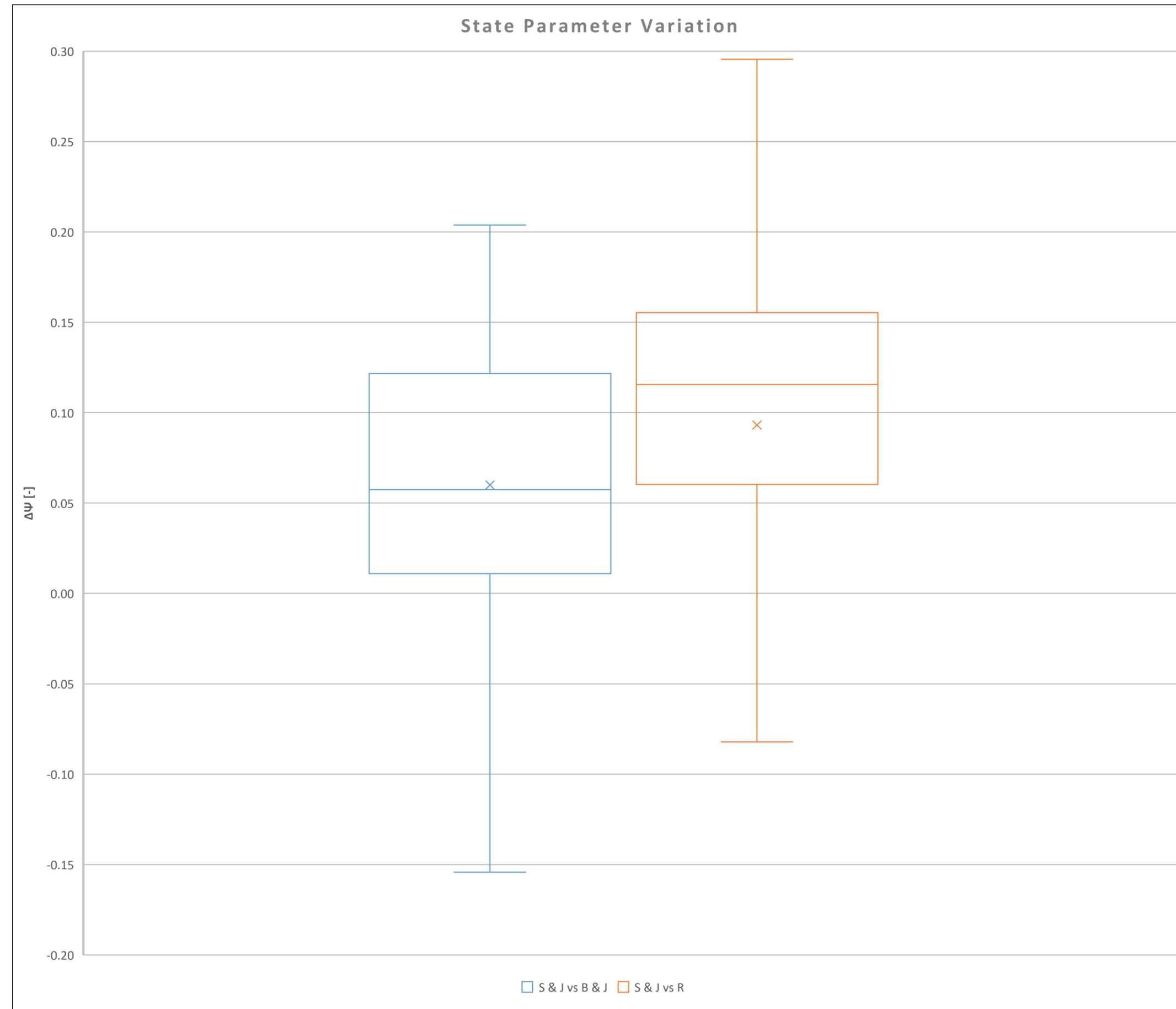




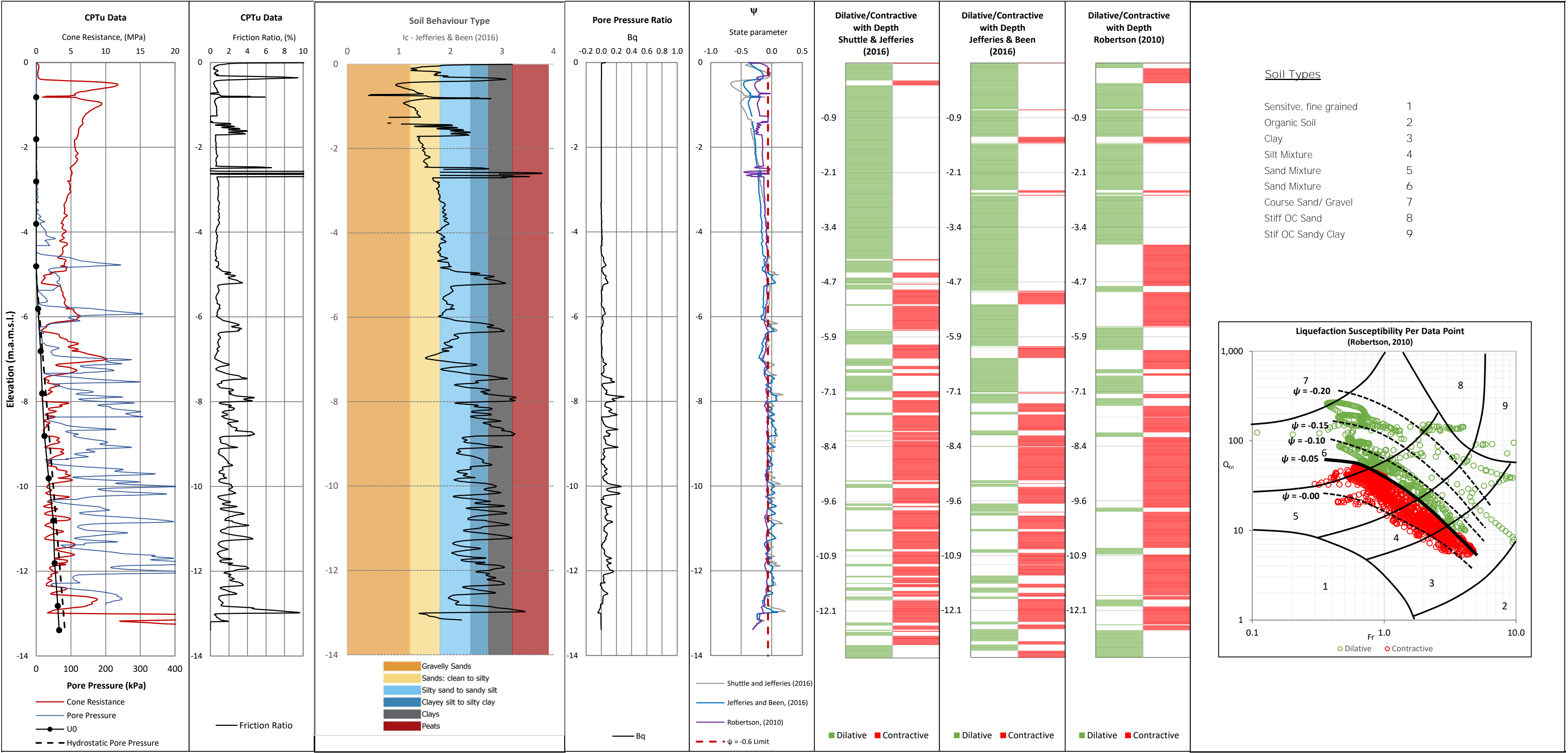
CPTu PC14



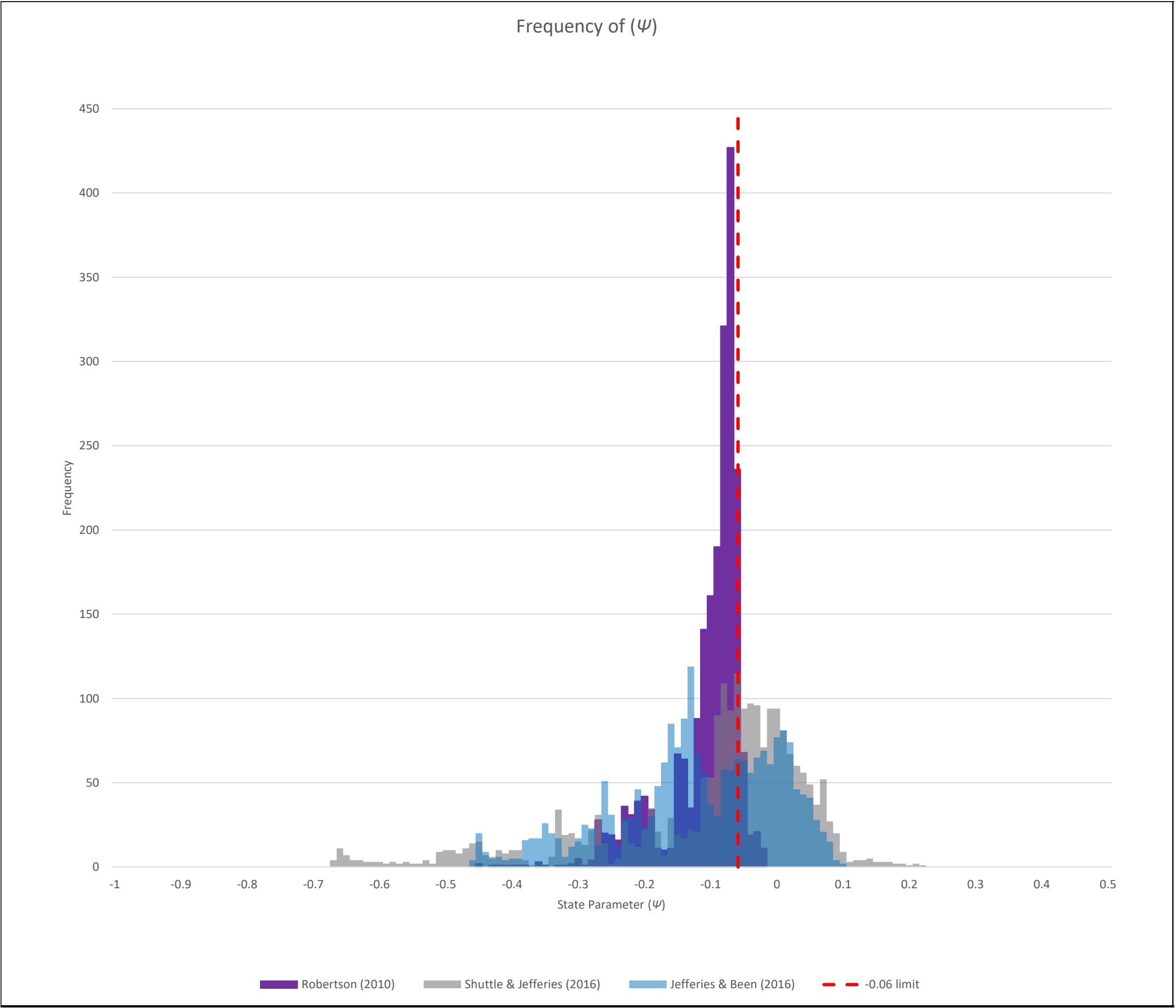
# CPTu PC14



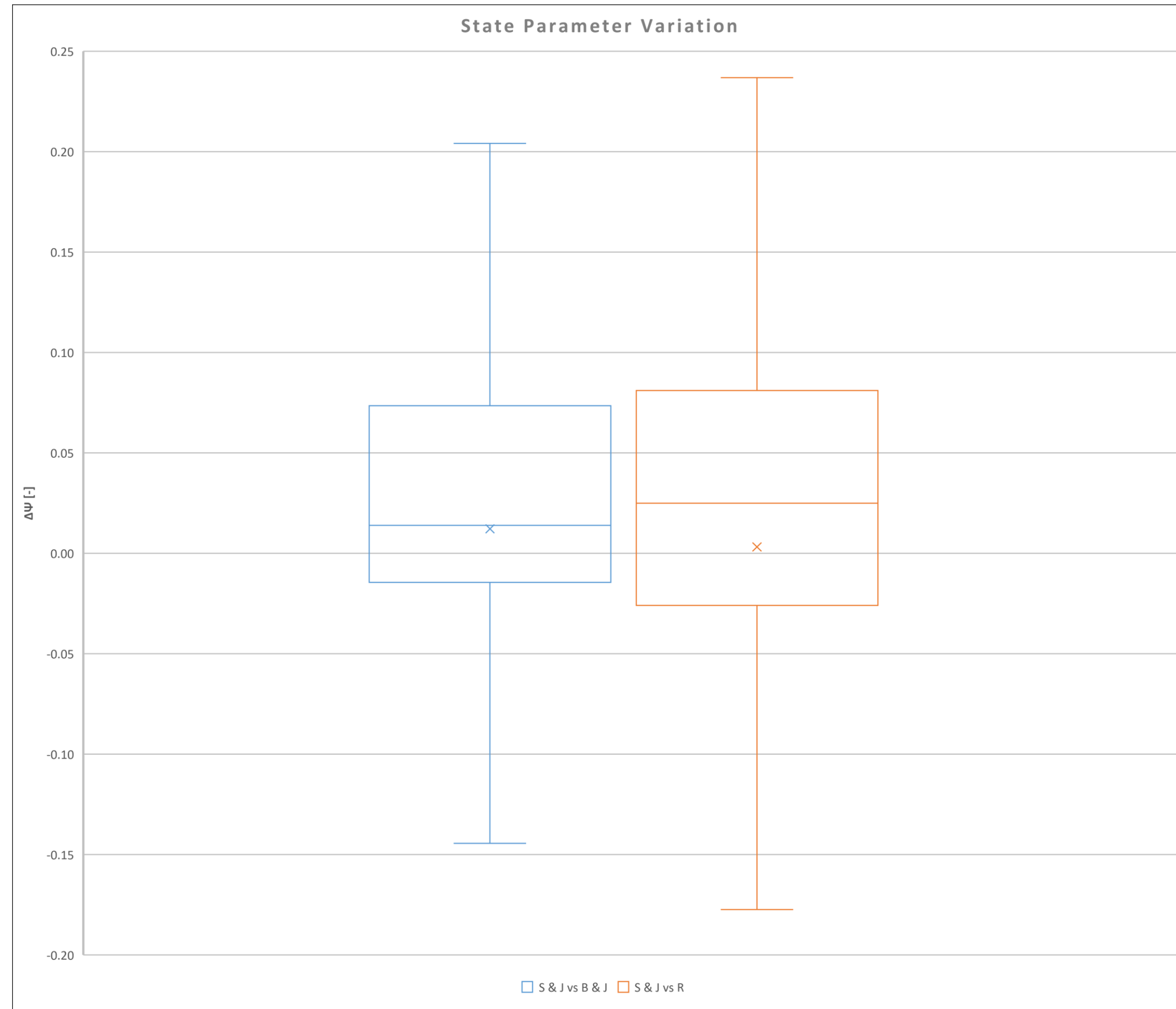
PC29-Q3\_CPTu



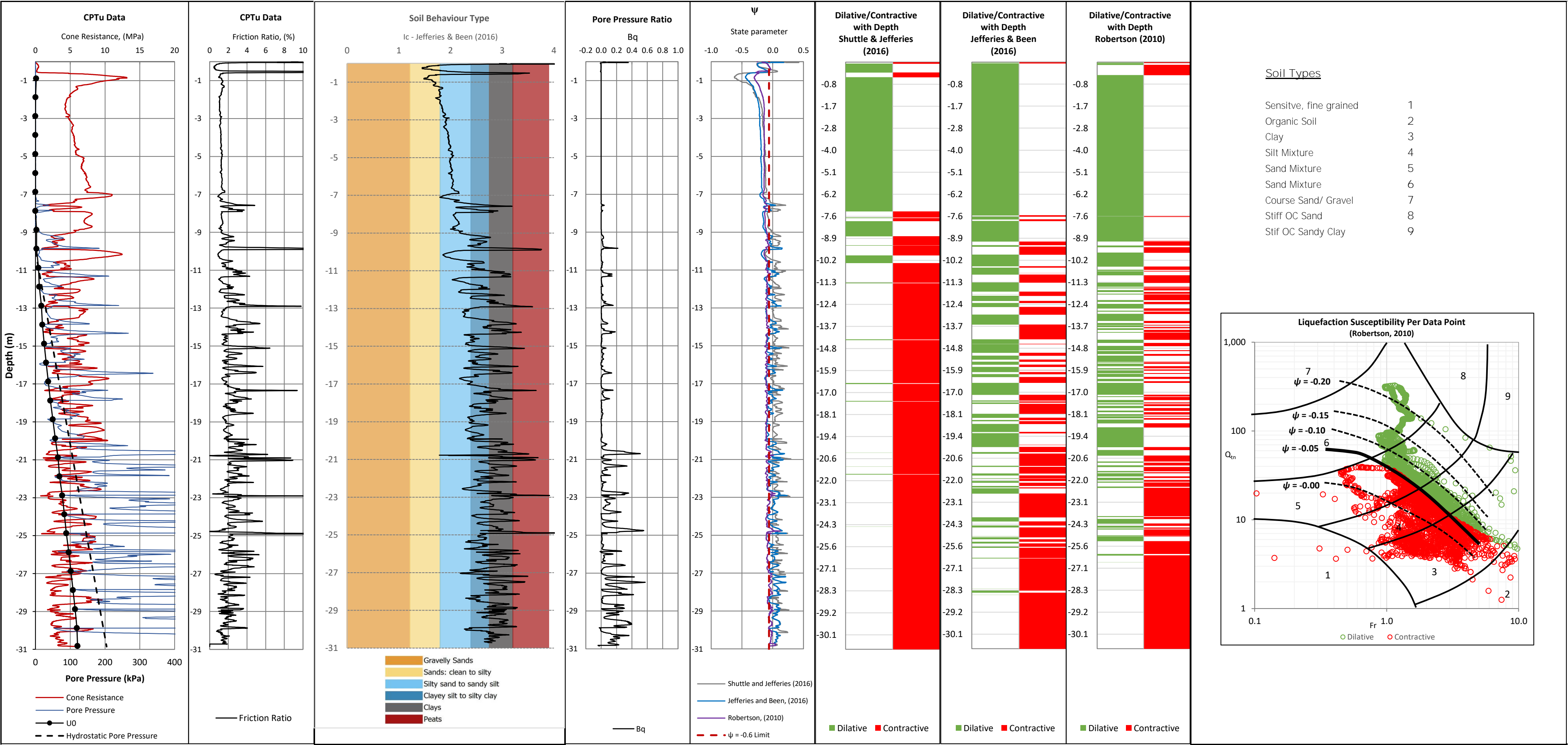
PC29-Q3\_CPTu



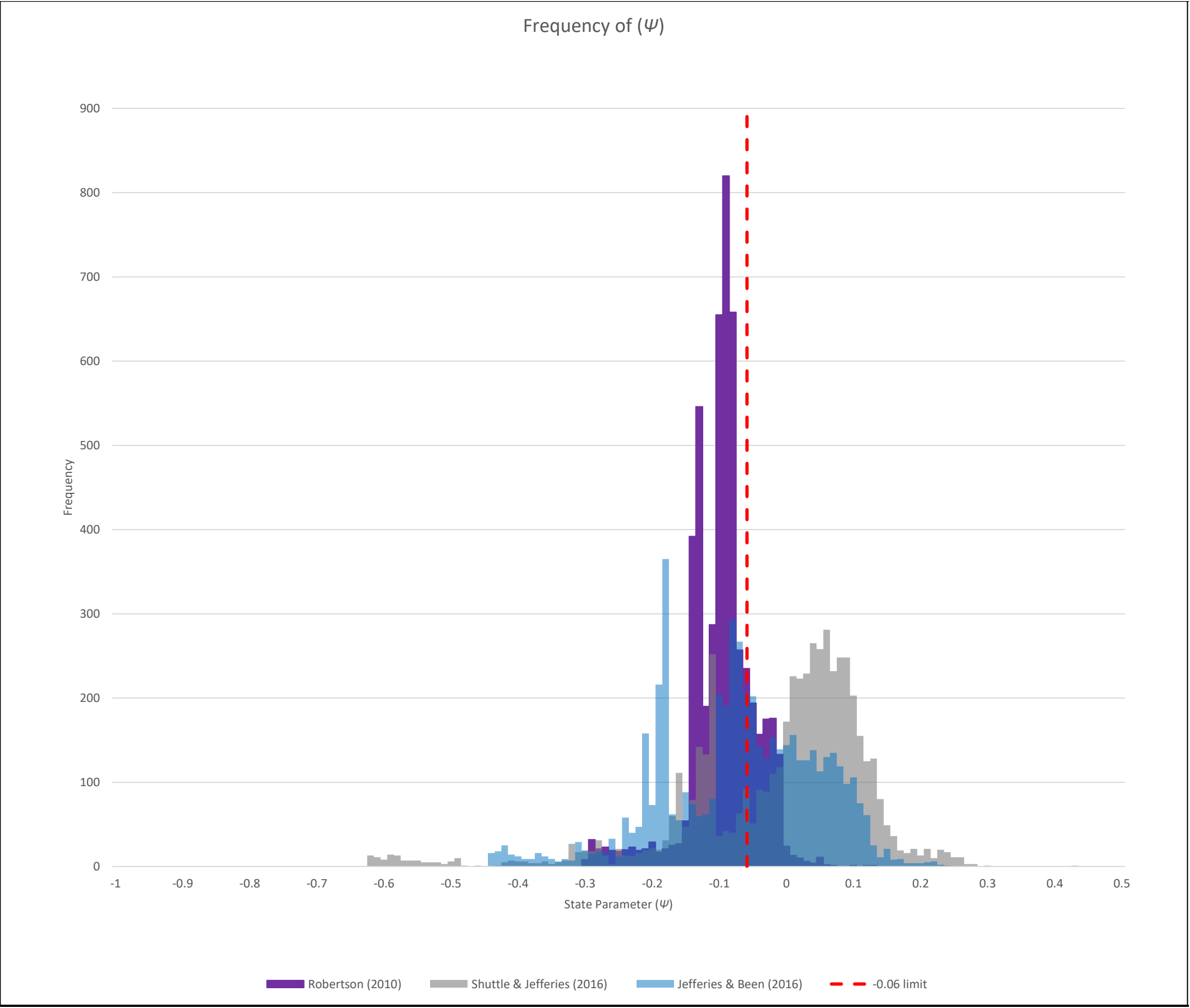
# PC29-Q3\_CPTu



PCD2

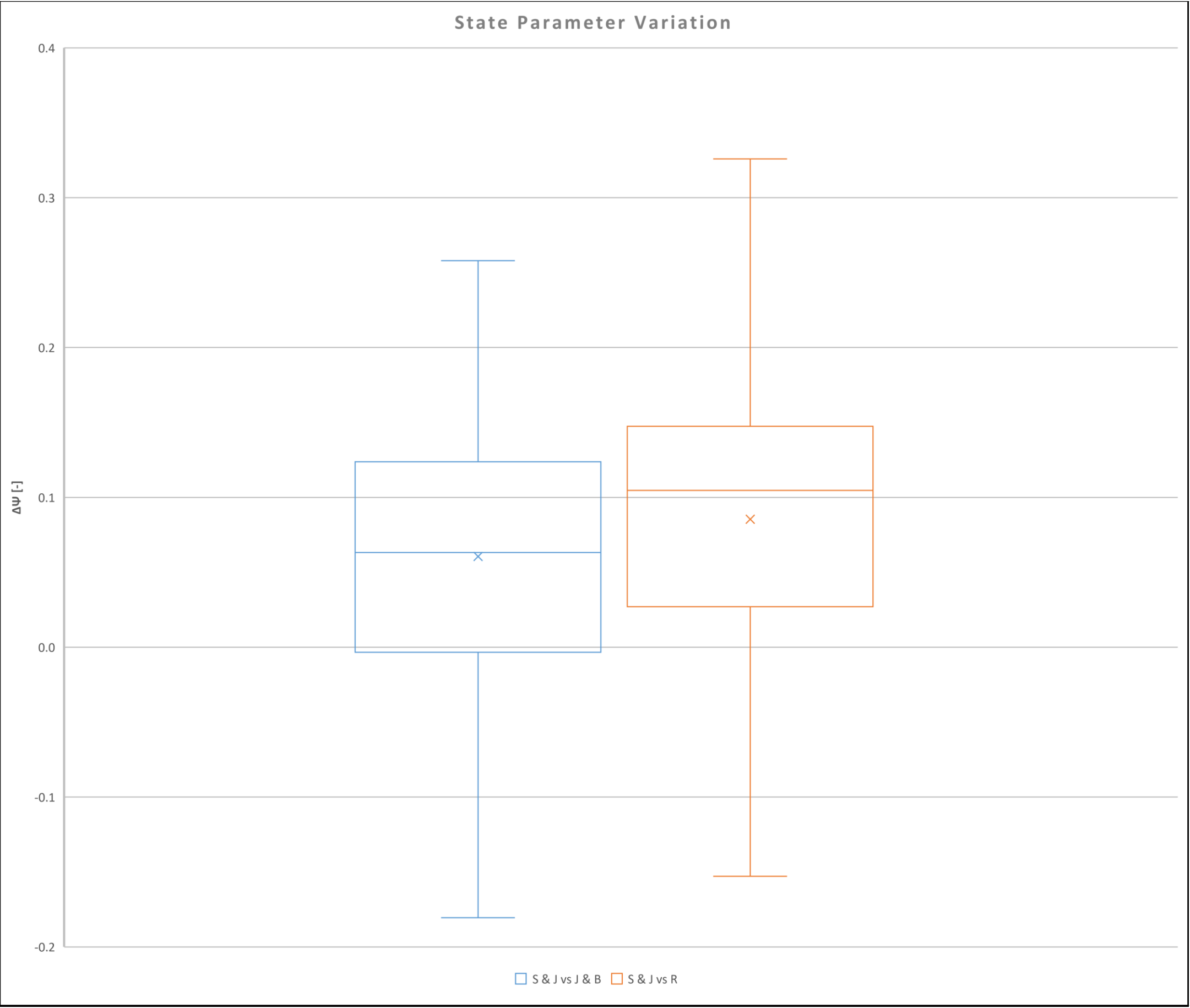


PCD2

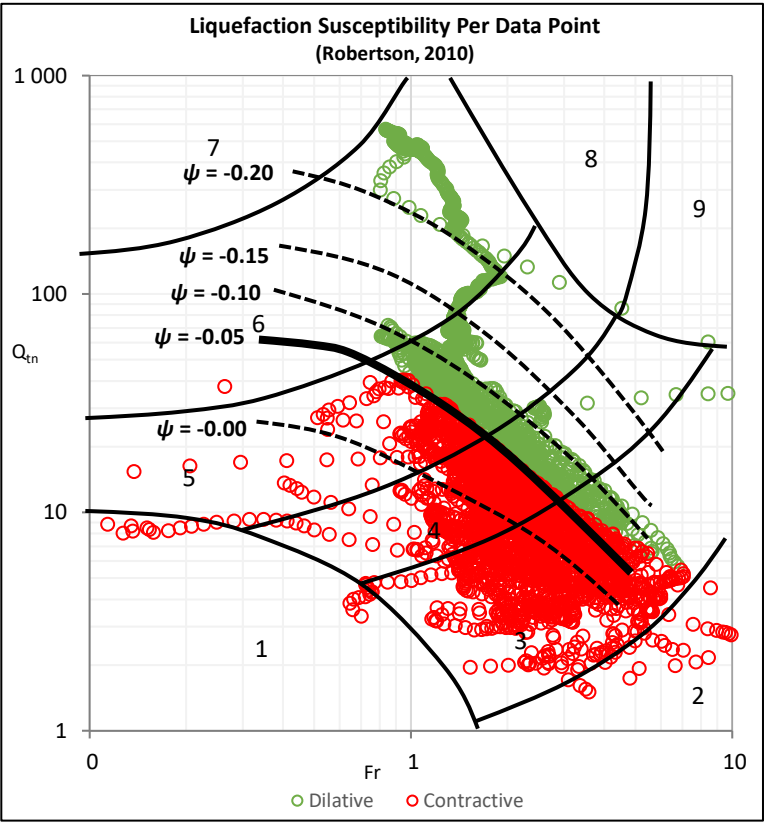




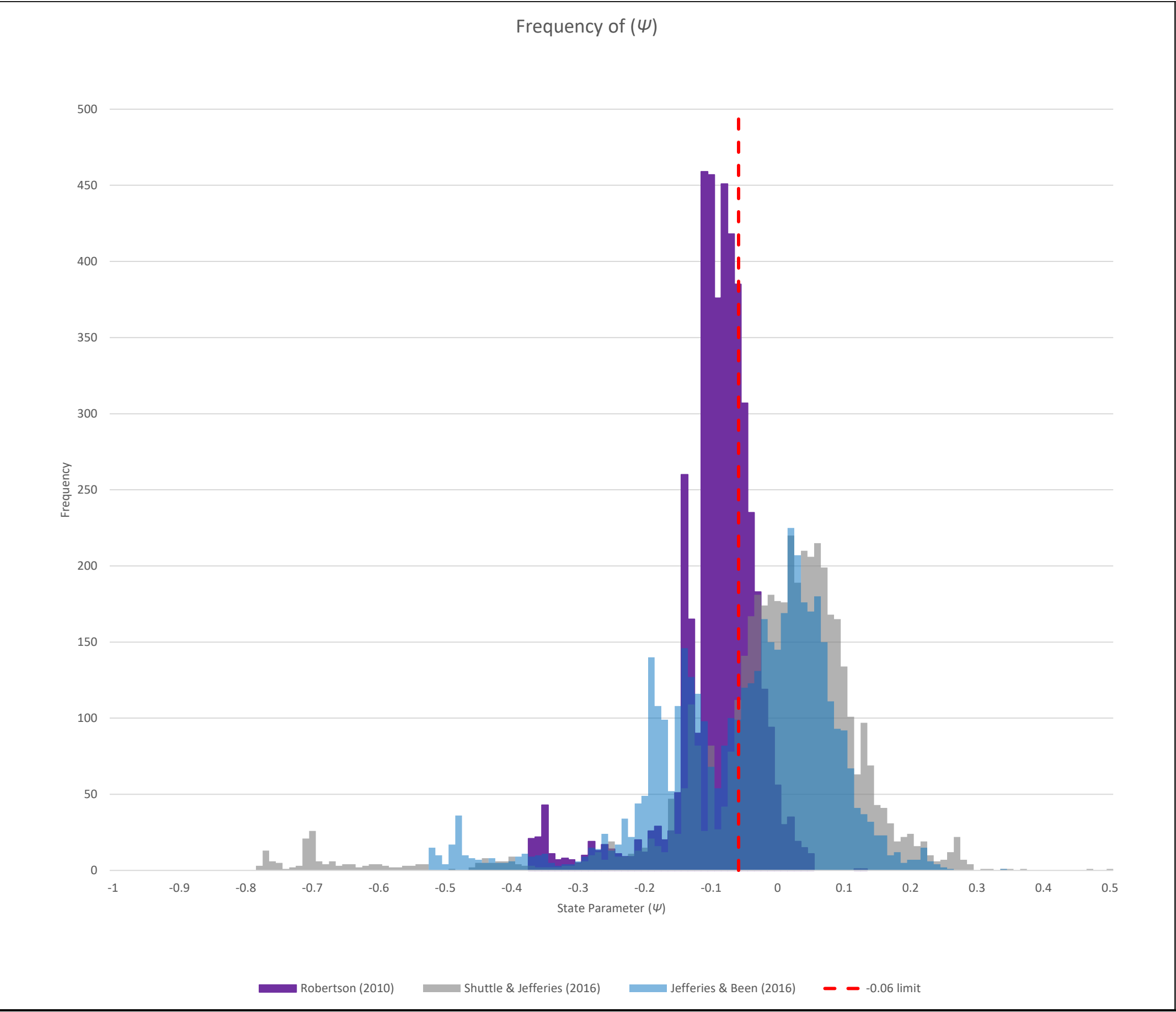
PCD2



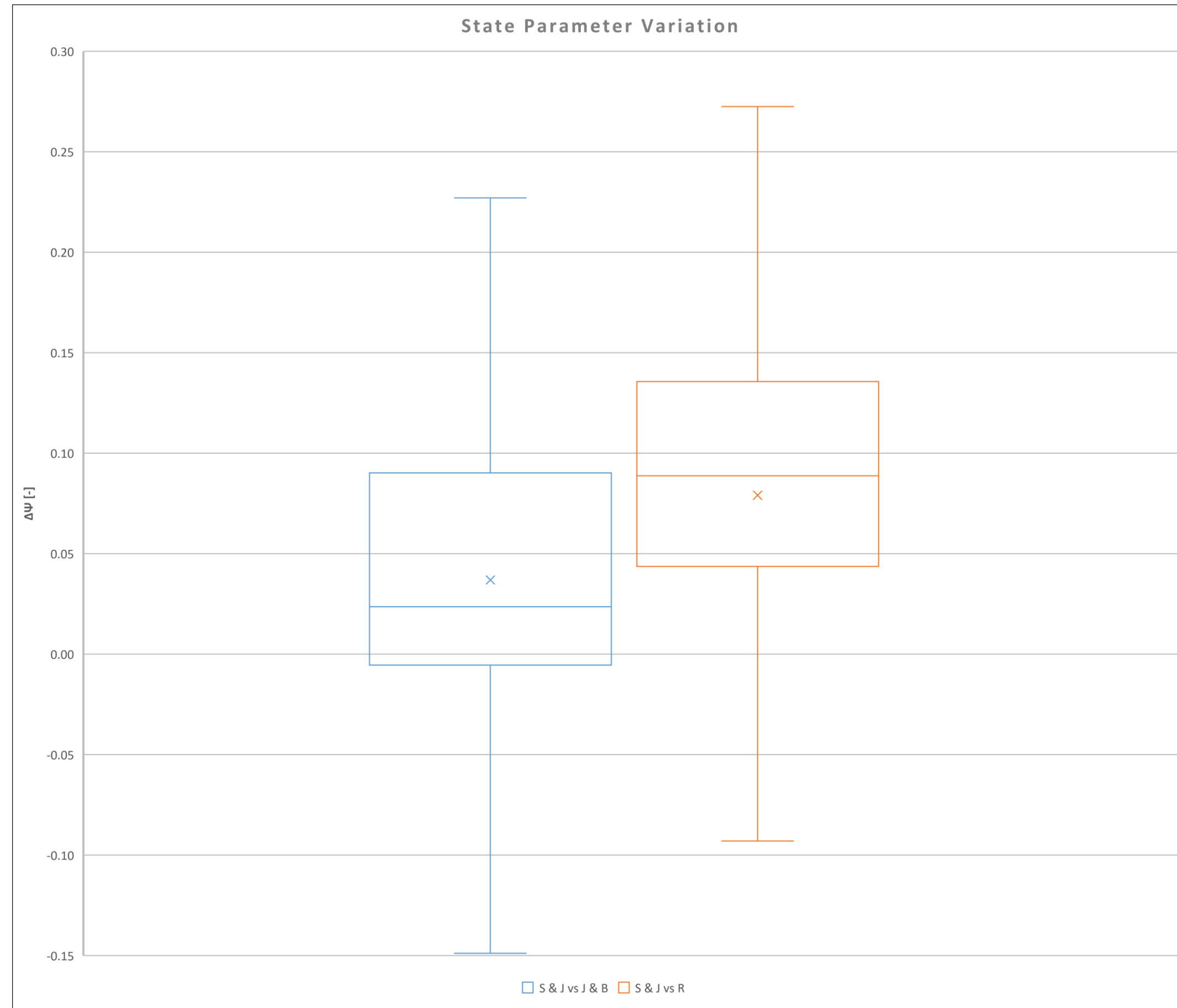
## **Appendix E: CPTu Interpretation – Monitoring Line E**



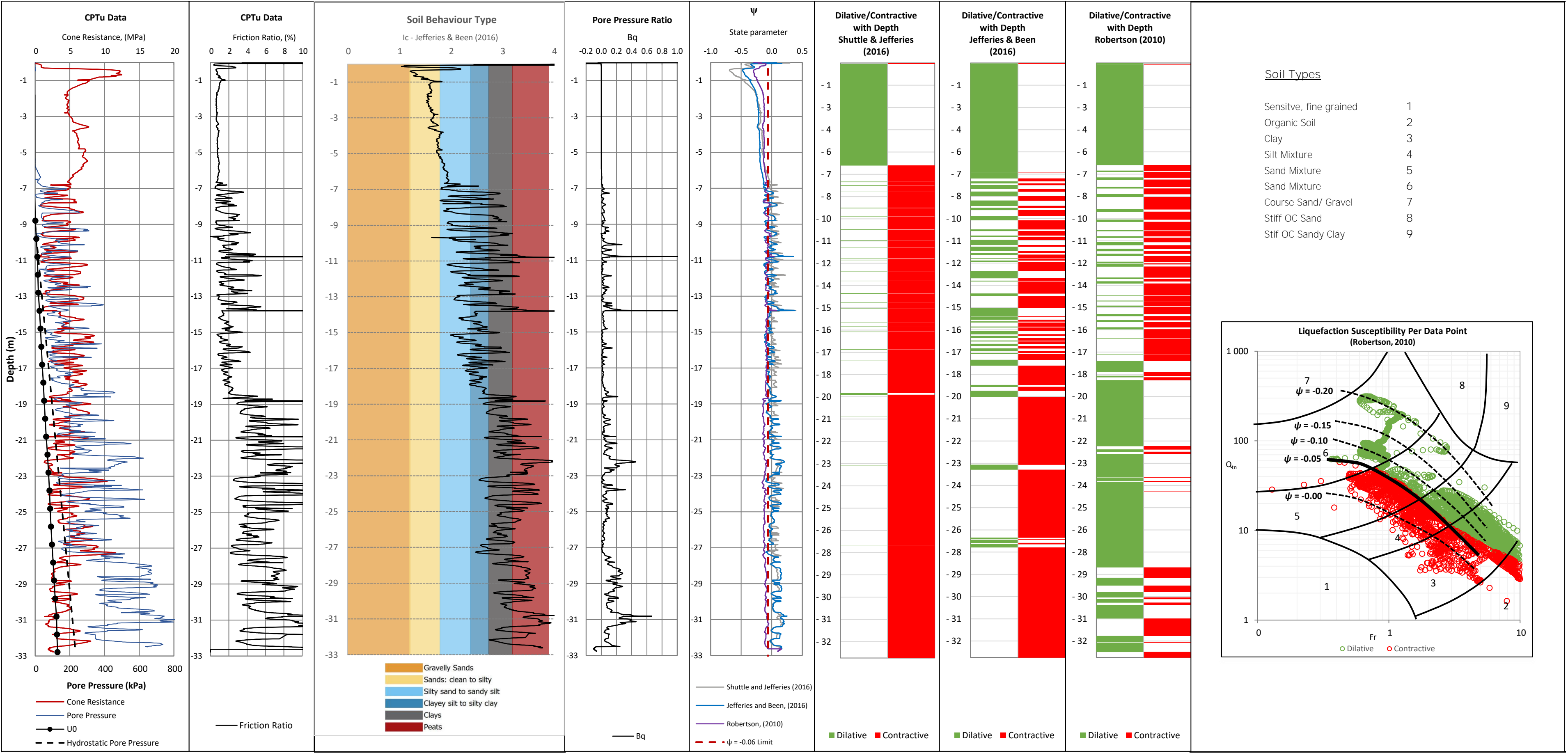
CPTu PC11



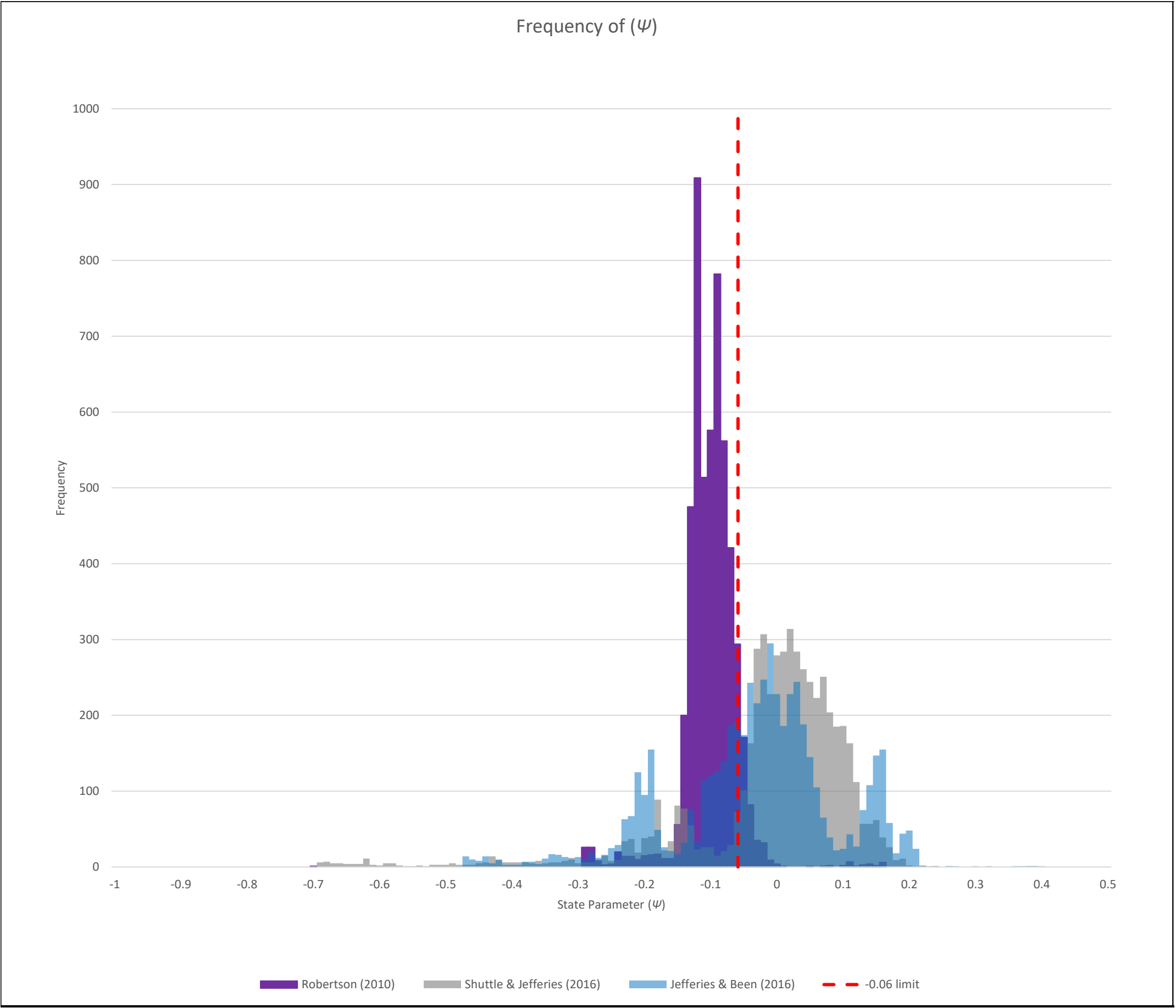
# CPTu PC11



CPTu PC12

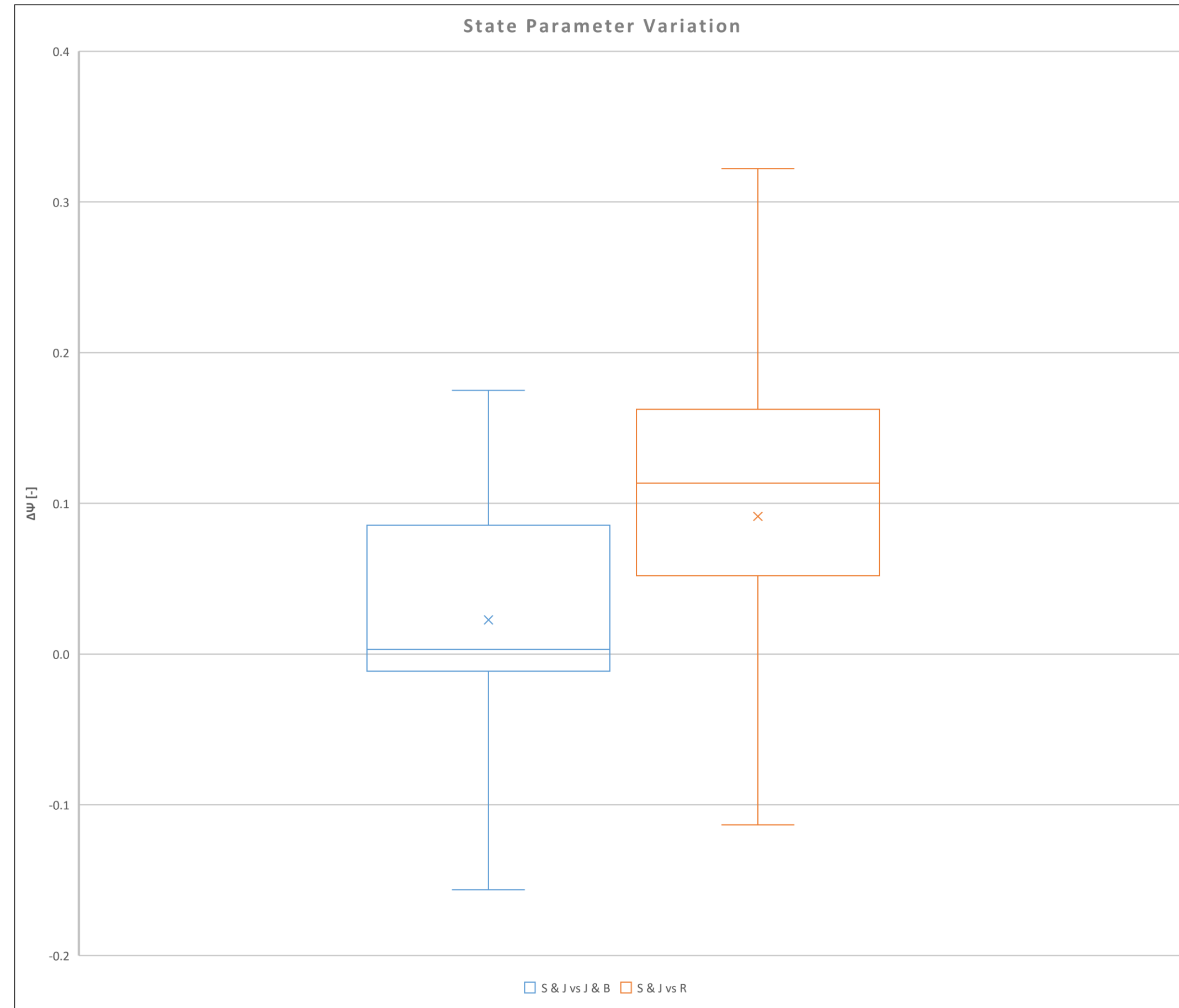


CPTu PC12

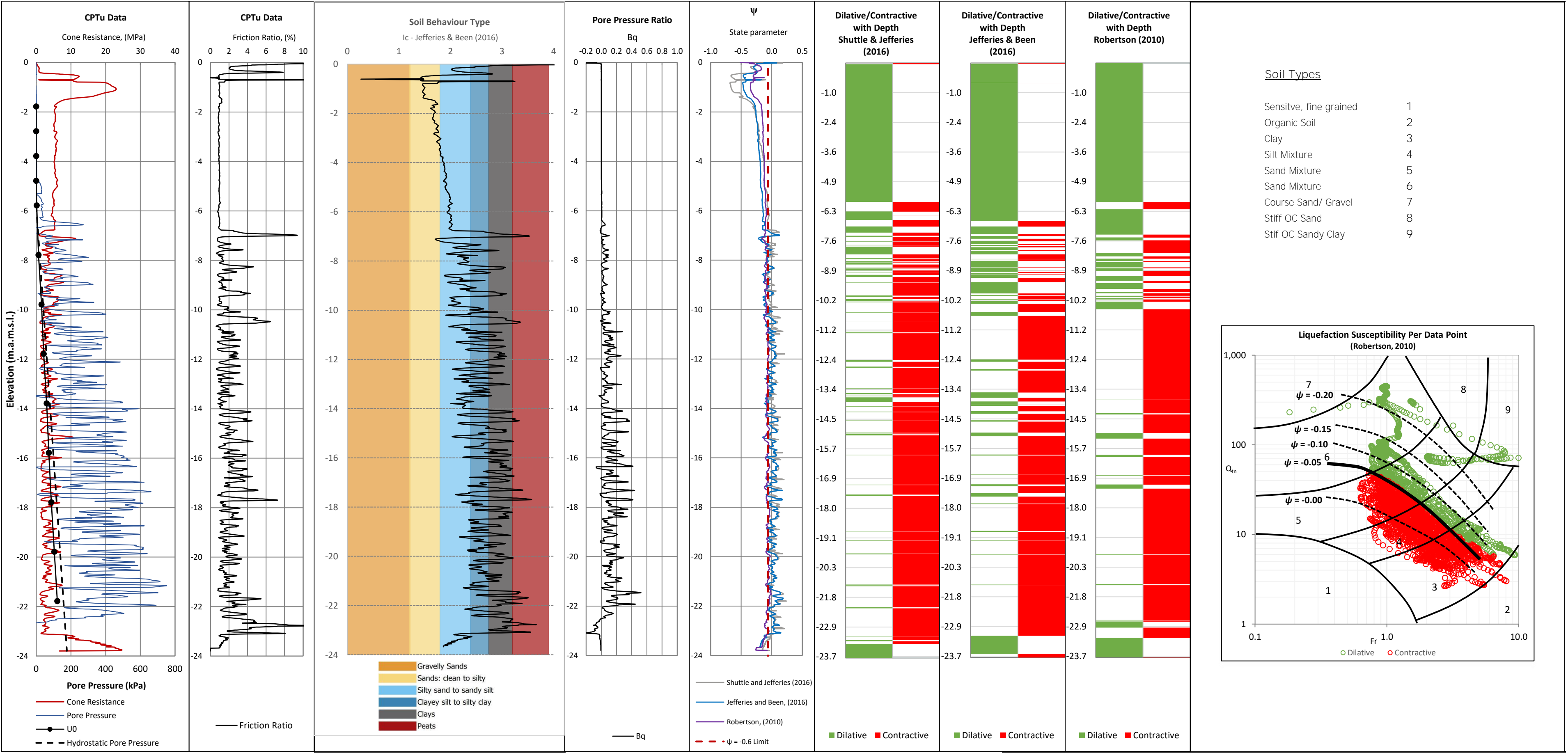




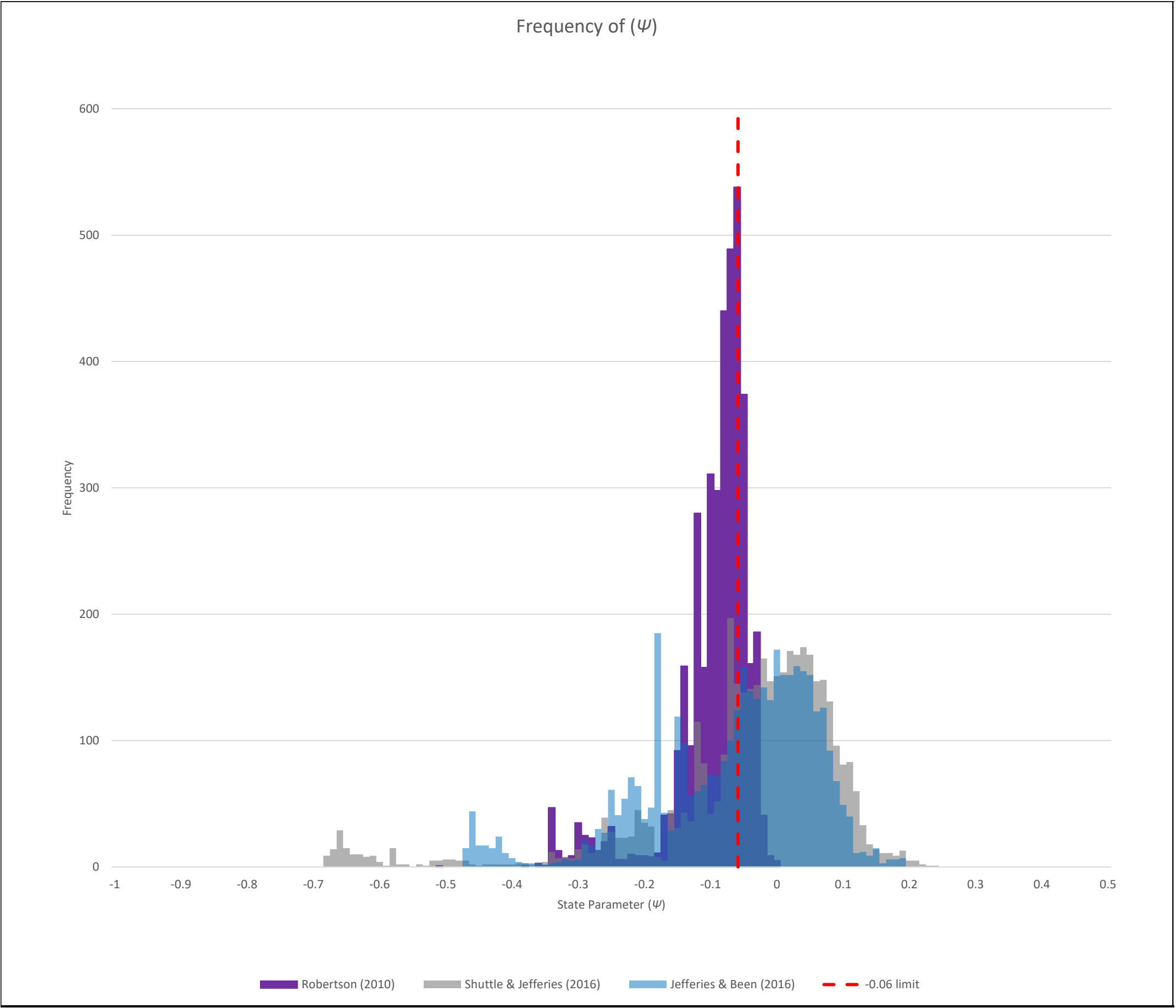
# CPTu PC12



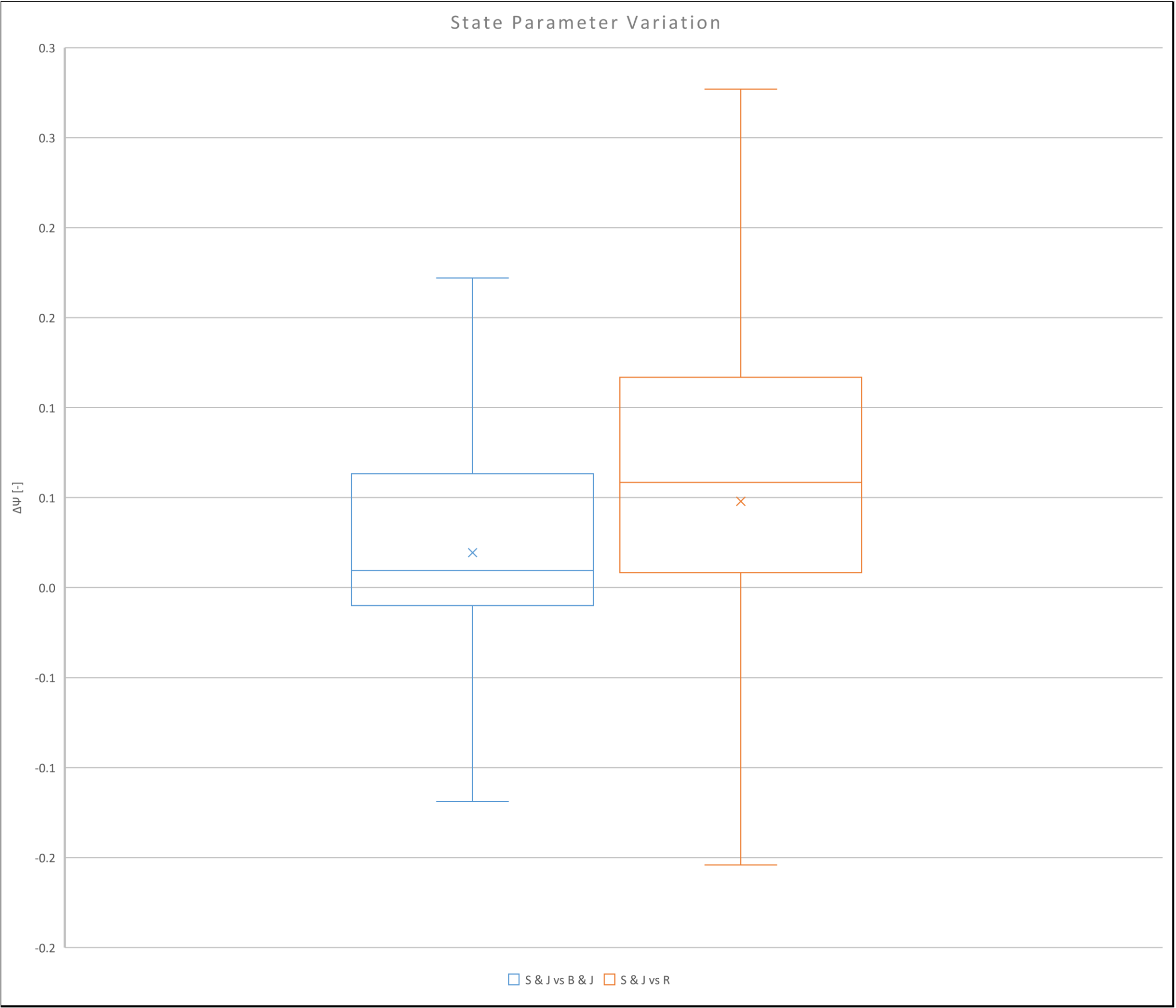
PC11-Q3\_CPTu



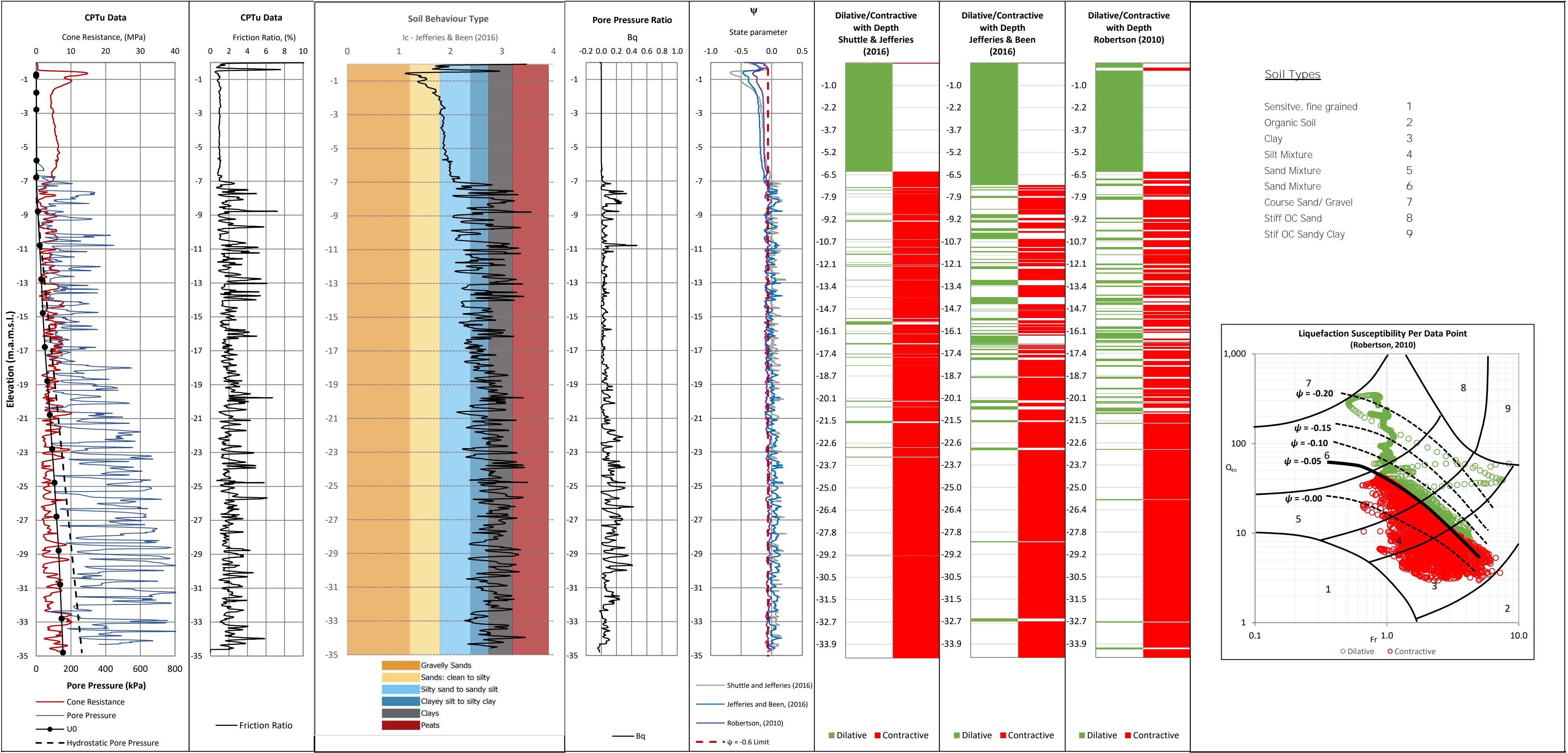
PC11-Q3\_CPTu



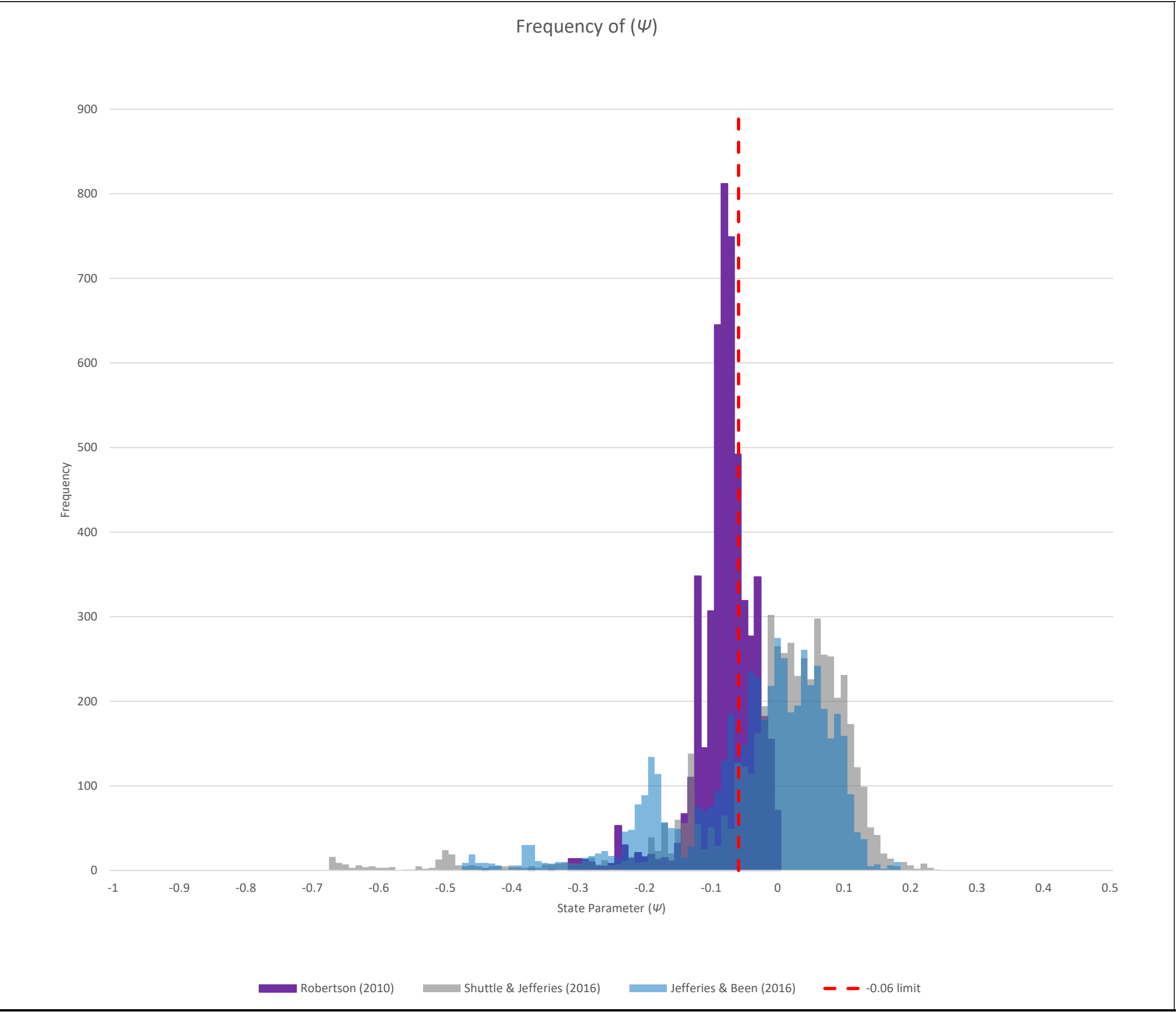
PC11-Q3\_CPTu



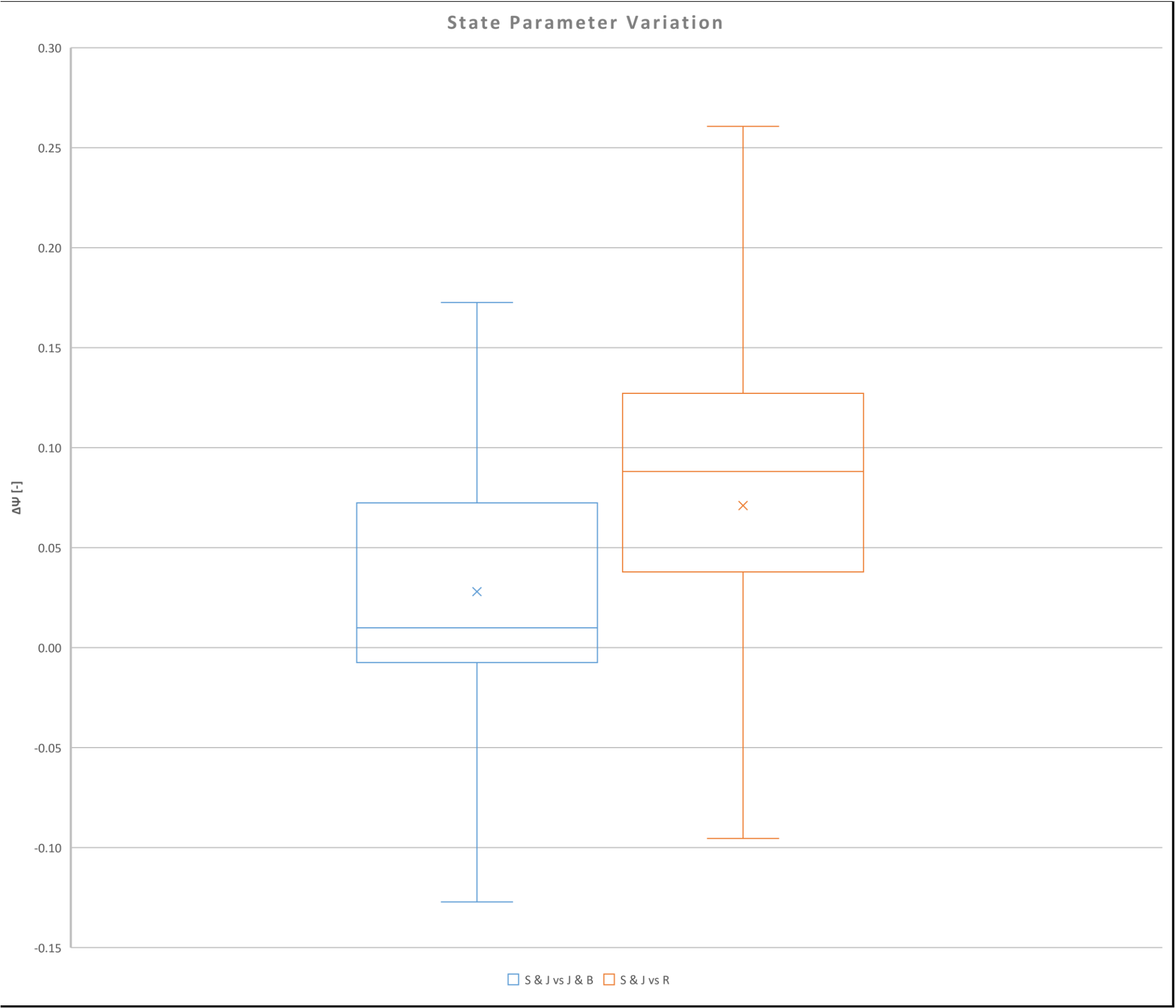
PC12-Q3\_CPTu



PC12-Q3\_CPTu

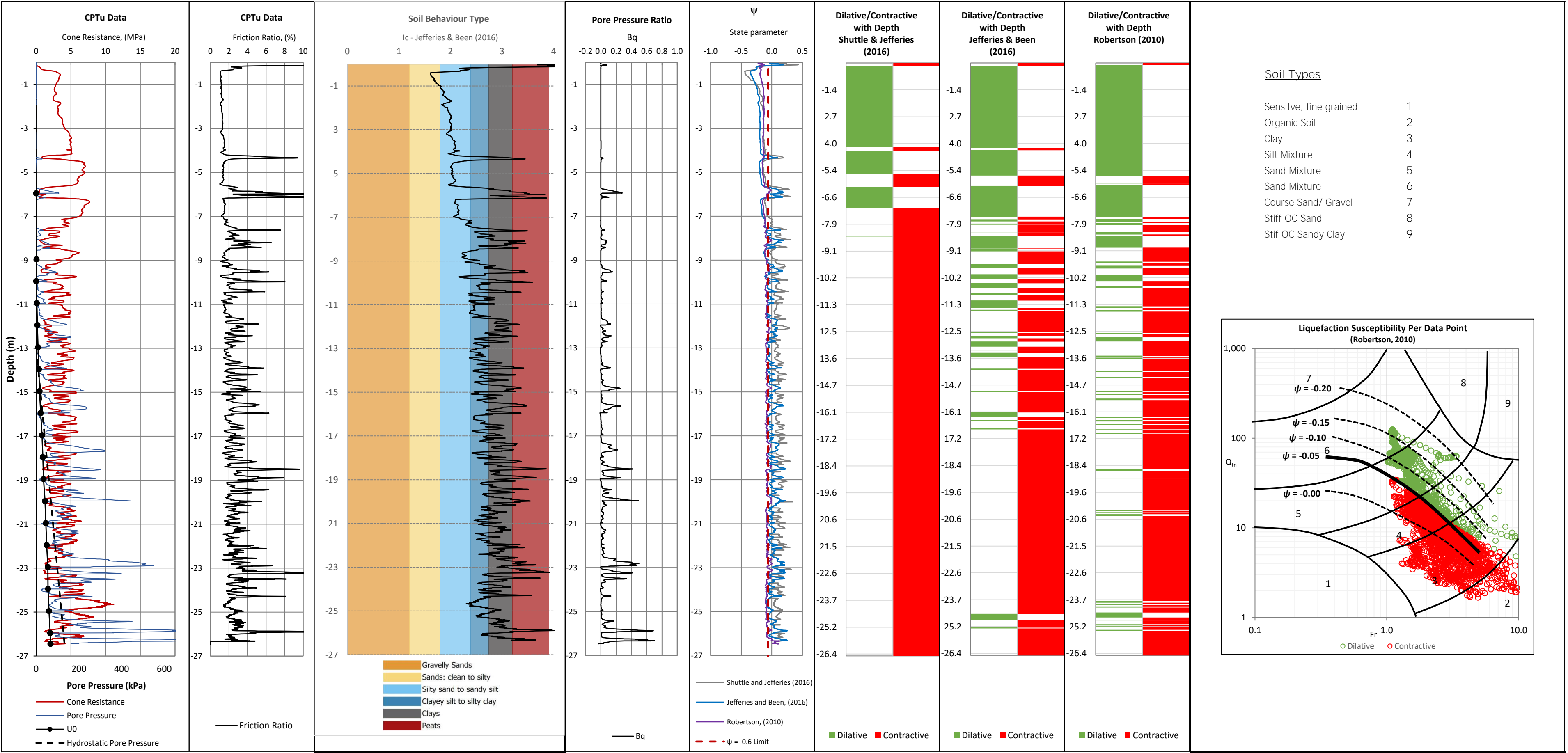


PC12-Q3\_CPTu

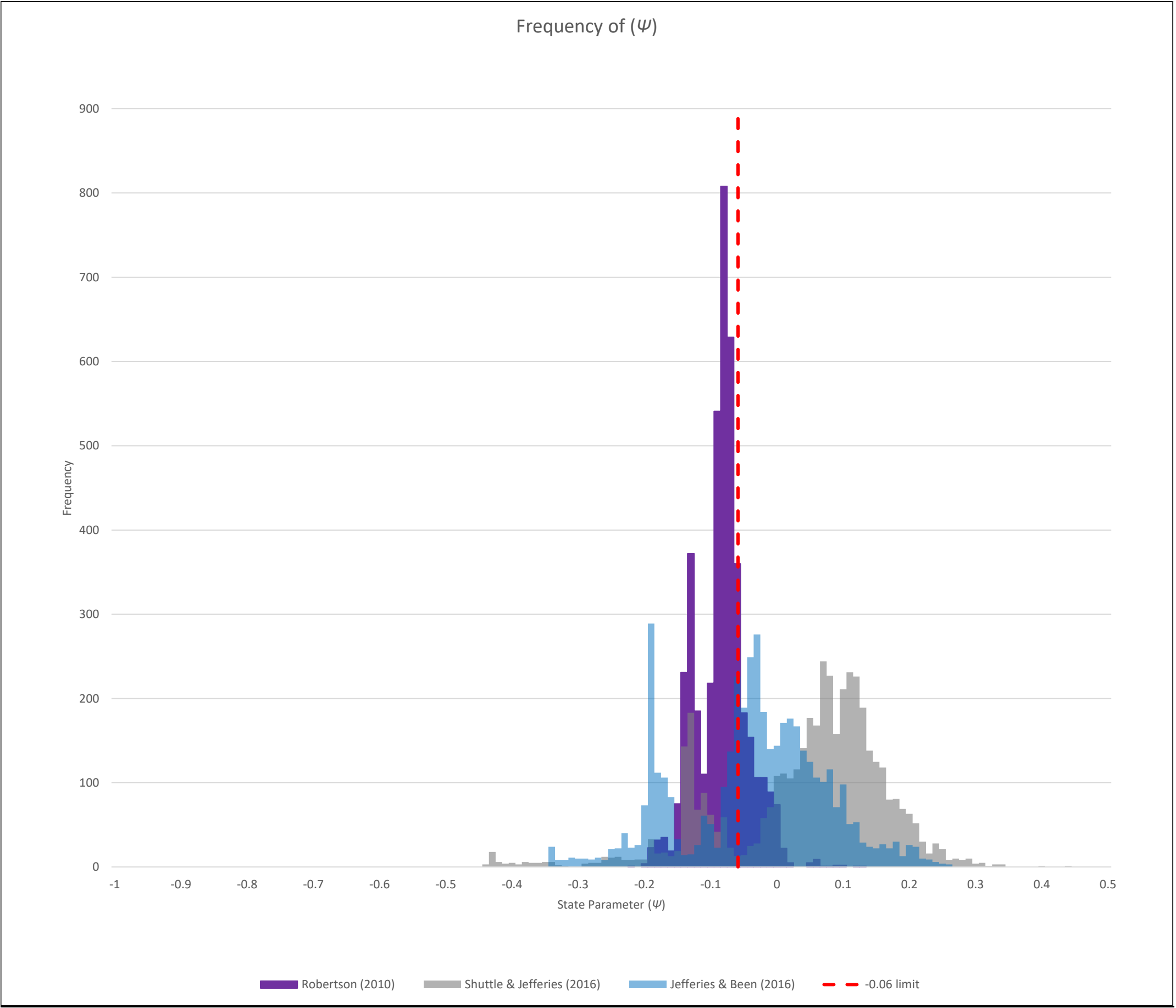




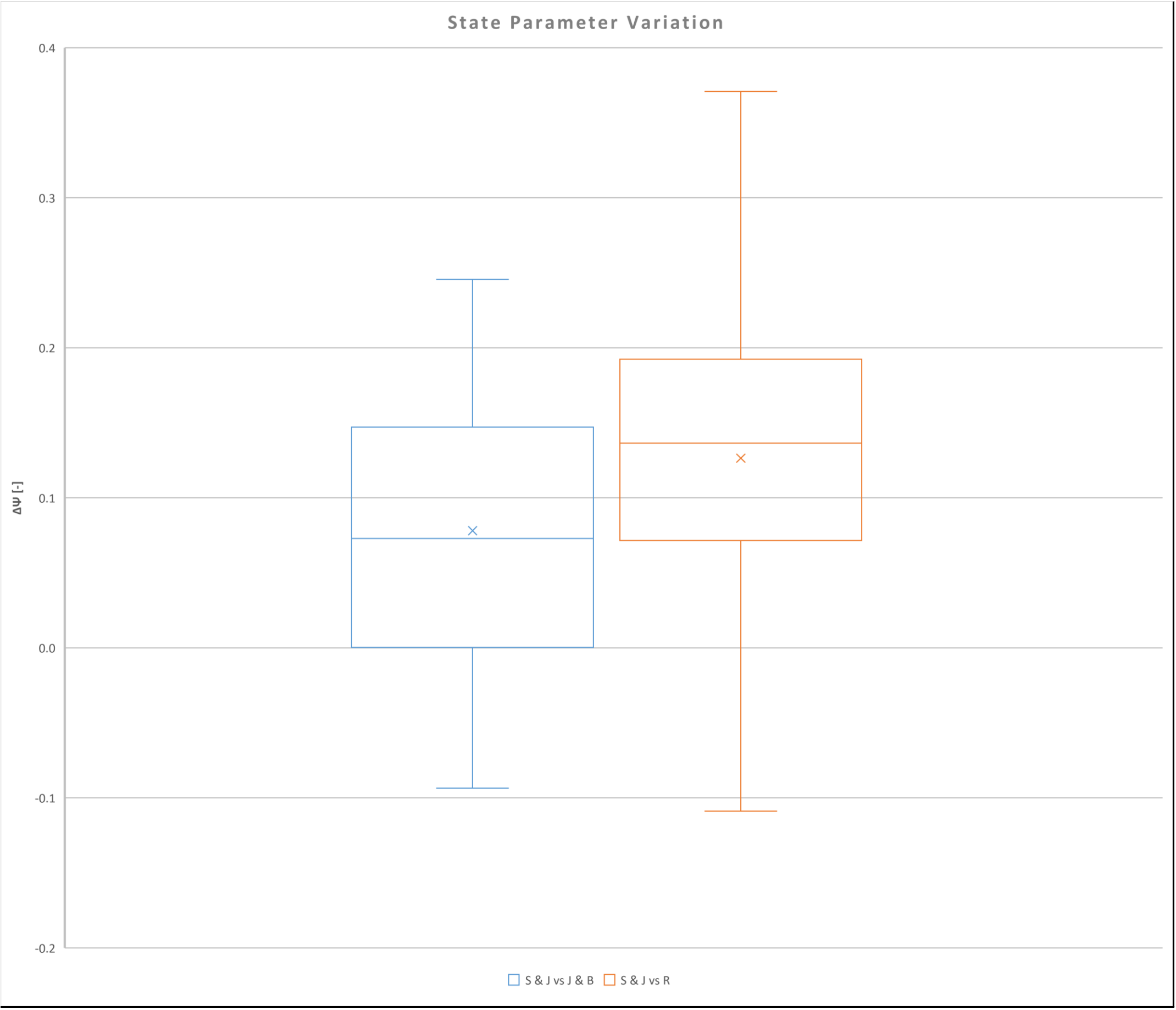
PCE1

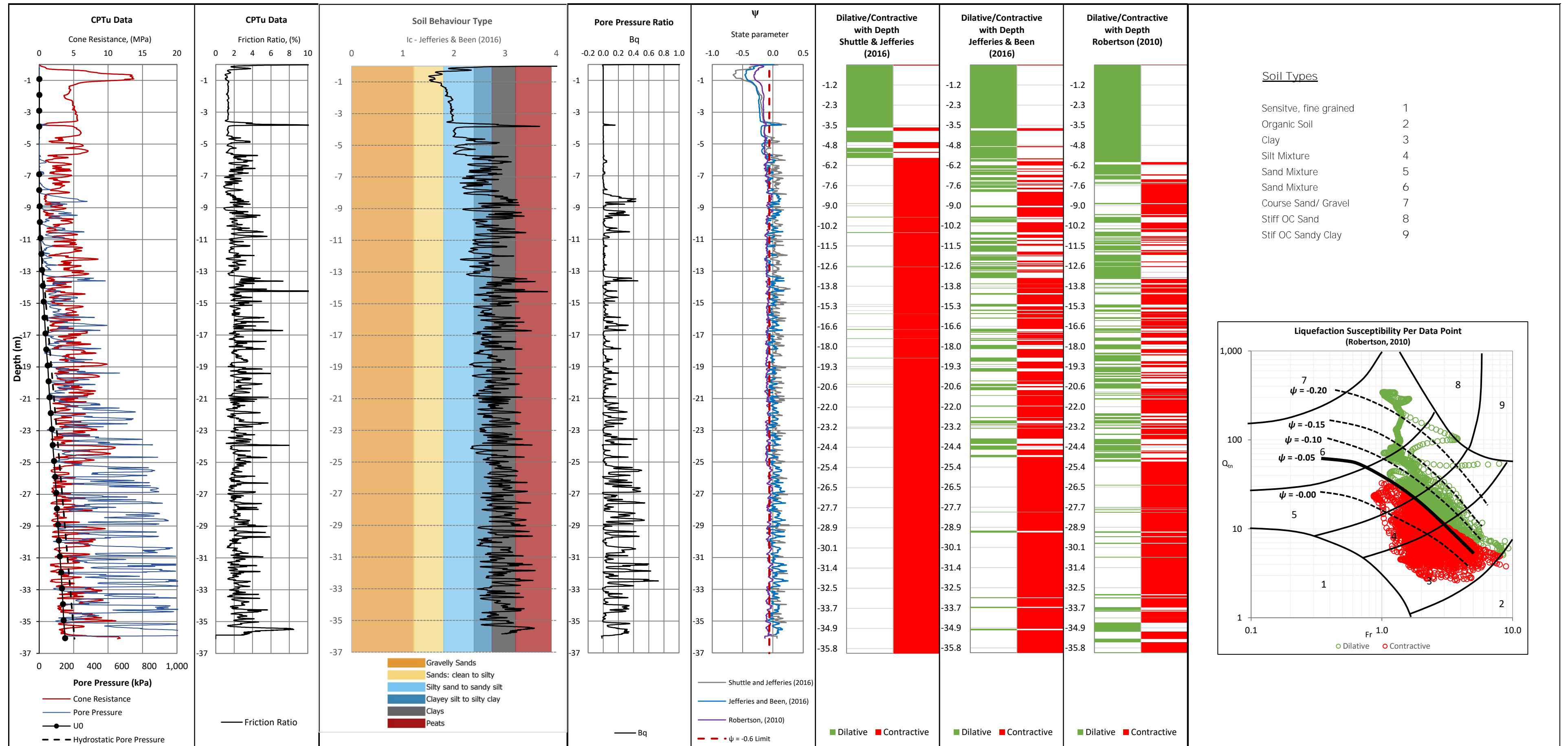


PCE1

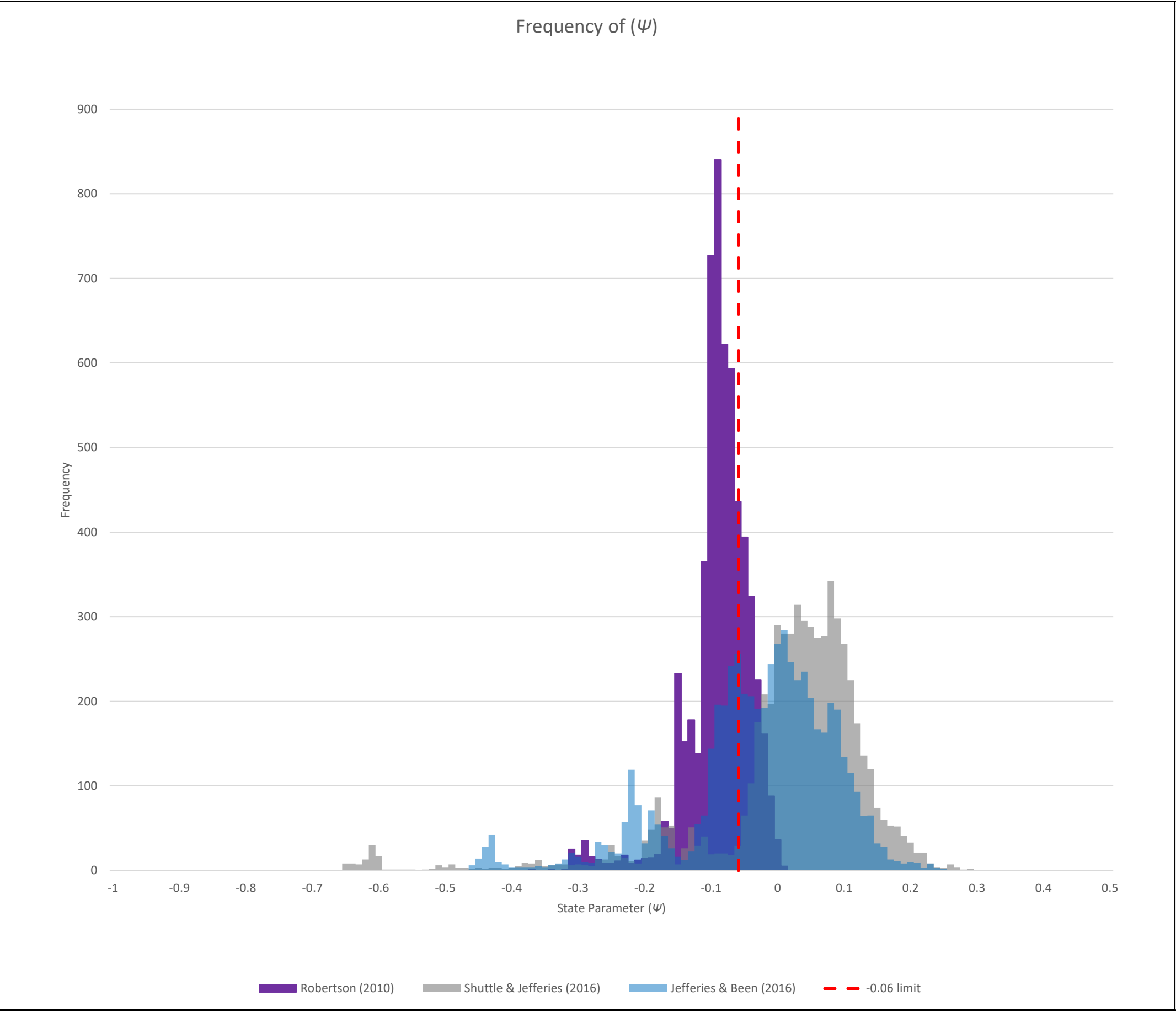


PCE1

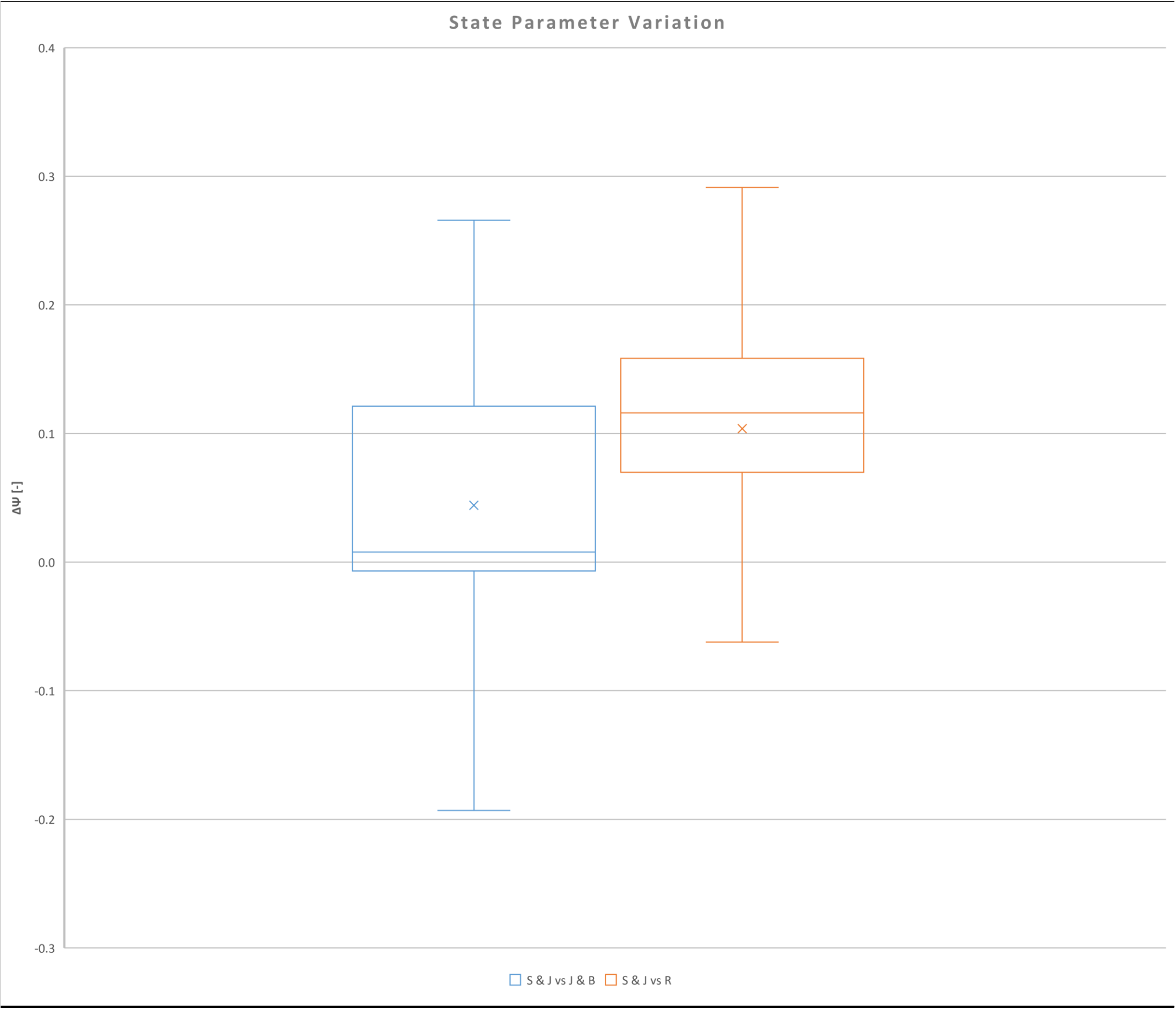




PCE2



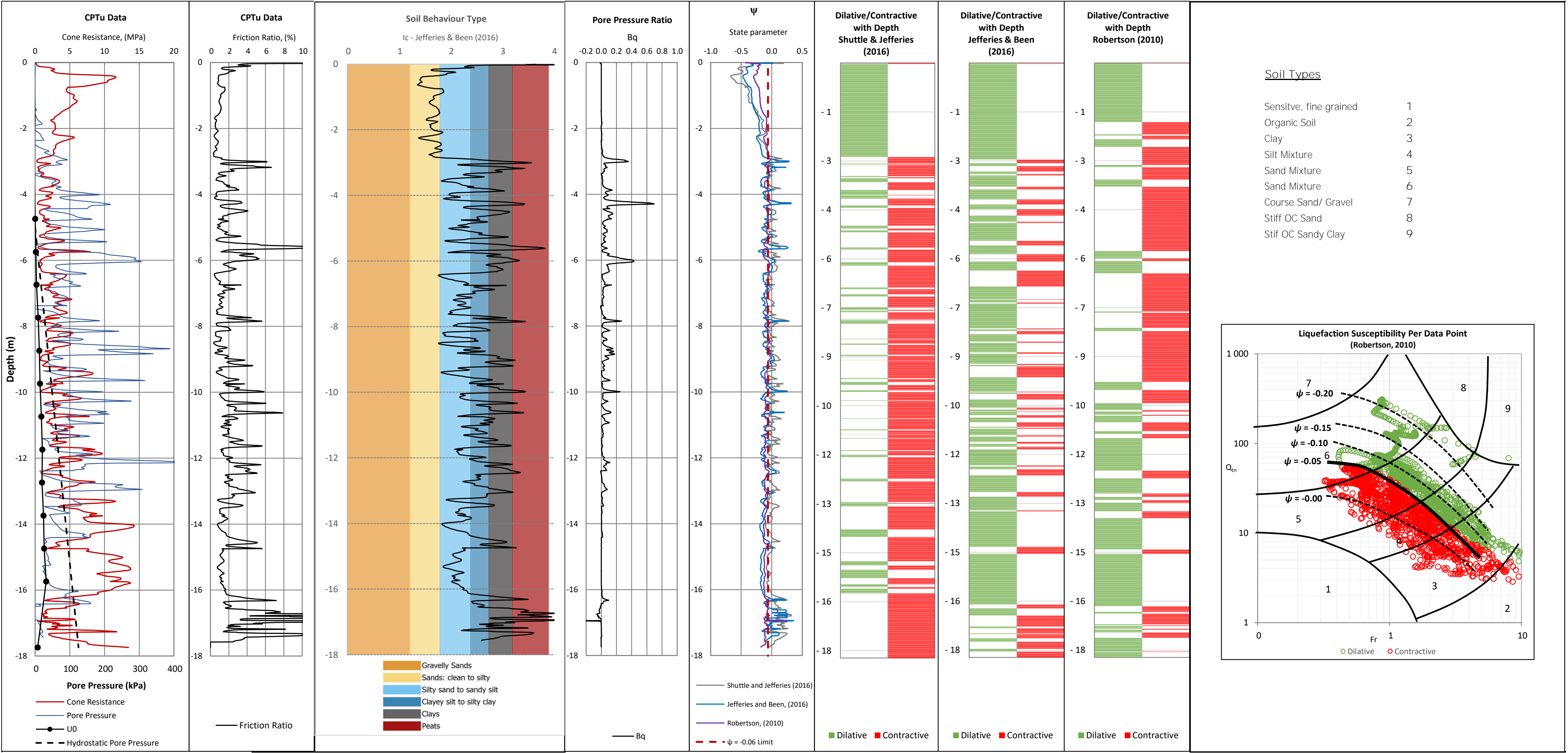
PCE2



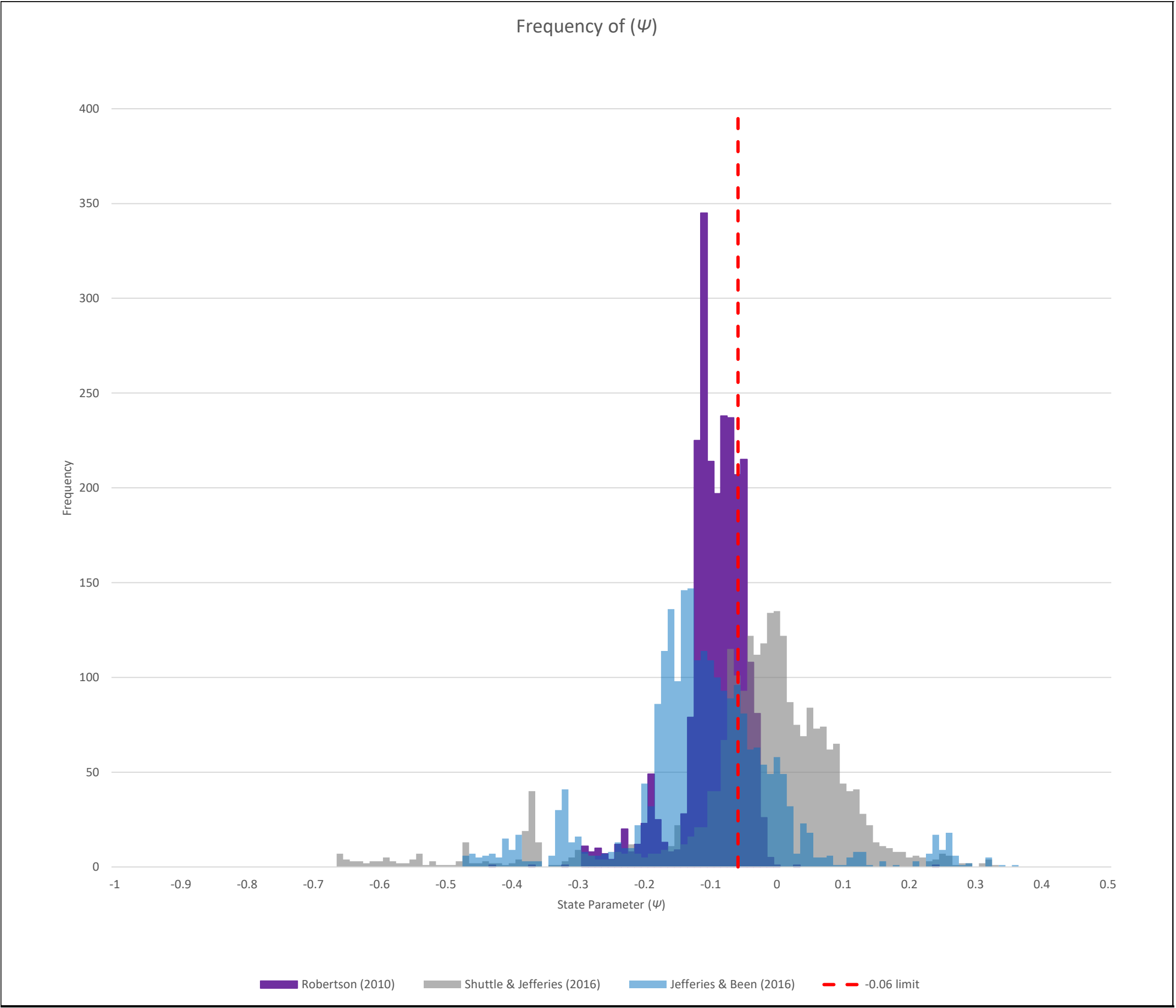
## **Appendix F: CPTu Interpretation – Monitoring Line F**



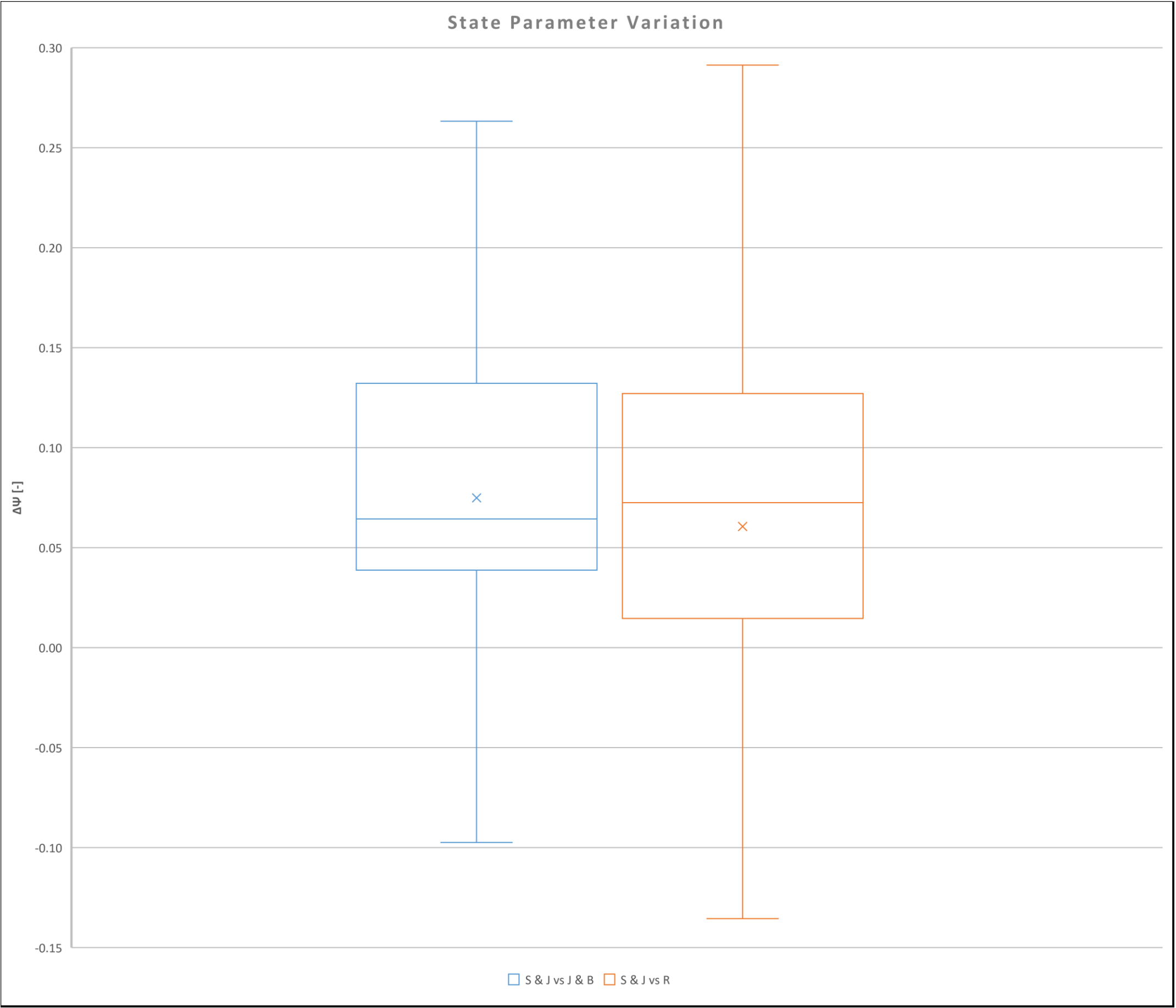
CPTu PC8



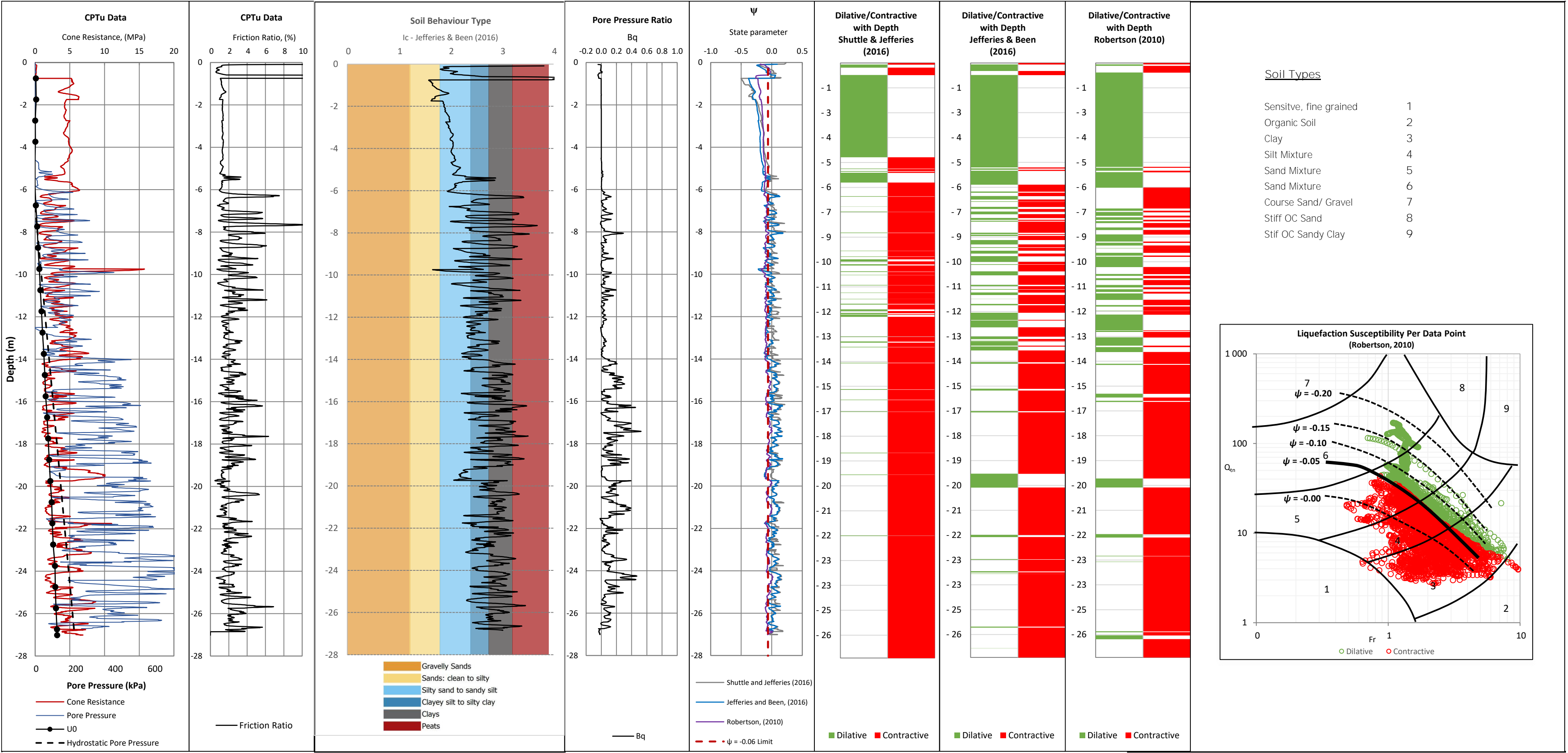
CPTu PC8



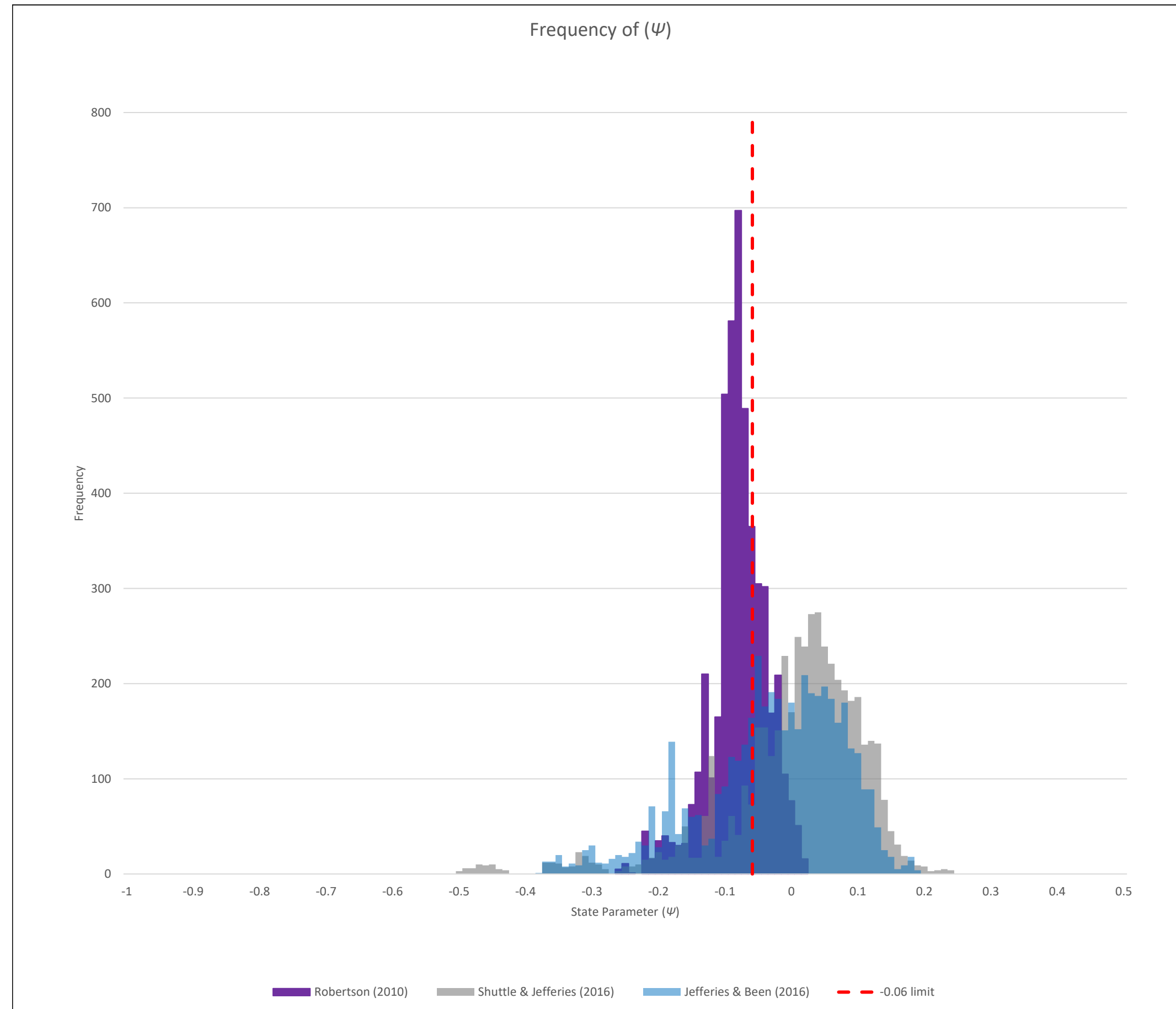
CPTu PC8



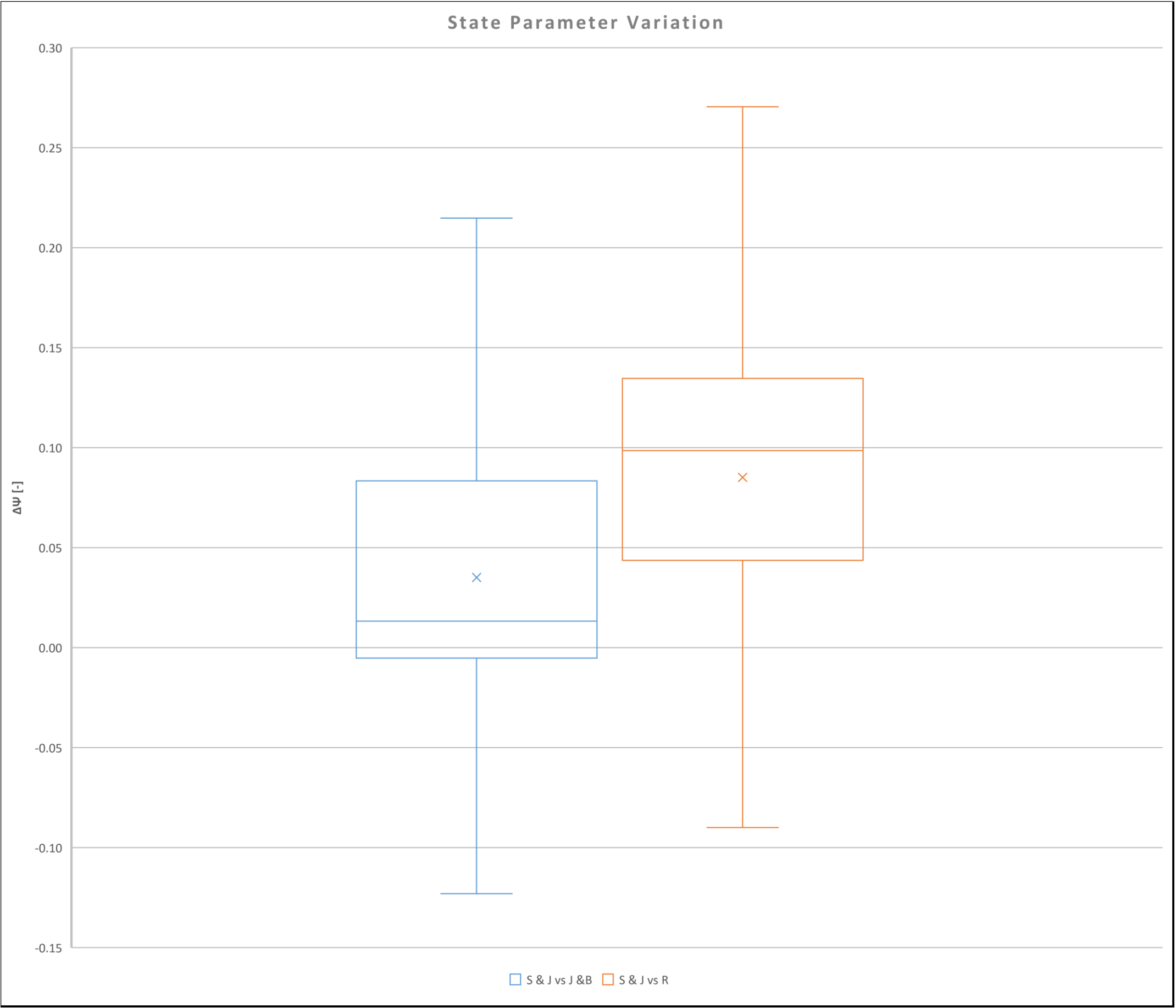
CPTu PC9



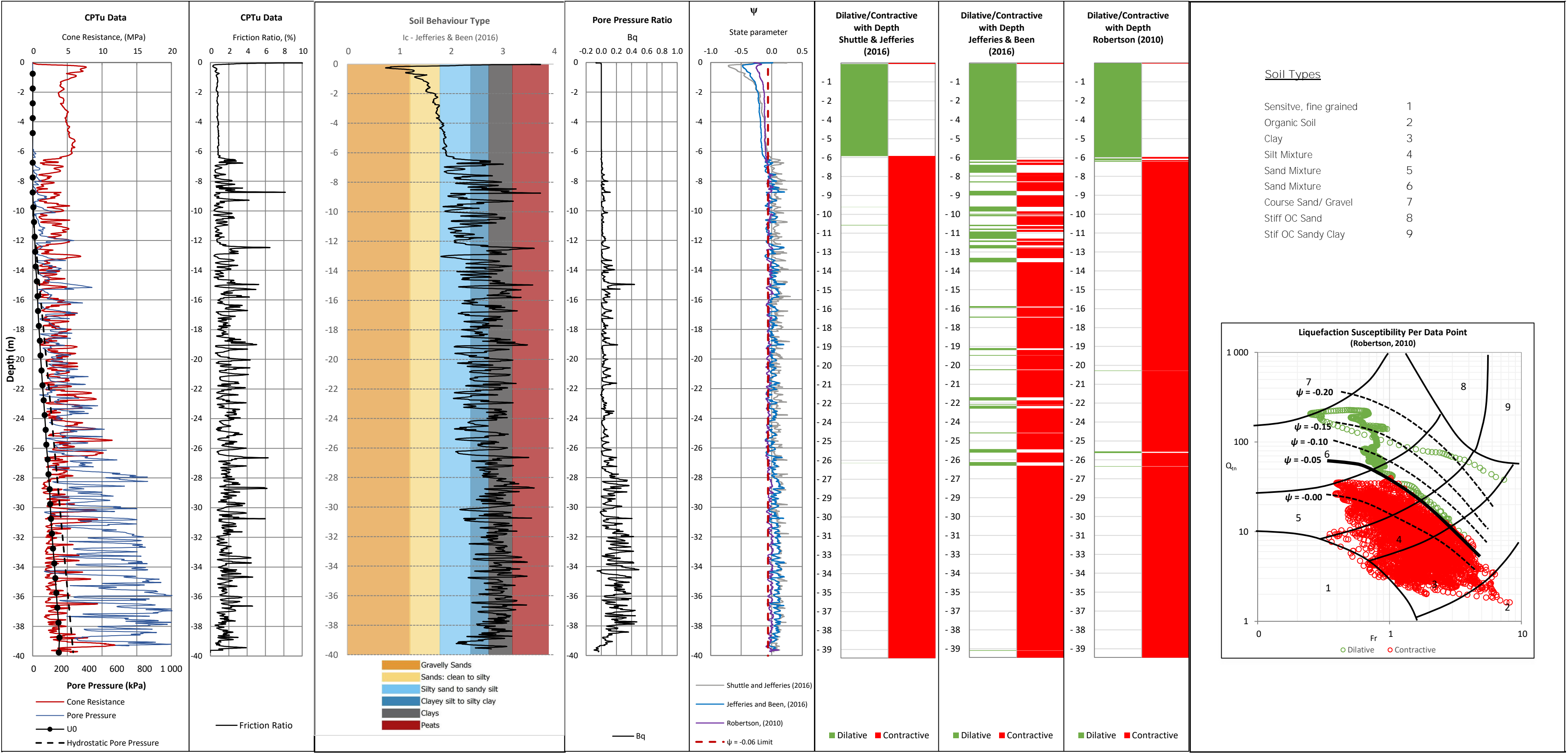
# CPTu PC9



CPTu PC9

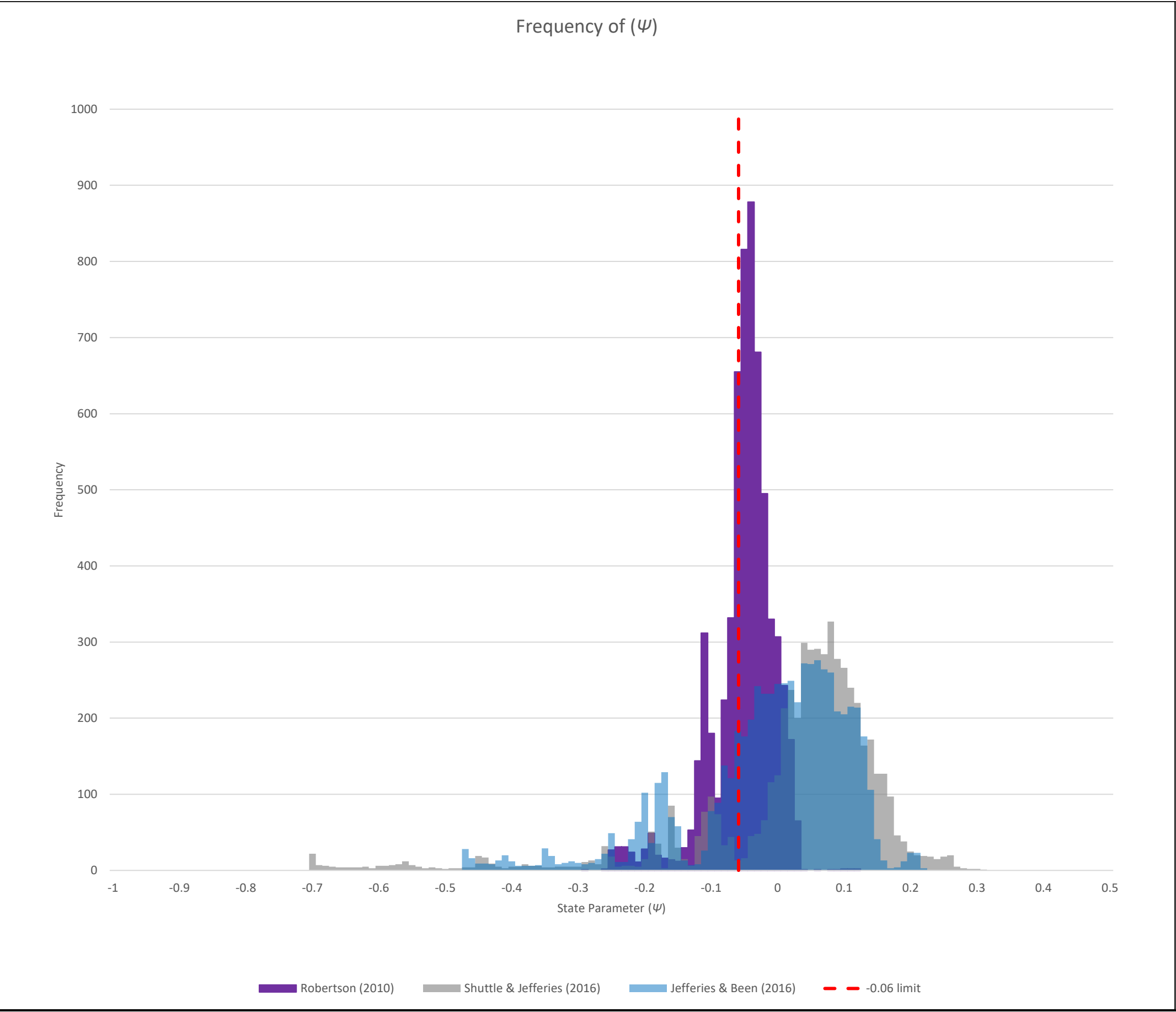


CPTu PC10

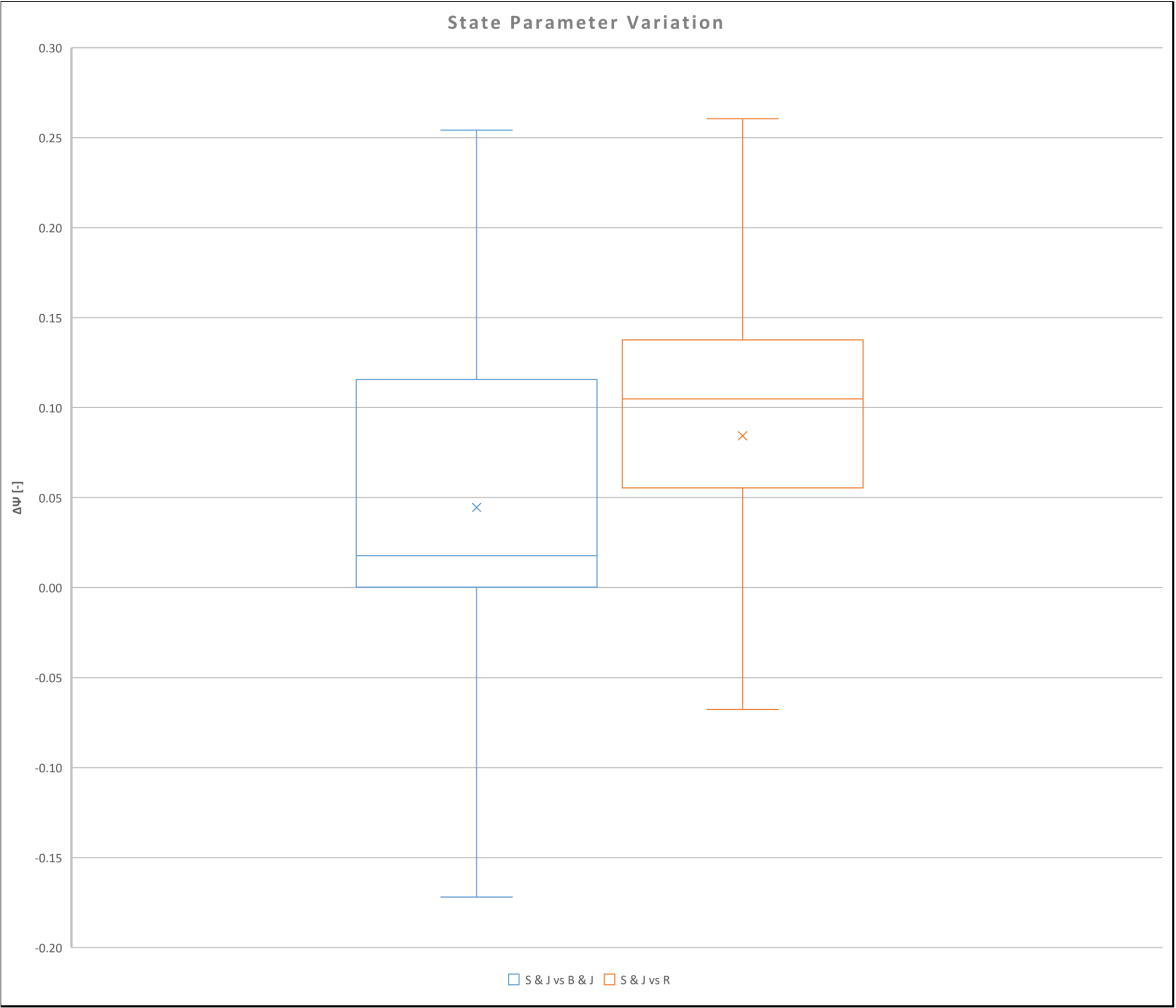




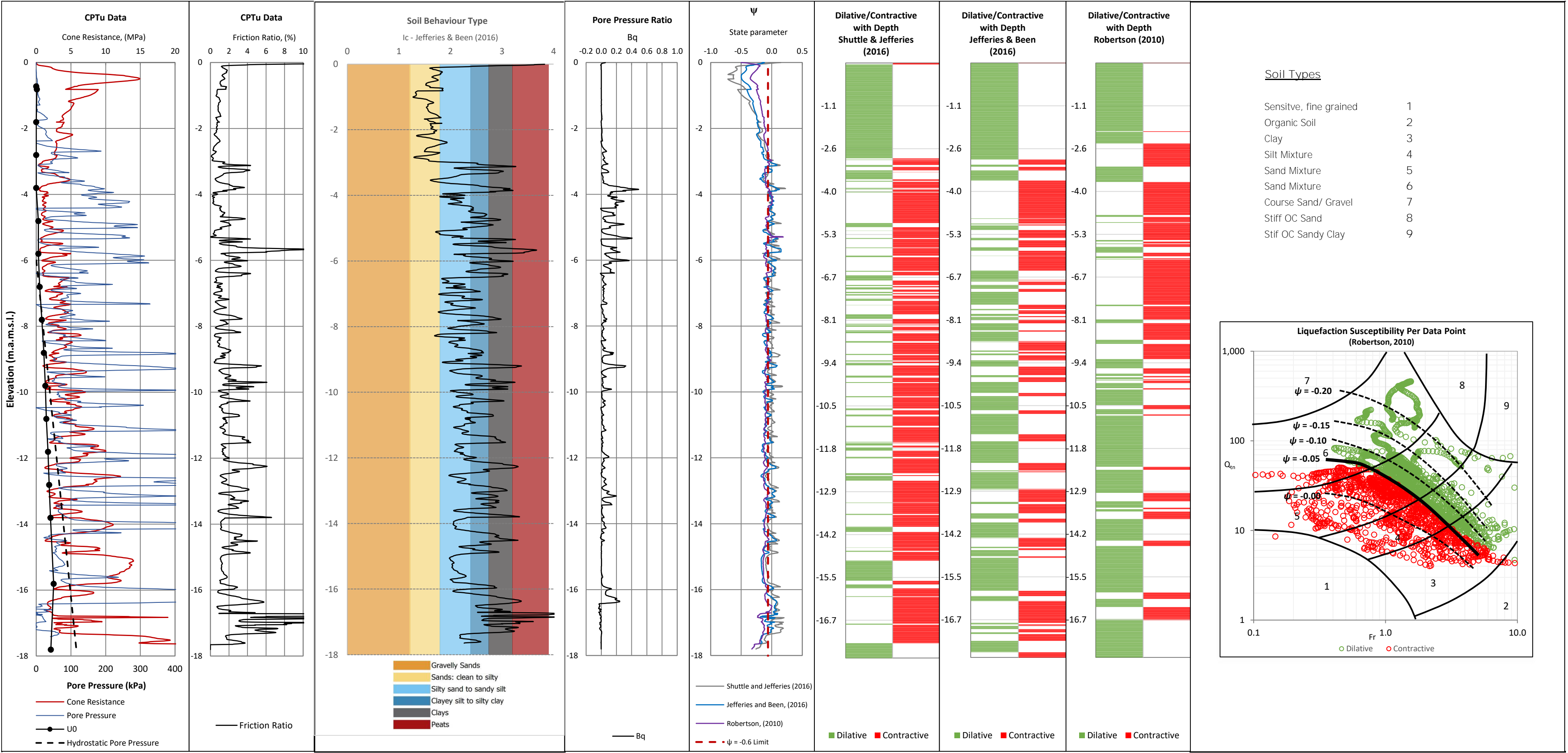
CPTu PC10



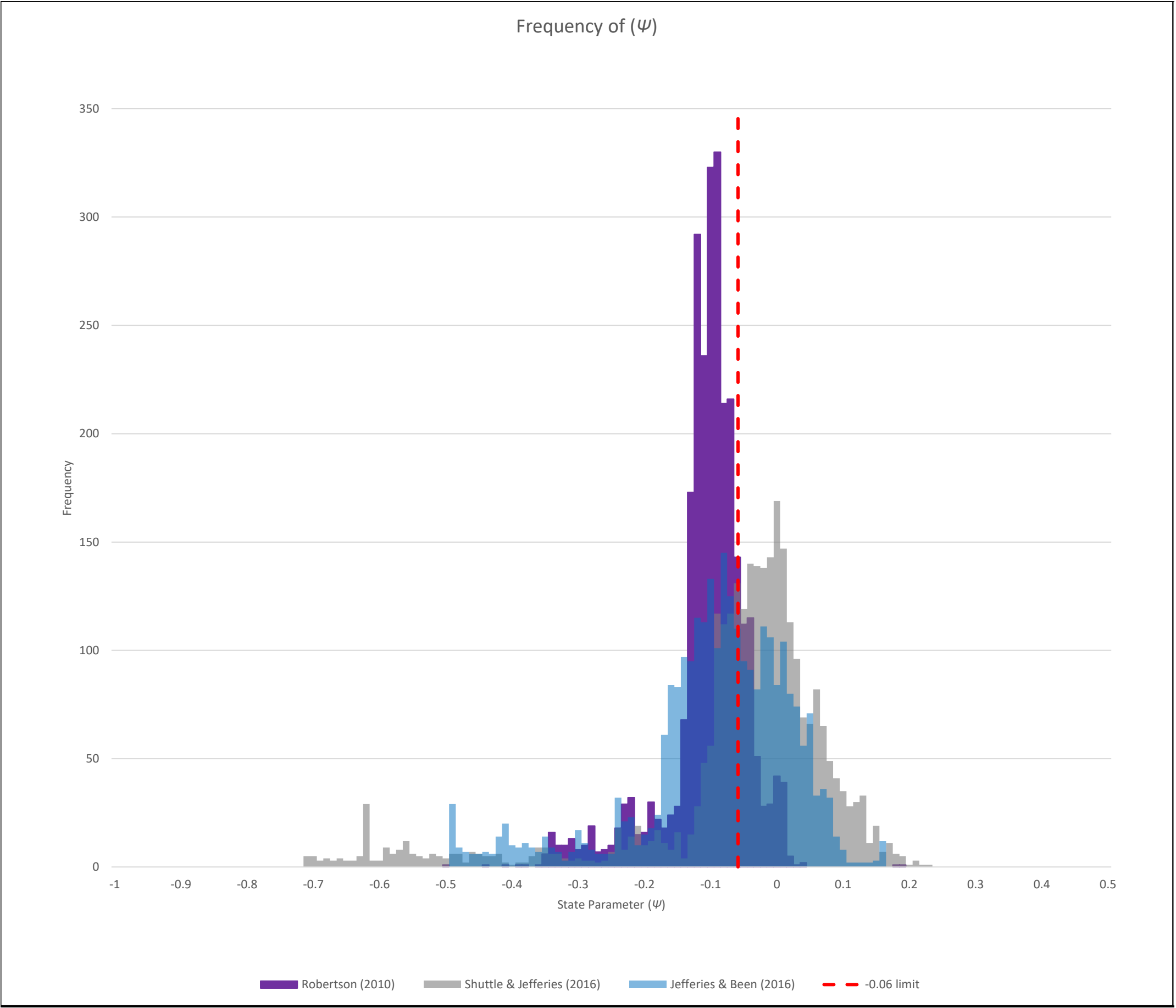
CPTu PC10



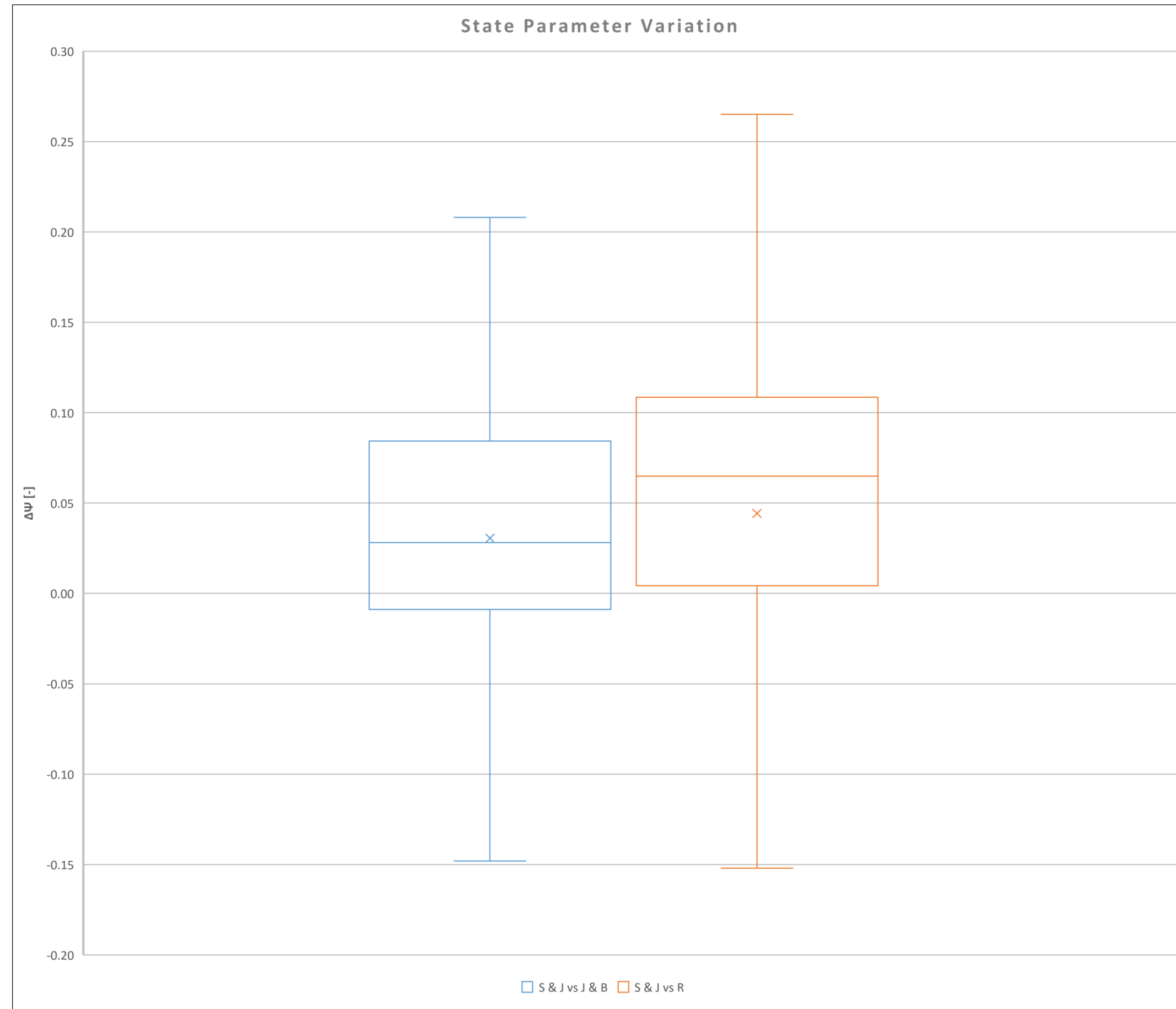
PC8-Q3\_CPTu



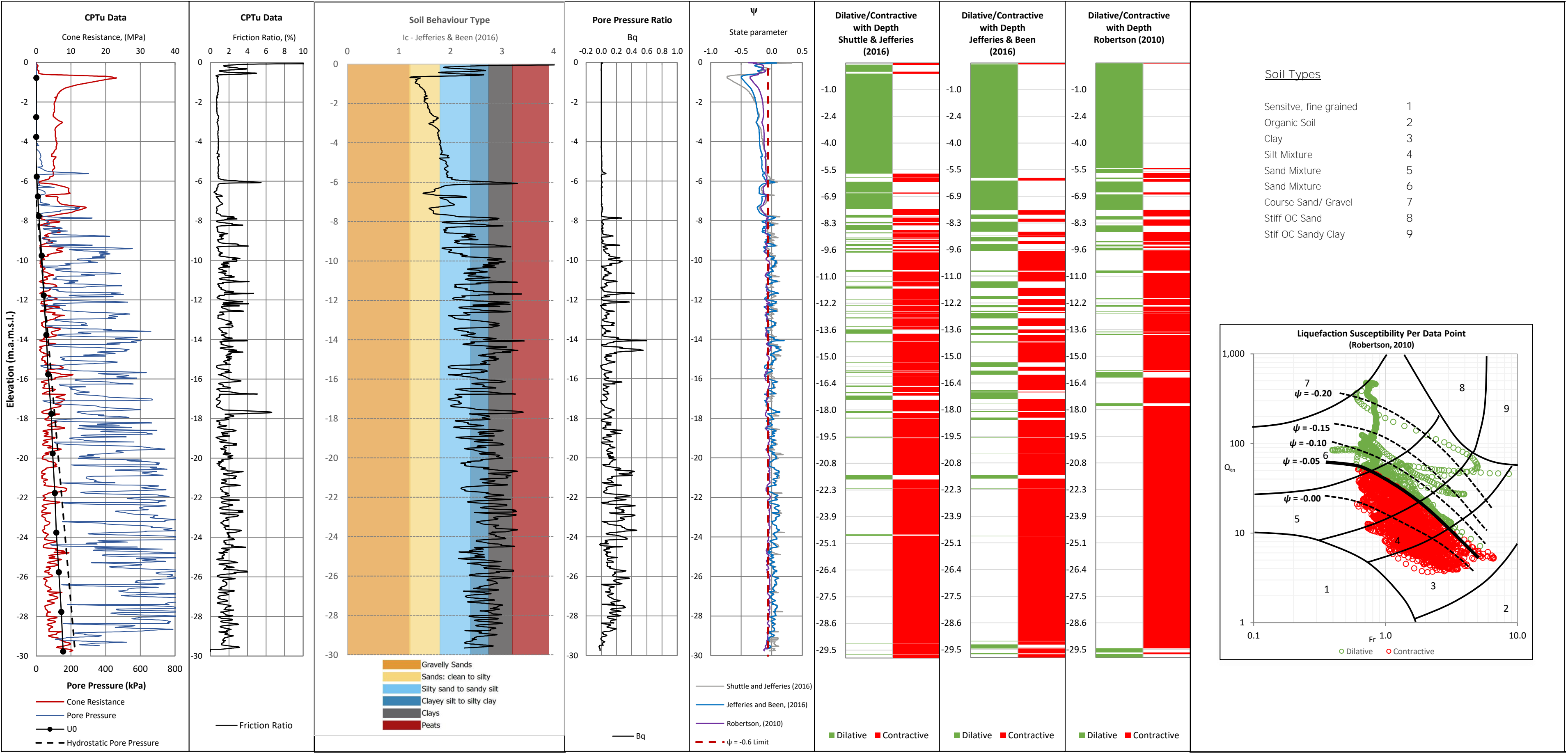
PC8-Q3\_CPTu



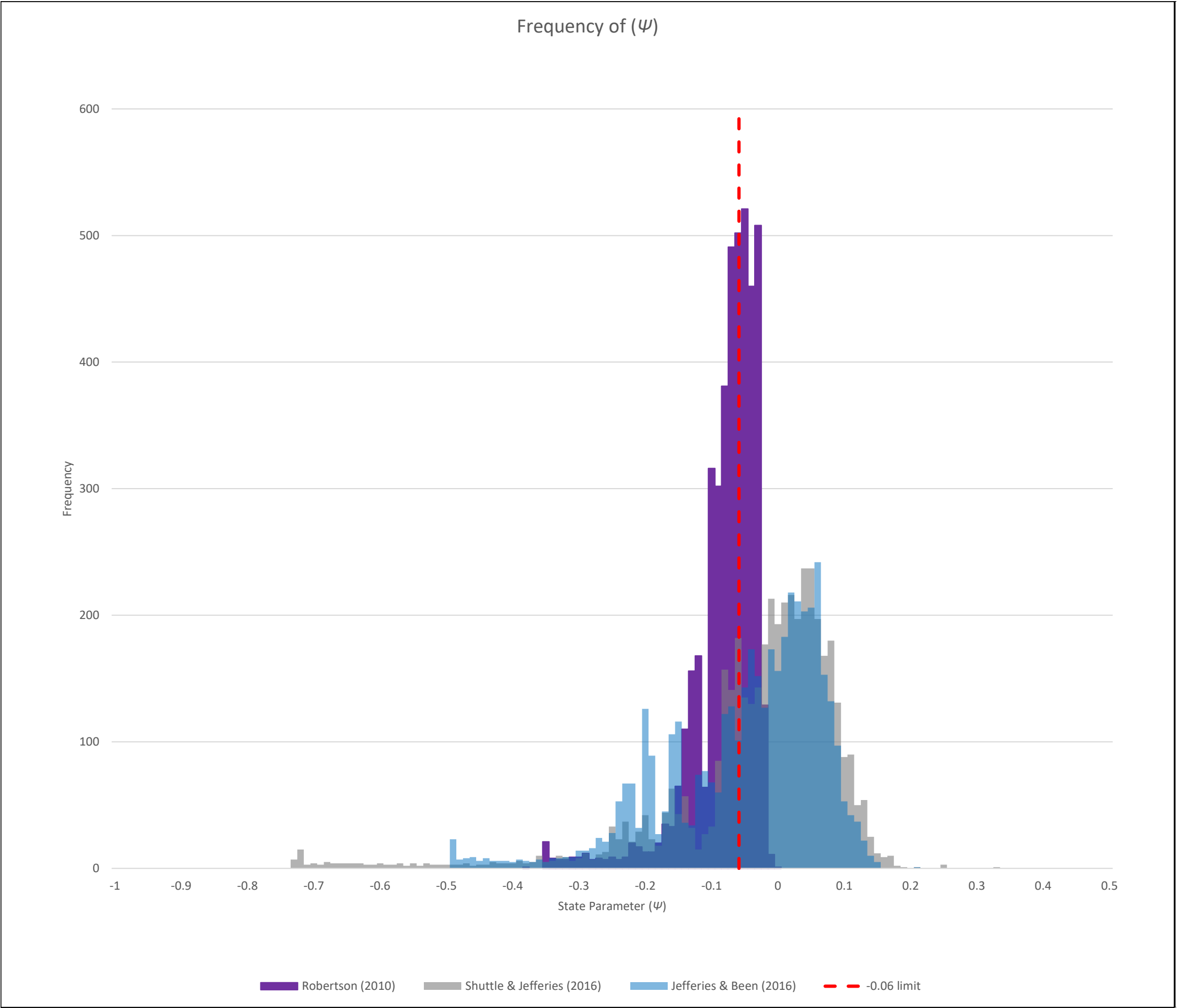
## PC8-Q3\_CPTu



PC9-Q3\_CPTu

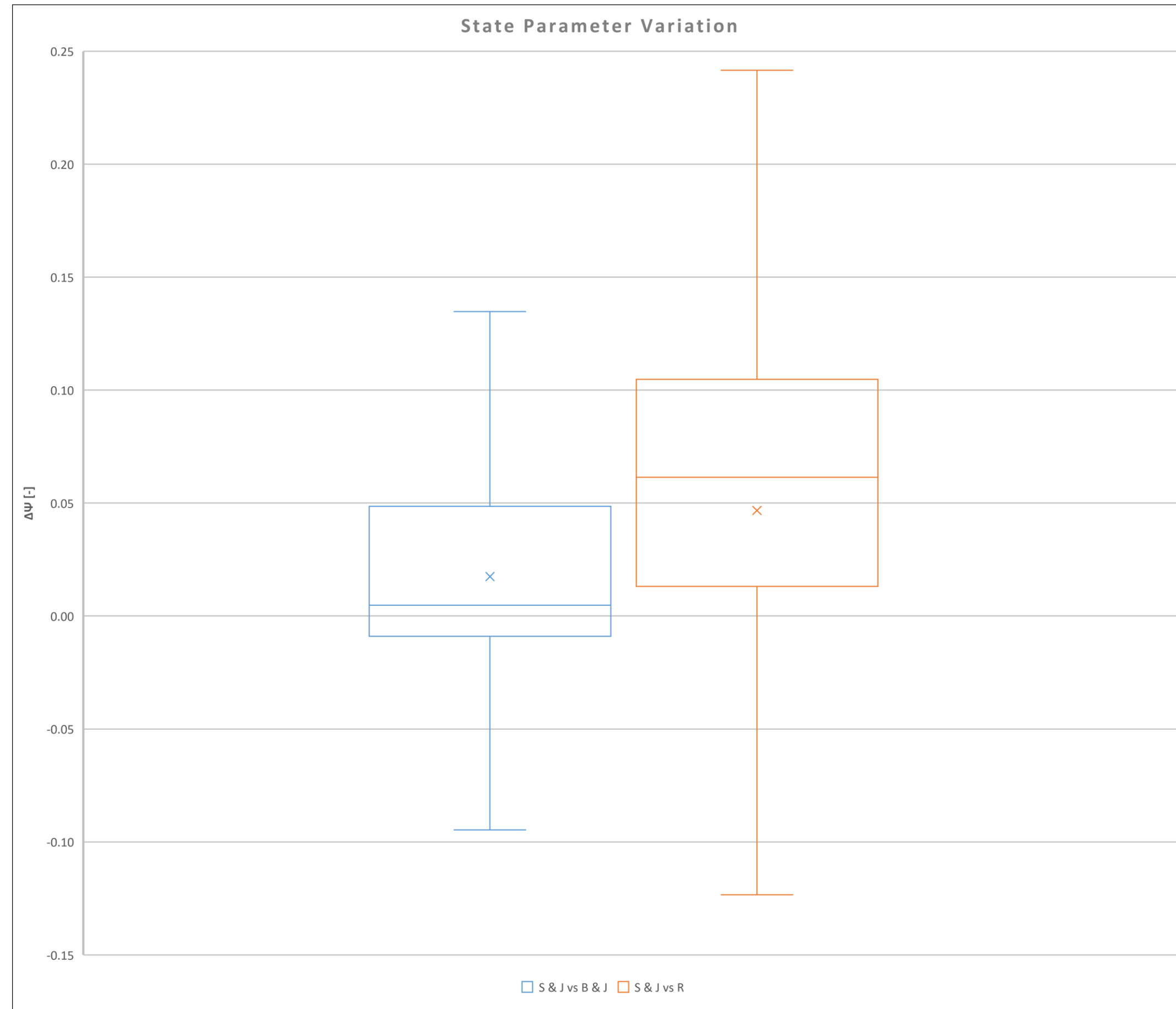


PC9-Q3\_CPTu

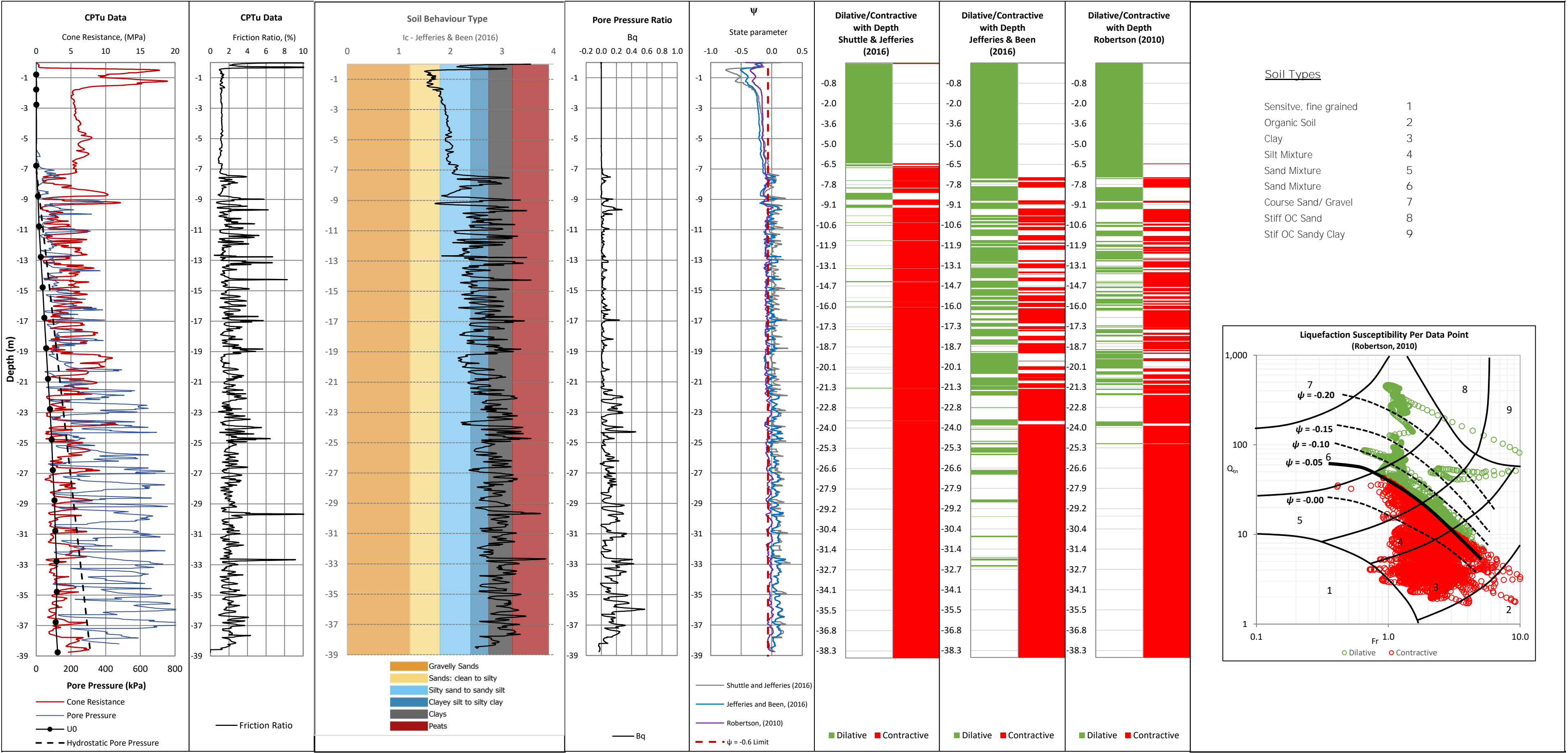




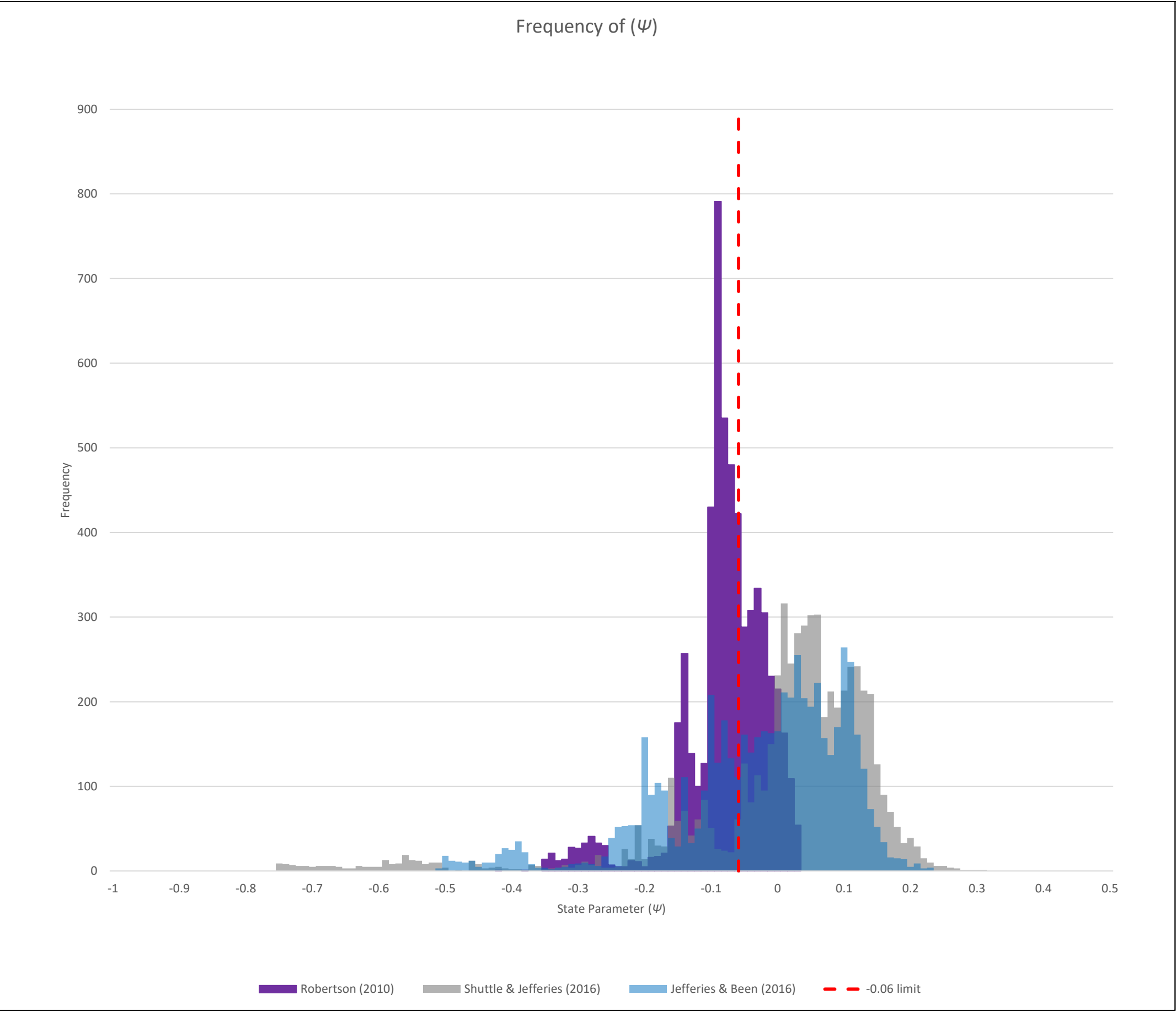
## PC9-Q3\_CPTu



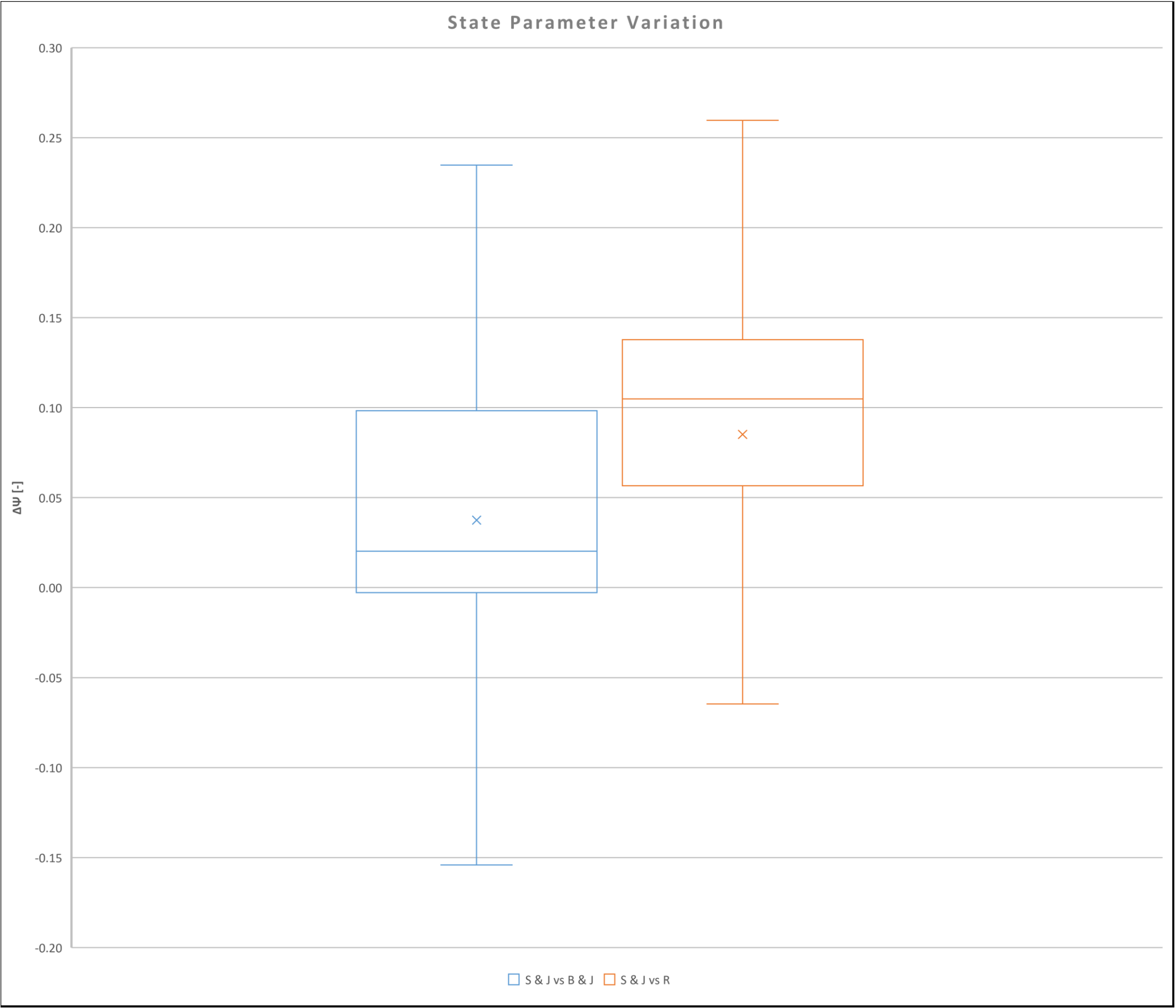
PC10-Q3\_CPTu



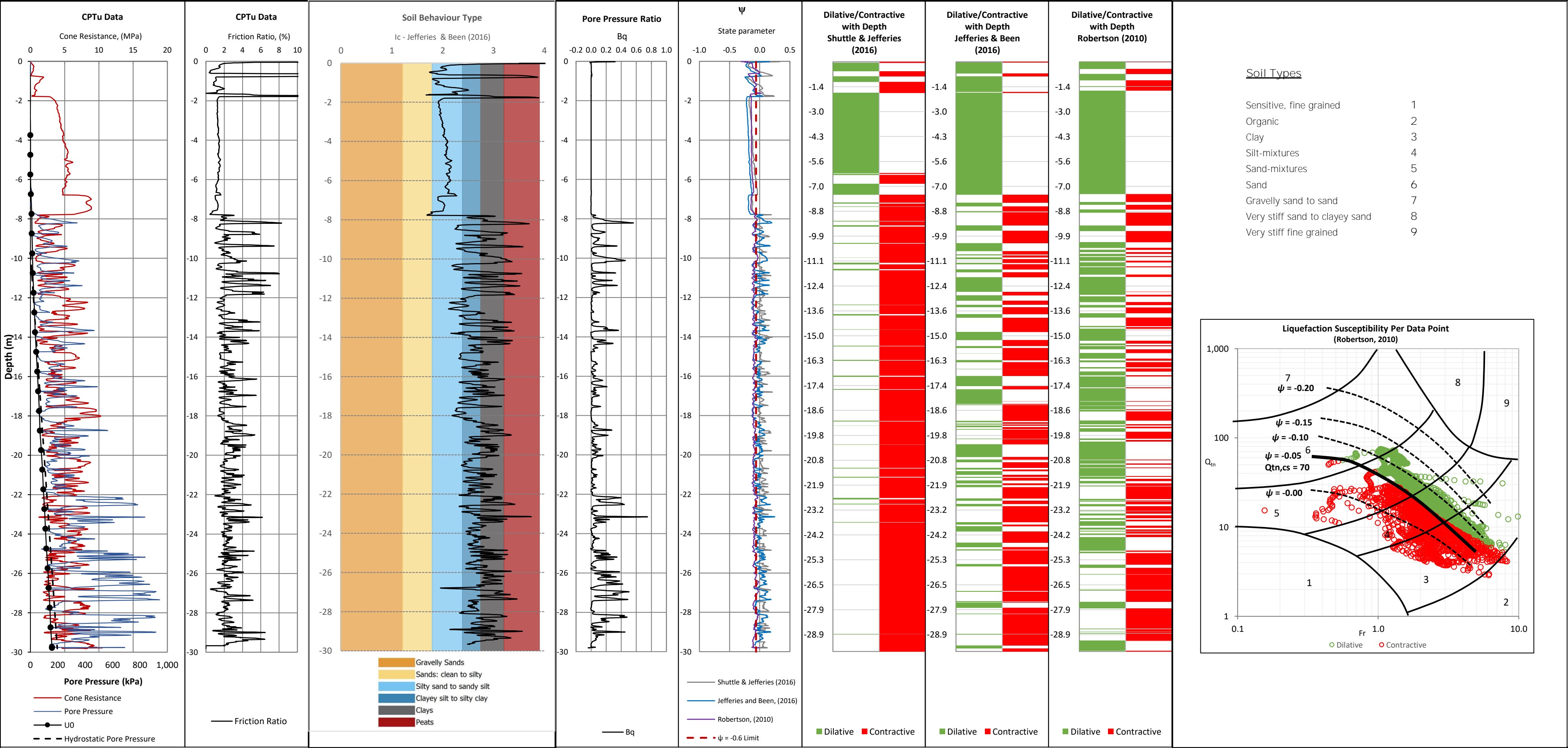
PC10-Q3\_CPTu



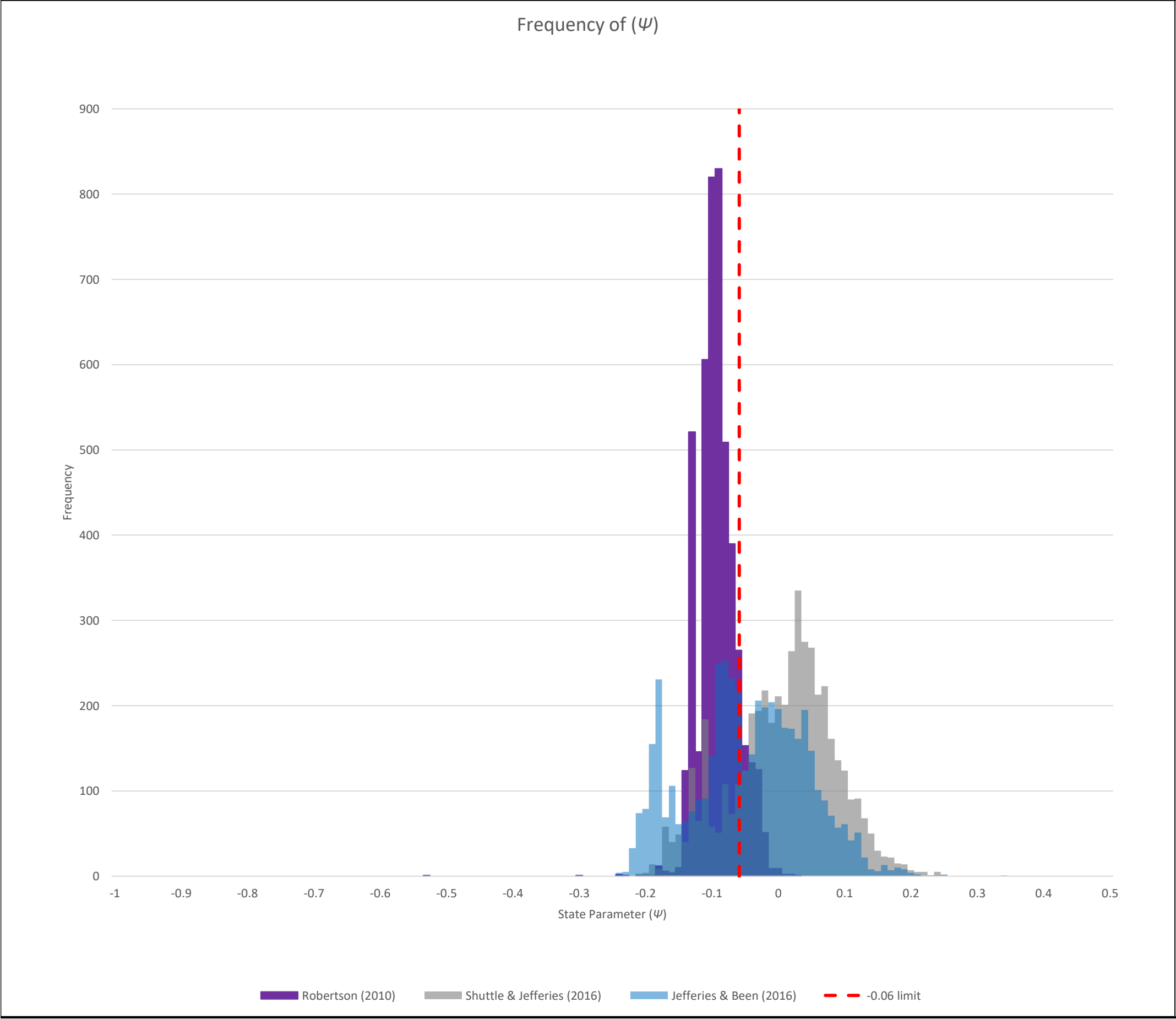
PC10-Q3\_CPTu



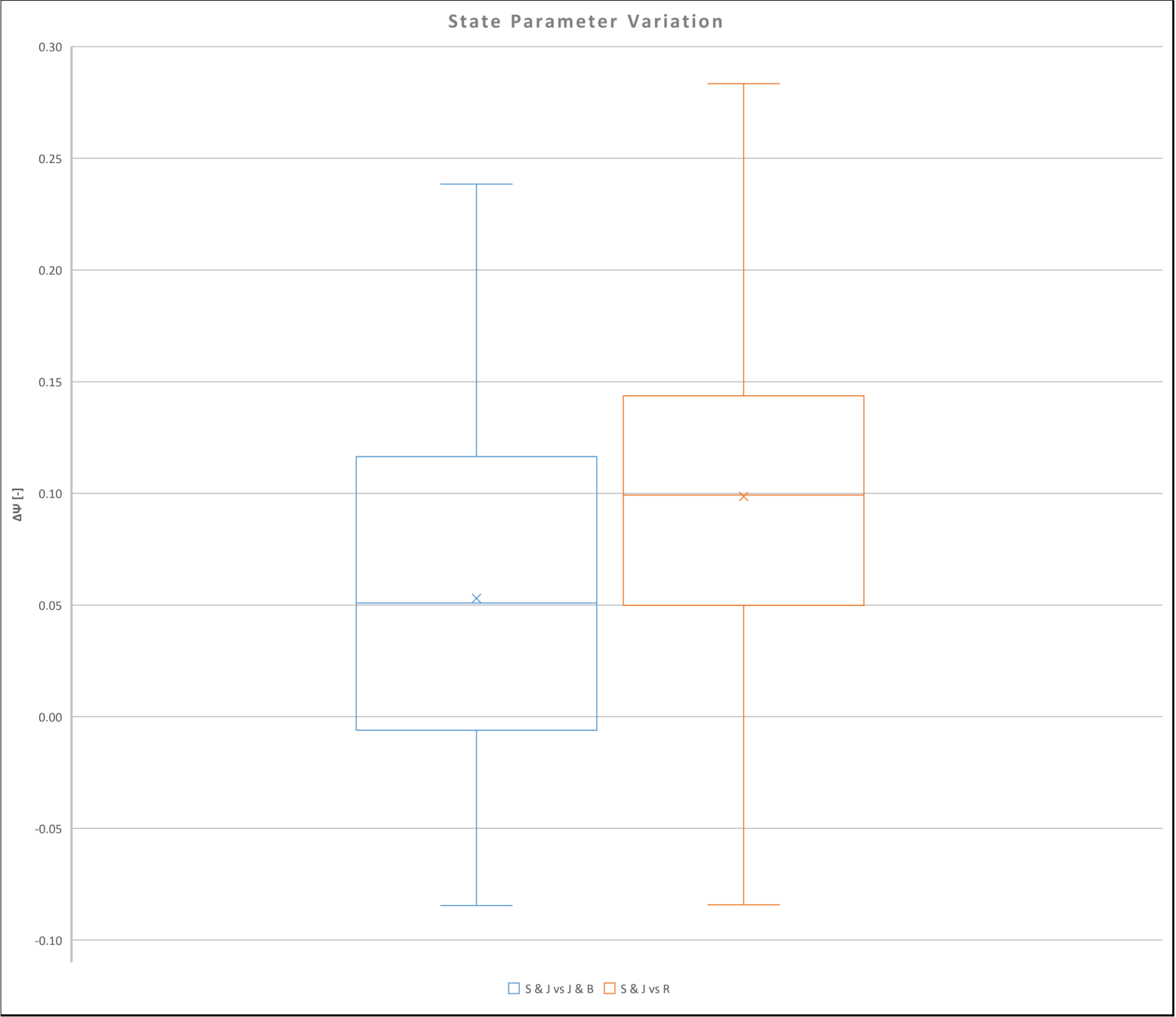
PCF1



PCF1

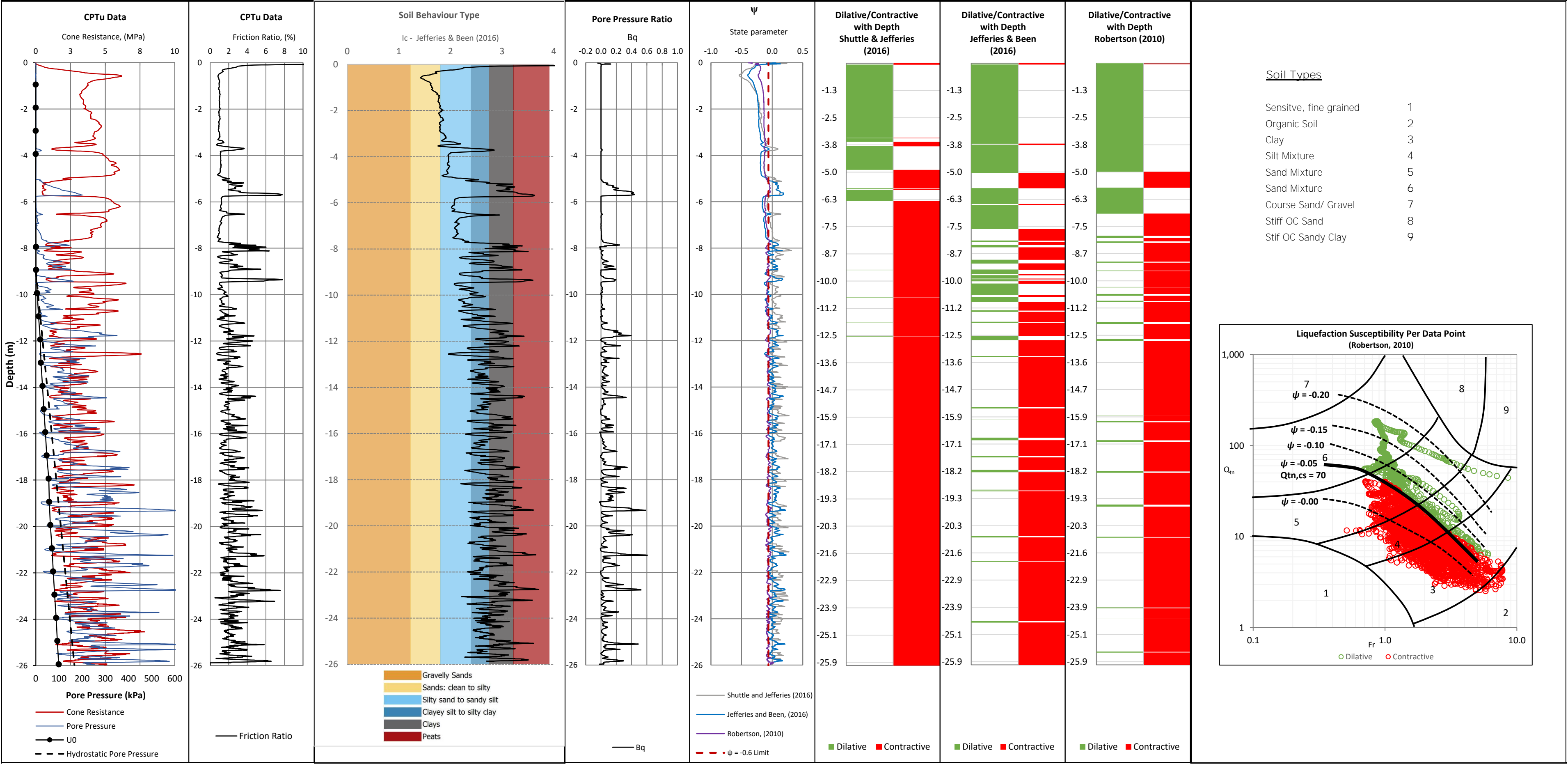


PCF1





PCF2



$\Psi$

State parameter

-1.0

-0.5

0.0

0.5

0

-2

-4

-6

-8

-10

-12

-14

-16

-18

-20

-22

-24

-26

Shuttle and Jefferies (2016)

Jefferies and Been, (2016)

Robertson, (2010)

$\Psi = -0.6$  Limit

Dilative/Contractive with Depth Shuttle & Jefferies (2016)

Dilative/Contractive with Depth Jefferies & Been (2016)

Dilative/Contractive with Depth Robertson (2010)

-1.3

-2.5

-3.8

-5.0

-6.3

-7.5

-8.7

-10.0

-11.2

-12.5

-13.6

-14.7

-15.9

-17.1

-18.2

-19.3

-20.3

-21.6

-22.9

-23.9

-25.1

-25.9

Dilative

Contractive

-1.3

-2.5

-3.8

-5.0

-6.3

-7.5

-8.7

-10.0

-11.2

-12.5

-13.6

-14.7

-15.9

-17.1

-18.2

-19.3

-20.3

-21.6

-22.9

-23.9

-25.1

-25.9

Dilative

Contractive

-1.3

-2.5

-3.8

-5.0

-6.3

-7.5

-8.7

-10.0

-11.2

-12.5

-13.6

-14.7

-15.9

-17.1

-18.2

-19.3

-20.3

-21.6

-22.9

-23.9

-25.1

-25.9

Dilative

Contractive

Soil Types

Sensitive, fine grained

1

Organic Soil

2

Clay

3

Silt Mixture

4

Sand Mixture

5

Sand Mixture

6

Course Sand/ Gravel

7

Stiff OC Sand

8

Stif OC Sandy Clay

9

Liquefaction Susceptibility Per Data Point (Robertson, 2010)

1,000

100

10

1

0.1

1.0

10.0

7

$\psi = -0.20$

8

9

6

$\psi = -0.15$

5

$\psi = -0.10$

4

$\psi = -0.05$

3

$\psi = -0.00$

2

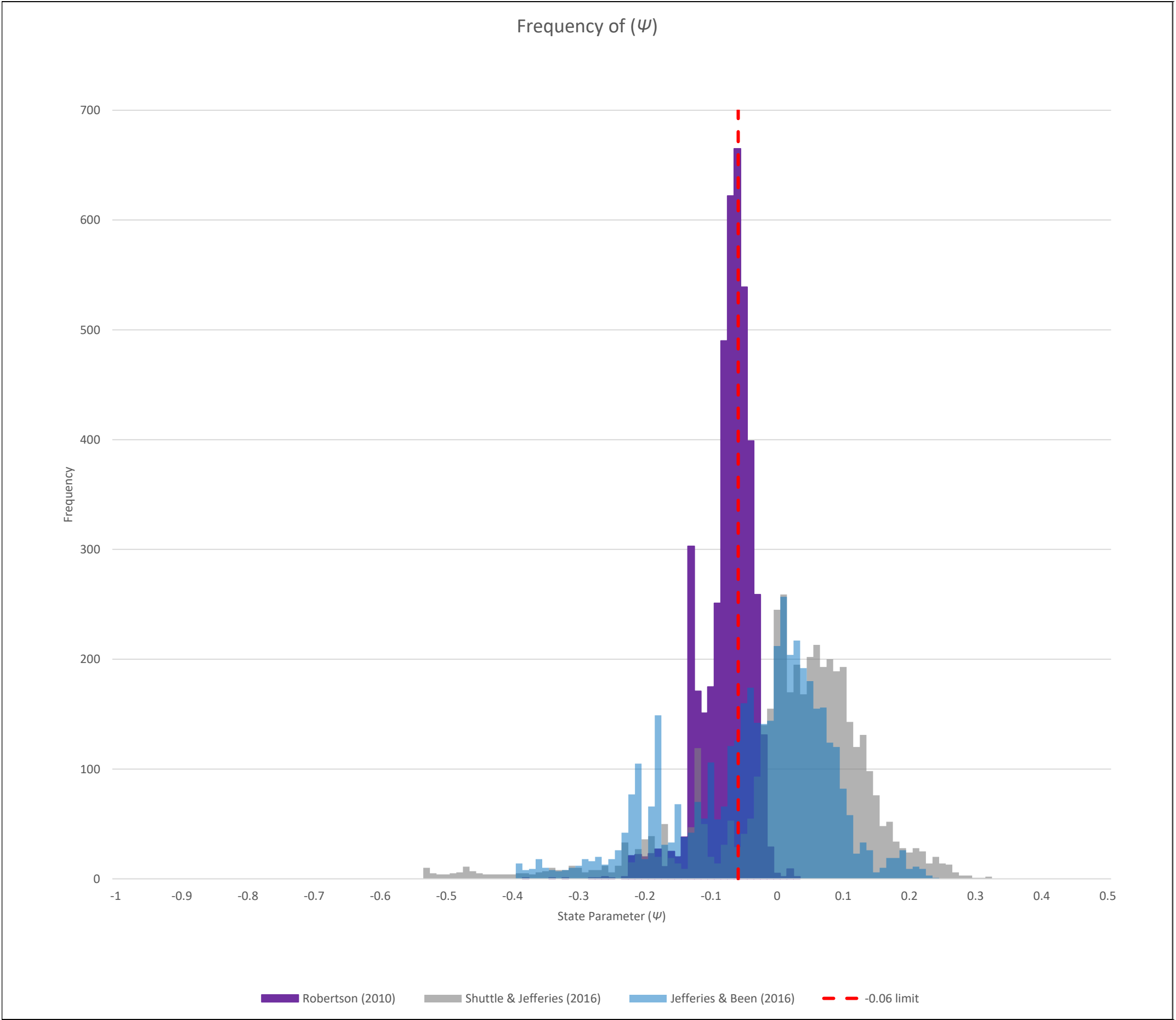
1

$Q_{tn,cs} = 70$

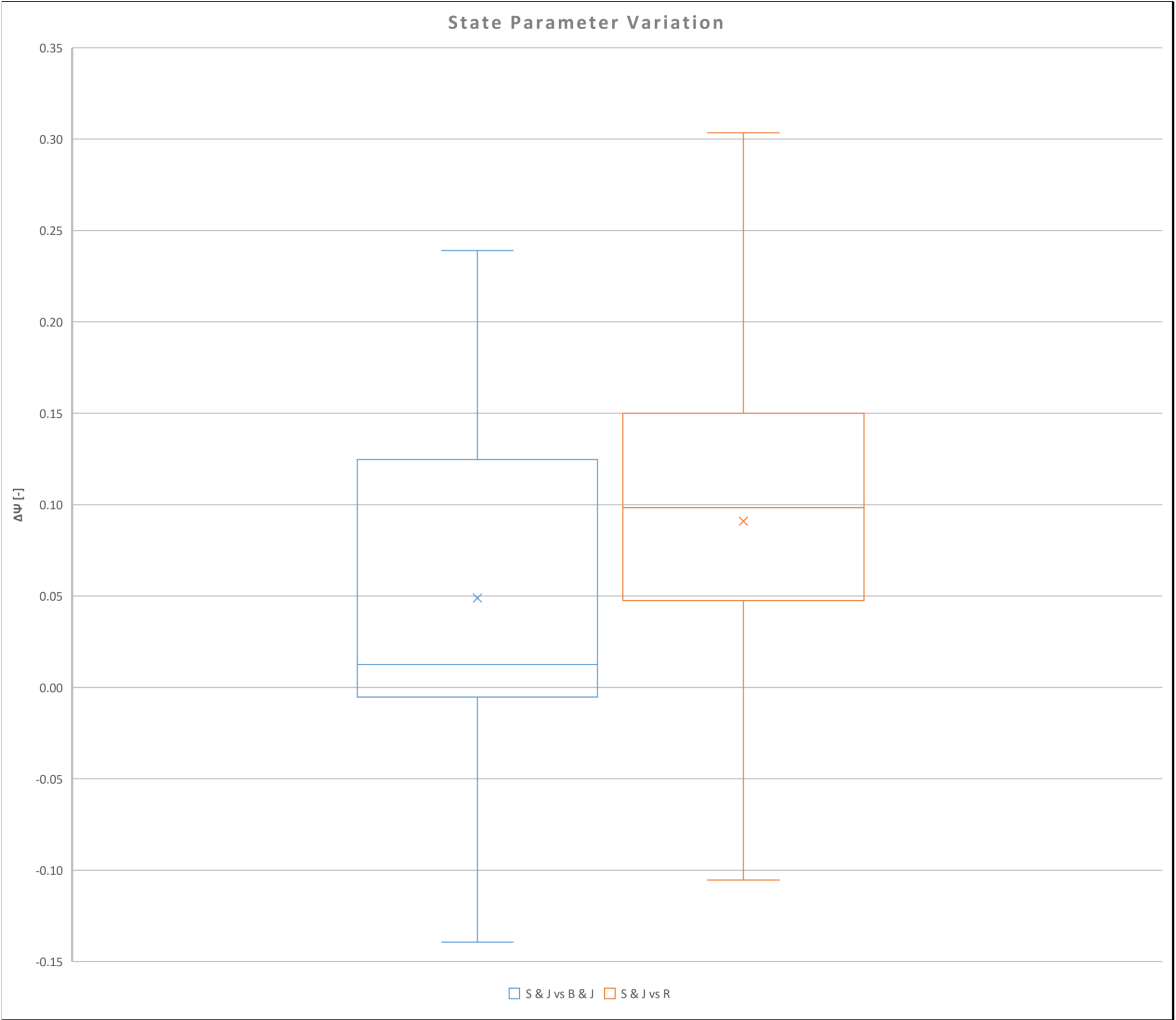
Dilative

Contractive

PCF2

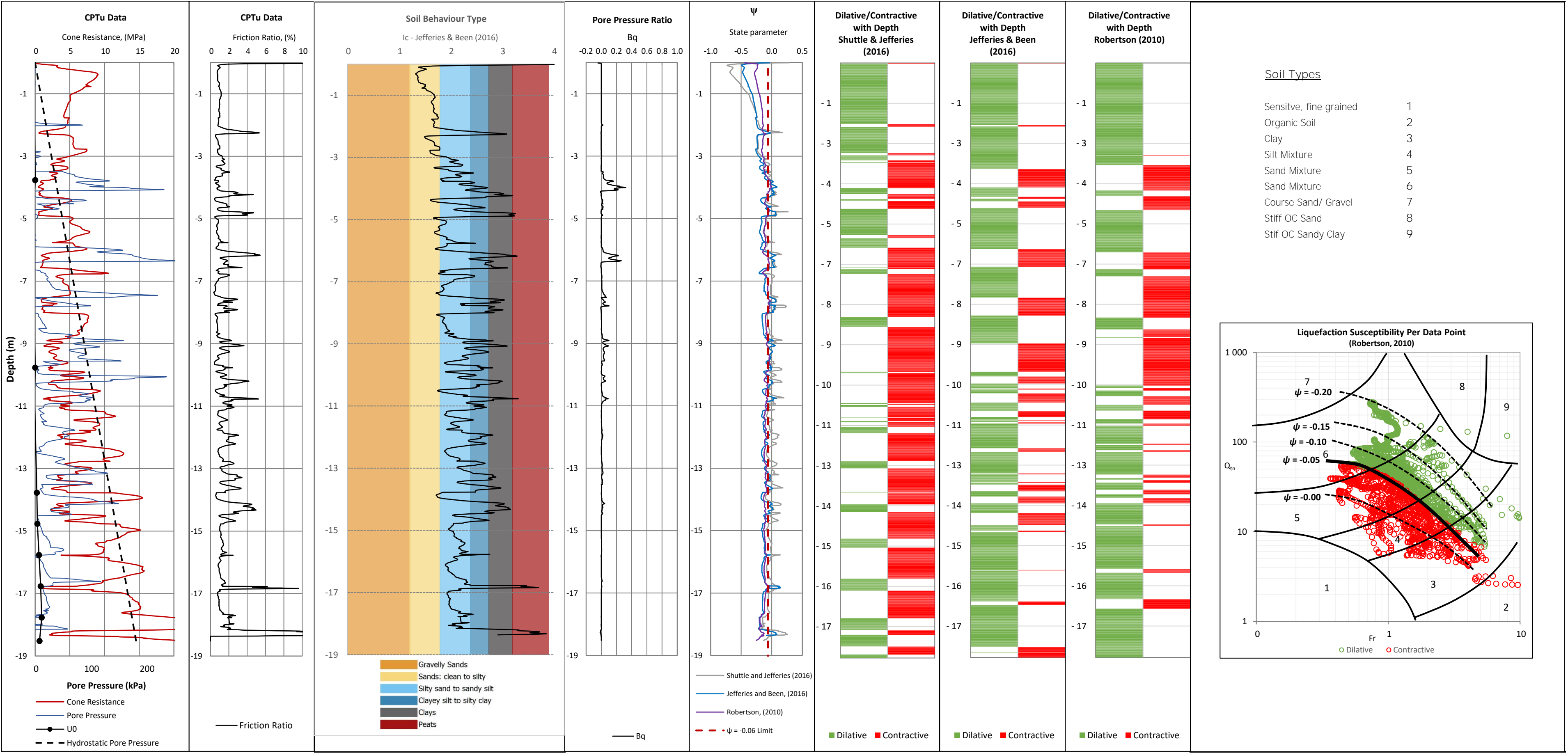


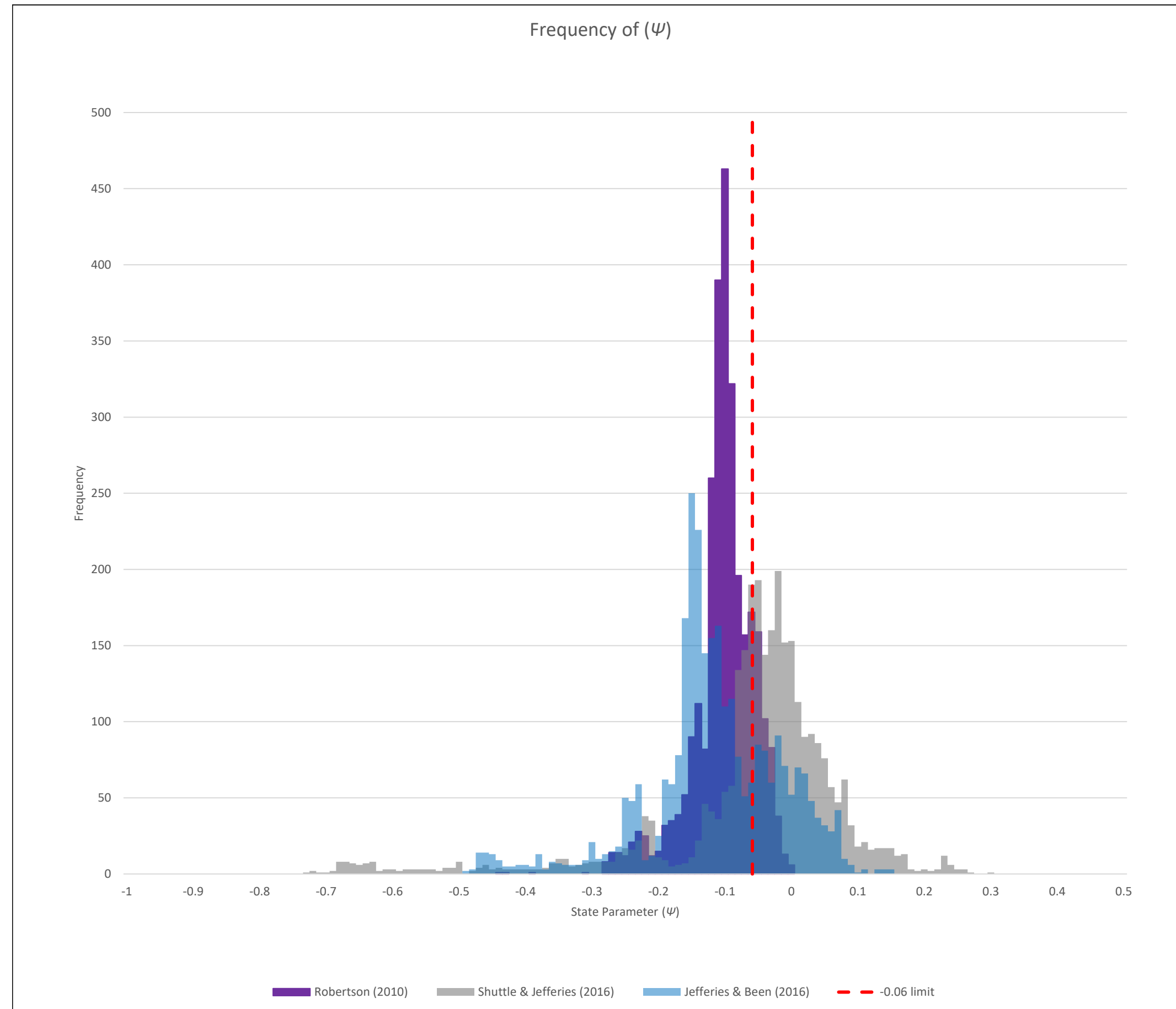
PCF2



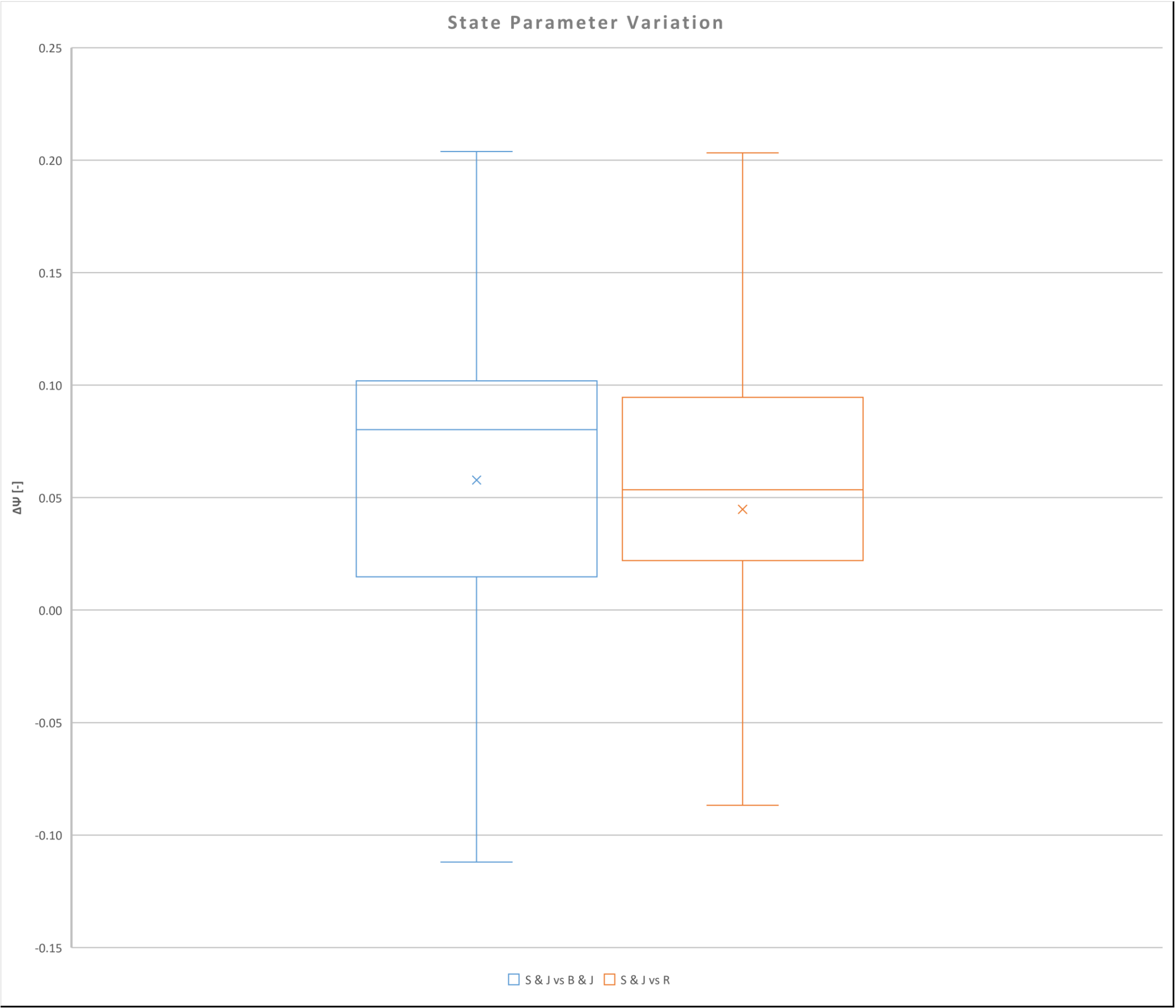
## **Appendix G: CPTu Interpretation – Monitoring Line G**

CPTu PC5



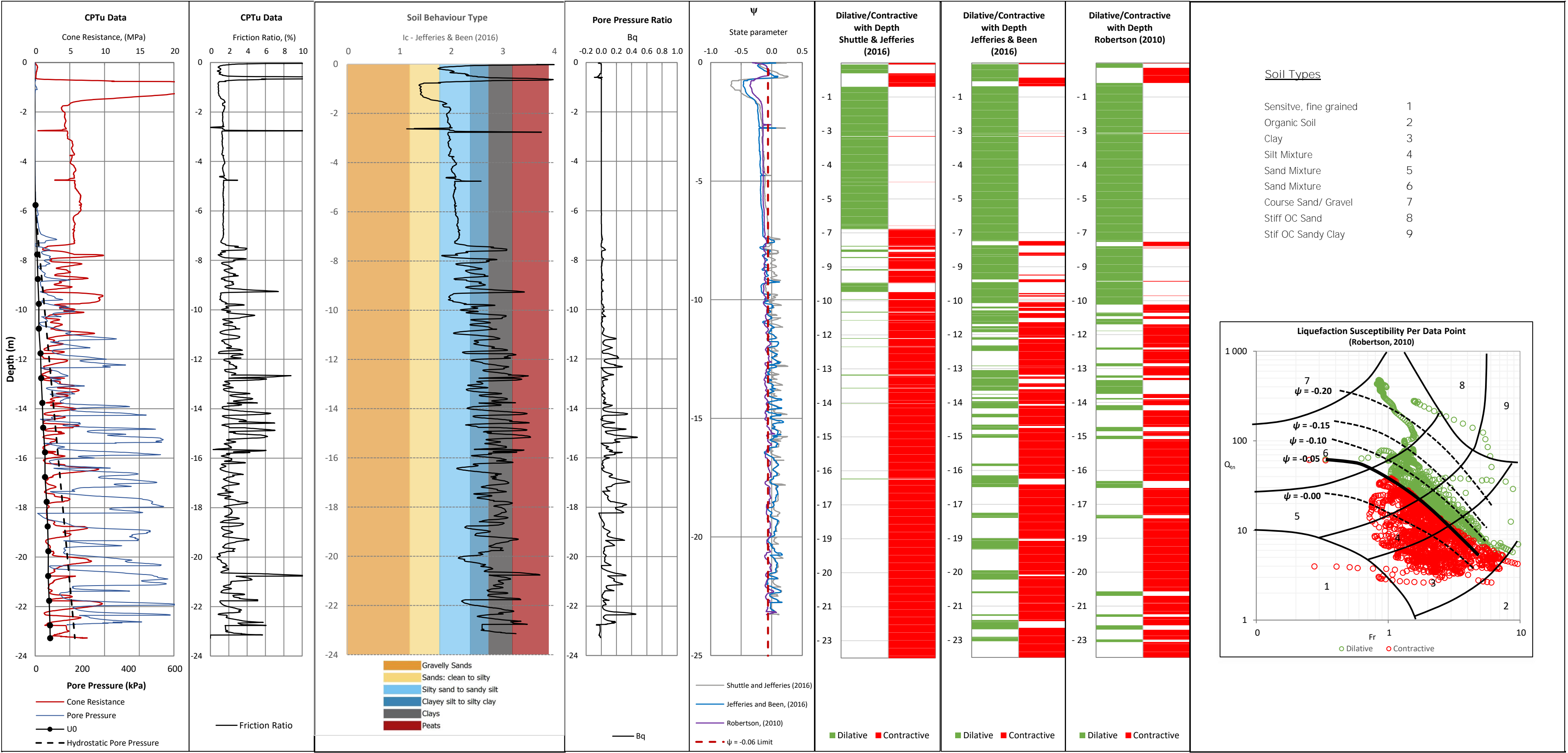
**CPTu PC5**

CPTu PC5

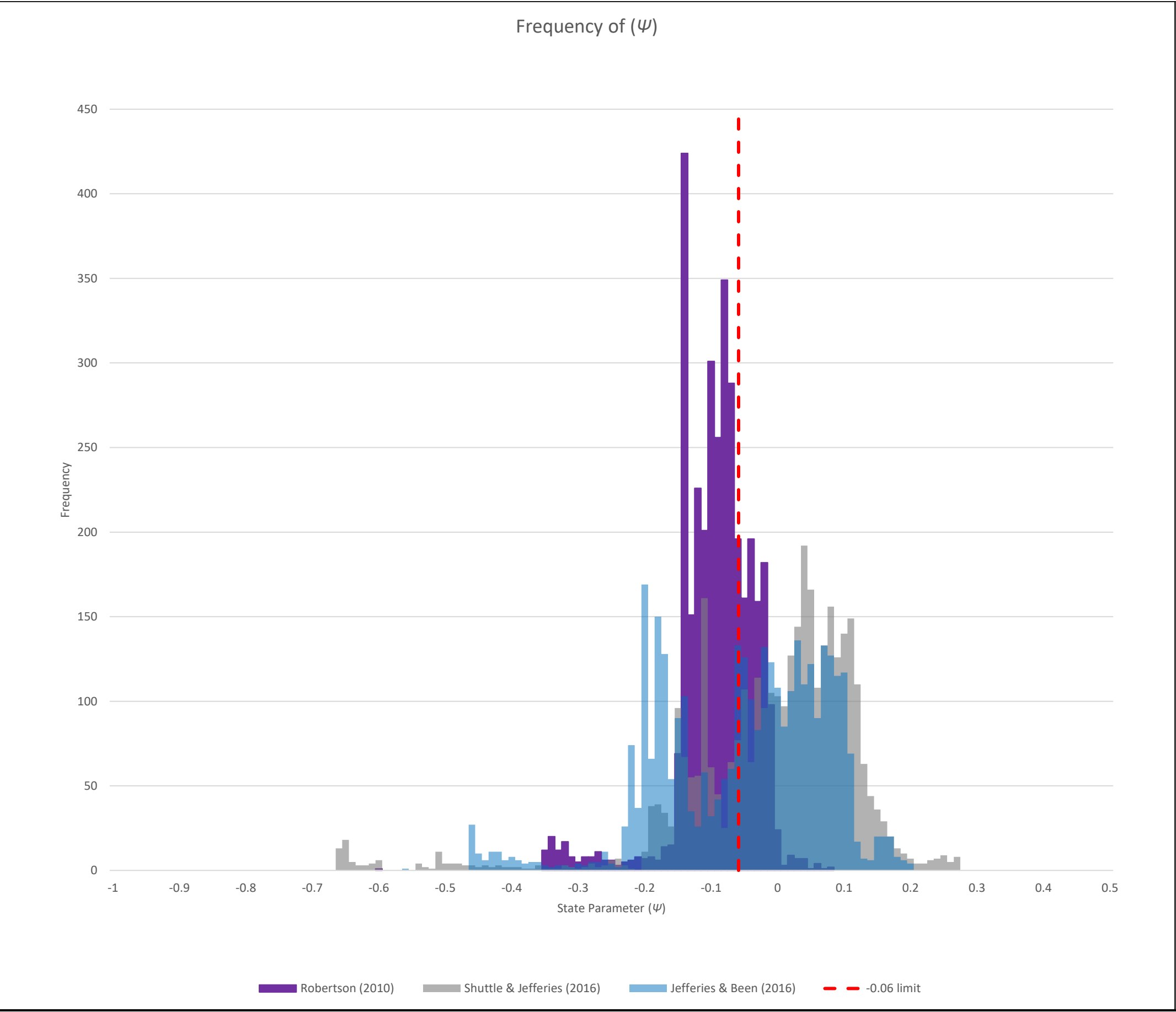


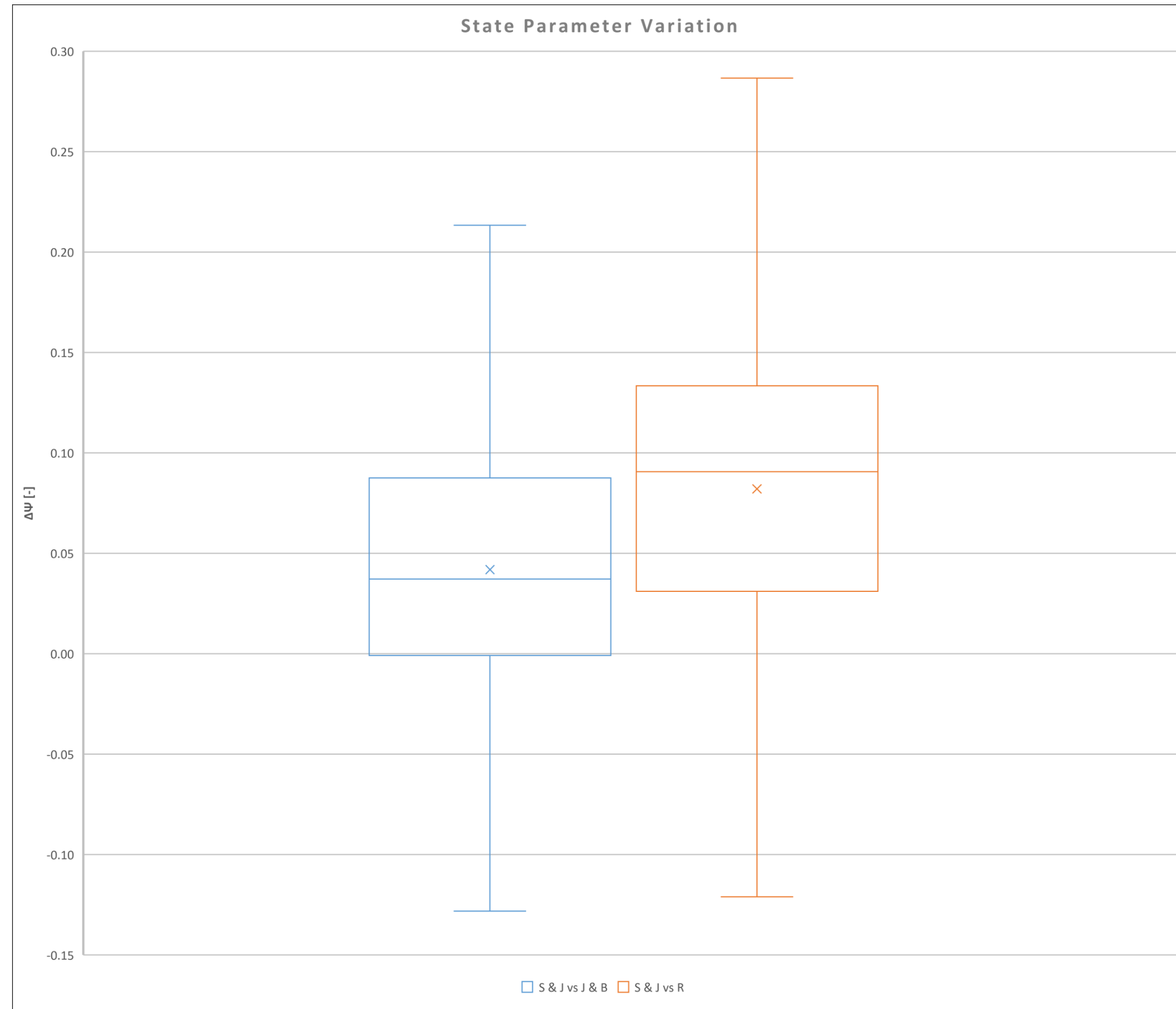


CPTu PC6

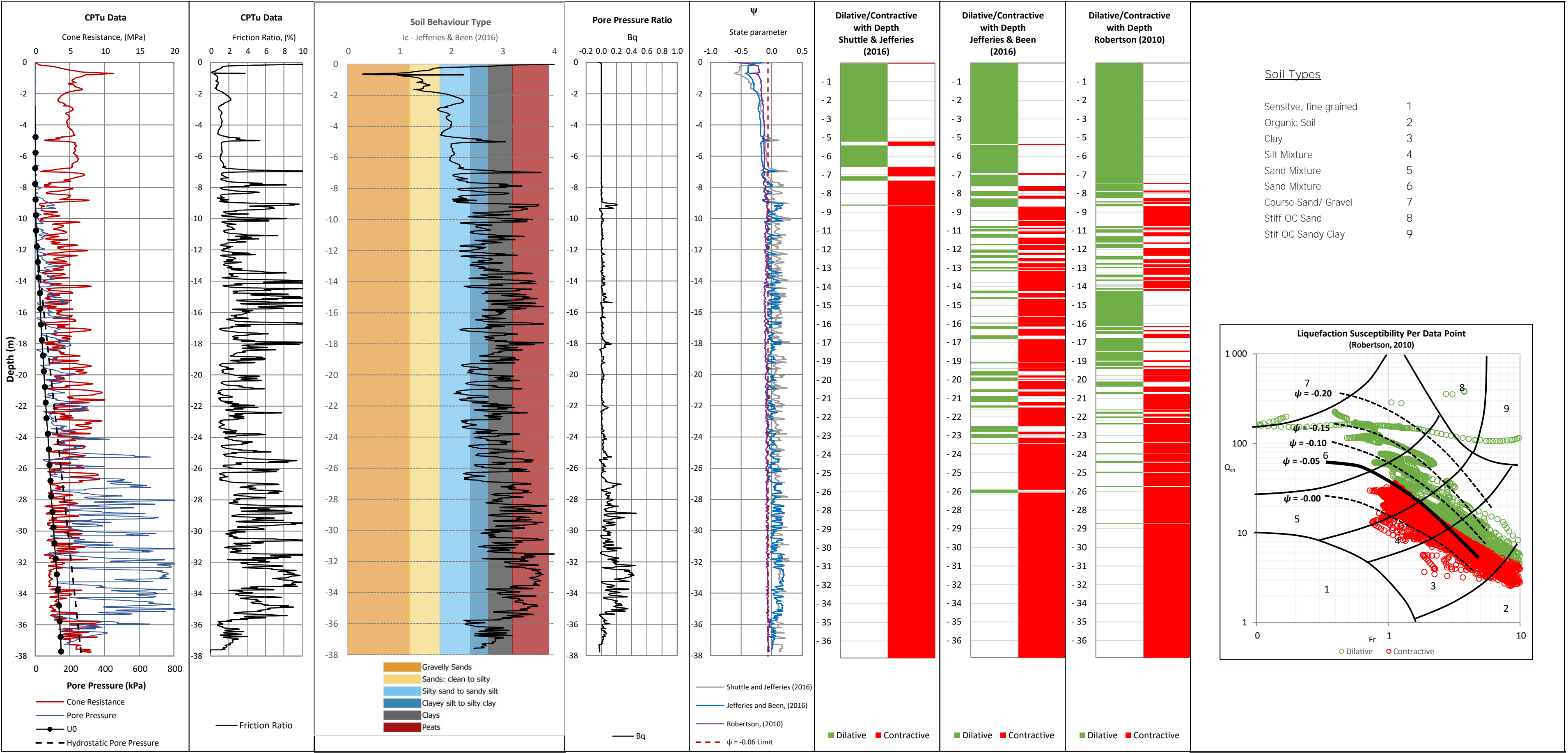


CPTu PC6

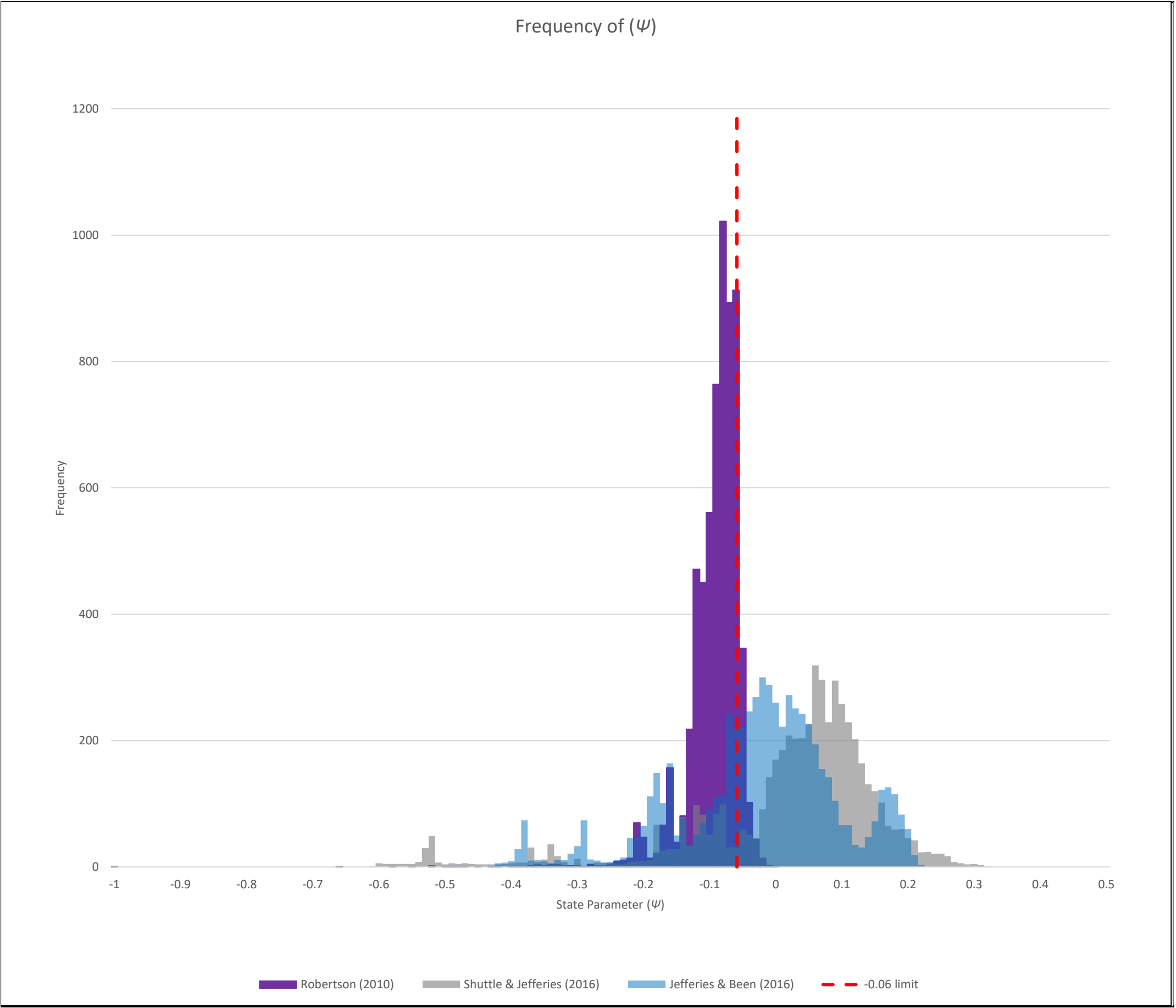


**CPTu PC6**

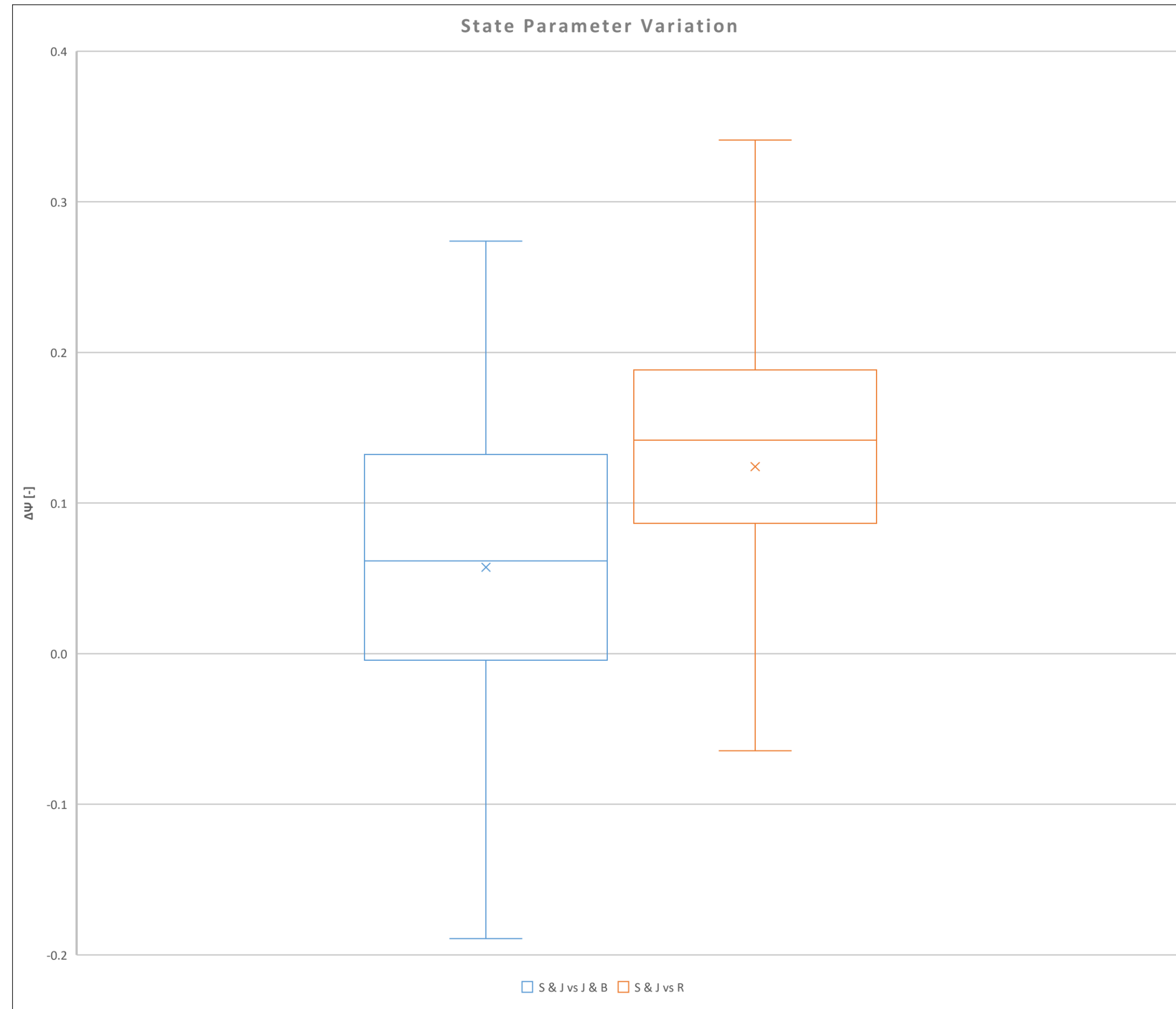
CPTu PC7



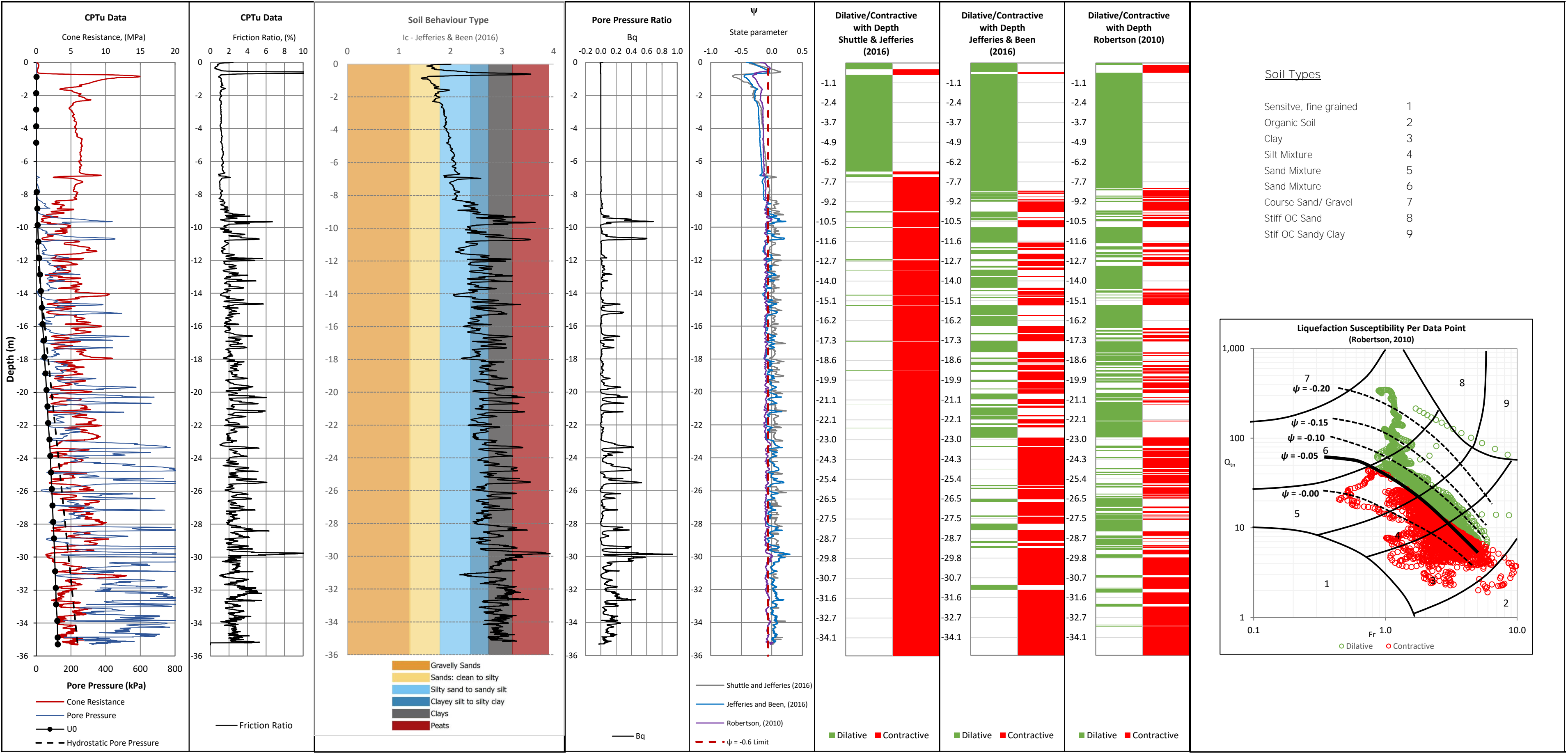
CPTu PC7



## CPTu PC7

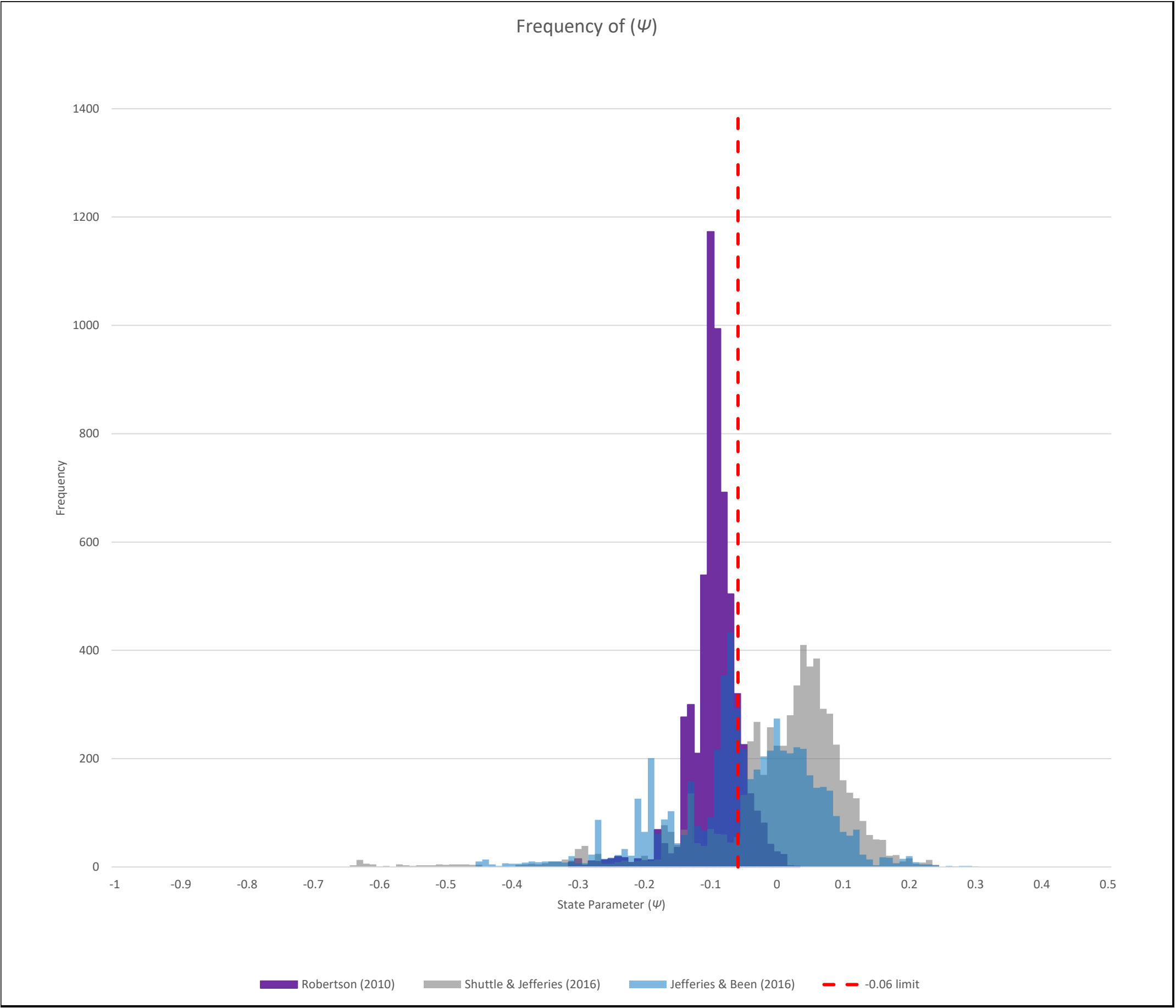


PCG1

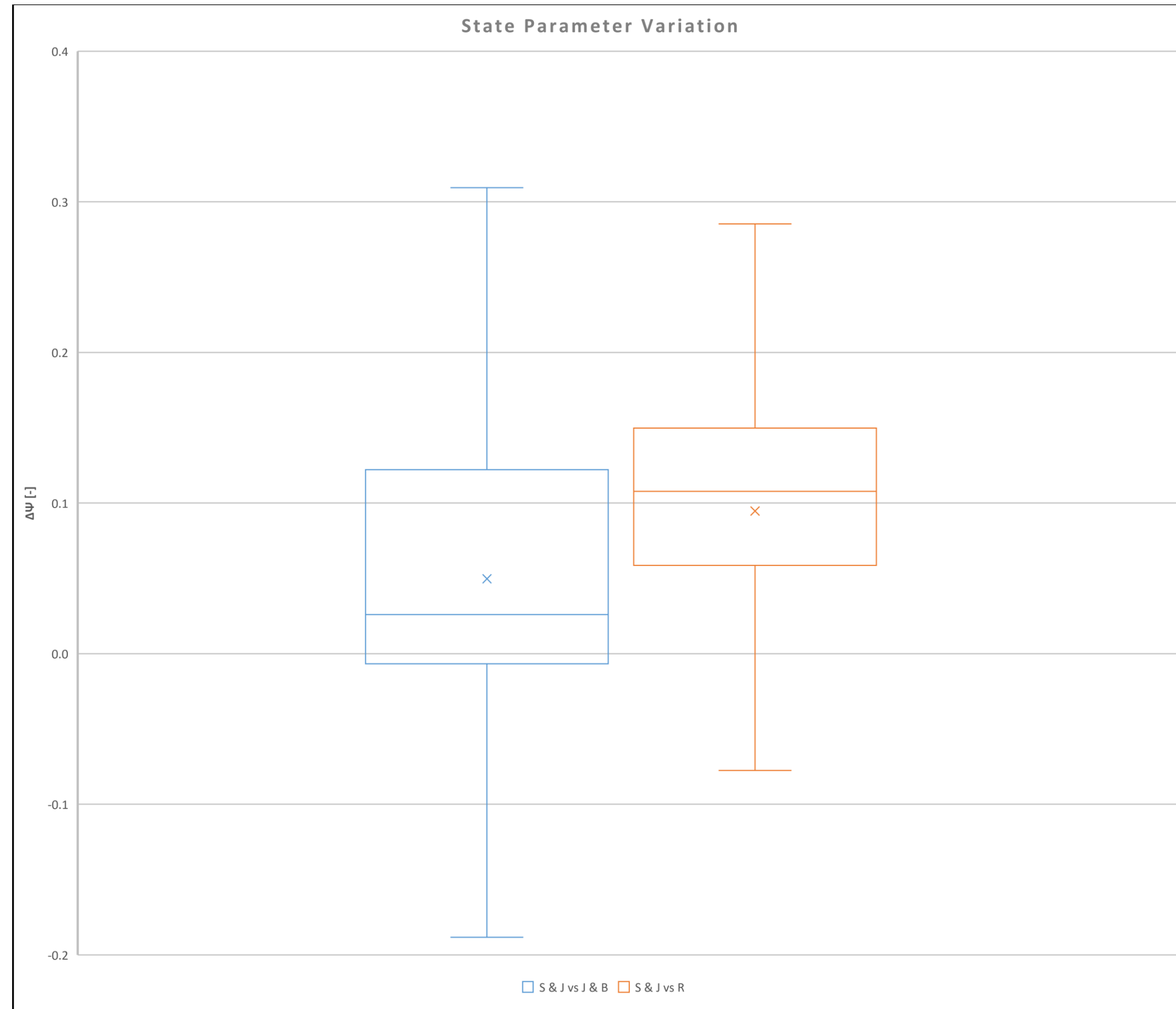




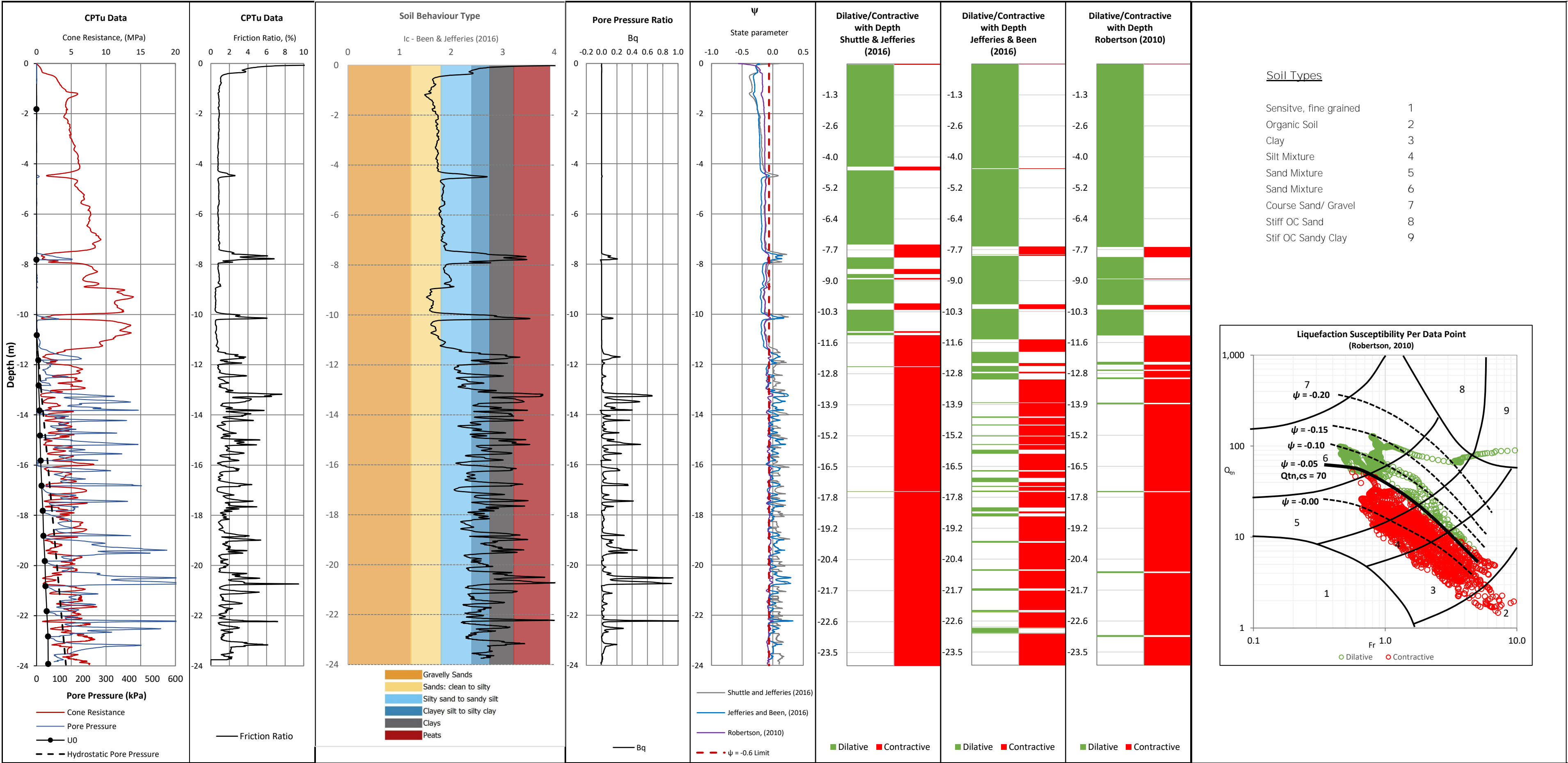
PCG1



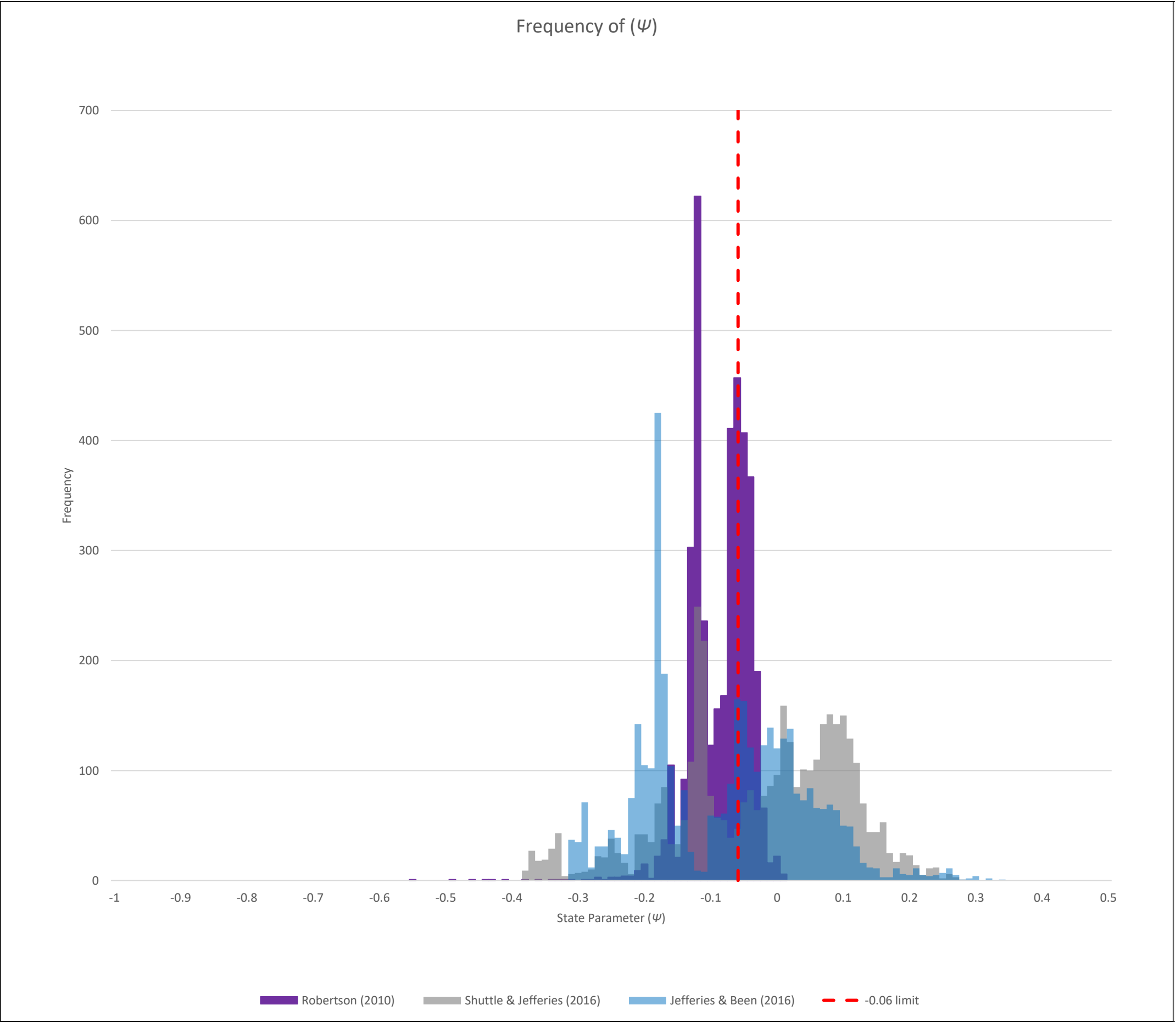
# PCG1



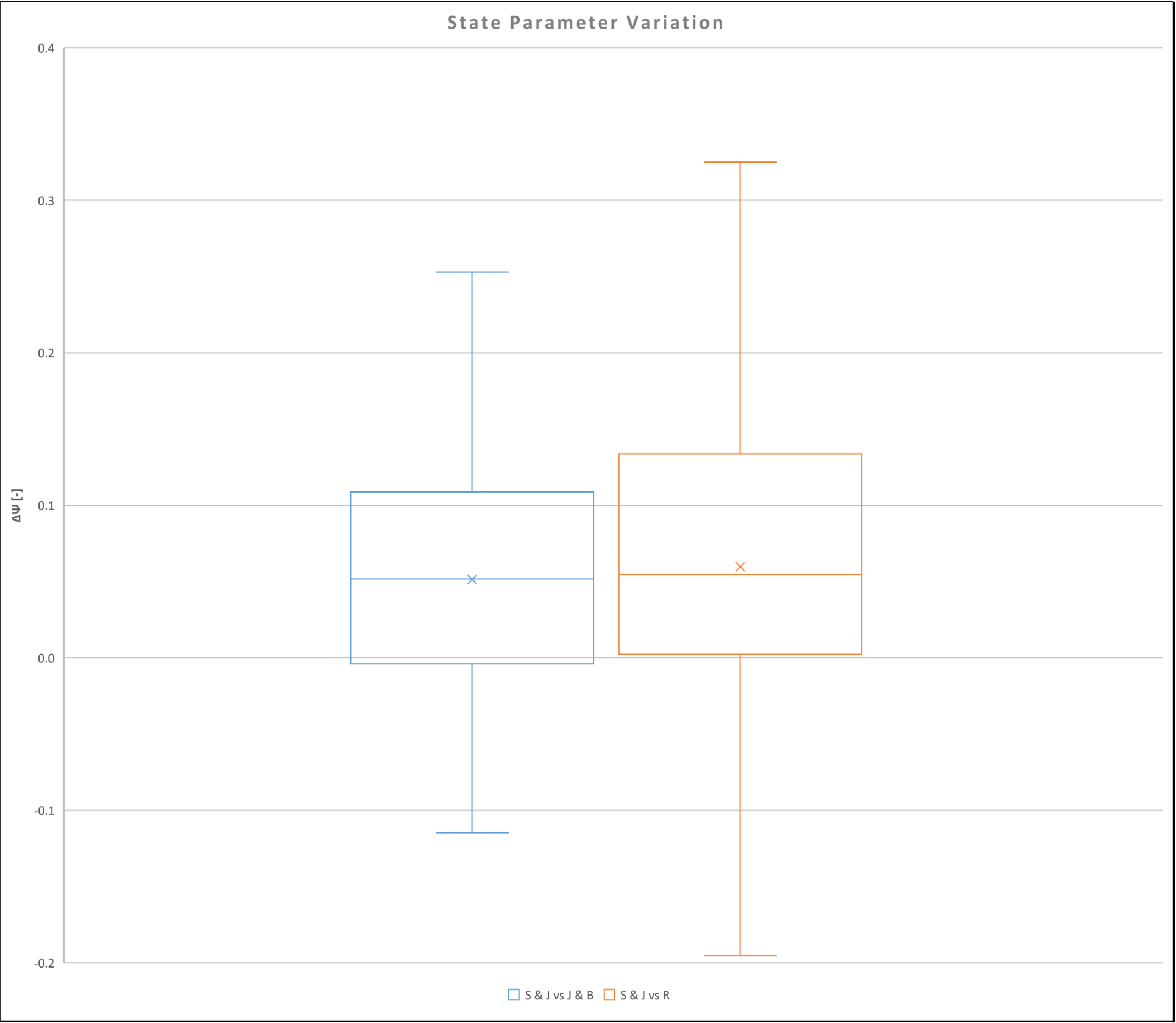
PCG2



PCG2

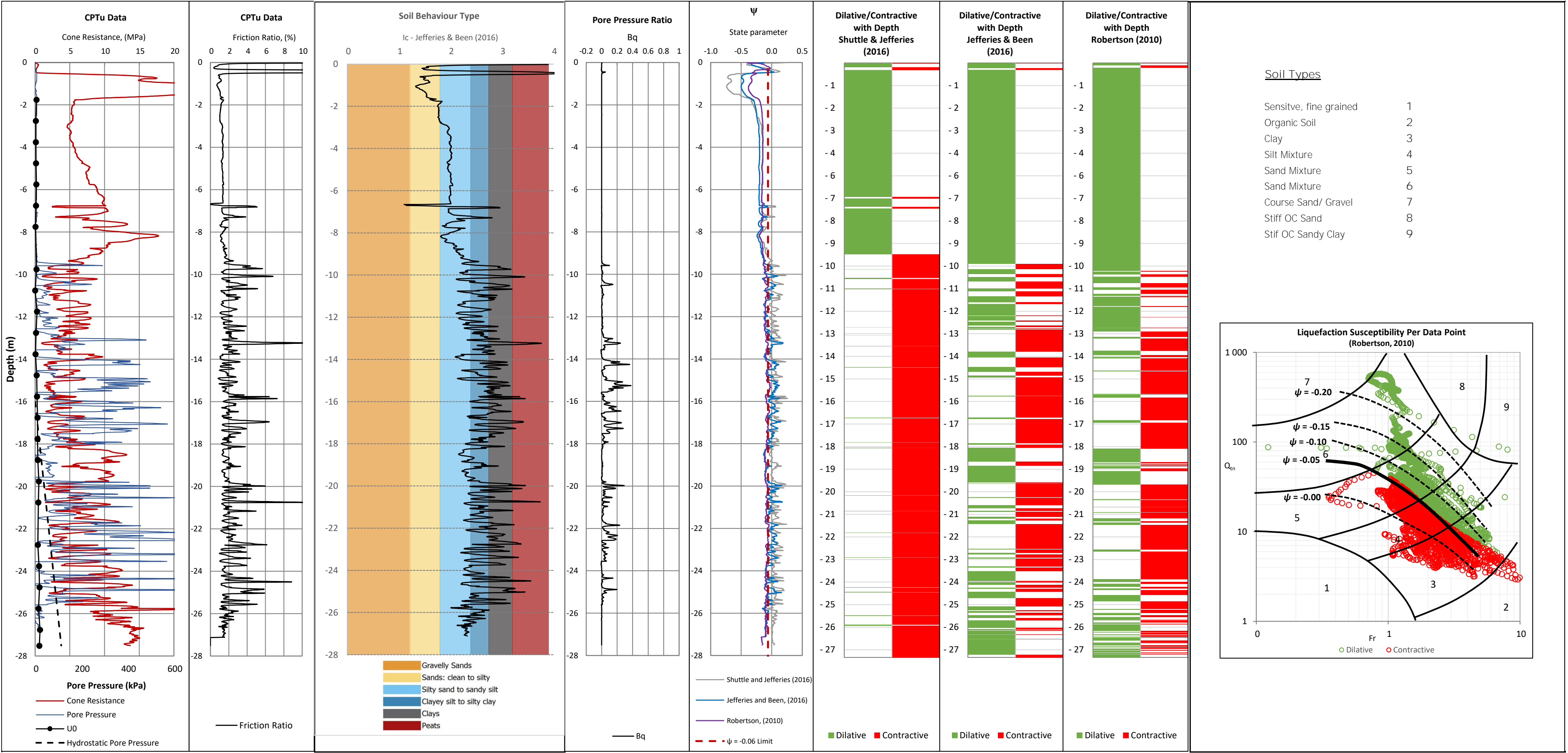


PCG2



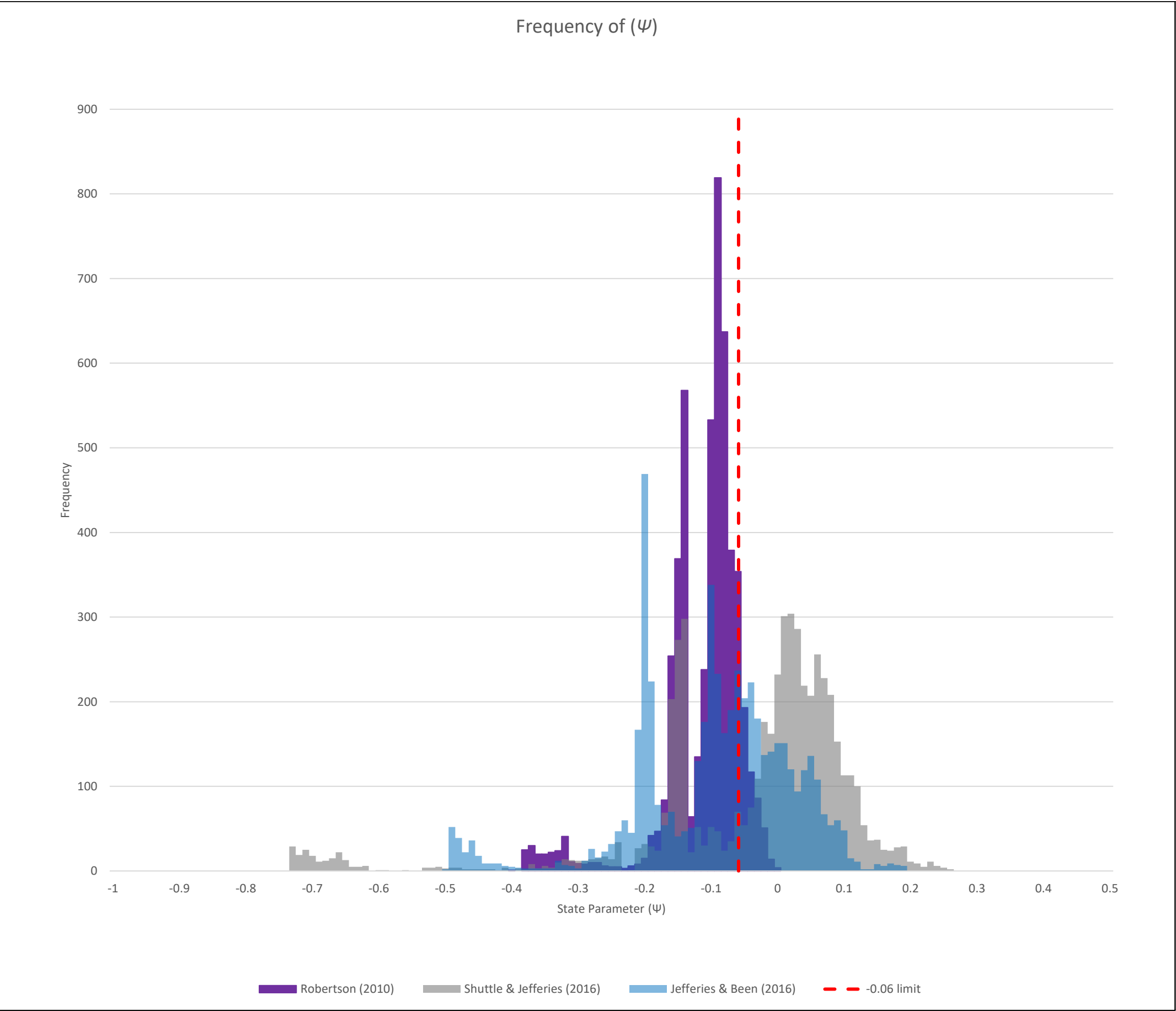
## **Appendix H: CPTu Interpretation – Monitoring Line H**

CPTu PC3

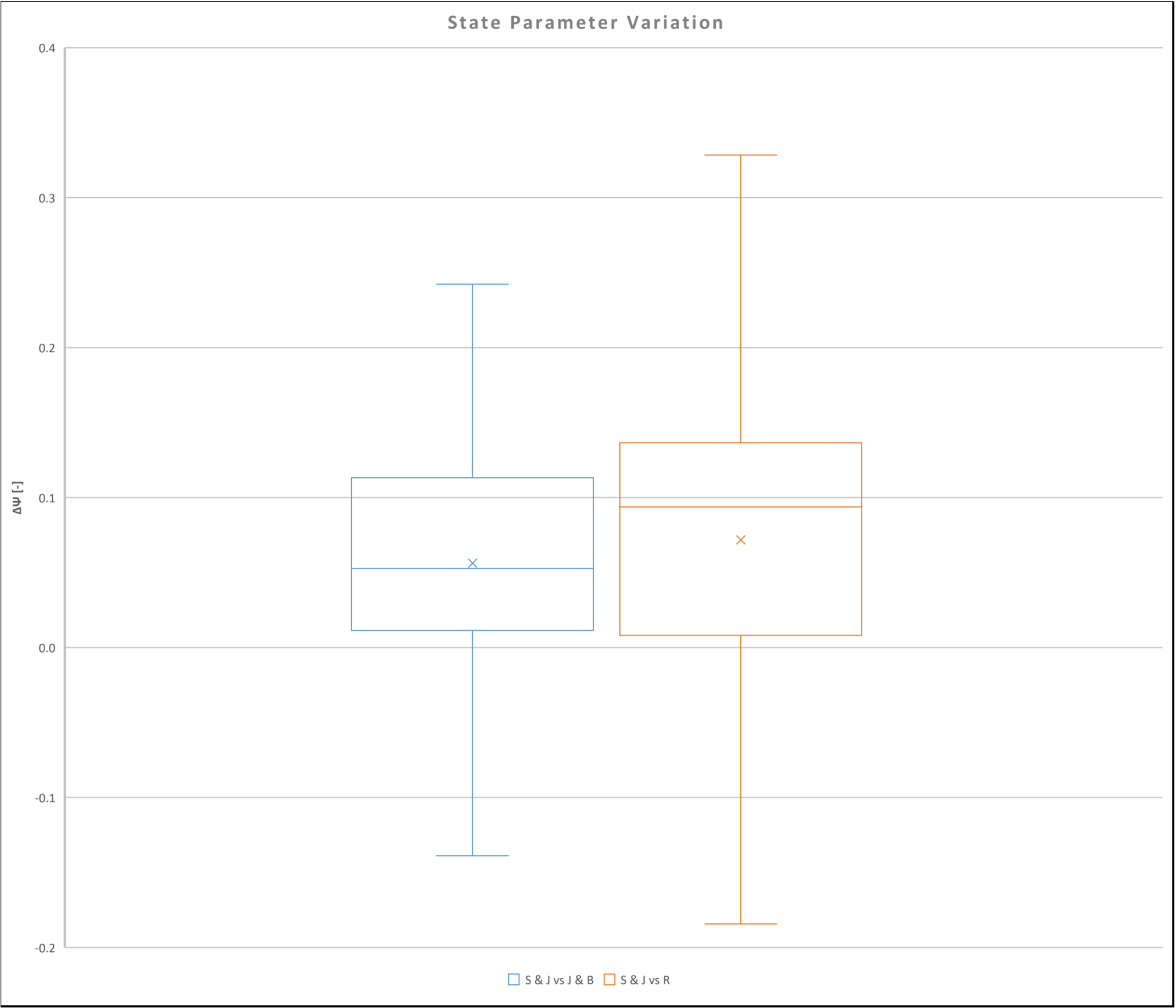


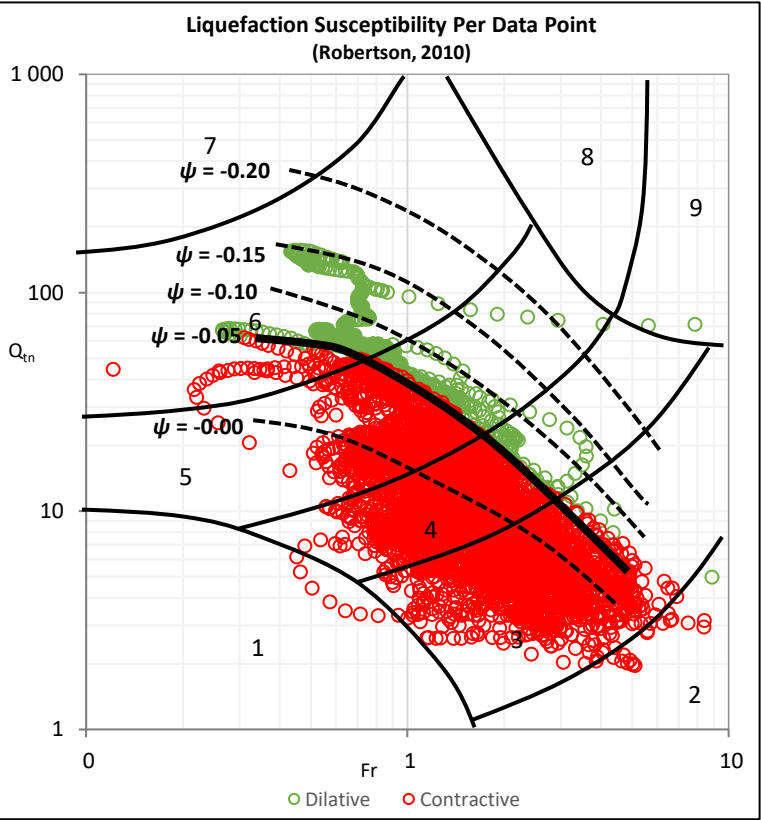


CPTu PC3

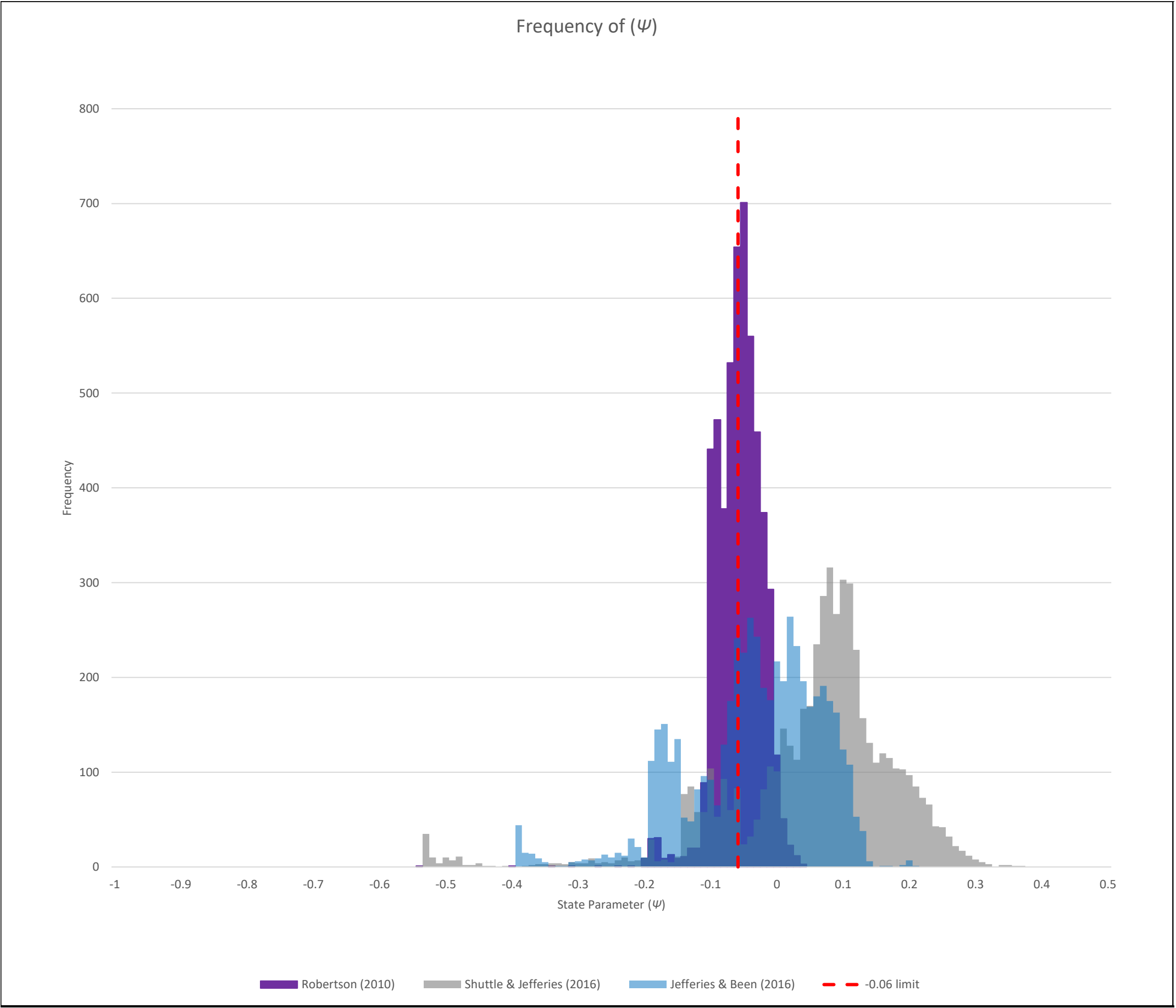


CPTu PC3

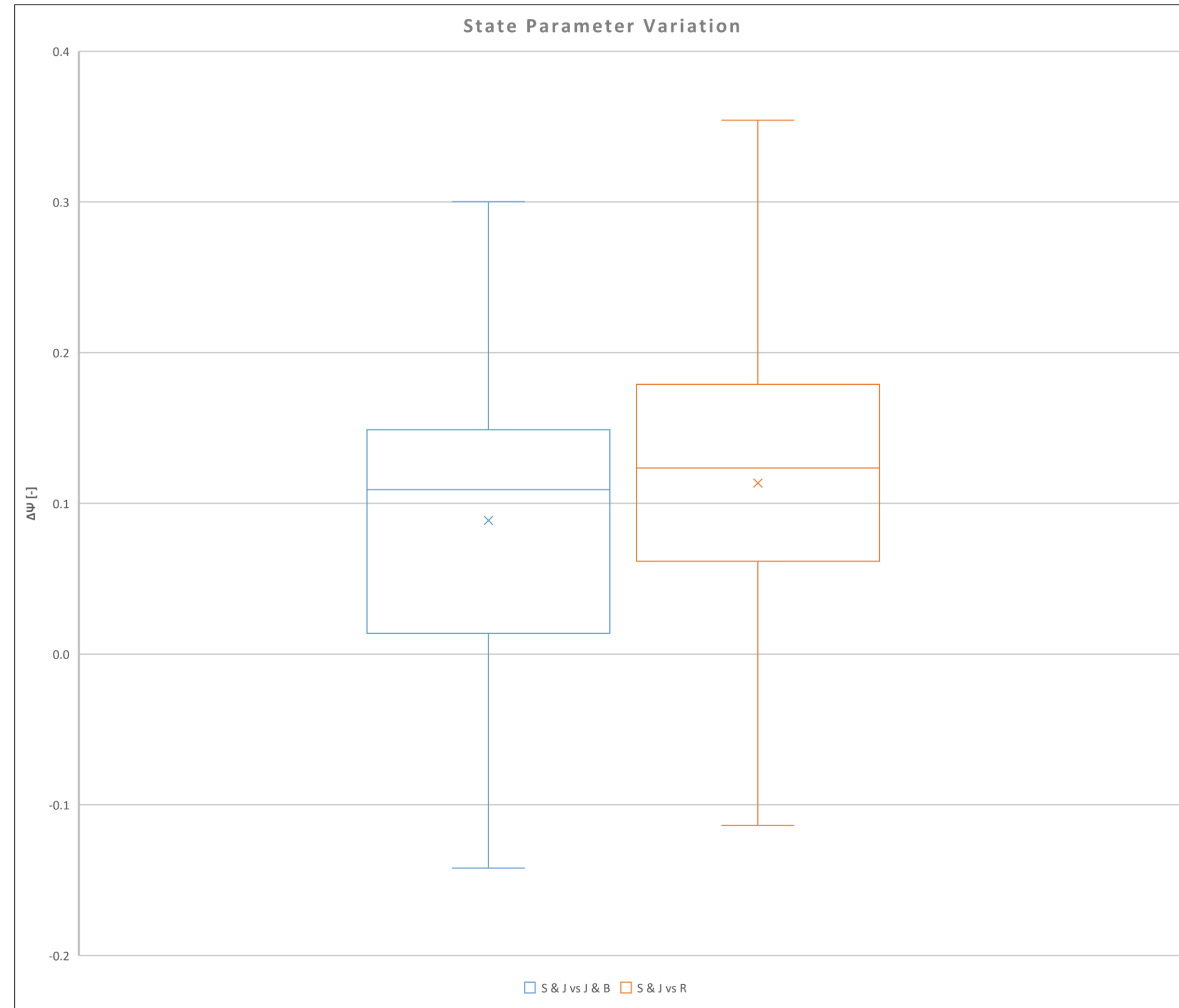




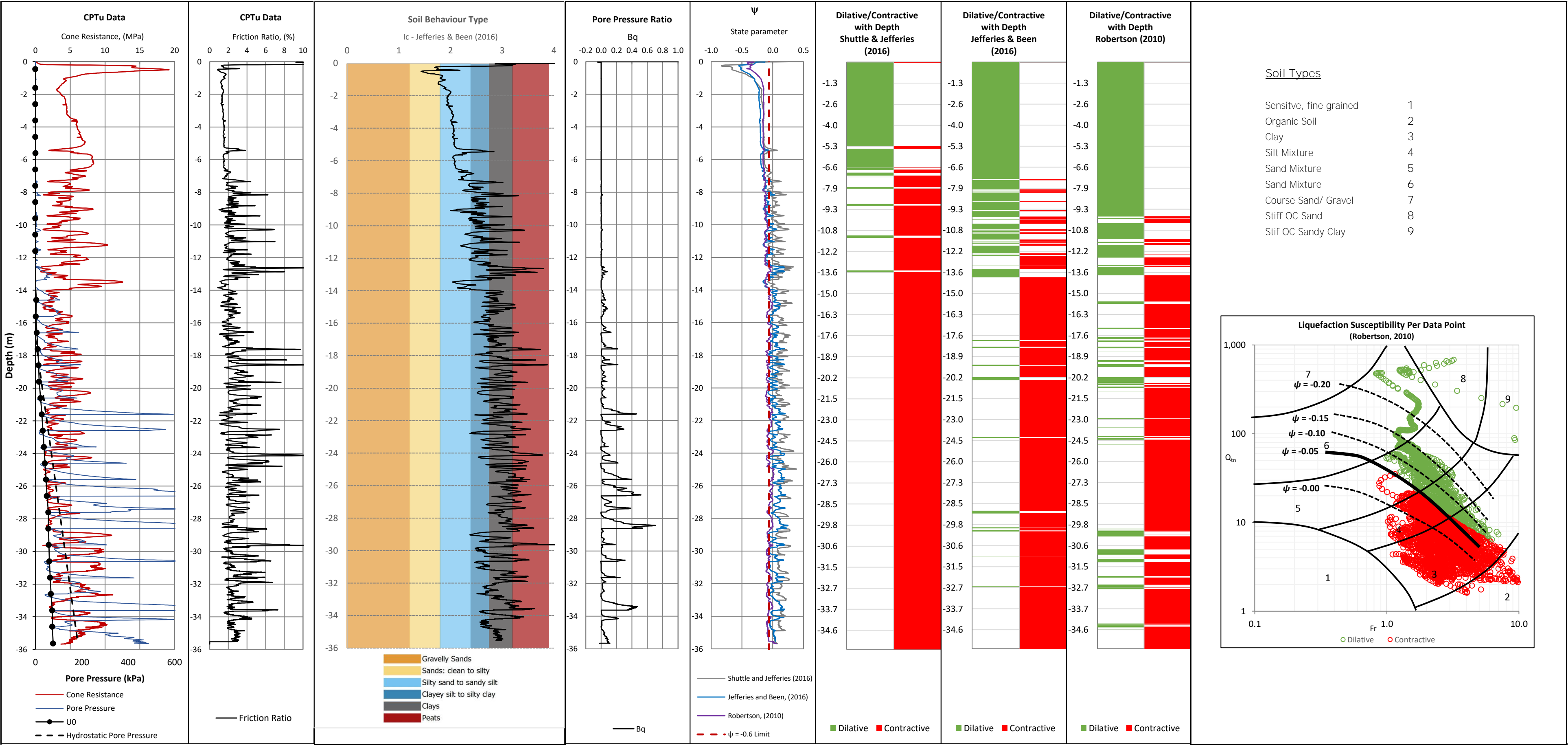
CPTu PC4



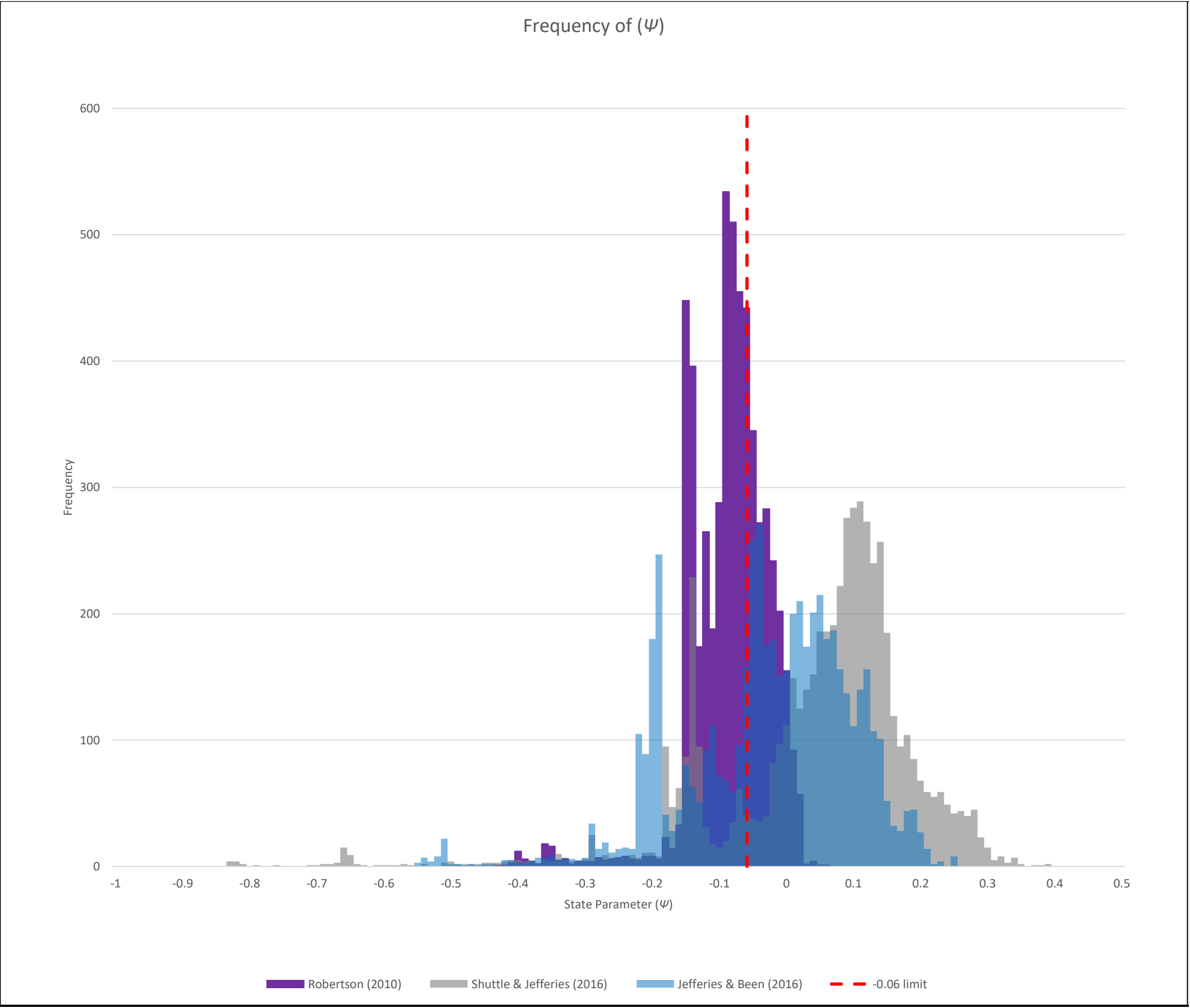
## CPTu PC4



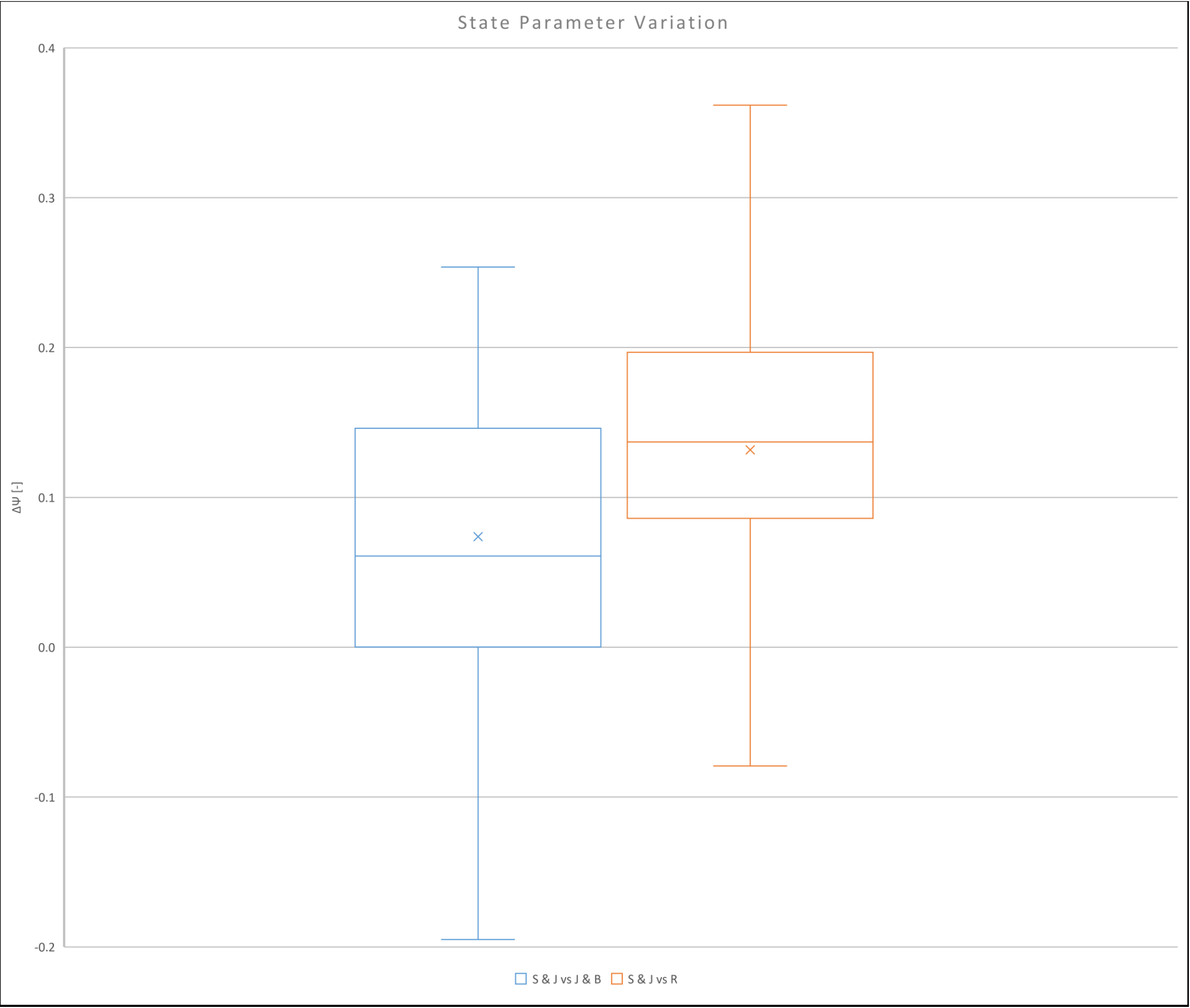
PCH1



PCH1

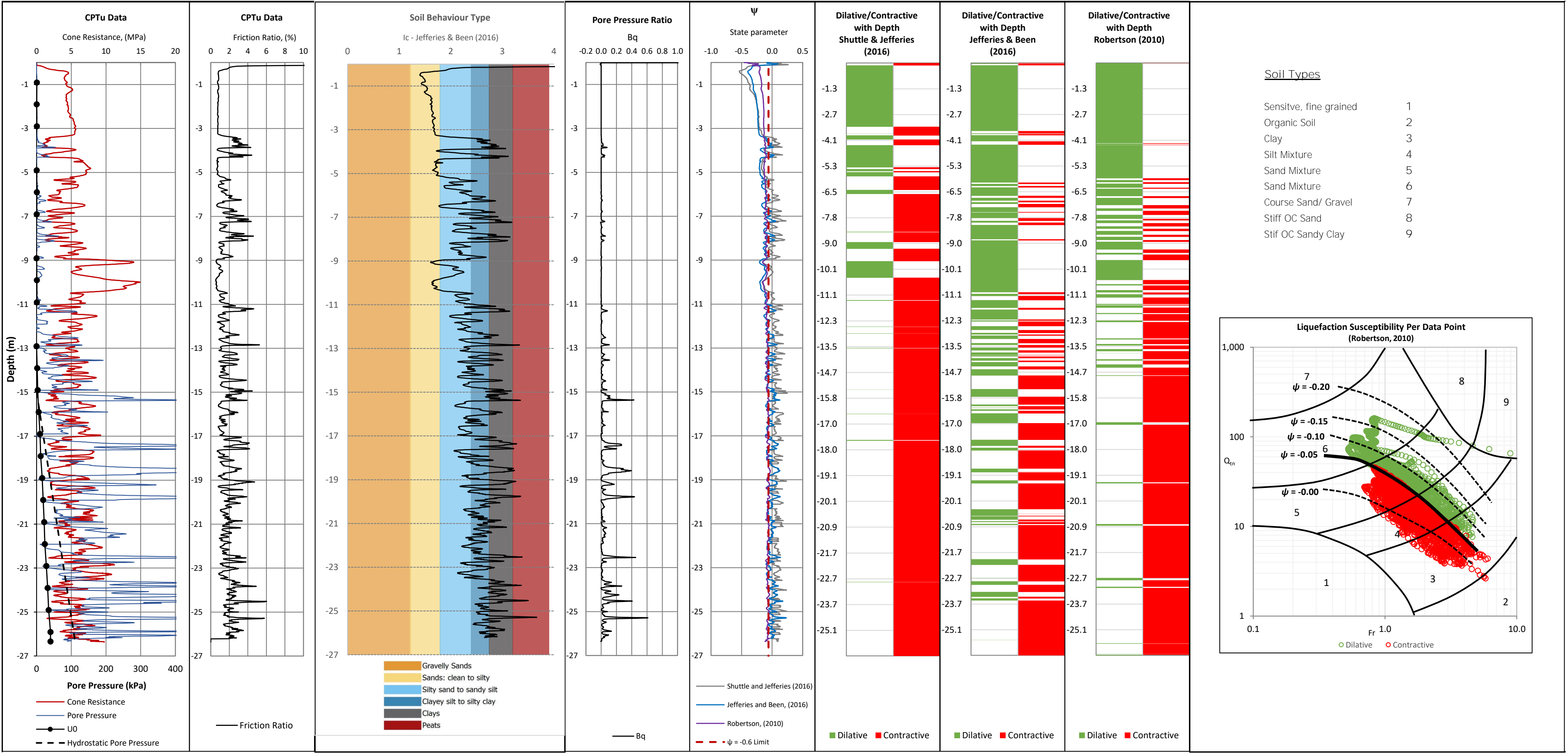


PCH1

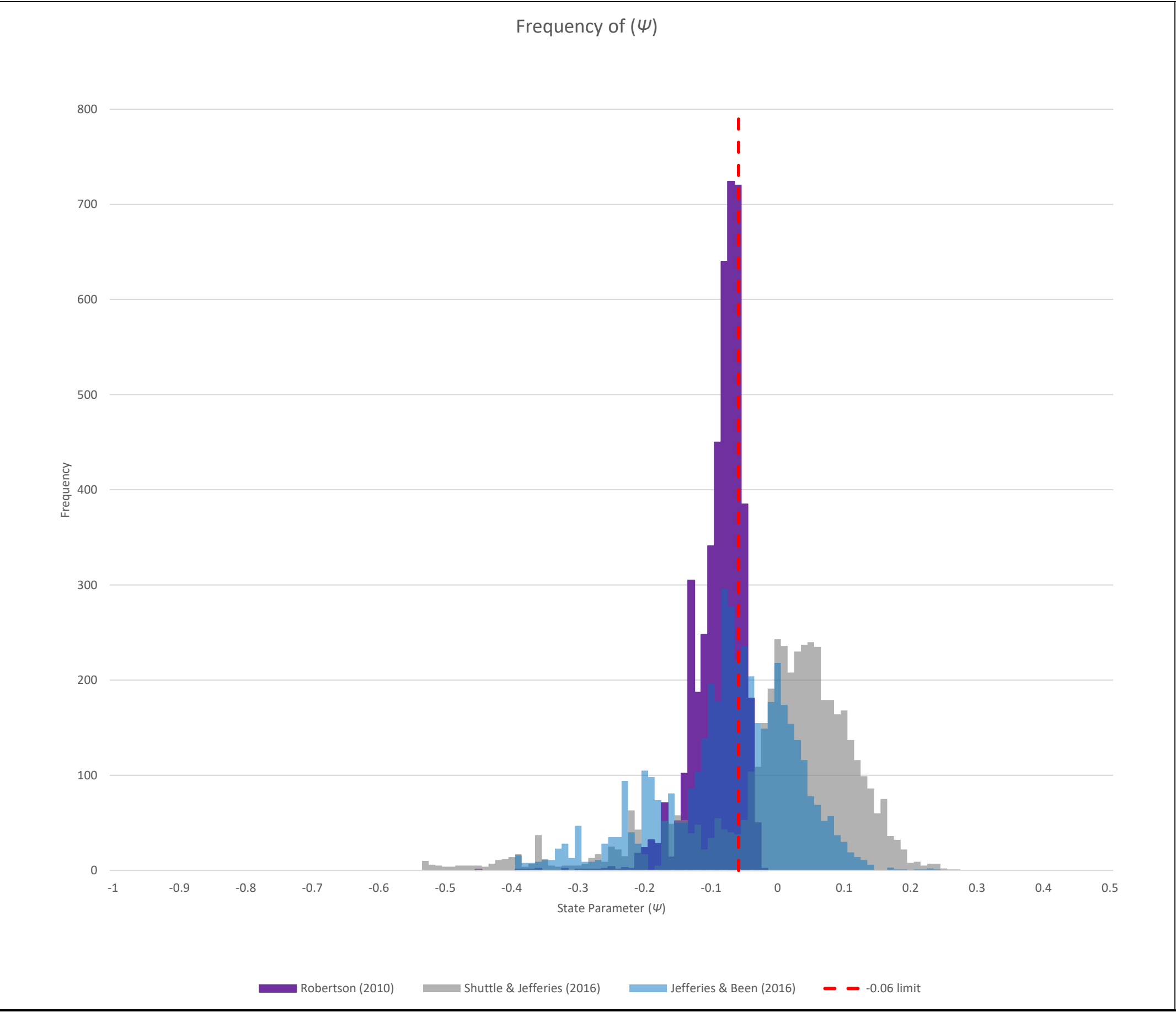




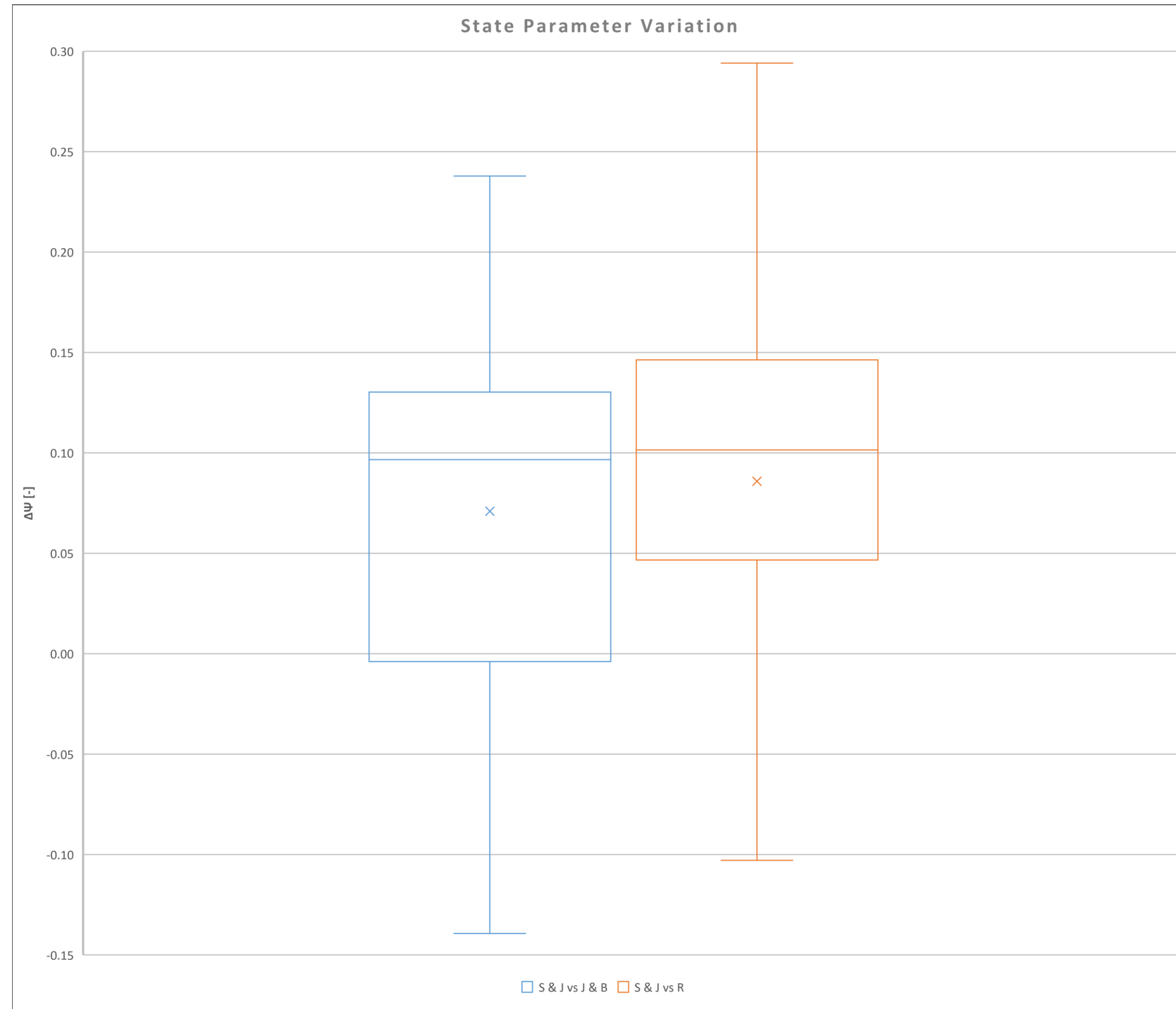
PCH3



PCH3

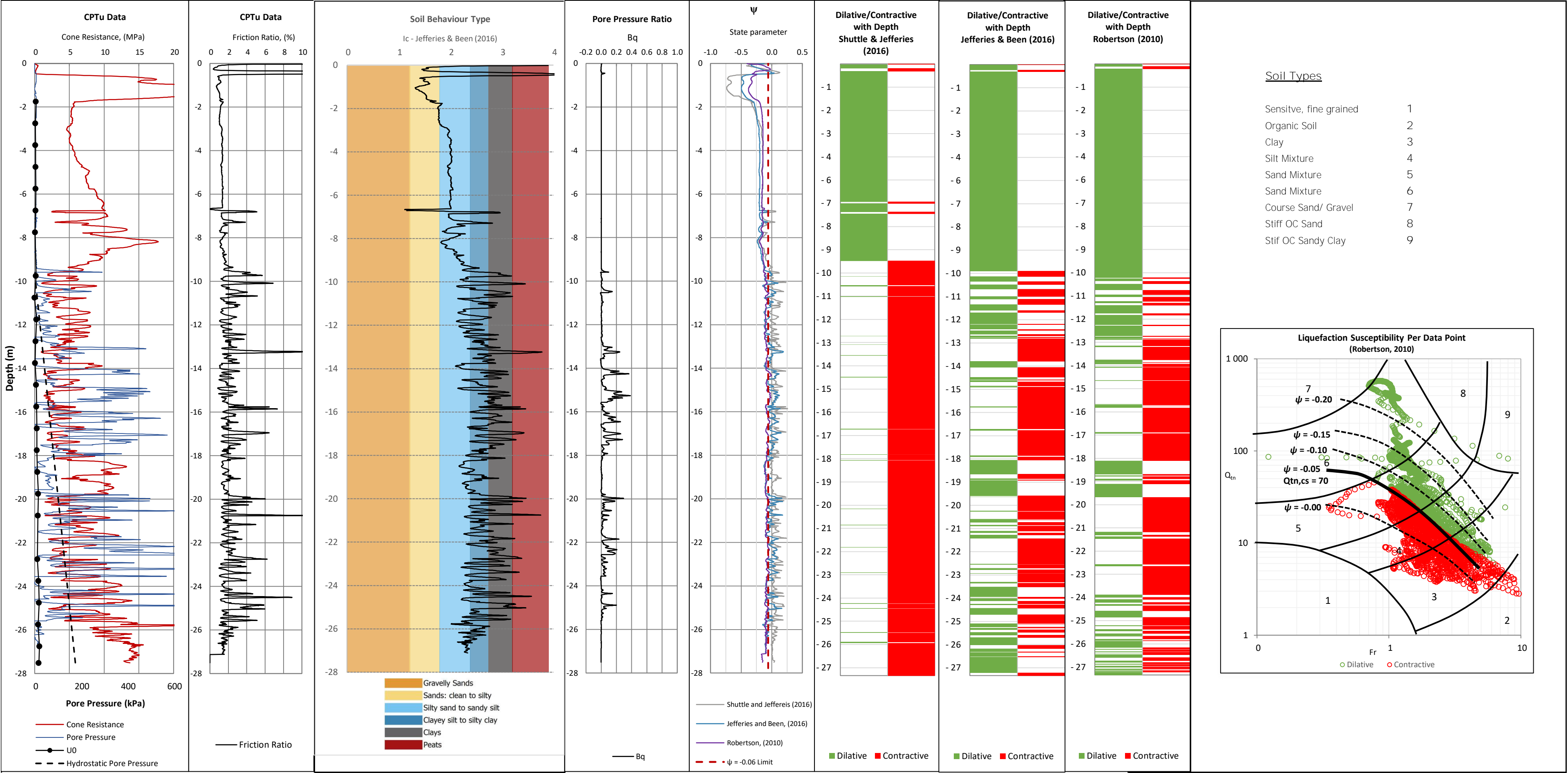


# PCH3

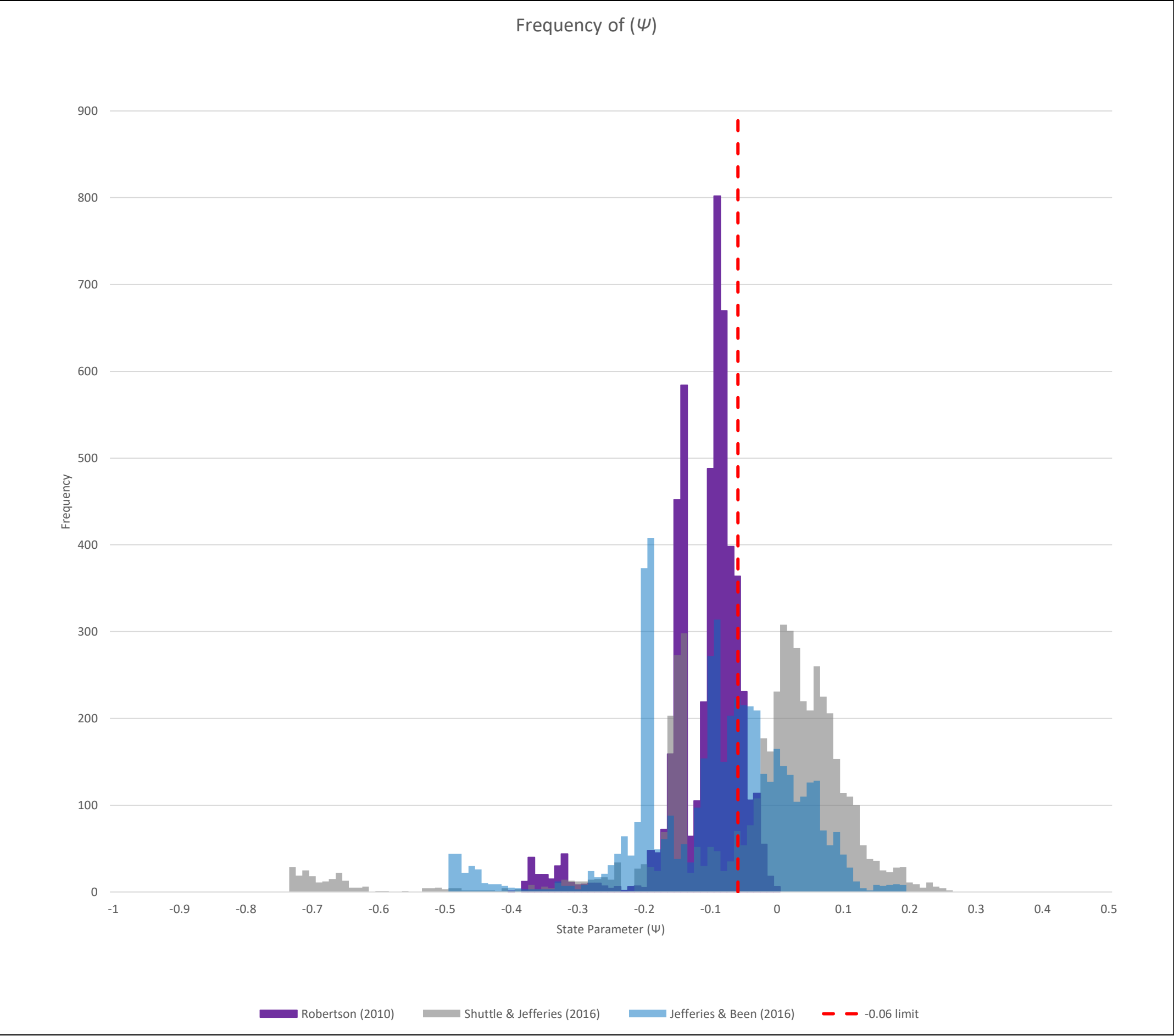


## **Appendix I: CPTu Interpretation – Monitoring Line I**

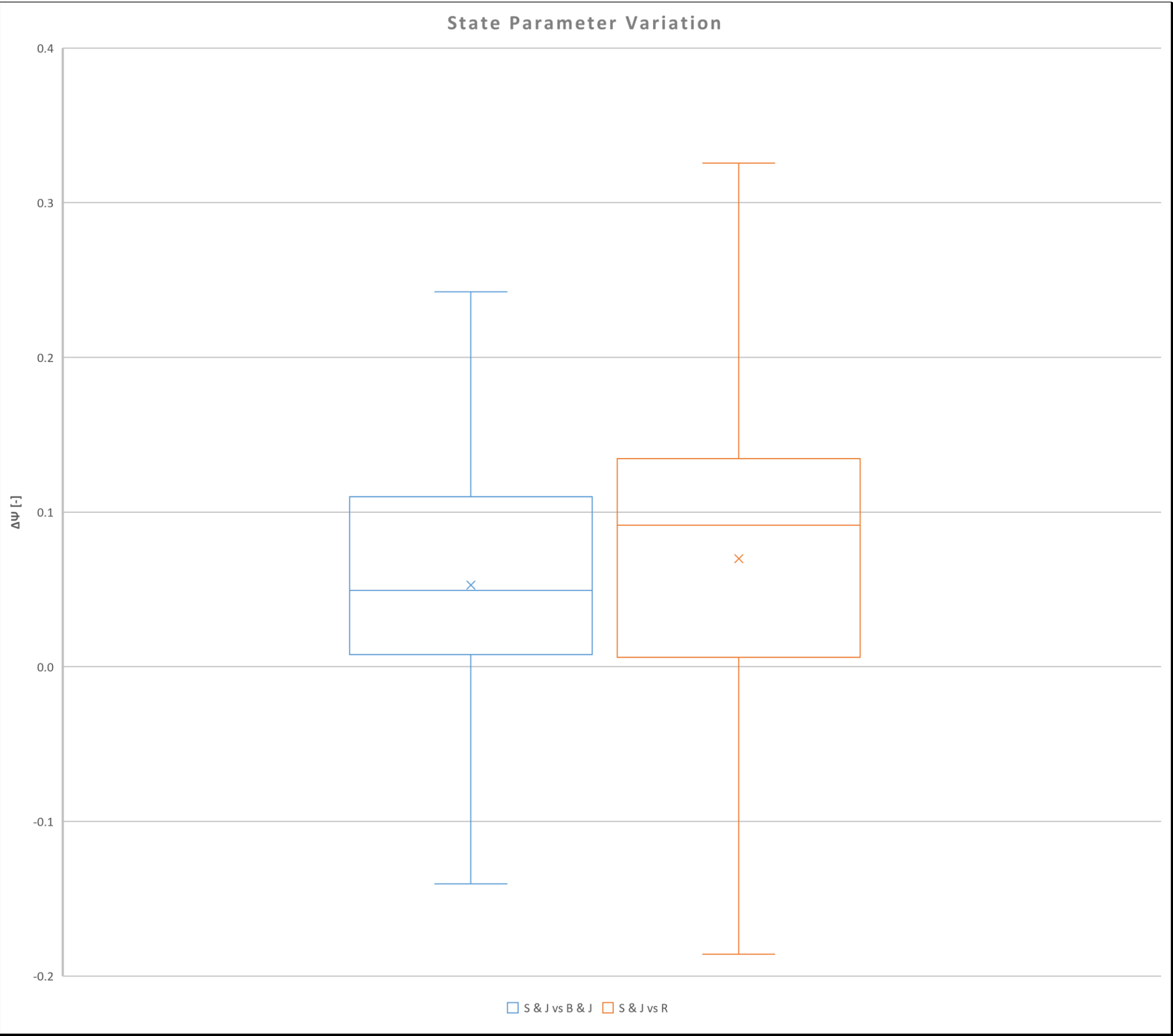
CPTu PC1



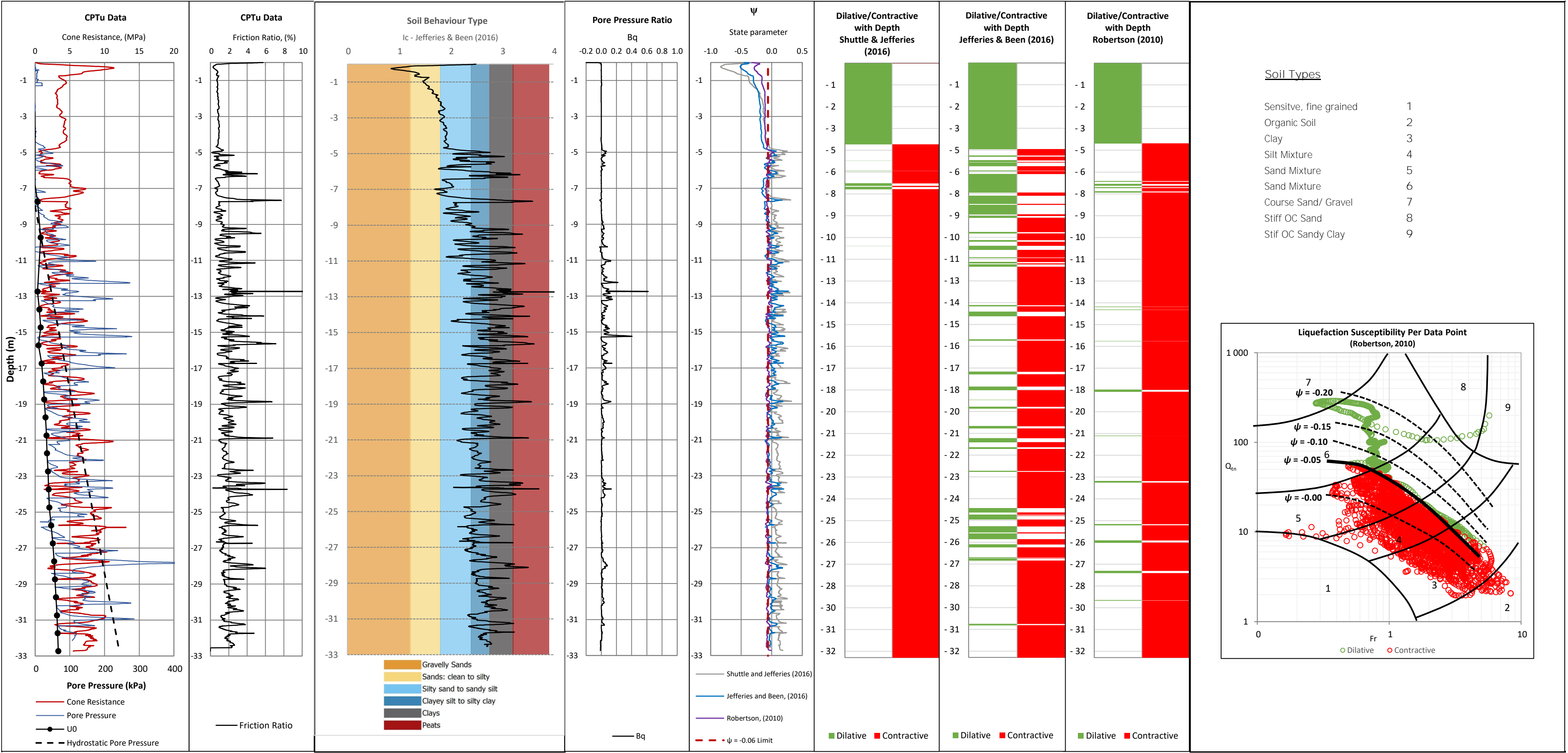
CPTu PC1



CPTu PC1

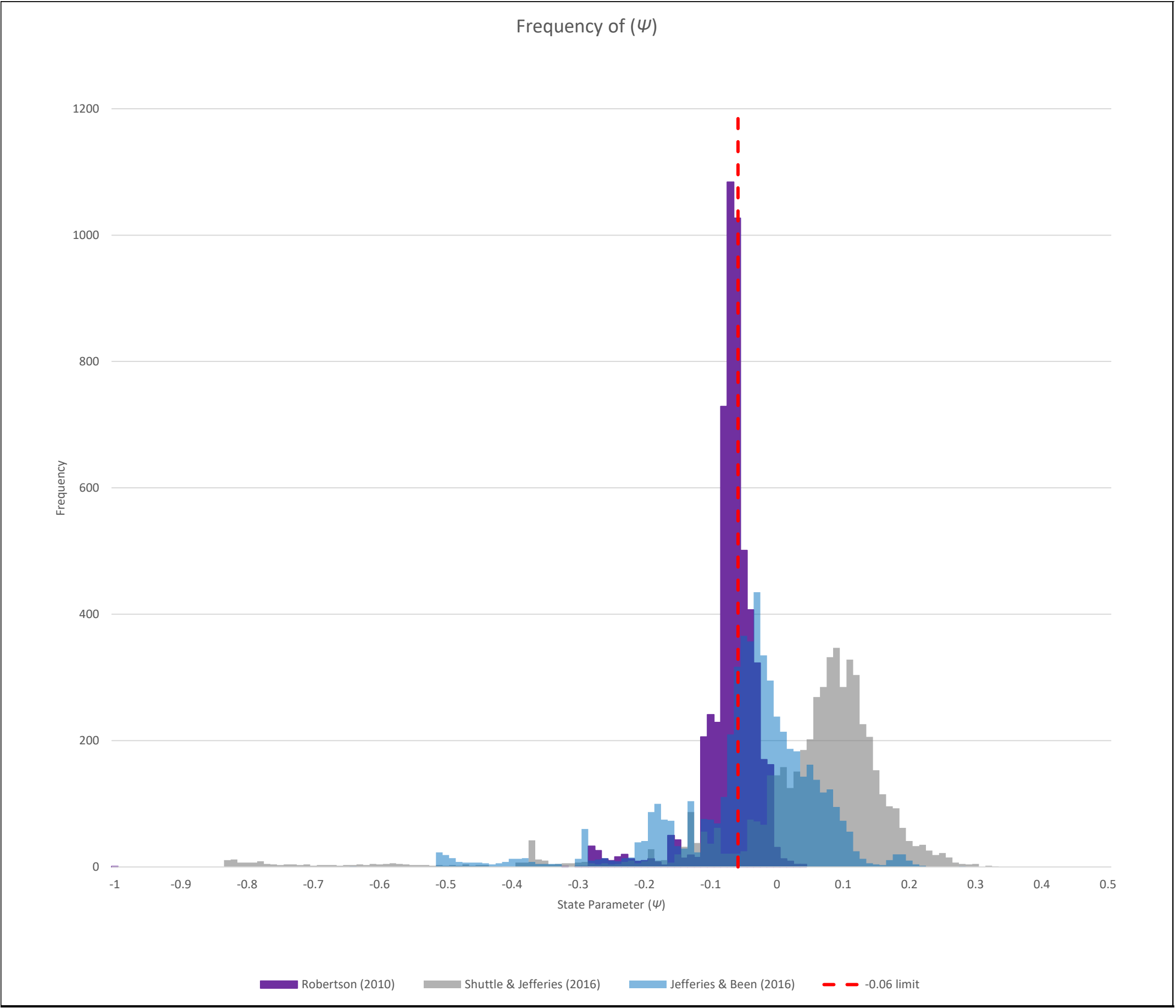


CPTu PC2

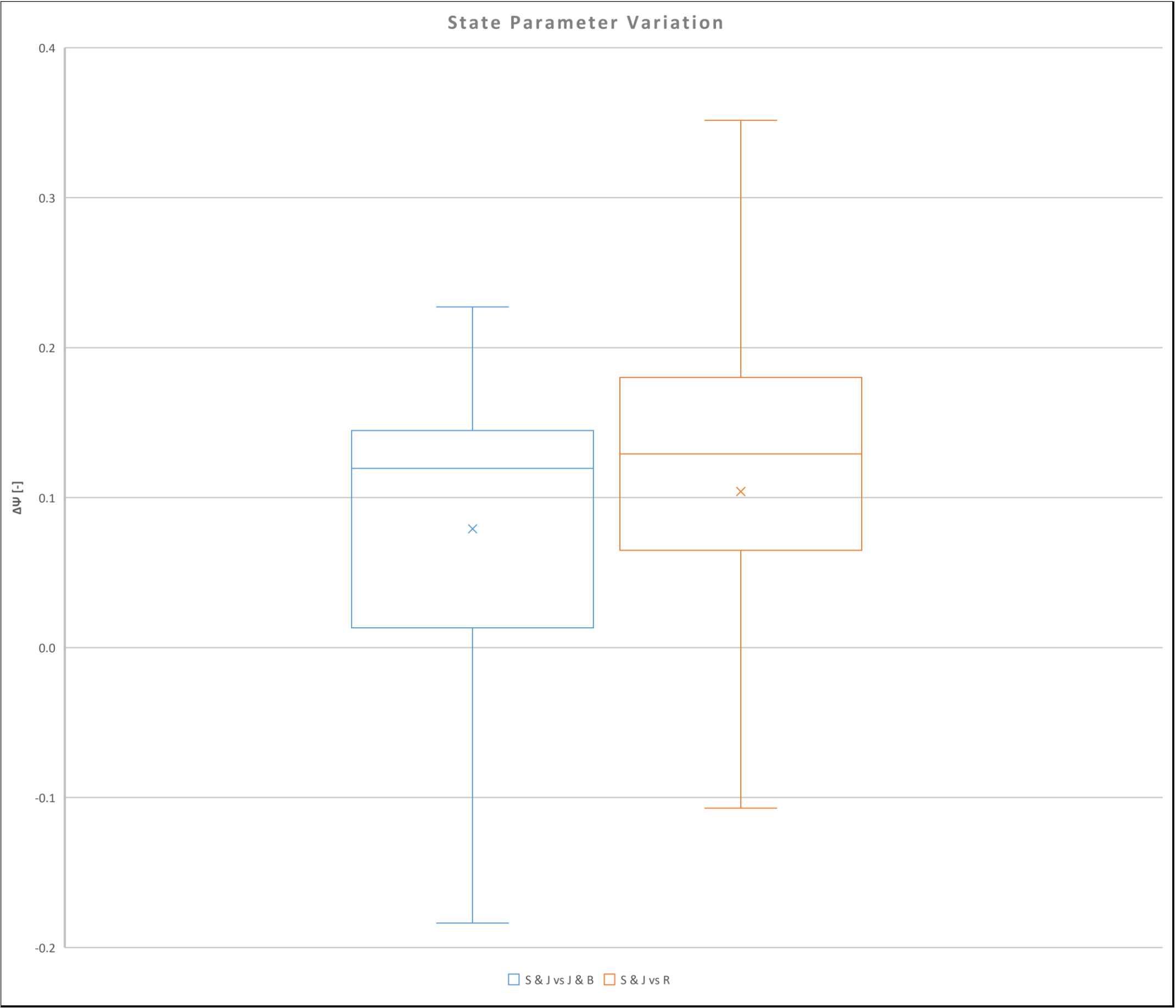




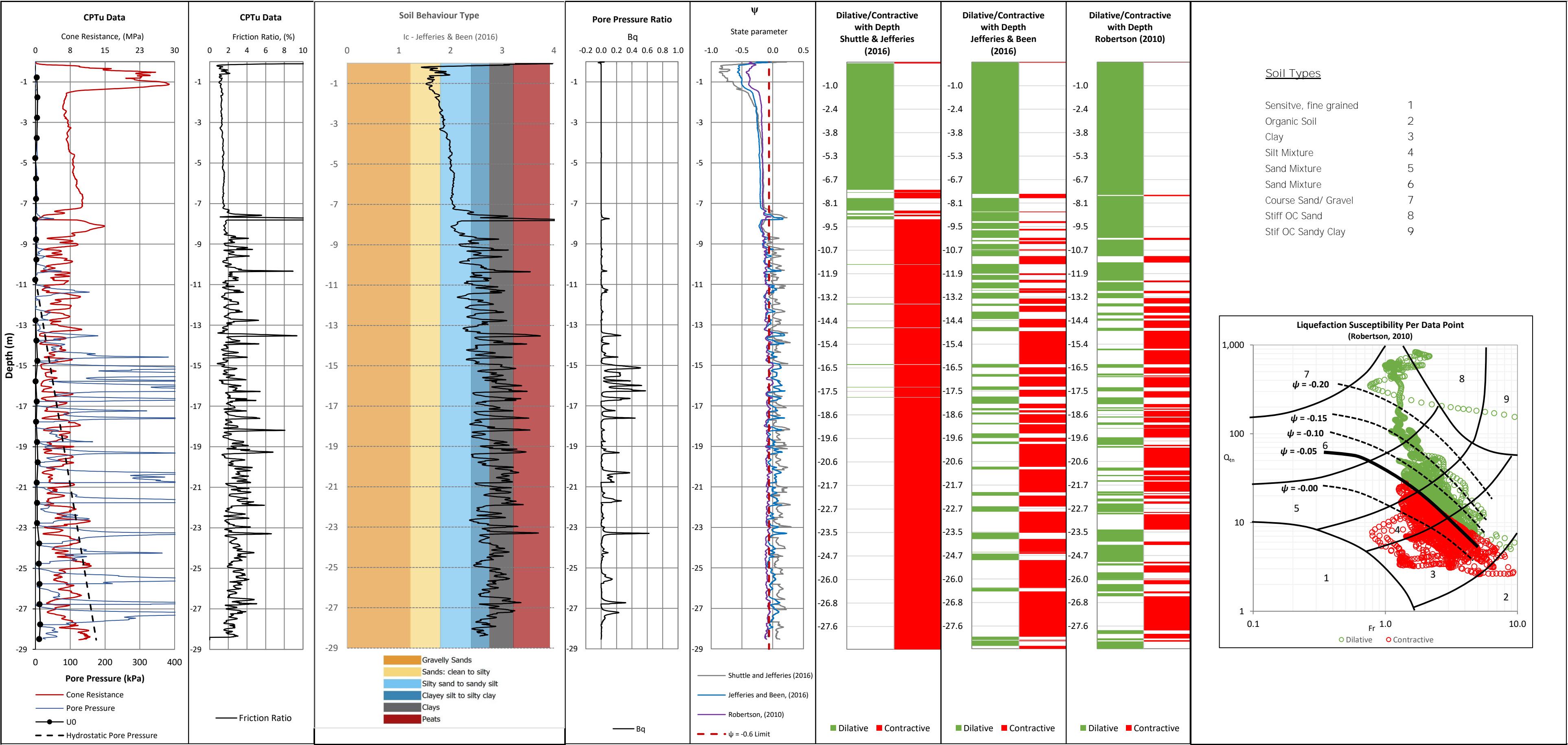
CPTu PC2



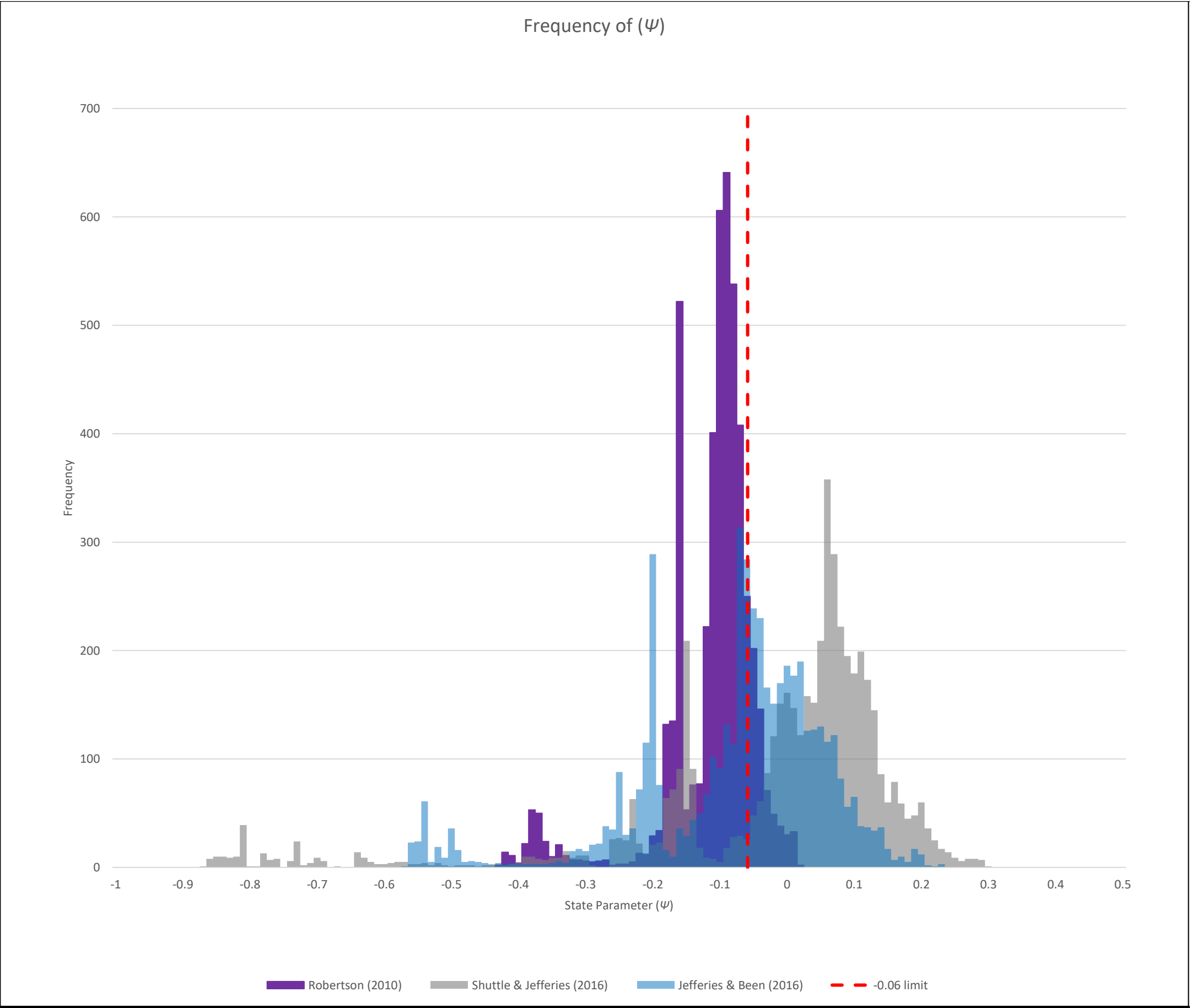
CPTu PC2



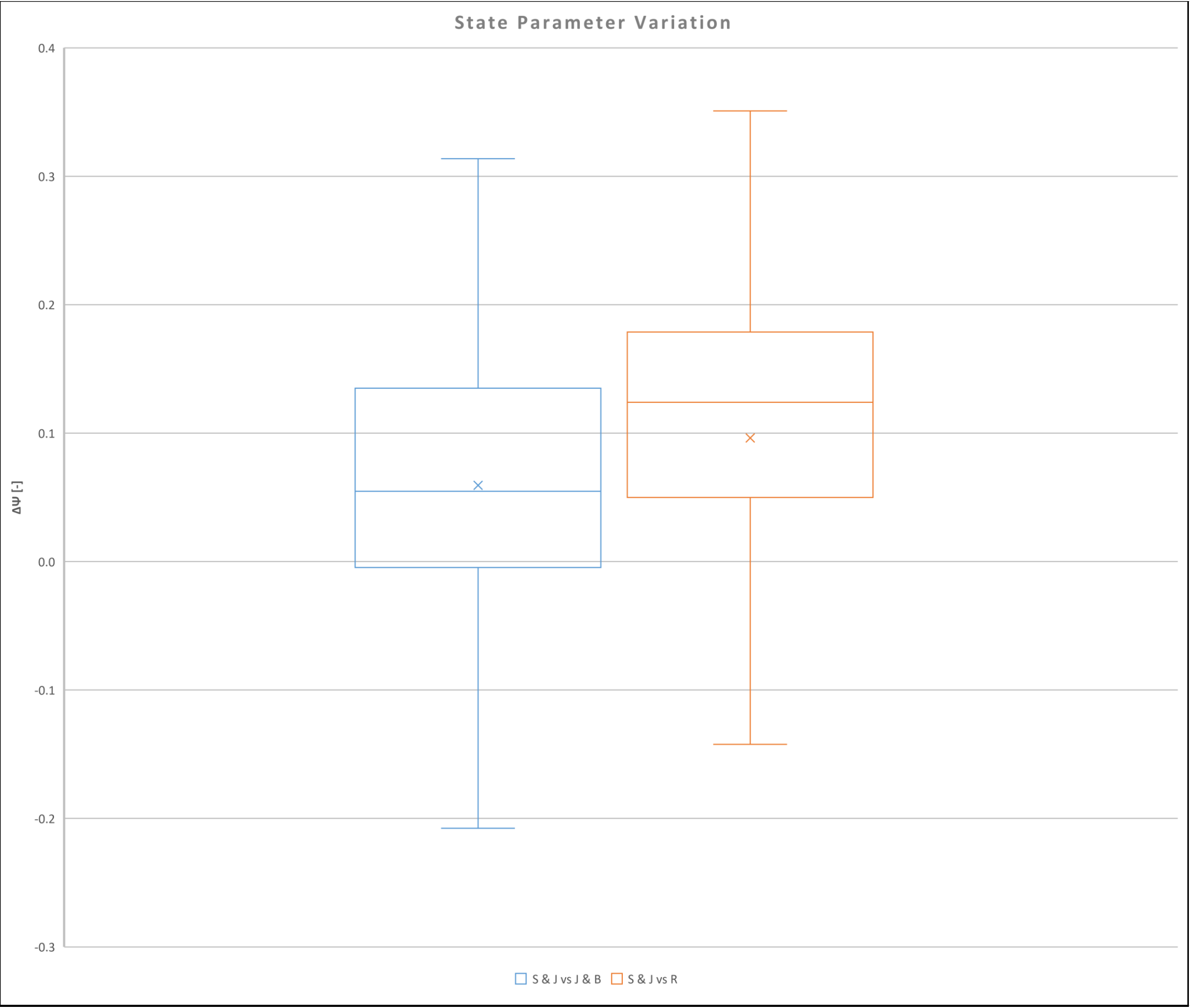
PCI1

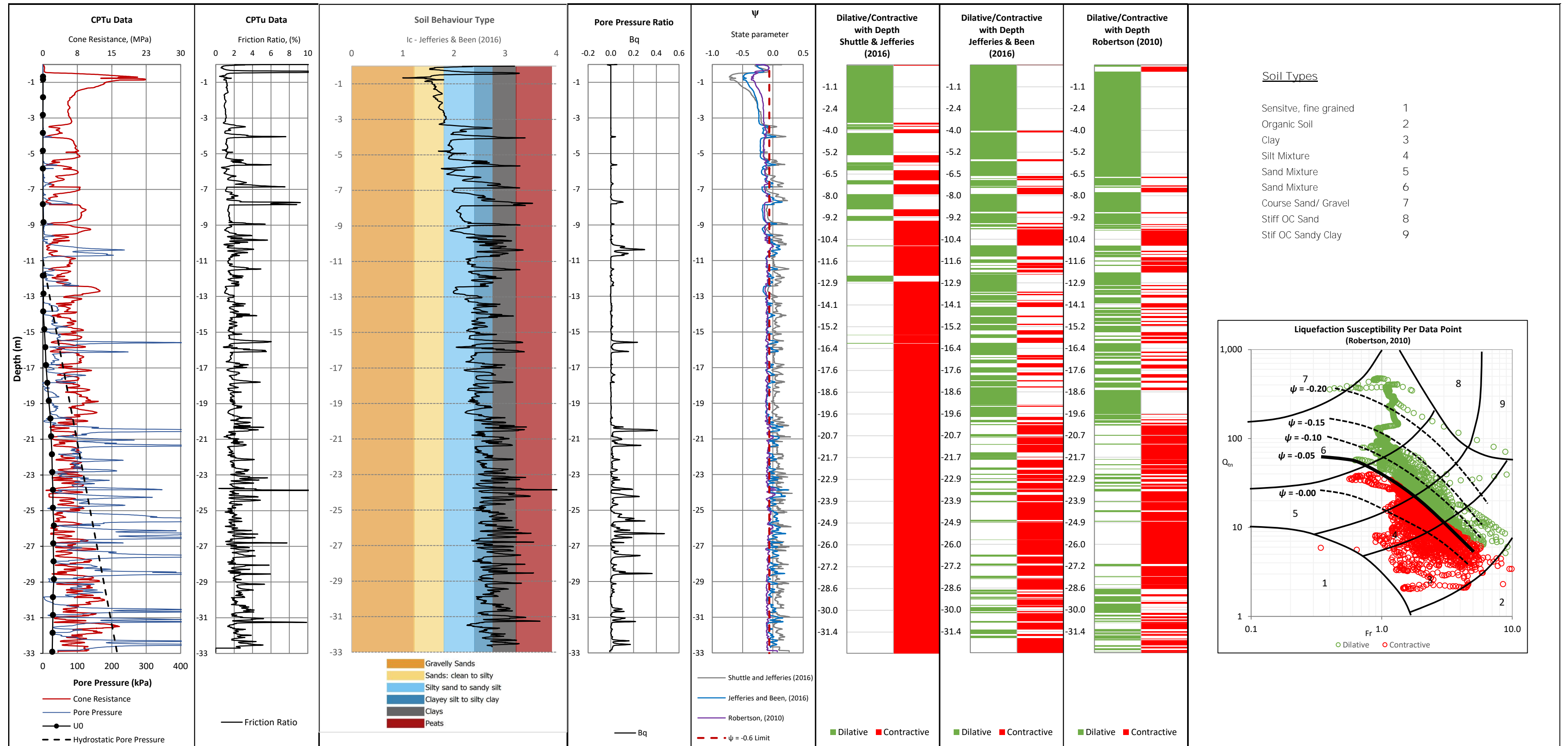


PCI1

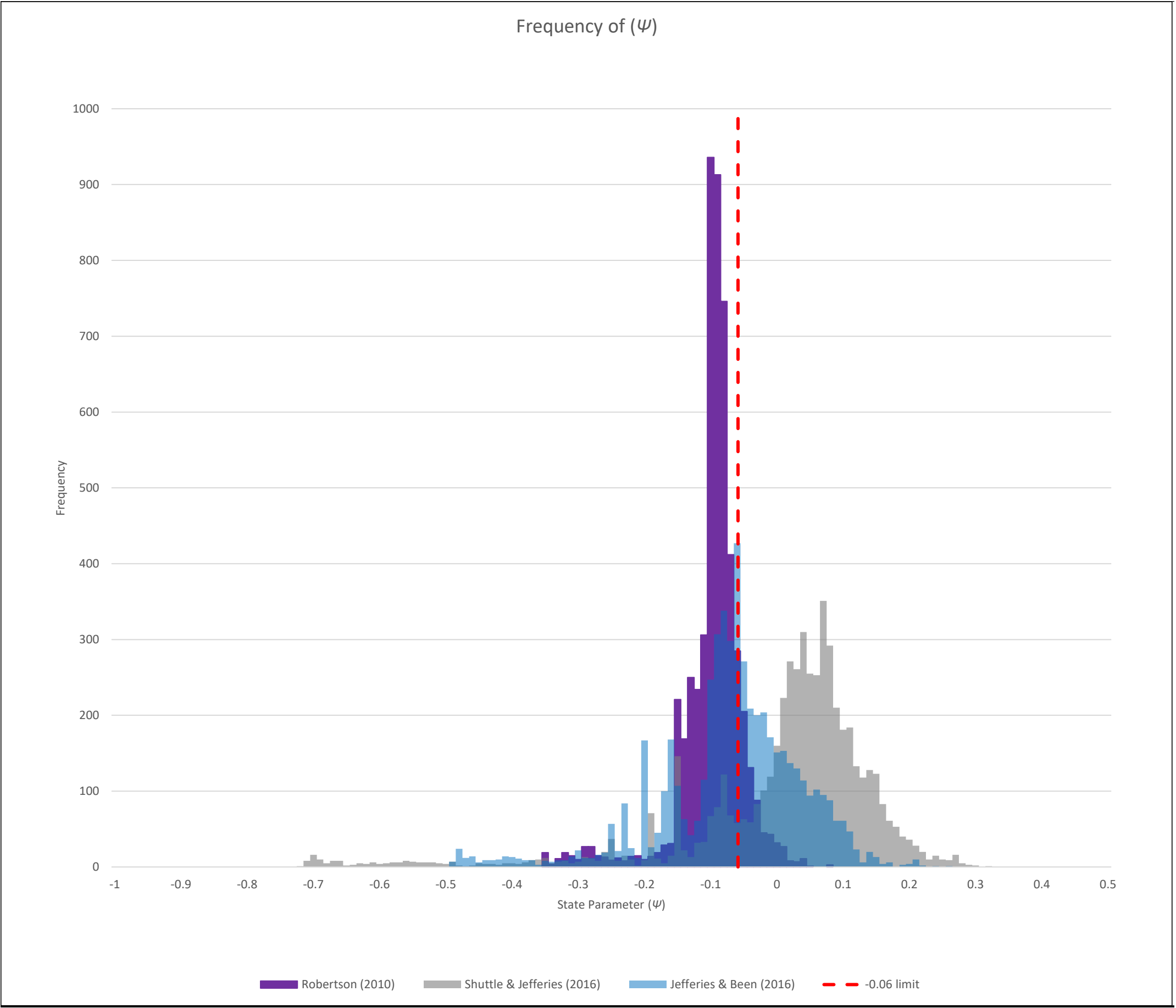


PCI1

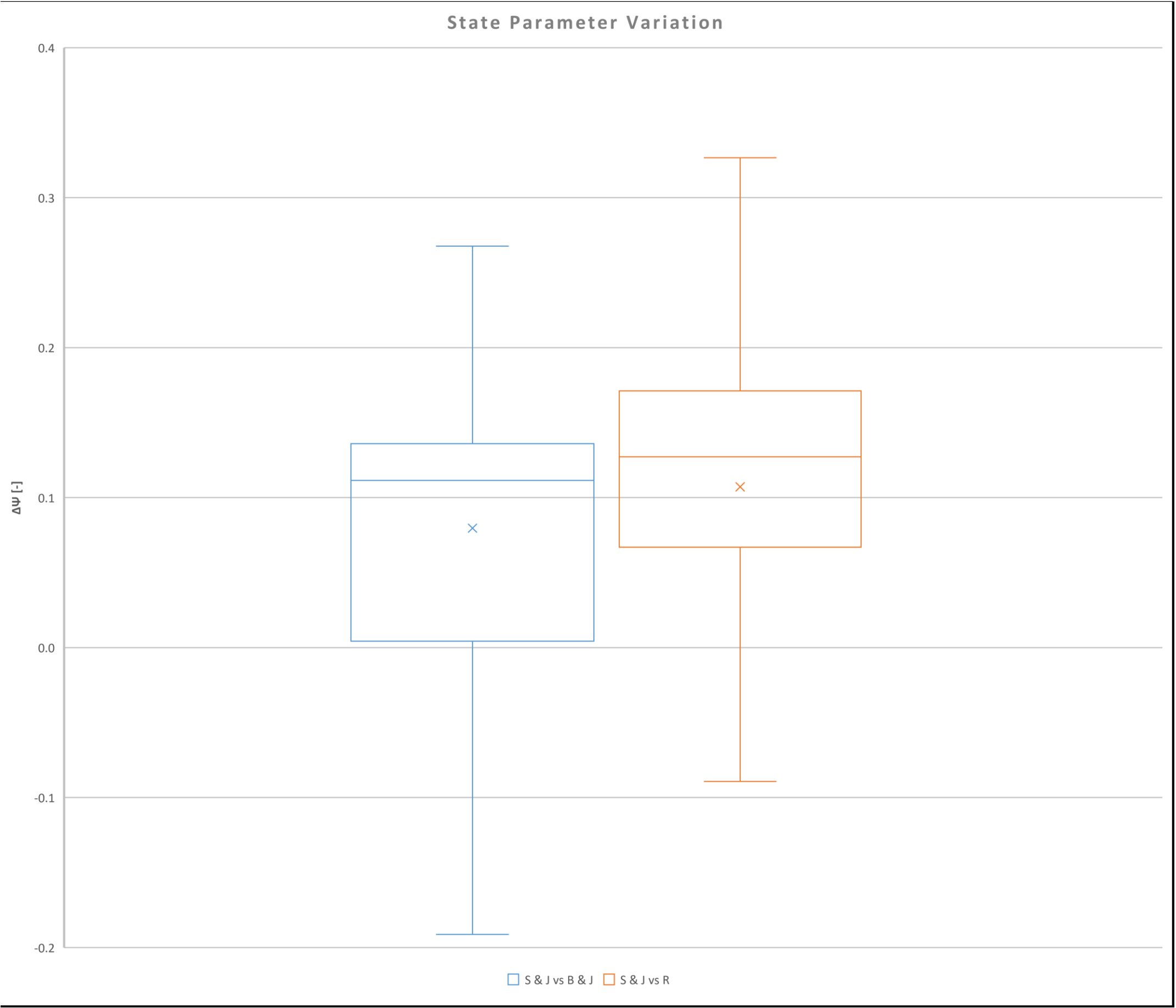




PCI2

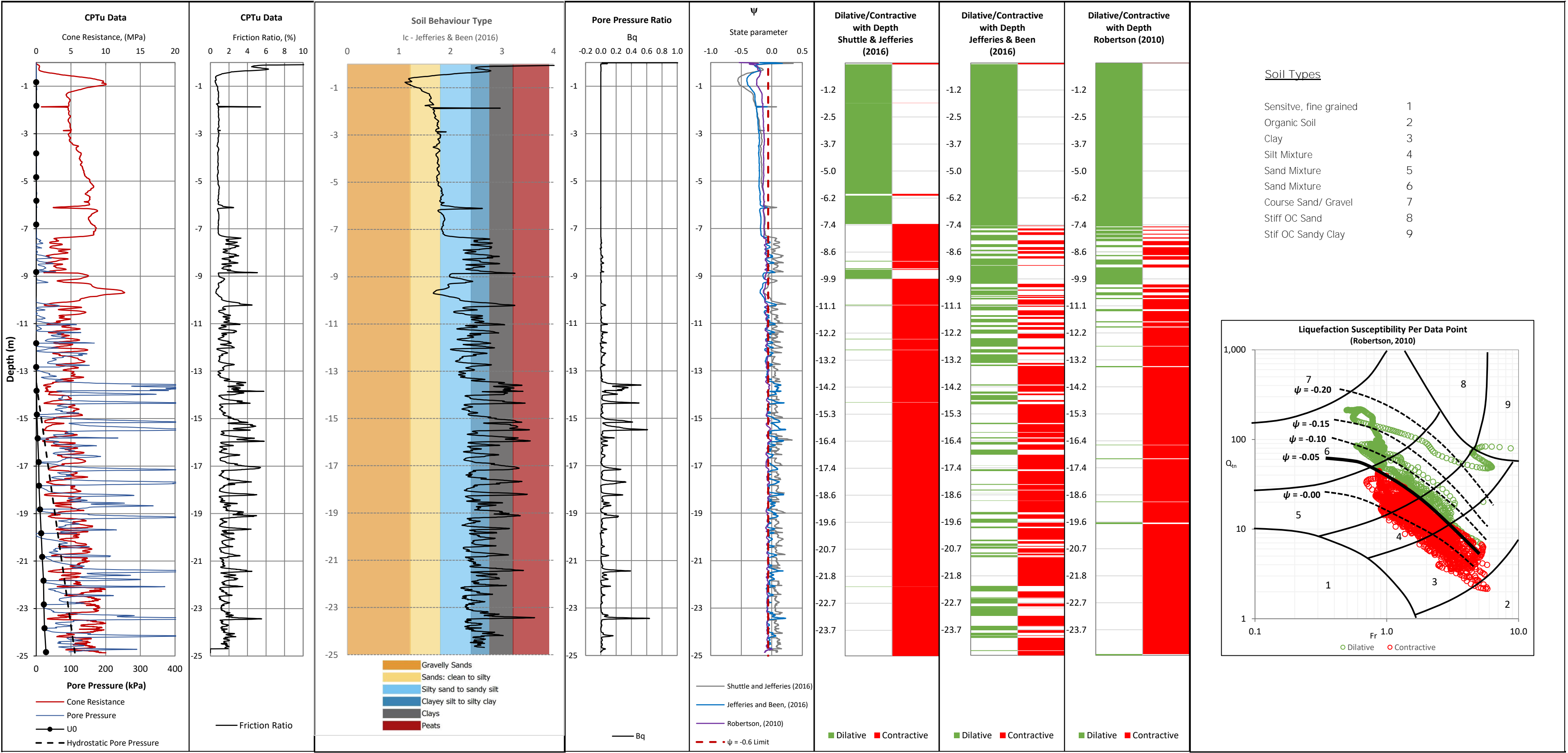


PCI2

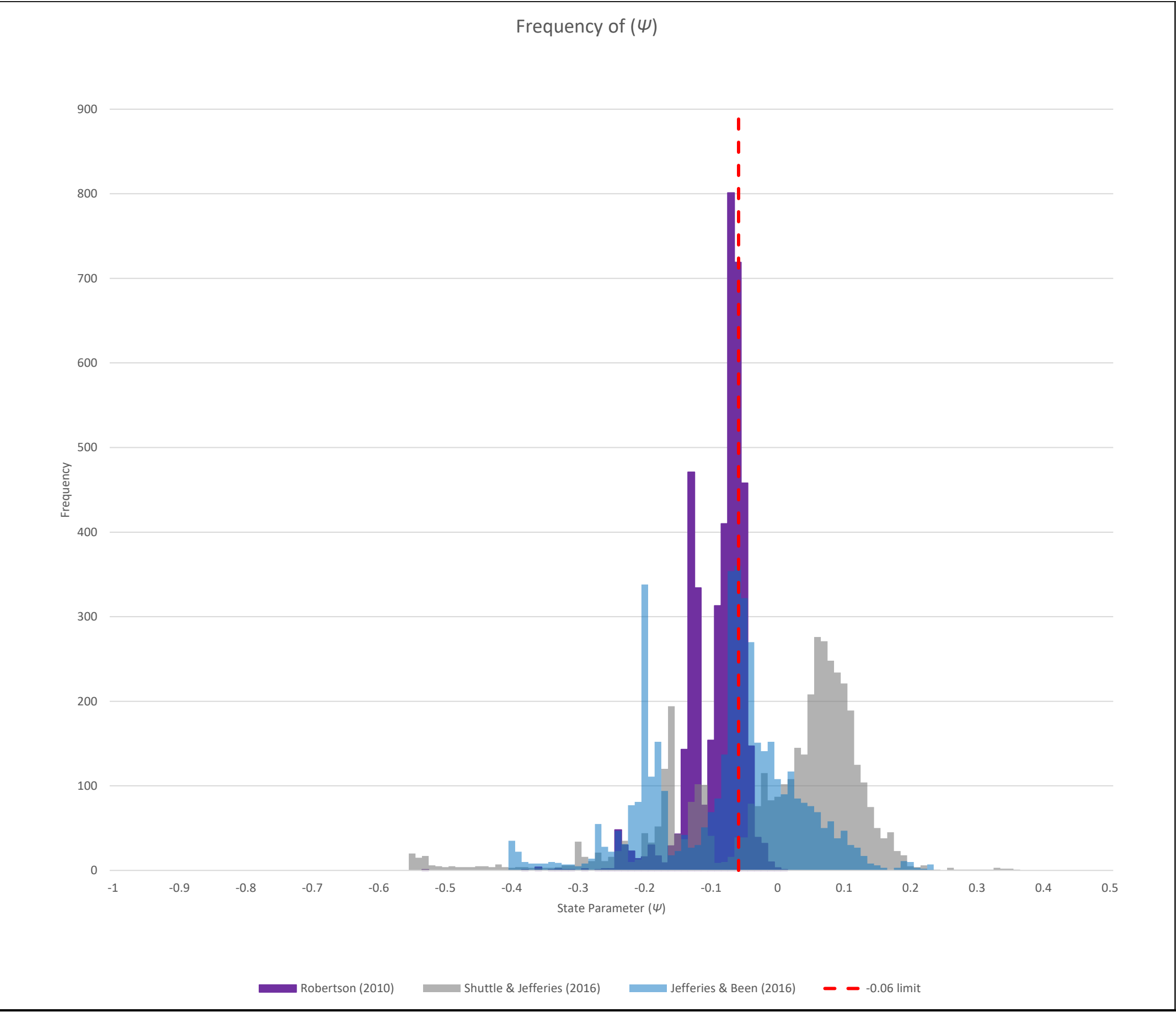




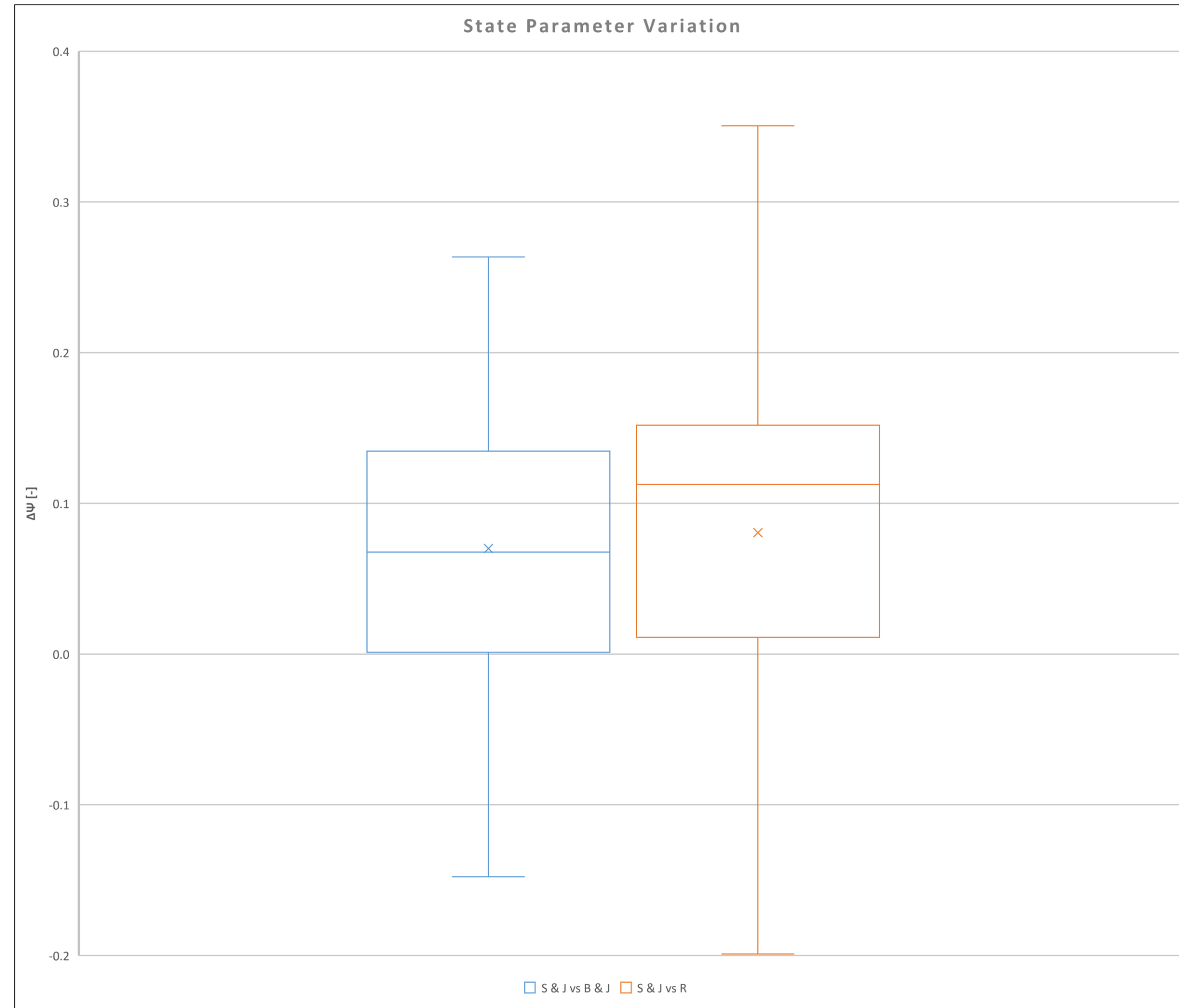
PCI3



PCI3

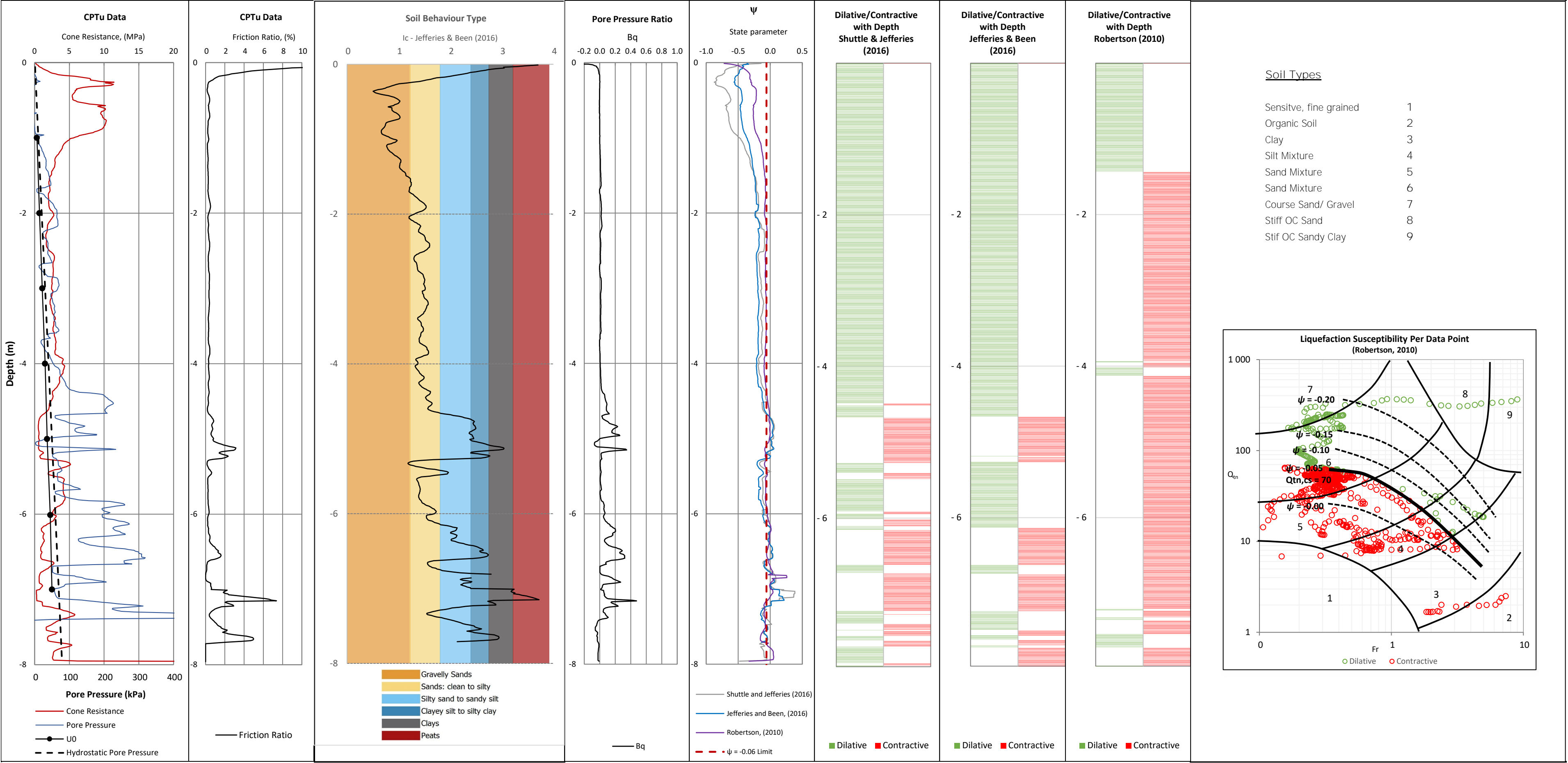


# PCI3

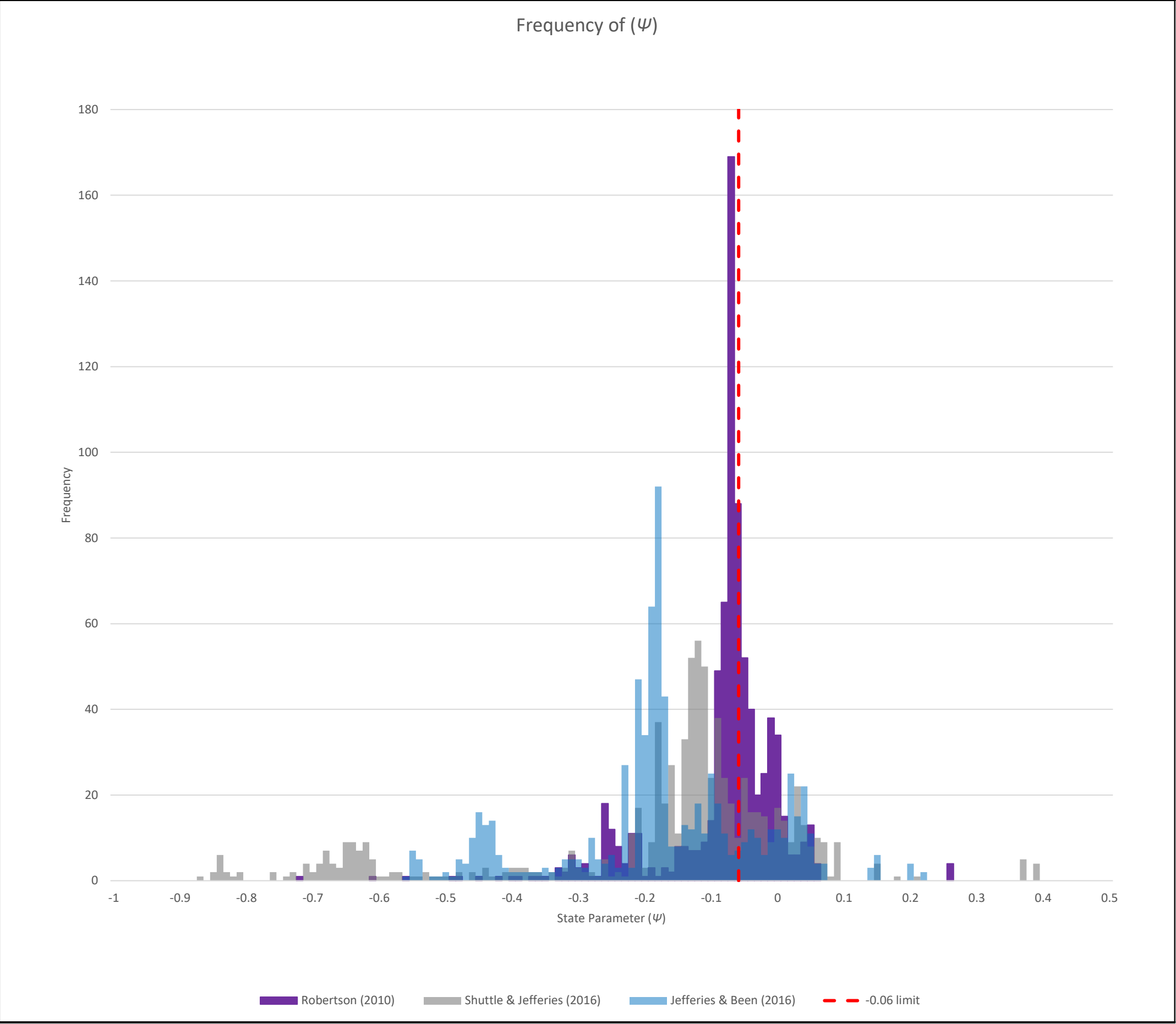


## **Appendix J: CPTu Interpretation – Monitoring Line O**

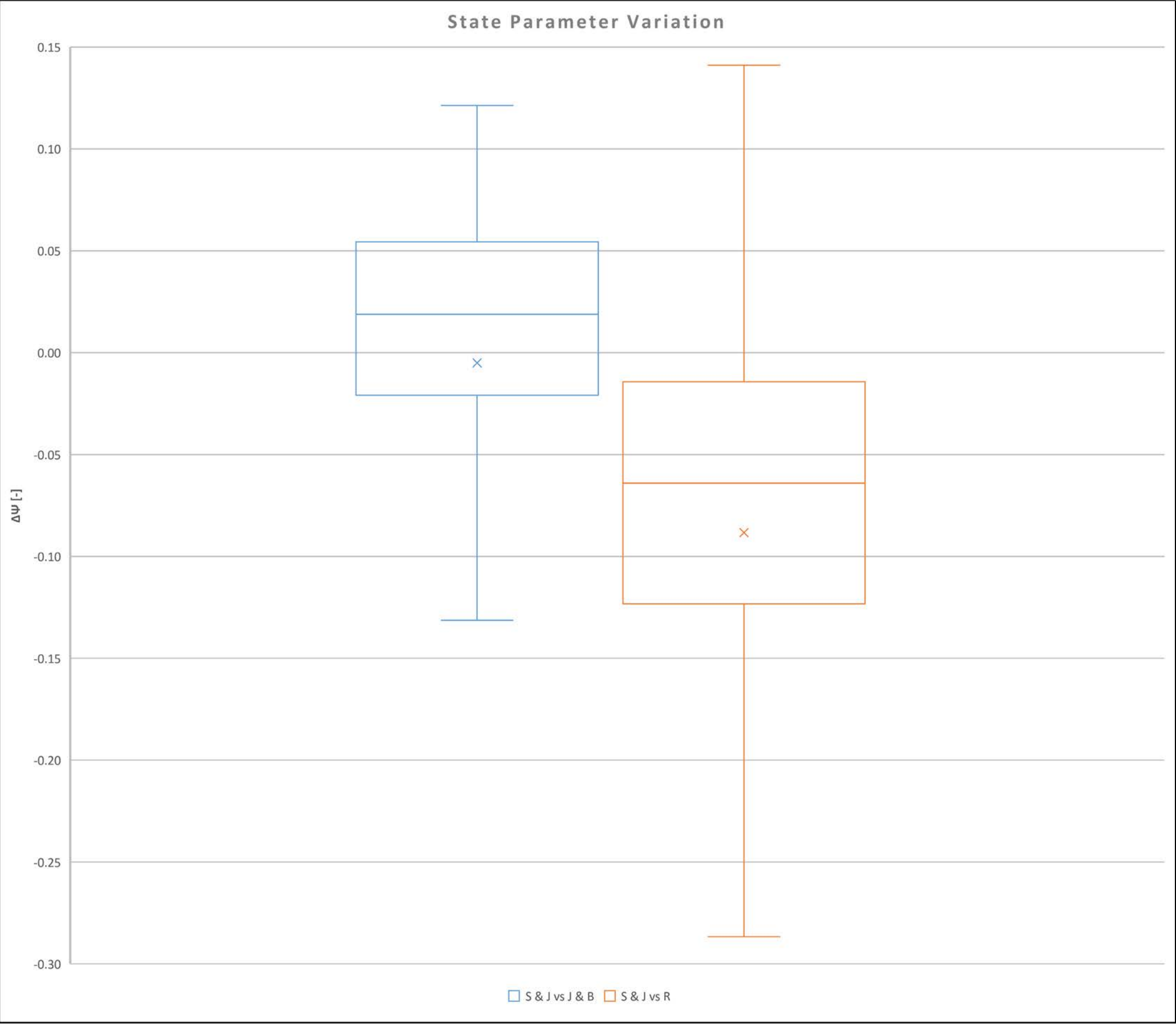
CPTu PC22

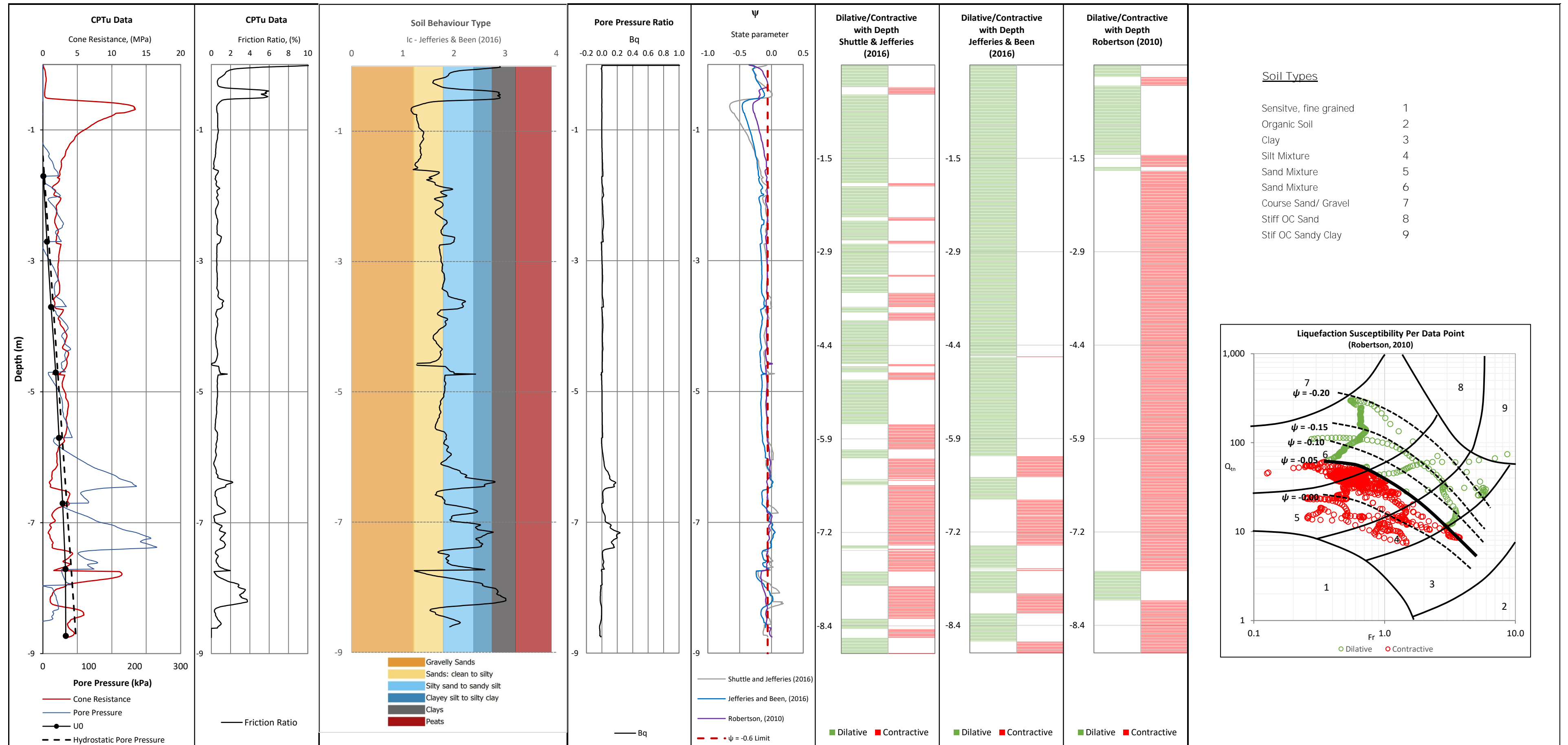


CPTu PC22



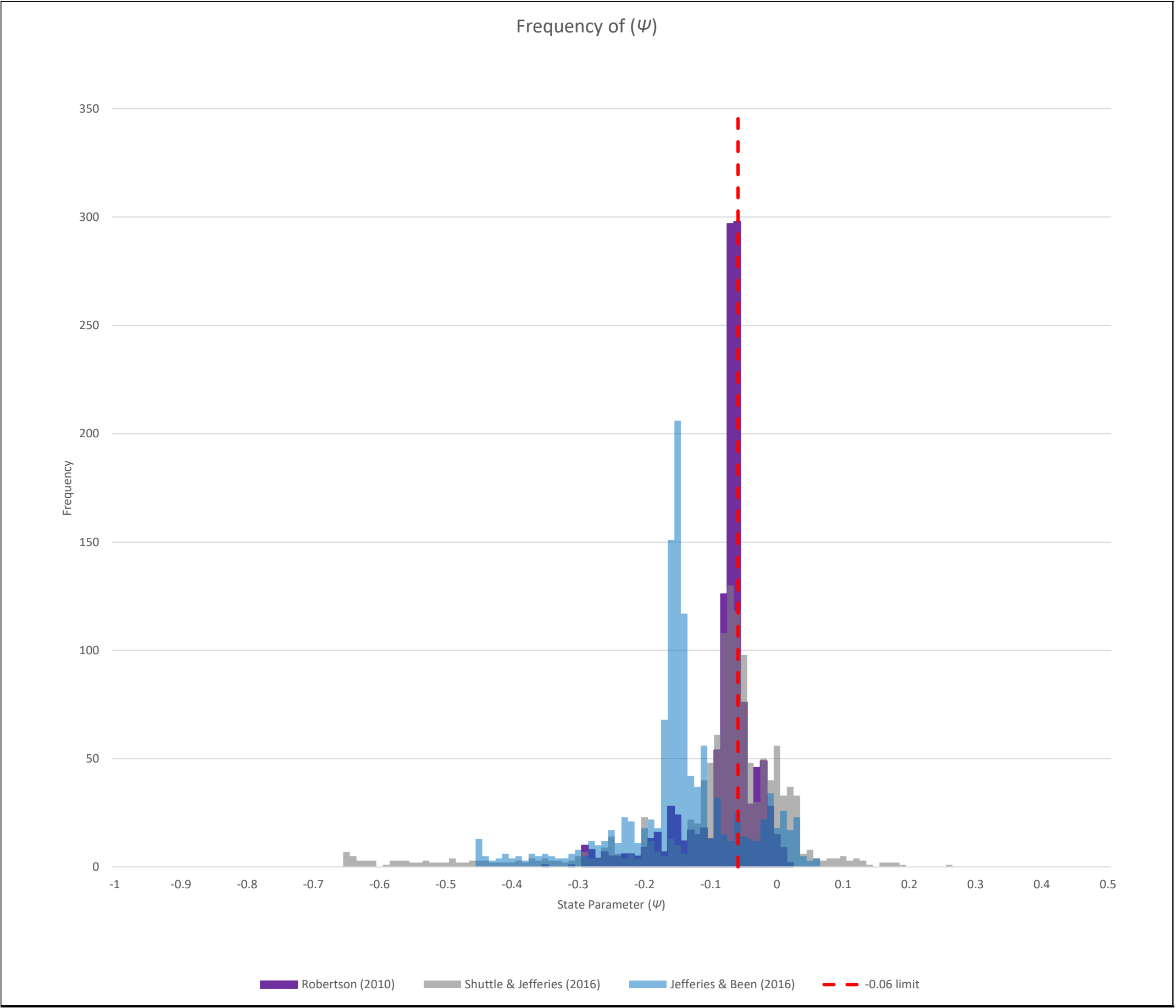
CPTu PC22



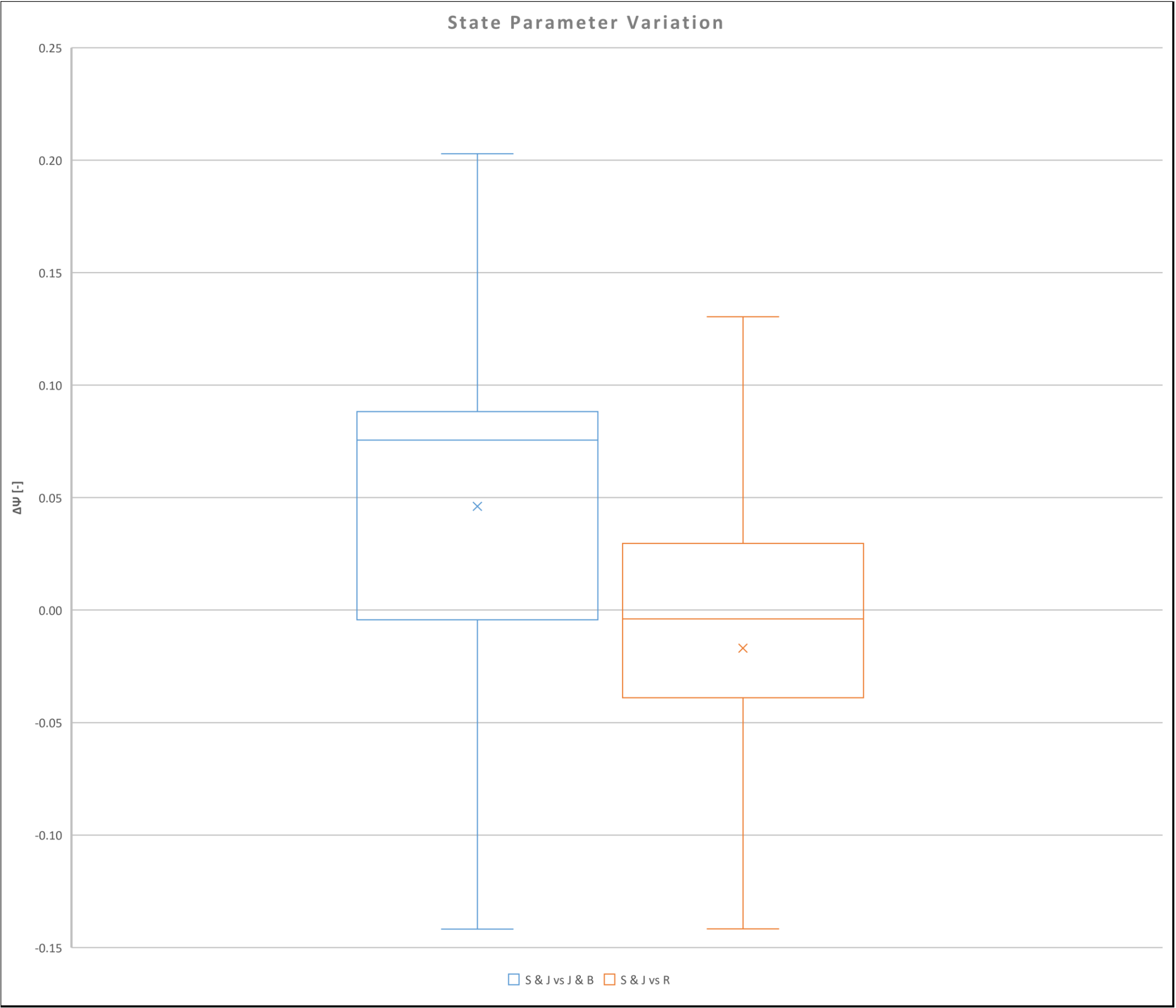




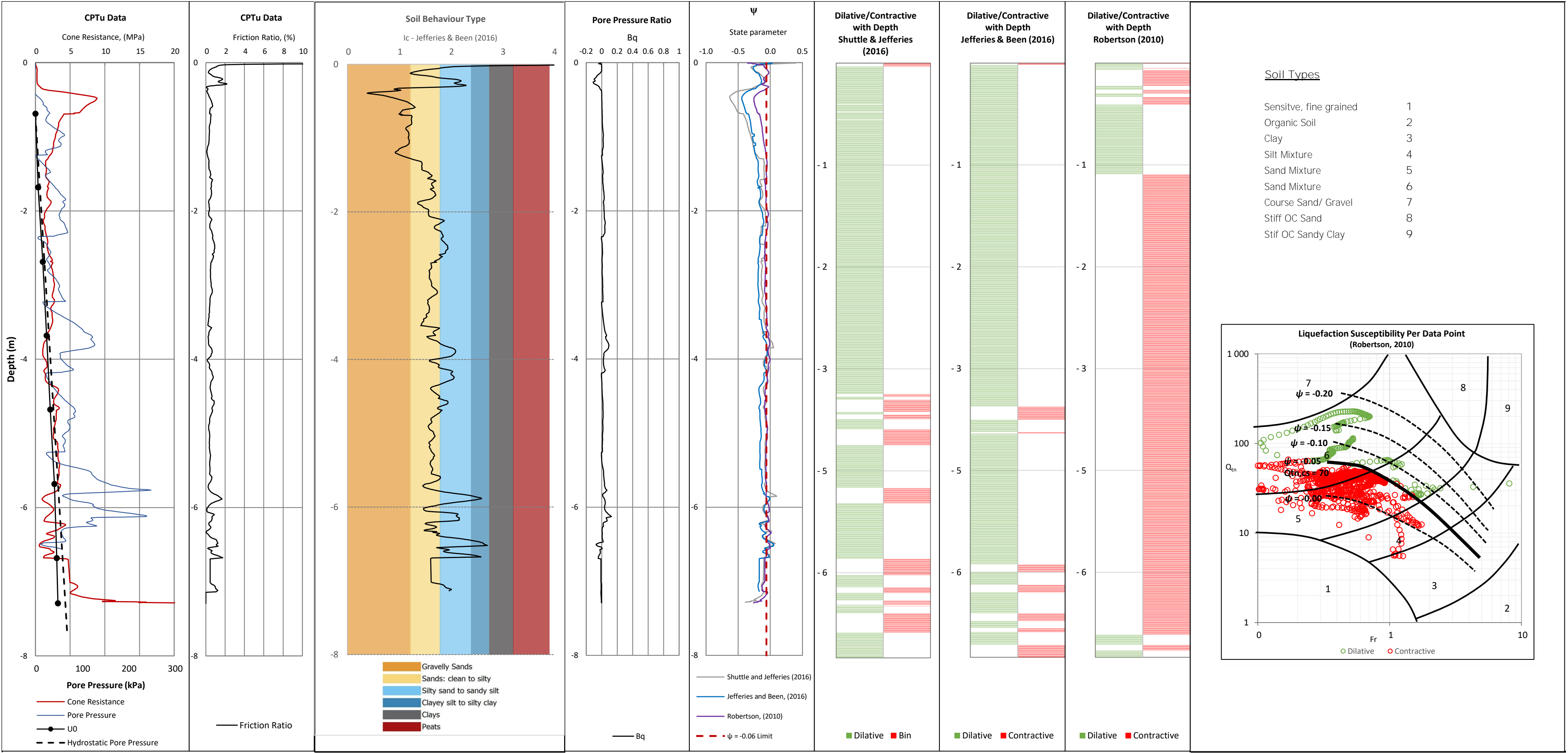
CPTu PC22ADTS



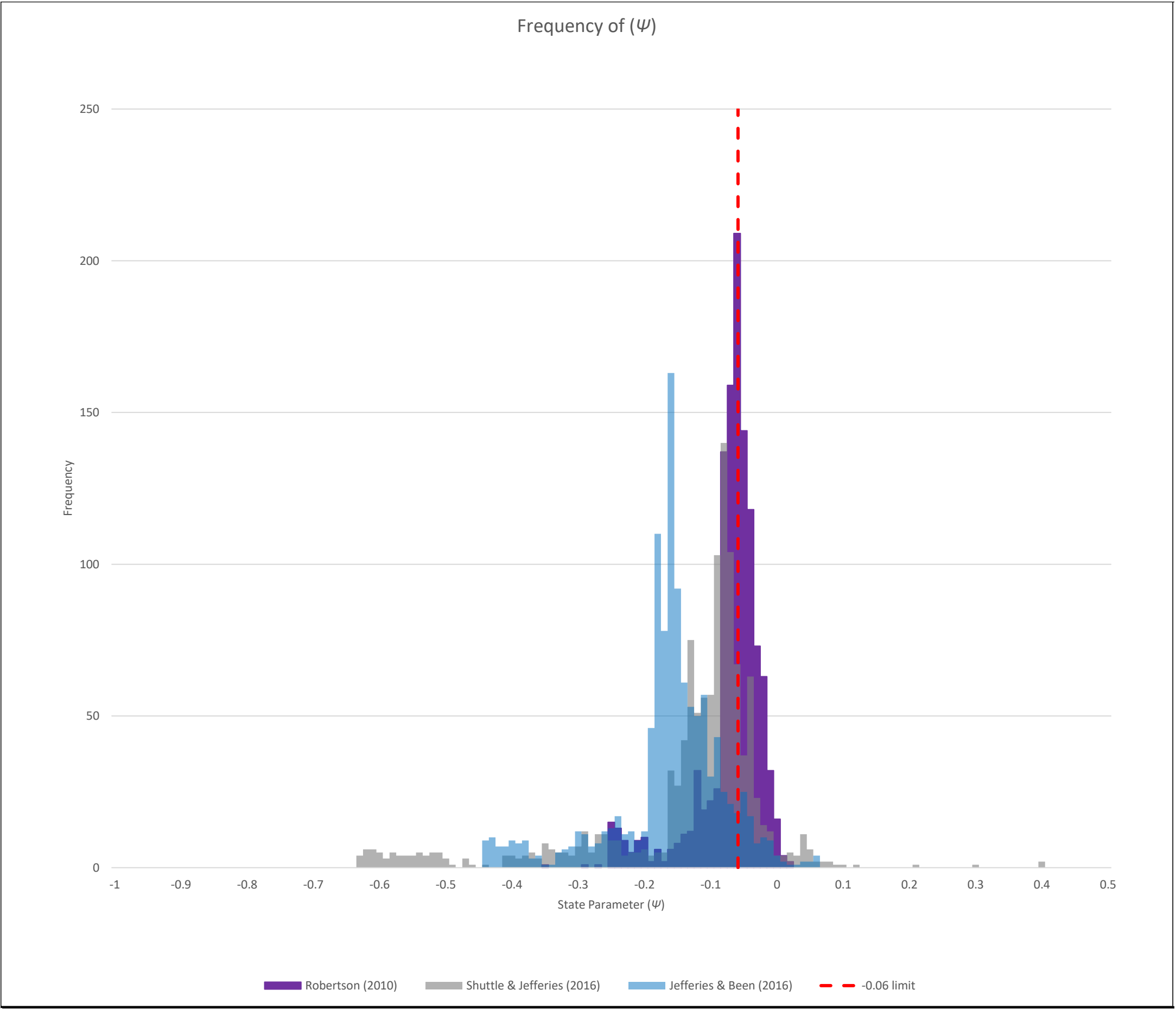
CPTu PC22ADTS



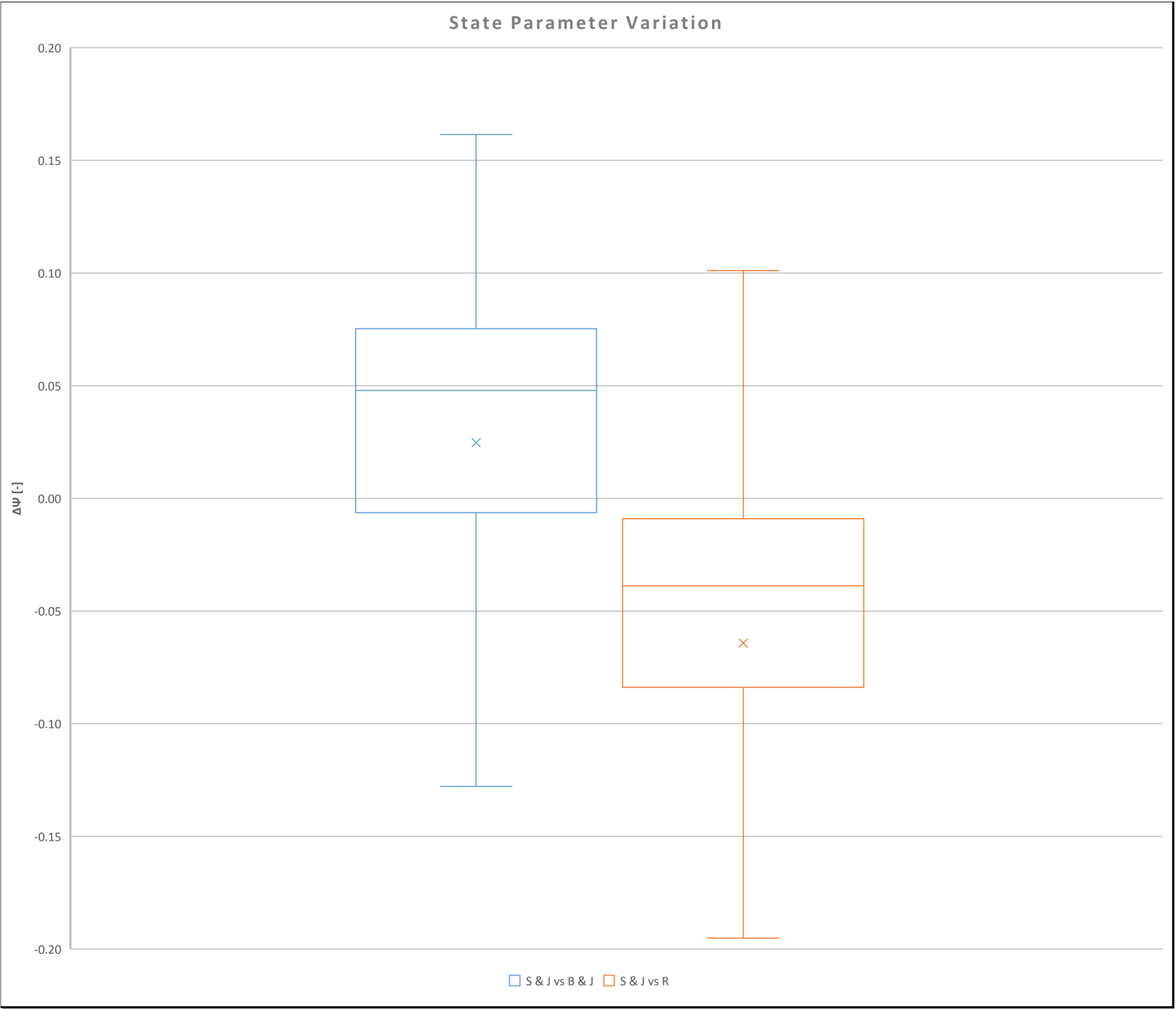
CPTu PC22B



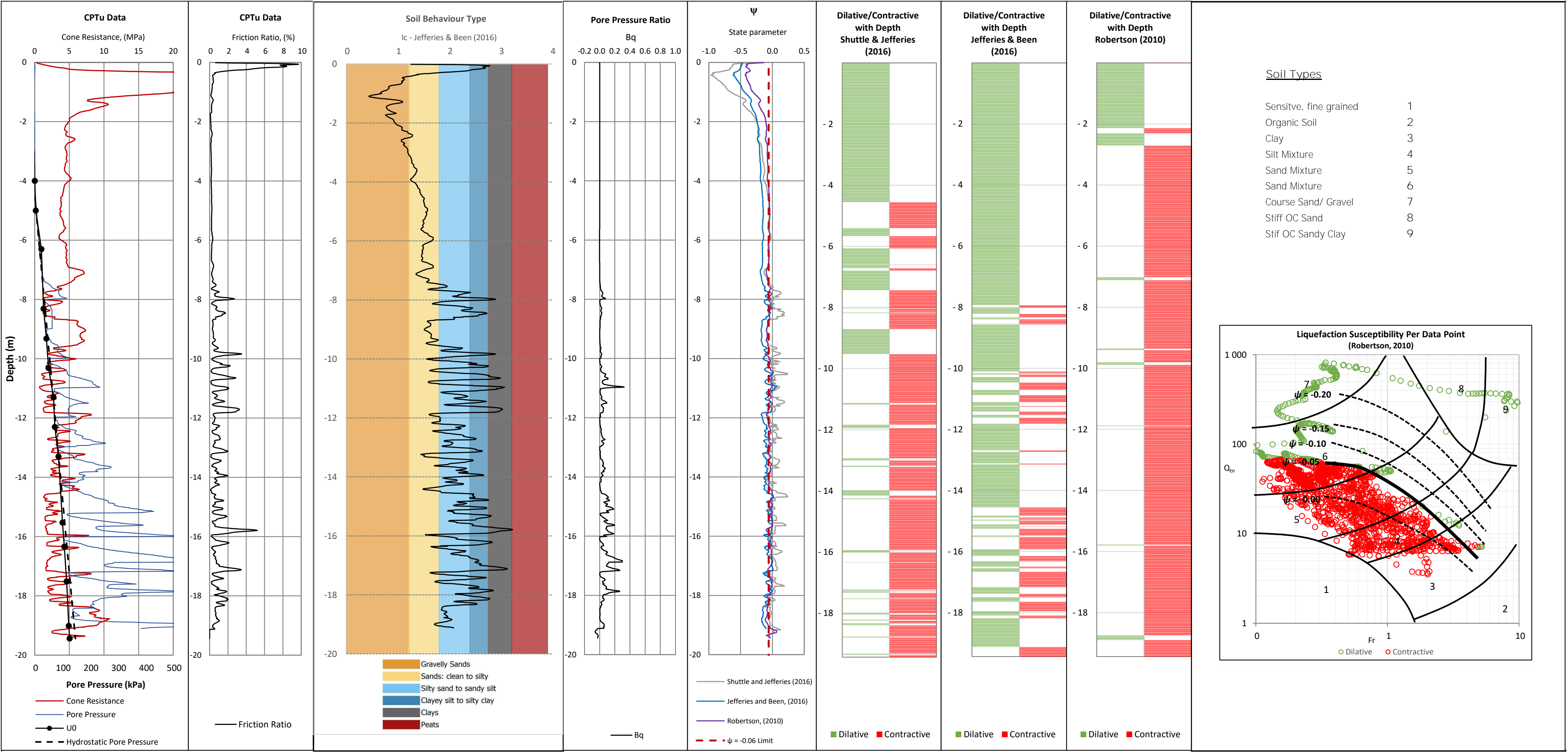
CPTu PC22B



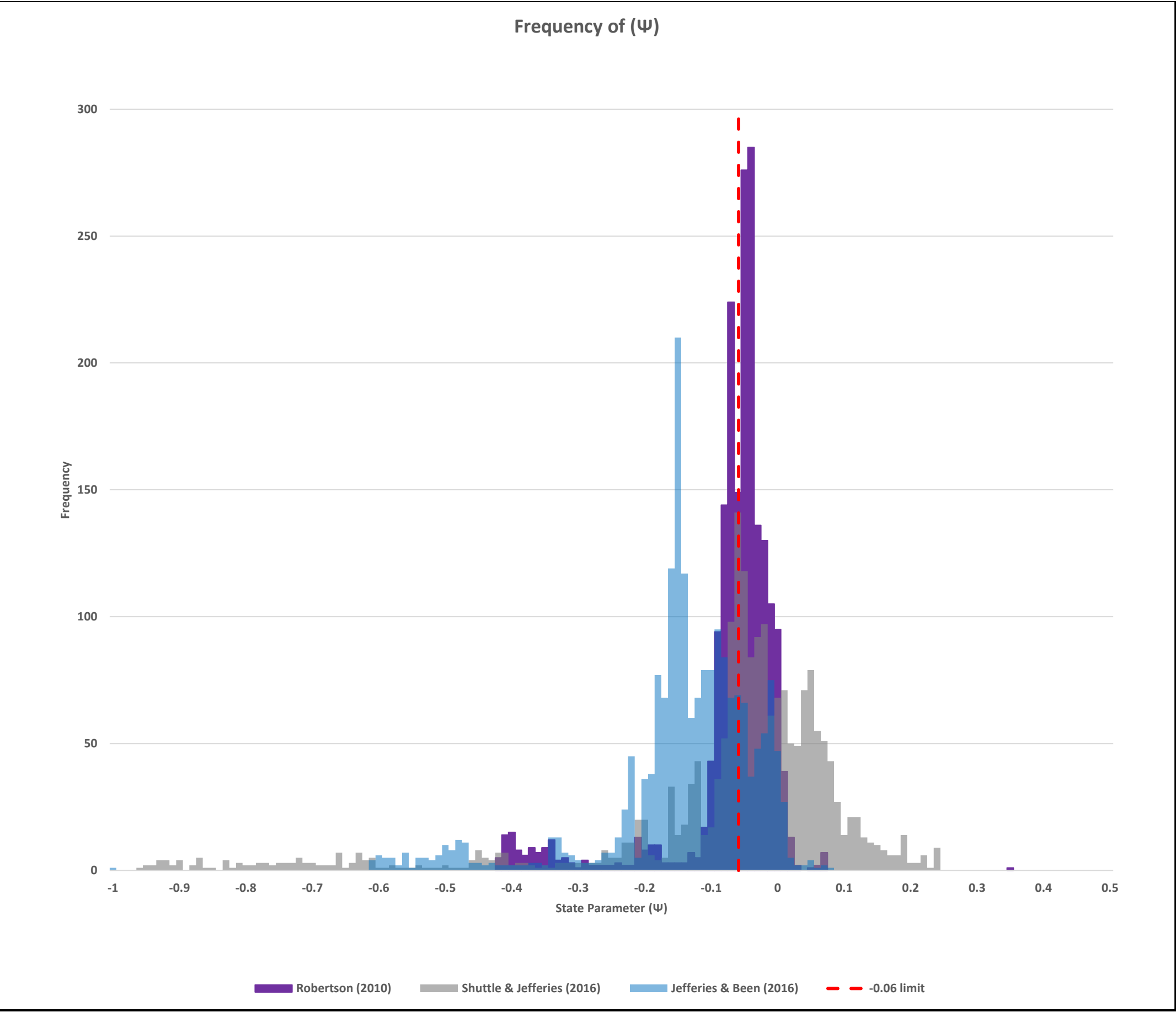
CPTu PC22B



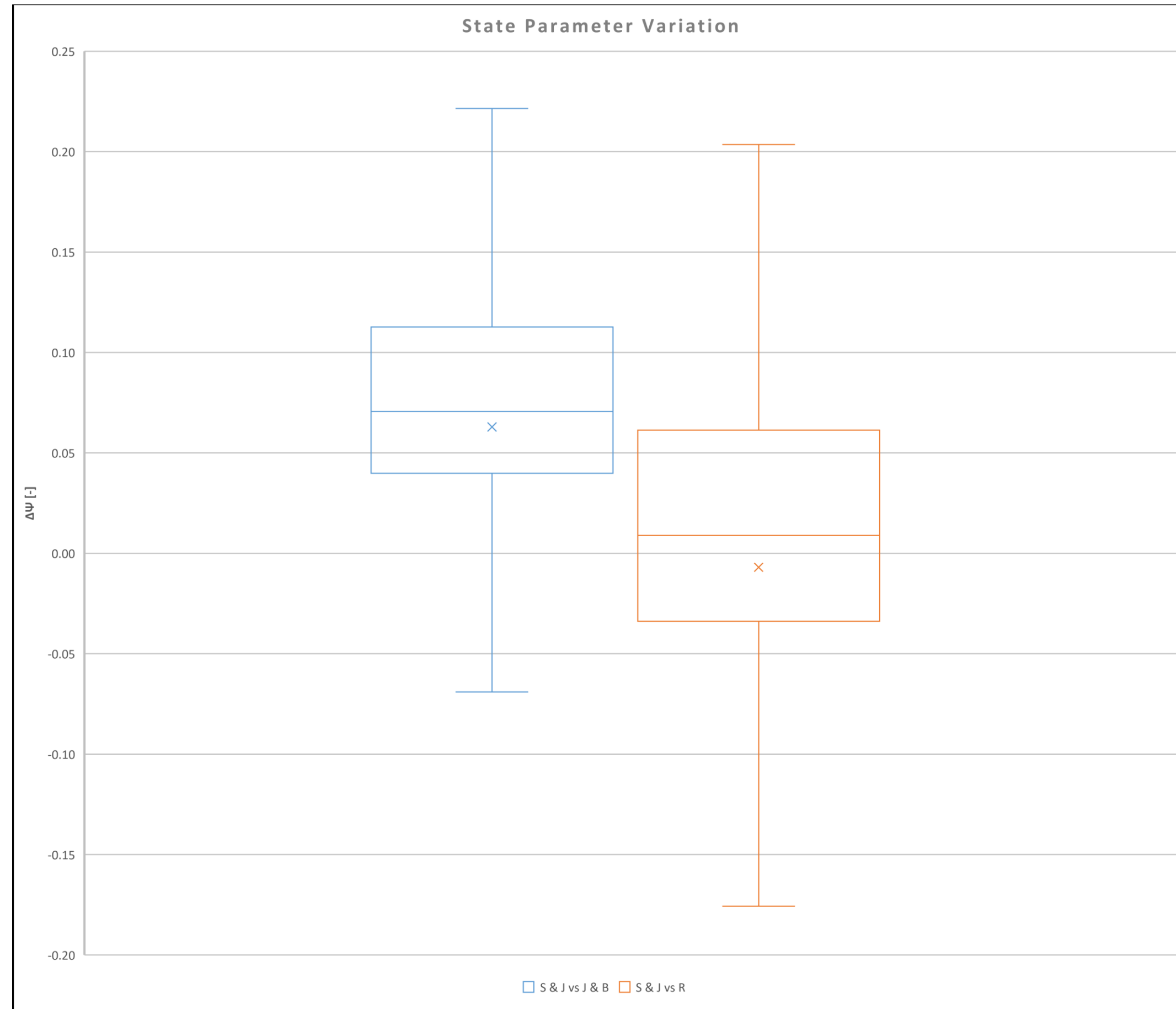
CPTu PC23



CPTu PC23

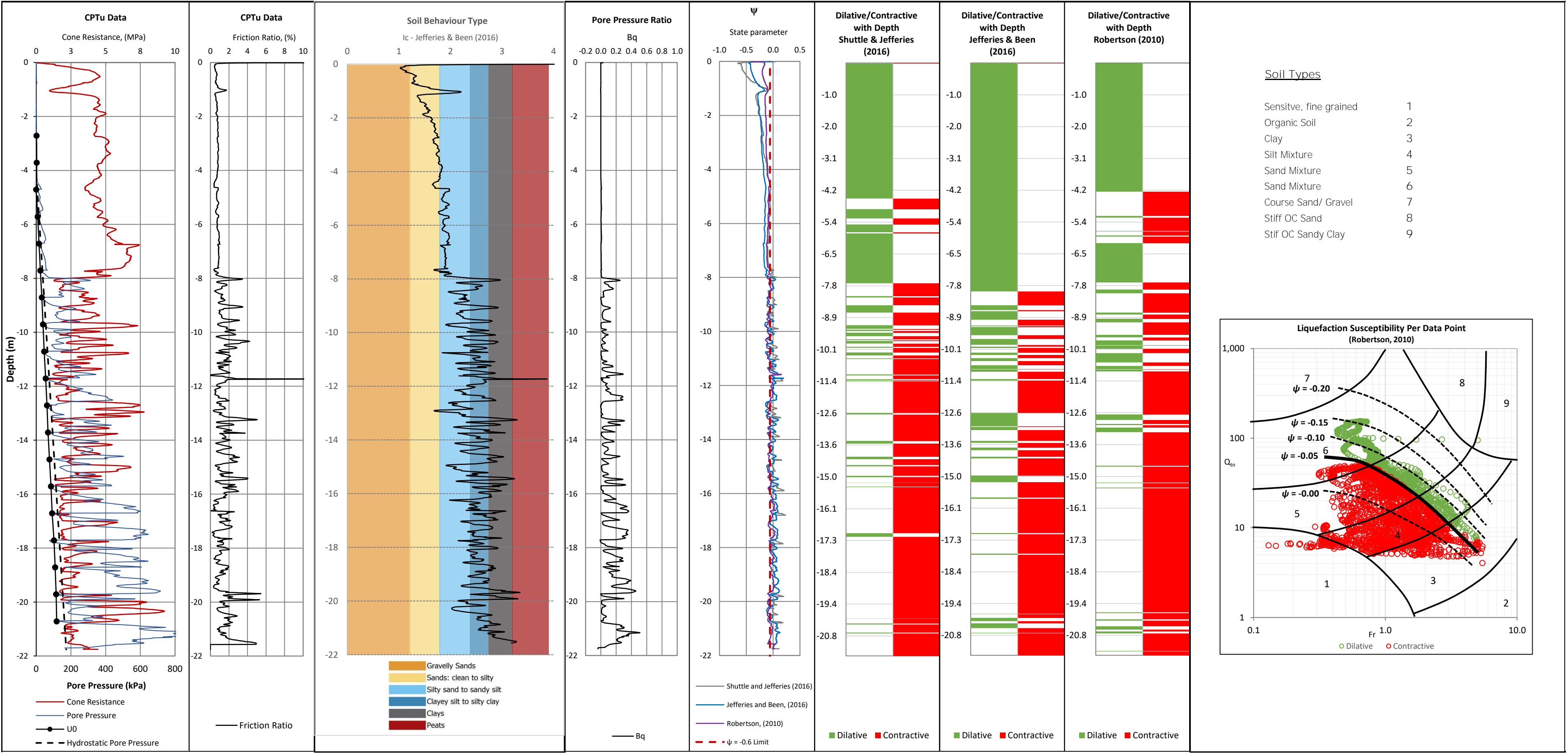


# CPTu PC23

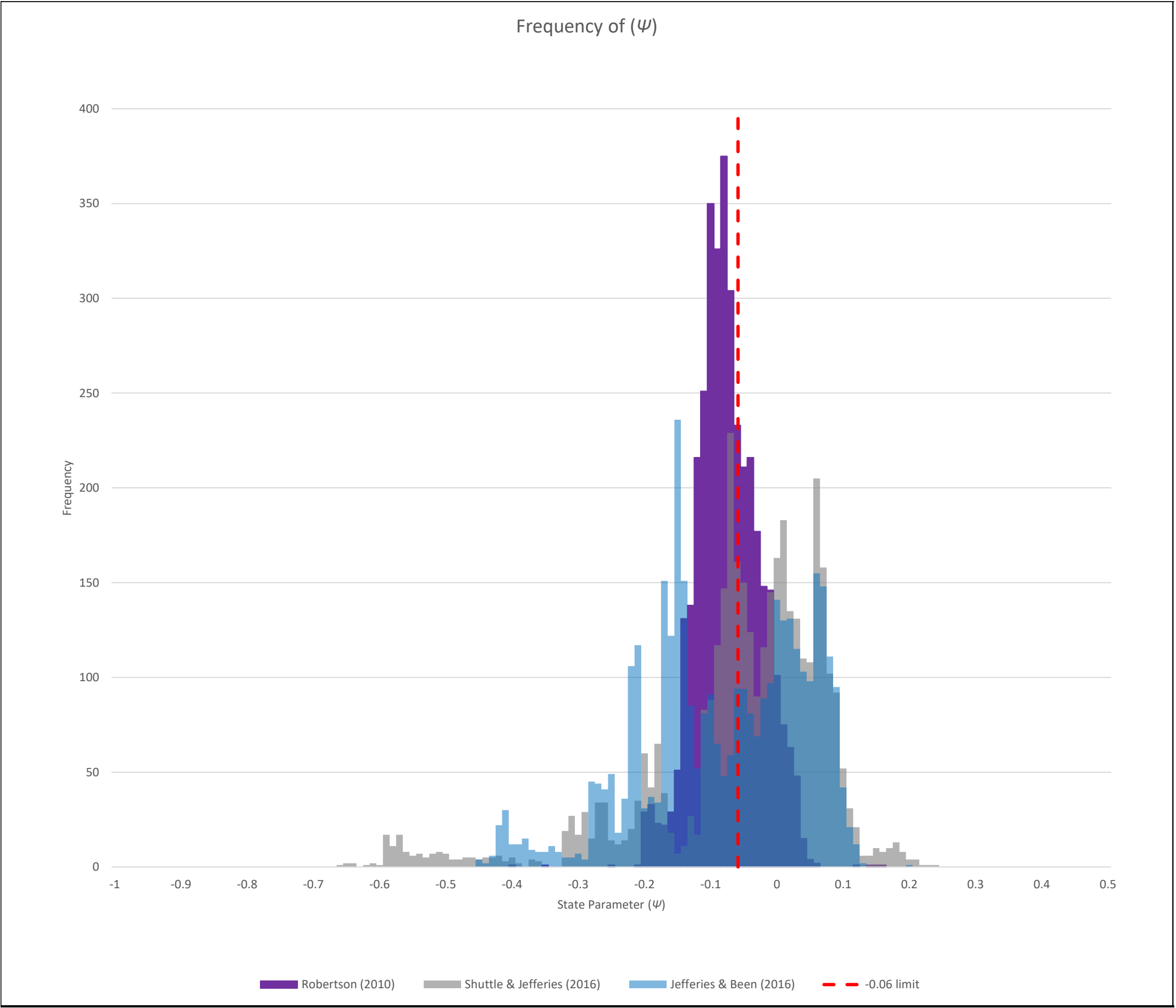




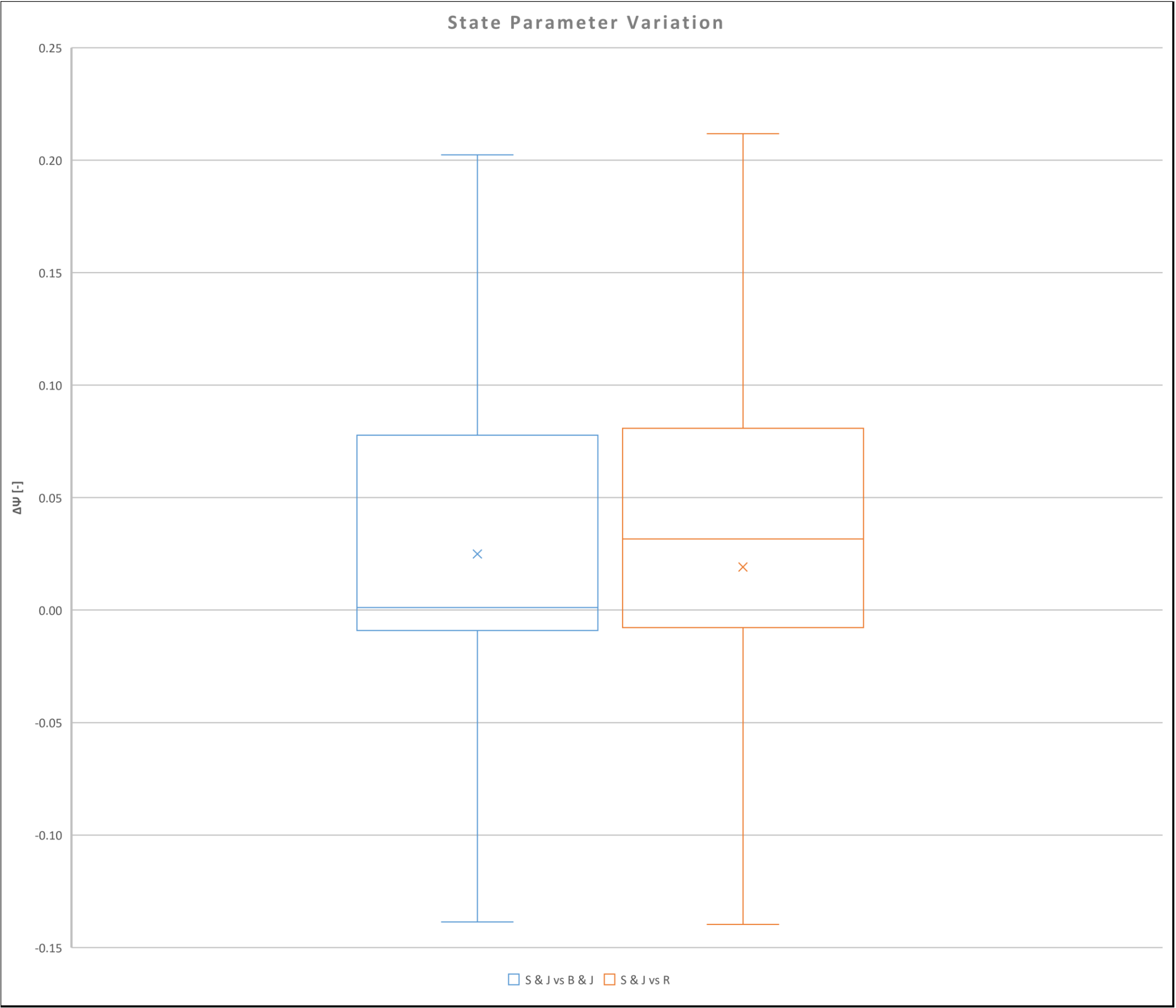
CPTu PC23AD



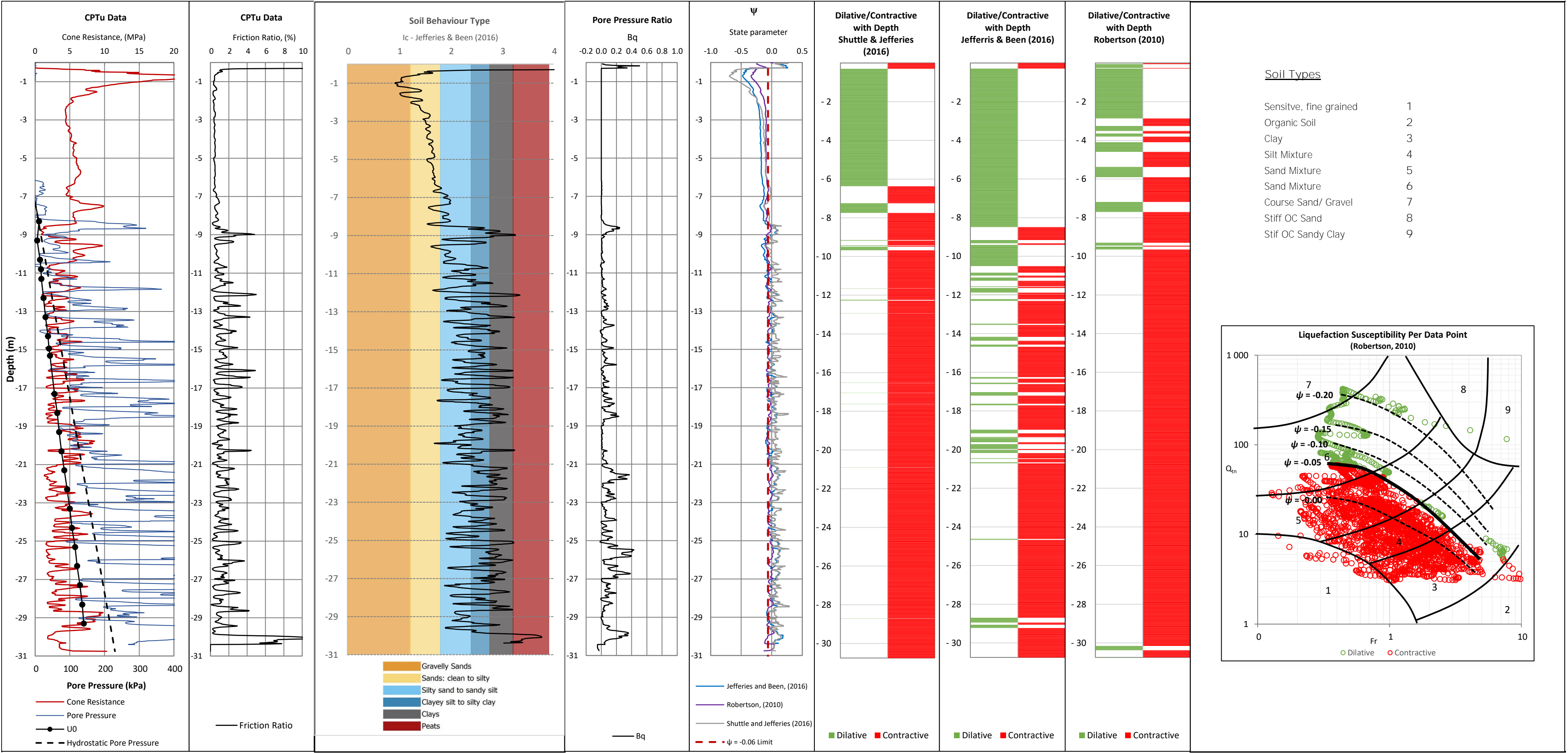
CPTu PC23AD



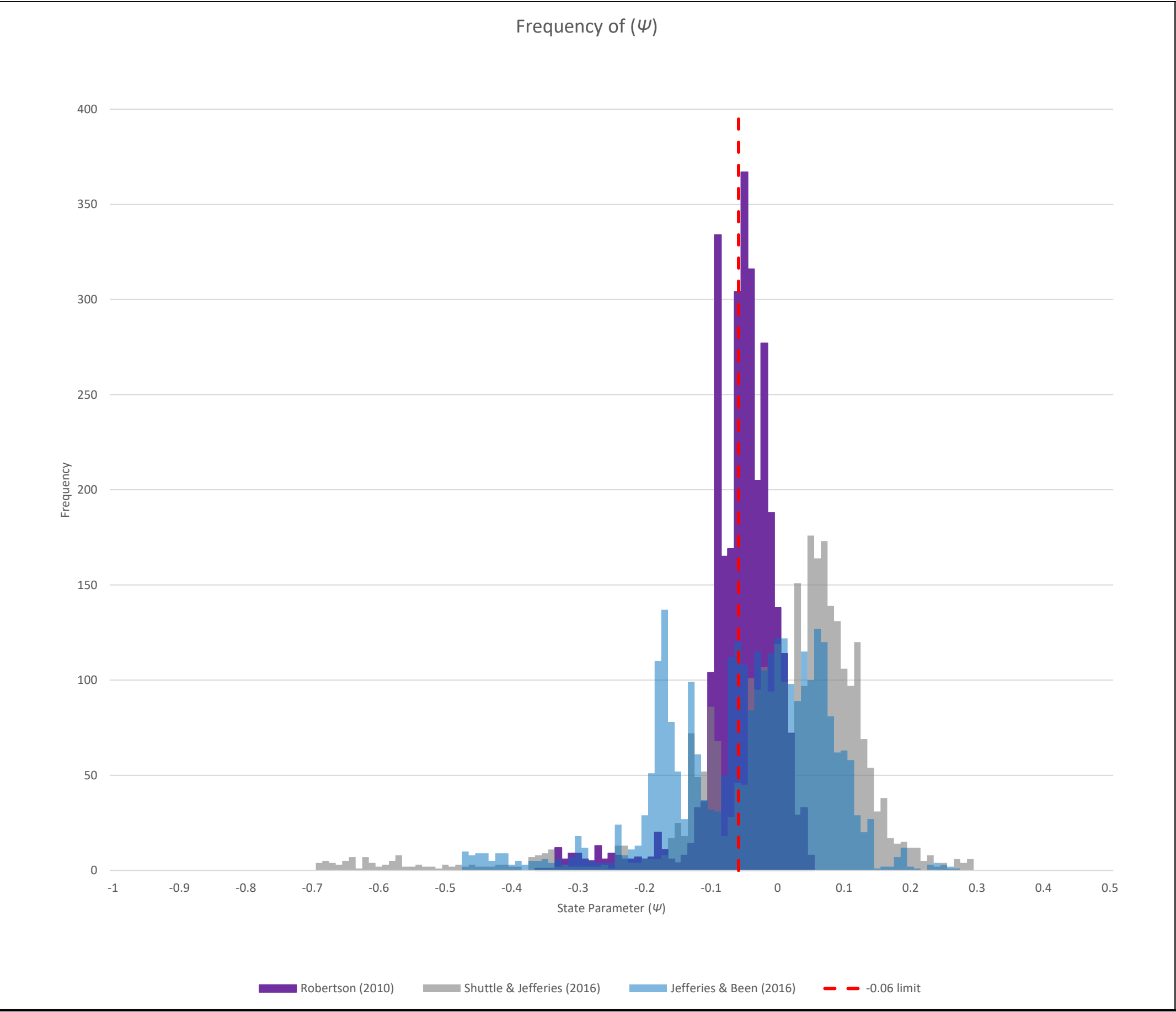
CPTu PC23AD



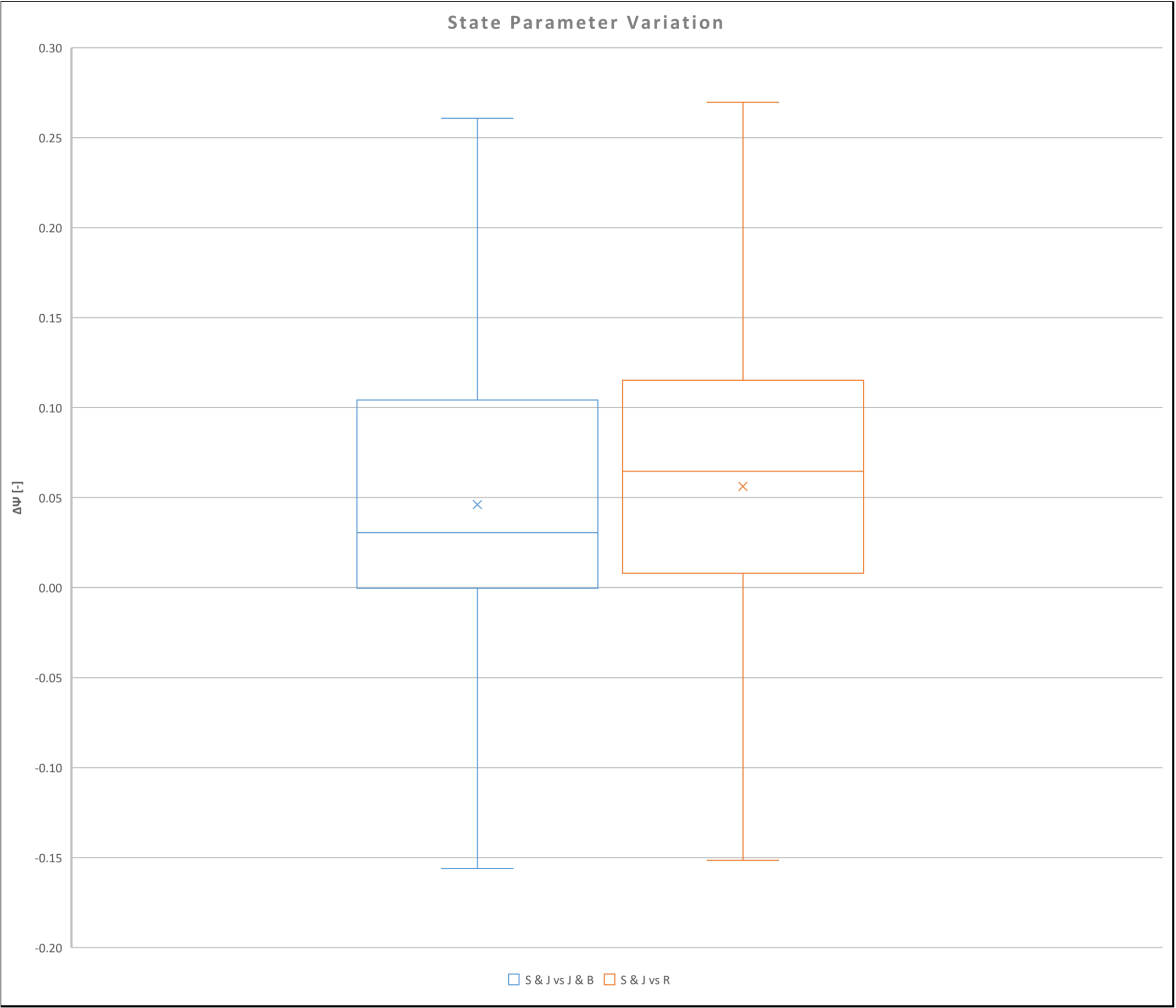
CPTu PC24



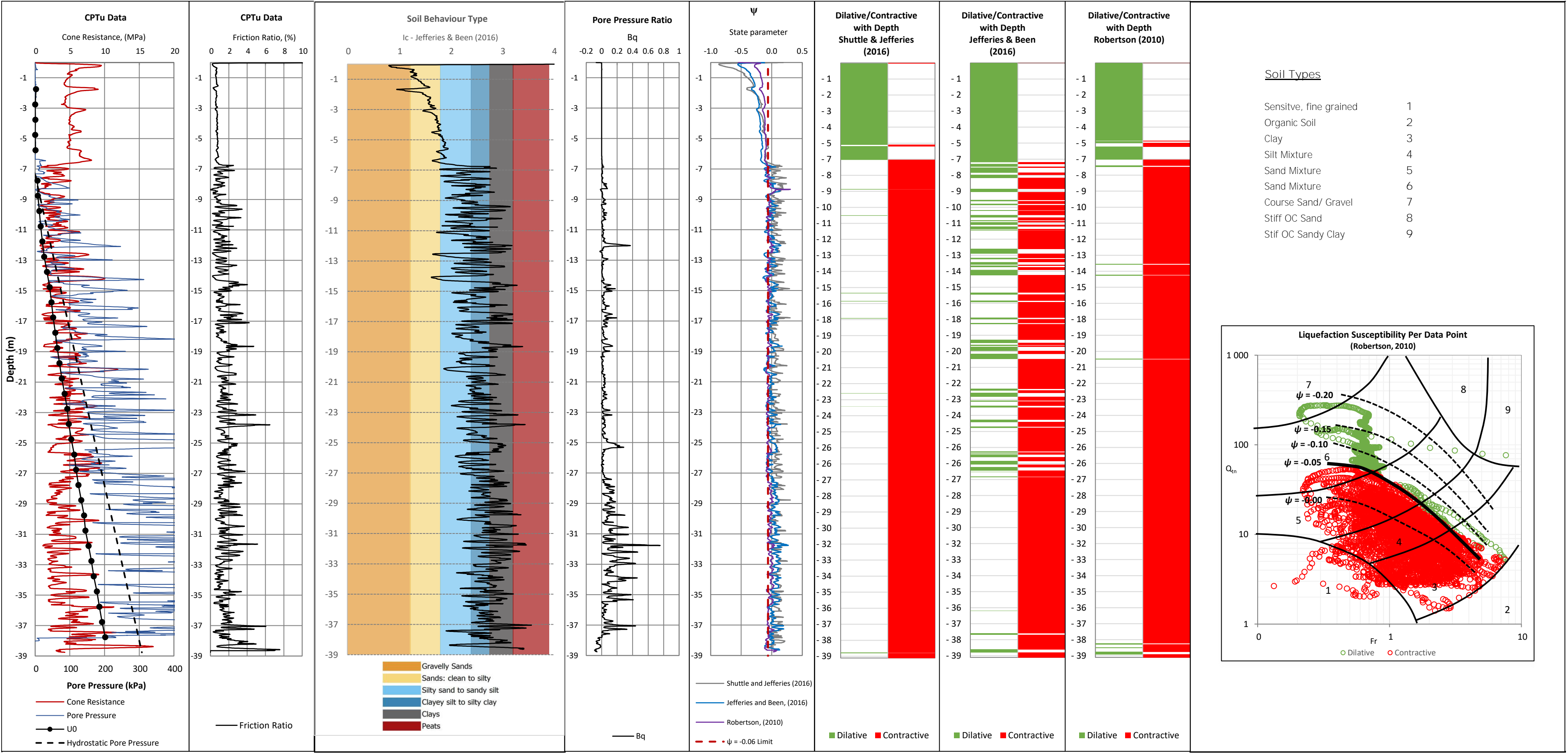
CPTu PC24



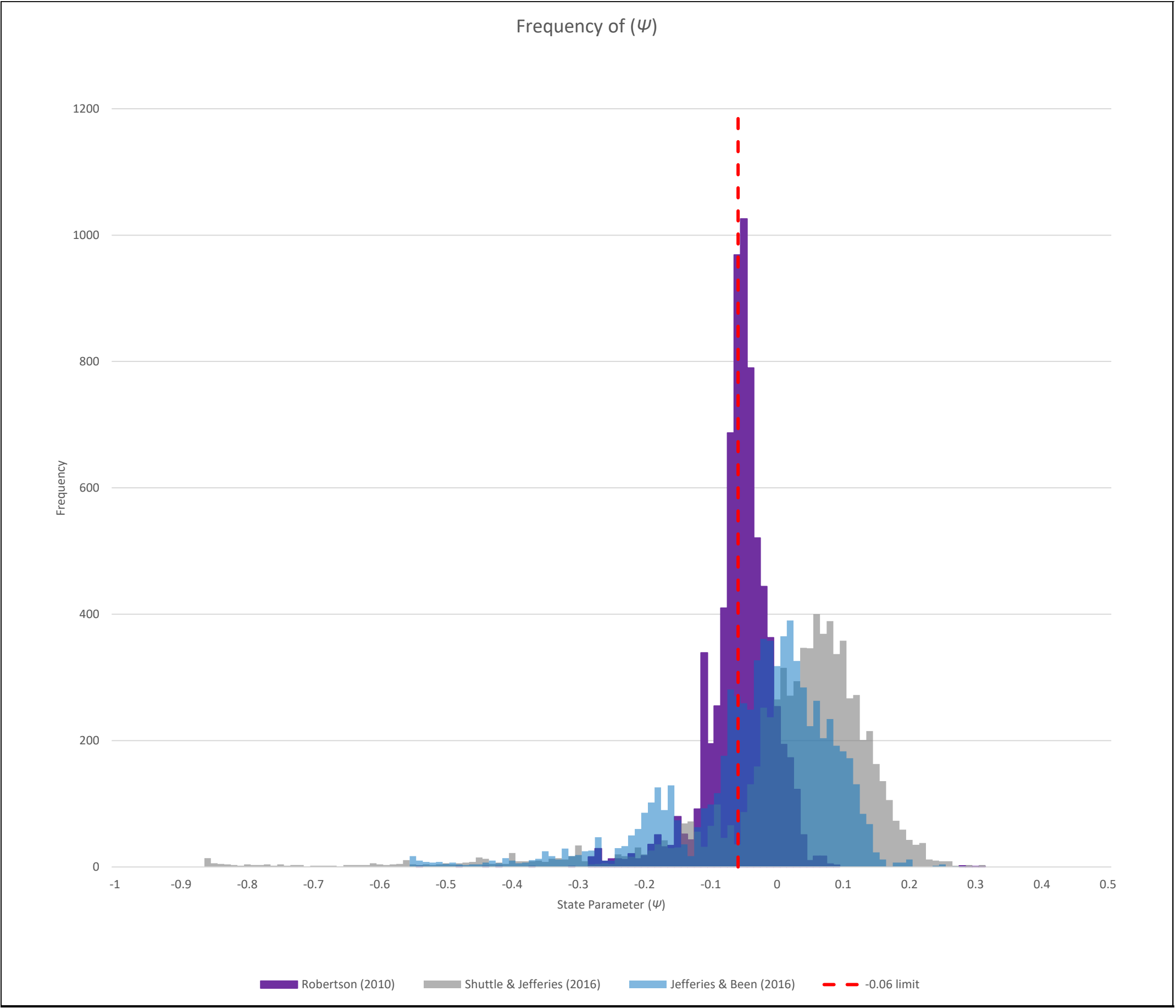
CPTu PC24



CPTu PC24AD

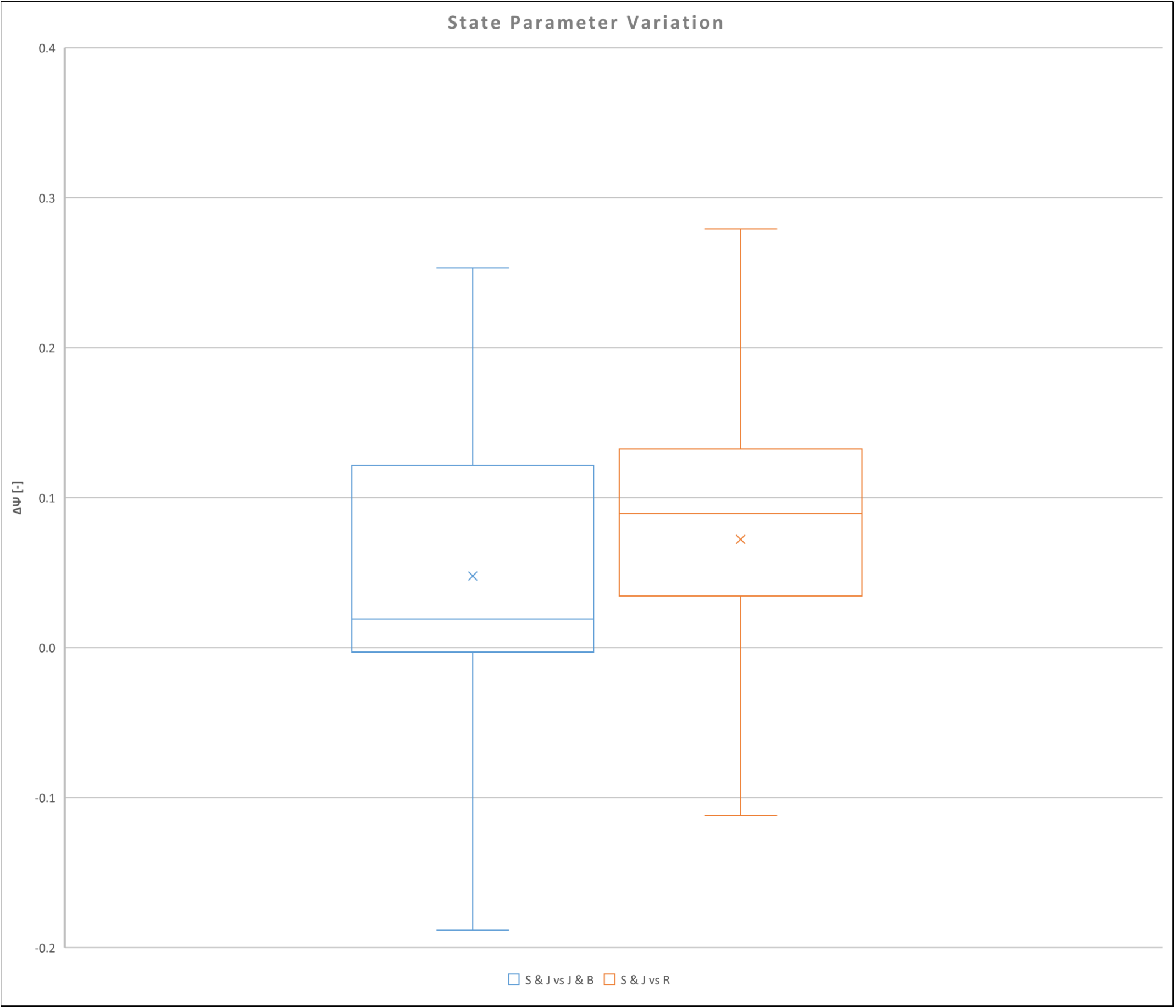


CPTu PC24AD



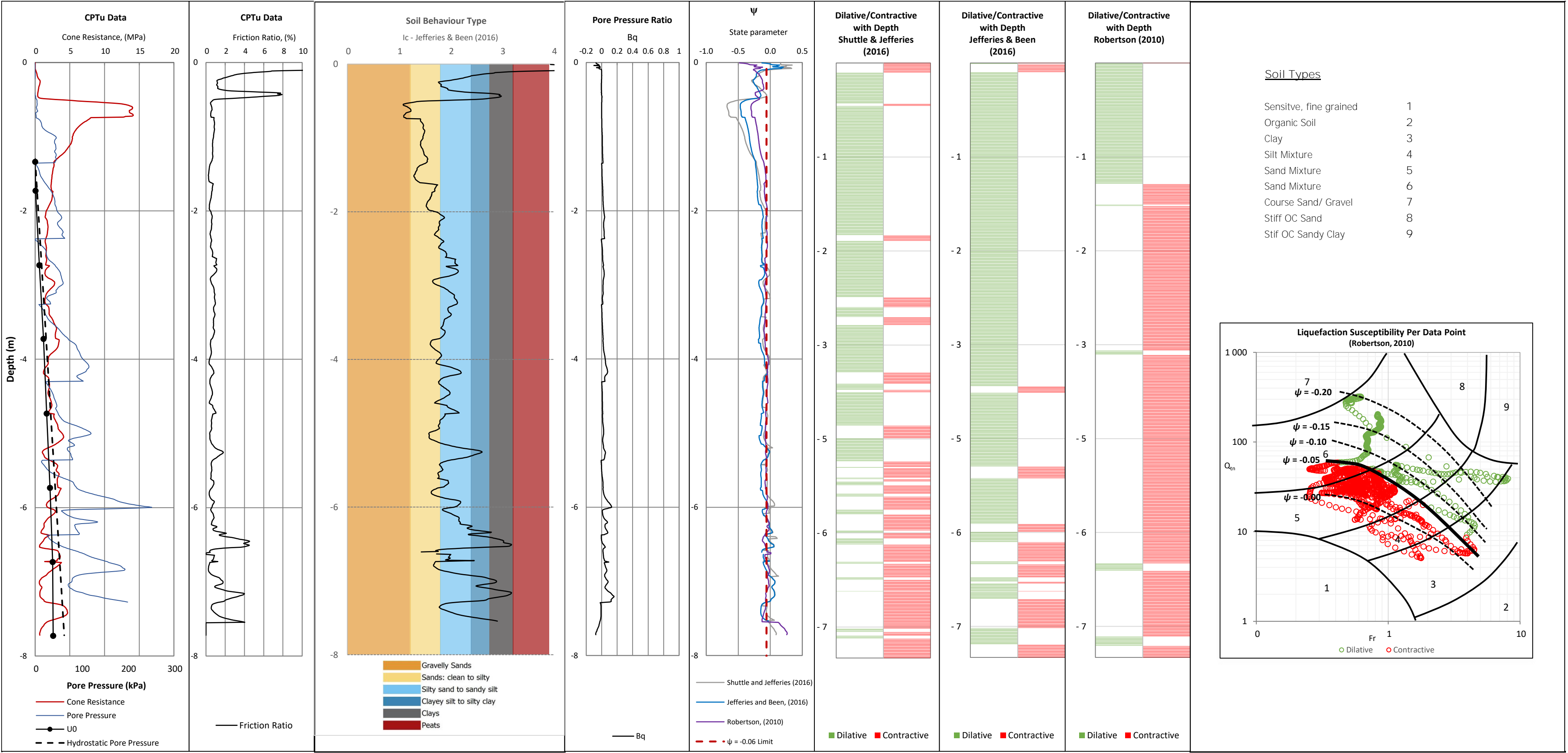


CPTu PC24AD

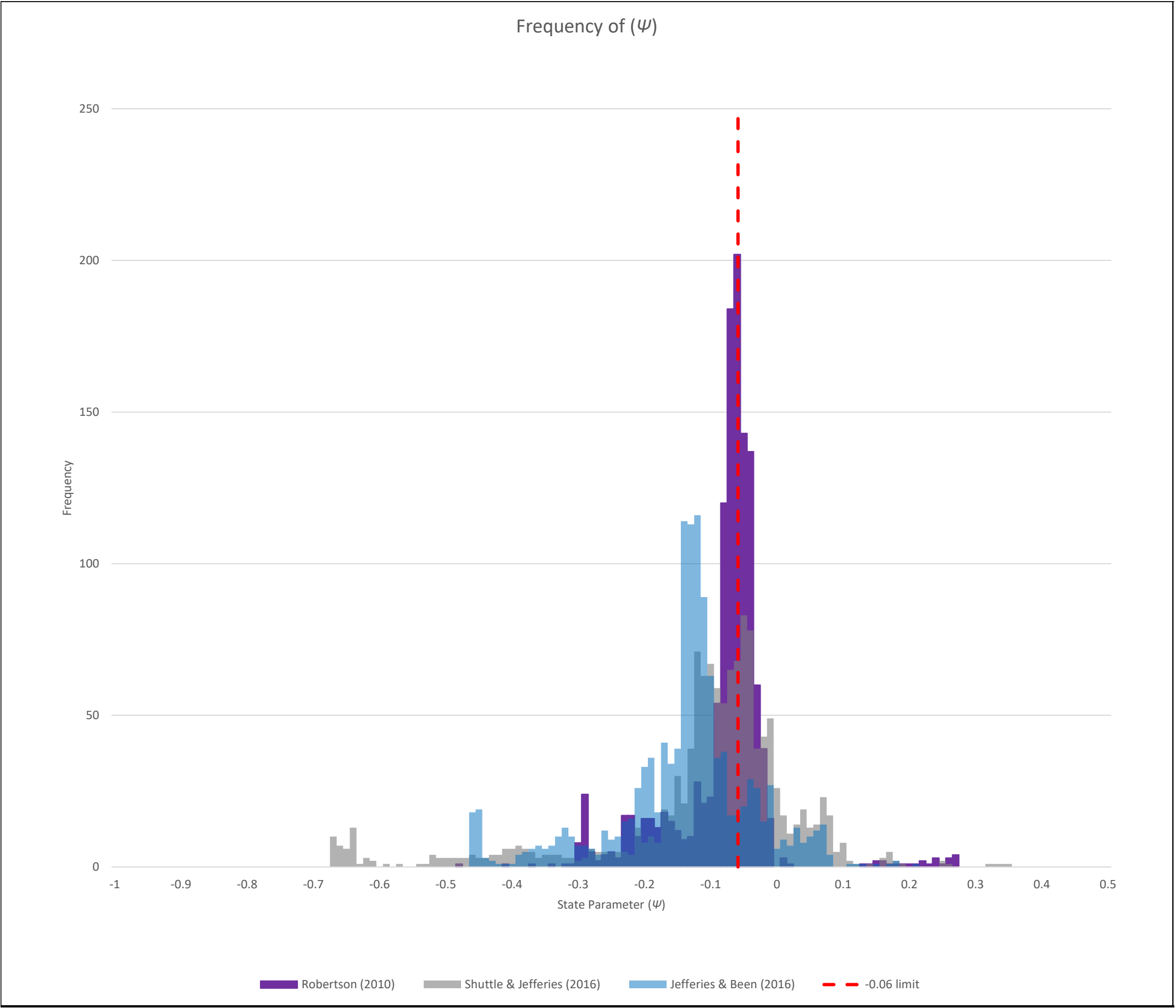


## **Appendix K: CPTu Interpretation – Monitoring Line P**

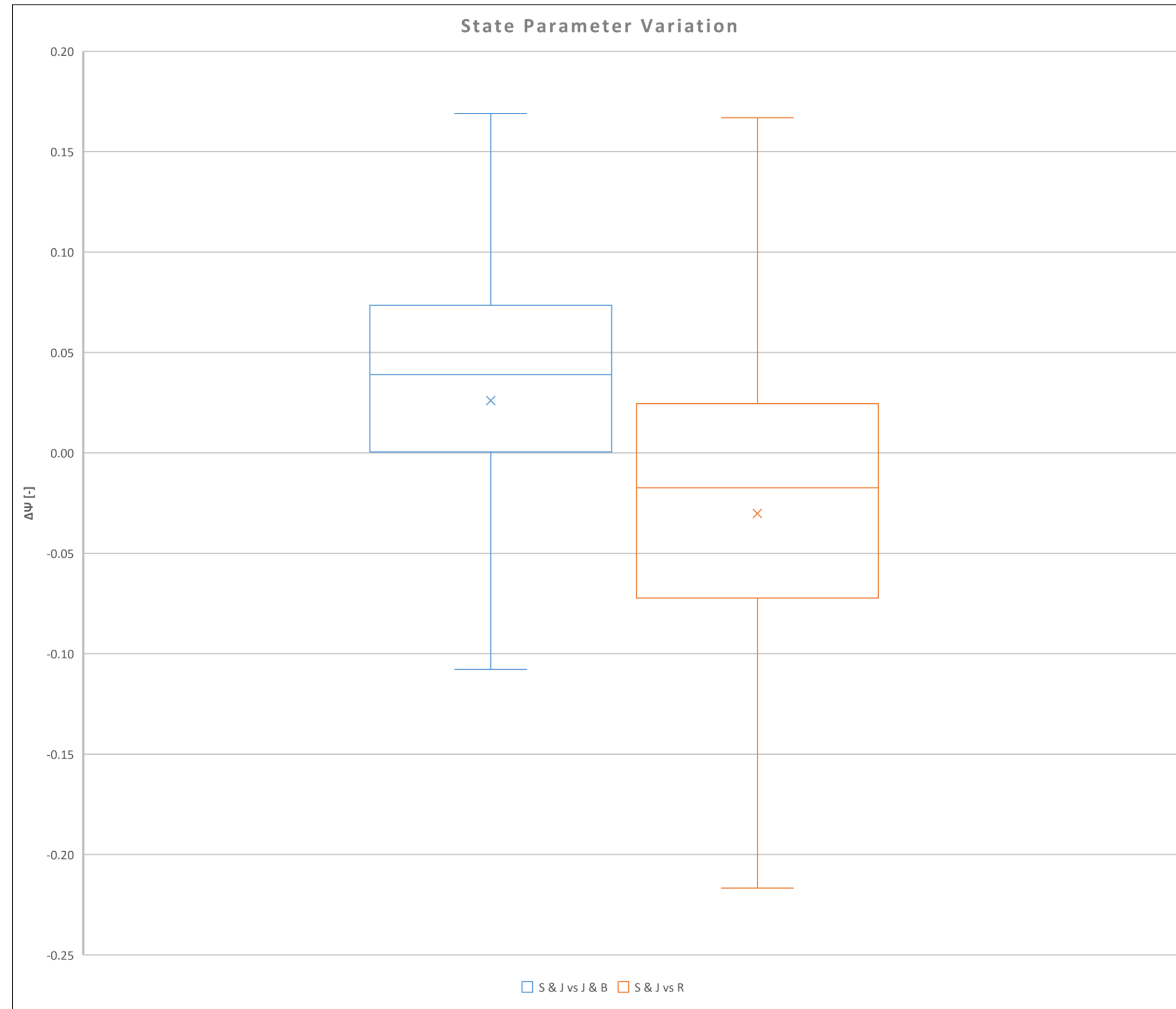
CPTu PC25

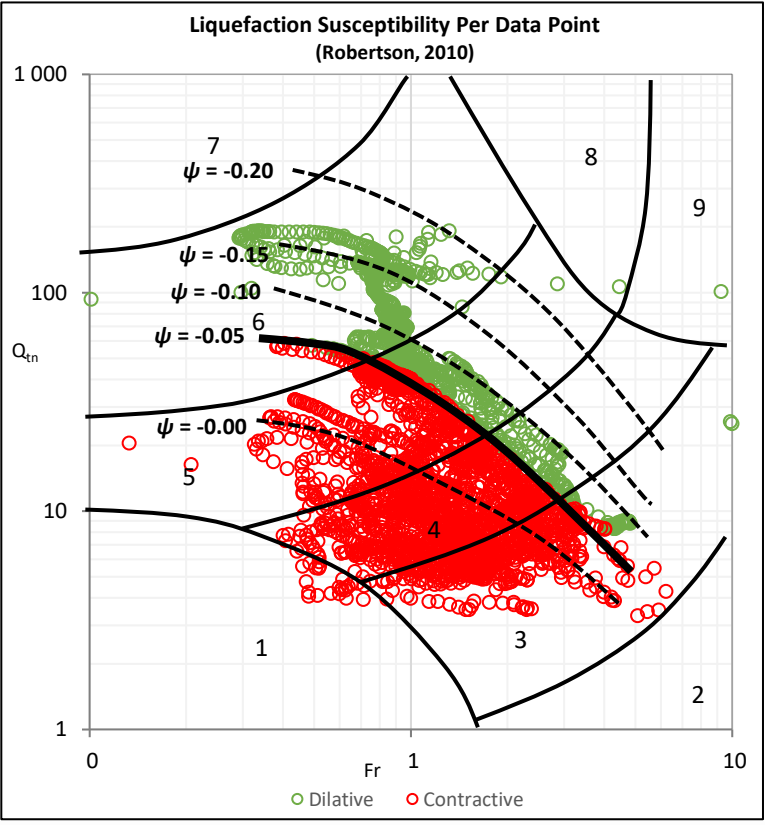


CPTu PC25

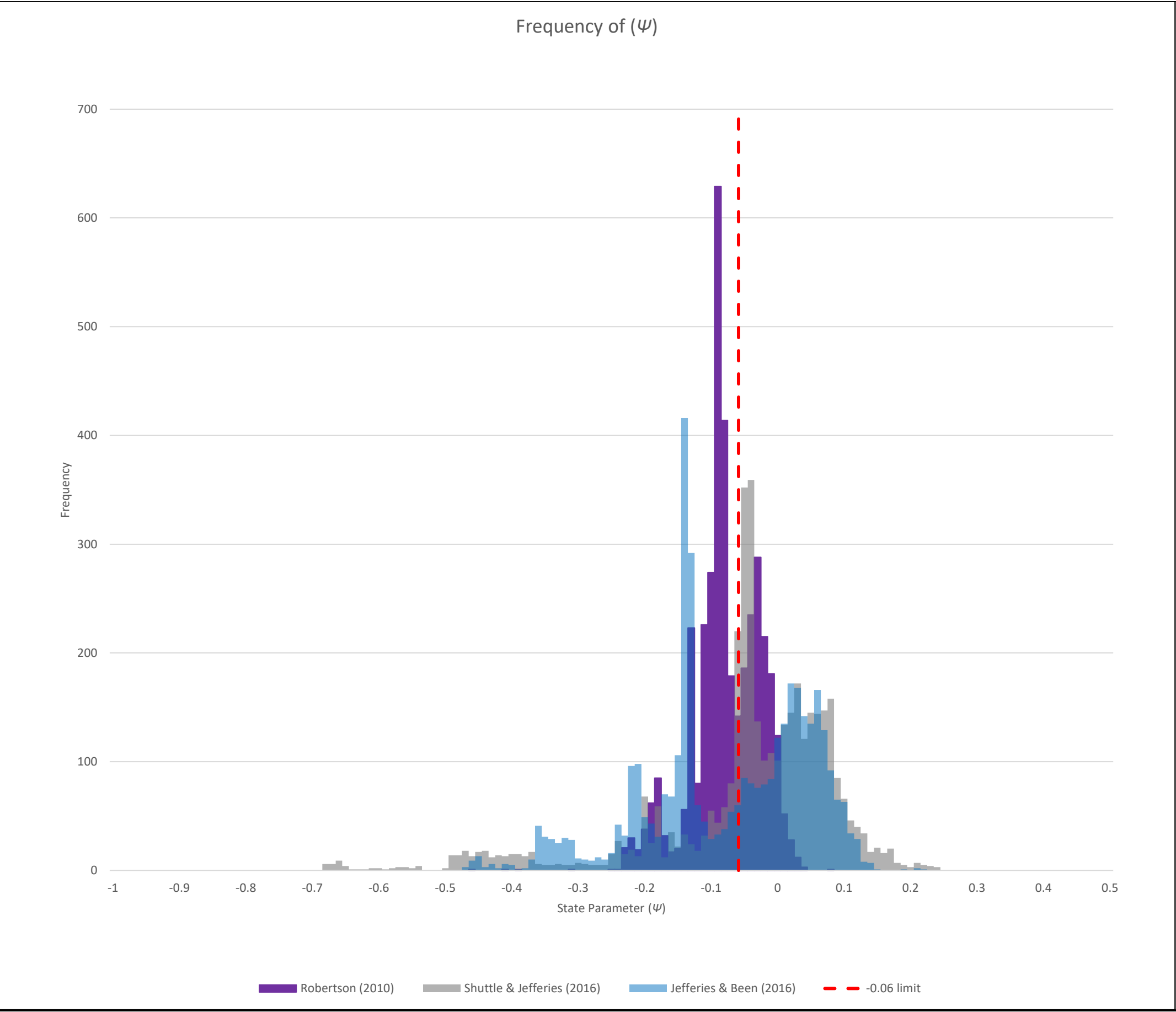


# CPTu PC25

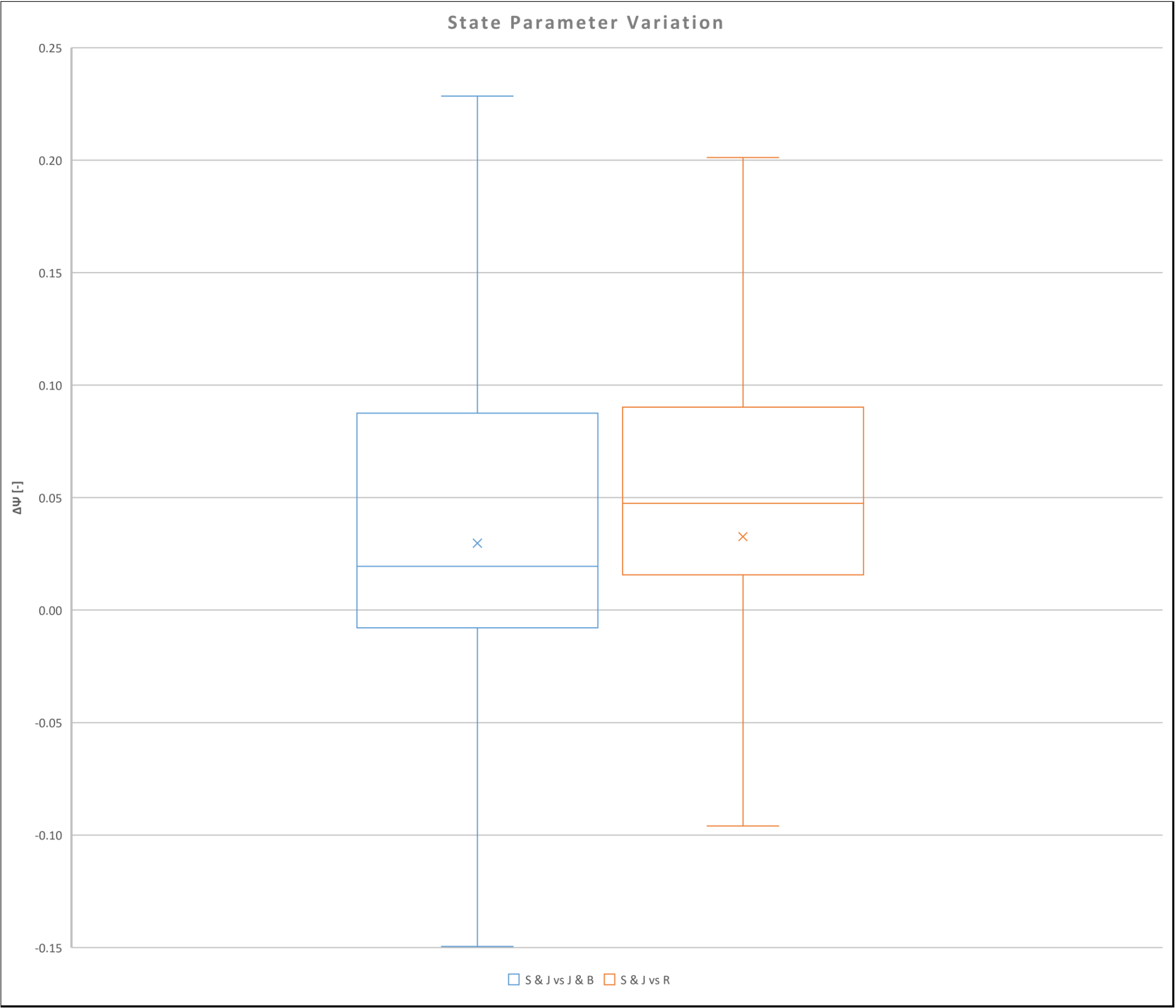




CPTu PC26

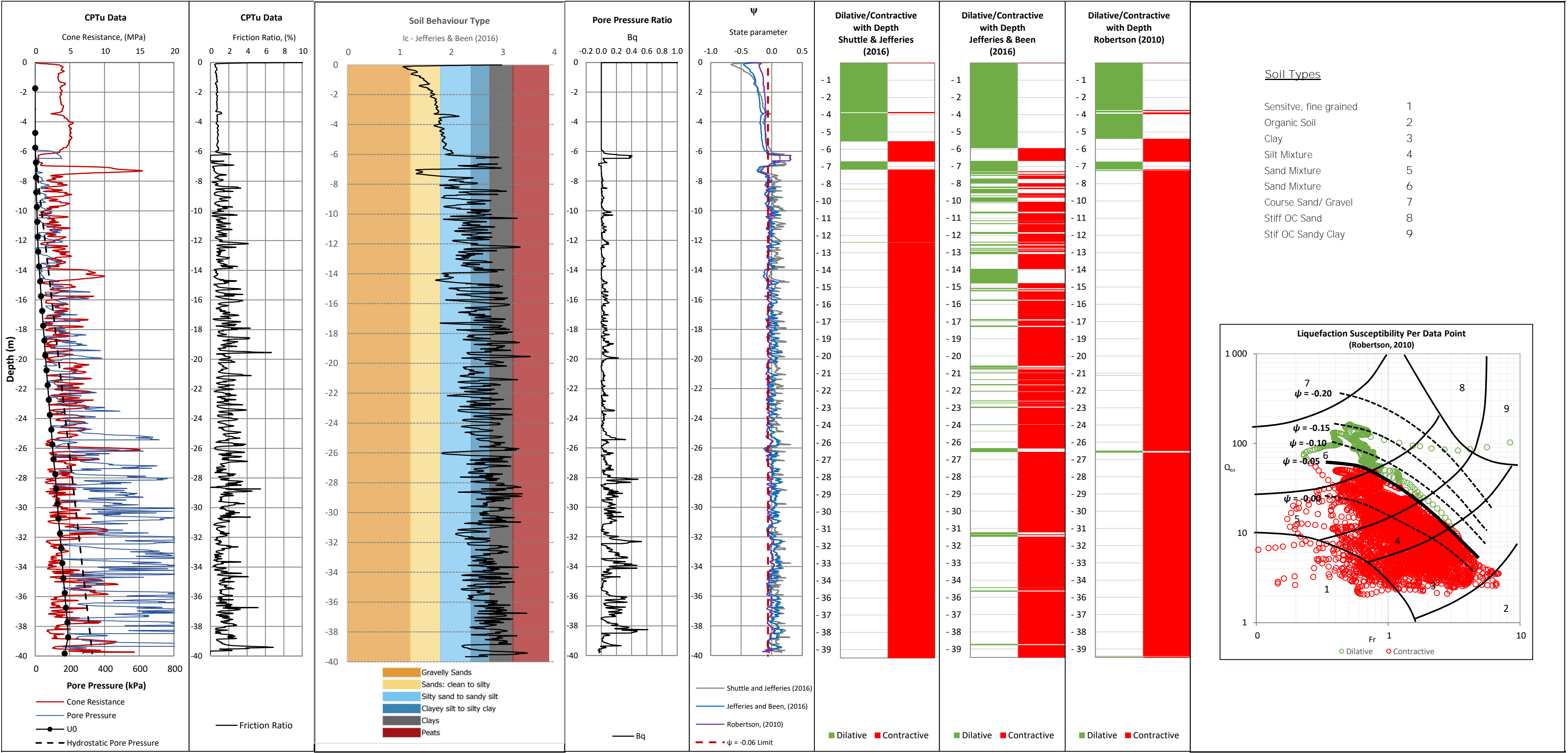


CPTu PC26

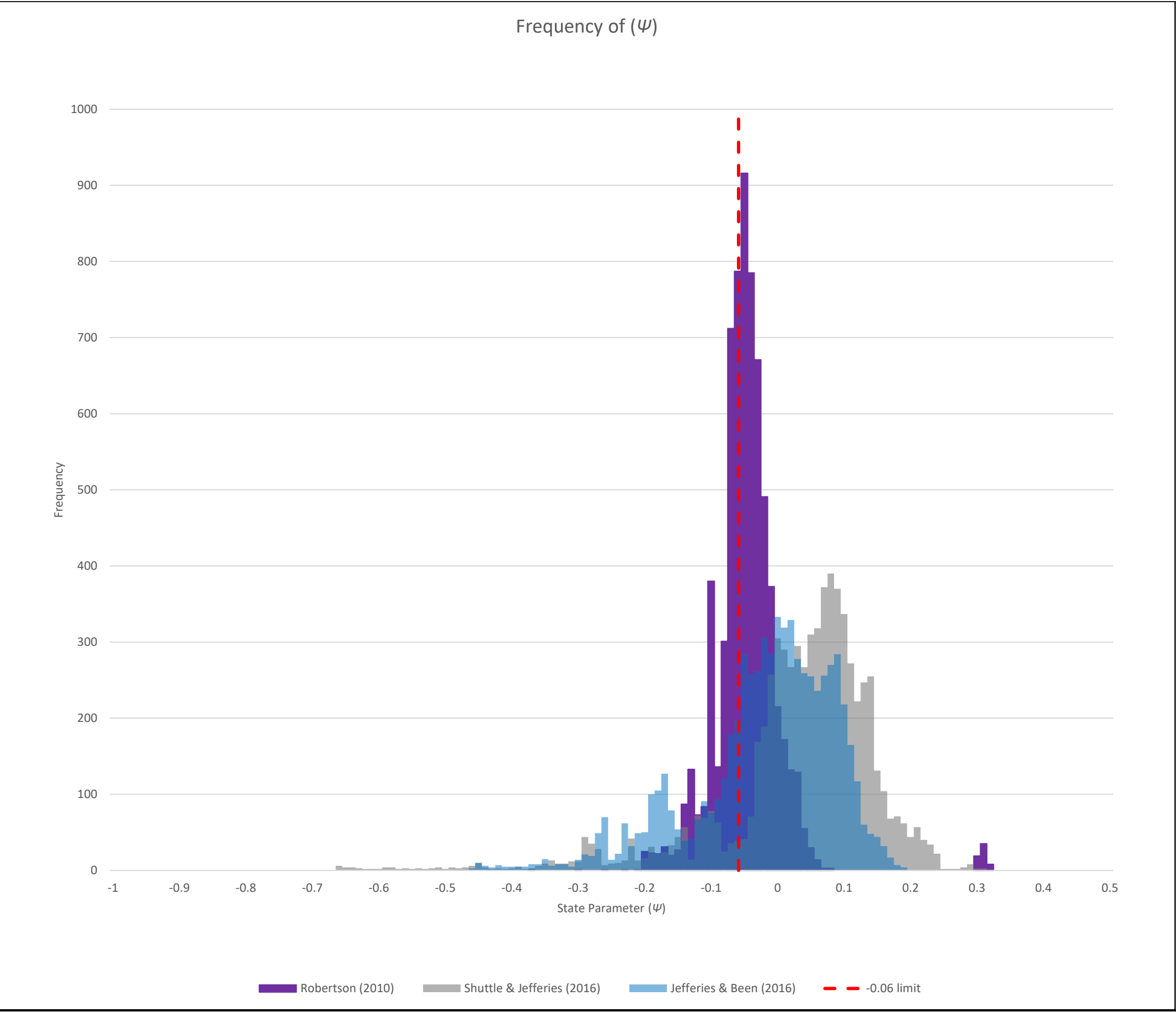




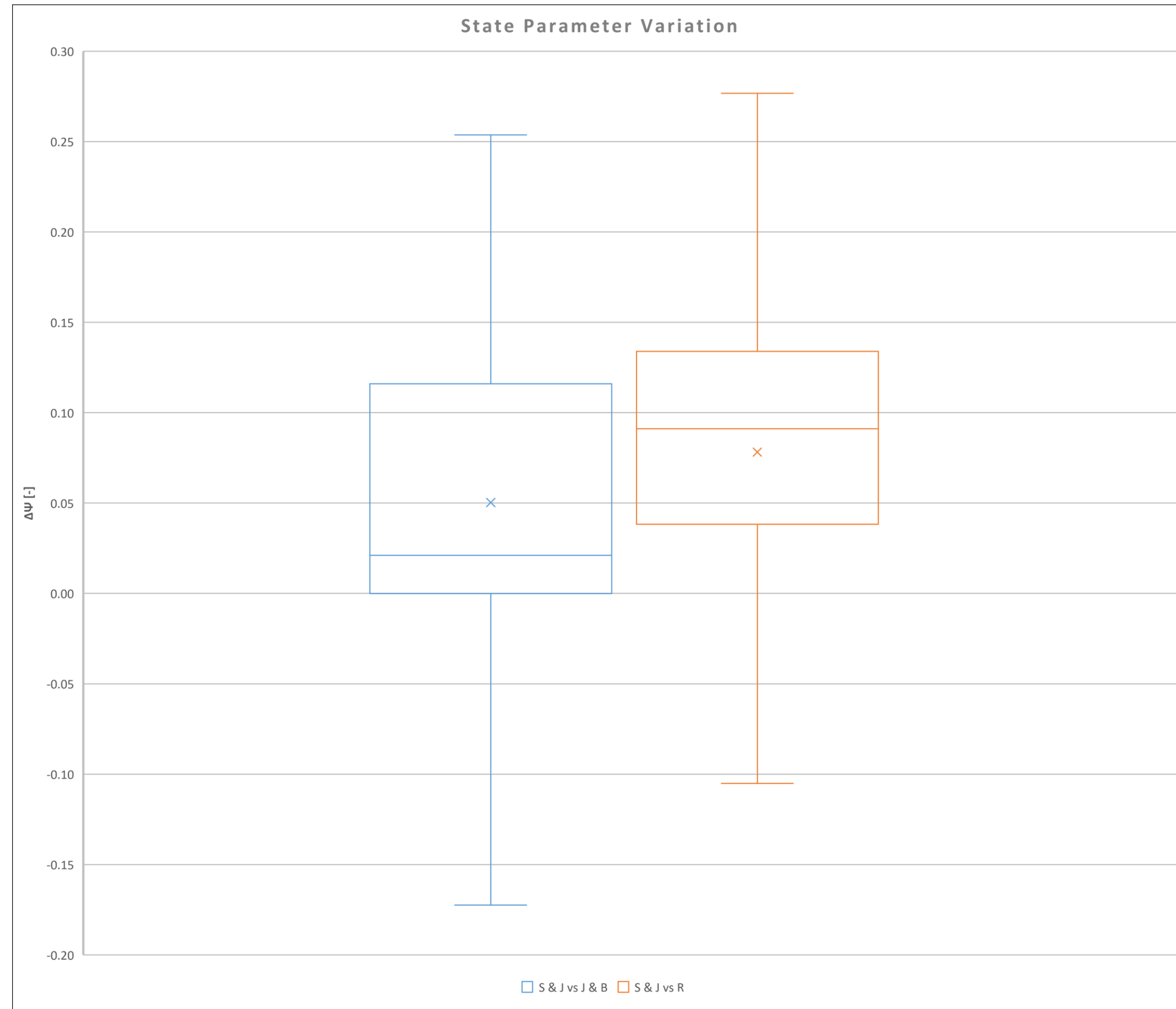
CPTu PC27



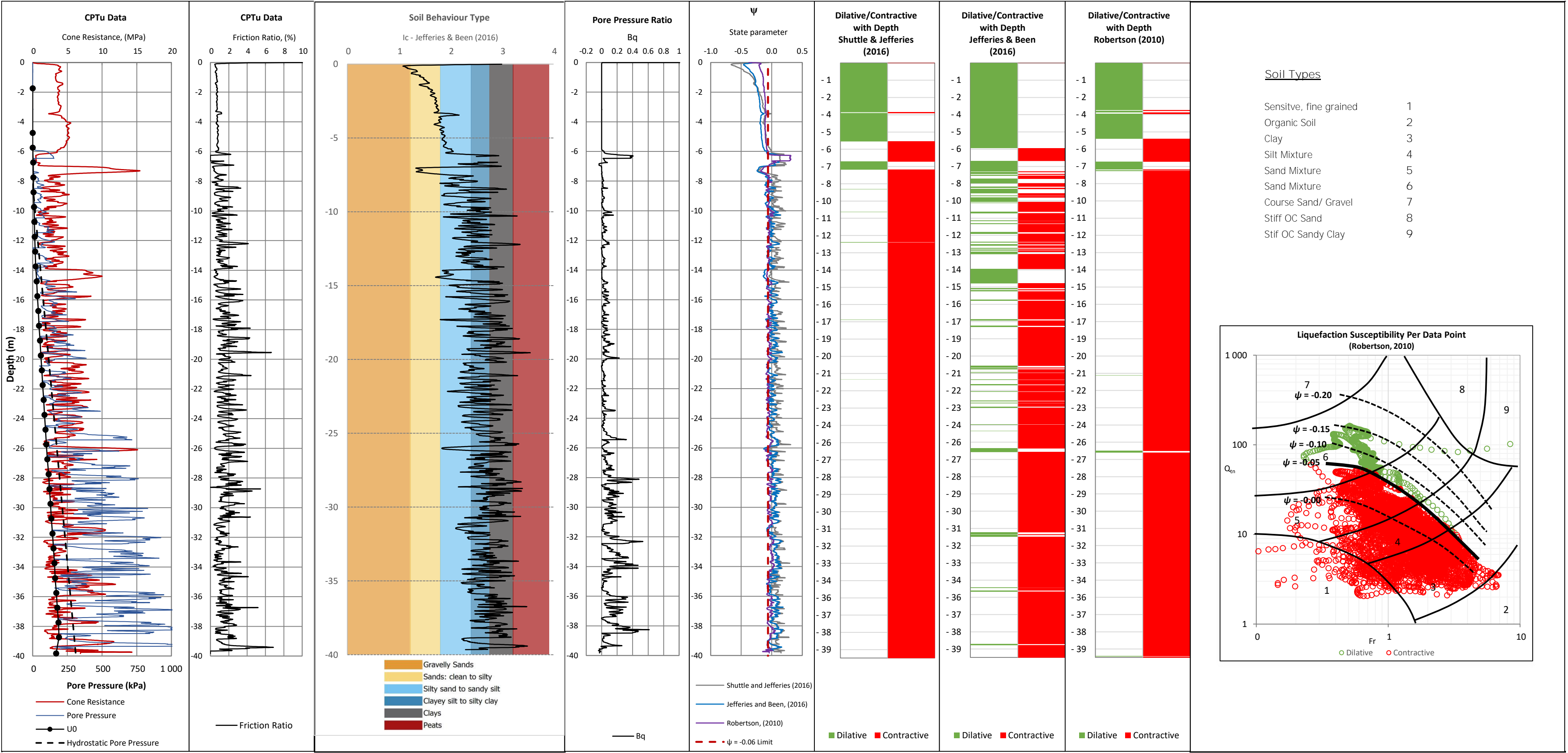
CPTu PC27



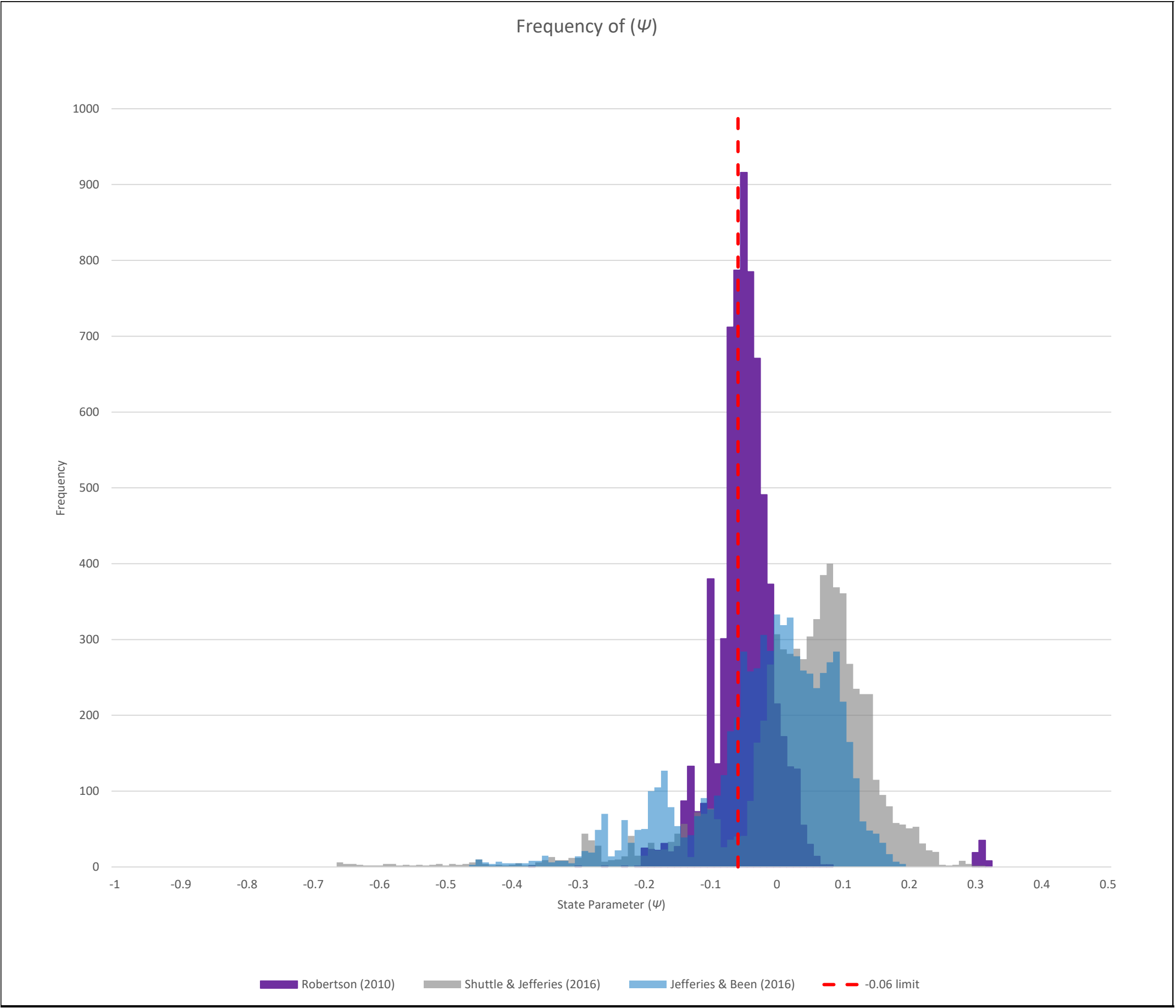
# CPTu PC27



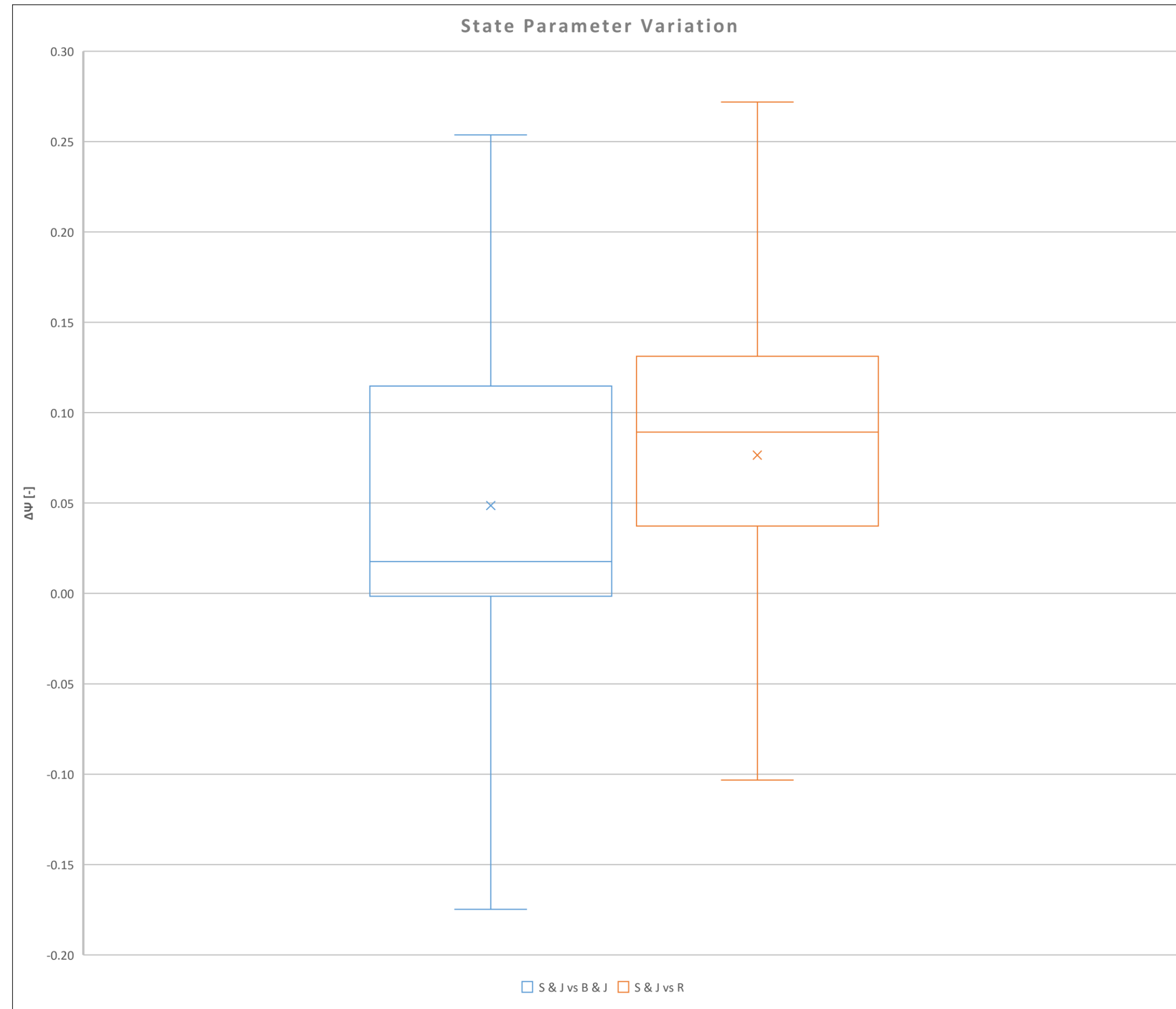
CPTu PC28



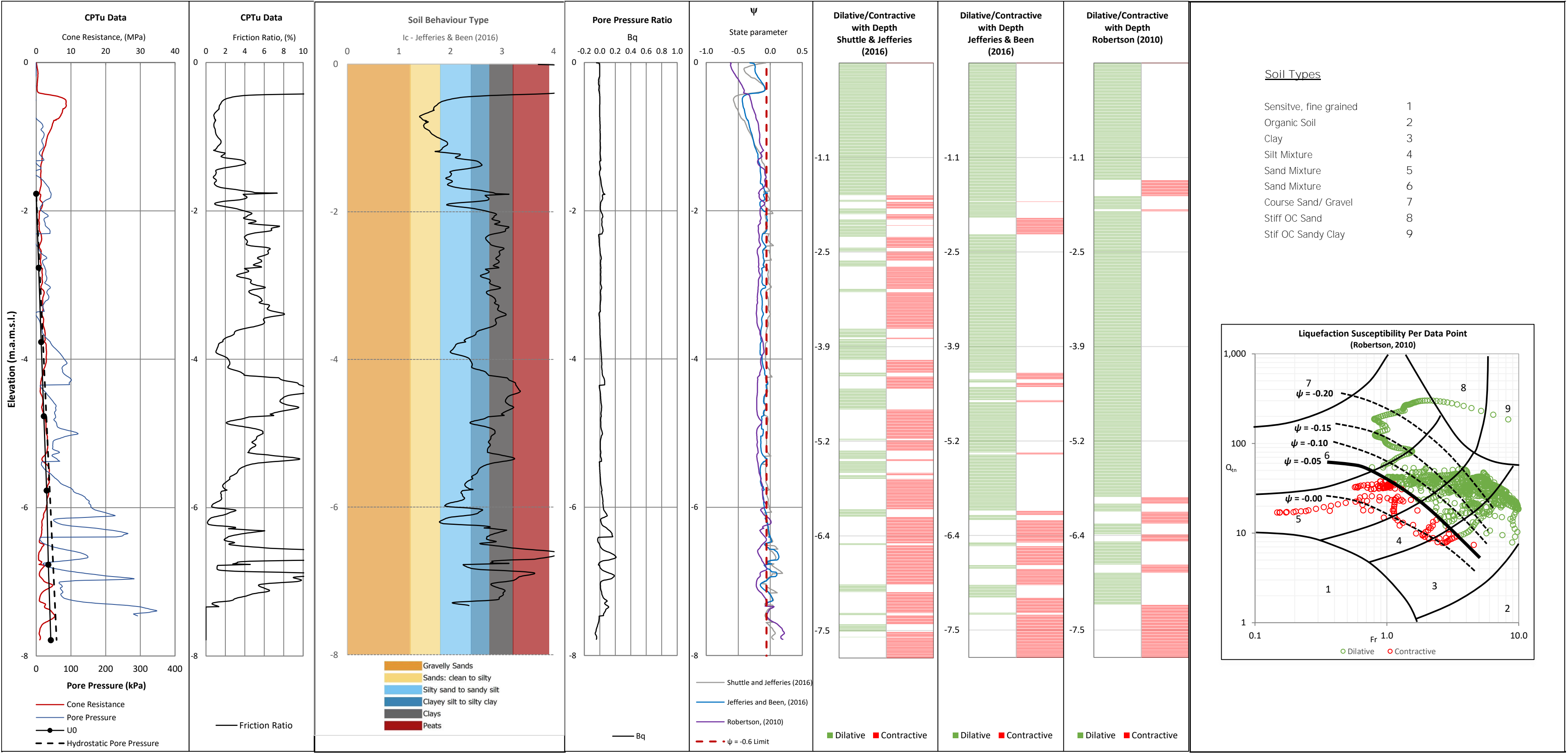
CPTu PC28



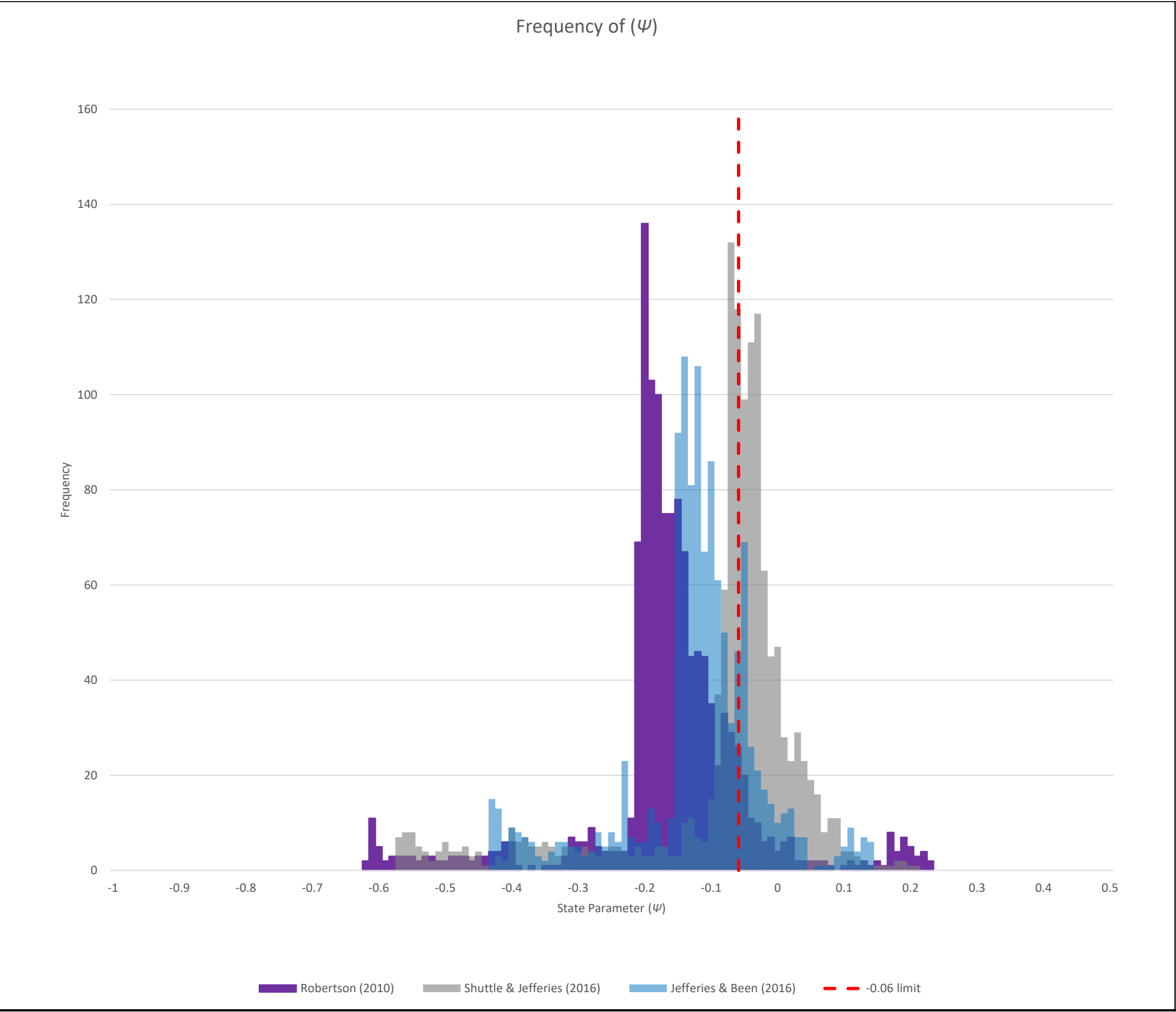
# CPTu PC28



PC25-Q3\_CPTu

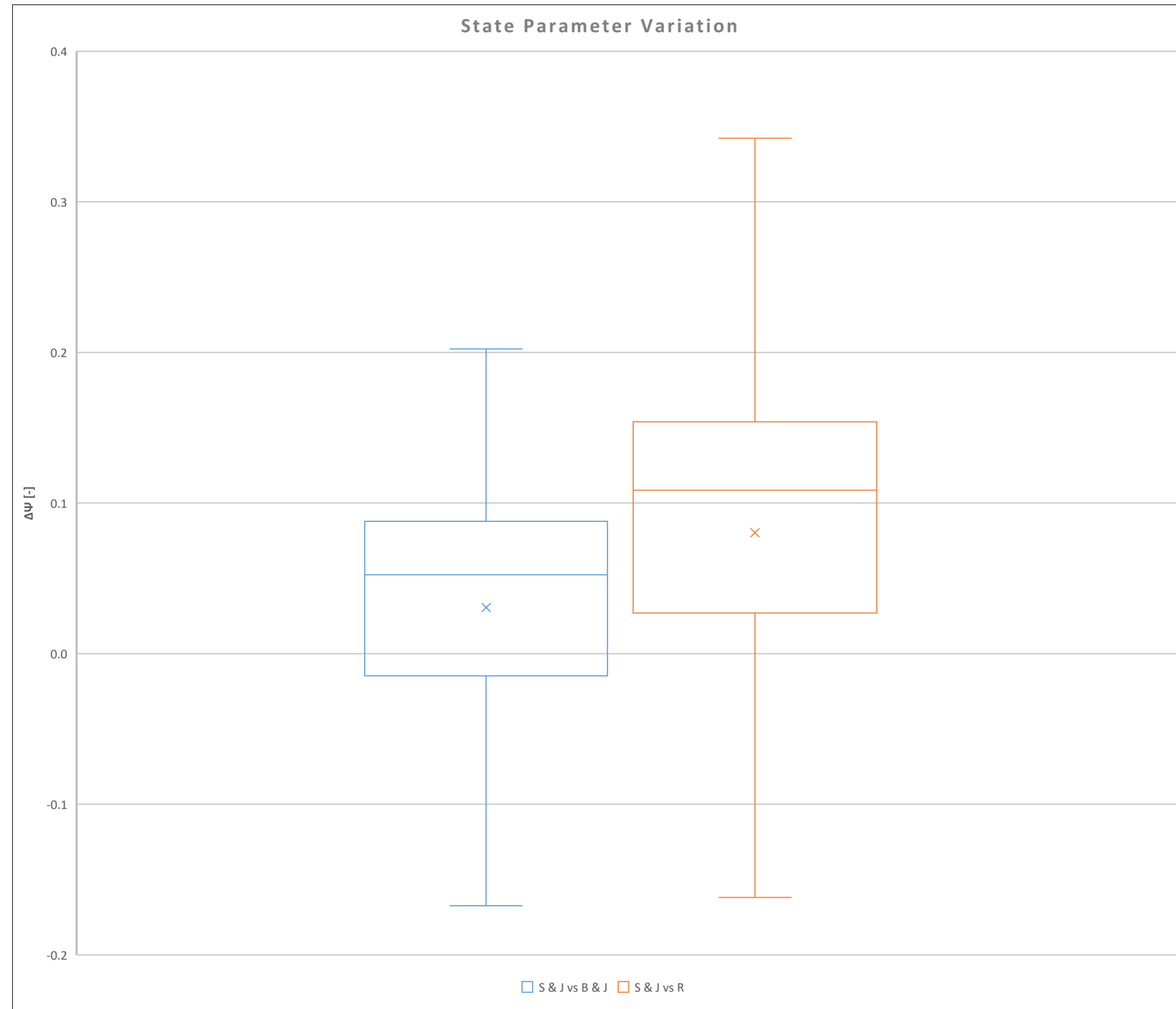


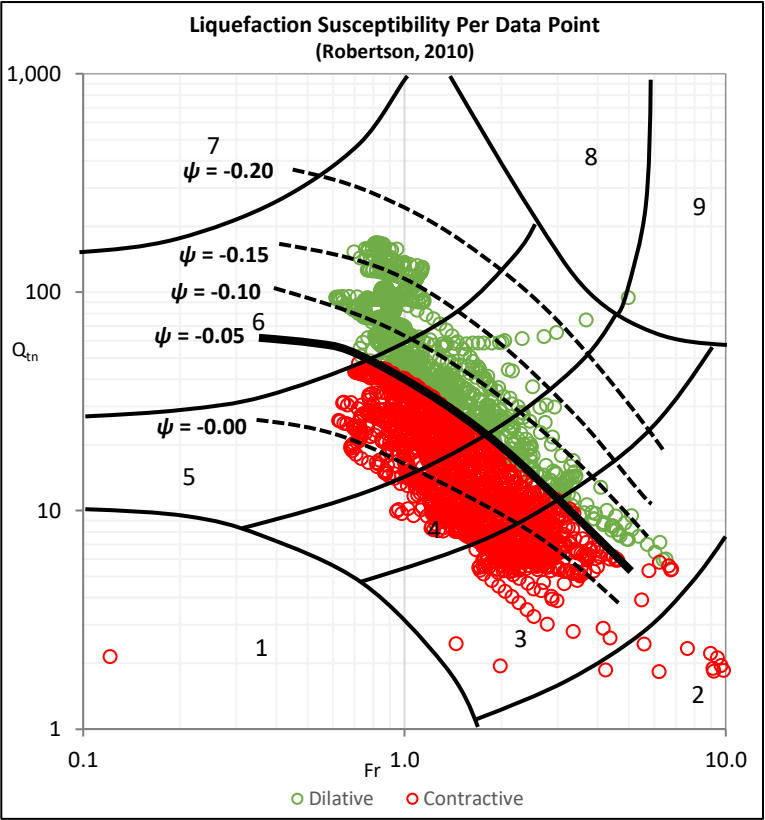
PC25-Q3\_CPTu



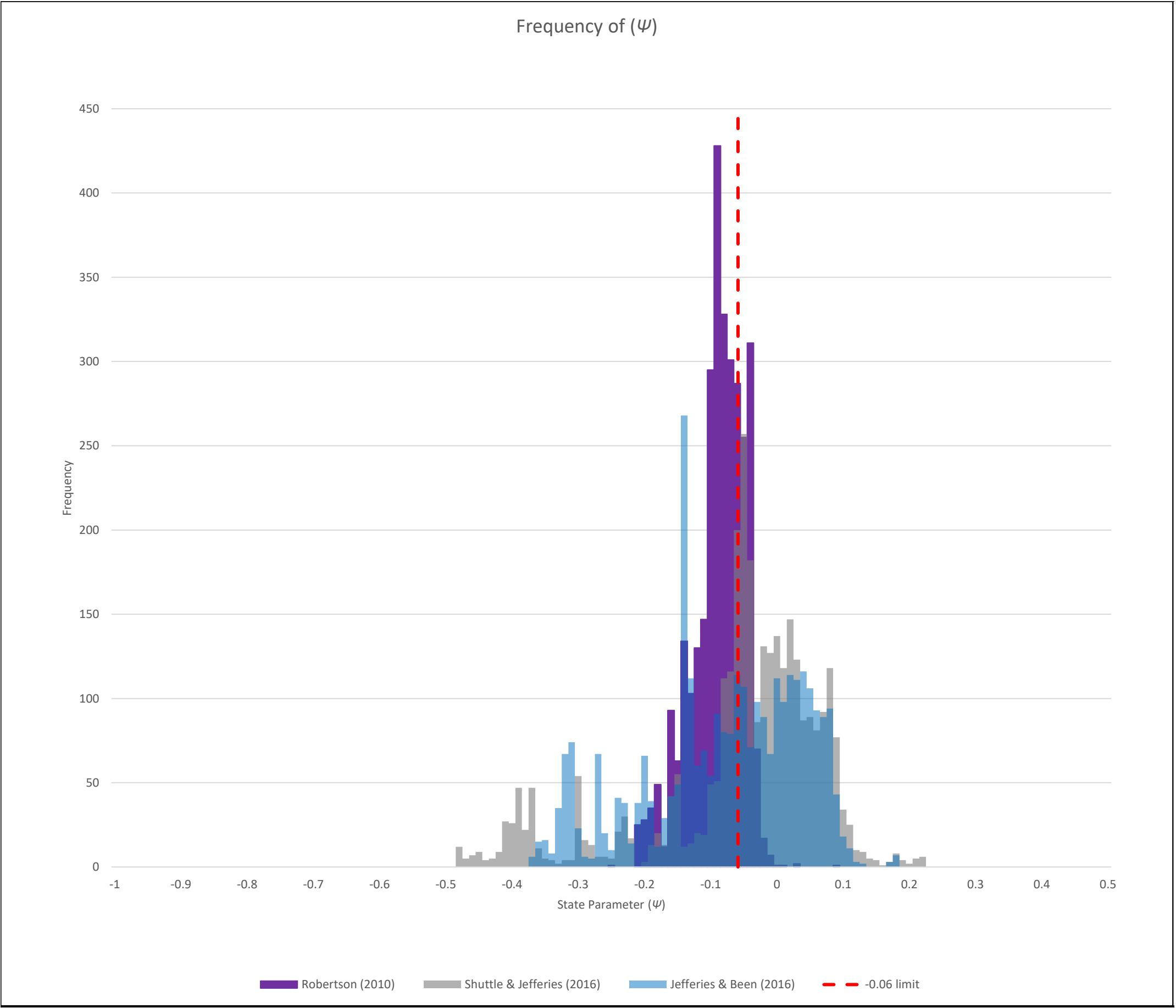


## PC25-Q3\_CPTu

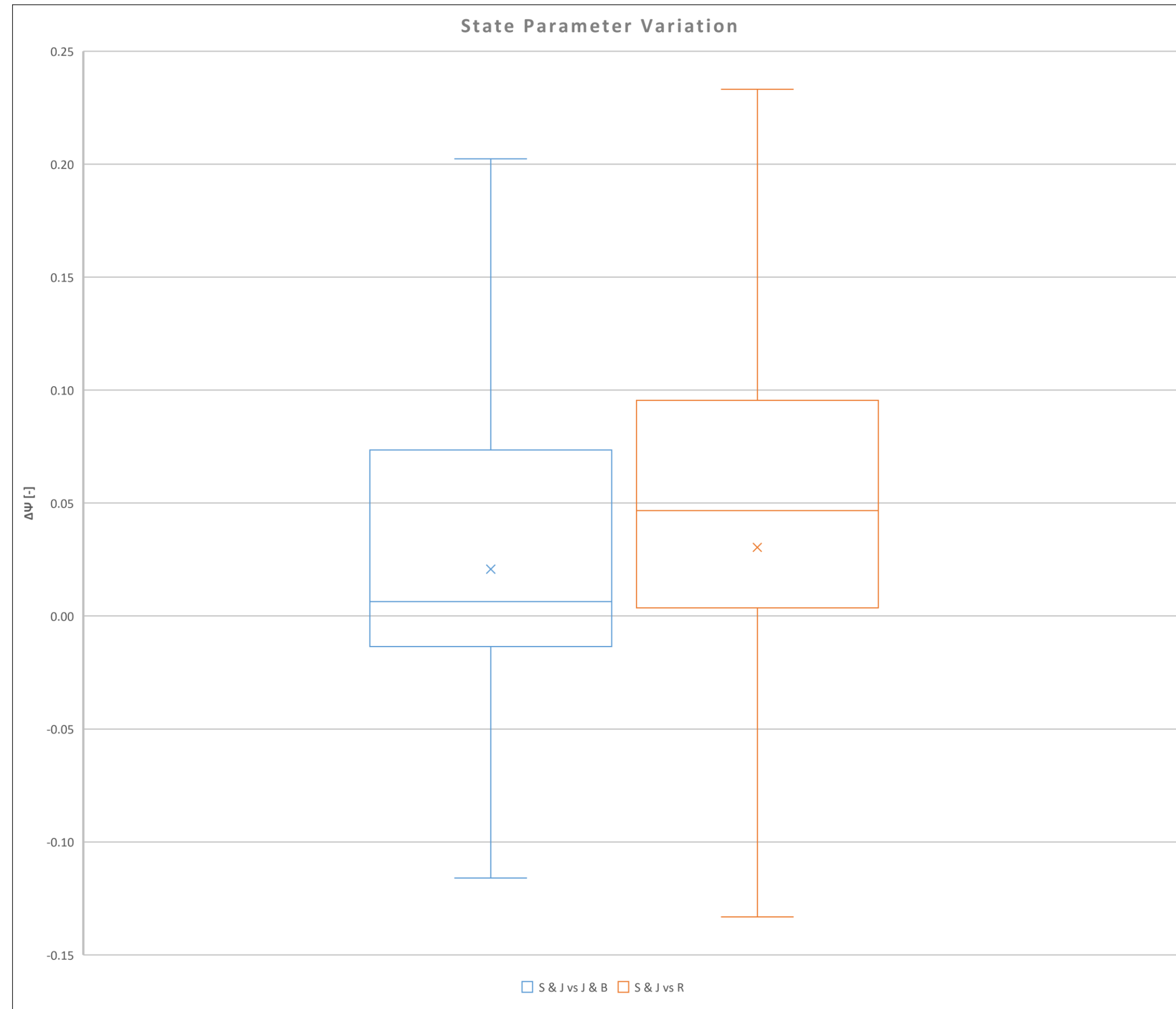




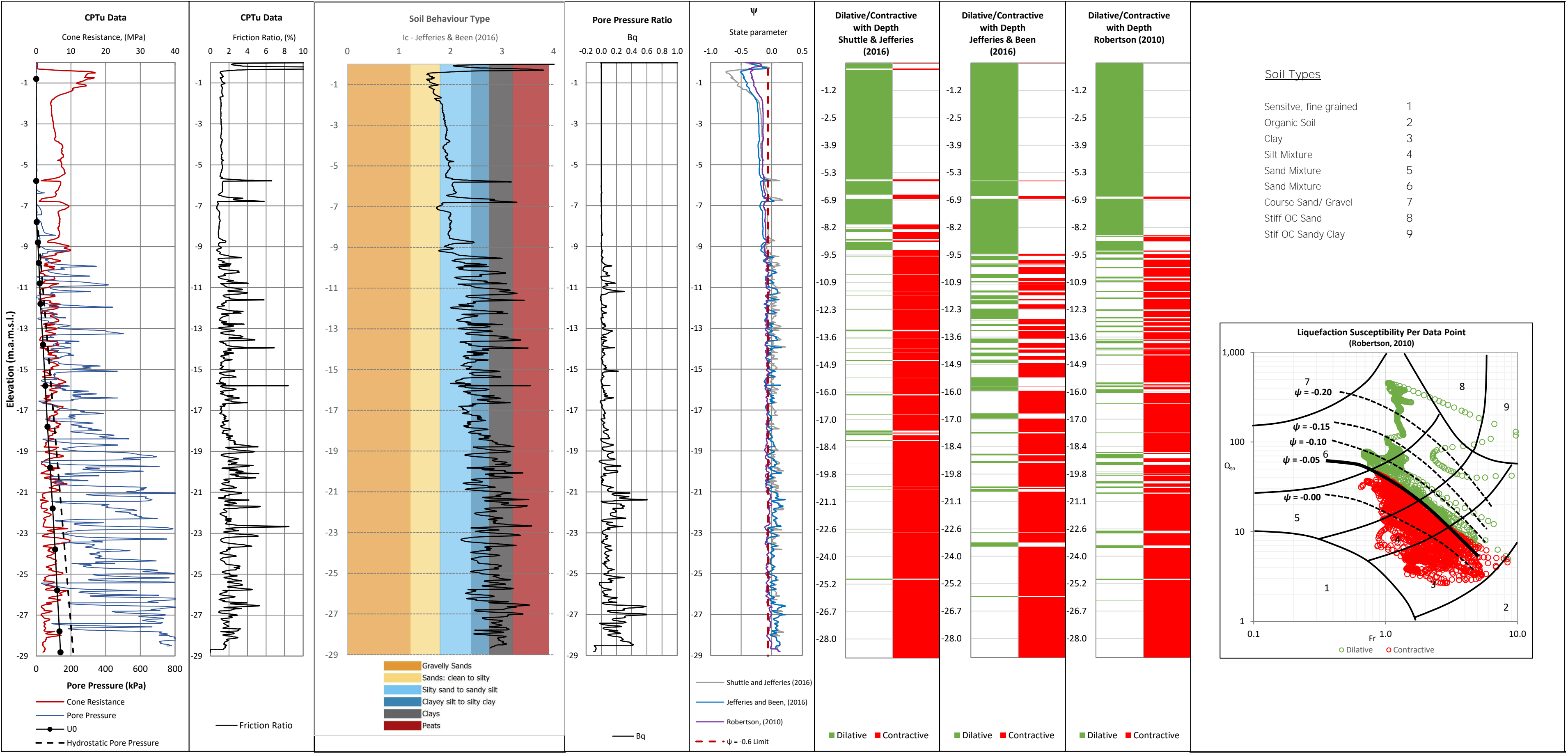
PC26-Q3\_CPTu



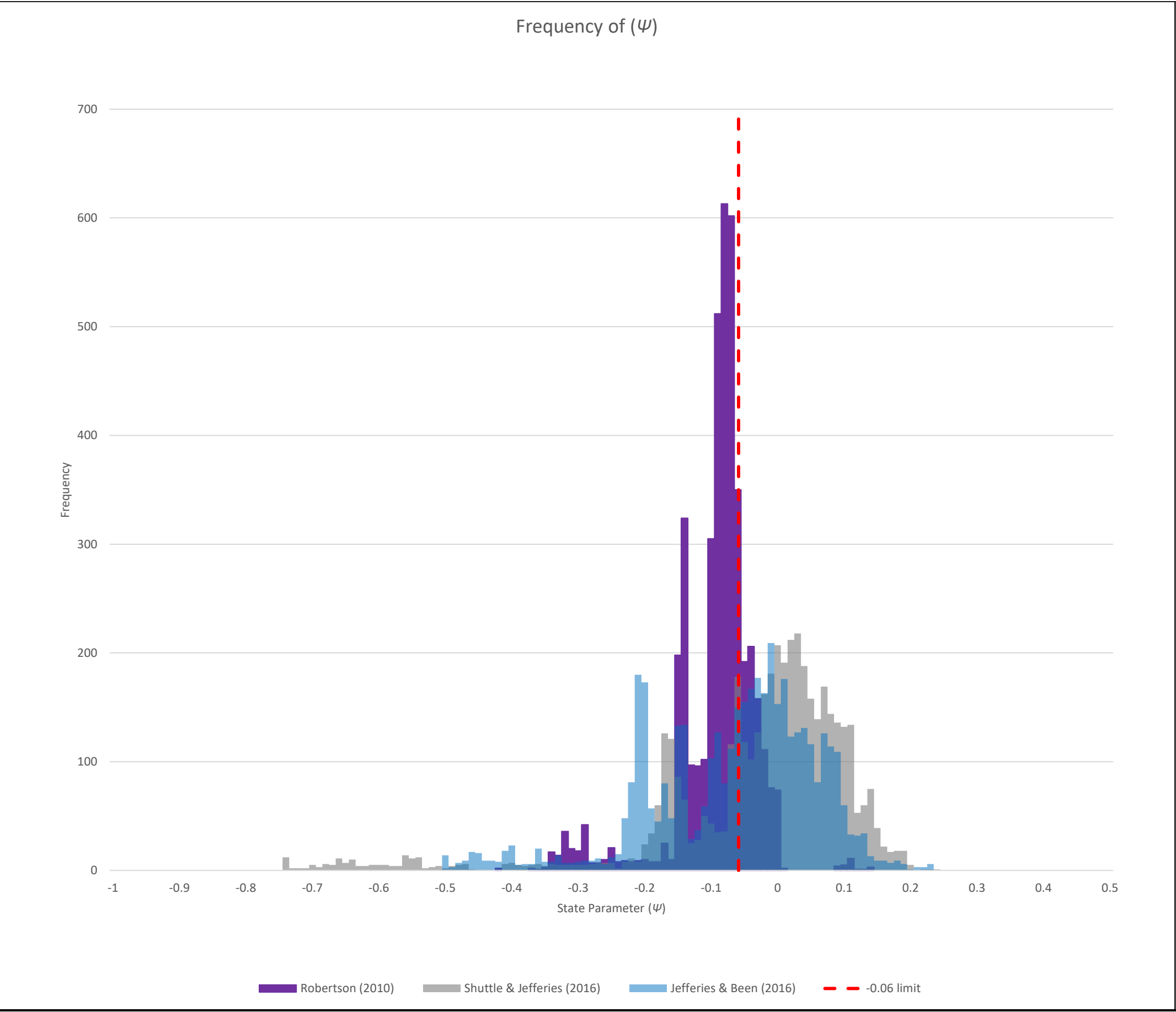
## PC26-Q3\_CPTu



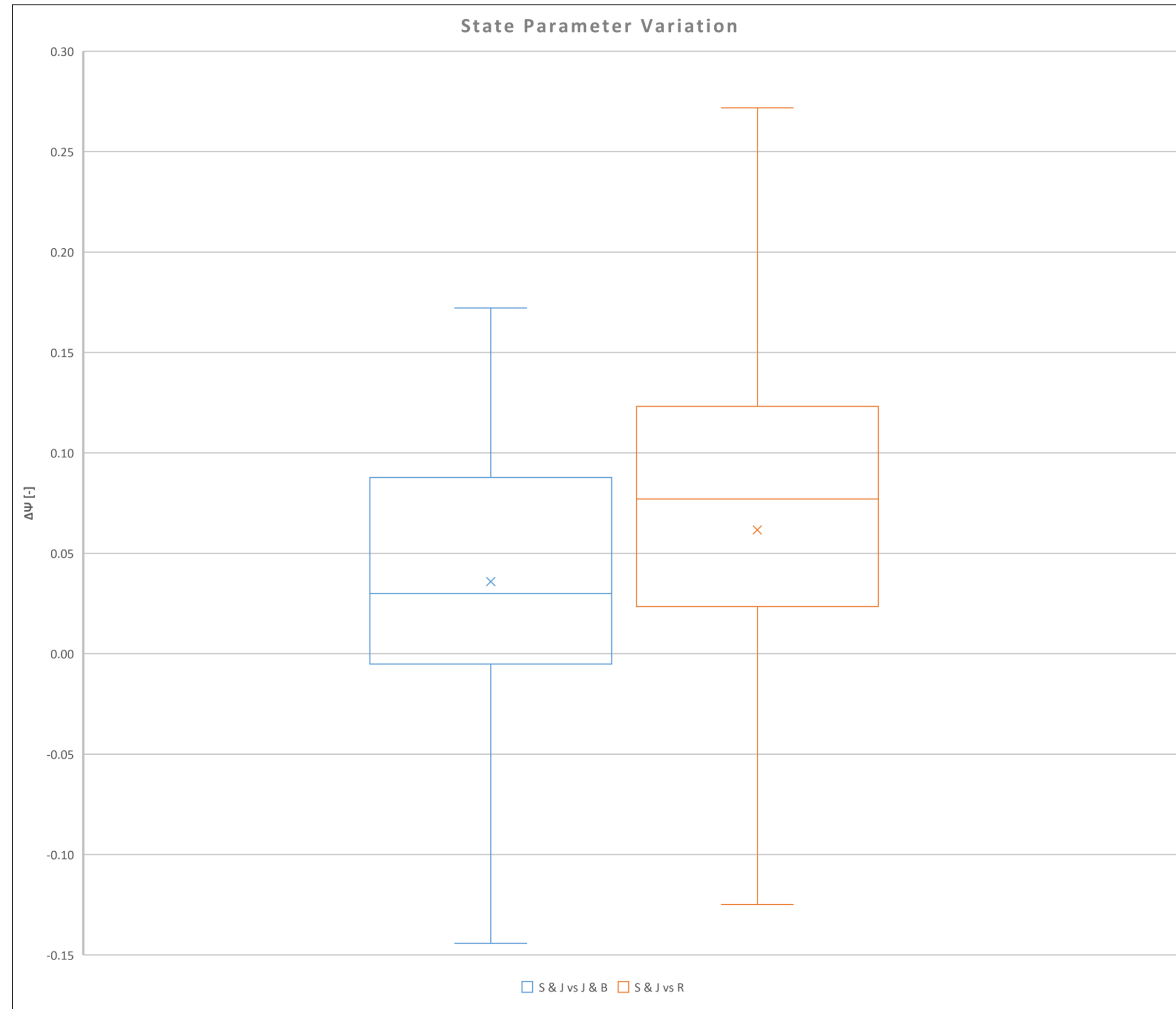
PC27-Q3\_CPTu



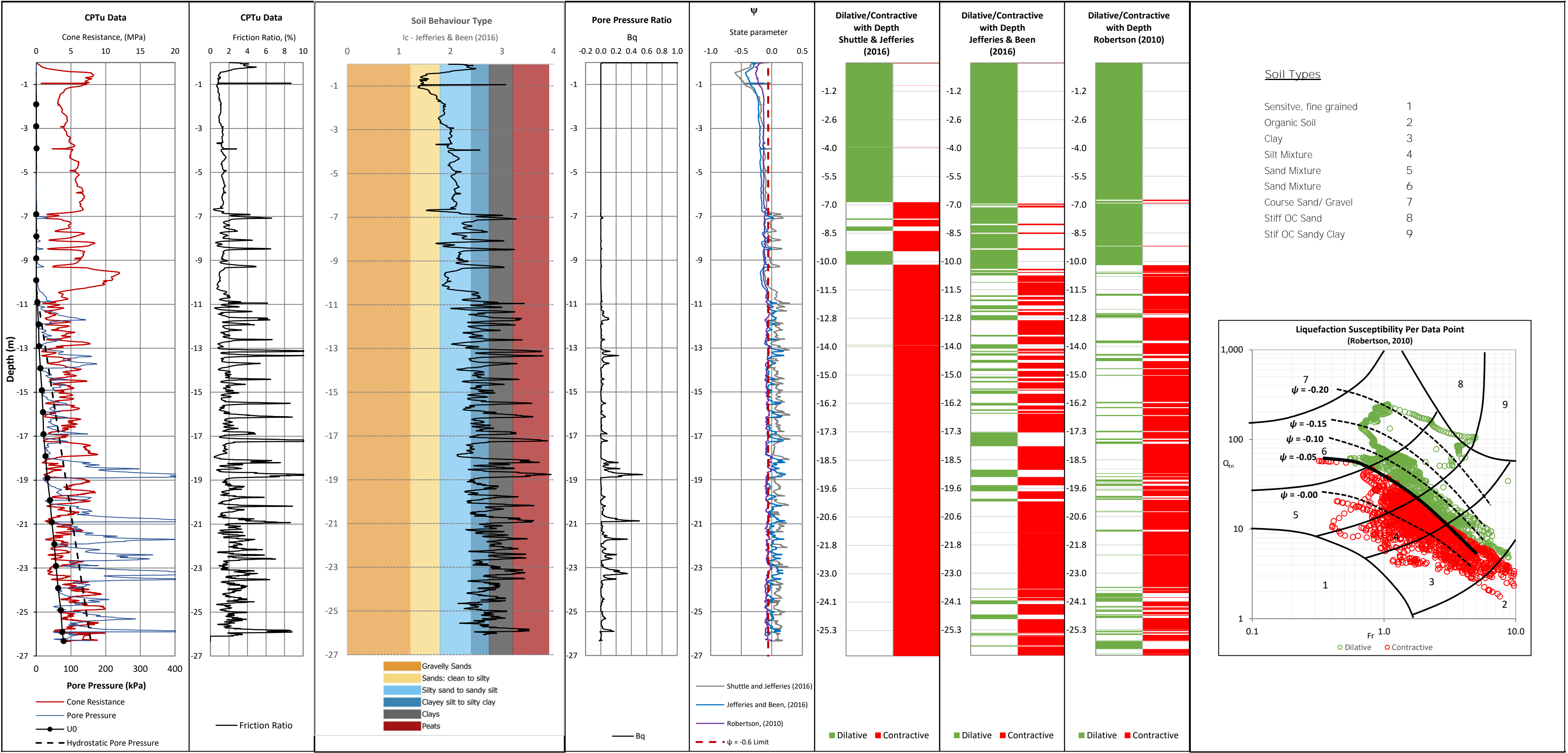
PC27-Q3\_CPTu



## PC27-Q3\_CPTu

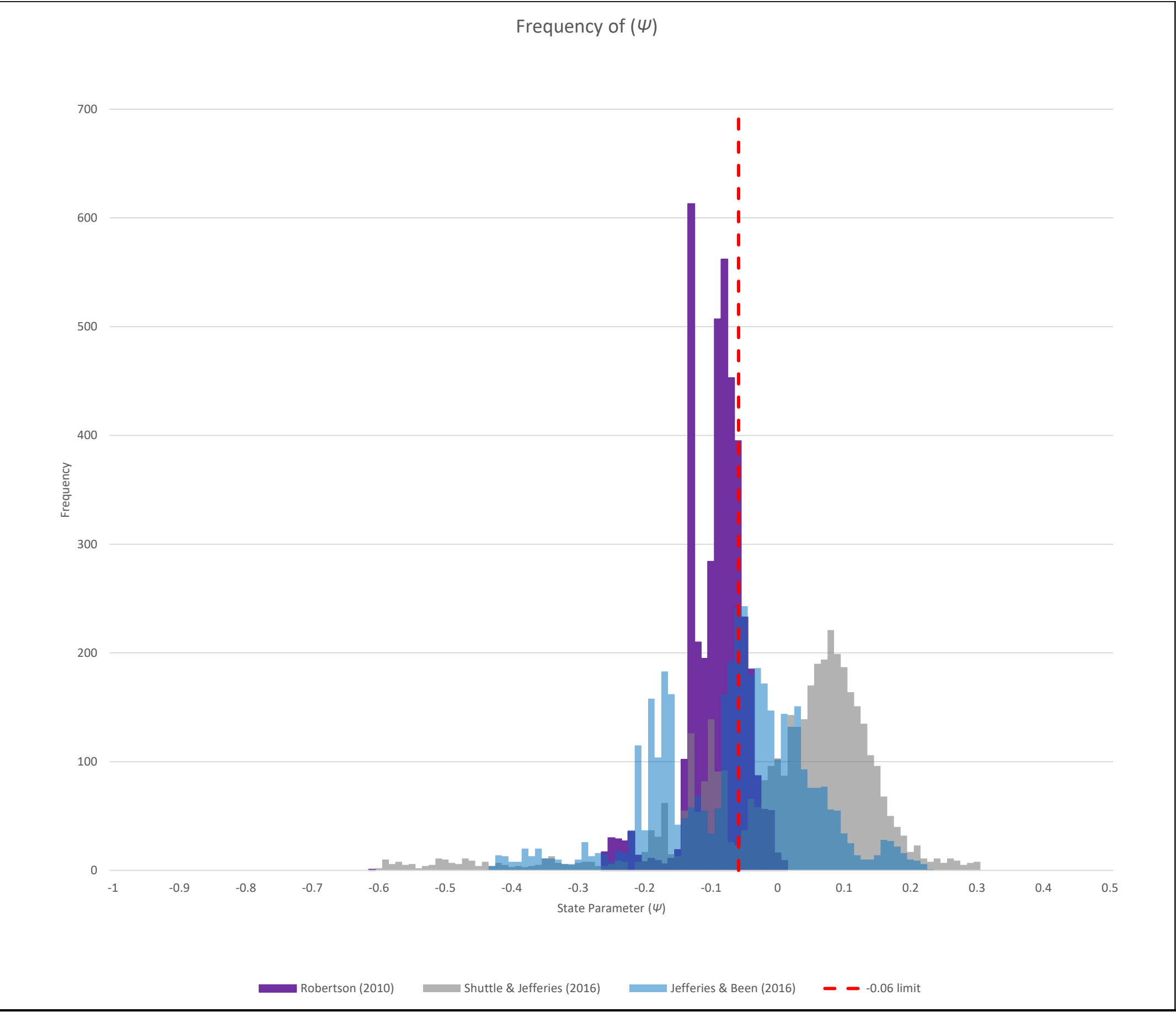


PCP3





PCP3



# PCP3

